

1127 21
146

JOURNAL OF COLLOID SCIENCE

EDITOR-IN-CHIEF

VICTOR K. LA MER
Columbia University, New York

ADVISORY BOARD

A. E. ALEXANDER	JOHN D. FERRY	THEODORE SHEDLOVSKY
STEPHEN BRUNAUER	J. J. HERMANS	ROBERT SIMHA
J. A. CHRISTIANSEN	L. G. LONGSWORTH	HARRY SOBOTKA
P. J. W. DEBYE	S. G. MASON	JACINTO STEINHARDT
B. DERJAGUIN	KAROL J. MYSELS	TORSTEN TEORELL
D. G. DERVICHIAN	J. TH. G. OVERBEEK	A. C. ZETTMLOYER
JOHN T. EDSALL	J. H. SCHULMAN	BRUNO H. ZIMM
I. FANKUCHEN	LEO SHEDLOVSKY	W. A. ZISMAN

Volume 16
1961



ACADEMIC PRESS
New York and London

THE EFFECT OF ADSORPTION ON THE VAN DER WAALS INTERACTION OF SPHERICAL COLLOIDAL PARTICLES

Marjorie J. Vold

*Department of Chemistry, University of Southern California,
Los Angeles, California*

Received March 25, 1960

ABSTRACT

A general formula has been derived for the interaction of spherical particles surrounded by any number of concentric shells of adsorbed material. The net interaction energy seems to be invariably negative (attraction) regardless of the magnitude of the van der Waals' constants of the materials comprising the particle, medium, and adsorbed substances. This result is demonstrated for one and for two adsorbed layers (i.e., a single layer of oriented amphipathic molecules), although it was not found feasible to develop a general proof. The interaction energy of solvated particles may be reduced by factors of the order of 5 to 50 compared to that of unsolvated particles. However, if current estimates of the magnitude of the van der Waals' constants are correct, flocculation can be inhibited by solvation alone only for small particles (<ca. 500 Å. radius) and quite thick layers (> ca. 20 Å.). Stabilization is most effective when the van der Waals' constant for the adsorbed material is either greater or less than the van der Waals' constants for both particle and medium.

INTRODUCTION

According to the currently accepted (1) working hypothesis of the mechanism of flocculation of colloidal suspensions, the forces responsible for particle association are, in most cases, van der Waals' forces. The total van der Waals' attraction between particles in contact is given by the sum of the London-van der Waals' interaction of all the atoms in the system in the flocculated state less the sum of the London-van der Waals' interaction of all the atoms in the system in the disperse state. Hamaker (2) has shown that the resultant is always negative (attractive) for identical homogeneous particles in a homogeneous medium, assuming that the attraction between two atoms (*i* and *j*) at a distance *r* apart is given by

$$V = -\frac{\lambda_{ij}}{r^6} \quad [1]$$

and that the interaction constant for unlike atoms is the geometric mean of those for pairs of corresponding like atoms. For two spherical particles

of radius $R_1 < R_2$ of composition P in a medium M with a separation Δ between surfaces

$$-12V = (A_P^{1/2} - A_M^{1/2})^2 H\left(\frac{\Delta}{2R_1}, \frac{R_2}{R_1}\right), \quad [2]$$

where the quantities A_P and A_M are constants depending on the compositions of particle and medium, and the function $H(x, y)$ (i.e., x is written for $\Delta/2R_1$, y for R_2/R_1) is given by

$$H(x, y) = \frac{y}{x^2 + xy + x} + \frac{y}{x^2 + xy + x + y} + 2 \ln \frac{x^2 + xy + x}{x^2 + xy + x + y}. \quad [3]$$

The constant A for a given homogeneous material with q_i, q_j , etc., kinds of atom per cubic centimeter is defined as

$$A = \pi^2 \sum_i \sum_j q_i q_j \lambda_{ij}. \quad [4]$$

The function $H(x, y)$ is always positive, decreasing from its limiting value for $x \ll 1$ to 0 as x gets very large.

$$\lim_{x \rightarrow 0} H(x, y) = \frac{y}{x(1 + y)}. \quad [5]$$

In flocculated systems the primary particles are in contact so that the separation of surfaces, Δ , is of the order of the minimum distance from each other of atom centers, at most a few Angstrom units. For colloidal particles a few hundreds of Angstrom units in radius, the function H is thus a number of the order of 100 or more at contact, so that the interaction energy will be large enough to guarantee flocculation unless its coefficient is small. For example, for $\Delta = 3$ A., $R_1 = R_2 = 500$ A., and $(A_P^{1/2} - A_M^{1/2})^2 = 5 \times 10^{-13}$ erg, $kT = 4 \times 10^{-14}$ erg, $V = 174$ in multiples of kT .

Since the interaction energies are so high, it has long been recognized (1, 3) that lyophobic suspensions owe their temporal persistence in a deflocculated state to repulsive interactions which result in a potential barrier to close approach, even though they are not large enough at close approach to overcome the London-van der Waals' interaction and give a truly stable colloid.

The classical view requires modification for systems in which the particles are partially or completely covered with an adsorbate the adsorption energy of which is high enough to prevent contact between bare particles. As the particles approach, an additional repulsion whose range is of the order of the length of the adsorbed molecule (3) arises from their interference

with each other's motion and the consequent decrease in entropy. In addition the presence of the adsorbed molecules modifies the van der Waals' interaction.

This paper examines the validity of the basic premises that the London-van der Waals' interaction is always negative and always large at surface contact, for spherical particles surrounded by concentric shells of adsorbed material. By surface contact is meant separation of the centers of the surface atoms in the solvate shells by distances of the order of a few Angstrom units (e.g., 3 Å.) since the electronic repulsion becomes rapidly very high in this range. Expressions for the interaction energy V are derived for particles surrounded by single shells and for particles surrounded by two shells such as could represent adsorbed amphipathic molecules. The case for two concentric shells can be generalized to any number by inspection.

Interaction of Spherical Particles Having a Homogeneous Adsorbed Layer

The net interaction energy is given by

$$V = V_F - 2V_D, \quad [6]$$

where V_F is the sum of the interaction of two solvated particles in contact and the interaction energy of two phantom particles with the composition of the medium, and V_D is the interaction of a phantom particle and a real solvated particle in contact. The configurations are shown in Fig. 1. The radius of the particle is R and the thickness of its adsorbed shell δ . The radius of the phantom particle, which is the medium to be displaced if flocculation occurs, is $R + \delta$.

For a sphere of radius $(R + \delta)$ composed entirely of the material of the adsorbate (S) and a second sphere of the same radius composed of the medium (M) the London-van der Waals' interaction energy V_1 at contact would be

$$-12V_1 = A_{MS} H \left(\frac{\Delta}{2(R + \delta)}, 1 \right) \quad [5]$$

where A is an interaction constant defined in a way analogous to Eq. [4] as

$$A_{MS} = \pi^2 \sum_i \sum_j q_i(M) q_j(S) \lambda_{ij}, \quad [6]$$

with $q_i(M)$ the atom density of the i^{th} kind of atom in the material M and $q_j(S)$ that of the j^{th} kind of atom in material S. It follows from this definition that A_{MS} is the geometric mean of A_M and A_S .

If, now, a sphere of radius R is imagined to be withdrawn from the center of the sphere of adsorbate, the interaction energy is reduced by

$$-12V_2 = A_{MS} H \left(\frac{\Delta + \delta}{2R}, \frac{R + \delta}{R} \right) \quad [5a]$$

which is the interaction energy of the sphere which has been withdrawn for the phantom particle. The particle (P) is then imagined to be placed in the void, augmenting the interaction energy by

$$-12V_3 = A_{PM} H \left(\frac{\Delta + \delta}{2R} \quad \frac{R + \delta}{R} \right) \quad [5b]$$

The total interaction energy of two dispersed particles which will be lost if they become flocculated is given by twice the three terms ([5], (5a), [5b]) together, yielding

$$-24V_D = 2(A_{MS}H_S - A_{MS}H_{PS} + A_{PS}H_{PS}), \quad [7]$$

where the symbol H_S is used for compactness to represent the H function for two spheres of radius $R + \delta$ and separation Δ , and H_{PS} is used for the H function for a sphere of radius R and one of radius $R + \delta$, separated by a distance $\delta + \Delta$. Later H_P , corresponding to two spheres of radius R , separated by a distance, $\Delta + 2\delta$, is required.

To deduce the value of the energy of the system in the flocculated state, start with a solvated particle and a sphere of adsorbate. The London-van der Waals' energy for this system can be written down as

$$-12V_4 = A_S H_S - A_S H_{PS} + A_{PS} H_{PS} \quad [8]$$

by analogy with Eq. [7]. If a sphere of radius R is now removed from the sphere of adsorbate the energy is reduced by

$$-12V_5 = A_S H_{PS} - A_S H_P + A_{PS} H_P, \quad [8a]$$

and, on filling the void with a particle, it is again increased by

$$-12V_6 = A_{PS} H_{PS} - A_{PS} H_P + A_{PP} H_P. \quad [8b]$$

To these three terms must be added the interaction energy of the phantom particles of medium yielding

$$\begin{aligned} -12V_F = (A_S + A_M)H_S + 2(A_{PS} - A_S)H_{PS} \\ + (A_{PP} - 2A_{PS} + A_S)H_P. \quad [9] \end{aligned}$$

Combining Eqs. [7] and [9] and using the relationships $A_{PS}^2 = A_P A_S$ and $A_{MS}^2 = A_M A_S$, which follow from their definition, yields the final result for the interaction energy controlling flocculation

$$\begin{aligned} -12V = (A_M^{\frac{1}{2}} - A_S^{\frac{1}{2}})^2 H_S + (A_S^{\frac{1}{2}} - A_P^{\frac{1}{2}})^2 H_P \\ + 2(A_M^{\frac{1}{2}} - A_S^{\frac{1}{2}})(A_S^{\frac{1}{2}} - A_P^{\frac{1}{2}})H_{PS}. \quad [10] \end{aligned}$$

Inspection of Eq. [10] shows that it is equivalent to the sum of the interaction energies for flocculation of two hypothetical solvate particles of radius $(R + \delta)$ separated by a distance Δ in the medium and two unsolvated

particles of radius R separated by a distance $\Delta + 2\delta$ in a medium composed of the adsorbed solvating material, plus a correction term which accounts for the fact that the hypothetical solvate particles giving the first term and the hypothetical medium involved in the second term are only shells.

Interaction of Spherical Particles Having an Adsorbed Layer of Oriented Molecules

The configuration and nomenclature for this case is also shown in Fig. 1 if the symbol I for inner, O for outer, and P for particle replace the integers 1, 2, 3, etc. The adsorbed layer of oriented molecules is treated as two shells, an inner one with a London-van der Waals' constant A_I and thickness δ_I and an outer one with a London-van der Waals' constant A_O . The total interaction energy of the system in the dispersed state which is lost upon flocculation is given by

$$\begin{aligned}
 -24V_D = 2 \bigg[& A_{MO} H \left(\frac{\Delta}{2(R + \delta_I + \delta_O)}, 1 \right) \\
 & - A_{MO} H \left(\frac{\Delta + \delta_O}{2(R + \delta_I)}, \frac{R + \delta_I + \delta_O}{R + \delta_I} \right) \\
 & + A_{MI} H \left(\frac{\Delta + \delta_O}{2(R + \delta_I)}, \frac{R + \delta_I + \delta_O}{R + \delta_I} \right) \\
 & - A_{MI} H \left(\frac{\Delta + \delta_O + \delta_I}{2R}, \frac{R + \delta_I + \delta_O}{R} \right) \\
 & + A_{PM} H \left(\frac{\Delta + \delta_O + \delta_I}{2R}, \frac{R + \delta_I + \delta_O}{R} \right) \bigg] \quad [11]
 \end{aligned}$$

following exactly the scheme used in the preceding derivation starting with a hypothetical sphere of radius $R + \delta_I + \delta_O$ composed of the material of the outermost shell (O), interacting with a phantom particle of medium of the same radius and removing a sphere of radius $R + \delta_I$ from it, replacing it with one composed of material of the inner shell, removing a sphere of radius R from this and replacing it with the unsolvated particle.

The London-van der Waals' interaction energy for the flocculated system is derived in a completely analogous manner starting with two spheres of radius $R + \delta_I + \delta_O$ separated by the distance Δ . When the result is combined with Eq. [12] and the general relation $A_{\alpha\beta}^2 = A_\alpha A_\beta$ inserted the net interaction energy becomes

$$\begin{aligned}
 -12V = & (A_O^{\frac{1}{2}} - A_M^{\frac{1}{2}})^2 H_O + (A_I^{\frac{1}{2}} - A_O^{\frac{1}{2}})^2 H_I \\
 & + (A_P^{\frac{1}{2}} - A_I^{\frac{1}{2}})^2 H_P + 2(A_O^{\frac{1}{2}} - A_M^{\frac{1}{2}})(A_I^{\frac{1}{2}} - A_O^{\frac{1}{2}}) H_{IO} \\
 & + 2(A_I^{\frac{1}{2}} - A_O^{\frac{1}{2}})(A_P^{\frac{1}{2}} - A_I^{\frac{1}{2}}) H_{IP} \\
 & + 2(A_O^{\frac{1}{2}} - A_M^{\frac{1}{2}})(A_I^{\frac{1}{2}} - A_I^{\frac{1}{2}}) H_{OP} . \quad [12]
 \end{aligned}$$

In the notation used above for compactness, the subscripts of the interaction constants A refer to the composition of the particle, medium, and inner and outer layers, and the same subscripts of the H functions refer to the radii of corresponding spheres and their separations as indicated in Fig. 1.

The structure of the expression for the interaction energy is similar to that derived for particles with a single shell. It is the sum of pairwise interaction of spheres of radius $R + \delta_I + \delta_O$, $R + \delta_I$, and R , supposing each pair to be made entirely of the material of its outer part and immersed in a homogeneous medium whose composition is that of the layer next to it, plus correction terms. The expression can readily be generalized to encompass adsorbed layers of any degree of complexity provided their composition is a function only of distance from the center of a spherical adsorbing particle. The result can be written compactly as

$$-12V = \sum_{i,j=1,n} a_i a_j H_{ij}, \quad [13]$$

where the subscript zero is assigned to the medium and the successive layers of adsorbed material are numbered from the outside inward as 1, 2, \dots , $n - 1$, the unsolvated particle being numbered n

$$a_i = (A_i^{\frac{1}{2}} - A_{i-1}^{\frac{1}{2}}) \quad [14a]$$

$$H_{ij} = H_{ji} = H \left(\frac{\delta_{ij}}{2R_K} \frac{R_L}{R_K} \right), \quad [14b]$$

where R_K is the radius of whichever shell, i or j , has the smaller radius, R_L is the radius of the other, and δ_{ij} is the separation of the surfaces of the two spheres.

Argument that the Net Interaction Energy Must Always be Negative

The author is unable to provide a general proof that the right-hand member of Eq. [13] is always positive. If the equation is regarded as a quadratic equation for any one of the van der Waals' constants, say a_1 , it can be written

$$a_1 = - \sum_{K=2}^n \frac{a_K H_{1K}}{H_{11}} + \frac{1}{H_{11}} \left[\sum_{K=2,L}^n a_K a_L (H_{1K} H_{1L} - H_{KL} H_{11}) - 12V H_{11} \right]^{\frac{1}{2}}. \quad [15]$$

Since a_1 is real the double summation appearing in the discriminant must be positive if the interaction V is to be positive. For $n = 2$, corresponding to a single adsorbed layer, the critical sum (Σ) reduces to

$$\Sigma = a_2^2 (H_{12}^2 - H_{22} H_{11}) \quad [16]$$

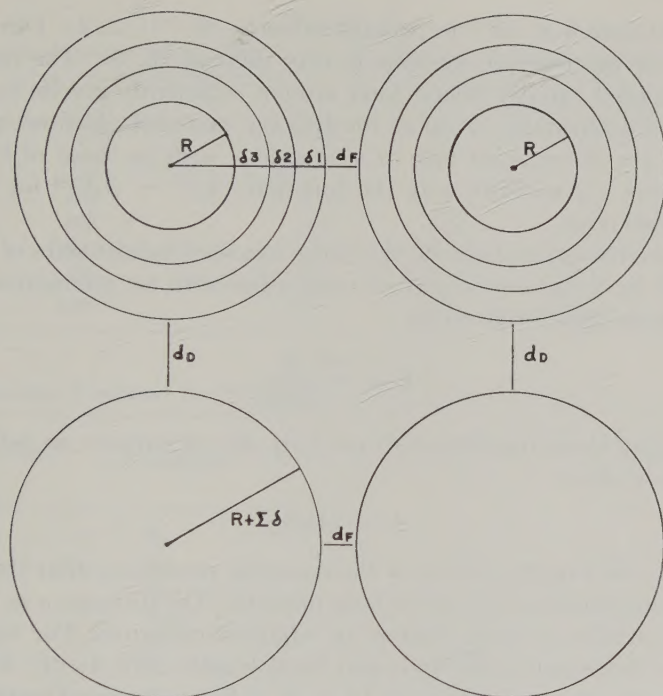


FIG. 1 Nomenclature for calculation of the van der Waals' energy of solvated particles. The particles have always the radius R and are separated by d_F augmented by the thickness of intervening adsorbed layers. Phantom particles of medium are also represented. In flocculation d_F is small (Δ) and d_D is infinite. In the disperse state the reverse is true. The shells are numbered $1, 2 \dots n-1$, the particle n , and the medium 0 .

while for $n = 3$, corresponding to an oriental adsorbed layer of amphipathic molecules,

$$\Sigma = (a_2 H_{12} + a_3 H_{13})^2 - H_{11}(a_2^2 H_{22} + 2a_2 a_3 H_{23} + a_3^2 H_{33}). \quad [17]$$

A very large number of systematic numerical calculations suggest that Σ is invariably negative for $n = 2$ and $n = 3$ at least. Hence V must be negative for these cases.

Order of Magnitude of the London-van der Waals' Constant

Equation [13] for the total interaction energy is a sum of terms each involving a constitutive part ($a_i a_j$) and a geometric part (H_{ij}) along with the numerical factor $1/12$. The following discussion is primarily justification for the guess that $1/12 a_i a_j$ is at most $10 kT$ at room temperature, and very likely more usually $0.5-1 kT$.

Theoretical estimates of the parameter A , as defined in Eq. [4], range

downward from 5×10^{-12} to perhaps as low as 10^{-13} (1, 2, 4). Direct measurement in macroscopic systems is very difficult (5, 6). The results for the unretarded van der Waals' force are not sufficiently precise to provide a means of determining A values for different materials. Indirect measures based on the flocculation rate of suspensions such as those of Overbeek and Reerink (7) measure only the function $(A_1^{1/2} - A_2^{1/2})^2$ for two different substances.

Overbeek has pointed out (8) that since two semi-infinite slabs of material separated by a distance a attract each other with an interaction energy per square centimeter given by

$$V = -\frac{A}{12\pi a^2}$$

and bringing them together destroys 2 sq. cm. of surface, an estimate of A can be made as

$$A = 24\pi a^2 \gamma,$$

where γ is the surface tension of the material, presuming that the surface has the same composition as the bulk material. The distance a in this case is the separation of atom centers in adjacent molecules. For water this should be presumably the hydrogen bond length, 2.76 Å. (9). Since γ is 72 dynes/cm., A is estimated as 4.15×10^{-12} . For a saturated hydrocarbon, twice the van der Waals' radius of the H atom should be a reasonable choice, yielding, for a surface tension of 20 dynes/cm., 2.17×10^{-13} .

From the flocculation rate of silver iodide solutions, Overbeek and Reerink found $(A_1^{1/2} - A_2^{1/2})^2$ for silver iodide and water to be 5×10^{-13} . If the value for water is 4.15×10^{-12} , that for silver iodide is either 1.8×10^{-12} or 7.3×10^{-12} , an arbitrary choice of sign being necessary. The higher value seems more plausible considering the high polarizability of iodide ion.

Values of A lying between 2×10^{-13} and 8×10^{-12} for individual materials mean that the coefficients $a_i a_j / 12$ of individual H functions in Eq. [13] can vary from virtually zero to a probable maximum of 5×10^{-13} erg or about $10 kT$ at room temperature.

Order of Magnitude of the Interaction Energy of Solvated Spherical Particles

For the special case that the solvate shell is a layer of bound medium, the total interaction energy given by Eq. [10] reduces to

$$V = -\frac{1}{12} (A_M^{1/2} - A_P^{1/2})^2 H \left(\frac{\Delta + 2\delta}{2R}, 1 \right), \quad [18]$$

where δ is the thickness of the layer of bound medium and R is the particle radius. The distance of closest approach of the solvated surfaces, Δ , has

TABLE I

Values of the Hamaker Function for Solvated Spherical Particles Separated by 3 Å.

Particle radius (Å.)	Thickness of the solvate shell (Å.)			
	0	5	10	20
100	27.0	4.1	1.7	0.5
200	58.9	10.9	5.0	1.8
300	94	17.4	8.6	3.6
500	167	31.9	16.2	7.3
1000	333	70	36.7	17.6

TABLE II

Hamaker Functions for Protected Colloidal Particles Separated by 3 Å.

Particle radius (Å.)	<i>H</i> functions	Layer thickness (Å.)			
		0	5	10	20
200	H_P	58.9	10.9	5.0	1.8
	H_S	—	60.1	62.0	66
	H_{PS}	—	19.5	10.8	5.2
	H'_{min}^a	—	8.2	4.3	1.6
300	H_P	94	17.4	8.6	3.6
	H_S	—	96	98	100
	H_{PS}	—	31.3	18.1	8.8
	H'_{min}^a	—	12.7	6.3	3.3
500	H_P	167	31.9	16.2	7.3
	H_S	—	168	169	173
	H_{PS}	—	55.3	32.2	16.6
	H'_{min}^a	—	25.7	14.1	6.8
1000	H_P	333	70	36.7	17.6
	H_S	—	335	336	340
	H_{PS}	—	125	70	37.1
	H'_{min}^a	—	57.7	32.0	16.3

^a From Eq. [20].

been arbitrarily chosen to be 3 Å. and the thickness of the bound layer chosen to be 5, 10, and 20 Å. Corresponding values of H for particles of various radii are given in Table I. Presumably the total interaction energy must be of the order of kT for preservation of a dispersed state. If the coefficient has a small enough value, particles up to 1000 Å. in radius can be stabilized in dispersion by bound medium, but for values of the order of say 5×10^{-13} , Table I shows that only very small particles with thick solvate shells can be stabilized in this way. For example, if $\frac{1}{12} (A_P^{1/2} - A_M^{1/2})^2 = kT$, and $10 kT$ is regarded as sufficient to prevent thermal redispersion, particles of 100 Å. radius can be easily stabilized, particles of 200 Å. radius only with adsorbed layers thicker than 5 Å., particles of

TABLE III

Hamaker Functions for Colloidal Particles of 500 A. Radius 3 A. Apart Protected by Oriented Amphipathic Molecules of Variable Chain Length^a

Function ^b	$\delta = 0$	Chain length		
		$\delta = 5$ A.	$\delta = 10$ A.	$\delta = 20$ A.
H_{11}	168	170	172	174
H_{12}	168	56.4	32.5	16.8
H_{13}	55.6	32.2	22.2	13.0
H_{22}	168	32.2	16.4	7.4
H_{23}	55.6	21.9	12.8	6.3
H_{33}^c	31.9	16.2	10.3	5.4
H'_{\min}	31.9	9.3	3.3	2.0
H'_{\min}^d	25.7	14.1	9.7	4.3

^a The "head" is given a length of 5 A. and adjoins the particle.

^b For notation see Eq. [14].

^c Applies to a layer of bound medium of thickness ($\delta + 5$).

^d From Table II for optimum layer of thickness ($\delta + 5$), interpolated or extrapolated as required.

500 A. radius only with adsorbed layers thicker than 10 A., etc. It is of course assumed throughout that the particles are not able to desorb the adsorbed molecules.

Particles with Adsorbed Molecules

The values of the required Hamaker functions for application to Eq. [11] for which the adsorbed layer differs in composition from the medium, for varying layer thicknesses and particle radii, are given in Table II. It is easy to show that for the same composition of particle and medium, a value for the van der Waals' constant of the solvent can be selected which yields a minimum value for the net attraction, which is less than that for particles with an equally thick layer of bound medium. The results are:

$$A_s^{1/2} = \frac{A_M^{1/2}(H_P - H_{PS}) + A_P^{1/2}(H_S - H_{PS})}{H_P - 2H_{PS} + H_S}; \quad [19]$$

$$\begin{aligned} -12V &= (A_P^{1/2} - A_M^{1/2})^2 H_{\min} \\ &= (A_P^{1/2} - A_M^{1/2})^2 \left(H_P - \frac{(H_P - H_{PS})^2}{H_P - 2H_{PS} + H_S} \right). \quad [20] \end{aligned}$$

Numerical results are given in Table II for the same range of particle sizes and layer thicknesses considered under solvation. Although it is possible by proper choice of adsorbed material to reduce the van der Waals' attraction somewhat, the maximum effect is not much over 20%, and it remains true that pronounced stabilization can occur only for small

TABLE IV

Hamaker Functions for Colloidal Particles of 500 Å. Radius 3 Å. Apart Protected by Oriented Amphipathic Molecules of Variable Chain Length^a

Function ^b	Chain length			
	$\delta = 0 \text{ Å.}$	$\delta = 5 \text{ Å.}$	$\delta = 10 \text{ Å.}$	$\delta = 20 \text{ Å.}$
H_{11}	168	170	172	174
H_{12}	55.6	56.1	57.0	58.4
H_{13}	55.6	32.2	22.1	12.9
H_{22}	32.0	32.3	32.9	33.6
H_{23}	55.6	21.9	16.1	10.6
H_{33}^c	31.9	16.2	10.3	5.4
H'_{\min}	31.9	9.3	6.7	3.9
H'_{\min}^d	25.7	14.1	9.7	4.3

^a The "head" is given a length of 5 Å. and adjoins the medium.

^b For notation see Eq. [14].

^c Applies to bound medium of thickness ($\delta + 5$).

^d From Table II for an optimum layer of thickness ($\delta + 5$), interpolated or extrapolated as required.

particles or for particles coated with thick adsorbed layers. Compare H_P and H'_{\min} to see this effect.

Particles with Adsorbed Oriented Molecules

Numerical investigation of the effect of oriented adsorbed layers has been carried out for amphipathic molecules at a single value of the particle radius, first with the "head" of the molecule adsorbed, and the "tail" of variable length directed toward the medium and having the same van der Waals' constant as the medium, choosing the optimum relation between the van der Waals' constants for the particle and the adsorbed heads as was used for adsorbed unoriented or homogeneous molecules. The results given in Table III show that it is theoretically possible to stabilize a particle more effectively with such oriented adsorption than with a layer of bound medium of equal thickness or an adsorbed unoriented layer of equal thickness. The application of Eq. [13] gives for this case

$$\frac{-12V}{(a_P - a_M)^2} = H'_{\min.} = H_{33} - \frac{(H_{33} - H_{23})^2}{(H_{22} + H_{33} - 2H_{23})}. \quad [21]$$

For oriented molecules with the "head" outwards, having the same van der Waals' constant as the medium, Eq. [21] also applies but the arguments of the H functions differ. The results given in Table IV show that in this case also adsorption of appropriately selected oriented molecules is more effective than a corresponding layer of bound medium or than adsorption of a single homogeneous layer.

General Discussion

All the numbers in Tables I–IV have to be combined with numerical values of van der Waals' constants of the sort defined in Eq. [4], before the question can be answered as to whether or not association of particles protected by adsorbed layers can ever involve such weak interaction that ordinary thermal motions can be expected to keep them largely dispersed. However, unless the A values are substantially smaller than is currently thought probable, any such phenomenon can be expected only for very small particles or for thick layers of adsorbed material.

If the protection involves a layer of bound medium, the interaction energy can be reduced by a factor of from 5 to 50 depending on the thickness of the adsorbed layer and on the particle radius. It may also be observed that the difference in interaction energies between small and large particles is greatly reduced by solvation.

Finally, investigation of Eq. [19] shows that to obtain maximum protection for a given layer thickness of adsorbed material the van der Waals' constants for particle, medium, and sorbate must be in the order $A_M < A_P < A_S$ or $A_M > A_P > A_S$. In the latter case also there will be some values of A_M/A_P for which no optimum positive A_S can be found.

ACKNOWLEDGMENTS

Financial support of this Project by the Office of Ordnance Research is gratefully acknowledged. Numerical computations were facilitated by the preparation of an extensive table of values of the H function on the IBM 709 computer of the Western Data Processing Center, University of California at Los Angeles. The author is especially grateful to Professor J. Th. G. Overbeek for valuable assistance throughout the course of this work.

REFERENCES

1. VERWEY, E. J. W., AND OVERBEEK, J. Th. G., "Theory of the Stability of Lyophobic Colloids." Elsevier, Amsterdam, 1948.
2. HAMAKER, H. C., *Physica* **4**, 1058 (1937).
3. MACKOR, E. L., AND VAN DER WAALS, J. H., *J. Colloid Sci.* **7**, 535 (1952).
4. KOELMANS, H., AND OVERBEEK, J. Th. G., *Discussions Faraday Soc.* **18**, 52 (1954).
5. DERJAGUIN, B. V., TITJEVSKAIA, A. S., ABRICOSSOVA, I. I., AND MALKINA, A. D., *Discussions Faraday Soc.* **18**, 24 (1954).
6. DE JONGH, J. G. V., Thesis, University of Utrecht, 1958.
7. REERINK, H., AND OVERBEEK, H. Th. G., *Discussions Faraday Soc.* **18**, 74 (1954).
8. OVERBEEK, J. Th. G., private communication.
9. PAULING, L., "Nature of the Chemical Bond," p. 281. Cornell University Press, Ithaca, New York, 1939.

RHEOLOGICAL PROPERTIES OF MONODISPERSE LATEX SYSTEMS

I. CONCENTRATION DEPENDENCE OF RELATIVE VISCOSITY¹

Frank L. Saunders

Plastics Basic Research Laboratory, The Dow Chemical Company, Midland, Michigan

Received June 22, 1959, revised September 13, 1960

ABSTRACT

The relations of relative viscosity η_r to volume fraction ϕ for a series of monodisperse polystyrene latexes were determined for particle diameters between 990 Å and 8710 Å. Volume fractions up to about 0.25 were considered above which the latexes were non-Newtonian as indicated from flow curves obtained with a rotational viscometer. Experimental results obtained with a capillary viscometer appeared to fit the general equation $\eta_r = \exp. \alpha_0 \phi / 1 - k\phi$ with a value of 2.504 for α_0 in good agreement with the Einstein coefficient of 5/2. The constant α_0 was found to be independent of particle diameter provided the measured volume fraction was corrected for an adsorbed layer of emulsifier. The interaction coefficient k varied from 1.118 to 1.357 increasing with decreasing particle diameter.

INTRODUCTION

The rheological properties of synthetic latex systems have been studied in recent years to obtain information on the flow behavior of stable colloidal suspensions. Synthetic latexes represent a fairly uniform dispersion of spherical colloidal particles of small particle size and can be prepared to give very narrow particle-size distributions. With the availability of monodisperse polystyrene latexes of different particle diameters, it was of interest to investigate the relative viscosity of these latexes as a function of concentration and particle size.

A great variety of theoretical and empirical equations have been developed to predict the concentration dependence of the viscosity of colloidal systems, a number of which have been reviewed by Ward (1). Whereas no one equation has been found to adequately represent all systems, many of the equations can be expressed as a power series

$$\eta_r = 1 + \alpha_0 \phi + \alpha_1 \phi^2 + \alpha_2 \phi^3 + \dots \quad [1]$$

¹ Presented in part before the Division of Colloid Chemistry at the 131st Meeting of the American Chemical Society, Miami, Florida, April, 1957.

where ϕ is the volume fraction; η_r the relative viscosity; α_0 the Einstein coefficient ($= 5/2$); and α_1 and α_2 interaction coefficients. Equation [1] is an extension to finite concentration of the well-known Einstein viscosity equation at infinite dilution (2). The present work was undertaken to determine the viscosity-concentration dependence of monodisperse latexes of different particle size and the effect of particle size on the value of α_0 and the interaction coefficients at finite concentration.

EXPERIMENTAL

A series of monodisperse polystyrene latexes of different particle sizes similar to those described by Bradford and Vanderhoff (3) were used for the viscosity measurements. The average particle size was determined by electron microscopy as described in reference 3. The particle size ranged from 990 to 8710 Å and the latexes were essentially monodisperse.

The latexes were formulated to the surface tension minimum to obtain surface coverage of the particles with the same emulsifier used in the polymerization of the latex. The various concentrations were obtained by dilution of the latex with a solution of the same emulsifier at its surface tension minimum to minimize desorption of the adsorbed emulsifier with dilution and to maintain the viscosity of the aqueous phase constant.

The viscosities of the latexes were measured by two methods; Oswald-Fenske viscometer, and a rotational viscometer similar in design to that described by Oldroyd *et al.* (4). The measurements made in the capillary viscometer are those recorded for the relative viscosity-concentration dependence. The measurements were made at $25.00^\circ \pm .02^\circ\text{C}$. The rotational viscometer was used to determine the concentration at which the latex systems were non-Newtonian as indicated by a nonlinear relationship between rate of shear and shearing stress as described by Krieger and Maron (5). Only those systems that gave Newtonian flow were considered here, thus limited to volume fractions less than 0.25.

The measured volume fraction, C , of the latex was obtained from the partial specific volume (1/1.052) and the dry weight concentration correcting for salt and emulsifier concentration. The relative viscosity was determined from the measured efflux time of the latex and that of the aqueous phase containing the emulsifier.

RESULTS AND DISCUSSION

To indicate the concentration range in which the latex systems show Newtonian flow, the flow curves of the latexes were determined with the rotational viscometer by measuring the shearing stress at various rates of shear up to 256 sec^{-1} . A linear relationship between rate of shear and shearing stress is indicative of Newtonian flow. To indicate the deviation from

Newtonian behavior, the flow curves were plotted in the form of an exponential equation

$$F^N = \eta' S \quad [2]$$

as described by Krieger and Maron (5). The index of non-Newtonian behavior is given by N , with F the shearing stress, S the rate of shear, and η' the viscosity at unit shearing stress. For a Newtonian system, N is unity. From suitable logarithmic plots of Eq. [2] at various volume fractions, the coefficient N can be determined. In Fig. 1 are shown the data for a typical monodisperse latex (2510 Å) up to a volume fraction of 0.40. These results indicate that below a volume fraction of about 0.25 the latex is Newtonian in agreement with the result found by Krieger and Maron (5). Similar data obtained with latexes of different particle size showed very little change in the concentration at which non-Newtonian flow was observed. There was a slight trend towards lower concentrations with decreasing particle size; however, the difference was not considered significant in terms of the method by which N was determined. This point may be worthy of further consideration with a more sensitive method of determining non-Newtonian flow.

The viscosity-concentration data for a series of monodisperse polystyrene latexes are given in Table I. In Fig. 2 is a plot of η_{sp}/C vs. C indicating a nonlinear dependence over the concentration range of 0.023–0.24 volume fraction.

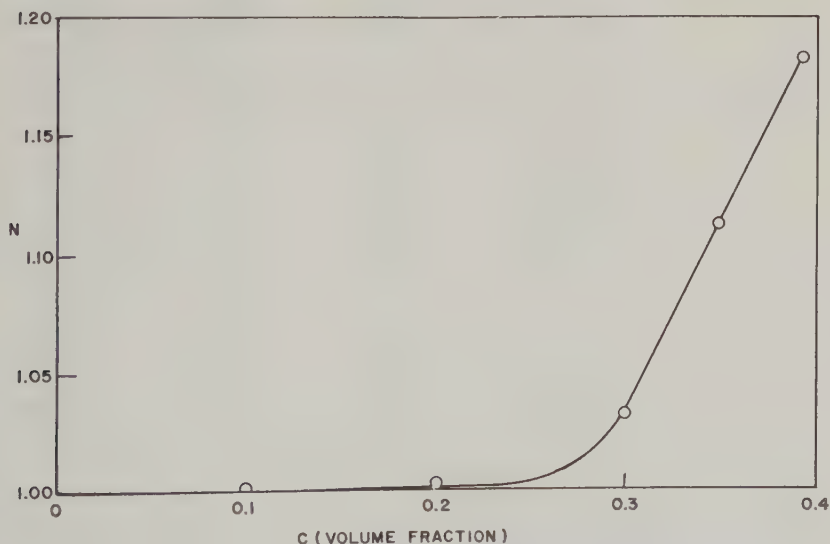


FIG. 1. Variation of N with volume fraction of monodisperse latex.

TABLE I
Viscosity-Concentration Data for Monodisperse Polystyrene Latexes

Diam (<i>A</i>)	<i>C</i>	η_r	<i>C</i> /log η_r	η_{sp}/C
990	0.2394	2.620	0.5723	6.767
	0.1915	2.009	0.6321	5.269
	0.1436	1.613	0.6916	4.269
	0.09576	1.339	0.7553	3.540
	0.04788	1.145	0.8141	3.028
	0.02394	1.068	0.8379	2.840
1480	0.2422	2.490	0.6112	6.152
	0.1938	1.945	0.6709	4.876
	0.1453	1.584	0.7278	4.019
	0.09688	1.331	0.7795	3.412
	0.04844	1.143	0.8346	2.952
	0.02422	1.067	0.8601	2.766
2490	0.2372	2.311	0.6520	5.527
	0.1897	1.886	0.6885	4.671
	0.1423	1.553	0.7444	3.886
	0.09487	1.315	0.7979	3.320
	0.04744	1.137	0.8508	2.888
	0.02372	1.064	0.8805	2.698
3420	0.2348	2.271	0.6591	5.413
	0.1878	1.847	0.7101	4.510
	0.1409	1.538	0.7530	3.818
	0.09390	1.306	0.8098	3.259
	0.04695	1.135	0.8536	2.875
	0.02348	1.063	0.8846	2.683
4240	0.2332	2.242	0.6651	5.326
	0.1866	1.827	0.7129	4.432
	0.1399	1.529	0.7586	3.781
	0.09328	1.302	0.8139	3.238
	0.04664	1.133	0.8600	2.852
	0.02332	1.063	0.8790	2.702
8710	0.2411	2.329	0.6566	5.512
	0.1929	1.851	0.7214	4.412
	0.1447	1.543	0.7682	3.753
	0.09645	1.312	0.8179	3.325
	0.04823	1.137	0.8649	2.841
	0.02411	1.065	0.8815	2.696

There also appears to be a definite effect of particle diameter on the viscosity-concentration relationship.

To express the data in a form suitable for evaluation of the Einstein

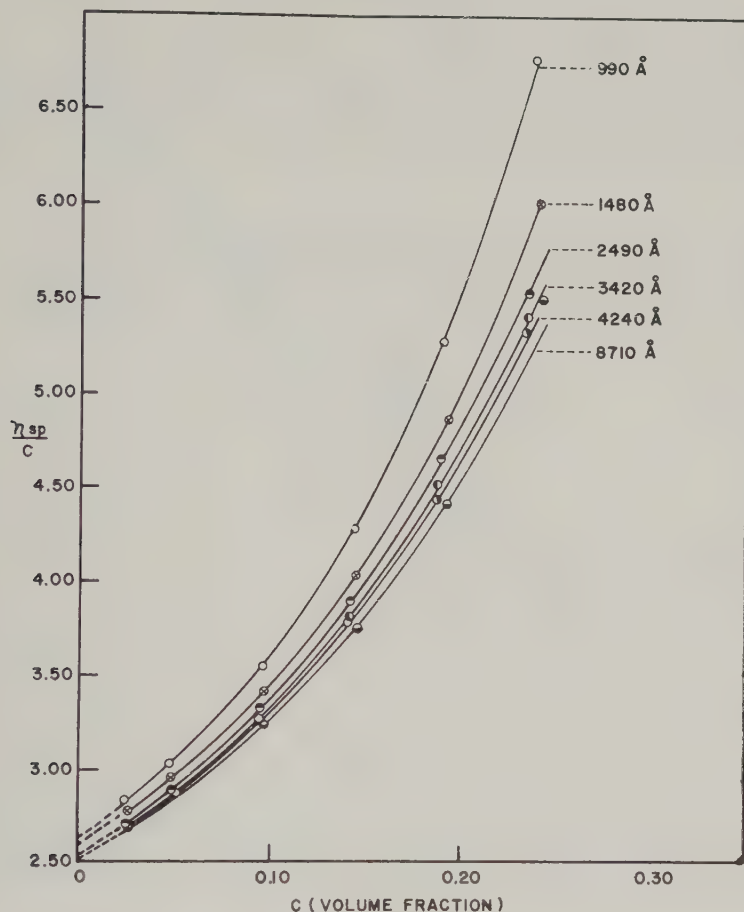


FIG. 2. Reduced viscosity-concentration plot for monodisperse latexes.

coefficient and interaction constants, the following general exponential equation was used:

$$\eta_r = \exp \frac{(\alpha_0 \phi)}{(1 - k\phi)}, \quad [3]$$

where η_r is the relative viscosity, α_0 and k are constants, and ϕ is the effective volume fraction. Equation [3] is of the form theoretically derived by Vand (6) with α_0 corresponding to Vand's shape factor, and k the hydrodynamic interaction constant. Mooney's (7) equation is also of the form of Eq. [3] with α_0 equivalent to Einstein's constant of 2.50, and k the self-crowding factor which Mooney estimates should be about 1.35 for mono-

disperse systems from consideration of geometric packing of densely packed spheres.

It has been shown (8-15) that colloidal suspensions may have an adsorbed layer that increase the measured volume fraction, C , such that the effective volume fraction, ϕ , is given by

$$\phi = fC, \quad [4]$$

where f is a factor to correct for the adsorbed layer.

Substitution of Eq. [4] in Eq. [3] and expressing as a logarithmic function, Eq. [3] becomes

$$\frac{C}{\log \eta_r} = \frac{2.303}{\alpha_0 f} - \frac{(2.303k)}{(\alpha_0)} C \quad [5]$$

or

$$\frac{C}{\log \eta_r} = mC + B, \quad [6]$$

where the slope constant

$$m = -\frac{2.303k}{\alpha_0}, \quad [6a]$$

and the intercept

$$B = \frac{2.303}{\alpha_0 f}. \quad [6b]$$

A linear plot of $C/\log \eta_r$ vs. C can be used to determine the constants m and B . It has been shown (8, 14) that the ratio ϕ/C , or f (from Eq. [4]) is given by

$$\frac{\phi}{C} = f = 1 + \frac{6\Delta}{D} \quad [7]$$

where Δ is the thickness of the adsorbed layer and D the particle diameter.

If in Eq. [5] or [6] we let

$$\alpha = \alpha_0 f, \quad [8]$$

and substitute in Eq. [7] we obtain

$$\alpha = \alpha_0 \frac{6}{D} \Delta + \alpha_0. \quad [9]$$

Since α can be determined from the intercept of Eq. [6], for each particle size, the values of α_0 and Δ can be obtained from a linear plot of α vs. $1/D$.

From the above Eqs. [6] and [9], the values of α_0 , Δ , and k can be determined from viscosity-concentration data on monodisperse latexes of different particle diameters.

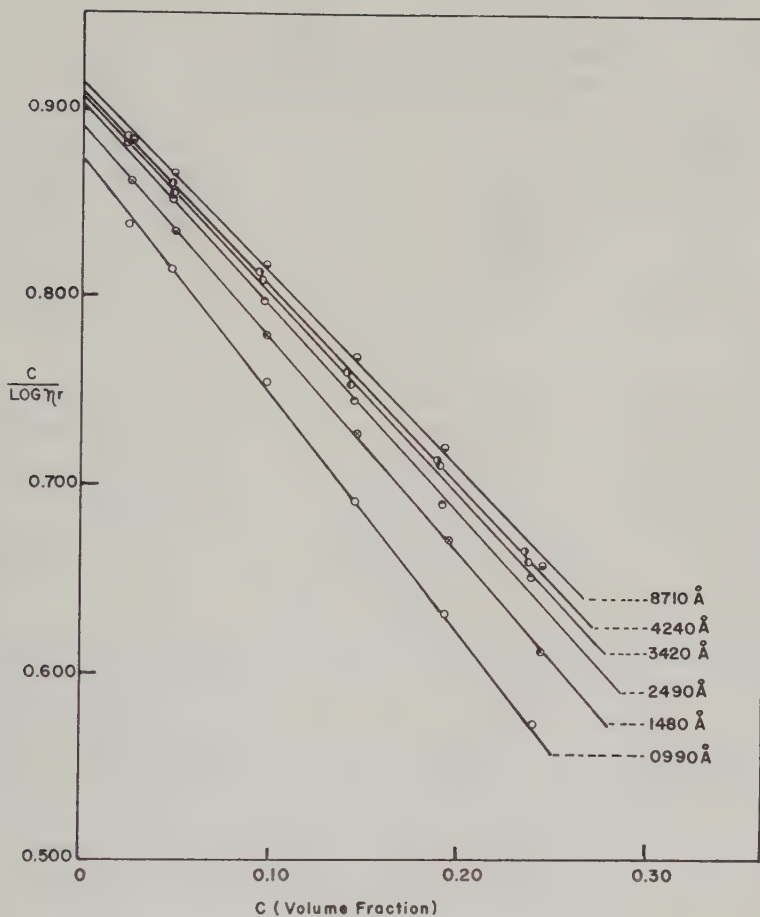


FIG. 3. Plot of $\frac{C}{\log \eta_r}$ vs. C for monodisperse latexes.

In Fig. 3 is shown a plot of $C/\log \eta_r$ vs. C for monodisperse latexes of different particle diameter indicating a reasonably good linear relationship for each particle size. The data depicted in Fig. 3 are given in Table I. The straight line drawn through the experimental points for each particle size was determined by the method of least squares. In Table II, the slope and intercept constants are given with the corresponding values of α and k as given by Eqs. [6a] and [6b] using the value of 2.504 for α_0 as determined below.

With the experimental determined value of α for each particle size, a plot of α vs. $1/D$ should be linear as given by Eq. [9]. Such a plot is shown in Fig. 4 with the straight line being determined by the method of least squares. From this line the value of α_0 was found to be 2.504 ± 0.046 , and $\Delta = 9 \text{ \AA}$, where the precision of α_0 is expressed as the 95 % confidence limits

TABLE II
*Constants for Eq. [6] Relating Viscosity and
 Concentration for Monodisperse Latexes*

Diam (<i>A</i>)	<i>B</i>	$-m$	α	k
990	0.8715	1.248	2.642	1.357
1480	0.8895	1.136	2.589	1.235
2490	0.9024	1.089	2.552	1.184
3420	0.9065	1.056	2.541	1.148
4240	0.9066	1.039	2.540	1.130
8710	0.9132	1.028	2.522	1.118

calculated from the residual variations around the regression line. The value of 2.504 for α_0 is in good agreement with the Einstein value of 2.500. The calculated value of Δ for the thickness of the adsorbed layer is rather small compared with other emulsifiers; however, the value of about 9 Å is reasonably close to the thickness of the emulsifier layer as indicated by scaled Fisher-Hirschfelder Models and unpublished data by the author on the molecular adsorption area of this emulsifier.

The values of k as given in Table II indicate a dependence of this interaction or crowding factor on particle size, decreasing with increasing particle diameter. Attempts were made to graphically determine this function; however, the experimental k values do not appear to be precise enough to give a reliable fit and distinguish between a number of possible equations.

The value of 1.357 obtained for k with the small particle size latex is close to Mooney's value of 1.35; however, k decreases with increasing particle size as indicated above. Thus, k appears to be determined by other factors in addition to simple geometric packing considerations, this being especially true for highly charged particles such as considered here. The electroviscous effect and other interactions may be involved which would increase with decreasing particle size and affect k in the manner indicated by the data. In addition, there may also be an effect due to immobilization of the aqueous phase by aggregation as the concentration increases. This effect would tend to increase the observed viscosity and also increase with decreasing particle diameter (15).

Sweeny and Geckler (16) have studied the rheological properties of glass spheres and find the value of k to vary from 1.000 to 1.470. Their data also indicate a particle-size dependence with the larger particles giving lower k values.

If the general equation [3] is expanded into a power series

$$\frac{\eta_r - 1}{\phi} = \frac{\eta_{sp}}{\phi} = \alpha_0 + \alpha_1 \phi + \alpha_2 \phi^2 + \dots \quad [10]$$

the interaction coefficients, α_1 and α_2 , are dependent on particle size. Data

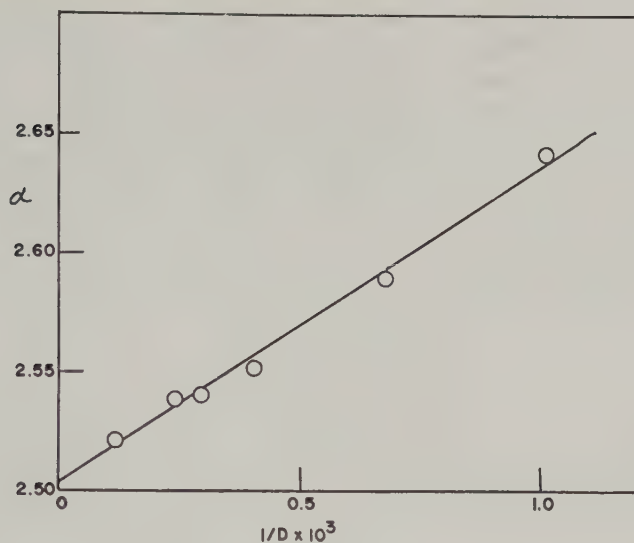


FIG. 4. Variation of α with $1/D$ as given by Eq. [9].

from the present work in the particle size range considered result in values of 6.29–7.64 for α_1 and 26.9–36.3 for α_2 , the smaller values corresponding to the larger particle size.

The value of the interaction constant α_1 is in good agreement with the value 7.35 obtained by Vand (6), and a value of 7.5 theoretically derived by Kynch (17); however, it is lower than the 10.05 obtained by Manley and Mason (18) on modification of Vand's theory, and the 12.6 resulting from Simha's treatment (19, 20). The data of Cheng and Schachman (21) on polystyrene latex also appear to give values higher than those obtained here.

Maron *et al.* (12, 13) have applied the generalized flow theory of Ree and Eyring to latex viscosity behavior and obtained a value of 2.60 for α_0 , and for the second and third coefficients values of 5.80 and 11.8. Nawab and Mason (22) have recalculated Maron's data without a volume correction and from a linear plot of η_{sp}/ϕ vs. ϕ obtain values of 2.53 for α_0 and 11.7 for α_1 .

The values reported for α_1 will depend on whether or not α_2 and higher terms are significant and are included in the power series equation. The data reported here indicate a significant curvature when plotted as η_{sp}/ϕ vs. ϕ (Fig. 2); therefore, the complete equation [3] was used and the values for α_1 and α_2 were calculated.

SUMMARY

The results of the above experimental work indicate that Eq. [3] is applicable to these monodisperse latex systems in predicting the viscosity-

concentration dependence in the Newtonian range and with particle sizes between 990 and 8710 Å. The Einstein coefficient obtained by extrapolation to zero concentration based upon the measured volume fractions was found to be greater than 2.50 and increased with decreasing particle size; however, correcting the volume fraction for an adsorbed layer of emulsifier gave a value of 2.504 ± 0.046 and independent of particle size. For particle sizes greater than 1 micron, the contribution of an adsorbed layer of emulsifier in affecting the volume fraction is probably negligible. The interaction or self-crowding factor k was found to vary from 1.118 to 1.357, depending on particle size, decreasing with increasing diameter.

ACKNOWLEDGMENTS

The author wishes to thank Dr. J. W. Vanderhoff and E. B. Bradford for the supply of monodisperse latexes and electron microscopy data, and J. H. Oswald and E. H. Richardson for assistance in obtaining experimental data. The author also expresses sincere appreciation to Dr. R. Simha, Dr. S. G. Mason, and Dr. T. Gillespie for helpful discussions of this work.

REFERENCES

1. WARD, S. G., *J. O. & Colour Chemists' Assoc.* **38**, 9 (1955).
2. EINSTEIN, A., *Ann. Physik* **19**, 289 (1906).
3. BRADFORD, E. B., AND VANDERHOFF, J. W., *J. Appl. Phys.* **26**, 864 (1955).
4. OLDROYD, J. G., STRAWBRIDGE, D. J., AND TOMS, B. A., *Proc. Phys. Soc. (London)* **B64**, 44 (1951).
5. KRIEGER, I. M., AND MARON, S. H., *J. Colloid Sci.* **6**, 528 (1951).
6. VAND, V., *J. Phys. & Colloid Chem.* **52**, 277 (1948).
7. MOONEY, M., *J. Colloid Sci.* **6**, 162 (1951).
8. MARON, S. H., MADOW, B. P., AND KRIEGER, I. M., *J. Colloid Sci.* **6**, 584 (1951).
9. MARON, S. H., AND MADOW, B. P., *J. Colloid Sci.* **8**, 130 (1952).
10. MARON, S. H., AND FOK, S. M., *J. Colloid Sci.* **10**, 482 (1955).
11. MARON, S. H., AND BELNER, R. J., *J. Colloid Sci.* **10**, 523 (1955).
12. MARON, S. H., AND PIERCE, P. E., *J. Colloid Sci.* **11**, 80 (1956).
13. MARON, S. H., AND SISCO, A. W., *J. Colloid Sci.* **12**, 99 (1957).
14. MOONEY, M., AND HERMONAT, W. A., *J. Colloid Sci.* **10**, 121 (1955).
15. ZETTMAYER, A. C., AND LOWER, G. W., *J. Colloid Sci.* **10**, 29 (1955).
16. SWEENEY, K. H., AND GECKLER, R. D., *J. Appl. Phys.* **25**, 1135 (1954).
17. KYNCH, G. J., *Proc. Roy. Soc. (London)* **A237**, 90 (1956).
18. MANLEY, R. ST. J., AND MASON, S. G., *Can. J. Chem.* **32**, 763 (1954).
19. GUTH, E., AND SIMHA, R., *Kolloid-Z.* **74**, 266 (1936).
20. SIMHA, R., *J. Appl. Phys.* **23**, 1020 (1952).
21. CHENG, P. Y., AND SCHACHMAN, H. K., *J. Polymer Sci.* **16**, 19 (1955).
22. NAWAB, M. A., AND MASON, S. G., *Trans Faraday Soc.* **54**, 1 (1958).

POLYELECTROLYTE ADSORPTION ON MERCURY SURFACES. DIFFERENTIAL CAPACITY IN THE PRESENCE OF POLY 2- AND 4-VINYL PYRIDINES

I. R. Miller and D. C. Grahame¹

*Weizmann Institute of Science, Rehovoth, and Amherst College,
Amherst, Massachusetts*

Received April 25, 1960

ABSTRACT

The differential capacity of the double layer on a mercury water interface in the presence of poly-vinyl pyridine (2 P.V.P.) and of poly 4-vinyl pyridine (4 P.V.P.) was measured. The supporting electrolyte in most cases was 0.1 HNO₃ or 0.09 NaNO₃ + 0.01 HNO₃. The nature of the monovalent cation is of no or very little importance.

Adsorption peaks at potentials -0.030 v. and -0.130 v. relative to a 1 *N* calomel electrode were observed in the case of 4 P.V.P. and 2 P.V.P., respectively, 4 P.V.P. giving the higher peak. Thus, in spite of its higher polarity and water solubility, 4 P.V.P. is more surface active. In both cases, however, full coverage is approached at very low bulk concentrations. The phenomenon is discussed in the light of the orientation abilities of both polymers in the surface.

Surface tension values as calculated from the differential capacity curves decrease linearly with concentration at small concentrations when equilibrium is not yet reached. They remain constant at intermediate concentrations and start increasing again at the highest measured polymer concentrations. From the time-dependent results at low polymer concentrations, the adsorption kinetics can be obtained. The equilibrium values, on the other hand, indicate that the adsorbed polymer molecules form a surface phase which may be a hundred or more angstrom units thick.

Surface activity of the counter anion facilitates the adsorption of the polybase at positive potentials, and vice versa, the polybase enhances adsorption of the counterion at negative potentials. This was proved by exchanging NO₃⁻ by the more surface-active Cl⁻ and Br⁻.

INTRODUCTION

The behavior of polyelectrolytes at charged mercury surfaces is conveniently studied by measuring the capacity of the double layer which is formed on growing mercury droplets. In previous publications (1, 2) the influence of ionized polyacids on the differential capacity of the electrical double layer was described. The differential capacity data indicated very pronounced adsorption at positive polarization, whereas no influence of the added polyacid on the differential capacity could be observed, when

¹ This work was completed after the death of D. C. Grahame.

the mercury surface was negatively charged. These results suggest that the polyacids are adsorbed on the positively charged surface whereas they are repelled from the negatively charged surface. The assumption of anodic adsorption was confirmed by the electrocapillary curves (unpublished results). Nevertheless it could not be decided whether the adsorption is merely electrostatic or both electrostatic and specific in nature. The difference in the pattern of the differential capacity of polyacrylic and polymethacrylic acid does suggest, however, that the adsorption forces are significantly specific.

In the present paper we report on the effect of two polybases poly 2- and 4-vinyl pyridines (2 P.V.P. and 4 P.V.P.) on the electrocapacity phenomenon. In these cases we may assume *a priori* that specific adsorption will be weak. This assumption is based on the fact that unlike ammonia and primary amines, the tendency of pyridine to form complexes with the mercury ion is weak (3). The chances of forming specific attachment between the planar mercury surface and the sterically hindered pyridine residues in P.V.P. should be even smaller. On the other hand, by varying the anion of the supporting electrolyte, which serves as counter ion to the P.V.P., differences in specific interaction can be brought into play.

EXPERIMENTAL

Materials

Unfractionated samples of 2 P.V.P. and 4 P.V.P. of various molecular weights were used in these experiments. The variation in molecular weight was achieved by varying the amount of the polymerization catalyst 2,2'-azobisisobutyronitrile.

It turned out that the differential capacity curves of polymers having a wide range of intrinsic viscosities were practically identical. Only the P.V.P. of the lowest degree of polymerization ($z = 600$) showed a slight difference in behavior. No determination of the molecular weight of 2 P.V.P. was therefore made. The molecular weight of 4 P.V.P. was evaluated from viscosity measurements in 92% ethanol using the experimental formula given by Boyer and Strauss (4):

$$[\eta] = 1.20 \times 10^{-4} M^{0.73}.$$

The approximate degrees of polymerization of the three samples were: 600, 1500, 2300.

The polymers were purified by multiple precipitation from ethanol with ethyl ether. The solvents were freshly distilled before use.

The water used for making up the solutions was tridistilled and the salts and acids used were of analar grade.

Apparatus

The differential capacity of the electrical double layer was measured by the dropping mercury method. Part of the measurements were made in Amherst with an apparatus described elsewhere (5). The other part of the measurements was carried out in Rehovoth with a similar but slightly modified apparatus.

The measurement involves the building up of an adsorption layer on a nascent mercury drop from a solution containing the materials to be investigated. The solution has a 1 *N* calomel electrode dipping into it, and an adjustable electrical potential is applied between the mercury reservoir and the calomel electrode. At the same time the value of the capacitor (differential capacity) represented by the double layer on the growing drop is measured by a separate bridge circuit at a certain measured time after the start of drop (i.e., double layer) formation. A full description of the method has been given elsewhere (5).

Thermodynamic, i.e., equilibrium, relations can be derived for the capacities so measured, provided three conditions are fulfilled. These are:

1. The double layer must have reached its equilibrium build-up at the same time the capacity is measured.
2. The variation in adsorption may not lag behind the variations in potential of the alternating current imposed on the bridge and make the measurements frequency dependent.
3. No current may flow across the double layer, that is, the mercury electrode must be ideally polarized. This means in effect that no electrode processes are allowed.

For diffusion-controlled monomeric adsorption the conditions (1) and (2) are closely related (6). This is not true for adsorbing polymeric molecules. Even when the surface coverage depends on the age of the surface, no frequency effect has necessarily to be observed. This follows from the none or all principle of the polymeric adsorption. Wherever a segment is adsorbed, a whole polymeric molecule lies in the surface and the local concentration is of the order of the internal concentration of a polymeric molecule. The uncovered parts of the surface obviously do not exhibit any frequency effect. One could of course argue that for very low frequencies (order of 1 cycle or less) diffusion of whole polymeric molecules from and to the surface would affect the measured capacity data. However, no measurements at those low frequencies could be made.

It is clear that at equilibrium, the same differential capacities will be measured on equal surface areas irrespective of drop age. In order to maintain approximately the same area for each measurement, the age of the drop was varied either by varying the mercurostatic pressure or by changing the capillary. Measurements were taken in a range of drop ages between

6 and 34 sec. In this range of time, the measured capacity data at P.V.P. concentrations of 0.0015 mono mole/liter and above remained constant. There was no significant difference in this respect between polyelectrolyte of different degrees of polymerization.

It should be noted that at polymer concentrations of 0.0015 mono mole/liter and above there is only a minute variation of the differential capacity curves with polymer concentration. At polymer concentrations of 0.00075 mono mole/liter and a drop age of 34 sec. the differential capacity curves become identical with those at the higher polymer concentrations. At still lower polymer concentrations and at 34 sec. the same curves are approached but not quite reached. At those low concentrations still higher drop ages would be required in order to reach equilibrium.

This behavior suggests that the equilibrium surface coverage for the given salt concentration (0.1 *N*) is complete even at extremely low polymer concentration.

The absence of transport across the double layer is shown by the fact that the differential capacity is frequency independent under almost all the conditions reported upon here. Under certain circumstances, however, corresponding to high positive potentials, variations of differential capacity with frequency were established and a high d.-c. current flow across the mercury surface was found. For this region of potentials the differential capacity measurements could not be simply interpreted but the direct electrocapillary determinations which were made could be used in order to elucidate the behavior.

The electrocapillary curves presented here were obtained by a modification of the capillary method. In this method the height of the mercury level required in order to squeeze out a mercury droplet from the capillary tip at a given potential is measured. It is important that the capillary be slightly conical, i.e., narrower at the tip. The measurements were actually carried out the other way round. The mercury was first set to a level at which no dropping occurred and the potential was close to the electrocapillary maximum. The potential was then changed, once towards higher and once towards lower potentials, until in both cases a mercury drop appeared. Thus for each potentials, until in both cases a mercury drop appeared. Thus for each potentials, until in both cases a mercury drop appeared. Thus for each potentials, until in both cases a mercury drop appeared. Thus for each potentials, until in both cases a mercury drop appeared. Thus for each potentials, until in both cases a mercury drop appeared.

The time required to reach equilibrium in these measurements was considerably higher (several minutes). The high time required to reach equilibrium follows probably from the access difficulties of the polymer molecule to the surface of the mercury meniscus adjacent to the capillary wall. The slowness of polymer adsorption in these experiments thus increases the degree of surface contamination by impurities.

Another uncertainty in the measured surface tension data follows from a possible influence of the adsorbed molecules on the contact angle. The

measured electrocapillary curves taken by themselves have thus only qualitative value. They are helpful, however, in supplying the integration constants necessary for establishing the electrocapillary curves from differential capacity measurements.

All the potentials cited in this paper are given relative to a 1 *N* calomel electrode.

RESULTS AND DISCUSSION

All the measurements summarized in this work were made in the presence of 0.1 *N* supporting electrolyte. The electrolyte solutions used contained usually 0.09 *N* sodium salt and 0.01 *N* acid of the same anion. In certain cases 0.1 *N* acid was used instead, but the differential capacity curves in the main region of potentials remained unaltered. The anions, NO_3^- , Cl^- , and Br^- , were chosen for these experiments.

The only data analyzed quantitatively are the differential capacity curves. Double integration of these curves with respect to the applied potentials gives the electrocapillary curves. The integrations, however, give rise to integration constants which have to be evaluated or assessed. To do this use is made of the fact that at sufficiently large positive potentials the electrocapillary curves and the surface charge density curves for the supporting electrolyte with or without added polybase should superimpose, as no polymer adsorption occurs in that region. Consequently also the differential capacity curves should correspond to that of the supporting electrolyte. Conversely a deviation of the differential capacity from the differential capacity value without polymer can be taken to reflect the effect of the polymer on the double layer on the mercury surface.

In the region of potentials where the surface is saturated by polymer molecules or the degree of coverage does not vary with potential a lowering in differential capacity is usually observed. This lowering is a result of the displacement of the more polar water molecules by the less polar organic components of the polymeric molecules particularly in the narrow layer immediately adjacent to the mercury surface. However, at the usually narrow ranges of potentials over which the adsorption process takes place, a peak in the differential capacity curves is developed owing to the invariably positive contribution when either charged or noncharged material is brought into the surface.

Following Frumkin *et al.* (6) we can separate the differential capacity into two terms as follows:

$$c = dq/dE = (\partial q/\partial E)_\Gamma + (\partial q/\partial \Gamma)_E (\partial \Gamma/\partial E)_q, \quad [1]$$

where q = surface charge density; E = potential; Γ = surface excess of surface-active substance.

The first term on the right side is called by Frumkin the true capacity,

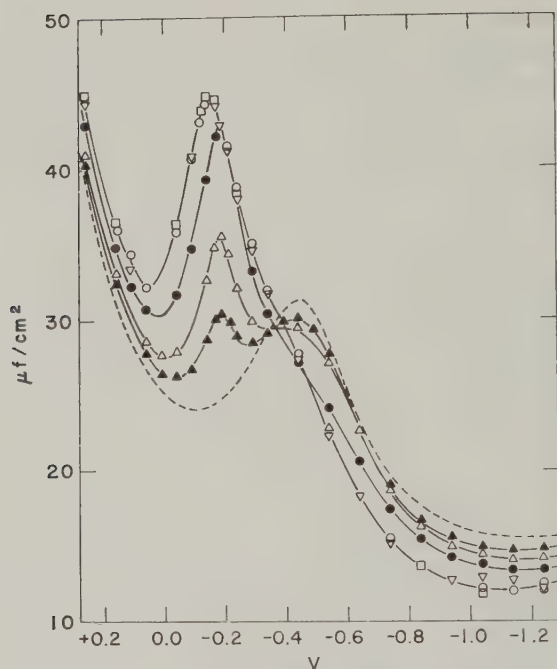


FIG. 1. Differential capacity versus potential relative to 1 *N* calomel electrode in the presence of 0.1 *N* HNO_3 and different concentrations of added 2 P.V.P. Dotted line—no P.V.P.; ▲—0.00019 *N*; △—0.00038 *N*; ●—0.00075 *N*; ○—0.0015 *N*; ▽—0.003 *N*; ◻—0.006 *N*.

whereas the second term is called the supplementary capacity. This second term is always positive, and it is responsible for the peak in differential capacity. It is zero when no variation of adsorption with potential takes place.

NO_3^- as Counter-Ion

a. Differential Capacity. The effect of poly 2- and poly 4-vinyl pyridine on the differential capacity of the electrical double layer in the presence of NO_3^- is given in Figs. 1 and 2, respectively. One sees that the effect of the two polybases on the differential capacity curve is quite similar. In both cases we have an adsorption peak starting at a potential which is positive by 0.5–0.6 volt with respect to the electrocapillary maximum of the pure salt solution. In other words, a potential of +0.5 v. or more is required in order to expel the positive poly-ions from the surface completely. However for corresponding polymer concentrations, the adsorption peak in the presence of 4 P.V.P. is located at a potential about 50 mv. more positive, than in the presence of 2 P.V.P. Similarly the adsorption peak of

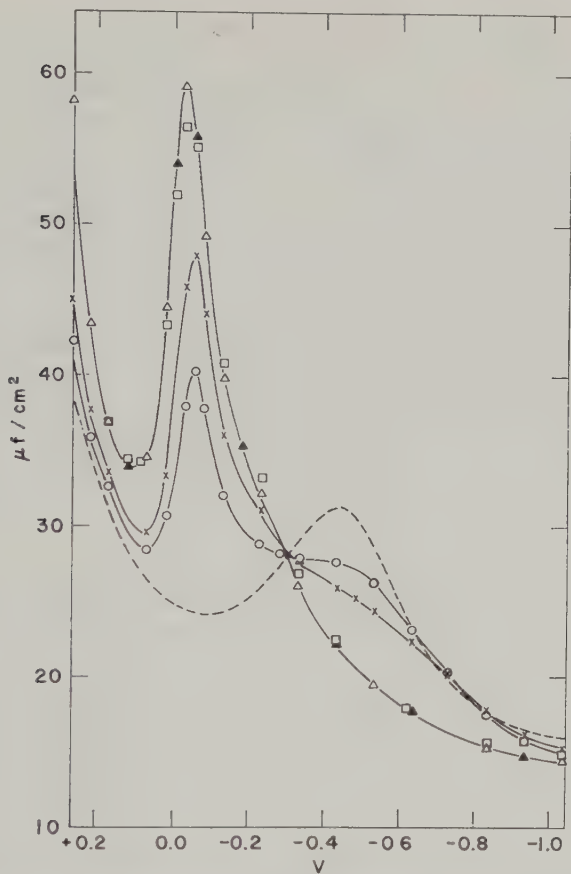


FIG. 2. Differential capacity curves for different concentrations of 4 P.V.P. in the presence of 0.1 N HNO_3 as supporting electrolyte. Dotted line—no 4 P.V.P. added; \circ —0.00038 N ; \times —0.00075 N ; \square —0.0015; \triangle —0.003 N , and \blacktriangle —0.006 N 4 P.V.P.

4 P.V.P. is considerably (by about 15 $\mu f./cm.^2$) higher than that of 2 P.V.P.

From the location of the capacity peaks in Figs. 1 and 2 two important facts are evident: (a) Adsorption of positively charged molecules starts on a still positively charged surface; (b) 4 P.V.P. is more strongly adsorbed than 2 P.V.P.

From the adsorption of positively charged molecules to a positively charged surface we may conclude that the adsorption is at least partly specific in character. This is also confirmed by the lowering in differential capacity caused by the adsorbed P.V.P., at potentials negative with respect to the adsorption peak. Evidently the decrease in dielectric constant near the surface due to the noncharged parts of the polymer in this case

overweighs the influence of the charges carried by the polyelectrolyte to the mercury surface.

The fact that 4 P.V.P. is more readily adsorbed than 2 P.V.P. seems surprising in view of the hydrophobic character of adsorption. It is known that 4 P.V.P. is more polar and more water soluble than 2 P.V.P. One would have expected therefore that 2 P.V.P. should have the larger tendency to leave the water solution. However, this consideration does not take into account the total change of energy of the two polymers in going from the dissolved to the adsorbed state. It can easily be seen that 4 P.V.P. can assume a state in adsorption, of considerably lower energy than 2 P.V.P. The adsorbed monomer units of 4 P.V.P. can adjust themselves in a layer with all the polar groups oriented towards the water and with all the hydrocarbon parts towards the mercury surface, to give a fairly compact 7 Å. thick hydrocarbon layer. Under similar circumstances 2 P.V.P. can form a layer about 4 Å. thick but one which leaves a large area of contact between the hydrocarbon parts and water. In other words 4 P.V.P. is more detergent-like in the adsorption than 2 P.V.P.

The difference in the orienting ability of 2 P.V.P. and 4 P.V.P. is also responsible for different differential capacity lowerings at more negative potentials. It is convenient to compare the behavior of the two polymers in this respect at higher concentrations, where any increase in polymer concentration does not change the differential capacity curve significantly. At a potential of -0.5 v. relative to the 1 *N* calomel electrode the differential capacity is lowered by $10 \mu\text{f./cm.}^2$ and by $6 \mu\text{f./cm.}^2$ when 4 P.V.P. and 2 P.V.P., respectively, are added to 0.1 *N* HNO_3 solution. The lowering of the differential capacity by 2 P.V.P. moreover is roughly uniform over the whole range of potentials between -0.45 v. and -1.4 v. relative to the *N* calomel electrode; the reduction of the differential capacity by 4 P.V.P. on the other hand varies considerably with the potential. It is largest between the potentials -0.45 v. and -0.55 v. and decreases gradually with increasing negative potential. This behavior is in keeping with the picture which we have formed about the reorientation of the well-organized 4 P.V.P. According to the model it is adsorbed at positive potentials with its hydrocarbon parts towards the mercury surface. With the increasing negativity of the mercury surface the 4 P.V.P. molecules will tend to bring its charges nearer to the surface. The reorientation of the less organized layer of 2 P.V.P., on the other hand, may be expected to have a considerably smaller and more uniform effect on differential capacity as found (see Fig. 1).

As we have pointed out already at potentials more positive than $+0.1$ v. only negligible polymer adsorption should take place and the differential capacity should be constant. This stands in contradiction to the observed elevation of the differential capacity by P.V.P. at those positive potentials.

After a minimum at $+(0.1 \leftrightarrow 0.2)v$, the differential capacity elevation increases with increasing positive potential. However, a close check of other data obtained from the impedance bridge makes it clear that a break down of the conditions at the mercury surface takes place and that we are dealing with a case of pseudo capacity.² The nature of the electrode process taking place under these conditions is not yet known.

b. Electrocapillary Data. Confirmation that the observed elevation in differential capacity at high positive potentials is due to pseudo capacity can be obtained from the electrocapillary curves. The surface tension versus potential curves for various concentrations of either 4 P.V.P. or 2 P.V.P. converge at positive potentials ($+0.05$ relative to 1 *N* calomel electrode). Addition of P.V.P. would have lowered the interfacial tensions at these potentials if the measured differential capacities had been of thermodynamic significance. Although the measured electrocapillary curves are of poor quantitative validity and for that reason are not presented, their convergence at positive potentials may be regarded as well established.

The electrocapillary curves which are presented here (Fig. 3) have been obtained by a more reliable procedure involving the double integration of the differential capacity curves, starting at the potential ($+0.1 v$.) where both the surface charge and electrocapillary curves converge. We note that at concentrations high enough to give equilibrium values (0.0015 mono mole/liter and above), there is practically no additional lowering of surface tension with polymer concentration. Moreover, at the highest polymer concentration surface tension starts rising slightly. This suggests that the Gibbs adsorption relation cannot be used to determine the surface excess of polymer molecules.

The Gibbs adsorption isotherm derived for our system containing a polyelectrolyte and a uni-univalent salt (neglecting $\Gamma_w d\mu_w$ for the water) (7) and introducing a model for the polyelectrolyte as proposed by Katchalsky, Alexandrowicz, and Kedem (8) is given by:

$$-d\gamma/d\ln c_p =$$

$$RT\{\Gamma_{p+}[1 + (g^2\nu^2c_p/c_i + g\nu c_p)] + (\Gamma_- - \nu\Gamma_{p+})(g\nu c_p/c_i + g\nu c_p)\}. \quad [2]$$

In the above formula is the surface tension, c_p and c_i are the polymer and salt concentrations, respectively, Γ_{p+} , Γ_+ , and Γ_- are the surface excesses of the poly-ions (in polymeric units), of the free co-ions, and of the counter-ions, respectively, ν is the number of ionized groups per poly-ion, and g is the internal osmotic factor (9).

When the surface is practically saturated with polymer molecules and

² The d.-c. current across the mercury surface and the bridge resistance increase abruptly in this potential region. The capacity data are strongly frequency dependent.

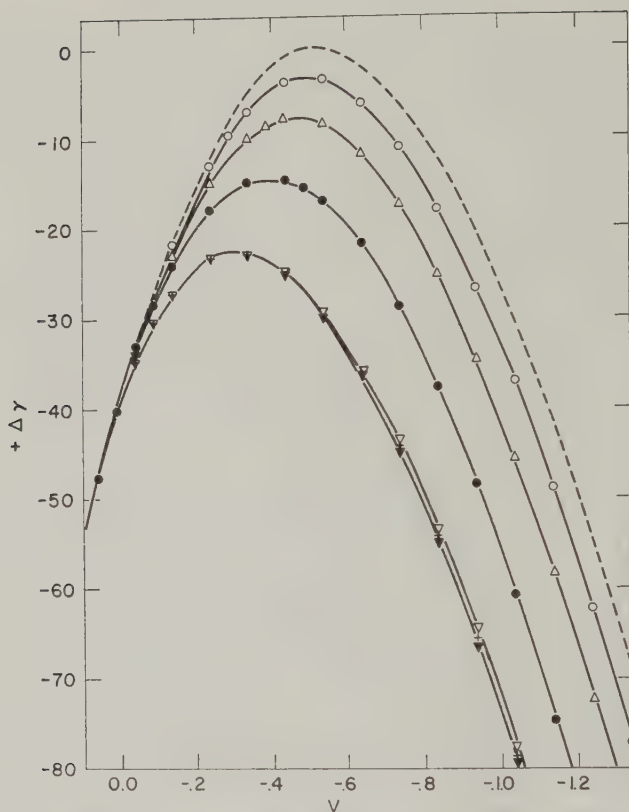


FIG. 3. Electrocapillary curves calculated from differential capacity data for various concentrations of 4 P.V.P. The supporting electrolyte is 0.1 N HNO_3 . 4 P.V.P. concentrations:—dotted line—no polymer; \circ —0.00019 N ; \triangle —0.00038 N ; \bullet —0.00075 N ; \blacktriangledown —0.0015 N ; $+$ —0.003 N ; ∇ —0.006 N .

the adsorption of the small ions on the surface proper is negligible, Eq. [2] can be simplified, and we shall discuss two limiting cases.

Case 1. The polymer molecules are fully spread on the surface:

$$-(d\gamma/d\ln c_p) = RT\Gamma_p\{1 - (1-g)(g\gamma^2 c_p/c_i + gvc_p)\}. \quad [3]$$

Case 2. The polymer molecules in the surface are highly compressed and only a negligible portion of the charge is neutralized by the surface. In this case $\Gamma_- = \Gamma_+ + \nu\Gamma_{p+}$, where Γ_- and Γ_+ are the number of anions and cations in 1 cm^2 of the surface phase, respectively, as determined by Donnan equilibrium less the number of anions and cations in the same volume of bulk solution. However, the cation concentration in the surface phase is small when compared with the bulk and $gvc_p \ll c_i$. Hence

$$-d\gamma/d\ln c_p = RT\{\Gamma_p(1 + g^2 v^2 c_p/c_i) - \delta g v c_p\}, \quad [4]$$

where δ is the thickness of the surface phase.

Equation [3] predicts an increase in surface tension with polymer concentration, whereas Eq. [4] on the contrary indicates negative values for $d\gamma/d\ln c_p$.

In both cases, however, the expected variations of surface tension with $\ln c_p$ under the given experimental conditions are so small as to be within the experimental error. This is typical for cases of polymer adsorption; it is clear therefore that the Gibbs adsorption equation is not suitable for determining the polymer surface excess.

Surface concentrations can, however, be obtained from kinetic experiments at polymer concentration and drop times where adsorption is not complete. If we assume that the adsorption tendency is high, then all polymer molecules which reach the nascent mercury surface will be adsorbed, and the following relation holds (9):

$$\Gamma_p(t) = 0.736 c_p t^{\frac{1}{2}} D^{\frac{1}{2}}, \quad [5]$$

where D is the diffusion constant, and t is the age of the mercury drop at the time of the measurement.

Figure 4 shows that at low polymer concentrations the surface tension decreases linearly with increasing polymer concentration. The surface tension, moreover, for the same polymer concentration decreases linearly with the square root of the age of the mercury droplet (not shown). Thus surface tension and surface concentration are evidently linearly related.

We may therefore assume that the surface contains patches which are occupied and patches which are unoccupied by the polymer.

Areas which are covered will have the surface energy corresponding to the surface tension γ of the saturated surface; areas which are uncovered will contribute the surface energy γ_0 of the surface without polymer. The surface tension (energy) at surface age t is thus given by

$$\gamma(t) = \gamma_0 \frac{\Gamma_p - \Gamma_p^{(t)}}{\Gamma_p} + \frac{\Gamma_p^{(t)}}{\Gamma_p} = \gamma_0 + (\gamma - \gamma_0) \frac{\Gamma_p^{(t)}}{\Gamma_p}$$

or

$$\Delta\gamma(t) = \Delta\gamma \frac{\Gamma_p^{(t)}}{\Gamma_p}. \quad [6]$$

Ordinarily Eq. [6] would be incomplete, as an entropy term has to be added which allows for the different arrangement of the polymers into differently shaped and arranged patches in the surface. In the case of polymers, however, this contribution is negligible as compared with the adsorption energies involved. The internal entropies of rearrangement accompanying the adsorption of a single polymer molecule is included in $\Delta\gamma$.

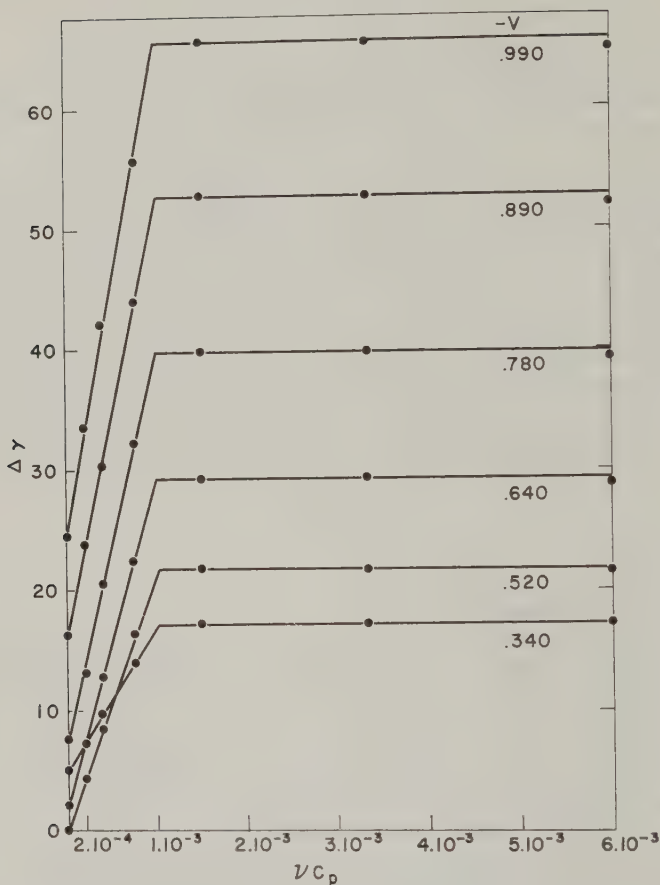


FIG. 4. Lowering of surface tension $\Delta\gamma$ versus 2 P.V.P. concentration in mono moles/liter at various potentials.

From the diffusion constant of the polyelectrolyte at the experimental salt concentration $\Gamma_p(t)$ as well as Γ_p can be calculated (Γ_p from the intercept of the two straight lines in Fig. 4.). The surface concentration Γ_p of the saturated but noncompressed surface layer calculated from the intercepts in Fig. 4 using Eqs. [5] and [6] is $(7 \pm 1) \times 10^{-10}$ mono mole/cm.². It turns out that the same value is found over wide ranges of applied potential and of charge density.

At a potential of -0.990 v. no. NO_3^- is adsorbed and the double layer consists almost exclusively of cations. At this potential, however, the number of charges in the surface (q/F) is only one-fifth of the number of positive charges on the poly-ions adsorbed per square centimeter. It is clear therefore that no more than one-fifth of the monomer units in the chain

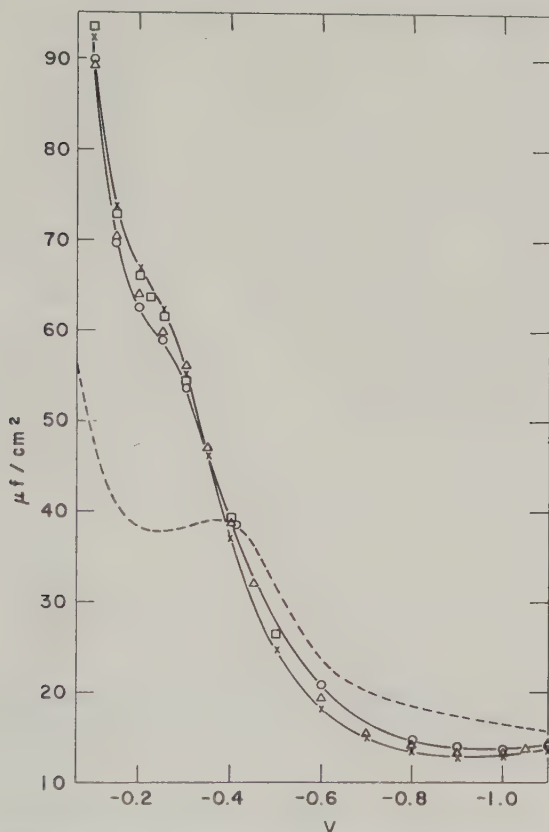


FIG. 5. Differential capacity curves in the presence of 0.09 *N* NaCl + 0.01 *N* HCl and various concentrations of 4 P.V.P. ($z = 600$). 4 P.V.P. concentrations: dotted line—no polymer; O—0.00029; Δ —0.00096 *N*; \times —0.008 *N*; \square —0.029 *N*.

are actually attached closely to the surface.* At less negative potentials this fraction is probably even smaller. The major parts of the polymer molecules protrude therefore into the solution and form a surface phase. The thickness of the surface phase can be estimated, assuming that its polymer concentration is equal to the internal concentration of a polymer molecule in the bulk sphere. The thickness of the surface phase found this way is approximately 100 Å. For higher polymer concentrations, when the surface layer becomes compressed, the surface thickness probably increases.

* NOTE ADDED IN PROOF: q/F gives only the number of monomer units which are actually mentioned by the surface charge. Another fraction of the monomeric units probably adheres to the surface due to van der Waals interaction, turning their polar N^+ groups towards the aqueous solution. In the discussion given these units are considered to be part of the "surface phase".

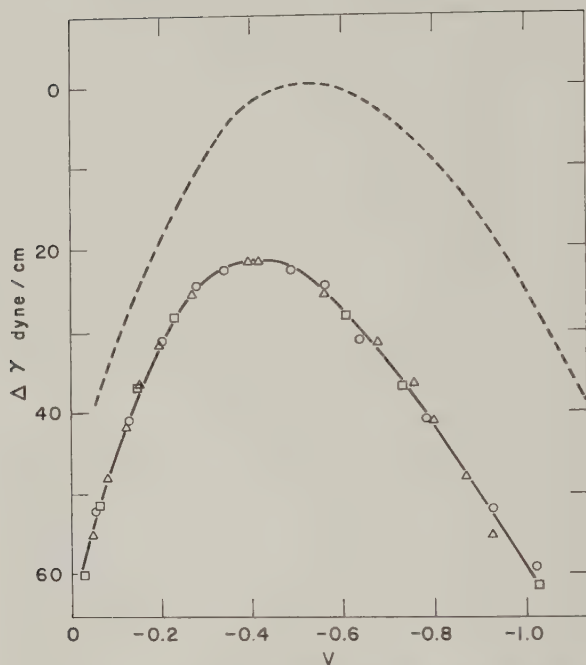


FIG. 6. Electrocapillary curves in the presence of various concentrations of 4 P.V.P. ($z = 600$). The supporting electrolyte is 0.09 NaCl + 0.01 HCl. Polymer concentration: dotted line—no polymer; \circ —0.0046 N ; \triangle —0.0014 N ; \square —0.004 N .

Exchange of NO_3^- by More Surface-Active Anions

In the following experiments the NO_3^- of the supporting electrolyte was exchanged for Cl^- or Br^- .

a. 0.09 NaCl + 0.01 N HCl as Supporting Electrolytes. The differential capacity curves in the presence of 0.1 N Cl^- and of various concentrations of ionized 4 P.V.P. are given in Fig. 5. The elevation of the differential capacity by 4 P.V.P. as compared with the pure salt solution in the presence of Cl^- begins 90 mv. more negatively than in the presence of NO_3^- . This behavior can be explained by the stronger adsorption of Cl^- superimposed on its tendency to form ion pairs with pyridonium residues.

Ion pair formation of polyelectrolytes with counter-ions is indicated by the observation of Alexandrowicz (8) that the osmotic factor of a polyelectrolyte is affected only when the salt concentration approaches 0.5–1 N . At these salt concentrations $1/\kappa$ is of the order of magnitude of the distance between the opposite charges in the ion pair (4 Å and less).

From this it is seen that the adsorbed P.V.P. is accompanied into the surface by its counter-ions. The more surface-active the counter-ion, the more negative are the potentials of the mercury surface at which the

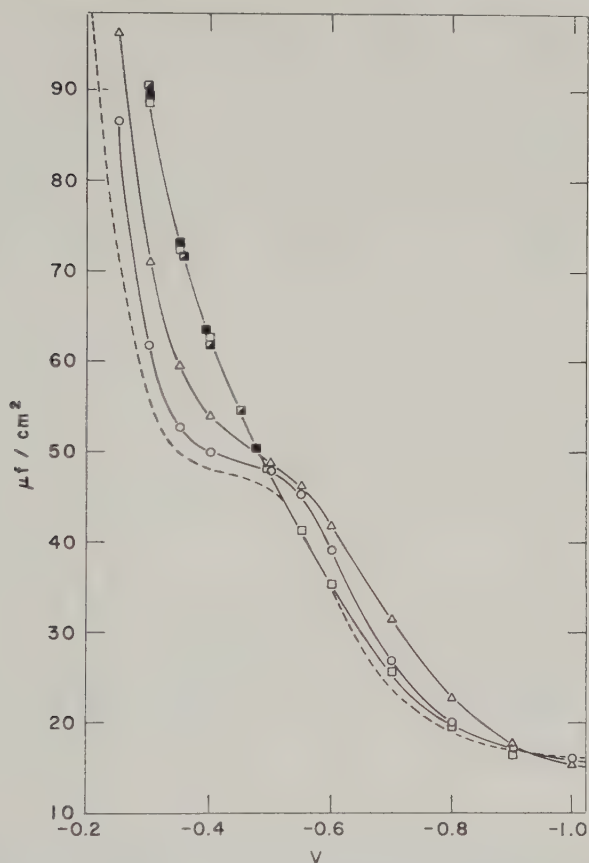


Fig. 7. Differential capacity versus potential (relative to 1 *N* calomel electrode). The medium is 0.09 *N* NaBr + 0.01 *N* HBr containing various concentrations of 4 P.V.P. ($z = 600$): dotted line—no P.V.P.; \circ — 1.9×10^{-5} *N*; \triangle — 9×10^{-5} *N*; \blacksquare — 2.9×10^{-4} *N*; \blacksquare — 2.4×10^{-3} *N*; \square — 8×10^{-3} *N*.

counter-ions get attached to it and the greater is the increase in differential capacity due to the adsorbed polysalt. On the other hand, even at the largest positive potentials used in this case no desorption was observed. It is found that the differential capacity increase due to added polymer increases when the potential becomes more positive. This suggests that polyvinyl 4 pyridonium chloride is not desorbed from the mercury surface even at very high positive potentials. Unlike NO_3^- at high positive potentials, the capacities here are real in the entire range of potentials investigated. The thermodynamic significance of the capacity data can be proved by direct electrocapillarity measurements.

The directly measured electrocapillary curves are presented in Fig. 6 and

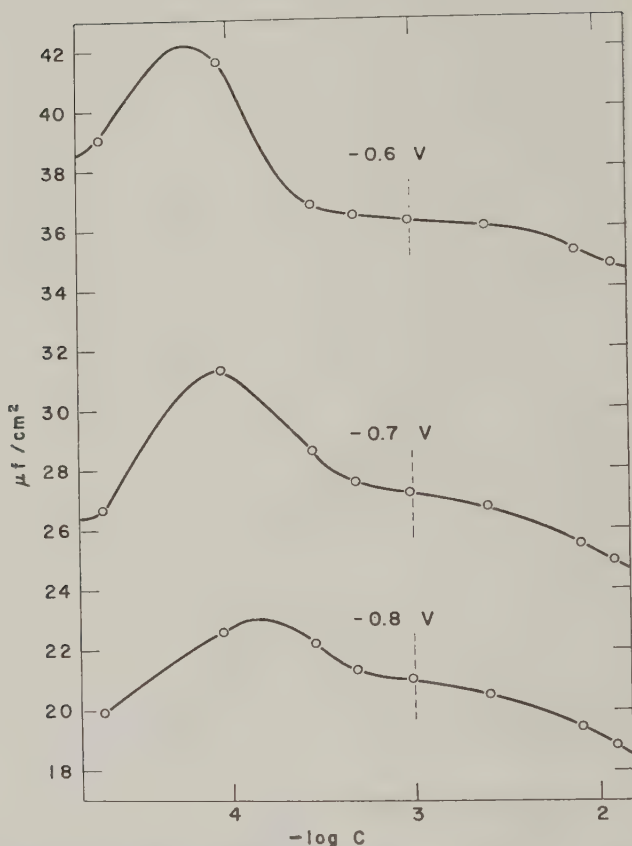


FIG. 8. Differential capacity versus logarithm of 4 P.V.P. (600) concentration at constant potentials (noted in the figure).

show a lowering of the surface tension by P.V.P.+Cl⁻ at all potentials. Cl⁻ here is a bridging agent between the charged surface and the polyelectrolyte of the same sign of charge, the polybase being attracted to the negatively charged inner Helmholtz layer (10).

b. 0.09 N NaBr + 0.01 N HBr as Supporting Electrolytes. As is well known, Br⁻ is more strongly adsorbed on a mercury surface than Cl⁻. It follows from the previous consideration that this should bring about a rise in differential capacity at even more negative potentials. As seen from Fig. 7 the large elevation in differential capacity in the case of NaBr ends at -0.5 v., which is 100 mv. more negative than the elevation in the presence of Cl⁻. The electrocapillary curve (not presented) also shows that the lowering of surface tension is stronger and more symmetrical with respect to potential than in the presence of Cl⁻. In fact even at the more negative

potentials (between -0.6 and -0.9 v.) the differential capacity values in the presence of several concentrations of added 4 P.V.P. are higher than in the presence of pure bromide solution only. In this case 4 P.V.P. performs a double function. At the beginning it raises the differential capacity by facilitating the entry of anions (11) into the adsorption layer. Then it lowers it again by lowering the dielectric constant in the double layer. The dependence of the differential capacity on the logarithm of polymer concentration in this potential region is given by Fig. 8. Small concentration of added 4 P.V.P. cause a strong elevation in the capacity value. At small polymer concentrations in the surface, the highly surface-active Br^- ions which are carried along with the polybase are free to adhere to the surface and to increase the differential capacity. The capacity data are again lowered with increased polymer concentration. The possible causes of this subsequent capacity lowering could be: steric hindrance, decrease of dielectric constant in the double layer, and decrease of free ($\text{NaBr} + \text{HBr}$) in the surface phase. The capacity lowering slope is steep at low concentrations; it then flattens out and becomes steeper again at still higher concentrations.

The first steep capacity lowering slope results probably from the decrease of the dielectric constant and from the restriction of the freedom of the pyridonium residues to orient with the Br^- counter-ion toward the mercury surface in the course of surface saturation by polymer. The decrease in free ($\text{NaBr} + \text{HBr}$) concentration in the surface phase is probably responsible for the slow changes in differential capacity at the higher polymer concentrations.

The lowering in the concentration of the free NaBr in the surface phase is expected when taking into account the probable increase in the polymer concentration in the surface phase when its bulk concentration increases. The increase in the polymer surface concentration may be accompanied by a more complex mechanism. Such a mechanism might involve structural changes in the surface phase as a result of which more polymer molecules would be attached to the surface, but the number of actual contact points between an adsorbed polymer molecule and the mercury surface would decrease. Increasing polymer concentration in the surface phase causes, owing to Donnan equilibrium, a decrease in co-ion (free $\text{HBr} + \text{NaBr}$) concentration. The adsorption of Br^- in the mercury surface as well as its contribution to the differential capacity is likely to decrease with the decrease of ($\text{NaBr} + \text{HBr}$) concentration in the surface phase.

ACKNOWLEDGMENT

One of the authors (I. R. Miller) is grateful to Dr. A. Silberberg for reading and discussing the manuscript.

REFERENCES

1. MILLER, I. R., AND GRAHAME, D. C., *J. Am. Chem. Soc.* **79**, 3006 (1957).
2. MILLER, I. R., "Electrochemical phenomena," *Proc. 2nd Intern. Congr. Surface Activity 1957*, p. 53.
3. BJERRUM, J., *Chem. Revs.* **46**, 381 (1950).
4. BOYER, A. G., AND STRAUSS, V. P., *J. Polymer Sci.* **22**, 463 (1956).
5. GRAHAME, D. C., *J. Am. Chem. Soc.* **71**, 2975 (1949).
6. FRUMKIN, A., AND MELIK-GAIKAZYAN, V. I., *Doklady Akad. Nauk S.S.S.R.* **77**, 855 (1951).
7. MILLER, I. R., AND SILBERBERG, A., in preparation.
8. KATCHALSKY, A., ALEXANDROWICZ, Z., AND KEDEM, O., *Advances in Chem. Phys.*, in preparation.
9. DELAHAY, P., AND TRACHTENBERG, I., *J. Am. Chem. Soc.* **79**, 2355 (1957).
10. GRAHAME, D. C., *Chem. Revs.* **41**, 488 (Fig. 16), (1947).
11. FRUMKIN, A., NIKOLAJEVA-FEDOROVICH, N., AND IVANOVA, R., *Can. J. Chem.* **37**, 253 (1959).

STUDIES ON ULTRASONIC EMULSIFICATION

R. S. Krishnan, V. S. Venkatasubramanian, and E. S. Rajagopal

Physics Department, Indian Institute of Science, Bangalore-12, India

Received May 8, 1959

ABSTRACT

An experimental setup suitable for a quantitative study of the ultrasonic emulsification is described. The methods of producing a well-defined sound field, of measuring the sound intensity, and of following the emulsion concentration are discussed critically. The good reproducibility resulting from the improved experimental techniques is examined.

I. INTRODUCTION

The phenomenon of ultrasonic emulsification has been studied by Wood, Loomis, Richards, Harvey, and Sollner, among others, and the basic mechanisms are known qualitatively (1). The quantitative studies of Bondy and Sollner (2) and Claus and Schmidt (3) were not very successful, since the poor reproducibility achieved ($\sim 20\%$) did not allow quantitative interpretations. The present studies aim at improving the experimental methods and the theoretical interpretations.

II. THE ULTRASONIC GENERATOR

Among the many methods of producing high-intensity sound waves, the piezoelectric generators can give well-defined controllable and reproducible ultrasonic fields because of the higher frequencies and greater intensities and energies. Other factors are the sharpness of the beam, the absence of transmission losses, and the simplicity of the electronic design (4-6).

The present generator (950 k.c.s. and 500 watts) follows the design of Smith and Stumpf (7), who have discussed the various components in detail. X-Cut quartz crystals, prepared in the usual way (8, 9), are used, and the crystal holder used is a slight modification of that of Smith and Stumpf (7), Laufer (10), Noltingk (11), and Rust (12). Figures 1 and 2 explain the general arrangement very fully.

III. MEASUREMENT OF ULTRASONIC INTENSITY

There has been little study of the correlation between the ultrasonic intensity and the effects produced (13, 14) mainly because of the difficulty

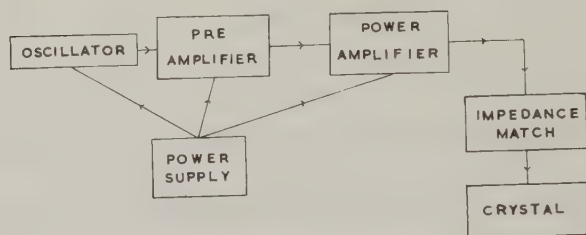


FIG. 1. Block diagram of the ultrasonic generator.

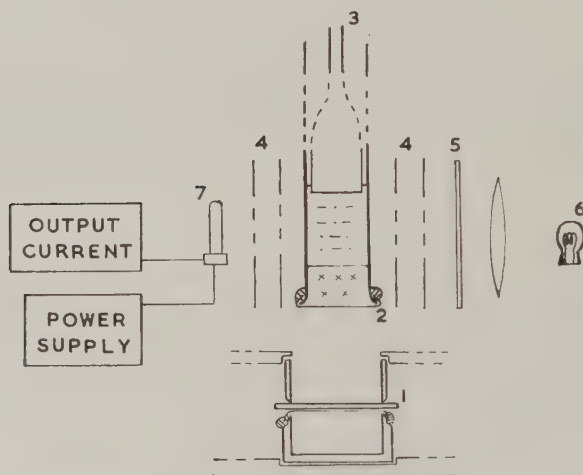


FIG. 2. Arrangement for producing and observing the emulsions: (1) transducer; (2) emulsion chamber; (3) reflector; (4) slits for observation; (5) light filters; (6) light source; (7) RCA 931-A Photomultiplier.

of intensity measurements at high power levels. Among the various techniques (15, 16) the absolute radiation pressure method is adaptable for mapping the field. However, for much work, only a constant field is needed, and this is easily achieved, for example, through voltage or current measurements in the electronic part of the generator.

The intensities are measured under the same conditions in emulsification. Because of the practical difficulties in maintaining progressive waves at high intensities over long lengths of time, sound reflectors are used. But owing to the inhomogeneities caused by the scattering by the liquid droplets and cavitation nuclei, multiple reflections, etc., strictly stationary waves are not formed. So the pressure on the reflector, measured with a balance, is equated to $2I_{eq}/v$ to give the intensity I_{eq} of an equivalent progressive wave.

The experimental arrangement (except the reflector for intensity measure-

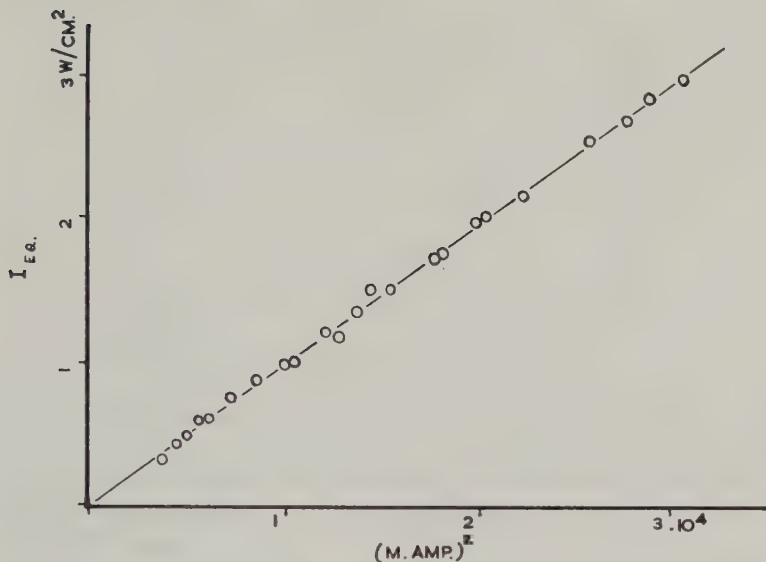


Fig. 3. Dependence of the ultrasonic intensity on the output of the electronic generator.

ments) is shown in Fig. 2. I.C.I. Alkathene paper, not affected by most of the liquids, serves as the acoustic window ($\sim 90\%$ transmission), and the method of sealing it to the glass emulsion chamber with Araldite resin is also indicated. Several precautions and corrections have to be observed, and the relative accuracy is $\sim 5\%$, whereas the absolute values have much greater errors for various obvious reasons. The same situation is present in all measurements of high-intensity sound waves. See also Beal and Skauen (30).

A rough check on the intensity measurements can be made by a comparison with the electrical power output. If the other parameters are not altered, the acoustic output is nearly proportional to the square of the anode current of the power amplifier, as is indeed the case (Fig. 3). The variation of the intensity inside the emulsion chamber is of interest (Fig. 4). There is little absorption in the water phase and some reduction of intensity at the interface and in the emulsion, as expected. The absorption coefficient for a 1% emulsion is $\sim 0.03 \text{ cm.}^{-1}$, while the theoretical value (17) for hard spheres is $\sim 0.01 \text{ cm.}^{-1}$, including that in benzene. This order of magnitude agreement is all that can be expected, since the particles are liquid spheres and since the sound field is complex.

IV. MEASUREMENT OF THE CONCENTRATION OF THE EMULSION

The bulk concentrations of the emulsions are estimated, absolutely through the specific gravity and relatively by the optical transmission

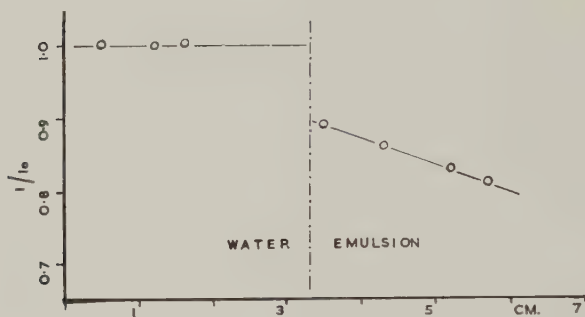


FIG. 4. Variation of intensity inside the emulsion chamber.

method. The other methods (18) are not rapid or adoptable. Since the solubility effects are negligible (the benzene used was also not "dry") the percentage composition by volume of the dispersed phase of density ρ_1 in the emulsion of density ρ_0 (density of the dispersion medium ρ_2) is $c = (\rho_0 - \rho_2)/(\rho_1 - \rho_2) \times 100\%$. The technique is straightforward and with the usual precautions (19) an accuracy of 2%–3% is easily achieved.

The relative concentrations are found without disturbing the arrangement by the light absorption method (20, 21). The experimental arrangement (Fig. 2) consists of the usual (22) nearly monochromatic source, the photomultiplier unit, and a number of slits to get an axial pencil of light passing only through the emulsion. One then uses the Lambert-Beer's law $\log(i_0/i) = kc$, to get the relative value of c .

It is very essential to check the validity of Beer's law in the actual setup used, as in Fig. 5. Up to $\sim 3\%$ the linearity is good, but at higher c , deviations occur, the effective absorption being less. The deviation is explained by Amiot and Blondeau (23) as due to multiple scattering, but it may also be due to any stray light falling on the photomultiplier. In any case, this nonlinearity sets a limit to convenient measurements. The reliability of the light absorption method (24) can be evaluated from the particle size measurements (25) and is $\sim 5\%$, just sufficient for the present purpose.

V. REPRODUCIBILITY OF THE EXPERIMENTS

The water-benzene system is chosen with magnesium oleate (26) emulsifier. Since the water-in-benzene emulsion is formed above the clear water phase, the reduction of the intensity at the interface by the passage through the emulsion is avoided, and the optical measurements can be made without interference from the oil bath, Araldite sealing, etc. The emulsion chamber is lined vertically with a constant uniform field acting on the interface. As the emulsion is being formed, the photomultiplier current decreases, reaching finally a constant value corresponding to c_∞ . Now the

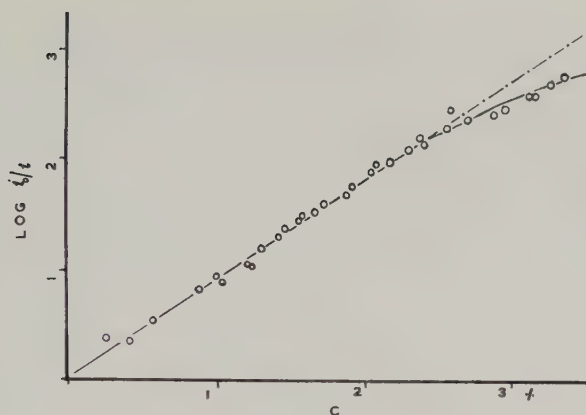


FIG. 5. Test of the validity of Beer's law.

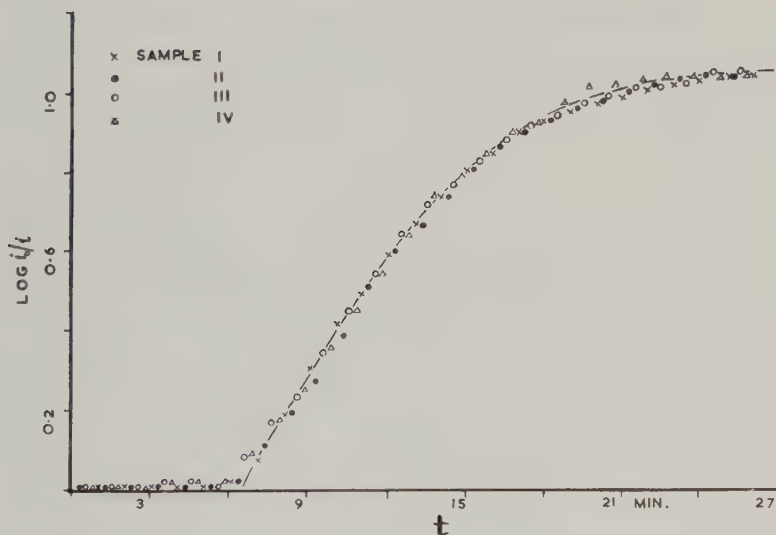


FIG. 6. Reproducibility of the experiments. Results of four runs are given.

ultrasonic intensity in the water phase is measured, and the emulsion is filled into a pycnometer for density measurements.

The reproducibility of the measurements is evaluated by the observations on different samples under the same conditions. The results of four specimens (4 ml. of water + 8 ml. of benzene at energy density $\bar{E} = 64$ ergs/ml.; $A = 2.38$ cm.²) are illustrated in Fig. 6, and all the points cluster very closely about the mean line, deviating by no more than $\pm 3\%$ from the mean. The characteristic features of Fig. 6 (27) are: a definite nucleation

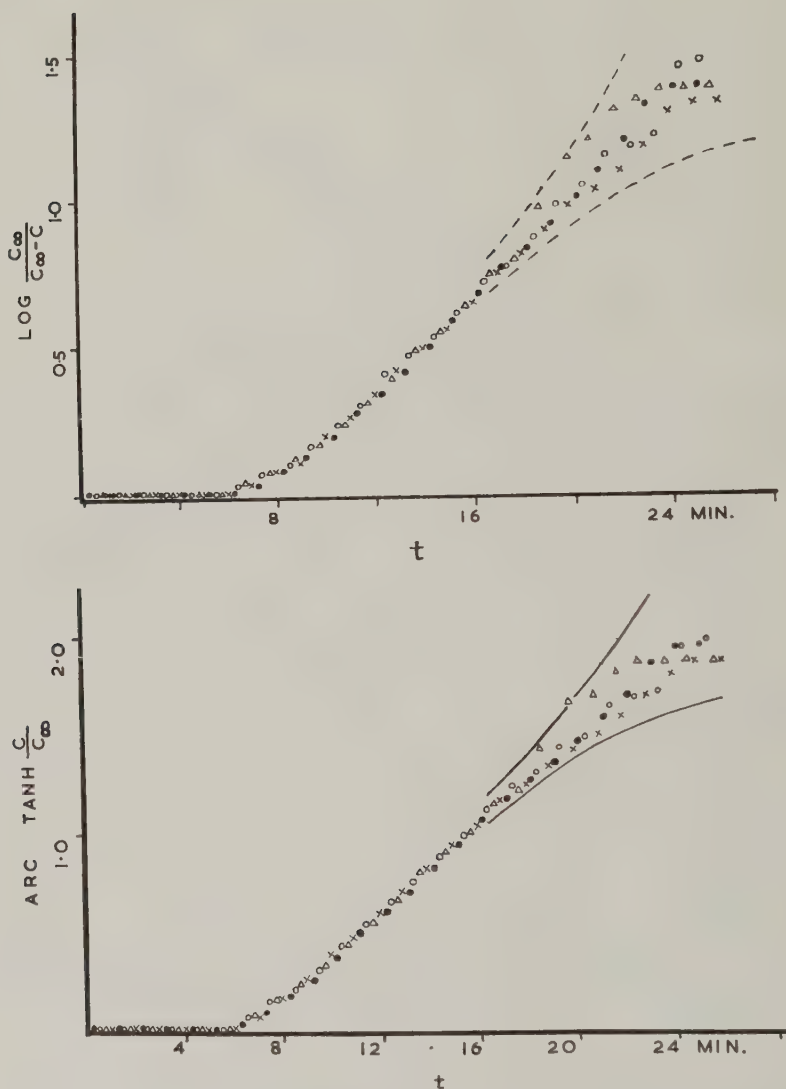


FIG. 7. Plot of (a) $\log [c_{\infty}/(c_{\infty} - c)]$ vs. t and (b) $\text{arctanh } (c/c_{\infty})$ vs. t . Dotted lines are $\pm 3\%$ deviations from the mean.

time t_N during which no emulsion is formed, followed by a sudden onset of emulsion, which sometimes is somewhat rounded off, with the concentration rising rapidly at first and soon leveling to c_{∞} . The emulsification rate can be compared with the elementary theory (28) by drawing the $\log [c_{\infty}/(c_{\infty} - c)]$ vs. t and the $\text{arctanh } (c/c_{\infty})$ vs. t plots, as done in Fig. 7a and b. The lines showing $\pm 3\%$ deviation from the mean are also drawn.

The points are satisfactorily inside this band, giving the reproducibility as $\sim 5\%$. But even this accuracy is not sufficient to resolve between the two cases, without additional analysis (31).

The improved consistency of the experiments is principally due to the well-defined sound field. In the earlier experiments (for example, ref. 2) the liquids were taken in a test tube and simply dipped in the oil fountain. Reflections from the irregular liquid-air interface and the excitation of the cross modes of vibrations in the transmission through the glass tube distort the sound field and renders the alignment very critical. A second factor is the use of dry emulsion chambers. If they are wet, emulsification occurs at these contacts making the area of the interface uncertain, as noted by Richards (29) himself. Another cause is the presence of reflectors preventing irregular mound formations at the liquid surfaces—a fact elaborated by Lindstrom (14). The use of optical methods, not disturbing the arrangements, is also significant.

ACKNOWLEDGMENTS

We thank the Indian Council of Medical Research for financial assistance and for the award of a Junior Research Fellowship to the junior author. We also thank the referees for their suggestions.

REFERENCES

1. SOLLNER, K., in J. Alexander, ed., "Colloid Chemistry," Vol. 5, p. 337. Reinhold, New York, 1944.
2. BONDY, C., AND SOLLNER, K., *Trans. Faraday Soc.* **32**, 556 (1936).
3. CLAUS, B., AND SCHMIDT, E., *Kolloid-Beih.* **45**, 41 (1936).
4. CRAWFORD, A. E., "Ultrasonic Engineering." T. Butterworth, London, 1955.
5. HUETER, T. F., AND BOLT, R. H., "Sonics." Wiley, New York, 1955.
6. NOLTINGK, B. E., AND TERRY, N. B., in E. G. Richardson, ed., "Technical Aspects of Sound," Vol. 2, Elsevier, Amsterdam, 1957.
7. SMITH, F. W., AND STUMPF, P. K., *Electronics* **19**, 116 (April, 1946).
8. HEISING, R., "Quartz Crystals for Electrical Circuits," Van Nostrand, New York, 1947.
9. VIGOREUX, P., AND BOOTH, C. F., "Quartz Vibrators and Their Applications." His Majesty's Stationary Office, London, 1950.
10. LAUFER, A. R., *Electronics* **24**, 82 (March, 1951).
11. NOLTINGK, B. E., *J. Brit. Inst. Radio Engrs.* **11**, 11 (1951).
12. RUST, H. H., *Naturwissenschaften* **38**, 235 (1951).
13. WEISSLER, A., *J. Acoust. Soc. Amer.* **25**, 651 (1953).
14. LINDSTROM, O., *J. Acoust. Soc. Amer.* **27**, 654 (1955).
15. MARKHAM, J. J., BEYER, R. T., AND LINDSAY, R. B., *Revs. Mod. Phys.* **23**, 386 (1951).
16. BERGMANN, L., "Der Ultraschall." Springer, Berlin, 1954.
17. URICK, R. J., *J. Acoust. Soc. Amer.* **20**, 283 (1948).
18. BERKMANN, S., AND EGLOFF, G., "Emulsions and Foams." Reinhold, New York, 1941.
19. BAUER, N., A. Weissberger, ed., "Technique of Organic Chemistry," Vol. 1. Interscience, New York, 1949.

20. GRIBNAU, F. B., KRUYT, H. R., AND ORNSTEIN, L. N., *Kolloid-Z.* **75**, 262 (1936).
21. STRONG, F. C., *Anal. Chem.* **24**, 338, 2013 (1952).
22. SVEDBERG, T., AND LINDE, H., *J. Am. Chem. Soc.* **45**, 943 (1923).
23. AMIOT, R., AND BLONDEAU, L., *Compt. rend.* **239**, 264 (1954).
24. GOULDEN, J. D. S., *Trans. Faraday Soc.* **54**, 941 (1958).
25. RAJAGOPAL, E. S., *Proc. Ind. Acad. Sci.* **49A**, 333 (1959).
26. PINK, R. C., *J. Chem. Soc.* **1938**, 1252.
27. PIFFAULT, C., MOUNIER, J., BLANQUET, P., DALLIES, G., AND MEYNIEL, G., *Bull. soc. pharm. Bordeaux* **96**, 6 (1957).
28. RAJAGOPAL, E. S., *Current Sci. (India)* **26**, 142 (1957).
29. RICHARDS, W. T., *J. Am. Chem. Soc.*, **51**, 1724 (1929).
30. BEAL, H. M., AND SKAUVEN, D. M., *J. Am. Pharm. Assoc., Sci. Ed.* **44**, 487 (1955).
31. RAJAGOPAL, E. S., *Kolloid-Z.*, in press.

NONIONIC SURFACE-ACTIVE COMPOUNDS

IV. MICELLE FORMATION BY POLYOXYETHYLENE ALKANOLS AND ALKYL PHENOLS IN AQUEOUS SOLUTION

Paul Becher

Chemical Research Department, Atlas Powder Co., Wilmington, Delaware

Received July 5, 1960

ABSTRACT

Critical micelle concentrations and micellar molecular weights, determined by light scattering, are presented for a series of commercially prepared polyoxyethylene lauryl alcohols and nonyl phenols. A relationship is shown to exist between average aggregation number and ethylene oxide mole ratio, and, on the basis of some simple assumptions, a rod-shaped micelle is shown to be most likely at long ethylene oxide chain lengths, whereas there is little to choose between a rod, disc, or sphere for short polyoxyethylene chains.

INTRODUCTION

In the previous paper in this series (1), data were presented on micelle formation for several pure, homogeneous nonionic surface-active compounds in benzene solution. Unfortunately, the preparation of homogeneous water-soluble nonionics is a formidable synthetic problem, and, initially, at least, we must be content to learn what we can from the behavior of the heterogeneous compounds prepared commercially.

Luckily, as has been pointed out by the writer (2), although these materials are heterogeneous, they appear to be reproducibly so, and from this point of view they can be regarded as pure materials.

The present paper describes a study of the effect of structure on micelle formation in aqueous solution for a series of polyoxyethylene lauryl alcohols and polyoxyethylene nonyl phenols as determined by light-scattering measurements.

METHODS AND MATERIALS

The light-scattering determinations were carried out in a conventional Brice-Phoenix Light-Scattering Photometer¹ using the standard 40 × 40 × 120 mm. semioctagonal cell. Measurements were carried out at 436

¹ Phoenix Precision Instrument Co., Philadelphia, Pennsylvania.

mμ. Solutions were clarified by pressure filtration under dry nitrogen through a Corning UF sintered glass disc directly into the cell. The usual precautions to exclude dust and other extraneous matter were taken.

The refractive index increments were determined using a Phoenix Automatic Recording Differential Refractometer.¹

The materials studied were commercial ethylene oxide adducts of lauryl alcohol containing 8, 12, 18, and 23 moles of ethylene oxide per mole of alcohol, and adducts of nonyl phenol containing 10, 15, and 30 moles of ethylene oxide per mole of alkyl phenol. These materials were used as is. Solutions were made up volumetrically in distilled water, and allowed to equilibrate (usually over night) before measurement, in order to insure micellar equilibrium (2).

Micellar molecular weights were calculated from the relation

$$H(c - c_0)/(\tau - \tau_0) = 1/M_m + 2Bc. \quad [1]$$

Here τ_0 is the turbidity excess at the critical micelle concentration, c_0 , and the other terms have their well-known meanings. The critical micelle concentrations for the lauryl alcohol derivatives obtained from light-scattering measurements were in agreement with those obtained previously for these compounds by the iodine solubilization method (3); the values for the nonyl phenol derivatives were also in agreement with values obtained by that method, and are comparable with those obtained by Hsiao, Dunning, and Lorenz (4) by surface tension measurements for a similar series.

The aggregation numbers, n , were calculated from the micellar molecular weight by using the average molecular weight for the compound as obtained from composition data. They thus represent an average value.

The light-scattering data show no appreciable dissymmetry, and the slope of the $Hc/(\tau - \tau_0)$ vs. c plot is in all cases zero, corresponding to a zero value for the constant B in Eq. [1]. These results are consistent with the small size of the micelles. No "monomer saturation effect," as reported by Kushner and Hubbard (5), was observed, possibly because of the long equilibration time allowed each solution prior to measurement.

RESULTS AND DISCUSSION

The critical micelle concentrations, micellar molecular weights, and average aggregation numbers obtained for these compounds are reported in Table I. The trends observed with increasing ethylene oxide content (and hence increased water solubility) are about what one would expect, i.e., higher c.m.c., lower micellar weight, and aggregation.

However, it is interesting to note that a straight-line relationship exists if one plots the aggregation number as a function of the reciprocal of the ethylene oxide mole ratio, as shown in Fig. 1. The equations for the straight lines are, respectively:

TABLE I
Summary of Light-Scattering Results
 (dn/dc in ml./g.; c_0 in g./dl.)

Hydrophobe	R	dn/dc	$M_m \times 10^{-3}$	n	$c_0 \times 10^3$
Lauryl alcohol	8	0.134	68.2	123	5.9
	12	0.136	58.9	81	6.5
	18	0.137	50.6	51	8.0
	23	0.139	48.8	40	11.0
Nonyl phenol	10	0.158	66.3	100	6.4
	15	0.155	45.0	52	7.7
	30	0.143	29.7	19	23.6

Lauryl alcohol derivatives:

$$n = 1025/R - 5.1.$$

Nonyl phenol derivatives:

$$n = 1215/R - 22.5,$$

where n is the aggregation number and R is the ethylene oxide mole ratio, i.e., moles ethylene oxide per mole of hydrophobe.

These relations predict an infinitely large micelle, i.e., complete insolubility, for $R = 0$. On the other hand, they predict an aggregation number of unity, i.e., complete solubility, at a value $R = 168$ for the lauryl alcohol derivatives, and $R = 44$ for the nonyl phenol adducts. It is interesting to speculate whether this difference, if it is significant at all, is ascribable to a difference in solubility of the hydrophobic portion of the molecule.

It is interesting to note that the decrease in aggregation number with increase in ethylene oxide chain length has been noted for polyoxyethylene isooctyl phenols by Kushner, Hubbard, and Doan (6) and for polyoxyethylene dodecyl alcohol by Stauff and Rasper (7). However, in both these cases, the measurements were made on materials obtained by the fractionation of a single sample. Since there is no reason to expect the polymer distribution in the fractionated samples to be the same as in a directly polyoxyethylated material of the same average molecular weight, the results are not strictly comparable with our data. The micellar molecular weights are of the same order of magnitude, however.

Although, as noted, the micelles are so small that dissymmetry measurements can give us no clue to the shape of the micelle, certain conclusions may be drawn on the basis of some simple assumptions.

One may first arrive at an estimate of the volume of the micelle from the following considerations. The volume of the molecules which make up the micelle from the well-known relation for the molar volume, namely,

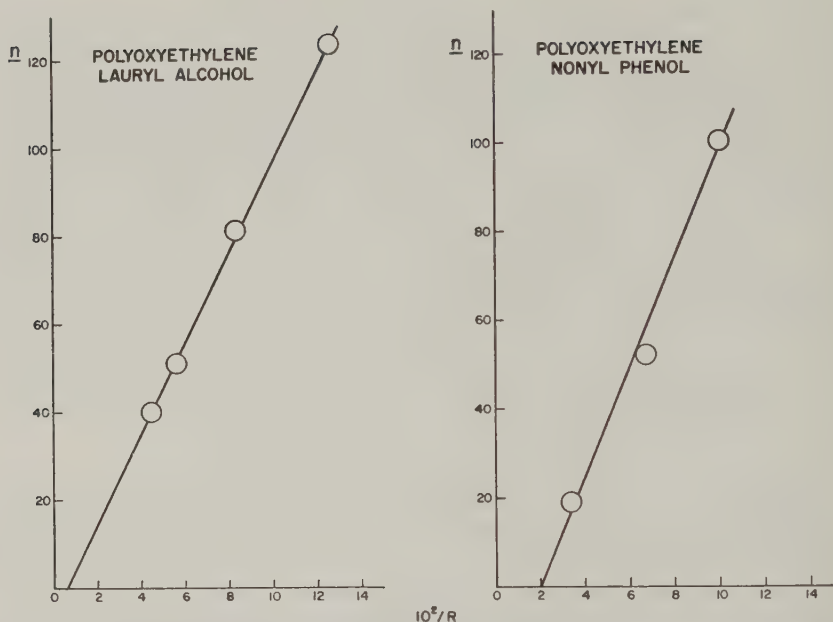


FIG. 1. Dependence of aggregation number (n) on ethylene oxide mole ratio (R) for polyoxyethylene lauryl alcohol and nonyl phenol. The R -axis is multiplied by a factor of 100 for convenience in plotting.

$$v = \frac{10^{-24}}{N} \left[\frac{M}{d} \right], \quad [2]$$

where v is the molar volume in cubic Angstroms, N is Avogadro's number, M is the average molecular weight, and d is the density in grams per milliliter. For most of the compounds under consideration, d may be taken as unity with only a small error.

In calculating the volume of the micelle it must be remembered that the ether-oxygens of the polyoxyethylene chain are hydrated, and that other water molecules are kinetically trapped in the network formed by the water-soluble chains which extend out from the center of the micelle. The viscosity data of Kushner and Hubbard (5) on a nonyl phenol derivative suggests that the average amount of water contained in the micelle amounts to about 4.5 molecules per ether oxygen.

Thus, the volume of the micelle may be expressed as

$$V_m = n(v_d + 4.5Rv_{H_2O}), \quad [3]$$

where V_m is the micellar volume, n the aggregation number, v_d the molar volume of the detergent monomer, v_{H_2O} the molar volume of water, and R the ethylene oxide mole ratio. The results of this calculation are shown in the fourth column of Table II.

TABLE II
Micelle Shape Calculations
 (V_m , V_s in \AA^3 ; r , h , L in \AA .)

Hydrophobe	R	L	$V_m \times 10^{-3}$	$V_s \times 10^{-3}$	r	h
Lauryl alcohol	8	42	247	311	30	54
	12	55	240	697	26	25
	18	75	209	1,770	21	12
	23	91	210	3,160	19	8
Nonyl phenol	10	43	257	321	31	45
	15	59	192	861	23	18
	30	108	130	5,290	14	4

It is now necessary to relate this figure to that of some suitably chosen model. The simplest assumption is that of a spherical micelle, which was successfully applied to their data by Kushner and Hubbard (5). From the known bond distances and angles an average molecular length L can be estimated for each molecule of surface-active compound studies. These are listed in the third column of Table II.

With this value, the volume of the spherical micelle can be calculated from the relation:

$$V_s = \frac{4}{3}\pi L^3 \quad [4]$$

and compared with V_m . The thus calculated values of V_s are shown in the fifth column of Table II. As can be seen, the volume calculated from the spherical model shows only rough agreement at the very lowest ethylene oxide contents, and soon becomes unreasonably large. Indeed, the trend is actually in the wrong direction. The model thus cannot be considered suitable for the larger molecules.

Two other micellar models may be considered, the rod and the disc. These are both cylindrical in shape, but differ in the orientation of the molecules comprising the micelle. In the rod, the altitude of the cylinder is twice the length of a monomer molecule, i.e., $2L$. In the disc, it is the diameter of the cylinder that is equal to $2L$.

Unfortunately, the other dimension of these models cannot be readily estimated, so that an absolute calculation of the corresponding volumes is impossible. However, if one assumes the correctness of the quantity V_m (derived ultimately from the light-scattering data), it is possible to calculate the radius r of the rod-shaped micelle and the height h of the disc from the relations

$$r = (V_m/2\pi L)^{1/2}; \quad [5]$$

$$h = V_m/\pi L^2. \quad [6]$$

TABLE III
Surface Areas of Micellar Models (A.²)

Hydrophobe	<i>R</i>	$S_s \times 10^{-3}$	$S_r \times 10^{-3}$	$S_d \times 10^{-3}$
Lauryl alcohol	8	22.1	21.5	25.3
	12	38.1	22.2	27.7
	18	70.9	22.6	40.9
	23	104.0	24.0	56.6
Nonyl phenol	10	22.7	22.6	22.5
	15	43.7	20.4	28.6
	30	135.0	20.2	76.0

One may then decide which of the so calculated dimensions seems most reasonable in view of the known geometry of the molecules. The calculated values are tabulated in the sixth and seventh columns of Table II. Again it does not appear that there is much to choose between the models for low values of the ethylene oxide mole ratio; but for the higher members of the series, the disc model seems to give disc heights which are unreasonably low.

Another method of determining which model seems most reasonable would be to use the dimensions derived in Table II to calculate the surface area of the micelle, since, from thermodynamic considerations, the micelle of minimum surface would probably be the most stable. The following relations can be used to calculate the surface areas of micelles

$$S_s = 4\pi L^2; \quad [7]$$

$$S_r = 2\pi r(2L + r); \quad [8]$$

$$S_d = 2\pi L(L + h); \quad [9]$$

where S_s , S_r , and S_d are the surface areas of the sphere, rod, and disc, respectively, and r and h have been calculated from Eqs. [5] and [6].

The results of these calculations are shown in Table III. Here the differences are quite clear-cut. There is nothing to choose between the three models for the polyoxyethylene (8) lauryl alcohol and the polyoxyethylene (10) nonyl phenol. However, for all the other compounds the rod model gives much the lowest surface area; indeed, it is interesting to note that the rod model gives a surface area which is practically independent of the size of the monomer molecule.

One other interesting result can be derived from a consideration of the rod-shaped micelle. Since the cross section of the rod contains, on the average, $n/2$ molecules, and since the cross-sectional area of the rod can be calculated, using the derived value of r , the average cross-sectional area per

TABLE IV
Cross-Sectional Areas of Molecules (\AA^2)

Hydrophobe	<i>R</i>	In the micelle	At the solution/ air interface
Lauryl alcohol	8	49	46
	12	54	57
	18	56	72
	23	58	74
Nonyl phenol	10	60	60
	15	64	72
	30	62	101

molecule in the micelle can be calculated. The result of this calculation is shown in Table IV and is compared with values of the cross-sectional area occupied by the same molecules at the air solution interface, as calculated from surface tension data. The values for the lauryl alcohol derivatives are calculated from unpublished surface-tension data obtained in this laboratory; the values for the nonyl phenol derivatives are taken from Hsiao, Dunning, and Lorenz (4). The values agree quite well at low ethylene oxide content but diverge at higher values. This is consistent with the fact that at the solution/air interface one would expect the longer polyoxyethylene chains to "thrash about" more and thus cause the molecule to occupy a larger area. On the other hand, the molecules in the micelle might well be expected to be rather constrained and thus show little, if any, change in molecular cross-sectional area occupied.

Although the above calculations are based on somewhat naive assumptions, the results are sufficiently consistent so that we may conclude that for molecules containing fairly short ethylene oxide chains, there is nothing to choose between a rod, disc, or sphere model for the micelle, whereas at higher chain lengths the data favor the assumption of at least a rod-like micelle.

The relationship reported between the aggregation number and the ethylene oxide mole ratio may be expressed in the broad generalization that the more soluble the material, the smaller the micelle. It may be remarked that the overall behavior observed is broadly consistent with the statistical mechanical theory of micelle formation of Hoeve and Benson (8).

ACKNOWLEDGMENT

Most of the measurements reported herein were carried out by Mrs. N. C. Soistmann and Mr. M. J. Megraw.

REFERENCES

1. BECHER, P., *J. Phys. Chem.* **64**, 1221 (1960).
2. BECHER, P., AND CLIFTON, N. K., *J. Colloid Sci.* **14**, 519 (1959).
3. BECHER, P., *J. Phys. Chem.* **63**, 1675 (1959).
4. HSIAO, L., DUNNING, H. N., AND LORENZ, P. B., *J. Phys. Chem.* **60**, 657 (1956).
5. KUSHNER, L. M., AND HUBBARD, W. D., *J. Phys. Chem.* **58**, 1163 (1954).
6. KUSHNER, L. M., HUBBARD, W. D., AND DOAN, A. S., *J. Phys. Chem.* **61**, 371 (1957).
7. STAUFF, J., AND RASPER, J., *Kolloid-Z.* **151**, 148 (1957).
8. HOEVE, C. A. J., AND BENSON, G. C., *J. Phys. Chem.* **61**, 1149 (1957).

THE EFFECT OF SUCROSE ON PROTEIN FILMS

I. SPREAD MONOLAYERS

F. MacRitchie and A. E. Alexander

Department of Physical Chemistry, The University of Sydney, Sydney, Australia

Received June 1, 1960

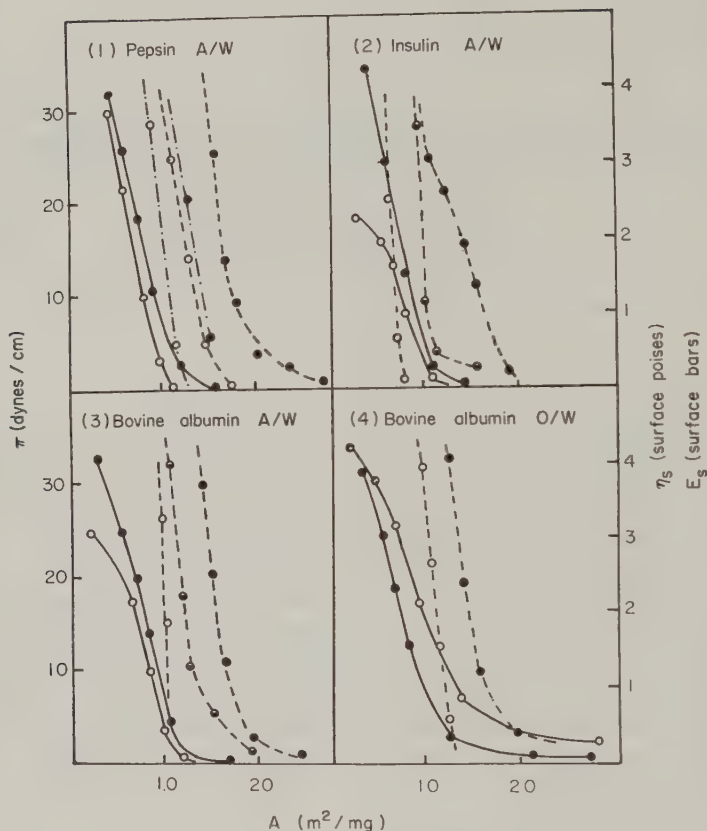
Although much work has been done in the past on protein films (1), comparatively little attention has been paid to the effect of agents which influence hydrogen bonding, in view of the great importance of this bond in proteins. The effect of urea has been studied to some extent (2) but mainly as regards surface pressure changes, which, however, are much less sensitive than the mechanical properties (surface viscosity and elasticity) for detecting changes in molecular bonding. Sucrose offers the advantage of high solubility in water without affecting the pH or ionic strength, factors which are known to influence protein films. The study of the effects of sucrose on protein films is also relevant to certain technological systems in which foams and emulsions are stabilized by proteins in the presence of sugars. In this work, protein films have been studied as spread monolayers and as films adsorbed from solution, together with some bulk foam measurements.

EXPERIMENTAL

Measurements of surface pressure (II) were made by the Wilhelmy dipping-plate method, surface potential (ΔV) by the standard polonium air-electrode method, and surface viscosity (η_s) and elasticity (E_s) by means of a torsion pendulum viscometer employing a platinum needle oscillating in the interface. For monolayer measurements at the A x W interface, a Perspex (Leucite) trough 30 cm. x 20 cm. was used. To prevent movement by rigid films, the plate and needle were centered in the trough and the films compressed simultaneously from both sides.

Bubbles were injected beneath the monolayers by means of an Agla micrometer syringe and the average lifetime was found by timing at least eight bubbles.

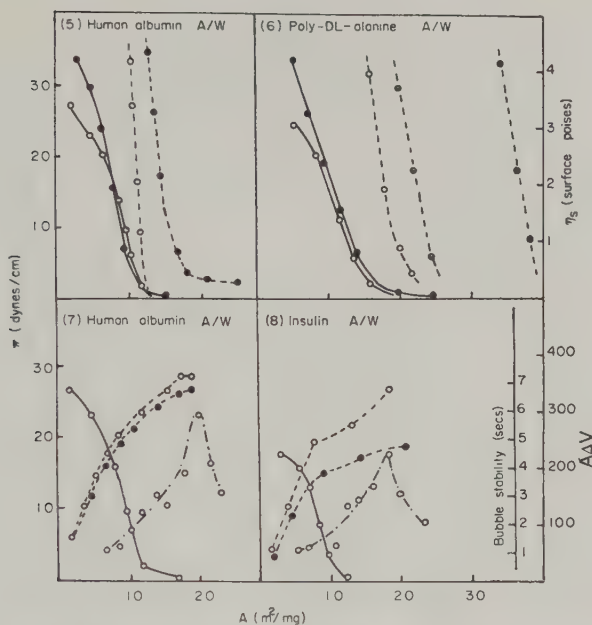
A circular glass dish (14.0 cm. in diameter) was used for measurements at the O/W interface and for studying adsorbed films. Temperatures were maintained to $\pm 0.1^\circ\text{C}$. by circulating water from a thermostat through glass coils. Unless otherwise stated all measurements were made at 25°C .



FIGS. 1, 2, 3, and 4. Typical data for protein monolayers on sucrose solutions. — pressure; ---- viscosity; ---- elasticity. Sucrose concentrations are: ○ none; ◐ 100 g./100 g. water; ● 150 g./100 g. water.

The extrapolated areas from Π - A curves were reproducible to within $\pm 1\%$ and potentials to within ± 5 mv. in the stable region. Viscosity-area curves on purely aqueous substrates generally agreed to within $\pm 1\%$; on strong sucrose solutions the reproducibility was not as good.

The proteins used were pure materials from Armour and Co. and the Commonwealth Serum Laboratories, Melbourne. All proteins and poly-L-alanine were spread from 0.03% solutions in 50% aqueous propanol containing 0.5 M sodium acetate by means of an all-glass Agla micrometer syringe with its tip placed in the interface. Other polymers used were spread from benzene solution. It was found unnecessary to allow the films to stand for more than 2 min. after spreading before taking measurements. Since monolayers of proteins and many polymers tend to show some decrease in pressure with time, measurements were standardized by recording pressures 1 min. after compression.



FIGS. 5, 6, 7, and 8. Typical data for protein monolayers on sucrose solutions. Legend same as for Figs. 1-4 except in Figs. 7 and 8 where: --- $A\Delta V$; ---- bubble stability (seconds).

Sucrose used was the highest purity available commercially. All sucrose solutions were shaken with activated charcoal and filtered, and gave no measurable surface pressure on bringing the movable barriers together after 10 min. standing. Their pH differed by less than 0.2 unit from the distilled water used. No sucrose solution was used which was more than one week old.

RESULTS

Π - A , ΔV - A , η_s - A , and E_s - A curves for pepsin, insulin, trypsin, lysozyme, bovine and human albumin, and polyalanine, were measured on distilled water (pH 6.0) and on sucrose solutions up to concentrations of 150 g./100 g. water. Insulin gave no measurable E_s ; the other proteins and polyalanine were similar to pepsin. Some typical results are shown in Figs. 1-8. (In Figs. 7 and 8 the product $A \cdot \Delta V$ is plotted, this quantity being proportional to the surface moment.)

A comparison between the A/W and an O/W interface is given in Figs. 3 and 4, for bovine albumin. Other proteins studied (pepsin, insulin, lysozyme, and human albumin) behaved similarly.

A range of sucrose concentrations (50, 75, 100, and 150 g./100 g. water) was used with insulin, bovine albumin, and polyalanine; in other cases only the highest concentration was employed.

TABLE I
Boundary Tensions at 20°C.

Aqueous phase	Against air (dynes/cm.)	Against pet. ether (dynes/cm.)
Water	72.5 \pm 0.2	44.2 \pm 0.2
Sucrose solution (150 g./100 g. water)	77.4 \pm 0.2	42.3 \pm 0.2

In the case of polyvinyl acetate and polyvinyl stearate even the highest sucrose concentration produced no appreciable change in surface properties; no figures have therefore been given. These compounds were chosen since no hydrogen bonding between their molecules is possible, and in particular the latter gives a rigid film resembling those of proteins.

Strong sucrose solutions modify the boundary tension as shown in Table I, these measurements being made with a du Nouy tensiometer. Similar results have been found by Douglas (3), using paraffins as the oil phase.

Typical data showing the stability pattern of surface bubbles liberated beneath monolayers are shown in Figs. 7 and 8. Despite the poor reproducibility of bubble lifetimes, the general pattern was quite clear and the film area giving maximum stability could be found quite accurately. In all cases, maximum stability occurred at a film area greater (by about 80 %) than that of a close-packed monolayer. This stability pattern has been found previously for a number of compounds (4).

On sucrose solutions bubble stabilities increased from several seconds to many minutes. Owing to the length and variability of the lifetimes, no definite optimum area could be found, although stability definitely decreased at low areas, suggesting a pattern similar to that found on water.

DISCUSSION

It is seen from the data presented above that with proteins and polyalanine the addition of sucrose produces marked changes in η_s and E_s together with much smaller effects upon Π and $A\Delta V$. At the A/W interface the Π - A curves are displaced to slightly higher areas and the films are appreciably more stable at the higher pressures. Similar effects have been previously noted for polypeptides on strong urea solution (2).

At the O/W interface, on the other hand, sucrose has the opposite effect on the Π - A curve. The difference may be related to the opposite effects of sucrose on the boundary tensions, as shown in Table I.

Since sucrose has no effect at all on the film properties of polyvinyl acetate and polyvinyl stearate but does influence polyalanine to the same extent as the proteins it seems logical to conclude that sucrose exerts its influence by modifying the hydrogen bonding between keto-imido groups

on neighboring chains. Possibly sucrose binds water molecules, thus preventing the latter from participating in hydrogen bonding with C=O and N—H groups which are then free to associate; this would tend to increase both η_s and E_s . The thermodynamic properties of sucrose solutions indicate, according to Taylor and Rowlinson (5), strong hydrogen bonding between sucrose and water molecules, this bonding being stronger or more abundant than that between water molecules themselves. (At a sucrose concentration of 150 g./100 g. water the mole ratio is *ca.* 1/12, i.e., about one water molecule to each O atom in the sugar molecule.)

REFERENCES

1. CUMPER, C. W. N., AND ALEXANDER, A. E., *Revs. Pure and Appl. Chem. (Australia)* **1**, 121 (1951). CHEESMAN, D. F., AND DAVIES, J. T., *Advances in Protein Chem.* **9**, 440 (1954).
2. MISHUCK, E., AND EIRICH, F. R., *J. Polymer Sci.* **16**, 397 (1955). ISEMURA, T., AND HAMAGUCHI, K., *Ann. Rept. Sci. Works* **5**, 65 (1957).
3. DOUGLAS, H. W., *Trans. Faraday Soc.* **46**, 1082 (1950).
4. TALMUD, D., AND SUCHOWOLSKAJA, S., *Z. physik. Chem.* **154**, 227, (1931). TRAPEZNIKOV, A. A., *Acta Physicochim. U.R.S.S.* **13**, 265 (1940).
5. TAYLOR, J. B., AND ROWLINSON, J. S., *Trans. Faraday Soc.* **51**, 1183 (1955).

THE EFFECT OF SUCROSE ON PROTEIN FILMS

II. ADSORBED FILMS

F. MacRitchie and A. E. Alexander

Department of Physical Chemistry, The University of Sydney, Sydney, Australia

Received June 1, 1960

EXPERIMENTAL

The adsorption of the proteins at the air/aqueous interface was followed by measurements of the mechanical properties of the adsorbed film. With the use of previous monolayer results, it was possible from measurements of η_s and E_s to estimate the thickness of the surface denatured layer. The proteins used for study were chosen so as to include ones with isoelectric points near the pH of the solutions (bovine and human albumins, 5.5) and on either side (pepsin, *ca.* 2, trypsin *ca.* 8, and lysozyme, *ca.* 11).

The method used was found to be a critical factor. The one first employed was to make up a solution, pour it into a dish, and commence measurements, assuming that a new interface had been formed on completion of pouring. However, low concentrations of sucrose did not appear to be increasing the rate of adsorption of protein as was anticipated from foam

TABLE I
Adsorption Times (τ)
(in Minutes)

Protein	Sucrose concentration (g./100 g. water)		
	0	50	150
Bovine albumin	$< \frac{1}{2}$	$< \frac{1}{2}$	10
Human albumin	10	$< \frac{1}{2}$	5
Pepsin	$>> 30$	3	—
Lysozyme	> 30	2	—

measurements. The effect of removing by suction the films formed and observing the subsequent adsorption was then tried. The rate of build-up of the denatured layer was then seen to decrease on removal of the first film or films (depending on the protein) until it reached an approximately constant value, after which reproducible adsorption rates were obtained for subsequent film removals. This phenomenon was probably due to some surface denaturation occurring during the mixing and pouring operations, the denatured protein then appearing at the interface. For bovine and human albumins with isoelectric points close to the pH of the solution, several films had to be removed from the surface before true values for the adsorption rate could be obtained.

Foam measurements were made in a graduated cylinder fitted with a porous septum of sintered glass, through which compressed air, previously filtered through cotton wool, was passed. The volume of air introduced was measured with a flow meter previously calibrated by the downward displacement of water in a 1-liter measuring cylinder.

Foam heights were recorded during bubbling for a period of 60 sec., and after ceasing bubbling for a suitable time, depending on the rate of collapse. From the figures, the ease of formation and the half-life of the foam were calculated.

The materials used were the same as in the preceding paper. Purification of the sugar was essential since its surface-active impurities greatly influenced the formation and stability of foams from protein solutions.

RESULTS

1. *Films Adsorbed from Solution*

The adsorption data for the various proteins in solutions of different sucrose concentrations at $25^\circ \pm 0.2^\circ\text{C}$. is summarized in Table I. Here, τ shows the time required for 1 mg. per square meter of denatured protein to be formed at the surface. The concentration of protein was 0.03 % as for the bulk foam experiments described later.

A more detailed study of the effect of sucrose concentration on the adsorption of human albumin and poly-DL-alanine is shown in Table II.

TABLE II
Adsorption Times (τ)
(in Minutes)

Compound	Sucrose concentration (g./100 g. water)					
	0	10	20	50	100	150
Human albumin	31	8	4½	4	4	30
Poly-DL-alanine	3¼	—	3¼	6½	12	52

Low concentrations (human albumin—0.01 % and poly-DL-alanine—0.002 %) were chosen so as to make the measurements more sensitive.

2. Bulk Foams

A summary of the results for a range of sucrose concentrations and for several proteins at a constant concentration (0.03 %) at room temperature ($24^\circ \pm 2^\circ\text{C.}$) is given in Table III. In the table F.H. is the foam height in millimeters after 60 sec. bubbling; $\tau_{1/2}$ is the half-life of the foam, and Q is an estimate of the "quality" of the foam as assessed visually by the size and uniformity of the bubbles.

The effect of protein concentration in purely aqueous solution was studied in the case of bovine serum albumin; the results are given in Table IV.

DISCUSSION

1. Adsorption of Proteins

Cumper and Alexander (1) have made an extensive study of the effects, on the rate of adsorption, of protein concentration, nature of interface, pH, ionic strength, and temperature. All these factors influence the rate of build-up of a denatured layer, although at a particular interface for a sufficient protein concentration, pH is probably the major one. The adsorption-pH curves show a maximum near the isoelectric point, falling away steeply on either side.

In the build-up of a denatured protein film at an interface we have three factors to consider—adsorption, surface denaturation, and surface coagulation. It is generally accepted that the process of surface denaturation occurs by adsorption in the globular form followed by an unfolding caused by the asymmetric surface forces. It is also widely held that the surface denaturation step is practically instantaneous. There is good evidence (2) that this is so under certain conditions, but this does not mean that it is necessarily so under all conditions.

At pH's away from the isoelectric point, adsorption of proteins is believed to be retarded by repulsive forces arising from the charged molecules at the surface. Since sucrose would not be expected to reduce this barrier,

TABLE III

Sucrose concentration (g./100 g. water)	0		25		50		100		150							
	F.H.	$\tau_{1/2}$	Q	F.H.	$\tau_{1/2}$	Q	F.H.	$\tau_{1/2}$	Q	F.H.	$\tau_{1/2}$	Q				
Bovine albumin	100	1 min.	Fair	80	>30 mins.	Very good	90	>30 mins.	Very good	80	ca. 32 mins.	Good	Poor foam, large bubbles which collapse quickly	80	ca. 2	Very poor
Human albumin	No foaming			110	ca. 18 mins.	Good	120	ca. 30 mins.	Very good	120	ca. 20 mins.	Good				
Trypsin	100	ca. $\frac{1}{2}$ min.	Poor	About same as for water			100	ca. 1 min.	Fair	80	ca. 3 mins.	Fair				
Pepsin	No foaming						80	ca. 3 mins.	Fair	80	ca. 3 mins.	Fair				
Lysozyme	No foaming						10	Few secs.	Poor	Same as for previous concn.						

TABLE IV

Protein concentration (%)	F.H.	$\tau_{1/2}$	Q
0.005	80	Few sec.	Poor
0.01	80	Few sec.	Poor
0.03	90	1 min.	Fair
1.0	85	11 mins.	Very good
4.0	80	25 mins.	Excellent

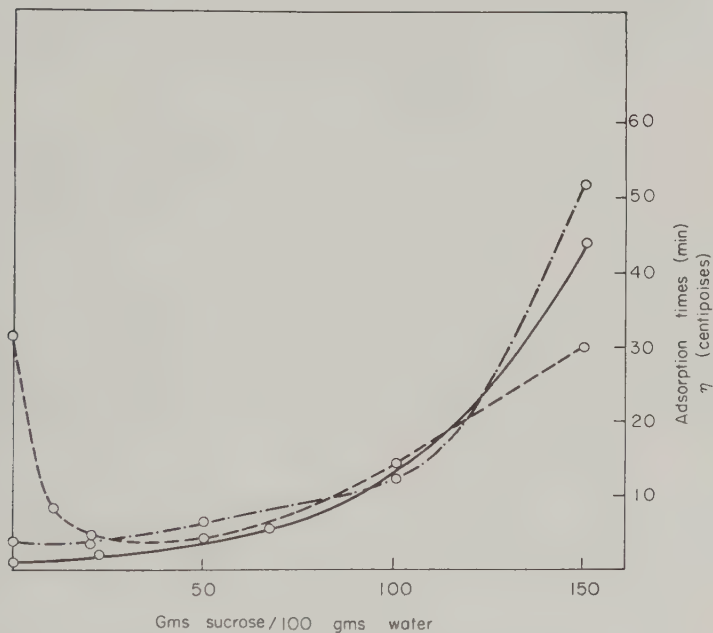


FIG. 1. Bulk viscosity of pure sucrose solutions and adsorption data for human albumin and poly-DL-alanine as a function of sucrose concentration. — bulk viscosity curve; - - - adsorption times for human albumin; - · - · - adsorption times for poly-DL-alanine.

some other reasons must be sought for the increased rate of adsorption produced by low concentrations of sucrose. Possible ones would be:

- An increased rate of diffusion of the molecules to the interface.
- An increased rate of surface denaturation of the adsorbed globular molecules.
- Unfolding of the molecules in *bulk* solution with a subsequent rapid adsorption of denatured protein.

The only likely way in which sucrose could increase the rate of diffusion is by reducing the hydration of the protein molecules. However, this effect could not be large, and it seems probable that sucrose acts only in

hindering diffusion by the bulk viscosity of its solutions. This is supported by the data shown in Fig. 1, where the adsorption times of human albumin and polyalanine and the bulk viscosity of sucrose solutions are plotted against sucrose concentration. In the case of polyalanine, where denaturation is not possible, the correlation is seen to be very close.

It would, therefore, appear that sucrose influences adsorption by assisting unfolding of the protein molecules either at the surface or in the bulk. That this unfolding may occur is suggested by the following evidence.

a). Unfolding of protein molecules is known (3) to be brought about by hydrogen-bonding agents (e.g., urea and guanidine hydrochloride). By virtue of the number of hydrogen-bonding groups in its molecule, it is quite likely that sucrose could also cause such unfolding.

b). In preliminary adsorption studies, it was apparent that protein which had been surface denatured during mixing of solutions adsorbed very rapidly afterwards. Although elongated molecules would have lower diffusion coefficients than globular ones, the important factor here could be the exposure of hydrophobic sidechains, which would certainly promote rapid adsorption.

c). The adsorption of polyalanine, the molecule of which closely resembles an unfolded protein molecule, is only decreased by sucrose, as shown in Fig. 1. If such changes occur in the bulk solution they should become apparent in studies of molecular shape, using the standard techniques of sedimentation, diffusion, and light scattering. Such studies do not appear, however, to have been made.

That the rate of build-up of the protein film decreases above a certain sucrose concentration does not mean that the effect of sucrose declines at this point but merely reflects the point at which the effect of bulk viscosity on the diffusion becomes predominant.

2. Bulk Foams

From Table III, the general effects of sucrose are seen to be: an overall increase in foam stability and an increase in the ease of formation up to a point beyond which higher concentrations depress the foaminess. The adsorption data in Tables I and II provide the key for explaining the bulk foam measurements in Table III.

In foam considerations it is usual to separate the factors of ease of formation and of stability. For protein-stabilized foams the former depends on the rapid formation of a denatured layer of protein at the A/W interface, and any factor which enhances this initial adsorption should therefore increase the foaminess. On the assumption that the data for human albumin are typical for proteins, as is indicated by Tables I and II, the foaminess should be a maximum at a sucrose concentration of about 50 g./100 g. water. The foam height data in Table III are seen to give reasonable support to this conclusion.

The second factor, foam stability, also depends on the quality and thus the concentration of denatured film at the interface, as is seen from Table IV, where stability increases with protein concentration.

If bubble studies under monolayers are to be taken as a guide, stability should decrease at a certain concentration of film molecules and thus the stability-concentration curve for foams should pass through a maximum. Owing to shortage of material the stability of foams for protein concentrations greater than 4% was not investigated. The average lifetimes of bubbles in foams are considerably higher than those under monolayers, and although there are basic differences to be expected in view of the techniques used, it would appear that the structure of the stabilizing adsorbed film cannot be strictly compared with that of a spread monolayer. Bubble studies under monolayers therefore do not seem to be very useful for interpreting bulk foam properties, although they may prove a sensitive means of investigating monolayer structure.

It is quite clear that sucrose does not impart high stability to protein foams merely through its influence on adsorption. Providing that the rate of adsorption remains the same, increasing sucrose concentration appears to increase foam stability. This seems to be due to its forming very stable lamellae, as can be seen by suspending them in wire frames; the factor which is important here is probably the bulk viscosity. Drainage of films usually occurs exponentially until a film remains which undergoes practically no further thinning. At this stage such factors as vibration and evaporation become important in the breakdown of the films.

We therefore have various factors to consider when deciding optimum conditions for a stable protein foam in the presence of sucrose. One is to have an intermediate sucrose concentration giving the maximum rate of adsorption. Using higher sucrose concentrations will theoretically increase the stability but, since it will also depress the rate of adsorption, it will do so only if the original adsorption rate is retained by altering other factors such as protein concentration and pH.

It has not been possible to make a definite correlation of monolayer properties with bulk foams but it is quite conceivable that the changes in monolayer properties brought about by strong sucrose solutions could be important factors in the stability of foams in these concentrated solutions. Both increased surface viscosity and pressure stability would be expected to add stability to the films by hindering the surface coagulation process.

REFERENCES

1. CUMPER, C. W. N., AND ALEXANDER, A. E., *Trans. Faraday Soc.* **46**, 235 (1950).
2. BULL, H. B., *J. Biol. Chem.* **123**, 17 (1938).
3. KAUZMANN, W., *Advances in Protein Chem.* **14**, 1 (1959).

MEASUREMENT OF THE ANGULAR VARIATION OF LIGHT SCATTERED FROM SINGLE AEROSOL DROPLETS¹

Frank T. Gucker and James J. Egan²

*Contribution No. 972 from The Chemical Laboratory of Indiana University,
Bloomington, Indiana*

Received July 11, 1960

ABSTRACT

An instrument was constructed to measure the intensity of light scattered at various angles from a single droplet of dioctyl phthalate of about one micron radius or larger, illuminated by radiation of 436 millimicrons wavelength.

The general principle of the measurement is to suspend a charged particle between two electrostatic plates, illuminate it with a parallel beam of monochromatic light, and measure with a sensitive photometer the light scattered at various angles from the incident beam. Scattering curves for four particles varying in size from 0.7 to 1.5 microns radius are presented and compared with curves calculated from Mie's electromagnetic theory. In general the agreement is satisfactory.

INTRODUCTION

The problem of the scattering of a plane electromagnetic wave from an isotropic sphere was originally solved with Maxwell's field equations by Mie (1) in 1908 and Debye (2) in 1909. Since that time the theory has found numerous applications in various branches of science. The colloid chemist has used light scattering extensively in measuring particle sizes of both sols and aerosols; and the polymer chemist, extending the theory, has been able to measure the molecular weights and shapes of polymers. Astronomers and physicists are also currently engaged in the study of atmospheric dust and microwave scattering, both of which apply the theory of Mie and Debye.

Although the experimental methods of measuring scattering vary greatly from case to case, most of the measurements have been made on systems containing several particles. It was thus believed useful to devise a method

¹ The research reported in this paper has been made possible through support and sponsorship extended by the Geophysics Research Division of the Air Force Cambridge Research Center, under Contract No. AF-19(122)-375 with the Research Division of the Indiana University Foundation.

² Present address: Brookhaven National Laboratory, Upton, Long Island, New York.

whereby a single particle could be isolated, and the light scattered from this particle measured with a sensitive photometer.

THEORY OF SCATTERING FROM SPHERES

A brief statement of some results of Mie's work will give a more precise significance to the measured quantities and serve to define the notation used later.

A sphere of radius r is illuminated by a plane wave of natural light having unit intensity and a wavelength λ . The intensity of light scattered into a unit area at an angle θ , measured from the *forward* direction of propagation of the incident beam, is given by

$$I_\theta = \frac{\lambda^2}{8\pi^2 R^2} (i_1 + i_2), \quad [1]$$

where R is the distance from the sphere to the unit area collecting the scattered radiation. Here i_1 is proportional to the intensity of light plane polarized with the electric vector perpendicular to the plane of observation (formed by the incident beam and the point of observation), and i_2 is proportional to the intensity of light plane polarized perpendicular to i_1 .

Using the notation suggested by Gucker and Cohn (3), the analytical expressions for i_1 and i_2 are given in terms of the following convergent series:

$$i_1 = \left| \sum_{n=1}^{\infty} a_n \Pi_n(\cos \theta) + b_n T_n(\cos \theta) \right|^2. \quad [2]$$

$$i_2 = \left| \sum_{n=1}^{\infty} a_n T_n(\cos \theta) + b_n \Pi_n(\cos \theta) \right|^2. \quad [3]$$

$$a_n = \frac{S_n'(\beta) S_n(\alpha) - m S_n'(\alpha) S_n(\beta)}{S_n'(\beta) \Phi_n(\alpha) - m \Phi_n'(\alpha) S_n(\beta)}. \quad [4]$$

$$b_n = \frac{m S_n'(\beta) S_n(\alpha) - S_n'(\alpha) S_n(\beta)}{m S_n'(\beta) \Phi_n(\alpha) - \Phi_n'(\alpha) S_n(\beta)}. \quad [5]$$

$$S_n(\alpha) = \sqrt{\pi\alpha/2} J_{n+1/2}(\alpha). \quad [6]$$

$$C_n(\alpha) = (-1)^n \sqrt{\pi\alpha/2} J_{-(n+1/2)}(\alpha). \quad [7]$$

$$\Phi_n(\alpha) = S_n(\alpha) + i C_n(\alpha). \quad [8]$$

$$\Pi_n = \frac{2n+1}{n(n+1)} \pi_n(x) = \frac{2n+1}{n(n+1)} P_n'(x). \quad [9]$$

$$T_n = \frac{2n+1}{n(n+1)} \tau_n(x) = \frac{2n+1}{n(n+1)} [x P_n'(x) - (1-x^2) P_n''(x)]. \quad [10]$$

In these equations m is the refractive index of the scattering material referred to the medium, $\alpha = 2\pi r/\lambda$, $\beta = m\alpha$, $S_n(\alpha)$ and $\Phi_n(\alpha)$ are Riccati-Bessel functions of order n , J_n is an ordinary Bessel function, $P_n(x)$ is a Legendre polynomial of order n , $x = \cos \theta$, the prime denotes the first derivative with respect to the argument, and the double prime the second.

When the particle is illuminated with polarized light of unit intensity with the electric vector first perpendicular to the plane of observation and second in this plane, the corresponding intensities (1, 10) scattered at angle θ are:

$$I_{\theta}^{(1)} = (\lambda^2/4\pi^2 R^2) i_1 \quad \text{and} \quad I_{\theta}^{(2)} = (\lambda^2/4\pi^2 R^2) i_2. \quad [11]$$

DESCRIPTION OF THE APPARATUS

General Description

The general principle of the method is to suspend a charged particle between two electrostatic plates, illuminate it with a parallel beam of monochromatic light, and measure the light scattered at various angles from the incident beam with a 1P21 photomultiplier. The two major problems encountered in the design and construction of such an instrument are the reduction of background light to the very low level comparable with scattering from a single aerosol particle, and the elimination of convection or air currents so as to allow accurate centering of the particle in the incident beam. The instrument will be described under three main headings; the illuminating system, the scattering cell, and the photometer.

The illuminating system produces an intense beam of parallel light of small cross-sectional area. It has been designed to allow convenient interchange of different optical filters and can be used with a variety of light sources. The scattering cell consists of two electrostatic plates surrounded by an anticonvection jacket with appropriate windows. The cell and the photomultiplier tube are enclosed in a brass chamber, surrounded by an oil bath which keeps the entire system at a uniform temperature and thus reduces convection currents inside the brass chamber. The photometer consists of a 1P21 photomultiplier in conjunction with a Leeds and Northrup micromicroampere amplifier and Speedomax recorder. In order to limit the field of view of the photometer, a lens system collects the light scattered into a small solid angle and focuses it on the photocathode of the photomultiplier.

Illuminating System

The illuminating system is shown in Fig. 1. The aspheric lenses L_1 and L_2 , of 63 mm. diameter and 57 mm. focal length, are placed 57 mm. from the source and the stop S_1 , respectively. They form an image of the source at S_1 , a circular stop 1 mm. in diameter which acts as a secondary source.

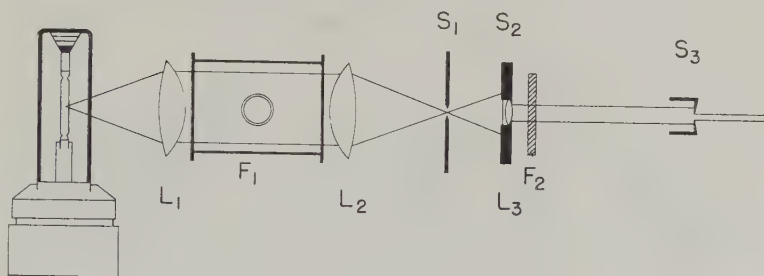


FIG. 1. Top view of illuminating system.

This arrangement can be used with a source of any shape, as long as the most intense part is focused at the opening of S_1 . A filter cell F_1 , 7.5 cm. long, containing a 1% copper chloride solution, is used to absorb the longer wavelengths and thus reduce any possible convection caused by the heat of the beam. The lens L_3 , which produces the desired parallel beam, is a coated achromat with a diameter of 14 mm. and a focal length of 36 mm. Since this lens has a thickness of approximately 2 mm., it is supported in a holder S_2 having a sharp-edged stop in contact with the lens; otherwise the emerging beam will be surrounded by a "halo" of light due to the scattering from the edges of the lens. All these parts are supported on a conventional optical bench not shown in Fig. 1. The stop S_3 , placed very close to the inlet window of the scattering cell, has a diameter of 3 mm. and serves to reduce the cross-sectional area of the incident beam, so as to prevent its striking the electrostatic plates and thus scattering light. To obtain an effective illuminating system, all the stops must be very sharp and all the lenses must either have sharp edges like L_1 and L_2 or be stopped like L_3 . Without such care, a sharply defined beam cannot be obtained. The angular divergence of the beam is $0^\circ 48'$.

Filter F_2 is a Schott narrow-band metallic interference filter obtained from the Fish-Schurman Corporation, New York. According to the manufacturer, it has a peak transmission of 24% at 436 millimicrons and a half-band width of 9.5 millimicrons. Later work in our Laboratory by R. L. Rowell has shown that the half-band width is 3.4 millimicrons.

Filter F_2 must be removed from the beam intermittently in order to view the particle through the microscope, but the heat filter F_1 is kept in the beam at all times.

Brass Chamber and Scattering Cell: General

An overall view of the brass chamber B and scattering cell C may be obtained from Fig. 2. The design of the brass chamber itself is similar to that of Millikan (4). The illuminating beam enters from the left, passing through the window W_1 , not shown in Fig. 1, the stop S_3 , and the window

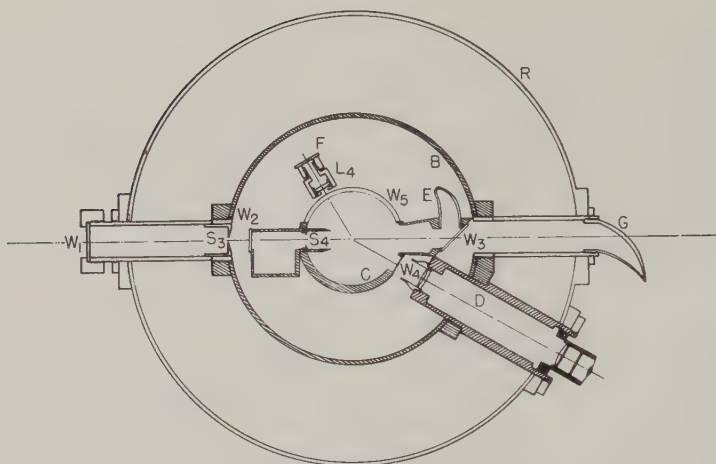


FIG. 2. Horizontal section through center of scattering cell.

W_2 to enter the scattering cell C . Thence it passes through a 45° window W_3 into the light trap G . The particle is held at the center of the scattering cell C , and the light which it scatters is collected by the lens L_4 of the photometer system and reflected down upon the photomultiplier by the mirror F , which cuts the plane of Fig. 2 at about 60° , as shown in the side view of Fig. 3. The microscope D is used to observe the particle through the plane window W_4 and to center it.

The brass chamber B is held in the center of the vessel R containing the oil bath designed to keep it at a uniform temperature. The brass chamber has a diameter of 20 cm. and a height of 22 cm., while the vessel R is 38 cm. in diameter and 38 cm. in height. The oil is stirred with a propellor driven by a Sargent cone-drive stirring motor.

Anticonvection Jacket

Unfortunately the oil bath will not completely eliminate air currents within a volume as large as the brass chamber. In order to check the remaining convection, a cylindrical Lucite jacket C (Figs. 2 and 3), lined with black felt, was fitted around the electrostatic plates. Its wall is fitted with a cylindrical window, W_5 , which permits photometric measurements over a large range of angles.

Two Lucite tubes attached to the anticonvection jacket have glass windows W_2 , W_3 mounted on the ends to allow the incident beam from the projector to enter and leave the scattering cell. These tubes are designed to intercept light scattered by small imperfections in the windows and to prevent it from reaching the photometer and increasing the background. These precautions are necessary, since the intensity of the incident beam is

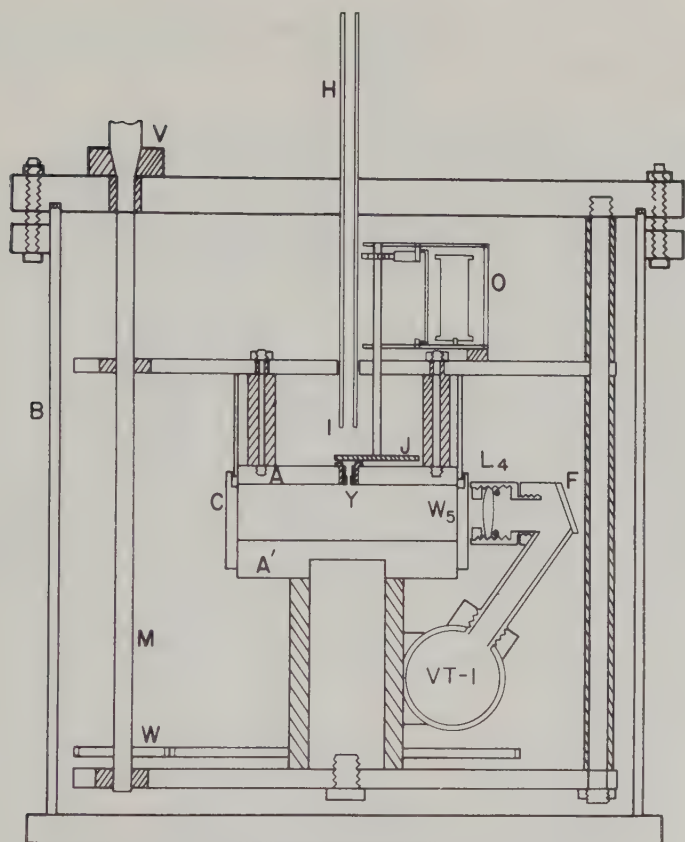


FIG. 3. Side view of scattering cell and brass chamber.

millions of times greater than that of the light scattered from a single particle, and stray light from windows and the edges of stops could completely obscure the scattered light.

As shown in Fig. 2, the inlet tube holding W_2 was made much wider than the incident beam so that no light can be reflected from its wall into the scattering cell. S_4 is a glare stop, slightly larger in diameter than the incident beam, which prevents any light diffracted by stop S_3 from entering the scattering cell.

The window W_3 of the outlet tube is placed at 45° to the light beam so that light reflected from its surface will not reach the photocell. Instead, it is reflected into a very efficient glass light trap E , coated on the outside surface with an optical black paint.

These precautions were essential and helped to reduce the background light considerably. The greatest deficiency of the anticonvection jacket is that the phototube can "see" the outlet window W_3 at values of θ above

145°. The small amount of back scattering from defects in this window increases the background light to a level which makes measurements impossible in this region.

Introduction of the Particle into the Scattering Cell

The aerosol particles used in these experiments were generated in a nebulizer. Dioctyl phthalate (DOP) was used as the aerosol material because of its low vapor pressure, approximately 1.5×10^{-7} mm. at 25°C. The particles were transferred from their source to the apparatus by means of a large syringe.

The aerosol is introduced into the apparatus through rubber tubing attached to a 3 mm. copper tube *H* (Fig. 3) which guides it into a chamber *I* above the top electrostatic plate. Here the particles fall freely toward a small pinhole in disc *Y* in the center of the top plate. This hole may be closed by a slotted circular disc *J*, attached to the pawl and ratchet-wheel mechanism of an impulse counter *O*, actuated by an electromagnet. The disc *J* covers the pinhole in alternate positions of the ratchet wheel. In intermediate positions a slot in the disc allows the particles to fall through the pinhole and into the space between the electrostatic plates. The pinhole is uncovered until a particle falls into the measuring cell, after which it is covered. The electromagnet is operated by 12 volts d.c. supplied from a selenium rectifier bridge connected through a step-down transformer to the a.-c. line. To determine whether the pinhole is open or closed, the circuit is connected to another impulse counter which registers odd or even values depending upon the position of the disc.

The advantage of the ratchet mechanism is that its operation entails no appreciable heating, since the solenoid dissipates energy only for the instant it is operated. The pinhole may be left open or closed for an indefinite time with no generation of heat.

Suspension and Centering of the Particle

The particle is suspended between two electrostatic plates *A*, *A'* shown in Fig. 3, which are 75 mm. in diameter and 19 mm. apart. They are kept parallel by a system of spacers. Three leveling screws attached to the bottom of the apparatus (*K*, Fig. 4) allow adjustment of the brass chamber to align the electrostatic and gravitational fields, so that the former can be adjusted to balance the force of gravity acting on the particle.

The voltage needed to suspend a particle, with the present plate separation, ranges from approximately 300 to 2000 v., depending on the size of the particle and its charge. A continuously variable power supply to deliver the needed voltage consists of five 300-v. batteries in series with five 67.5-v. batteries. A switch varies the voltage in steps of 300 v. and a Helipot across the 337.5-v. section gives a fine adjustment for intermediate values. A

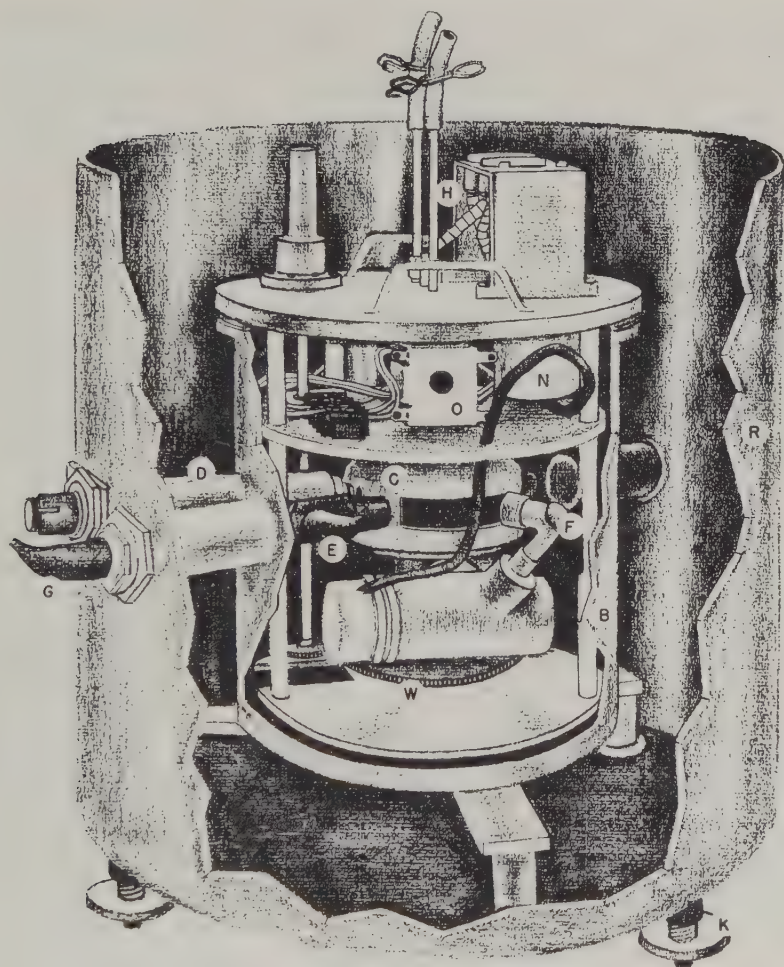


FIG. 4. Cutaway diagram of brass chamber.

switch is opened to disconnect the Helipot when the power supply is not in use, so as to avoid drain of the batteries. A reversing switch changes the polarity on the top and bottom plates so that particles with either a positive or a negative charge may be suspended.

A device introduced by Fletcher (5) is used to center the particle. As shown in Fig. 3 a small center disc *Y*, 3 mm. in diameter and insulated by the cross-hatched Bakelite ring, is inserted into the top electrostatic plate, *A*. When a particle drifts away from the center, a switch is turned to ground both *A* and *A'*, leaving *Y* at a high potential and thus attracting the particle to the center of the scattering cell. Since the particle falls somewhat during this process, it must be raised by application of a suitable potential

between plates A and A' . The procedure must be repeated several times before the particle is completely centered.

The position of the particle perpendicular to the line of sight of the microscope is determined with an eyepiece scale, while its position in the line of sight is read from the adjustable calibrated barrel length.

Measurement of Particle Size

Figure 2 offers the best view of the microscope D used to center the particle in the beam and to measure its size by its rate of fall. The optical components and dimensions are essentially those of a standard microscope. The objective is a $2\times$ achromat with a numerical aperture of 0.08 and a working distance of 53 mm., used in conjunction with a $10\times$ eyepiece which contains a reticle. Since the particle is seen against a black background, the reticle is illuminated by means of a miniature 3-v. flashlight bulb shining through a small hole in the side of the eyepiece.

An electric interval timer graduated to 0.1 second is used to measure the time required for a particle to fall a distance corresponding to that between two horizontal lines of the reticle. This operation may be repeated several times to obtain a more accurate value for the rate of fall, and the size of the particle then is calculated from Stokes' law. The distance corresponding to the separation of the reticle lines was determined by placing a stage micrometer at the focus of the microscope. Since the barrel length of the microscope can be changed, the distance between the reticle lines was calibrated for various settings of the barrel length. In this way the rate of fall can be measured for any particle within range of the objective of the microscope.

The eyepiece is covered during scattering measurements to prevent room light from entering the scattering cell through the microscope and increasing the background.

The Photometer

The basic plan of the amplifier and recorder section of the photometer is shown in Fig. 5. The output of the photomultiplier tube $VT-1$ is fed to a Leeds and Northrup No. 9836-A stabilized d.-c. micromicroampere amplifier. This instrument measures currents over eleven ranges varying from $0-1\times 10^{-9}$ to $0-2\times 10^{-6}$ ampere with a limit of error of $\pm 1.5\%$ of full scale, provided the current source has an output impedance of at least 1 megohm. Its action is basically that of a galvanometer, with the advantage that its power output is great enough to operate a standard recorder.

A compensating circuit attached to the input of this amplifier supplies a small "bucking" current to counteract the dark current of the phototube. A 1.5-v. battery B_1 may be connected through switch S_1 to supply a small current to this circuit. Most of this current is shunted through the 10-ohm

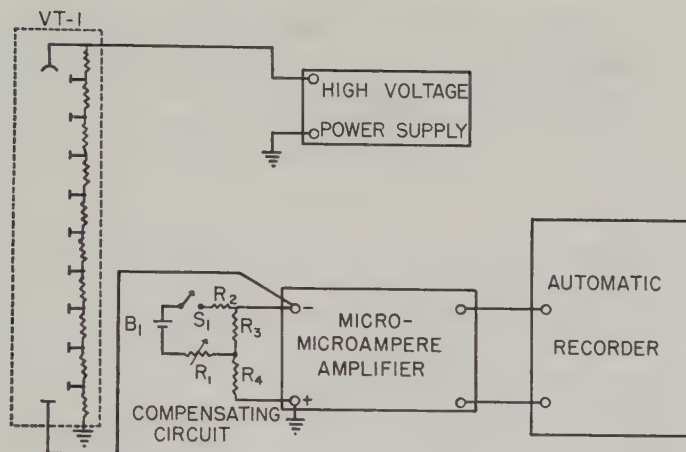


FIG. 5. Block diagram of photometer.

resistor R_3 , but a small fraction enters the amplifier proper with a polarity opposite to that from the phototube. The "bucking" current is adjusted by means of the 10-K variable resistor R_1 . R_4 has a value of 1 M and acts to increase the output impedance of the compensating circuit while R_2 is a 1-K resistor which helps to divide the voltage from B_1 when R_1 is set on zero.

The output from this amplifier in turn is measured and recorded by a Leeds and Northrup Speedomax G recorder, which yields a plot of the light intensity vs. time. Since the phototube is rotated by a synchronous motor, the intensity may be directly interpreted as a function of the angle.

The resistors shown inside the dashed lines of VT-1, each 470 K, could not be mounted in the usual position, directly beneath the photomultiplier socket, because the heat which they dissipate sets up convection currents which disturb the particle. Instead, they are supported in a Lucite container, N , Fig. 4, at the top of the brass chamber and connected to a 12-wire cable which supplies the proper voltage to the dynodes. The dynodes are supplied with 100 v. per stage by means of a Furst Model 710-2P regulated power supply, which has a ripple and noise of less than 0.01 % of the output voltage.

The mechanical design of the photometer can be seen in Figs. 3 and 4. The scattered light does not fall directly onto the photocathode but is collected by an achromatic lens L_4 with a focal length of 28.7 mm. and reflected by a mirror F onto the photomultiplier VT-1 located at the bottom of the brass chamber. This arrangement was necessitated by the small size of the brass chamber. An image of the particle is formed approximately on the photocathode surface. Since the sensitivity of the photomultiplier is known to vary when an image is focused at different

positions on its surface, care must be taken to keep the particle stationary during a measurement. In this way the image of the particle remains at one position on the photocathode and a true comparison of light scattered at different angles is obtained. The lens L_4 is covered with a rectangular stop the width of which subtends an angle of 5.3° at the center of the scattering cell.

The lens system and the photomultiplier tube are supported by a bearing mounted on the cylindrical base of the bottom electrostatic plate. For controlling the movement of the photometer, a vertical drive shaft (M , Fig. 3) extends through the cover and controls a pair of meshed gears W , one connected to the drive shaft and the other connected to the photometer system. At the cover a tapered ground joint V provides free movement of the drive shaft while maintaining a vacuum-tight seal.

These gears are powered by a synchronous motor mounted on a lid which fits over the entire apparatus. The lid also carries an indicator, graduated every 1° , for reading the angle at which the scattered light is being measured. This cover is not shown in Fig. 4. A microswitch is attached to each end of the angle indicator, preventing the motor from driving the phototube past any pre-set forward and backward angle. As an added precaution, two pegs located at the bottom of the brass chamber prevent the receiving lens L_4 from being driven into the inlet or outlet tubes of the scattering cell.

Factors Influencing the Accuracy of the Experiments

Since the aerosol droplets are suspended in an electrostatic field, they become optically anisotropic through the Kerr effect and are deformed from a spherical shape. Calculations were carried out to determine the magnitude of these effects, which prove to be negligible. The Kerr constant for DOP is not known, but it is less than 2×10^{-5} for similar liquids; hence the change in refractive index on this account is less than 10^{-9} . The deformation from spherical shape, calculated from the limiting law derived by O'Konski and Thacher (6), corresponded to an eccentricity of only 0.002.

The photometer is limited in accuracy by several properties of photomultiplier tubes, particularly their polarization selectivity and the variation of sensitivity over the photosurface. Clancy (7) has investigated the response of several 1P21 photomultiplier tubes to polarized light of various orientations. In general, the response is somewhat greater if the electric vector of the incident light is perpendicular to the longitudinal axis of the phototube instead of parallel to this axis. For the ratio of these two sensitivities, he found values of 1.014, 1.005, and 1.025 for three different tubes. Since the light scattered by aerosol particles is known to be partially plane polarized, the selectivity will affect the results but should not change the relative intensities by more than 1%.

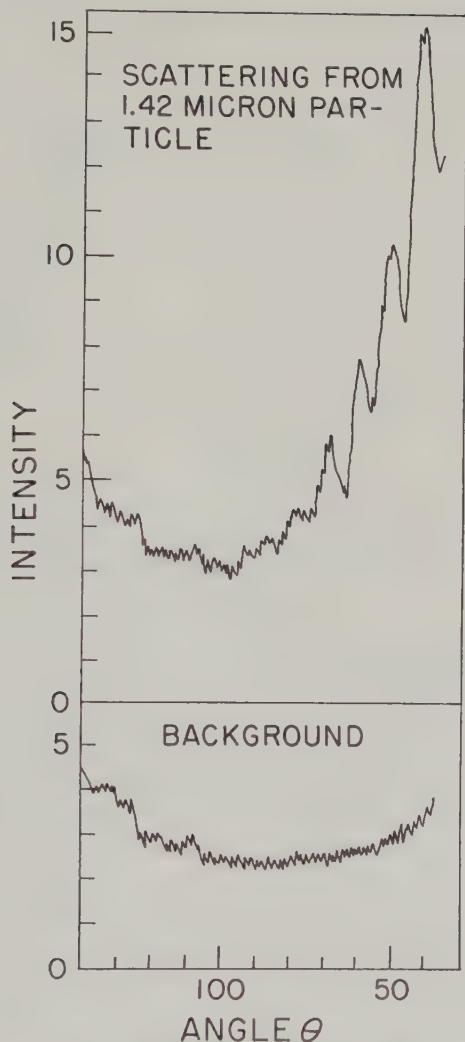


FIG. 6. Typical experimental records.

Errors larger than those due to polarization selectivity can result if the image of the particle moves near an edge of the photosurface, as shown by the studies of variation in sensitivity over the surface of the phototube made by Peterson and Holland (8). Around the point of maximum sensitivity on the photosurface there is a plateau averaging about 1.1 mm. in diameter, over which the response is constant to within 5%. In order to keep the image on this plateau, the particle was centered carefully with a cross-ruled reticle and allowed to fall until the maximum response appeared

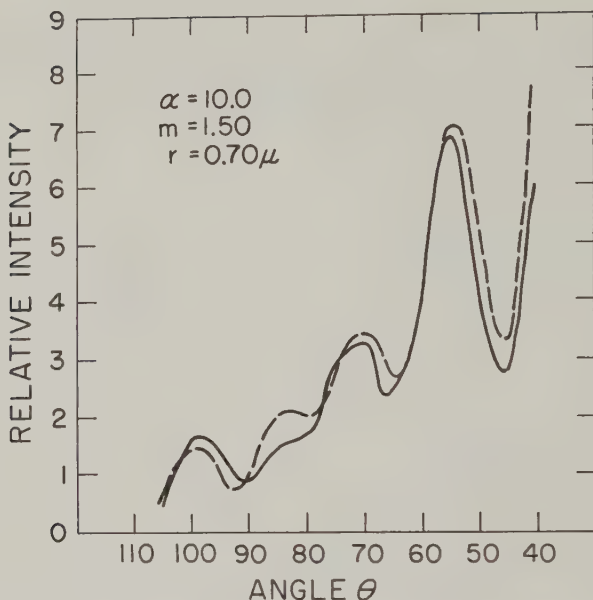


FIG. 7. Scattering diagram for particle of 0.70μ radius illuminated by unpolarized light. Solid line, experimental; dashed line, theoretical.

on the recorder. Thereafter the particle was not allowed to move more than 0.5 mm. during any one experiment. Several scattering curves were run with each particle, and we accepted only those which could be reproduced.

Previous studies (9) of photomultipliers show that the response will be linear to better than 3% at the low level of light striking the tube in these experiments.

Another effect of any motion of the particle during an experiment is to cause a change in the solid angle subtended by the lens system and therefore in the response of the photometer. The solid angle subtended by the 5.3° aperture, when the particle is centered, is 0.0171 steradian. A movement of the particle of 0.5 mm. in any direction will cause no more than a 4% change in the amount of light flux reaching the photometer lens.

Experimental Data and Conclusion

Scattering curves were measured for DOP droplets of various sizes between 0.7 and 1.5 micron radius, as determined from Stokes' law:

$$r = \sqrt{\frac{9\eta v}{2g(d - d_0)}} \quad [12]$$

Here η is the coefficient of viscosity of the gas, v is the velocity of the particle, g the acceleration of gravity, and d and d_0 , respectively, the densities of the particle and the gas.

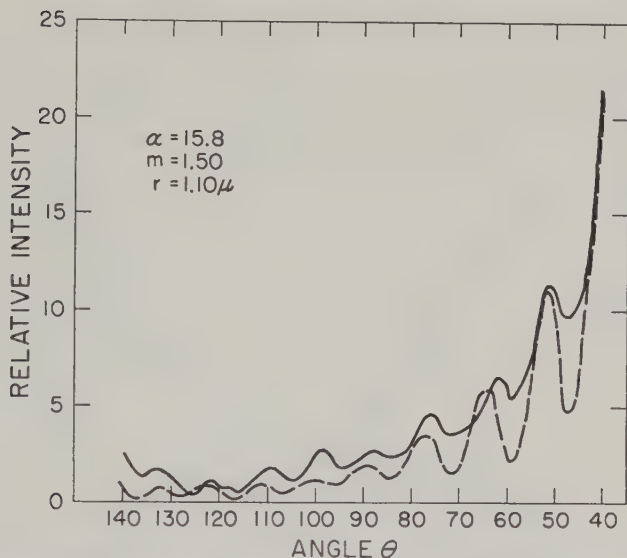


FIG. 8. Scattering diagram for particle of 1.10μ radius illuminated by unpolarized light. Solid line, experimental; dashed line, theoretical.

Figure 6 gives typical curves of the background and scattered light obtained on the recorder, which show the noise level of the photomultiplier tube. The curves were reproducible within the uncertainty of this noise level. Scattering curves for the particles were obtained by subtracting the background curve from those of the particle plus background. Figures 7 through 9 show scattering curves for particles of various size after the background has been subtracted. The relative intensity of scattered light is given for angles of about 40° to 140° measured from the incident beam, which in each case is unpolarized. Figures 10 and 11 give the scattering curves when the incident light is polarized with the electric vector respectively perpendicular and parallel to the plane of observation. In these last two figures the scattered light intensity should be proportional respectively to i_1 and i_2 , whereas the intensities in the other graphs should be proportional to $i_\theta = (i_1 + i_2)$. All these data exhibit typical diffraction patterns in which the number of maxima increases with particle size, as we would expect on the basis of previous work (10).

In order to compare our experimental results with the predictions of the Mie theory, we first measured the refractive index of DOP in an Abbé refractometer at 23°C . and found $m = 1.50$ for a wavelength of 436 millimicrons. Dr. Rudolph Penndorf of the Geophysics Research Division of the Air Force Cambridge Research Center kindly supplied us with values of i_1 and i_2 at 10° intervals and also of the scattering coefficients a_n and b_n for the particles of the radii which we studied. These values had been calculated by him and Bernice Goldberg and later were published (11). We then

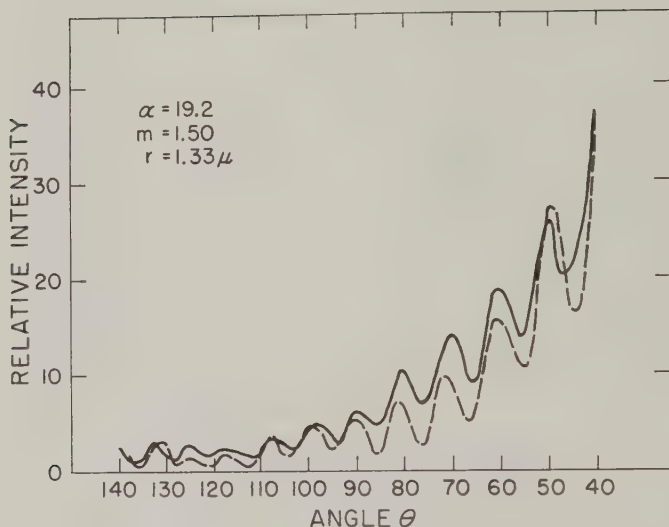


FIG. 9. Scattering diagram for particle of 1.33μ radius illuminated by unpolarized light. Solid line, experimental; dashed line, theoretical.

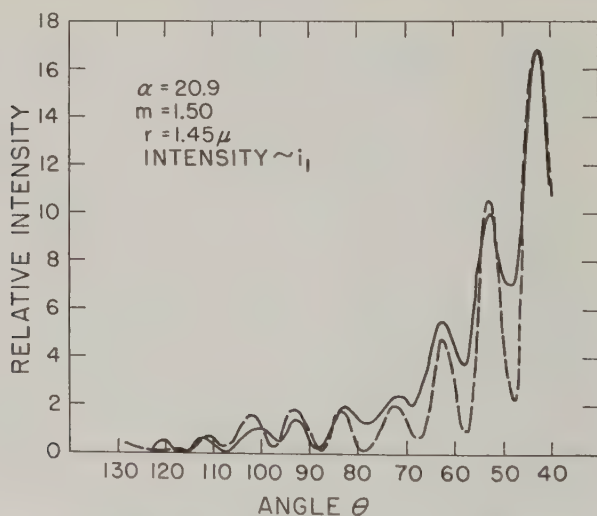


FIG. 10. Scattering diagram for particle of 1.45μ radius illuminated by plane polarized light with electric vector perpendicular to plane of observation. Solid line, experimental; dashed line, theoretical for i_1 .

calculated values of i_1 and i_2 at 2.5° intervals, using the values of π_n and τ_n previously reported from our Laboratory (3), extended to $n = 43$. The dashed curve on each graph is drawn through the theoretical points. Since each experimental curve gives only the *relative* intensities at various angles, the theoretical values are normalized to make the height of the first maxi-

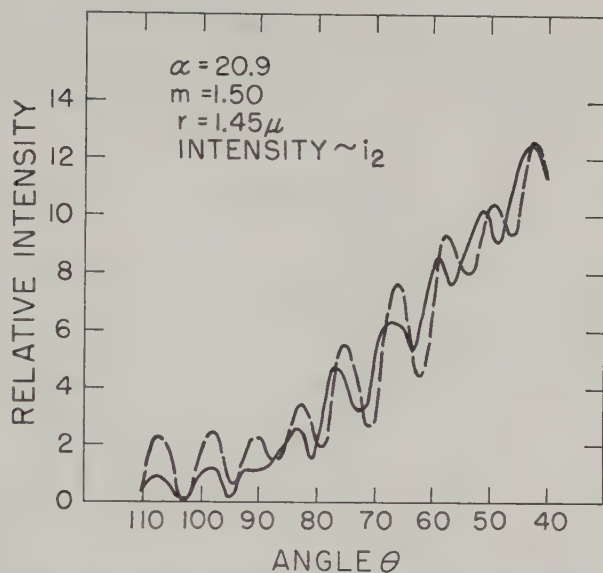


FIG. 11. Scattering diagram for particle of 1.45μ radius illuminated by plane polarized light with electric vector parallel to plane of observation. Solid line, experimental; dashed line, theoretical for i_2 .

mum (nearest $\theta = 0^\circ$) the same as that of the experimental curve. In general the agreement is satisfactory, and differences between the theoretical and experimental curves may be due to the following causes: (a) Each theoretical curve corresponds to the light collected by an infinitesimal aperture, whereas the experimental curve is obtained with a lens system which integrates the rapidly varying scattered intensity over a 5.3° range. (b) The theoretical curve corresponds to monochromatic light, whereas the experimental curve is obtained with light covering a range of about 7 millimicrons. Since r is fixed for any particle, α varies with λ and the photometer integrates the changing intensity over a range of wavelength corresponding to $\Delta\alpha = (\Delta\lambda/\lambda)\alpha = 0.016 \alpha$, the center of which is the α of the theoretical curve. (c) Any error in determining the particle size causes a corresponding error in the value of α assigned to the particle. This tends to shift the positions of the maxima (since the number of maxima increases with particle size) and also causes small differences in their amplitude. (d) Any motion of the particle during an experiment changes the solid angle subtended by the collecting lens or the position of the image on the photomultiplier and thus introduces small random deviations.

ACKNOWLEDGMENTS

It is a pleasure to acknowledge the support of the Air Force Cambridge Research Center and the courtesy of Dr. Rudolph Penndorf of the Geophysics Research Division, who sent us the theoretical values of the scattered intensities before their

publication. We also wish to express our appreciation to Maurice Williams for his help in the design and construction of the apparatus; to Ora May Engle in the Research Computing Center of Indiana University for the computations of the scattered intensities on the IBM 650; to John Minton for the drawing of Fig. 4; and to Robert L. Rowell for assistance in preparation of the article.

REFERENCES

1. MIE, G., *Ann. Physik* **25**, 377 (1908).
2. DEBYE, P., *Ann. Physik* **30**, 57 (1909).
3. GUCKER, F. T., JR., AND COHN, S. H., *J. Colloid Sci.* **8**, 555 (1953).
4. MILLIKAN, R. A., *Phys. Rev. [1]* **32**, 349 (1911).
5. FLETCHER, H., *Phys. Rev.* **4**, 440 (1914).
6. O'KONSKI, C. T., AND THACHER, H. C., *J. Phys. Chem.* **57**, 955 (1953).
7. CLANCY, E. P., *J. Opt. Soc. Amer.* **42**, 357 (1952).
8. PETERSON, E. W., AND HOLLAND, D. H., *J. Opt. Soc. Amer.* **40**, 253 (1950).
9. ENGSTROM, R. W., *J. Opt. Soc. Amer.* **37**, 420 (1947).
10. SINCLAIR, D., AND LA MER, V. K., *Chem. Revs.* **44**, 245 (1949).
11. PENNDORF, R., AND GOLDBERG, B., Geophysical Research Papers No. 45, "New Tables of Mie Scattering Functions for Spherical Particles," Part 5, "Values of Amplitude Functions a_m and b_m for Refractive Index $n = 1.50$ and Size Parameters $\alpha = 0(0.1)30$," ASTIA Document No. AD-98771, March, 1956, available through U. S. Department of Commerce, Office of Technical Services, Washington 25, D. C.

LETTERS TO THE EDITOR

DEMULSIFICATION BY THE USE OF ION-EXCHANGE
RESIN MEMBRANE

The possibility of destroying an emulsion which is stabilized by ionic surface-active agents by the use of an ion-exchange resin membrane has been examined. As an anion- (or cation-) exchange resin membrane selectively passes only anion (or cation) and not cation (or anion), we can either

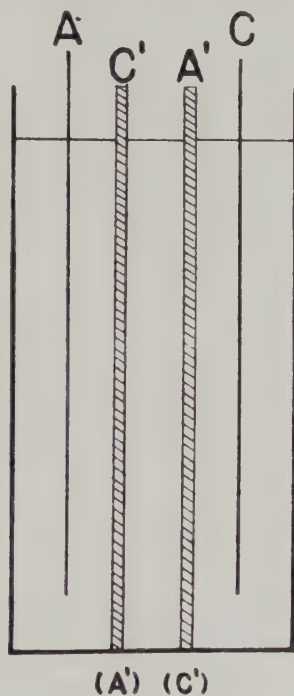


FIG. 1

concentrate or take off salt in solution separated by anion- and cation-exchange resin membrane by passing an electric current as shown in Fig. 1.

The same principle may be applied to the oil-in-water type emulsion stabilized by ionic agents. Figures 1 and 2 illustrate two kinds of elec-



FIG. 2

trolytic cells used for the experiments. Anode, A , was platinum plate and cathode, C , was nickel plate; A' and C' were the anion and cation exchange resin membranes, for example, Amber Plex A_1 and C_1 . Emulsified solution, consisting of 40 volume per cent of n -heptane and 60 volume per cent of water which contains 0.043% sodium dodecyl sulfate was introduced in the central cell of 5 mm. in thickness and the outer cells were filled with 0.25 N sodium chloride solution. The emulsion was almost destroyed after 10 minutes charging with 15 volts direct current, the density of which was 0.11 $A./dm.^2$, whereas the original solution remained stable over 48 hours. Instead of using one couple of ion-exchange resin membranes, we may use several couples of them in the same cell. If we interchange anion- and cation-exchange resin membranes and solutions in central and outer cells, demulsification proceeds in the cathode cell but not efficiently in the anode cell.

Then, demulsification was examined using only cation-exchange resin membrane as shown in Fig. 2. The cathode cell was filled with emulsified solution and the anode cell was filled with 0.25 N sodium chloride solution. Electrodes, solutions, membrane, etc., were the same materials as before.

The emulsion was destroyed after 10 minutes charging with 15 volts direct current the density of which was 0.17 A./dm.².

*Department of Chemistry,
Faculty of Engineering,
Yokohama National University,
Minamiku, Yokohama, Japan*

Kōzō SHINODA

Received October 10, 1960

TURBIDITY STANDARD

Correlation of test data gathered in our laboratory over long intervals has shown a need for a permanent turbidity standard. Such a standard would have to retain constant characteristics over an indefinite time period and be capable of accurate reproduction should the original standard be damaged or lost. We have developed a standard for use with the Fisher Nefluoro-Photometer that appears to meet the necessary requirements.

The Fisher Nefluoro-Photometer is an instrument capable of colorimetric, fluorometric, and nephelometric measurements. Measurements are made with a bridge circuit two legs of which are beams of light. The sample being measured modifies one beam of light while a reference, or standard, is used to modify the second beam. The reference used for fluorometric and nephelometric measurements is a prepared solution similar in nature to the unknown solution being measured. This reference solution is referred to as a "generator solution." These "generator solutions" are generally prepared just prior to a test run since their optical properties usually change with time. It is also common for supposedly identical "generator solutions" prepared at different times, to exhibit somewhat different optical properties. Hence, these solutions cannot be classed as true standards. The standard we have developed has eliminated these difficulties. It is for use during nephelometric measurements.

The theory of the standard is quite simple. It was assumed that light scattered from tightly packed, small spherical glass beads behaves similarly to light scattered from a turbid solution, if the beads are small enough. The light scattered by a large group is essentially independent of the orientation, position, and shape of the individual beads. It was also assumed that glass beads will retain the same light-scattering properties for a long time period. Based on these assumptions, preliminary experimental standards were constructed and tried. These standards showed the validity of the assumptions and resulted in the development of a final standard.

The final standard consists of three identically prepared test cells (i.e.,

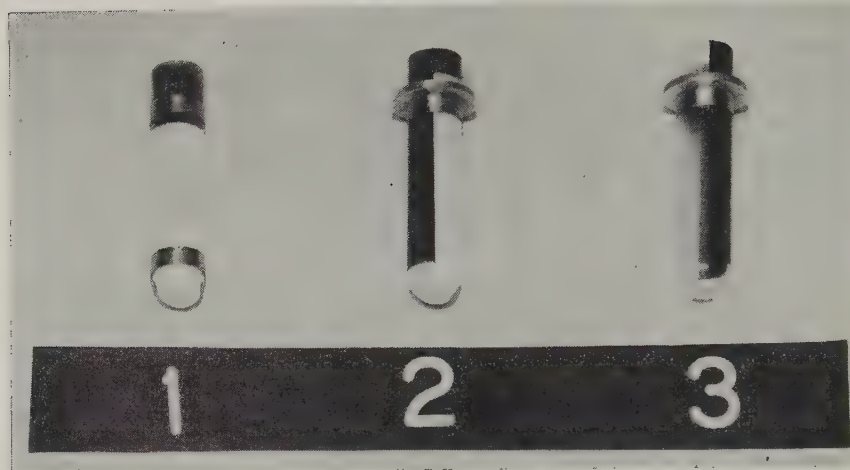


FIG. 1. (1) Generator solution; (2) standard cell; (3) blank cell

tubes); One cell, the "generator solution," is a standard, plain, $\frac{3}{4}$ -inch diameter photometric cell. The other two cells, each of which constitute the "standard solution," are standard $\frac{3}{4}$ -inch diameter black fritted cells. Each of these three cells is filled with glass beads of the same specifications and permanently sealed in the following manner:

1. All new tubes were used. These were cleaned with alcohol and with distilled water.

2. Glass beads¹ were classified with standard sieves. Beads with diameters between 0.0165 and 0.0117 inch were used after being cleaned in chromic acid solution and rinsed in distilled water. Examination of the beads showed that approximately 1% were oblong, and $\frac{1}{2}$ % were opaque.

3. The tubes (dry) were then filled to about $\frac{5}{8}$ inch from the top with the dry beads.

4. Round Neoprene plugs $\frac{3}{16}$ inch thick were placed in the tubes on top of the beads and the beads were then compacted by shaking the tube while applying pressure to the plug with a ram.

5. When the beads were tightly packed, the tubes were sealed by pouring melted jeweler's wax over the plugs. The tube had to be heated gently with a Bunsen burner to insure obtaining an airtight glass to wax seal. The Neoprene plug used was tight enough to prevent melted wax from mixing with the beads.

The two "standard solution" cells prepared in this manner were balanced against the "generator solution" at an instrument setting of 50%. The two standard solutions were found to compare favorably (within $\pm 10\%$). However, the readings on an individual cell were reproducible to only

¹ Patton Brothers, Inc., P.O. Box 14, Carlstadt, New Jersey.

$\pm 10\%$. This was due to the lack of accurate positioning of the cells by the instrument. To improve measurement accuracy through better positioning, $\frac{1}{4}$ inch wide brass strips (0.010 inch thick) were wrapped and glued to each cell just below the locating plate. An epoxy resin was used to bond the brass to the glass. Bands were glued to each end of the generator cell since it has no locating plate. Blank test cells were also prepared. The three types of cells are shown in Figure 1.

The two "standard solution" cells, balanced against the "generator solution," compared within 2%, while the individual "standard solution" cells gave readings better than $\pm 1\%$ when removed and replaced in the instrument. It appeared that the "standard solutions" were more accurate than the 2% indicated. This error is apparently due to a lack of identical placement of the two cells in the instrument.

It is believed that these standards have the necessary permanence required. The original standard and generator solution cells have been in use for more than six months and have as yet not deviated from the original comparison values. Calibrating the instrument at 50% scale reading with the generator solution and either standard produces a 1% scale reading for tap water. Since the "generator solution" is quite turbid, we have not yet had occasion to test samples which will produce a 100% scale reading.

Standards having different values of "turbidity" can be prepared. In general, large beads will produce cells of less "turbidity" and small beads will produce more "turbid cells." It may also be possible to change "turbidity" values by using colored beads if they are available. Since these standards can always be calibrated against more common but less permanent standards, they should be of value when making any type of turbidity measurements where a permanent standard would be desirable.

*Whirlpool Corporation,
Research Laboratories
St. Joseph, Michigan*

EDWARD C. PETERSON
ALLAN H. TINCHER

Received November 3, 1960

COMPRESSIONAL AND YOUNG'S MODULI IN MONOLAYERS

Recently Cheesman and Sten-Knudsen (1) described a method for the determination of the surface compressional (bulk) modulus by measuring the displacement of a mica float under a known applied force. The moduli calculated by them for actomyosin films yield surface coefficients of compressibility (reciprocal compressional moduli) which are over ten times higher than those normally found for protein films (2, 3) by the usual method of differentiation of the surface pressure—area isotherms. Cheesman and Sten-Knudsen's modulus B has the dimensions dyne/cm.² whereas

a surface compressional modulus should have the dimensions dyne/cm. (4). This indicates that an incorrectly derived formula must have been used.

Under their experimental conditions, if F is the applied force, a is the length of the float, and X is its displacement while d_1 and d_2 are the distances of the float from the edges of the trough, the surface compressional modulus

$$K_s = \frac{F}{aX (1/d_1 + 1/d_2)}, \quad [1]$$

since the surface stress (4) $\sigma_s = F/a$ and the strain $e = X(1/d_1 + 1/d_2)$, the relative change in area being

$$\frac{\Delta A}{A} = \frac{ad_1 - a(d_1 - X)}{ad_1} + \frac{a(d_2 + X) - ad_2}{ad_2}. \quad [2]$$

Maximum displacement will occur for $d_1 = d_2 = d$, when $K_s = Fd/2aX$. This should be compared with Cheesman and Sten-Knudsen's $B = F/2aX$. In their experiments d must have been close to 15 cm. If we correct their values accordingly, the coefficients of compressibility fall entirely within the range usually obtained with protein films.

It should be noted that a consideration of the relative change in length instead of the change in area leads to an expression for the surface Young's modulus Y_s (5) which is identical with Eq. [1]. Whether one measures Y_s or K_s depends in fact on the freedom of the film for lateral expansion (4). Under Cheesman and Sten-Knudsen's conditions, B , even using Eq. [1], would seem to be a modulus to which both Y_s and K_s contribute. If the film is rigid, the contribution by Y_s may become negligible.

The condition of no lateral freedom could probably be achieved with good approximation in the apparatus of Cheesman and Sten-Knudsen by using a long rectangular float leaving only negligible gaps between the ends and the trough. Such a modification, using Eq. [1], would provide a valuable experimental method for the direct determination of the surface compressional modulus and would allow a comparison with the modulus obtained from surface pressure—area isotherms.

REFERENCES

1. CHEESMAN, D. F., AND STEN-KNUDSEN, O., *Biochim. et Biophys. Acta* **33**, 158-163 (1959).
2. NEURATH, H., AND BULL, H. B., *Chem. Revs.* **23**, 391-435 (1938).
3. BULL, H. B., *Advances in Protein Chem.* **3**, 95-121 (1947).
4. TSCHOEGL, N. W., *J. Colloid Sci.* **13**, 500-507 (1958).
5. VAN WAZER, J. R., *J. Colloid Sci.* **2**, 223-236 (1947).

N. W. TSCHOEGL

*The Bread Research Institute of Australia,
North Ryde, New South Wales*

Received November 15, 1960

BOOK REVIEW

Introduction to Colloid Chemistry. KAROL J. MYSELS. Interscience, 475 pp. 1959. Price \$10.00.

The author is well known not only for his work in the field of colloids but also for the "Textbook Errors" column in the *Journal of Chemical Education*. He has written the present text with two audiences in mind; the college senior or beginning graduate student, for a one-semester introductory course, and the industrial chemist or executive desiring a concise survey of a field neglected in his academic career. (A reflection on many present-day courses in physical chemistry, not only in the United States!) Simplicity of presentation and development from fundamentals have been aimed at, and it is claimed that "a mastery of the material presented should give a basis for understanding the main factors involved in most practical problems and also for delving into the more advanced treatment of the whole field or of special topics." A range of problems is included after each chapter.

The basic approach is from the angle of the colloidal particle, considering particularly its interaction with electromagnetic radiation and the ways in which it is influenced by thermal motion and by mechanical, gravitational, coulombic, or van der Waals' forces.

Following two introductory chapters the author deals with sedimentation rate, flocculation (certain aspects), diffusion and Brownian motion, colligative properties, sedimentation equilibrium, sorption (two chapters), fluctuations and rubber elasticity, the preparation of colloids and rheology (two chapters). These are followed by four chapters dealing essentially with charge effects in colloids (the double layer, electrokinetics, etc.), and the book concludes with three chapters on optical phenomena (refraction and schlieren, interference and scattering).

The subject has been developed largely from fundamentals, as the author claims, although one might differ as regards choice of fundamentals in a number of cases. For example one and a half pages are taken up with the derivation of Poiseuille's equation, which the student should have met in his elementary physics or applied mathematics.

A great deal of thought has clearly been given to the presentation of material for student purposes and teachers of colloids will certainly benefit from the author's endeavors. Nevertheless the present book must, in the reviewer's opinion, be criticised on two main grounds.

Firstly, the student will find little link-up with the physical chemistry he meets in other parts of his course, and this will serve to emphasize the "separateness" of colloids which is still one of its major handicaps. For example, the consideration of the physical properties of soap solutions (association colloids), which probably is linked more closely with the student's study of solutions and of thermodynamics than any other branch of colloids, receives little attention and then only in scattered places.

The second major criticism and probably the more important one in view of the stated objectives of the book, concerns the scant attention given to surface chemistry. Thus Gibbs and his adsorption isotherm are not even mentioned, and Langmuir only in connection with his adsorption isotherm on solids. An understanding of the applicability and limitations of the Gibbs adsorption isotherm is certainly of major impor-

Journal

Editor-in-chief: J. C. Ke
Peterhouse, Cambridge, E

VOLUME 1 1959, \$14.00

- Geoffrey Zubay and Paul Doty. The Isolation and Properties of Deoxyribonucleoprotein Particles Containing Single Nucleic Acid Molecules
- V. Moses, O. Holm-Hansen, J. A. Bassham and M. Calvin. The Relationship between the Metabolic Pools of Photosynthetic and Respiratory Intermediates
- I. M. Dawson and D. H. Watson. An Electron Microscope Study of the Structure of Crystalline Ribonuclease
- Robert L. Sinsheimer. Purification and Properties of Bacteriophage ϕ X174
- Robert L. Sinsheimer. A Single-Stranded Deoxyribonucleic Acid from Bacteriophage ϕ X174
- D. W. Green and R. Aschaffenburg. Twofold symmetry of the β -lactoglobulin Molecule in Crystals
- M. S. Santanam. Calcification of Collagen
- Pauline M. Harrison. The Structures of Ferritin and Apoferritin: Some Preliminary X-Ray Data
- C. O. Doudney and F. L. Haas. Gene Replication and Mutation Induction in Bacteria
- R. W. Horne, S. Brenner, A. P. Waterson, P. Wildy. The Icosahedral Form of an Adenovirus
- Ernest Freese. The Specific Mutagenic Effect of Base Analogues on Phage T4
- Jacques R. Fresco. Polynucleotides II: The X-Ray Diffraction Patterns of Solutions of the Randomly Coiled and Helical Forms of Polyriboadenylic Acid
- Benjamin D. Hall and Paul Doty. The Preparation and Physical Chemical Properties of Ribonucleic Acid from Microsomal Particles
- V. Luzzati and A. Nicolaieff. Etude par Diffusion des Rayons X aux Petits Angles des Gels d'Acide Désoxyribonucléique et de Nucléoprotéines: (Note Préliminaire)
- Gunther S. Stent, Gordon H. S. Niels K. Jerne. Dispersal of Parental Nucleic Acid of Bacteriophage T4 among its Progeny
- Endre A. Balazs, Aksel A. Both and John Gergely. Proton Magnetic Resonance Studies on Water in the Presence of Various Macromolecular Substances
- R. E. Burge and R. D. Hynes. Thermal Denaturation of Collagen and its Structural Implications
- Arthur B. Pardee, François Jacob and Jacques Monod. The Genetic Control of "Cytoplasmic Expression of Inducibility" in the Synthesis of Lactosidase by *Escherichia coli*
- M. H. F. Wilkins, G. Zubay and Wilson. X-Ray Diffraction Studies of the Molecular Structure of Histone and Chromosomes
- Geoffrey Zubay. The Transition between Straight and Coiled-Coil Configurations of the α -Helix
- Richard S. Morgan and Robert Byrne. "Alkaline" Polyadenylation
- Hideo Kon and Norman Davidson. Clear Magnetic Relaxation of Protons by Ferrihemoglobin and Ferrimyoglobin
- Cecil E. Hall, Elizabeth C. MacLennan, Irwin Tessiman. Structure and Functions of Bacteriophage ϕ X174: Electron Microscopy
- Ellen Borenfreund, Herbert S. Kranz and Aaron Bendich. Studies on Deoxyribonucleic Acid after Exposure to Tritium Gas
- Masayasu Nomura and J. Drenth. Ribonucleoprotein Particles Inhibited by Chloromycetin in *Escherichia coli*
- Robert L. Sinsheimer. Is the Genetic Acid Message in a Two-Symbol

Molecular Biology

Board: P. Doty, A. F. Huxley, R. L. Sinsheimer,
J. D. Watson, M. H. F. Wilkins

ères, J. D. Watson, D. Schles-
and B. R. Hollingworth. Ribo-
protein Particles from *Escher-
coli*

orne, G. E. Russell and A. R.
High Resolution Electron Mi-
scopy of Beet Yellows Virus Fila-

hr and A. Tissières. Nucleotide
Position of Ribonucleoprotein
es from *Escherichia coli*

e Grunberg-Manago. Phospho-
et Configuration Macromo-
re des Polyribonucleotides
thétiques et des Acides Ribo-
ques

Koch and A. D. Hershey. Syn-
of Phage-Precursor Protein in
a Infected with T2

M. Smith and G. J. Hills.
Studies on the Electron
copy of the *Tipula* Iridescent

er, G. Streisinger, R. W. Horne,
hampe, L. Barnett, S. Benzer
W. Rees. Structural Compo-
of Bacteriophage

Donovan, Michael Laskowski,
Harold A. Scheraga. Carboxyl
Interactions in Lysozyme

L. Hayes, Jack C. Murchio,
T. Lindgren and Alex. V.
. A Determination of Lipopro-
molecular Weight by use of the
n Microscope

Lacks and François Gros. A
lic Study of the RNA-Amino
complexes in *Escherichia coli*

S. Friesen and Robert L.
mer. Partition Cell Analysis of
re Tobacco Mosaic Virus Nu-
id

C. E. Hall and H. S. Slayter. Electron
Microscopy of Ribonucleoprotein Par-
ticles from *Escherichia coli*

R. W. Horne and J. Nagington. Electron
Microscope Studies of the Develop-
ment and Structure of Poliomyelitis
Virus

E. A. Barnard and W. D. Stein. Histidine
Residue in the Active Center of Ribo-
nuclease. I: A Specific Reaction with
Bromoacetic Acid

W. D. Stein and E. A. Barnard. His-
tidine Residue in the Active Center
of Ribonuclease. II: The Position of
this Residue in the Primary Protein
Chain

Kazutomo Imahori and Jiro Tanaka.
Ultraviolet Absorption Spectra of
Poly-L-Glutamic Acid

A. Tissières. Some Properties of Soluble
Ribonucleic Acid from *Escherichia
coli*

Murray Vernon King. The Unit Cell and
Space Group of Cubic Glucagon

J. Weigle, Matthew Meselson and
Kenneth Paigen. Density alterations
Associated with Transducing Ability
in the Bacteriophage Lambda

R. D. B. Fraser and T. P. MacRae.
Molecular Organisation in Feather
Keratin

C. R. Worthington. Large Axial Spac-
ings in Striated Muscle

M. F. Perutz, L. K. Steinrauf, Anne
Stockell and A. D. Bangham. Chemi-
cal and Crystallographic Study of the
two Fractions of Adult Horse Haemo-
globin

Index.



ACADEMIC PRESS, London and New York

TOXIC PHOSPHORUS ESTERS

Chemistry, Metabolism,
and Biological Effects

By RICHARD D. O'BRIEN

*Pesticide Research Institute
Canada Department of Agriculture
London, Ontario**

September 1960, 434 pp., illus., \$14.50

THIS BOOK gives a full account of the mode of action of phosphorus anticholinesterases in mammals and insects, and of their metabolism in mammals, insects and plants. A chapter is also devoted to their chemical properties, with emphasis both on properties which contribute to an understanding of the biochemical aspects and on those of which a knowledge is necessary for the utilization of these compounds.

Besides providing a synthesis of the enormous literature in the field, the author has integrated this material by showing how the chemistry of the phosphorus esters permits an understanding of their reactivity with enzymes, how this reactivity accounts for effects upon the various tissues, and how these in turn explain the effects of organophosphates in the whole animal, in which such processes as detoxification, detoxification, enzyme inhibition, aging, and regeneration are active in the process of poisoning. Finally, the author suggests how knowledge of these processes can be used to produce new organophosphates with predictable properties.

CONTENTS:

Introduction

Nonenzymic Reactions

Hydrolysis—Isomerization—
Transalkylation—Oxidation—
Dehydrohalogenation—Effects of Light

The Reaction with Cholinesterase *In Vitro*

Phosphorylation of the Enzyme—
Reversal of Inhibition (Reactivation)—
“Aging”—Selectivity for Different
Cholinesterases

Enzymic Degradation and Activation *In Vitro*

Degradation—Activation

Effects on Isolated Whole Tissues

Ion Permeability—Muscle
Contraction—Nerve Transmission

Effects in Mammals

Results of Poisoning—Protection and
Therapy—Synergism (“Potentiation”)—
Metabolism and Residues in Intact
Mammals

Effects in Insects

Results of Poisoning—Ovicidal
Action—Distribution—Metabolism—
Resistance—Antagonism and Synergism

Effects in Plants

Systemic Activity—Metabolism—
Residues—Phytotoxicity

Selective Toxicity

Absorption—Excretion and Storage—
Metabolism—Penetration to the
Target—Nature of the Target—Design
of New Selective Compounds

Techniques

Radio Tracer Synthesis—Analysis—
Spectroscopy—Refractive Index—
Esterase Determinations

Appendix 1. Electronic Interpretations

The Underlying Concepts—The
Inductive Effect—The Field Effect—
The Mesomeric Effect

Appendix 2. Structure of Organophosphates

AUTHOR INDEX—SUBJECT INDEX.

* Present address: New York State College of
Agriculture, Cornell University



ACADEMIC PRESS New York and London

111 Fifth Avenue, New York 3, New York

17 Old Queen Street, London, S. W. 1

THE RATE OF DESORPTION OF STEARIC ACID FROM PLANAR SURFACES—A NEW TECHNIQUE

R. L. Patrick* and G. O. Payne, Jr.

*Central Research & Engineering Division, Continental Can Company, Inc.,
Chicago 29, Illinois*

Received June 29, 1960; revised October 13, 1960

ABSTRACT

A novel method for continuously monitoring the rate of desorption of stearic acid from a planar surface is reported. Excellent reproducibility has been obtained for the desorption of radiolabeled stearic acid into toluene solution. The desorption follows the classical decay equation $\phi = \phi_E(1 - e^{-kt})$ at 3°C.

INTRODUCTION

Classical adsorption-desorption work has been carried out by many investigators including Hackerman (1, 2) and Greenhill (3). The usual method is to adsorb onto a carefully prepared powdered material and to observe the weight gained by the substrate, or to determine analytically the reduction in concentration of the very dilute solution. Desorption is carried out by simply reversing the system by placing the sample into fresh solvent followed by reweighing the powder or analyzing the solution. It was felt that the use of powdered substrates limited very markedly the usefulness of the adsorption-desorption technique. In addition, it was desired to examine the phenomena of desorption over the entire scale of time in order to get a more complete understanding of the manner in which desorption occurs.

It has been proposed by Patrick *et al.* (4) that the failure of adhesive bonds is not possible by merely mechanical means. The work reported in this paper is being carried out to lay the groundwork for a more complete analysis of adhesive systems and the mechanisms of failure of the metal-organic bonds. It is known that physical-chemical processes cause failure of the interfacial bond with disastrous results. This paper represents the initial stages of an extensive program to investigate the mechanisms of failure of adhesive films caused by solvolysis or chemical exchange.

We are reporting a technique in which a radiolabeled sample is placed in a desorbing medium and is monitored continuously until the system

* Present address, Alpha Research & Development, Inc., Blue Island, Ill.

reaches equilibrium, or at least until the trend is well established. Other work to be reported will discuss the desorption of stearic acid into solution using a static system. The samples were withdrawn from the desorbing medium and dried in air, and the dry samples were counted in a gas flow "Mylar" window counter. After counting, the samples were returned to the same solution for further desorption.

EXPERIMENTAL METHODS

The materials and apparatus used in the experiments were as follows:

Materials

1. Radiolabeled stearic acid -(C-14)-, Nuclear Chicago.
2. Stearic acid, m.p. 68°-69.5°C., Eastman Kodak Co. Recrystallized from hexane three times.
3. Toluene, A.C.S. grade, Fisher.
4. 2,5-Diphenyloxazole, Pilot Chemicals, Watertown, Mass.
5. 1,4-Di [2-(5-phenyloxazolyl)] benzene, Pilot Chemicals, Watertown, Mass.
6. Apollo Mirror Finish Chrome Ferrottype Plate, degreased with benzene, flamed to a clean surface.

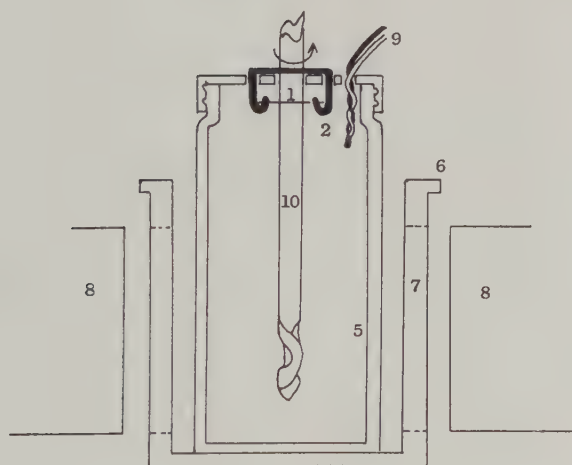
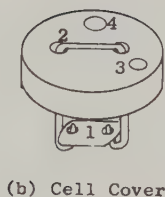
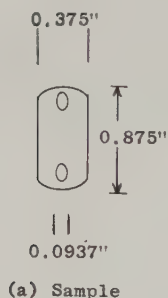
Apparatus

1. Tri-Carb Liquid Scintillation Spectrometer, Packard Instrument Co., LaGrange, Illinois.
2. Tracerlab Automatic Sample Changer utilizing the TCG-14 Carbon Counter ("Mylar" window—gas flow), Tracerlab Corp., Boston, Mass.

Small samples of ferrottype were die cut in the shape shown in Fig. 1a in order that they would conveniently fit into the round counting planchettes and, at the same time, pass through the narrow neck of the sample cell.

Radiolabeled stearic acid was deposited onto ferrottype samples from a 10^{-3} M solution in hexane. The samples were placed in the solution for one week during which time the vessel was occasionally shaken. The samples were withdrawn from solution and were drained onto lens tissue. As there was considerable solvent drag out, the samples were rubbed three times in each direction with lens tissue in as reproducible a manner as possible. The radioactivity of the samples was then determined in the usual manner utilizing the Tracerlab Carbon Counter. Following counting, the samples were again rubbed until the determination fell within a fairly narrow range of counting. Samples of nearly similar counts were paired and as often as possible were run together.

Liquid scintillation counting vials, which proved to be the most satisfactory, were readily prepared by drilling holes in the caps of two-ounce, wide-mouthed, screw-cap bottles. A copper wire was passed through two of



(c) Liquid Scintillator Optical Chamber

FIG. 1. Sample and liquid scintillator optical chamber with cell. 1. Sample. 2. Wire sample support. 3. Thermocouple hole. 4. Stirrer hole. 5. Liquid scintillator cell. 6. Liquid scintillator chamber. 7. Ports in chamber. 8. Phototubes. 9. Thermocouple. 10. Stirrer.

the holes and the ends were bent into hooks. The sample was laid across the two hooks with the highly reflective side facing the bottom of the cell. The additional holes allowed a small glass stirrer, as well as a thermocouple, to be placed in the solution.

A series of experiments was carried out to determine the optimum position of the sample as well as to determine the need for stirring the system. It was found that the reproducibility was most effective when the sample was held at the top of the vessel. In addition, it was found that stirring the system markedly increased the rate of desorption and made the system essentially diffusion independent.

Since the liquid scintillation counter required that the scintillating medium be refrigerated, the experiments were carried out in a refrigerated chest at 3°C. As it was necessary to stir the system, the cover of the lead shield was left up, resulting in a rather high background. However, good reproducibility was realized.

In every experiment, the background was counted with the sample suspended above the liquid; the cap was then screwed down allowing the sample to be submerged below the liquid level. The geometry of the cell was such that the sample was well above the ports in the cell cup and, therefore, out of direct line of sight of the phototubes (Fig. 1c).

The initial time (T_0) was noted as the sample was lowered into the solution. It was necessary to close the deep-freeze chest and apply power to the phototubes before counting could begin. A minute was allowed to elapse before counting began and readings were then taken at one-minute intervals. The counter indicated the cumulative count and as a result, the counts per minute for any given time were obtained by subtracting the preceding total from the total at that minute.

The spread of the data was remarkably low considering that the standard deviation equals \pm the square root of the count. In comparing the total count method with individual one-minute counts, at selected times, it was found that the spread was somewhat less at long times with the individual count method. However, the former method seemed simpler and was utilized in this work.

The desorbing solution was prepared as follows:

toluene	1 liter
2,5-diphenyloxazole	4 g.
1,4-di[2-(5-phenyloxazolyl)] benzene	50 mg.

It was necessary to utilize the solution described in order to optimize the scintillation counting efficiency of the system. Ideally, a system containing no extraneous material would be desirable; however, in order to achieve a high counting efficiency, these materials must be included.

RESULTS

Figure 2 represents a plot of the radioactivity, in counts per minute, of the desorbing solution versus the time in minutes. It may be seen that the

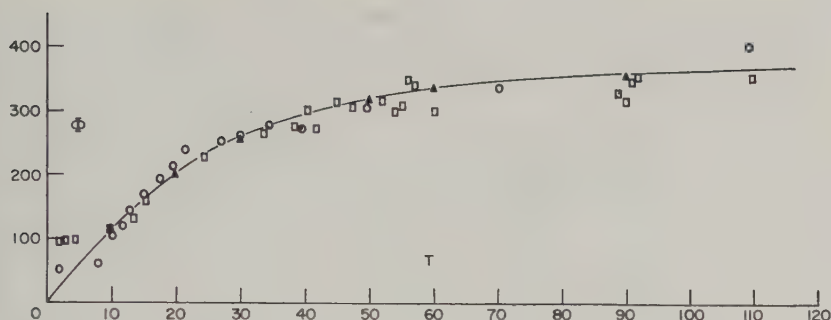


FIG. 2. Desorption isotherm—stearic acid into toluene solution at 3°C. Φ = net counts per minute, T = time in minutes. \circ —Experimental 1. \square —Experimental 2. \triangle —Calculated.

curve is a typical rate curve and, when the best calculated curve is drawn, the curve fits Eq. [1] very well indeed.

$$\phi = \phi_E(1 - e^{-kt}) \quad [1]$$

where

ϕ = counts per minute;

ϕ_E = equilibrium counts per minute;

k = rate constant;

t = time.

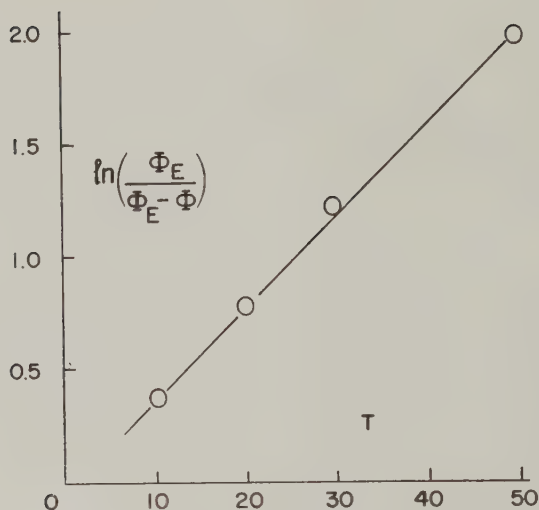
The equation is derived from the theory proposed by Langmuir (5) concerning the rate of adsorption of a gas on a free surface. In spite of the fact that the Langmuir equation was generated for gaseous materials adsorbing on free surfaces, the system discussed here seems to fit the equation extremely well. The curve shown represents two samples (samples 1 and 2); however, many samples have been examined and were found to fit the curve equally well.

By selecting values for ϕ , utilizing Fig. 2, and plotting the $\ln(\phi_E/\phi - \phi_E)$ versus time, a straight line results, as is shown in Fig. 3 (6).

As Eq. [1] is treated empirically, it is interesting to consider a more theoretical approach. By assuming the desorbing solution to be infinitely dilute, one may say that

$$\frac{d\theta}{dt} = -k\theta, \quad [2]$$

where the stearic acid leaving the surface will not, in all probability, return to the surface.

FIG. 3. Test of Eq. [1], $\phi = \phi_E[1 - e^{-kt}]$.

Integrating Eq. [2],

$$t = -\frac{1}{k} \ln \theta + C, \quad [3]$$

where θ = fraction of the surface covered.

At $t = 0$, $\theta = \theta_0$ and

$$C = \frac{1}{k} \ln \theta_0. \quad [4]$$

Then, substituting in Eq. [3]:

$$t = -\frac{1}{k} \ln \frac{\theta}{\theta_0}, \quad [5]$$

which may be rewritten

$$\theta = \theta_0 e^{-kt}. \quad [6]$$

Let $\theta_0 - \theta = \phi$, where ϕ represents the fraction which has entered the solution at any time, t . Then,

$$\phi = \theta_0 (1 - e^{-kt}), \quad [7]$$

which is the same as Eq. [1]. It is assumed that all the removable material is in the solution at $t = \infty$. To determine that Eq. [7] applies, θ_0 , ϕ , and t may be obtained from experimental data and when substituted in Eq. [5] the value for the rate constant, k , is obtained.

The differences in the actual number of layers of stearic acid on the metal

surface have an effect upon the absolute rate at which the stearic acid concentration in the solution increases. The more layers on a sample surface, the more rapidly the concentration in the solution will increase, all other variables being equal.

It should be made clear that the experiments were carried out to measure the rate at which the solution concentration is increasing and, by deduction, the rate at which the material is leaving the surface. It is not possible by using the technique described to know precisely, at any moment during the experiment, the fraction of stearic acid which is removed. Experiments are currently being carried out which entail the transfer of radiolabeled monolayers of stearic acid onto ferrotype samples. Desorption will be investigated using the technique described in this paper. The results will be reported at a later date.

As the samples discussed above were coated with approximately two layers of stearic acid (as determined by comparison with radiocounting of transferred films), a series of experiments with more layers of the acid were considered. Sample 3 had a radioactive count of 4100 c.p.m. using the "Mylar" window counter as compared to 2800 and 2600 c.p.m. for the previously discussed samples 1 and 2, respectively. Figure 4 represents the plot of the desorption data and indicates that the same phenomenon is occurring, as, again, the equation fits the data very well. The considerably higher count that is obtained is explained by the fact that the geometry of the liquid scintillation system is vastly more efficient than the dry counting systems. It is noteworthy that the value for the rate constant is, again, 0.04.

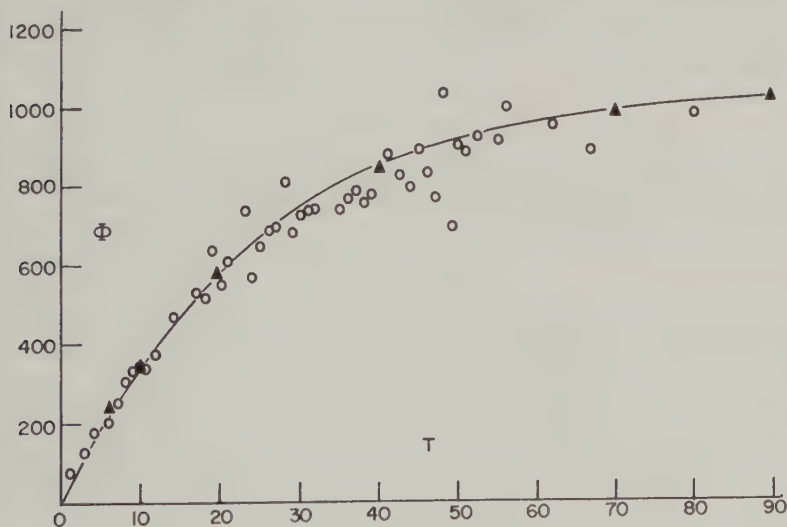


FIG. 4. Desorption isotherm—stearic acid into toluene solution at 3°C.—thicker adsorbed film. ○—Experimental 3. ▲—Calculated.

It was not deemed necessary in all cases to carry out the experiments to long periods of time. In no case was it possible to remove all the radio-labeled stearic acid from the surface. In all the desorption experiments it was indicated that equilibrium was attained before the calculated value for a residual monolayer was reached. In one experiment the sample was allowed to stay in the desorption cell and stirring was continued until desorption had, beyond all doubt, reached equilibrium. The dry count of the sample after desorption indicated slightly more than the calculated monolayer. Further attempts at desorption in fresh solution were negative; accordingly, one can say that the desorption which is recorded is the physio-desorption and that it concerns the removal of only the stearic acid which is not part of the interfacial monolayer. One may assume that removal of the interfacial monolayer would be accomplished by quite a different mechanism necessitating a considerably larger energy input. Furthermore, one would not expect the decay constant for the noninterfacial layers to be the same as the constant concerned with the interfacial molecules.

SUMMARY

A new technique for continuous examination of the desorption of a radiolabeled material from a planar surface has been investigated which provides useful information concerning the rate of desorption. When applied to more complex systems, this technique will be useful in determining the mechanism of physical-chemical degradation of interfacial bonds. Considerable work investigating the effect of a series of long-chain polar materials on the desorption rate has been planned. The effect of temperature on adsorption is currently being examined and will be reported at a later date.

ACKNOWLEDGMENTS

We are greatly indebted to Dr. R. B. Mesrobian and to Messrs. J. P. O'Meara and G. E. Novak, all of CCC Division's research organization, for many stimulating discussions and for help in preparing this paper.

REFERENCES

1. COOK, E. L., AND HACKERMAN, N., *J. Phys. Chem.* **55**, 549 (1951).
2. HACKERMAN, N., AND ROEBUCK, A. H., *Ind. Eng. Chem.* **46**, 1481 (1954).
3. GREENHILL, E. B., *Trans. Faraday Soc.* **45**, 625 (1949).
4. PATRICK, R. L., DOEDE, C. M., AND VAUGHN, W. A., *J. Phys. Chem.* **61**, 1036 (1957).
5. LANGMUIR, I., *J. Am. Chem. Soc.* **40**, 1361 (1918).
6. HARNED, H. S., *J. Am. Chem. Soc.* **42**, 372 (1920).

VISCOELASTIC DISPERSION OF POLYDIMETHYL SILOXANE IN THE RUBBERLIKE PLATEAU ZONE¹

Donald J. Plazek, Walter Dannhauser,² and John D. Ferry

*Department of Chemistry, University of Wisconsin, Madison, Wisconsin, and Mellon
Institute, Pittsburgh, Pennsylvania*

Received July 27, 1960

INTRODUCTION

As part of a continuing program to investigate the effect of polymer chain backbone structure on viscoelastic behavior, polydimethyl siloxane (PDMS) has now been studied over a wide range of time scale. Heretofore measurements on high molecular weight linear amorphous polymers in the region of relatively long times (beyond the primary relaxation transition) have indicated only quantitative differences in behavior. The kind of viscoelastic response observed in vinyl polymers, their concentrated solutions, and solutions of cellulose derivatives has been attributed to the interactions between the long chainlike molecules (1). Whereas the transition from glasslike to rubberlike consistency and those at still shorter times are molecular weight independent (2, 3), the single dispersion observed at long times is dependent on molecular weight and molecular weight distribution (4). Certain data for linear amorphous systems have been found to be well described by a form of Andrade's creep equation in this region of long times (5). The occurrence of Andrade creep in polymeric systems is by no means limited to this kind of system; in fact its presence had been established earlier in a number of polycrystalline systems (6, 7). It will be shown here that polydimethyl siloxane exhibits this kind of behavior but also that in the region measured it displays a response different from the single response usually found.

MATERIALS

All the polydimethyl siloxane samples studied in this investigation were generously supplied by the General Electric Research Laboratories through the kind assistance of Dr. Bruno H. Zimm. Three research samples of whole polymers with different molecular weight were supplied. They had been

¹ Presented in part at the Cleveland meeting of the American Chemical Society, April 12, 1960.

² Present address: University of Buffalo, Buffalo, New York.

TABLE I
Light-Scattering Results
 (Polydimethyl Siloxane in Toluene at 25°C.)

Stock	$\bar{M}_w^a \times 10^{-6}$	$A_2 \times 10^4$ (cm. ³ mole/g. ²)	$\sqrt{s^2}$ (Å).
IA	4.9	1.87	1,460
IB	4.1	2.31	1,390
IC	3.2	2.37	1,160
ID	2.2	2.15	1,010
II	1.34	2.82	760
III	0.41	4.07	405

^a Weight average molecular weight.

prepared by a KOH-catalyzed tetramer polymerization (8). The product in each case was finally washed with methanol to remove the KOH.

The stock of highest weight,³ I, was first studied. In searching for the proper molding conditions portions were kept in simple cavity molds for varying lengths of time at temperatures ranging from 80° to 120°C. The persistence of partial recovery after removal of the sample from the mold gave reason to keep one portion at 120°C, for two weeks. After mechanical property measurements were under way the results indicated the presence of unexpected degradation. This conclusion was first verified with intrinsic viscosity measurements and later by molecular weight determinations by light scattering. For this stock only room temperature molding for periods of one to three months was deemed safe and satisfactory. To utilize the valuable and interesting data obtained on the thermally degraded portions, measurements were continued to completion, and characterization by light scattering was carried out afterward. The results on four portions, IA, IB, IC, and ID, the molding temperatures of which range from 25° to 120°C, are presented herein.

PDMS stocks II and III⁴ were of lower molecular weight, \bar{M}_w , and exhibited no thermal sensitivity such as that found in stock I. The normal thermal stability found in these samples we take to be an indication of a more successful removal of the KOH catalyst. Intrinsic viscosities of stocks IA, IB, IC and ID were measured in a two-bulb viscometer in methyl ethyl ketone at the theta temperature 20°C. (9) and found to be 2.15, 1.70, 1.48, and 1.38 dl./g., respectively, at zero rate of shear. The extrapolation to zero rate of shear is not to be considered dependable and therefore the values given are to be considered approximate. The results of light-scattering measurements⁵ on all six samples are presented in Table I. The light-scattering measurements were carried out with a Brice-Phoenix

³ General Electric designation VT-32.

⁴ General Electric designations CP55-8C and CP57-9(1), respectively.

⁵ These measurements were made by Messrs. Harvey Notarius and Robert Kerwin.

photometer at 25°C. in reagent grade toluene, which was redistilled in a 48" \times 1" column packed with glass helices after being dried over Drierite. The values of the second virial coefficient, A_2 (mole cm.³/g.²), and the root-mean-square radius of gyration, $\sqrt{s^2}$, for these whole polymers appear reasonable but are somewhat larger than those found by Yavorsky (10) for fractions. Osmotic pressure measurements in methyl ethyl ketone were made⁶ on stock ID at 30°C. A number-average molecular weight, M_n , of 1.1×10^6 and an A_2 of 0.55×10^{-4} mole cm.³/gm.² were found. Further sample information will be included in the results section.

METHODS

Viscosities of stock III were determined by means of the falling ball method over the temperature range of -43° to 141° C.

The double transducer of Fitzgerald and Ferry (11) was used for the measurement of the dynamic shear moduli of stock IC at frequencies, ν , between 15 and 600 cycles/sec. at seven temperatures between -49° and 25° C.

Dynamic shear moduli of IA, IB, IC, and ID were measured in the freely oscillating torsion pendulum of Plazek, Vrancken, and Berge (12) between 0.05 and 10 cycles/sec. at temperatures from -25° to 75° C.

The corresponding measurements⁷ on stocks II and III were made utilizing the forced oscillation torsion pendulum of Morrisson, Zapas, and DeWitt (13) in the frequency range 0.0006 to 3 cycles/sec. at 25° C.

Torsional creep and recovery measurements were carried out in the freely oscillating torsion pendulum apparatus in a manner described elsewhere (12) on IA, IB, IC, and ID principally at 25° C.

Similar creep and recovery measurements were run on IA, ID, and II in the cone and plate viscometer of Markovitz *et al.* (14) at 25° C.

Measurements of creep and recovery in simple shear were carried out on stock IC at 25° C. in a simple sandwich instrument similar to that used by Van Holde and Williams (15).

RESULTS

Falling Ball Viscosities

Viscosities, η , of stock III were measured by the falling ball method at 12 temperatures from -42.7° to 140.8° C. The temperatures were held constant to $\pm 0.1^\circ$ C. Most of the measurements were made with stainless steel balls of 0.1590 cm. diameter in a cylindrical glass tube with a diameter of 2.9 cm. A check was made at 25.4° C. with a 0.0966 cm. ball. Checks were also made near 25° C. after the sample had been taken to the extreme tem-

⁶ Measured by Dr. Thomas Orofino and Mr. John Mickey.

⁷ These measurements were carried out in part by Mr. Haruo Nakayasu.

TABLE II
Falling Ball Viscosities of PDMS, Stock III

Temp. (°C.)	$\log \eta$	$\log a_T$	Temp. (°C.)	$\log \eta$	$\log a_T$
-42.7	5.790	0.961	34.1	4.861	-0.086
-38.4	5.703	0.872	40.6	4.803	-0.151
-21.3	5.436	0.564	55.8	4.688	-0.283
0.0	5.178	0.275	79.8	4.526	-0.471
25.0	4.936	0	100.7	4.403	-0.610
25.4	4.926	-0.010	120.2	4.280	-0.749
25.4 ^a	4.924	-0.012	140.8	4.172	-0.875

^a 0.0966 cm. ball used.

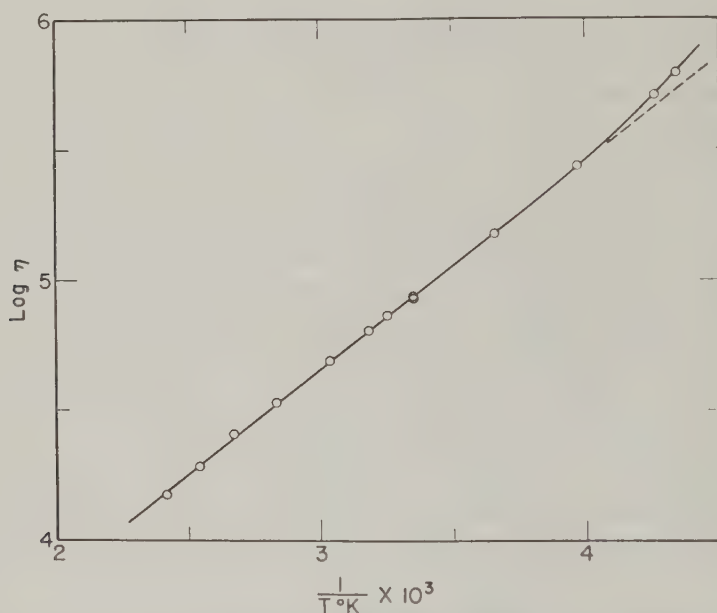


FIG. 1. Logarithms of falling ball viscosities (poises) of polydimethyl siloxane stock III plotted against reciprocal absolute temperature. Dashed line is extension of linear portion of line which extends from 141° to -21°C.

peratures. The Faxén correction (16) was used in the calculation of the viscosities; the results in poises are presented in Table II and are shown plotted logarithmically against the reciprocal absolute temperature in Fig. 1. Above -21°C. the temperature dependence is well represented by a constant apparent heat of activation of 3.65 kcal. The usual increase of this activation energy with decreasing temperature is observed at lower temperatures. Shown in Table II are a_T temperature dependence factors calculated from the expression $a_T = \eta \rho_0 T_0 / \eta_0 \rho T$, where the density, ρ_0 ,

at the reference temperature, $T_0 = 298.2^\circ\text{K.}$, is 0.974 g./cm.^3 and η_0 is 8.64×10^4 poises. The densities, ρ , at the other temperatures of measurement were obtained using an estimated thermal expansion coefficient of $7 \times 10^{-4} \text{ cm.}^3/\text{cm.}^3 \text{ }^\circ\text{C.}$

Since for high molecular weight materials a_T is independent of molecular weight (17) and since the accuracy of a_T values derived from dynamic mechanical property measurements would necessarily be limited, because of relatively low dispersion, values derived from Table II were used for the temperature reduction of data in all cases in this study.

DYNAMIC MEASUREMENTS

Dynamic measurements were carried out on samples of all the stocks, but not all in the same instruments and not under the same conditions. Table III summarizes most of the information concerning individual samples. Samples of stocks IA, IB, IC, and ID could be and were handled as solids, and those of II and III were handled as liquids.

The data from all the samples were treated in the usual manner (18) and appeared to behave normally for the plateau region. Because of the

TABLE III
Dynamic Measurements, Experimental Conditions

Sample	Nominal dimensions		Empirical modulus shift factor	Temperature range	Frequency range
	Ht. (in.)	Diam. (in.)	% increase	($^\circ\text{C.}$)	(cycles/sec.)
<i>Free Oscillation Torsion Pendulum</i>					
IA-1 ^a	$\frac{3}{8}$	$\frac{3}{4}$	9.6	-24-75	0.048-0.77
IA-2	$\frac{1}{32}$	$1\frac{1}{4}$	^b	-24-50	0.65-9.7
IB ^a	$\frac{3}{8}$	$\frac{1}{2}$	0	-24-25	0.046-0.18
IC-1 ^a	$\frac{1}{4}$	1	0	-24-55	0.22-1.0
IC-2 ^a	$\frac{1}{8}$	1	^b	-39-55	0.32-1.7
ID ^a	$\frac{9}{32}$	$1\frac{1}{8}$	0	-24-25	0.26-1.1
<i>Double Transducer</i>					
IC-3	$\frac{1}{8}$	$1\frac{1}{16}$	14.8	-49-25	15.0-600
<i>Forced Oscillation Torsion Pendulum</i>					
II	1.32	0.049 ^c	0	25	0.0010-2.8
III-1	1.55	0.049 ^c	0	25	0.013-3.5
III-2	1.45	0.127 ^c	0	25	0.0010-0.17
III-3	1.33	0.307 ^c	0	25	0.00066-0.086

^a Also used for creep measurements.

^b Completely empirical sample coefficient used.

^c Diameter of inner cylinder; outer cylinder in each case was 1.5 in.

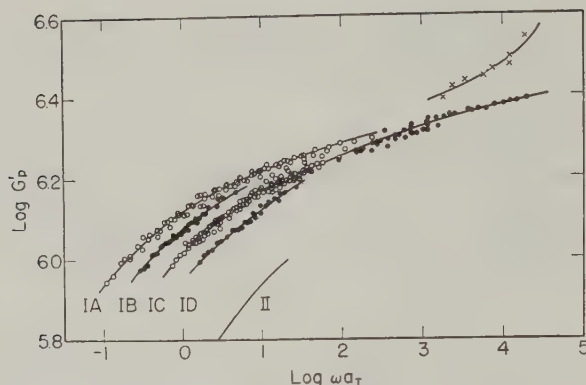


FIG. 2. Real part of the complex dynamic shear modulus reduced to 25°C., G'_p (dynes/cm.²), of four molecular weights of PDMS plotted logarithmically against reduced frequency (sec.⁻¹). Double transducer points measured above -49°C. are represented by filled-in points for stock IC above $\log \omega a_T$ equal to 2; at -49°C. by crosses. Line indicating position of results on stock II is shown for comparison.

small apparent heats of activation little difference in the frequency dependence of the storage modulus, G' (dynes/cm.²), and the loss tangent, G''/G' (where G'' is the loss modulus), was observed in the range of temperatures studied. However, temperature reduction was adequately checked and was found to hold over a range of 104°C. for stock IC (-49° to 55°C.) and for a 100°C. range for IA (-25° to 75°C.). In spite of the appreciable range the principal value of the temperature study was the check just mentioned. The resulting extension of the effective frequency range in this study is quite small, about a half a decade at each end of the curve in the above two cases.

Since little would be gained by presentation of the individual curves, the results for stocks IA, IB, IC, and ID are presented only in their reduced form. The storage modulus reduced to 298.2°K. [$G'_p = G'(T_0 \rho_0 / T \rho)$], is shown in Fig. 2 plotted logarithmically against the logarithm of the reduced frequency, ωa_T ; the pulsatace, ω , being equal to $2\pi\nu$. The corresponding results of the loss tangent determinations are shown in Fig. 3. The success of the reduction treatment is clear.

Two disc-shaped samples were studied in the free oscillation torsion pendulum to yield the data shown for stock IA. One similar sample of each was measured to obtain the curves indicating the behavior of IB and ID. Stock IC was the most thoroughly studied by far. A pair of discs was run in the double transducer. The results at temperatures above -49°C. are represented by the filled-in points at reduced frequencies greater than 100 radians per second in Figs. 2 and 3. The low degree of dispersion displayed in this region provides an unusual case which indicates the need for the

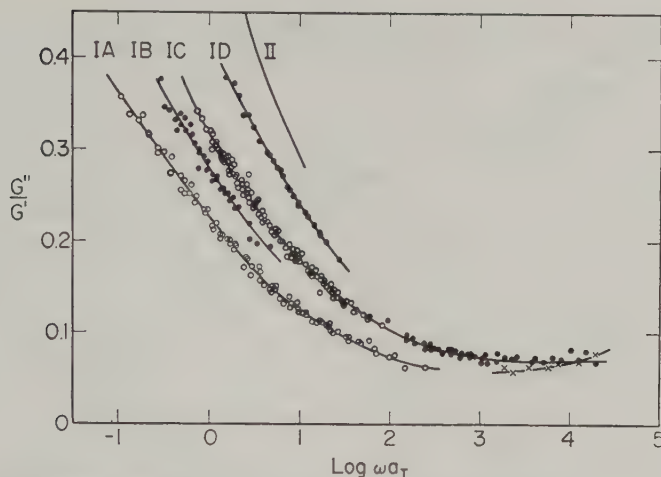


FIG. 3. Loss tangent results corresponding to moduli data seen and explained in Fig. 2.

often neglected vertical shift factor $T_0\rho_0/T\rho$ in the reduction procedure. The unreduced data from different temperatures describe curves which appear to superpose and an attempt to reduce utilizing the calculated a_T factors leads to a separation of the curves so the vertical shift factor is clearly necessary to achieve true superposition. The double transducer results at -49°C . are shown in these same figures by the crosses. Since the freezing point has been reported to be in the neighborhood of -40°C . (19) it is reasonable to connect this nonreducible behavior with the presence of crystallinity. It is evident that for PDMS in the amorphous state even the beginning of the transition from rubberlike to glasslike consistency was inaccessible to us. The lower frequency data of the IC curve was obtained from two disc-shaped samples in the free oscillation instrument. At this point of the analysis it would be customary to explain the increased dispersion to be due at least in part to the appreciable influence of irreversible flow. We shall see that this is not the case here. Over the entire reduced frequency range measured, G' increased from 1×10^6 to 4×10^6 dynes/cm.² while G''/G' decreased from 0.36 to 0.07 with increasing frequency and decreasing temperature.

Values of G' and the real component of the dynamic complex viscosity ($\eta' = G''/\omega$) of stocks II and III were obtained at 25°C . employing the forced oscillation torsion pendulum. Measurements were made utilizing the concentric cylinder configuration. A hundredfold change in the modulus of II required only a single combination of cylinders for the measurements over the conveniently accessible frequency range. To achieve a reasonable degree of accuracy over a range of modulus of 30,000, three inner cylinders

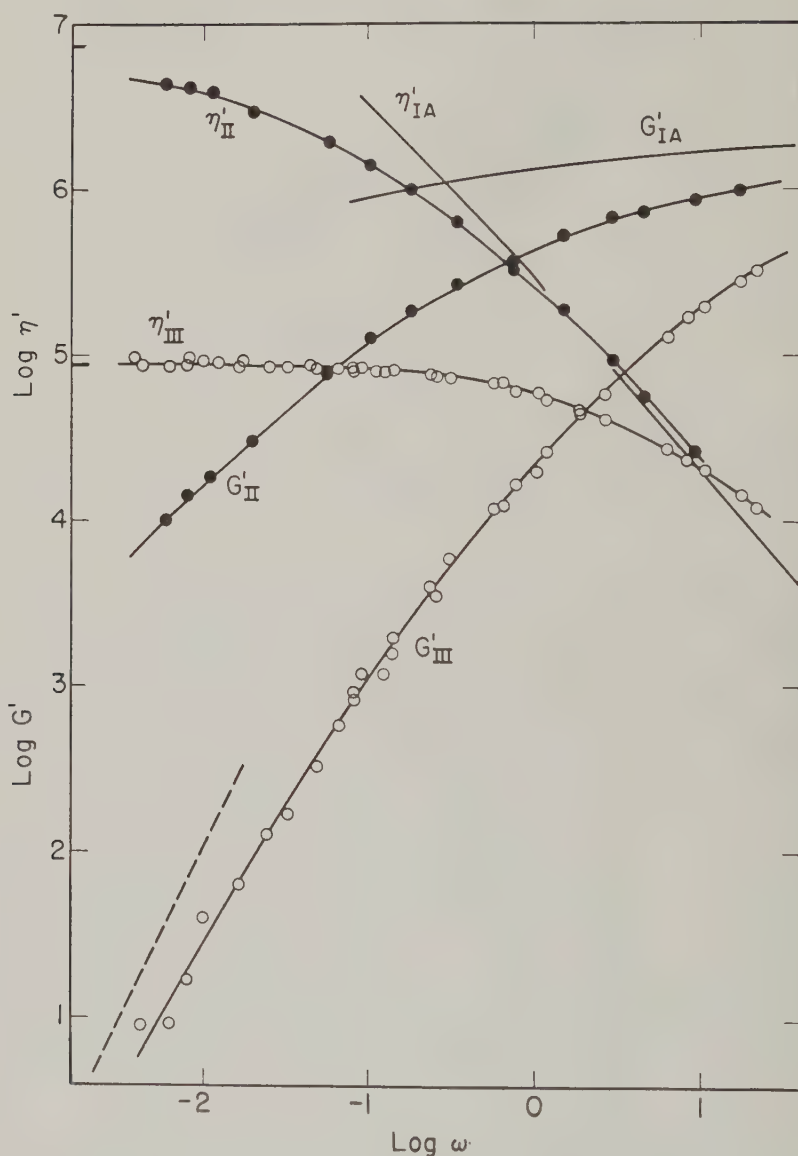


FIG. 4. Real components of the complex dynamic shear modulus G' and viscosity, η' (dyne sec./cm.²), at 25°C.: stock II, filled-in circles; stock III, open circles. Corresponding curves for IA are given for comparison. Short horizontal bars on the ordinate scale represent the steady-flow viscosities. Dashed line of slope 2 indicates the theoretical limiting slope of $\log G'$.

of varying diameter were used in measuring stock III. Logarithmically the results are presented in Fig. 4 versus the logarithm of the pulsatace. Short heavy bars indicate the values of the 25°C. viscosities. The falling ball result is used for stock III and that of 7.5×10^6 poises for stock II was obtained from creep measurements in the cone and plate viscometer. It is clear that within experimental error η'_{III} has reached its low frequency limiting value which is equal to the steady-state viscosity; whereas η'_{II} is still appreciably lower. Accordingly $\log G'_{III}$ has at low frequencies indeed come close to the slope of 2 which is predicted by phenomenological theory. A dashed line of slope 2 is provided for comparison. Curves corresponding to the behavior of IA are also shown to indicate the complete range of behavior measured.

CREEP AND RECOVERY MEASUREMENTS

Most of the creep measurements in the linear stress-strain region were made in torsion in the free oscillation instrument and the cone and plate viscometer. Three torsional creep and recovery runs were carried out on IB at 25°C. These can be used to show that deviations from stress-strain linearity are within the experimental uncertainty and to test adherence to Boltzmann superposition. The data for both creep and recovery are plotted linearly in Fig. 5 against the logarithm of the time of creep, t , and of recovery, $t - \theta$, where θ is the time at the end of the creep portion of the run. A range in maximum applied stress, \mathfrak{J}_m , of five fold is covered and a compliance curve, $J(t)$, is obtained with overall agreement to within 2%. The runs a, b, and c were performed consecutively, the total strains attained being about the same; see Table IV for the experimental conditions for these and the other creep measurements. The highest applied torque therefore gave the shortest run, a. Its recovery is seen to be complete. Run b also appears to be completely elastic. Unfortunately the recovery of c was measured only for a few minutes, but for over $2\frac{1}{2}$ decades of time it behaved as predicted by the superposition principle. The recovery lines drawn for these runs, calculated from the creep curve utilizing this principle, are

$$\gamma_r(t)/\mathfrak{J} = J(t) - J(t - \theta), \quad [1]$$

where the deformation is assumed to be entirely recoverable and $\gamma_r(t)$ is the strain remaining at time t . It was necessary to utilize an extrapolation of an analytical expression found for the long-time behavior of this stock to obtain recovery curve c. The agreement seen allows us to analyze these and similar measurements within the framework of existing phenomenological theory.

The results just discussed are also presented in Fig. 6 together with most of the results obtained on all the samples studied. The logarithm of

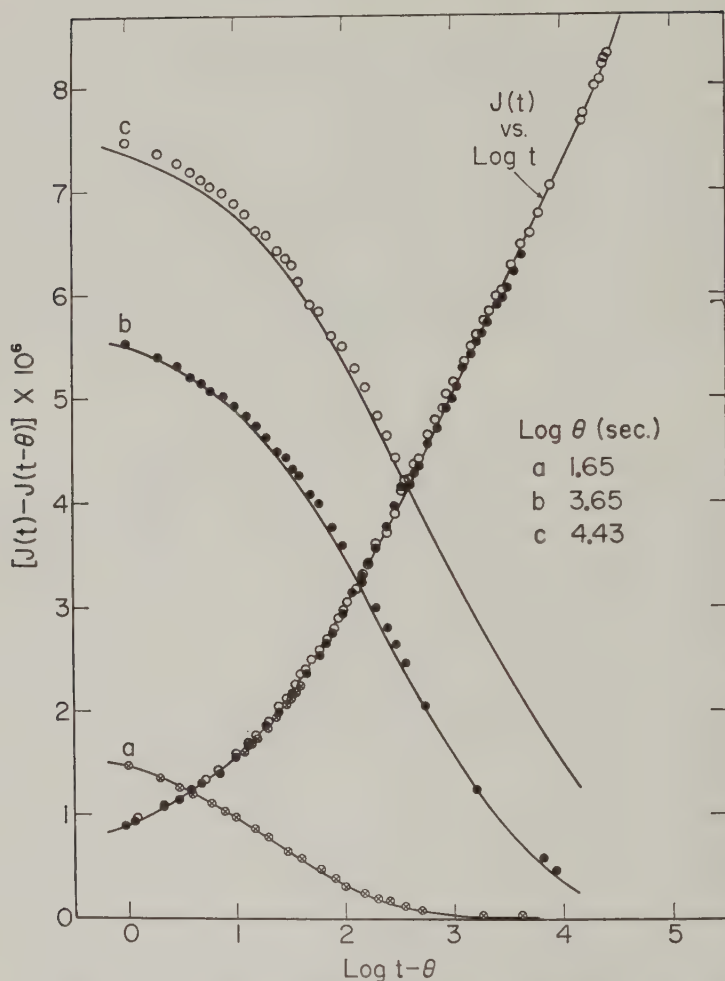


FIG. 5. Creep compliances and creep recoveries for three 25°C. runs at different stresses (see Table IV) on stock IB shown versus $\log t$ (time in seconds) and $\log (t - \theta)$, where θ is the duration of the creep portion of the run.

the creep compliance reduced to 25°C, $J_p(t)$, is shown as a function of the logarithm of reduced time, t/a_T . Of course the reduction has no effect on most of the results which were obtained at 25°C. All the directly measured $J_p(t)$ results are shown as open circles. The filled-in circles represent values of $J_p(t)$ calculated from the previously discussed dynamic results with the aid of the Ninomiya-Ferry approximation equation (20)

$$J(t) = J'(\omega) + 0.40J''(0.40\omega) - 0.014J''(10\omega)_{t=1/\omega}. \quad [2]$$

Smoothed values from the pertinent curves are used.

TABLE IV
Creep, Experimental Conditions, 25°C.^a

Sample	Empirical coefficient shift (%)	Max. strain $\times 10^2$	$\mathfrak{J}_m \times 10^{-3}$ (dynes/cm. ²)	Time of creep $\times 10^{-3}$ (sec.)	Time of recovery $\times 10^{-3}$ (sec.)	In- strument ^b
IA-1	9.6	2.30	2.66	165	2.7	T.P.
IB	0	1.12	4.88	0.045	4.2	T.P.
	0	1.05	1.74	4.4	8.7	T.P.
	0	0.79	1.00	27.2	0.37	T.P.
IC-1	0	3.55	0.580	3114	615	T.P.
IC-2	<i>c</i>	2.6	8.8	0.11	—	T.P.
	<i>c</i>	2.8	1.6	4.6	—	T.P.
IC-4	10.1	9.0	1.50	2365	1160	H.S.
	26.2	41.0	6.81	1883	2427	H.S.
	10.1	11.7	12.3	2.3	—	H.S.
	10.1	40.4	12.3	227	335	H.S.
	22.5	42.1	17.8	49.7	5300	H.S.
ID	4.6	8.1	1.52	194	—	T.P.
II	19.0	136	4.1	2.04	40.6	C.P.
	19.0	2140	4.1	39.4	10.8	C.P.

^a Runs on sample IC-2 were carried out at 55°C.

^b T. P., free oscillation torsion pendulum; H.S., horizontal sandwich; C.P., cone and plate.

^c Completely empirical sample coefficient.

Careful examination of the creep and recovery measurements made on samples from stocks IA, IB, IC, and ID in the range of stress-strain linearity surprisingly leads to the conclusion that within experimental scatter there is no definite evidence of viscous deformation. Complete recovery, of course, provides unambiguous proof of the absence of viscous flow, but following the long creep runs it was impossible to wait for the cessation of recovery. A convincing fact which attests to at least a very unusual viscosity behavior is that the viscous deformation predicted on the basis of the established viscosity-molecular weight relationship (21) for a 36-day run made on a sample from stock IC is 1600 times greater than the total deformation measured.

All the curves in Fig. 6 are converging at short times in accordance with the well-established fact that at very short times, starting with the primary relaxation dispersion, $J(t)$ along with many of the other mechanical parameters becomes independent of molecular weight. A point to be more fully discussed later is the presence of two elastic dispersion regions at long times most clearly seen in the curves for IC and ID. In linear amorphous polymers this is unexpected; heretofore theories (22-24) have dealt only with a single kind of mechanism beyond the intrachain modes of cooperation involved in the primary transition. A compliance greater than that exhibited by IB which is reached by IA, the highest molecular weight

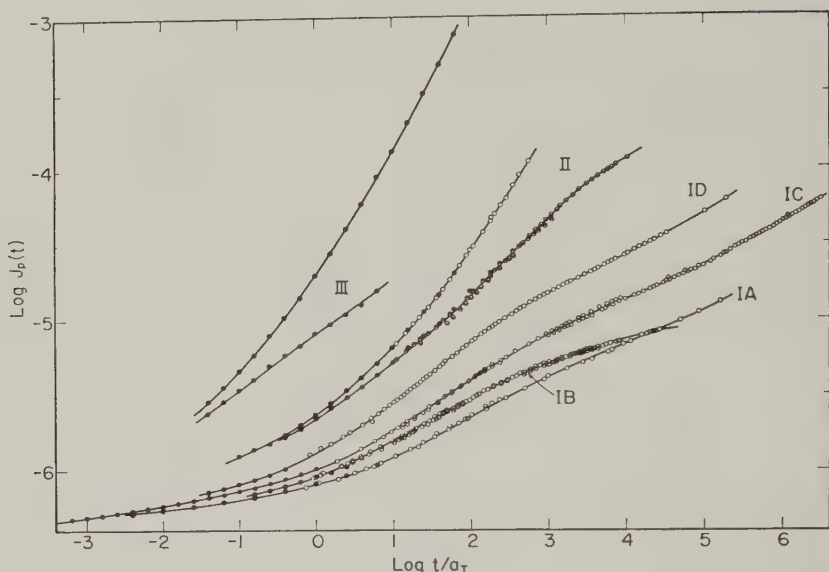


FIG. 6. Creep compliances of all samples of PDMS, reduced to 25°C. (logarithmic). Open circles, directly measured values; filled-in circles, converted from dynamic measurements. Bottom black points, $J(t) - t/\eta$ (retarded elastic compliance) measured in recovery; top black values, calculated from measured values of $J(t)$ and η . Crossed circles represent the same quantity obtained from $J(t)$ values calculated from the dynamic measurements.

stock, is attributed to a presumed narrower molecular weight distribution of the latter.

Although, as mentioned above, no discernible viscous flow occurs in stocks IA through ID, the presence of flow in stocks II and III is readily seen. Therefore, for these stocks the retarded elastic compliance,⁸ $J(t) - t/\eta$, was also calculated using the values of η given above. Points for $J(t) - t/\eta$ are presented in Fig. 6 where they exceed 15% of $J(t)$. For both stocks the crossed circles represent results obtained by subtracting the viscous contribution from the creep compliance points calculated from dynamic data. Direct creep and recovery measurements were also carried out on stock II. The retarded elastic contribution calculated from the former is described by the top black points and that calculated from the latter is represented by the bottom black points. These measurements were carried out in the cone and plate viscometer where the moving member, the plate, is supported by a shaft which rides in a pair of miniature precision ball bearings. In spite of a very low amount of friction in the instrument, 0.1 g. being able to turn the complete moving assembly, recovery measurements on systems that flow or are very compliant cannot be made with

⁸ The glassy compliance, J_g , contribution is negligible in this region.

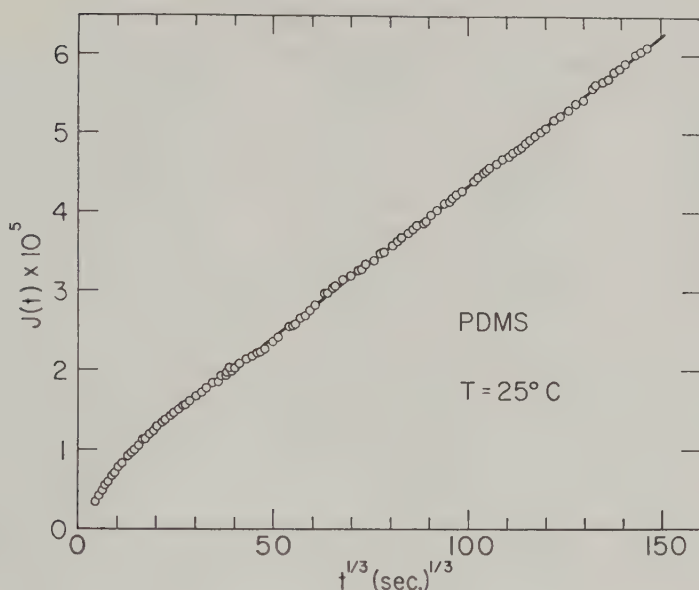


FIG. 7. Creep compliance of stock IC at 25°C. plotted against $t^{1/3}$.

dependability at very long times. In any creep instrument employing ball bearings the balls themselves in certain configurations can produce torques which erroneously enhance or diminish the amount the plate returns. It is for this reason that, although the creep preceding the partial recovery presented here is believed to have been sufficiently long to justify accepting this part of the recovery curve as representing the true retarded elastic compliance, that portion standing alone beyond 3 on the abscissa scale is viewed with incomplete trust. The preceding creep, though not measured throughout its course because of experimental barriers, ran to 3.9×10^4 sec.

To clarify the character of the very long time behavior of the higher molecular weight PDMS samples, a 36-day run on IC is shown in Fig. 7, where $J(t)$ is plotted against the cube root of time. The linearity of $J(t)$ extending from about 8000 sec. to the end of the run is a convincing example of the occurrence of Andrade creep in a polymeric system. For about fifty years Andrade and his associates have shown the existence of and claimed the significance of creep behavior of metal and metal alloy systems (25, 26) similar in form to

$$J(t) = J_A + \beta t^{1/3} + t/\eta. \quad [3]$$

Here J_A and β are characterizing constants. Within the past ten years a number of crystalline and cross-linked polymers have also been found to creep in a manner amenable to description by Eq. [3] with η being con-

TABLE V
Parameters of Andrade Equation at 25°C.

Stock No.	$M_w \times 10^{-6}$	$J_A \times 10^6$	$\beta \times 10^6$	$\eta \times 10^{-6}$
IA	4.9	3.9	0.159	^a
IB	4.1	4.5	0.127	^a
IC	3.2	5.2	0.382	^a
ID	2.2	6.4	0.929	^a
II	1.34	~98	~1.5	7.5
III	0.41	—	—	0.0864

^a Infinite.

sidered infinite (6, 7). Recently the possibility has been suggested that linear amorphous polymers might also deform according to Eq. [3] with the presence of flow (5). Following a suggestion by Dr. K. E. Van Holde that the PDMS data be tested it was found to serve as one of the most recent additions to the growing list.

Less extensive runs on stocks IA, IB, and ID showed the same qualitative behavior. The characterizing constants for the behavior at long times for the above-mentioned samples are given in Table V. It is evident that J_A decreases monotonically with increasing molecular weight. So does β except for stock IA, where the higher compliance at long times (Fig. 6) which was attributed to molecular weight distribution is associated with its correspondingly high value of β .

The negative curvature at times less than 8000 sec. ($t^{1/3}$ less than 20) appears to be similar to that caused by the transition from rubberlike to glasslike consistency as seen in other systems (5); but as noted earlier the behavior at the highest frequencies measured does not reach this transition, so this deviation must reflect some different mechanism.

LOSS TANGENT BEHAVIOR

The influence of the mechanism just alluded to is the most marked and can be most clearly seen in the behavior of the loss tangent. Such behavior is presented for four of the stocks in Fig. 8. The directly measured data for IB and IC previously given in Fig. 3 are shown here by the short-dashed lines. The long-dashed lines represent values calculated from the dynamic measurements on II and III; see Fig. 4. Subtraction of the viscosity contribution to the loss compliance enables one to calculate a quantity, $(J'' - 1/\omega\eta)/J'$, which reflects the proportion of viscoelastic loss exclusive of flow. Measured values of the dynamic parameters and the viscosity are utilized here.

To obtain the values presented as filled circles the dynamic compliances were calculated with the approximation equations of Thor L. Smith (27),

$$J''(\omega) = 1/\omega\eta + (L\pi/2) \sec(n\pi/2), \quad -1 < n < 1, \quad [4]$$

and

$$J'(\omega) = J(t) + L[(\pi/2) \csc (n\pi/2) + \Gamma(-n)] - t/\eta, \\ -2 < n < 1. \quad [5]$$

Here L (a function of τ , the relaxation time) is the retardation spectrum, Γ the gamma function, and n the derivative $d \log L/d \log \tau$. The viscosity in the above equations was considered experimentally infinite. The values of $J'(\omega)$ obtained must be considered more accurate than those of $J''(\omega)$ since they are relatively close to those of $J(t)$. Because L is a derived quantity, obtained from approximate expressions which involve second derivatives of the experimental curves, the calculation of $J''(\omega)$ is subject to appreciable error. To dispel any doubt concerning the general shape of these derived curves, two values of $J''(\omega)$ of IC were calculated by means of graphical integration and are utilized in obtaining the loss tangent points represented by the crosses. Calculations on the IA and ID data yielded results which were in general agreement with the observed trends seen in Fig. 8 but with far greater scatter, thus reflecting somewhat poorly on the shapes of the early portions of the creep runs involved. For the sake

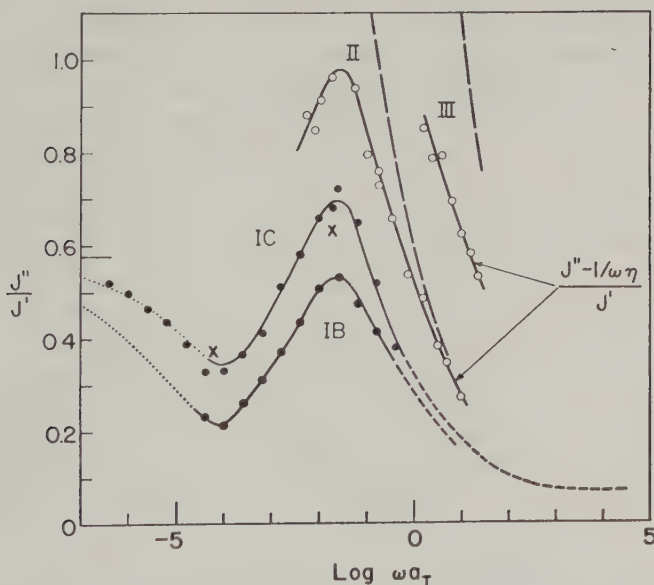


FIG. 8. Loss tangent values at 25°C. vs. logarithm of reduced frequency. Short-dashed lines, direct free oscillation torsion pendulum measurements; long-dashed lines, from forced oscillation measurements. Open circles are calculated from measured real (J') and imaginary (J'') components of the complex compliance and the viscosities. Filled-in circles are computed from $J(t)$ utilizing Eqs. [4] and [5]. Crosses involve J'' values obtained from graphical integration. Dotted lines are calculated from Eq. [3]. Long dash on ordinate shows low frequency limiting value of 0.577.

at higher and lower temperatures than water are melted. It is presumed to have a well-defined peak at a temperature of about 100°C, and which decreases in height with decreasing temperature. In the case of the polymer, the two peaks in Figure 1 are well separated.

In the case of the acid, it seems reasonable to take the curves obtained to follow the Debye-Hückel equation for strong electrolytes, approximately expressed as $\log f_{\pm} = -A\sqrt{c}$ at a given ionic strength. The A value for the solution predicted by the equation developed by Debye and Hückel is 0.509 for a solution of 0.1. The same value for a 0.1 solution of a weak electrolyte is 0.509, but the A value for a strong electrolyte will vary for the electrolyte under study.

Thermodynamic Properties

Thermodynamic data for the five polymers discussed might be obtained from the standard enthalpy of formation of the polymer. It is arranged along the Free Enthalpy method.¹⁰ The ΔG° values are calculated from the standard enthalpies of formation of the polymer, the heat of fusion, and the heat of vaporization. These values are then used to calculate ΔG° and ΔH° for the polymer. The ΔG° values are then used to calculate ΔH° and ΔS° for the polymer. The ΔH° values are then used to calculate ΔS° for the polymer. The ΔS° values are then used to calculate ΔG° for the polymer. The ΔG° values are then used to calculate ΔH° for the polymer. The ΔH° values are then used to calculate ΔS° for the polymer. The ΔS° values are then used to calculate ΔG° for the polymer.

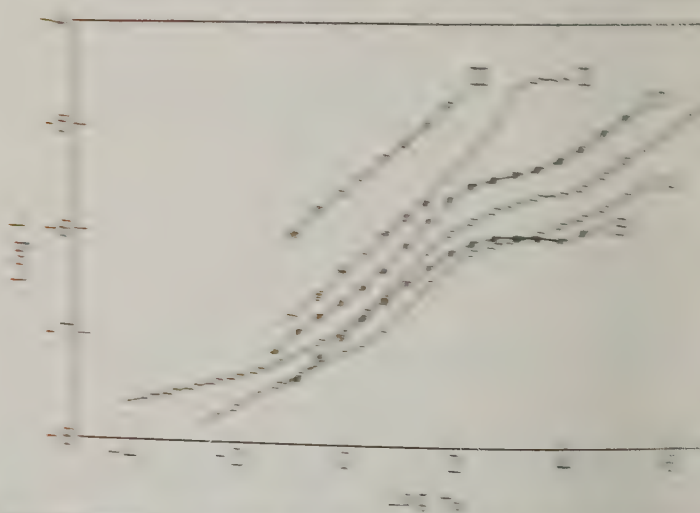


Figure 1. Thermodynamic data for 0.1% of all polymers studied in this study. The ΔG° values are calculated from the standard enthalpies of formation of the polymer, the heat of fusion, and the heat of vaporization. The ΔH° values are then used to calculate ΔS° for the polymer. The ΔS° values are then used to calculate ΔG° for the polymer.

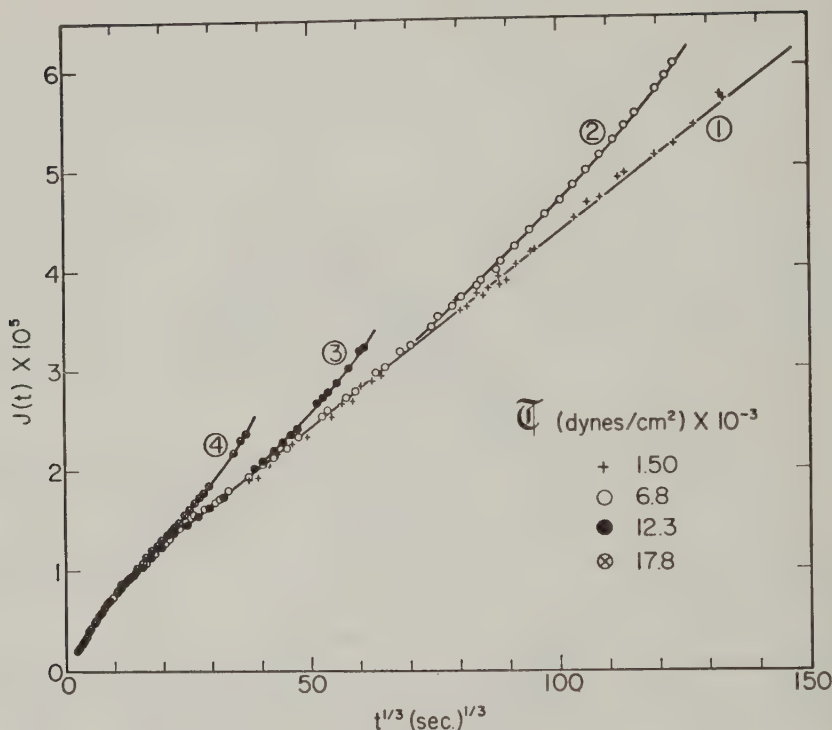


FIG. 11. Nonlinear creep compliance behavior at 25°C. of stock IC in simple shear given versus $t^{1/3}$, at various stresses as shown.

order of -10% is needed to bring compliances calculated by nominal geometrical relationships for simple shear into agreement with those obtained from other instruments. This correction is attributed to deviations from simple shear between the parallel plates, and in the present series was evaluated by matching the data at short times. The results are displayed in Fig. 11, where the torsional measurements, represented by the straight line, are in excellent agreement with the sandwich measurements at low stress, represented by the crosses, even out to very long times.

At higher stresses, however, deviations from the low-stress behavior eventually appeared, as shown by a study in the sandwich apparatus at different stresses as recorded in Table VI. Runs ① and ③ shown in Fig. 11 were made in direct sequence without removal of the samples and were calculated with the same sample coefficient; the coincidence of points at short times shows that there the behavior is truly linear with respect to stress. Runs ② and ④ involved reinstallation of samples with somewhat different sample coefficient corrections (Table IV), but for all these runs the corrected compliances at short times coincide exactly. The nonlinearity

TABLE VI
Parameters for Nonlinear Creep of Stock IC at 25°C.

Run	$\bar{\gamma} \times 10^{-3}$	$\xi \text{ (sec.)} \times 10^{-4}$	$\gamma_{\text{crit.}}$	η_D , obs. (poises), $\times 10^{-10}$	η_D , calc. Eq. [12], (poises), $\times 10^{-10}$
①	1.50	>240	—	—	—
②	6.81	34	0.22	20.4	20.4
③	12.3	4.8	0.23	5.0	5.1
④	17.8	0.32	0.21	1.05	1.02

with stress appears only after the lapse of longer times—the longer, the smaller the stress.

The creep compliances of ② and ③ appear at first glance to resemble qualitatively the behavior seen in polyisobutylene and a solution of cellulose nitrate in diethyl phthalate (5), two normally behaving linear amorphous polymers. Their behavior could be described by a more complete form of the Andrade equation where the characterizing constant J_A is multiplied by $\psi(t)$, a normalized retarded elasticity function, to account for the curvature present at short times. Deviations of the $J(t)$ values of ②, ③, and ④ from the torsional creep curve were examined as a function of time and are shown plotted linearly in Fig. 12. In each case the behavior appears to be linear with time, but instead of passing through the origin as would be the case with normal viscous flow, definite positive intercepts are observed. Interestingly enough these intercepts, ξ , which represent the onset of the nonlinear creep behavior, seem to occur at a critical strain of 22%. More exactly the strains at the pertinent times are 22%, 23%, and 21% for runs ②, ③, and ④, respectively. If the deviations are considered to be due to flow which begins only at a time $t = \xi$ and which is described by a delayed viscosity η_D , then the behavior observed may be described by the following two equations:

$$J(t) = J_A \psi(t) + \beta t^{1/3}, \quad \gamma < 0.22, \quad [6]$$

and

$$J(t) = J_A \psi(t) + \beta t^{1/3} + \frac{t - \xi(\bar{\gamma})}{\eta_D(\bar{\gamma})}, \quad \gamma > 0.22. \quad [7]$$

The time ξ and the delayed viscosity are functions of the applied stress, $\bar{\gamma}$. The values of these quantities obtained from the derived data in Fig. 12 are given in Table VI.

In an attempt to determine if the above deviations from stress-strain linearity lead in fact to irrecoverable deformation, the recovery of run ④, the run with the highest stress and shortest creep time, was followed to completion. The results of this and other recovery runs are presented in

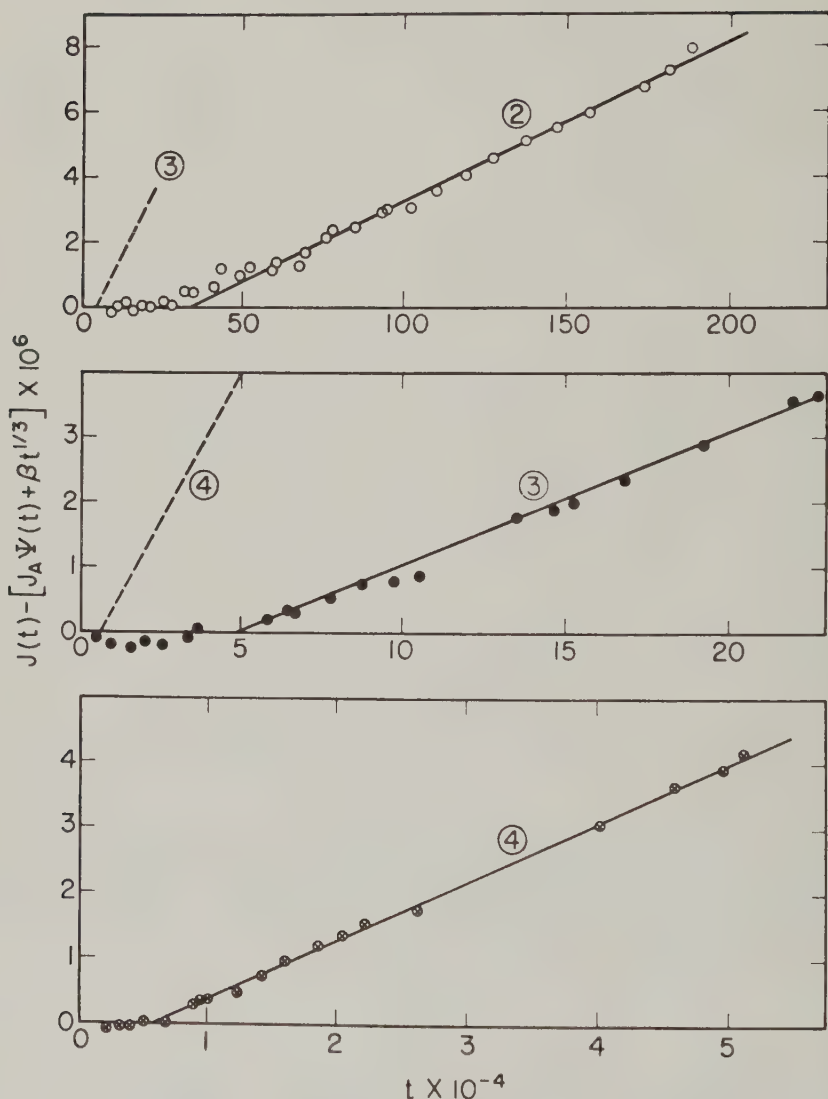


FIG. 12. Deviations from linear behavior of creep compliance values, plotted against linear time. Numbers correspond to runs shown in Fig. 11.

Fig. 13. The recovery of the torsional creep run shown in Fig. 7 is given and the lines drawn for this run and simple shear ① are calculated using Eq. [1]. Where nonlinear behavior is observed recovery curves cannot be calculated utilizing the Boltzmann superposition principle *per se*, but if the notion of a delayed viscosity is accepted the equation

$$\gamma_r(t)/5 = J(t)_{\text{linear}} - J(t - \theta)_{\text{linear}} + (\theta - \xi)/\eta_D \quad [8]$$

can be developed employing the underlying notions of the superposition principle. The lines drawn for runs (2), (3), and (4) were calculated using Eq. [8] where the linear compliance curve $J(t)_{\text{linear}}$ is assumed to represent the recoverable portion of the nonlinear compliance. Looking first at curve (4) we see that for a period of about the last 6 weeks that the recovery was observed there was no significant change in the amount of strain remaining. Therefore, the amount of permanent strain remaining can be taken to be 5.2%, which is 70% of the amount predicted. The disagreement existing between the other recoveries and their predicted curves do not permit any conclusive statements concerning the existence of a delayed viscous deformation. Further study will be necessary to eliminate the possibility that the nonlinear deformation is entirely recoverable.

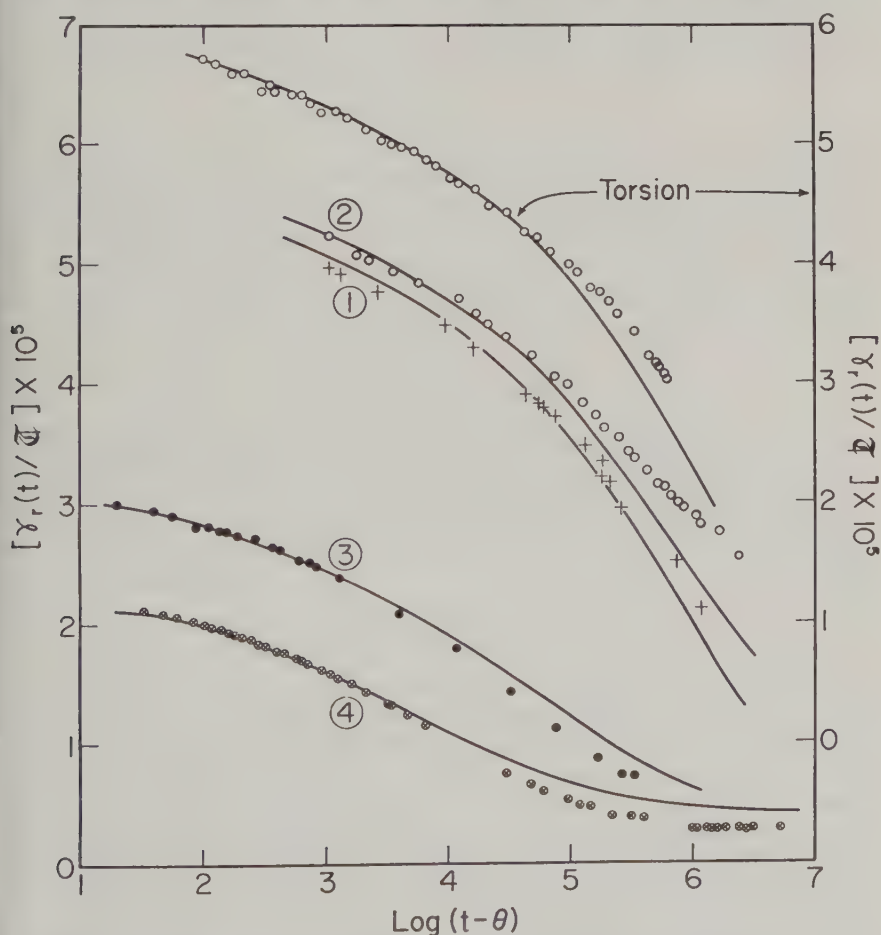


FIG. 13. Recovery measurements of runs displayed in Figs. 7 and 11 plotted versus $\log(t - \theta)$, the time of recovery. Lines are calculated; see text for details.

DISCUSSION

The Monomeric Friction Coefficient

Because of the well-known rubbery character of polydimethyl siloxane, presumably reflecting an unusually high chain mobility, the monomeric friction coefficient is of considerable interest. This quantity cannot be calculated from the relaxation spectrum in the usual manner (30), since the measurements did not extend into the transition zone. However, it can be estimated by an indirect method from the terminal zones of Stocks II and III as portrayed in Fig. 4.

The terminal Rouse relaxation time τ_1 can be estimated either by matching the dispersion of η' and G' in Fig. 4 to reduced logarithmic plots of the Rouse functions for these quantities (22, 31), or in accordance with the modified Rouse theory (22) directly from the molecular weight and viscosity by the equation

$$\tau_1 = 6\eta M / \pi^2 \rho RT. \quad [9]$$

Values obtained by both these methods are listed in Table VII, and are in quite good agreement for each of the two stocks. In the terminal zone, coupling entanglement causes the effective friction coefficient for long relaxation times to be larger by a factor Q_e than the friction coefficient applicable in the transition zone; following the concepts of Bueche (22, 32), Q_e can be calculated as

$$Q_e = (M/2M_e)^{2.4}, \quad [10]$$

where M_e is the molecular weight between coupling entanglements. Values of Q_e , taking M as the weight-average molecular weight and M_e as 17,600 from the compilation of Fox (21), are also given in Table VII. Finally, the modified Rouse theory (33) gives the monomeric friction coefficient ζ_0 in terms of τ_1 :

$$\zeta_0 = 6\pi^2 \tau_1 kT / a^2 Z^2 Q_e, \quad [11]$$

TABLE VII
Derived Calculations for Stocks II and III

	II	III
Log η	6.875	4.936
Log τ_1 from Eq. [9]	2.40	-0.05
Log τ_1 from matching dispersion	2.1 \pm 0.1	-0.16
Log Q_e from Eq. [10]	3.80	2.56
Log ζ_0 from Eq. [11]	-7.12	-7.30
Log ζ_0 from matching dispersion	-7.4 \pm 0.1	-7.40

where k is Boltzmann's constant, a^2 is the mean-square end-to-end length per monomer unit, taken from the measurements of Flory and associates in dilute solution (9) as $39.4A^2$, and Z is the degree of polymerization (M/M_0 , where M_0 is the monomer molecular weight). The values of ζ_0 in Table VII agree well for the two stocks. Since $\log \zeta_0$ is about -7.3 , it can be shown (18) that the rise in G' characteristic of the beginning of the transition zone should appear at about 5.7 on the logarithmic reduced frequency scale for all the stocks. This is not inconsistent with Fig. 2, where the measurements extend only to 4.2. $\log \zeta_0$ of -7.3 may be compared with -6.8 for unvulcanized Hevea rubber and -4.35 for polyisobutylene at 298°K . (18). At low temperatures, the friction coefficient of the PDMS will be very much less than those of the others because its temperature dependence is so small. Unfortunately, it is impossible to make the comparison at T_g , because the temperature dependence of ζ_0 for PDMS near T_g is completely unknown.

The Quasi-Permanent Network in High Molecular Weight PDMS

The absence of flow at strains below 22% in the four stocks of highest molecular weight is an unexpected result. The symptoms of this feature are apparent in Fig. 6, where the logarithmic plots of stocks IA to ID are clearly of a different character from the others; in Fig. 7, where the Andrade form of the time dependence is characteristic of systems without flow (5), and the total deformation is considerably smaller than would be predicted from the relation between η and M at lower molecular weights; and in Fig. 8, where the loss tangent at low frequencies approaches the limiting value characteristic of elastic Andrade creep instead of rising steeply. Further evidence is seen in Fig. 13, where curve ① and that labeled "Torsion" show recovery from creep runs in the low-strain range. The recovery corresponds to that calculated from the Boltzmann superposition principle except at the last stages, where the relatively small deviations are of uncertain origin.

The absence of flow indicates the presence of a quasi-permanent network with linkages which are stable over long periods of time even though they cannot be chemical cross-links, as evidenced by the complete solubility of these polymers in toluene, methyl ethyl ketone, and other solvents. They can hardly be crystallites, at 25°C ., since the melting point of PDMS appears to be near -40° (19). The spacing between these linkages, M_A , can be calculated from the Andrade intercepts J_A in Table V, assuming that these reflect an equivalent equilibrium compliance. The values of M_A decrease slightly with increasing M but can be extrapolated linearly as a function of $1/M$ to obtain $M_A = 75,000$ at infinite M . The relation between M_A and M_e will be discussed presently.

When the strain exceeds 22%, this network evidently begins to rupture

with the onset of flow. The delayed viscosity calculated from the flow is strongly dependent on stress; the rate of strain, $\dot{\gamma}$, follows a hyperbolic sine law (34),

$$\dot{\gamma} = 0.575 \times 10^{-8} \sinh 3.60 \times 10^{-4} \dot{\gamma}, \quad [12]$$

so that the extrapolated viscosity at vanishing stress is 4.8×10^{11} poises. Apparent viscosities ($\eta_D = \dot{\gamma}/\dot{\gamma}$) calculated from Eq. [12] are included in Table VI and agree very well with the measured values. The constants in Eq. [12] are presumably related to the breakage of network linkages. The extrapolated viscosity may be compared with the value of 3.2×10^7 calculated from the $\eta - M$ relation at low molecular weights (21), showing that an ordinary entanglement network would flow very much more readily.

Coupling Entanglements

In stocks II and III, the quasi-permanent network described in the preceding section does not appear, but there are coupling entanglements which have already been discussed in connection with the estimates of the monomeric friction coefficient. Such entanglements are spaced about five times more closely than the linkages of the quasi-permanent network. The value of $M_c = 17,600$ for the coupling entanglements from the molecular weight dependence of viscosity (21) is reinforced by the intercept of an Andrade type of plot obtained at much shorter times than those shown in Fig. 7, using $J(t)$ values derived from dynamic data by Eq. [2]. This intercept is $0.5_0 \times 10^{-6}$ cm.²/dyne, for all stocks except III, independent of molecular weight, corresponding to $M_c = 12,000$. The presence of such entanglements might be expected, on the basis of the Bueche theory for cross-linked networks (33), to give maximum contributions to L in the neighborhood of $\log \tau = -4$, while the quasi-permanent network should give similar contributions near $\log \tau = -2.5$. A broad plateau is observed in this range in Figs. 9 and 10. However, the origin of the maxima near $\log \tau = 2.5$ in Fig. 10 is still obscure.

SUMMARY

The viscoelastic properties of six stocks of polydimethyl siloxane, with molecular weights ranging from 0.41 to 4.9×10^6 , have been studied by dynamic and creep methods, between -49° and 75°C . and from a maximum frequency of 600 cycles/sec. to a maximum time of 36 days. The methods included the Fitzgerald transducer, Morrisson-DeWitt forced oscillation torsion pendulum, Plazek freely oscillating torsion pendulum, and creep and creep recovery in torsion and in simple shear. The temperature dependence of the viscosity of the stock of lowest molecular weight, between -21° and 141°C ., corresponded to an apparent heat of activation

for flow (ΔH_η) of 3.65 kcal. All dynamic measurements at different temperatures were successfully superposed by the method of reduced variables with shift factors calculated from the viscosity temperature dependence; all measurements were presumably too far above T_g for applicability of the WLF equation.

The measurements encompassed only the plateau and terminal zones of the viscoelastic time scale; because of the very high chain mobility, the transition between rubberlike and glasslike consistency was not entered at the highest frequency and the lowest temperature. At -49° , incipient crystallization apparently occurred. For the two stocks of lowest molecular weight, measurements were extended through the terminal zone to steady-state flow, and the results appeared to be normal for linear polymers of high molecular weight. By an indirect calculation involving the terminal relaxation times, the logarithm of the monomeric friction coefficient was estimated to be -7.3 at 25°C . For the other stocks ($M_w = 2.2$ to 4.9×10^6) no perceptible flow was observed at low stresses, even though their complete solubility demonstrated absence of cross-linking. Instead, their creep at long times followed the Andrade equation, $J(t) = J_A + \beta t^{1/3}$. The intercept J_A decreased somewhat with increasing molecular weight; so did β except for one discrepancy attributed to a broad molecular weight distribution.

At higher stresses, however, a flow contribution was observed which began after a critical deformation had been exceeded; this deformation was independent of the stress magnitude and for $M_w = 3.2 \times 10^6$ corresponded to a shear strain of 22% in the sample. The effective viscosity for this delayed flow was far higher than that extrapolated from the relation between η and M_w at lower molecular weights, and it decreased sharply with increasing stress. The results suggest the presence of a quasi-permanent network intermediate in character between chemically cross-linked and entanglement networks, the linkages of which yield when a critical strain has been exceeded.

ACKNOWLEDGMENTS

The work at the University of Wisconsin was supported in part by grants from Esso Research and Engineering Corporation and the National Science Foundation. We are indebted to Dr. Bruno H. Zimm for providing the polymers, and to Mrs. W. C. Frazier and Miss Rowena M. Green for making many of the calculations.

REFERENCES

1. FERRY, J. D., in H. A. Stuart, ed., "Die Physik der Hochpolymeren," Vol. 4, Chapter 6. Springer-Verlag, Berlin, 1956.
2. TOBOLSKY, A. V., AND McLOUGHLIN, J. R., *J. Polymer Sci.* **8**, 543 (1952).
3. CHILD, W. C., JR., AND FERRY, J. D., *J. Colloid Sci.* **12**, 327 (1957).
4. LEADERMAN, H., SMITH, R. G., AND WILLIAMS, L. C., *J. Polymer Sci.* **36**, 233 (1959).

5. PLAZEK, D. J., *J. Colloid Sci.* **15**, 50 (1960).
6. KENNEDY, A. J., *J. Mech. and Phys. Solids* **1**, 172 (1953).
7. VAN HOLDE, K., *J. Polymer Sci.* **24**, 417 (1957).
8. GRUBB, W. T., AND OSTHOFF, R. C., *J. Am. Chem. Soc.* **77**, 1405 (1955).
9. FLORY, P. J., MANDELKERN, L., KINSINGER, J. B., AND SHULTZ, W. B., *J. Am. Chem. Soc.* **74**, 3364 (1952).
10. YAVORSKY, P. M., Ph.D. Thesis, University of Pittsburgh, Pittsburgh, Pennsylvania, 1956.
11. FITZGERALD, E. R., AND FERRY, J. D., *J. Colloid Sci.* **8**, 1 (1953).
12. PLAZEK, D. J., VRANCKEN, M. N., AND BERGE, J. W., *Trans. Soc. Rheology* **2**, 39 (1958).
13. MORRISON, T. E., ZAPAS, L. J., AND DEWITT, T. W., *Rev. Sci. Instr.* **26**, 357 (1955).
14. MARKOVITZ, H., ELYASH, L. J., PADDEN, F. J., JR., AND DEWITT, T. W., *J. Colloid Sci.* **10**, 165 (1955).
15. VAN HOLDE, K. E., AND WILLIAMS, J. W., *J. Polymer Sci.* **11**, 243 (1953).
16. BACON, L. R., *J. Franklin Inst.* **221**, 251 (1936).
17. FOX, T. G., AND FLORY, P. J., *J. Am. Chem. Soc.* **70**, 2384 (1948).
18. FERRY, J. D., "Viscoelastic Properties of Polymers." Wiley, New York, 1961.
19. HUGGINS, C. M., ST. PIERRE, L. E., AND BUECHE, A. M., *J. Phys. Chem.* **64**, 1304 (1960).
20. NINOMIYA, K., AND FERRY, J. D., *J. Colloid Sci.* **14**, 36 (1959).
21. FOX, T. G., GRATCH, S., AND LOSHAEK, S., in F. R. Eirich, ed., "Rheology," Vol. 1, Chapter 12. Academic Press, New York, 1956.
22. FERRY, J. D., LANDEL, R. F., AND WILLIAMS, M. L., *J. Appl. Phys.* **26**, 359 (1955).
23. BUECHE, F., *J. Appl. Phys.* **26**, 738 (1955).
24. MARVIN, R. S., in J. T. Bergen, ed., "Viscoelasticity—Phenomenological Aspects," p. 27. Academic Press, New York, 1960.
25. ANDRADE, E. N. DA C., *Proc. Roy. Soc. (London)* **A84**, 1 (1910).
26. ANDRADE, E. N. DA C., *Proc. Roy. Soc. (London)* **A254**, 291 (1960).
27. SMITH, T. L., *Trans. Soc. Rheology* **2**, 131 (1958).
28. STERN, D. M., Ph.D. Thesis, University of Wisconsin, Madison, Wisconsin, 1957.
29. FERRY, J. D., AND WILLIAMS, M. L., *J. Colloid Sci.* **7**, 347 (1952).
30. FERRY, J. D., AND LANDEL, R. F., *Kolloid-Z.* **148**, 1 (1956).
31. ROUSE, P. E., JR., *J. Chem. Phys.* **21**, 1272 (1953).
32. BUECHE, F., *J. Chem. Phys.* **20**, 1959 (1952).
33. FERRY, J. D., in H. A. Stuart, ed., "Die Physik der Hochpolymeren," Vol. 4, p. 102. Springer-Verlag, Berlin, 1956.
34. REE, T., AND EYRING, H., in F. R. Eirich, ed., "Rheology," Vol. 2, Chapter 3. Academic Press, New York, 1958.

A THEORY OF SCHAEFER'S EXPANSION PATTERNS¹

R. H. Aranow and L. Witten

RIAS, 7212 Bellona Avenue, Baltimore 12, Maryland

Received November 6, 1959; revised July 27, 1960

ABSTRACT

An attempt is made to interpret theoretically the expansion patterns observed by Schaefer when an oil drop is deposited on a water surface covered with a protein layer. Schaefer observed that the line separating the oil from the protein could be smooth, rough circular, or star-shaped. The proposed interpretation involves a type of hydrodynamic instability known as the Rayleigh-Taylor instability. Jagged or star-shaped separations indicate the presence of these hydrodynamic instabilities. They require that small perturbations of the interfacial line from smooth circular will grow rapidly with time. Since these perturbations are always present the patterns for the unstable cases will be always jagged or star-shaped. The physical criteria for the presence of these instabilities are derived, and the difference between the rough circular and star-shaped patterns is discussed.

I. INTRODUCTION

Vincent J. Schaefer (1) discovered that the spreading pattern observed when an oil drop is deposited on a water surface covered with a protein layer could take one of three general types of pattern. The lines separating the protein from the oil could be smooth, jagged, or star-shaped. The patterns observed are characteristic of the protein used and the treatment the protein has received. No satisfactory explanation for these curious results has ever been given.

For details of the experimental methods used the reader is referred to Schaefer's original paper (1). The main features of the experiment are described by Schaefer as follows. Using the example of pepsin, Schaefer writes, "Distilled water at equilibrium with the air at pH 5.8 is placed in the tray. The surface is cleaned by sweeping several times with barriers and enough indicator oil is applied to cover three-quarters of the clean surface. A cleaned platinum wire transfers a small amount of pepsin in the form of powder to the center of the surface area. It spreads on the water, forming an invisible film whose advancing border will be seen as it

¹ This research was partially supported by the United States Air Force through the Air Force Office of Scientific Research of the Air Research and Development Command, under Contract Number AF 49(638)-735. Reproduction in whole or in part is permitted for any purpose of the United States Government.

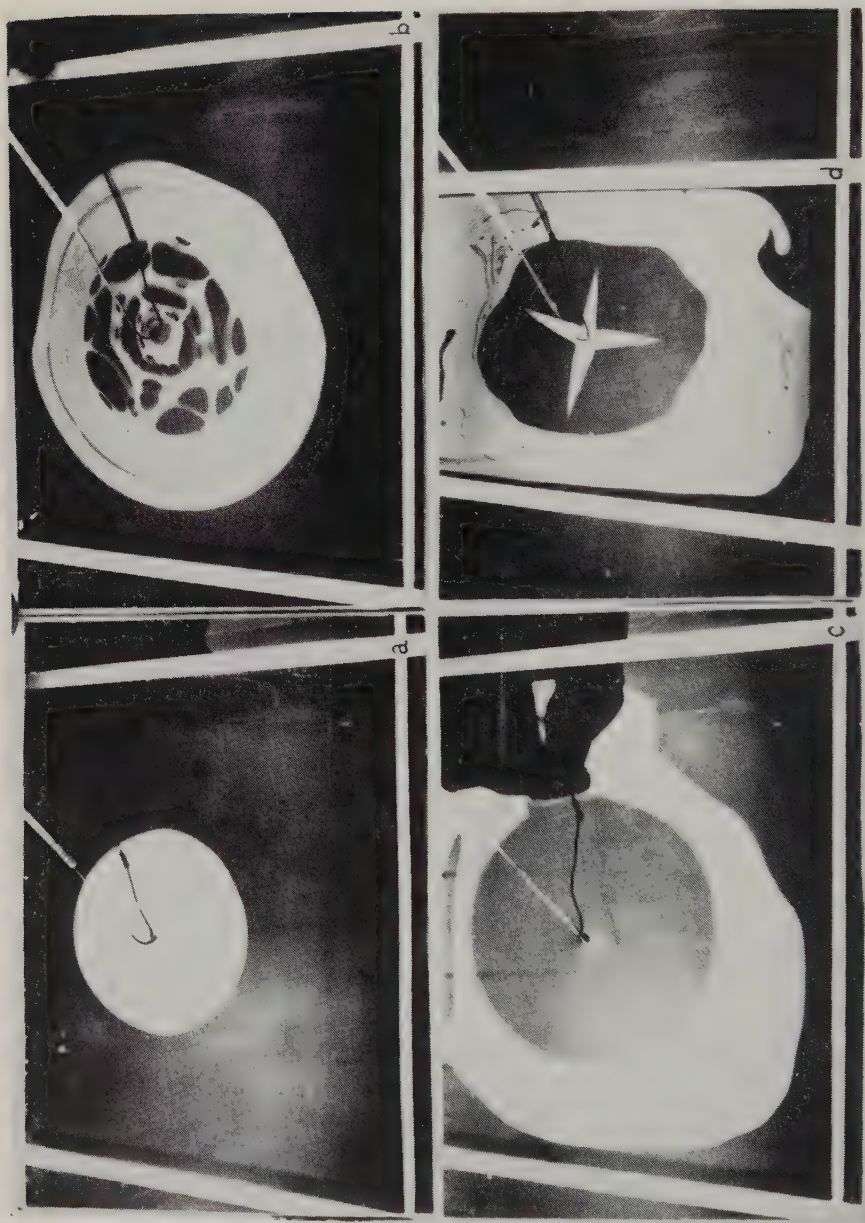


FIG. 1a. Formation of expansion pattern, *a*) Applying indicator oil, *b*) Indicator oils spreading, *c*) Applying and spreading protein, *d*) Expanding oil drop (star shape).

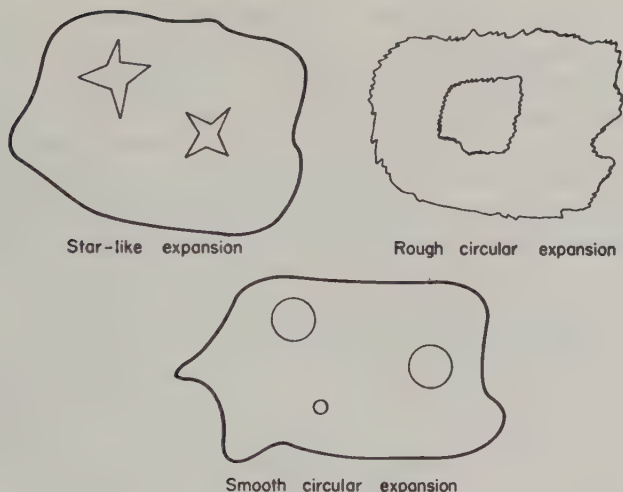


FIG. 1b. Types of spreading pattern observed by Schaefer.

drives the indicator oil ahead of it in radial directions. In the case of pepsin, this advancing film will be seen to present a smooth rounded concentric edge, of radius equal to the distance from the point of application. . . . After intimate contact is reached with the oil and the monolayer, a small drop of indicator oil is placed in the central portion and will in the case of pepsin expand to produce a geometrical figure of star-like form, with the indicator showing a peculiar gradation in color intensity appearing thinner than normal at the monolayer boundary. If other portions of the monolayer are treated in a similar way, patterns identical in every respect will be observed, indicating that the film possesses a structure which is uniform throughout, showing no memory of the point of formation." Figures 1a and 1b illustrate the experimental procedure and the types of patterns Schaefer obtained.

The purpose of this note is to propose as an explanation of these phenomena that they are manifestations of a hydrodynamic instability similar to the well-known Rayleigh-Taylor instability (2, 3). Imagine a light fluid and dense fluid in contact with each other and having a slightly irregular interface between them. The interface is subjected to an acceleration in a direction perpendicular to the interface. If the direction of the acceleration to which the boundary is subjected is from the less dense to the more dense fluid, the boundary will be unstable and will rapidly become more jagged. If the acceleration is directed from more dense to less dense the irregularities smooth out. (Note: the force per gram to which a system is subjected is equivalent in the equations of motion to an acceleration which is oppositely

directed. It is this "equivalent acceleration" to which we are referring above. Thus an upward acceleration of magnitude $|g|$ is equivalent in the equations of motion to the downward force per gram due to gravity.) The example frequently cited (3) is the glass of water at rest. The force of gravity is equivalent to an upward acceleration. The upward acceleration is directed from the more dense to the less dense medium. The surface of the water is stable and any irregularities smooth out. If the glass is inverted so that there is initially a layer of water above a layer of air, the boundary surface will be unstable. The water will fall, and the interface will become jagged and develop spikes owing to the instability. The upward acceleration is now directed from the less dense to the more dense medium.

In this paper, an analysis is made of the linearized hydrodynamic equations of motion in cylindrical coordinates for a simplified model of Schaefer's experiment. For this model the Rayleigh-Taylor type of instability occurs at the boundary under certain conditions leading to phenomena similar to that observed experimentally by Schaefer. The instability is not necessarily caused by the same mechanism as that which produces the Rayleigh-Taylor instability. In the latter case an acceleration is necessary from one medium to the second and the difference in density between the two media determines the existence of the instability. In Schaefer's experiments the lenses were so thin that on expansion the work done by surface tension becomes an important consideration. In fact the surface tension effects can possibly be far more important than gravity effects for the case here considered, as will be shown later.

The model to be studied consists of an incompressible liquid lens with circular symmetry containing two immiscible regions. The inner region (region one) has density ρ_1 . The outer region (region two), which is concentric to the first, has density ρ_2 . The lens lies on a flat plate. The objective is to study the behavior of the interface between the two regions when the interface is subjected to an arbitrary infinitesimal perturbation expressible as a Fourier series (for example, $P = \sum_{K=1} A_K \cos K\theta$). The lens is chosen so thin at the interface that its variation in behavior there with respect to the height, z , is negligible compared to the variation in behavior with respect to the radius, r , or the angle, θ , where r , θ , z are the cylindrical coordinates of a point.

We shall also study the limiting case of a monolayer (lying on a flat plate) which has two immiscible concentric regions. The compressible and incompressible monolayer will both be treated.

For the above models we solve the hydrodynamic equations of motion to first order assuming no viscous forces or surface tension. Then we treat the case with interfacial tension and surface tension and the case with viscous forces. Figure 2 shows the comparison between the mathematical

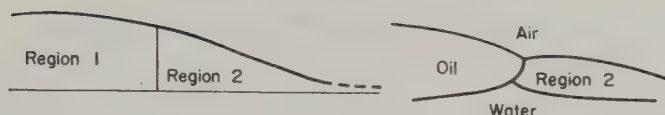


FIG. 2. Theoretical model of spreading oil drop and protein as compared with probable shape of actual spreading oil drop and protein.

model and a reasonable model of the four-phase system where all the components are mutually immiscible.

II. OUTLINE OF THE METHOD OF CALCULATION

The equation of continuity and the hydrodynamic equations of motion are to be solved.

1. Equation of continuity:

$$\operatorname{div}(\rho \mathbf{v}) = -\frac{\partial \rho}{\partial t}. \quad [1]$$

Here ρ is the density; \mathbf{v} is the velocity at the point; $\partial \rho / \partial t = 0$ for incompressible fluids.

2. Hydrodynamic equations of motion:

a. Motion in the absence of viscosity:

$$\frac{\partial \mathbf{v}}{\partial t} + (\mathbf{v} \cdot \nabla) \mathbf{v} = \mathbf{G} - \frac{1}{\rho} \operatorname{grad} P. \quad [2]$$

Here P is the pressure; G is the body force (force per gram) which for the z direction is the force due to gravity.

b. Motion of a viscous fluid:

$$\frac{\partial \mathbf{v}}{\partial t} + (\mathbf{v} \cdot \nabla) \mathbf{v} = \mathbf{G} - \frac{1}{\rho} \operatorname{grad} P - \frac{\mu}{\rho} \operatorname{curl} \operatorname{curl} \mathbf{v}, \quad [3]$$

where μ is the coefficient of viscosity.

The hydrodynamic equations of motion form a set of nonlinear differential equations which we shall solve by the method of perturbations. Expand the variables in a power series in ϵ .

$$\mathbf{v} = \mathbf{v}_0 + \epsilon \mathbf{v}_1 + \epsilon^2 \mathbf{v}_2 + \dots$$

$$P = P_0 + \epsilon P_1 + \epsilon^2 P_2 + \dots$$

$$\rho = \rho_0 + \epsilon \rho_1 + \epsilon^2 \rho_2 + \dots \quad \text{etc.}$$

The subscripts 0, 1, 2, etc., denote the "order" of the term. The various power series are then substituted in the hydrodynamic equations and the equations are solved to each order successively.

Thus, for the incompressible fluid where $\partial\rho/\partial t = 0$ and $\rho = \rho_0$, Eq [1] leads to the equations:

$$\operatorname{div} \mathbf{v}_0 = 0; \quad [4]$$

$$\operatorname{div} \mathbf{v}_1 = 0. \quad [5]$$

Equation [2] leads to the following set of equations:

$$\frac{\partial \mathbf{v}_0}{\partial t} + [\mathbf{v}_0 \cdot \nabla] \mathbf{v}_0 = \mathbf{G}_0 - \frac{1}{\rho_0} \operatorname{grad} P_0; \quad [6]$$

$$\frac{\partial \mathbf{v}_1}{\partial t} + [\mathbf{v}_0 \cdot \nabla] \mathbf{v}_1 + [\mathbf{v}_1 \cdot \nabla] \mathbf{v}_0 = \mathbf{G}_1 - \frac{1}{\rho_0} \operatorname{grad} P_1. \quad [7]$$

Here \mathbf{v}_0 and P_0 are solutions of the zeroth-order equations [4] and [6]. For mathematical simplicity we take as a solution $\mathbf{v}_0 = 0$. The essential characteristics of the instabilities we are studying are not changed by this choice of \mathbf{v}_0 while the first-order equations [5] and [7] become linear equations with constant coefficients.

The zeroth-order equation for P_0 and the first-order equations can now be solved and boundary conditions applied to the variables \mathbf{v} and P in order to determine the constants of the solution.

The boundary conditions suitable to our problem are as follows:

1. The radial velocities in medium one and two must be equal at the interface.

2. The radial velocity must be finite at $r = 0$ and $r = \infty$.

3. The pressure at a point at the interface must be the same in both media. Hence, the average pressures at the interface must also be the same in both media.

4. The velocity of the interface, $dr_i/dt = (\partial r_i/\partial \theta)\dot{\theta} + (\partial r_i/\partial Z)\dot{Z} + (\partial r_i/\partial t)$. Since $\mathbf{v}_0 = 0$, this equation imposes the requirement $dr_i/dt = \partial r_i/\partial t = v_{1r}$. (See appendix I. The appendix is not being published with this article. A copy is on file at the office of the editor of the *Journal of Colloid Science*.) Here v_{1r} is the r th component of velocity and r_i is the distance from the origin to a point on the interface. Thus $r_i = r_{i0} + \epsilon \int_0^t v_{1r} dt$.

5. The solution for angle θ must equal the solution for $\theta + 2\pi$ since the solution must be single valued.

When the effects of the boundary interfacial tension and lens surface tensions for our model are included, the boundary condition (3) is replaced by

$$(P_1 - P_2)_{\text{Average}} = \gamma_{12} \left(\frac{1}{R_1} + \frac{1}{R_2} \right) + \frac{\sqrt{(h'(r_i))^2 + 1}(\gamma_{1A} - \gamma_{2A}) + (\gamma_{1W} - \gamma_{2W})}{z_0 - h(r_i)},$$

where $z_0 - h(r_i)$ is the equation for the height of the lens at the interface; γ_{12} is the boundary interfacial tension. The subscript A refers to an interface with air and the subscript W refers to an interface with water. Here R_1 and R_2 are the radii of curvature (of two orthogonal curves at a point on and lying on the interfacial surface). The equation in the case of a very flat lens (where $h'(r_i) \ll 1$) reduces to

$$(P_1 - P_2)_{\text{Average}} = \frac{\gamma_{12}}{R_1} + \frac{(\gamma_{1A} - \gamma_{2A}) + (\gamma_{1W} - \gamma_{2W})}{z_0 - h(r_i)}.$$

This form of the boundary condition is the one which we shall use. The boundary condition equation may be easily derived by equating the work done in expanding an element of the interface, $\Delta P \cdot \Delta V$, to the work done against the surface tension on the upper and lower faces of lens plus the work done against the interfacial tension of the boundary.

For the case with viscous force conditions (1), (2), (4), and (5) are still used. In addition, the θ components of velocity and the components of the stress tensor at the interface must be equal in the two media. The interface is regarded as unstable if an arbitrary perturbation applied to the interface increases with time. If the perturbation diminishes or oscillates or remains unchanged with time the interface is stable. For the time-dependent part of the equation of the interface, r_i , a function such as $F = \exp(nt)/n$ or $G = (1/n) \cosh nt$ is used and n chosen to satisfy the appropriate boundary condition. A relationship is then established between n and the physical features of the problem: density, interfacial tension, viscosity, and wavelength (in the Fourier series expansion of the equation for the arbitrary perturbation). For $F(t) = \exp(nt)/n$ the perturbation at the interface will grow if n is positive and diminish if n is negative. For $G(t) = (\cosh nt)/n$ the interface will grow if n^2 is positive. If n^2 is negative the interface will be bounded (since $\cosh i|n|t = \cos nt$). From the relationship thus established between n and the physical features of the problem follows readily what physical conditions must be satisfied if the interface is to be stable or unstable.

The detailed calculations are given in the appendix. The results of the calculations will be stated in the following section of the paper.

III. SUMMARY OF MATHEMATICAL RESULTS

a. Lens model with no interfacial tension, no lens surface tension, and no viscosity. In the equation for the height of a point on the surface of the lens, $z_s = z_0 - h(r)$, where z_0 is the height of the center of the lens, $h(r)$ can be expanded in a Taylor's series. Thus at the interface:

$$z_{\text{interface}} = z_0 - [h(r_{i0}) + h'(r_{i0})(r_i - r_{i0}) + \dots], \quad [11]$$

where r_{i0} is the radius of the interface at zero time.

The equation for the interface is

$$r_i = r_{i0} + \epsilon \operatorname{Re} \int_0^t A_K \exp(-iK\theta) \frac{K}{r_{i0}} f(t) dt, \quad [12]$$

where the real part, denoted by the symbol Re , of $\epsilon A_K \exp(-iK\theta)$ is the expression for the applied perturbation, K being a positive integer.

If $f(t) = \sinh nt$, the equation for r_i is

$$r_i = r_{i0} + \epsilon \operatorname{Re} A_K e^{-iK\theta} \frac{K}{r_{i0}} \left[\frac{\cosh nt}{n} - 1 \right]. \quad [13]$$

From the boundary conditions we obtain (to first order) the relationship

$$n^2 = -\frac{G_0(\rho_2 - \rho_1)Kh'(r_{i0})}{2(\rho_2 + \rho_1)r_{i0}}, \quad [14]$$

where the positive constant G_0 is the magnitude of the acceleration due to gravity. For our model $h(r)$ is an increasing function of r . Hence, $h'(r_{i0})$ is a positive quantity. Thus n^2 can be positive only if $\rho_2 < \rho_1$. Hence, the interface will be unstable if the density of the inner lens is greater than that of the outer concentric lens.

b. Lens model with boundary interfacial tension and lens surface tension. The effect of adding interfacial and surface tension to the boundary conditions is that the equation for n^2 is now

$$n^2 = -\frac{\left[\frac{G_0}{2}(\rho_2 - \rho_1) + \frac{(\gamma_{1A} + \gamma_{1W}) - (\gamma_{2A} + \gamma_{2W})}{z_0 - h(r_{i0})} \right] Kh'(r_{i0})}{(\rho_2 + \rho_1)r_{i0}} + \frac{\gamma_{12}(K - K^3)}{r_{i0}^2(\rho_2 + \rho_1)}. \quad [15]$$

We see by inspection that a variety of cases governing $(\rho_2 - \rho_1)$ and the γ 's can be selected where n^2 is positive. All cases when n^2 is positive require that $\{(G_0/2)(\rho_2 - \rho_1) + [(\gamma_{1A} + \gamma_{1W}) - (\gamma_{2A} + \gamma_{2W})]/[z_0 - h(r_{i0})]\}$ be negative and the resultant first term greater than $\gamma_{12}(K - K^3)/r_{i0}^2(\rho_2 + \rho_1)$. The last requirement imposes a restriction on K . Thus

$$K < \left[1 + \left((\rho_1 - \rho_2) \frac{G_0}{2} + \frac{(\gamma_{2A} + \gamma_{2W}) - (\gamma_{1A} + \gamma_{1W})}{z_0 - h(r_{i0})} \right) \cdot \frac{h'(r_{i0})r_{i0}}{\gamma_{12}} \right]^{1/2}. \quad [16]$$

If the real part of $\epsilon A_K \exp(-iK\theta) = \epsilon A_K \cos K\theta$ (where A_K is real) is the equation for the applied perturbation, λ , the wavelength is $2\pi/K$.

The above limitation on K limits the wavelengths which are unstable to those λ such that

$$\lambda > \frac{2\pi}{\left[1 + \left(\rho_1 - \rho_2\right) \frac{G_0}{2} + \frac{(\gamma_{2A} + \gamma_{2W}) - (\gamma_{1A} + \gamma_{1W})}{z_0 - h(r_{i0})} \frac{h'(r_{i0})r_{i0}}{\gamma_{12}}\right]^{1/2}}. \quad [17]$$

The introduction of interfacial tension also limits the *rate* of growth as a function of K ; that is, a value of K can be found for which n^2 is a maximum by calculating $dn^2/dK = 0$.

$$K_{\max.} = \left[\frac{h'(r_{i0})r_{i0}}{3\gamma_{12}} \left(\rho_1 - \rho_2 \right) \frac{G_0}{2} + \frac{(\gamma_{2A} + \gamma_{2W}) - (\gamma_{1A} + \gamma_{1W})}{z_0 - h(r_{i0})} \right] + \frac{1}{3} \Bigg]^{3/2}; \quad [18]$$

and

$$n_{\max.}^2 = \frac{2\gamma_{12}}{(\rho_2 + \rho_1)r_{i0}^2} \left[\frac{(\rho_1 - \rho_2) \frac{G_0}{2} + \frac{(\gamma_{2A} + \gamma_{2W}) - (\gamma_{1A} + \gamma_{1W})}{z_0 - h(r_{i0})}}{3\gamma_{12}} + \frac{1}{3} \right]^{3/2}. \quad [19]$$

It must be noted again, however, that only integer values of K are permitted because of the periodicity condition on the θ function.

One important and interesting observation to be noted is that the lens surface tension term plays a role equivalent to a body force. Thus it is possible for instabilities to exist in systems where $\rho_1 \leq \rho_2$. This is, in fact, probably the situation for the case we are considering. The density of crystalline protein is more than the density of oil; we can perhaps suppose that in some cases the density of the denatured protein used by Schaefer is also more than the density of oil. Hence ρ_1 may be less than ρ_2 and, if this is so, the driving mechanism for the instabilities observed by Schaefer would be the lens surface tension effects.

c. Lens model with viscosity. The effect of viscosity is to inhibit the growth of high-frequency components in particular and all components in general of a perturbation. When, in addition, interfacial tension is also considered the effect of viscosity is to shift the maximum value of K to smaller K (and hence longer wavelengths). The details of the effect of surface (interfacial) tension combined with viscosity have been worked out by Bellman and Pennington (3) for a model where two infinite media are separated by an accelerated interface. The qualitative results for their model are expected to be the same as for ours. Figure 3 summarizes the relationships between n and K which were obtained by Bellman and Pennington.

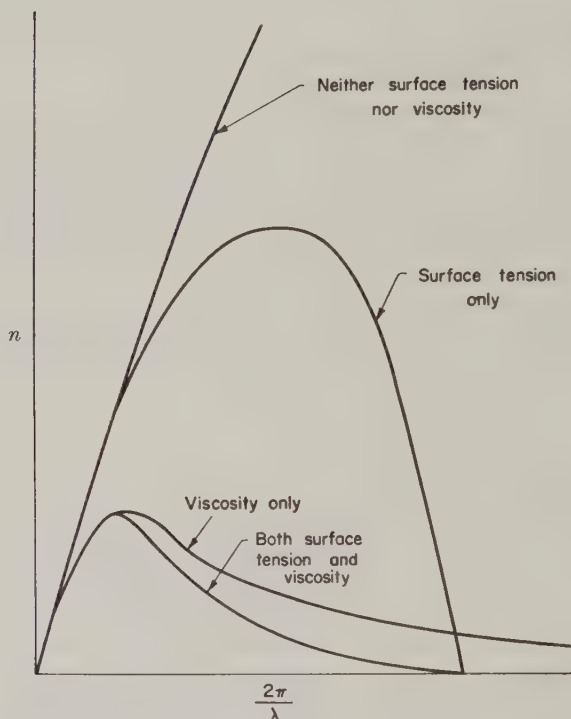


FIG. 3. Graph of n vs. wave number, where n is the coefficient in a function of time such as $f(t) = e^{nt}$. These results were obtained by Bellman and Pennington for a model of two infinite liquid media separated by an interface.

d. Monolayers. An arbitrary perturbation applied to the boundary (with or without boundary and surface tension) between the two media of this model will not grow. This result may be derived independently or considered as a special limiting case where $h'(r_{i0}) = 0$ and hence $n = 0$ (or $n < 0$ when boundary tension is considered). The result is the same for both the compressible and incompressible monolayer. Since $n = 0$ the perturbation will neither grow nor decay in time, and the interface will have a random appearance depending on the nature of the perturbations it experiences.

e. Compressible systems with no viscosity, interfacial tension, or surface tension. In order that an analysis of this case be possible it is necessary to know the equations of state of the two fluids. On the assumption that both fluids obey expressions of the adiabatic type, $P\rho_\rho^{-\gamma} = \text{constant}$ ($\gamma = \text{arbitrary positive parameter}$), an analysis has been made which shows that the interface will be unstable if the zeroth-order density, ρ_0 , of the inner lens is greater than the zeroth-order density of the outer lens. The analysis for this case is not included in the appendices because it is long and pro-

ceeds in a manner entirely analogous to the other calculations which are explicitly shown.

f. Discussion of the physical significance of the results. The model differs from reality in several features. The real system is not lying on a flat rigid plate but on a fluid immiscible subsystem, water, with which the real system interacts. The real system is a lens the curvature of which is governed by the air-oil, oil-water, air-protein, and water-protein interfacial tensions. However, qualitatively the model corresponds in many ways to the real system. For example, the gradation in color intensity of the oil star observed by Schaefer corresponds to a varying thickness of the oil layer and serves as visual proof of the existence of a thin "lens" of oil.

The model offers an explanation for the appearance of stars with a definite number of points. The number corresponds to that K for which the growth is a maximum. (Note: $K_{\max.}$ is a function of the density difference ($\rho_1 - \rho_2$) and surface tension differences, as well as other variables.) The model also explains why some proteins have starlike form with thin sharp spikes for points, whereas others have the same number of points but have broad "fat" spikes. If the Fourier expansion of the equation for the star be developed the sharper system will correspond to one with more high-frequency terms than the broader system. Also the rate of growth of comparable wavelengths must be greater for the sharper system than for the broader system. Since the introduction of viscosity has the effect of diminishing the rate of growth of high-frequency components in particular and all components in general, one might expect that a more viscous protein would exhibit broader star points.

The rough circular (or jagged) expansion figures of wheat gliadin may be explained as systems with low viscosity where the high-frequency cutoff (due to interfacial tension) occurs at very high wavelengths. The curve of n vs. K is thus broad around $K_{\max.}$, permitting many wavelengths to grow with equal rapidity. Hence, an arbitrary random perturbation will retain much of its arbitrary random character.

Truly circular smooth expansion patterns correspond to the stable interface.

Schaefer demonstrated the effect of heat denaturation of the protein pepsin. He first observed a broadening of the star spikes (probably the effect of increasing viscosity). After a long period of denaturation the oil drop took an elliptical form ($K_{\max.} = 1$) and then finally a smooth circular form. (Note: each of the above observations was made with a freshly introduced oil drop. The changes observed were not changes in a particular oil drop.) A shift in the value of $K_{\max.}$ from high to low either may be associated with a decrease in the density difference between protein and water for those cases where water has a greater density or may be associated with a decrease in surface tension terms ($\gamma_{2A} + \gamma_{2W}$) and a rise in the boundary

tension γ_{12} . Another effect of viscosity when the viscosity terms dominate the surface tension and density terms is to cause a shift of K_{\max} to lower values of K . Denaturation by ultraviolet light and by shaking may also be shown in these terms. Schaefer also observed changes in pattern observed when the protein was spread on solutions of different pH and different salt species and concentrations. The changes observed can most probably be correlated with changes in γ_{2W} and γ_{1W} .

The exact nature of the protein film that Schaefer observed is not well established, although it is generally assumed they were monolayers. Their density, viscosity, film thickness, and state of internal molecular randomness are all properties which have not been precisely determined. Moreover, the nature of the film at an advancing interface (a nonequilibrium situation) is not known. One question, for example, is whether or not there is local pile-up of protein molecules at the advancing interface. The precise meaning of the term $(\gamma_{2A} + \gamma_{2W})$ thus is in doubt. For example, for a monomolecular layer $(\gamma_{2A} + \gamma_{2W})$ reduces simply to the single γ associated with a monomolecular layer.

Until these issues have been resolved, our explanation of the expansion patterns can be offered only as a tentative explanation which has qualitative significance and which contains sufficient internal flexibility to offer reasons for all the physical phenomena Schaefer observed.

ACKNOWLEDGMENTS

The authors are grateful to Dr. Vincent J. Schaefer for providing us with the original photographs of his work and to Dr. C. H. Barkelew of Shell Development Company for his valuable suggestion concerning the treatment of lens surface tension.

Editors Note: Owing to limitations of space the appendix giving the detailed mathematical sequence of operations is not to be published. A copy is on file at the Editorial Office. The authors will communicate directly with those who are interested in the full proof.

REFERENCES

1. SCHAEFER, V. J., *J. Phys. Chem.* **42**, 1089 (1938).
2. TAYLOR, G. I., *Proc. Roy. Soc. (A)* **201**, 192 (1950).
3. BELLMAN, R. and PENNINGTON, R. H., *Quart. of Appl. Math.* **12**, 151 (1954).
4. PIPES, L. A., *Applied Mathematics for Engineers and Physicists*. McGraw-Hill, N. Y. 1946, p. 317.

ADSORPTION SELECTIVITY AND ELECTROSTATIC FIELDS OF RUTILE POWDERS

Luis A. Romo

*The Pigments Department, E. I. du Pont de Nemours and Company, Inc., Newport,
Delaware*

Received August 23, 1960; revised November 15, 1960

ABSTRACT

The surface properties of samples of rutile powder with different surface composition have been characterized by determining the preferential adsorption of *n*-butyl alcohol from binary solutions containing toluene and by estimating the electrostatic fields of the solid surfaces from heats of emersion obtained with liquids of various polarities. The surface polarity of rutile powders is greatly dependent on the chemical composition of the surfaces. These two methods can be used independently to characterize the polarity of solid surfaces since they lead to similar conclusions.

INTRODUCTION

A knowledge of the surface properties of finely divided powders is essential to the basic understanding of many processes which are controlled by the nature of the interface.

Heats of immersion have been used widely since the advent of high-precision calorimetry (1-3) in an attempt to characterize solid surfaces. The energy of adsorption, the affinity of a liquid for a solid, and the specific surface areas have been assessed by this technique (4, 5).

Harkins and Dahlstrom (1) were the first to establish that the heat of immersion of a powder increases with the polarity of the immersing liquids. More recently, Healey and co-workers (6) have used heat of immersion data obtained with liquids of various polarities to estimate the polarity of the surfaces of various powders.

However, there are factors which can complicate the interpretation of heat of immersion data. Thus, it appeared desirable to obtain, in addition, independent measurements of selective adsorption for polar molecules from binary solutions. These combined measurements should provide a meaningful characterization of those properties of the solid-surface which determine the nature of the interface with liquid media.

The lack of comprehensive information on the nature of powders used for surface studies greatly handicaps the evaluation of the results reported in the literature (1, 3-6, 10). Prior to any surface study, a characterization

of the powders used is essential because solid surfaces can be modified very significantly by additives.

This investigation was carried out to characterize by the methods mentioned above the surface properties of two samples of rutile titanium dioxide powders which were known to have surfaces which differ in chemical composition.

EXPERIMENTAL

A. Materials

Two samples of the rutile modification of titanium dioxide, R-40G and R-50G, were used. The former is rutile which received no surface treatment of any kind, whereas the latter received a surface treatment of silica and alumina hydrate. The relevant properties of these two powders are given in Table I.

The liquids used to measure the heats of immersion (11) were reagent grade *n*-heptane, *n*-butylamine, *n*-butyl alcohol, and *n*-butyl chloride which were dried by eluting them through a column of clean silica gel. The *n*-butyl alcohol and toluene used for the adsorption experiments were also dry reagent-grade chemicals.

B. Methods

1. Measurements of heats of immersion. The heats of immersion of these powders were measured following the techniques developed in our laboratory. Samples of 5.000 g. each were degassed and activated in thin glass bulbs of spherical shape at a temperature of $250^{\circ} \pm 1^{\circ}\text{C}$. by pulling a vacuum of 10^{-3} mm. Hg for 16 hours followed by 6 hours of a vacuum of 10^{-6} mm. Hg. A liquid nitrogen trap was used between the oil diffusion pump and the high vacuum manifold. The thin glass bulbs containing the activated powders were then sealed under vacuum *in situ* with a torch. Then, these bulbs were joined to glass stems before placing them in the calorimetric flasks containing 250.0 ml. of dry liquid. The calorimeter used is

TABLE I
Properties of Rutile Powders

Property	R-40G	R-50G
Rutile content of TiO_2	100%	100%
Mean particle size	0.22 ± 0.06 micron	0.22 ± 0.06 micron
Alumina content (Al_2O_3)	0.06%	1.95%
Silica content (SiO_2)	0	0.70%
pH of aqueous suspension	7.50	7.20
Resistivity of suspension	7500 ohm-cm.	8300 ohm-cm.
BET surface area	6.35 ± 0.07 m. ² /g.	11.20 ± 0.08 m. ² /g.

composed of two Dewar flasks of 500-ml. capacity which are imbedded into a cushion of polyurethane foam. The flasks are stoppered tightly with blocks of Lucite covered with aluminum foil. This cushion is placed inside an insulated wooden box on a moving platform which has a circular motion to shake the liquid in the flasks. For these measurements the box was thermostated to maintain a temperature $30.0^{\circ} \pm 0.10^{\circ}\text{C}$.

As the sensing element to detect the heat effects, a 10-junction thermocouple of iron-constantan calibrated with reference to a junction at 0°C . was used. The multijunction thermocouple emf's were measured by a Microspan multirange potentiometer with a maximum span of 10^{-8} volt per a recording division of 0.28 cm. In all our measurements, we have used an amplification which detects temperature changes of 0.00025°C . per division.

The errors which are due to the heat of bulk breaking (+), the heat of vaporization (-), and the work of atmospheric pressure (+), were determined by measuring the heat evolved by breaking evacuated bulks in the immersing liquids used for the heats of immersion measurements. The overall average systematic error is 0.06 cal. Thus, the quantity was subtracted from the total heats (calories) recorded for each sample of powder. Since traces of water significantly vitiate the heats of immersion (1), precautions were taken to maintain the Dewar flasks and reagents absolutely dry.

For calibration purposes, the small temperature changes recorded for the heats of immersion of the powders were compared with the temperature changes caused by a known amount of electrical energy which was introduced into the calorimeter by a suitable heater. An attempt was made to introduce amounts of heat which have a total curve height of similar magnitude to those recorded for the actual heats of immersion. The agreement between successive values of heat energy equivalents (calories/division) was within $\pm 1.0\%$.

The heats of emersion¹ of these two powders in *n*-butane derivatives with various dipole moments (7-9) are presented in Table II.

2. Measurement of adsorption selectivity. The adsorption exhibited by the two rutile powders for polar molecules was measured by equilibrating activated samples with binary solutions of dry *n*-butyl alcohol and toluene covering the concentration range of 0 to 1 mole fraction.

The solutions were prepared by weighing suitable aliquots of dry reagent-grade *n*-butyl alcohol with a sensitive analytical balance and making them to volume with dry reagent-grade toluene in flasks calibrated volumetrically at 25.0°C .

Each of a series of 5.000-g. samples of the powders used for the adsorption experiments was placed in a calibrated adsorption tube equipped with

¹ The heat of emersion, H_e (+), is opposite in sign to the heat of immersion, H_i (-).

TABLE II
Heats of Emersion of Activated Rutile Powders

Immersing liquids	Heats of emersion ^a	
	Rutile 40G (ergs cm. ⁻²)	Rutile 50G
<i>n</i> -Heptane	144 ± 7	150 ± 6
<i>n</i> -Butylamine	258 ± 4	322 ± 6
<i>n</i> -Butyl alcohol	303 ± 9	380 ± 10
<i>n</i> -Butyl chloride	350 ± 12	457 ± 17

^a Averages of three independent determinations.

a stopcock and a tapered joint for connection with a vacuum manifold. The tubes were joined to a high vacuum manifold and evacuated overnight at $120^\circ \pm 2^\circ\text{C}$. by pulling a vacuum of 10^{-3} mm. Hg followed by 6 hours of a vacuum of 10^{-6} mm. Hg. Then, the stopcocks were closed and the solutions added up to the 20.00 ml. calibration mark using the vacuum to suck in the liquids. The tubes were then sealed and shaken vigorously. They were allowed to stand at $25.0^\circ \pm 0.5^\circ\text{C}$. and shaken once everyday for two weeks to attain equilibrium.

The changes in concentration of *n*-butyl alcohol in the binary solutions effected by adsorption were determined with a Zeiss interferometer by comparing the interferometric readings of the solutions before and after adsorption. The actual values in moles were obtained from a previously established working curve where interferometric readings were plotted against corresponding small known changes in concentrations of *n*-butyl alcohol. The analytical values ΔC thus obtained computed for 1.000-g. samples of activated powders are given in Table IV, columns 4 and 5.

It should be noted that the ΔC values are the concentration changes due to the simultaneous adsorption of both *n*-butyl alcohol and toluene. Since there can be no concentration changes at $x_1 = 0$ and $x_1 = 1$, it follows that at these points, $\Delta C = 0$.

RESULTS

Electrostatic Field Strengths of the Surfaces

The plots of Fig. 1 show a linear relationship between H_e and μ . Therefore, their functional relationships can be expressed as follows:

$$H_e = H_0 + nP\mu,$$

where H_e is the heat of emersion, ergs cm.⁻², H_0 is the heat of emersion measured in a liquid with zero dipole moment, and n is the number of dipoles covering 1 cm.⁻² of solid surface. The significance of P can be evalu-

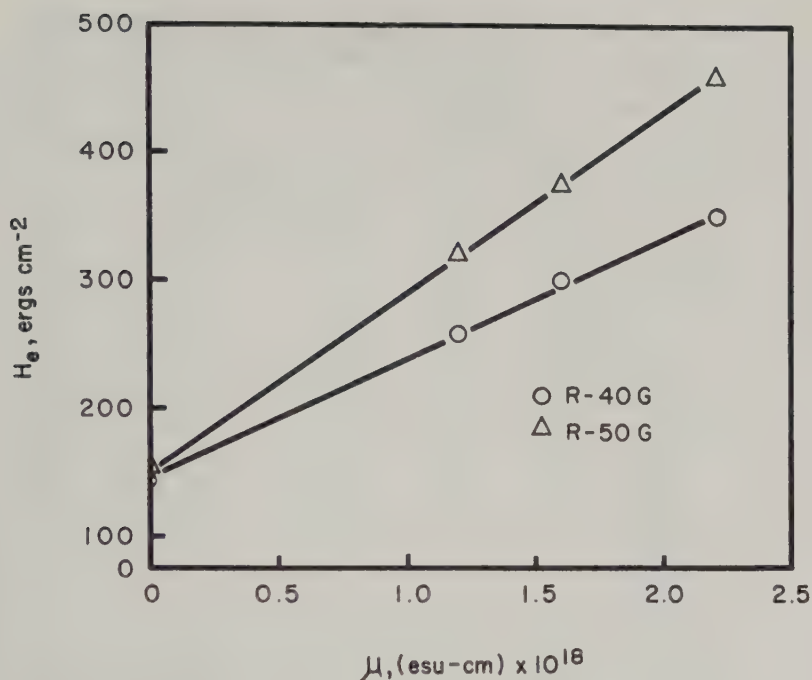


Fig. 1. Heats of emersion of rutiles vs. dipole moments of liquids.

TABLE III

The Electrostatic Field Strengths of the Surfaces of Activated Rutile Powders

Rutile powder	$\Delta H_e/\Delta\mu$	P -Factor (e.s.u.-cm. $^{-2}$)
Rutile 40G	0.91×10^{20}	2.00×10^5
Rutile 50G	1.44×10^{20}	3.18×10^5

ated by determining its dimensions since it is actually a ratio of H_e to μ . The c.g.s. dimensions of H_e are $ML^2T^{-2} \times L^{-2}$ and the c.g.s.-e.s.u. dimensions of μ are $E^{1/2}M^{1/2}L^{3/2}T^{-1} \times L$; consequently, the corresponding dimensions of P are $(E^{-1/2}M^{1/2}L^{-1/2}T^{-1})L^{-2}$. Thus, P has the dimensions of electrostatic field strength per unit of area. To find the value of P , one must know the areas of coverage of the *n*-butyl derivatives used to measure the heats of emersion. We have used a value of 22 \AA^2 as the average area of coverage of these molecular species. Therefore, $n = 4.55 \times 10^{14}$ molecules cm^{-2} . Consequently,

$$P = (\Delta H_e/\Delta\mu)/4.55 \times 10^{14}.$$

The values of P calculated on this basis are given in Table III.

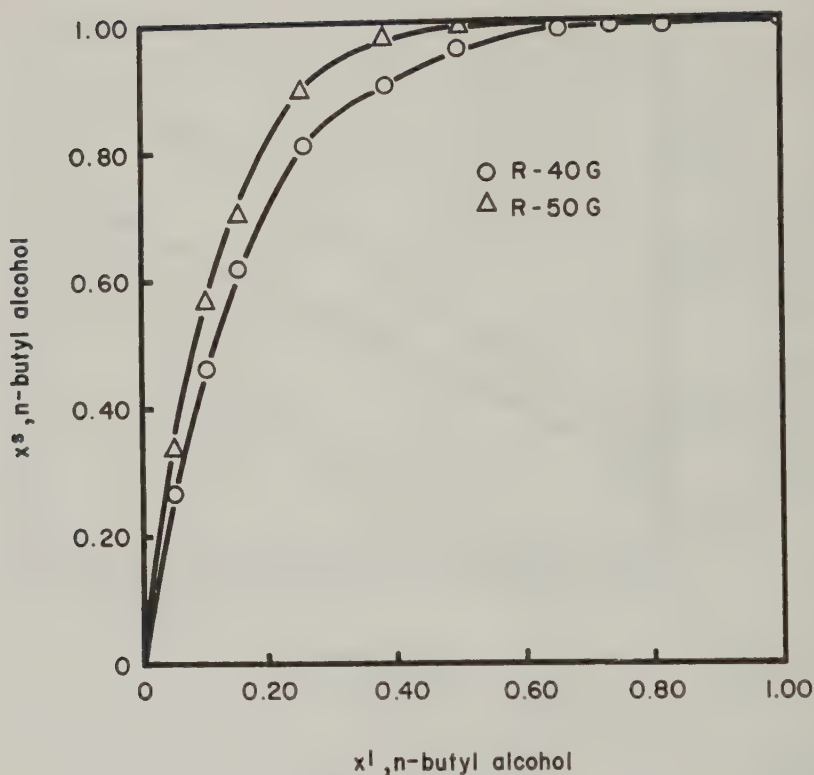


FIG. 2. Adsorption isotherms of *n*-butyl alcohol on rutiles from solutions containing toluene.

Adsorption Isotherms

The individual adsorption isotherms of *n*-butyl alcohol and toluene (Fig. 2) can be derived from the corresponding binary adsorption isotherms (Table IV, columns 3-6, 7).

For monolayer adsorption as proposed by Guggenheim and Adam (12)

$$a_1 n_1^s + a_2 n_2^s = a_p,$$

where n_1^s and n_2^s are the number of moles of *n*-butyl alcohol and toluene adsorbed by 1.000 g. of powder; a_1 and a_2 are the areas of monolayer coverage per mole of *n*-butyl alcohol and toluene; and a_p is the surface area of 1.000 g. of powder (Table I).

As has been shown previously (13), the concentration changes are related to the number of moles of components 1 and 2 adsorbed by the solid from the binary solutions by the equation:

$$(1 - x)n_1^s - xn_2^s = n_0 \Delta x,$$

TABLE IV

Molar Concentration Changes and Binary Adsorption of n-Butyl Alcohol and Toluene by Rutile Powders

n_1 , moles <i>n</i> -butyl alcohol	n_2 , moles toluene	x , m.f. <i>n</i> - butyl alcohol	ΔC moles/gram $\times 10^5$		$n_0 \Delta x$ /gram $\times 10^5$	
			R-40G	R-50G	R-40G	R-50G
0.00190	0.03343	0.0539	0.60	1.40	0.579	1.330
0.00386	0.03185	0.1082	1.20	3.00	1.028	2.636
0.00572	0.03036	0.1584	1.90	4.40	1.540	3.330
0.00952	0.02730	0.2587	3.00	6.50	2.228	4.831
0.01424	0.02270	0.3855	3.60	8.11	2.209	4.987
0.01905	0.01963	0.4925	4.00	9.00	2.130	4.777
0.02286	0.01657	0.5798	4.20	9.20	1.999	4.108
0.02667	0.01350	0.6640	4.50	9.10	1.912	3.463
0.03048	0.01044	0.7449	4.40	8.50	0.827	1.874
0.03430	0.00737	0.8231	3.70	7.10	0.821	1.425
0.03810	0.00431	0.8984	2.80	5.40	0.284	0.547
0.04150	0.00157	0.9635	1.40	3.20	0.103	0.116

where x is the mole fraction of *n*-butyl alcohol in the binary solutions; n_0 is the sum of the number of moles of the two components in the solutions (Table IV, columns 1, 2), and Δx is the apparent mole fraction change of *n*-butyl alcohol due to adsorption when 1.000 g. of powder is equilibrated with n_0 moles of binary solution.

In cases where monolayer adsorption prevails, these equations can be used to calculate the mole fraction of *n*-butyl alcohol and toluene adsorbed by the rutile powders

$$x_1^s = \frac{a_2 n_0 \Delta x + x a_p}{n_0 \Delta x (a_2 - a_1) + a_p}$$

and

$$x_2^s = 1 - x_1^s$$

In the calculations with these equations, values of 22.0 Å.² and 45.0 Å.² were used for the areas of coverage per molecule of *n*-butyl alcohol and toluene, respectively. These values are in fair agreement with those obtained by Harkins (4), Craig and co-workers (14), and Kisilev and co-workers (15). Therefore, the monolayer coverages per mole are: $a_1 = 1.32 \times 10^9$ cm.²/mole, $a_2 = 2.70 \times 10^9$ /mole. The specific surface areas a_p of the two powders (Table I) were determined on activated samples degassed at 120°C. for 2 hours with vacuum of 10^{-6} mm. Hg, by measuring their nitrogen adsorption following the B.E.T. method (16).

DISCUSSION

The electrostatic field strengths (P) of the solid surfaces were estimated by a direct analysis of the linear plots of the heats of emersion obtained with liquids of various dipole moments (Fig. 1). It appears that the linear relationship between H_e and μ arises because the surface polarizability, the angular orientation of the adsorbed dipoles on the surface, the number of *n*-butyl molecules adsorbed per unit of area, and the intermolecular interactions of the adsorbed dipoles must be approximately the same for rutile powders which have heteropolar surfaces (17, 18). Other workers (6) have used H_e - μ plots to estimate surface polarity of solids by analogy with the field equation $E = -\mu F \cos \theta$.

The similarity of the heats of emersion values of rutile powders immersed in heptane and other hydrocarbons² is attributed to the fact that in similar powders the ratios of heats of adsorption and the areas of coverage of adsorbed hydrocarbon molecules are fairly constant (19). Moreover, rutile powders with different surface electrostatic fields are characterized by a value of H_e which is constant when measured with a nonpolar hydrocarbon. This value of $H_0 = \lim_{\mu \rightarrow 0} H_e$ appears to be a parameter of the particular polar solid-nonpolar liquid interface.

It is interesting to observe that our average limiting value of $H_0 = 147 \pm 9$ ergs cm.⁻² (Table II) agrees very well with the value of 149 ± 9 ergs cm.⁻² reported by other workers (6) for a sample of rutile with a BET surface area of 7.3 m.²/gram.

The binary adsorption isotherms (Table IV, columns 3, 6, 7) indicate that both powders have adsorbed *n*-butyl alcohol preferentially throughout the whole concentration range. To determine whether the two rutile powders exhibit proportionally different preferential adsorptions for *n*-butyl alcohol from the binary solutions, the individual adsorption isotherms were calculated from the binary adsorption data. To do this, it was necessary to recognize that the solid surface is continuously covered by the liquid phase and to make two assumptions. The first is (a) that the areas of coverage of the two molecular species are constant in the adsorbed layer throughout the whole concentration range. However, since the geometry of the adsorbed layer may vary as the ratio of the two molecular species is changed in the binary solutions, the areas of coverage of the adsorbed molecules may change accordingly. To simplify the interpretation of adsorption data, it is customary to use the areas of coverage of the molecular species calculated from monolayer coverage of vapor adsorption isotherms or, as has been proposed more recently (15), to calculate the average areas of coverage of the adsorbed molecules from binary adsorption isotherms. The second as-

² The heats of emersion of these rutile powders in hexane and octane are 145 ± 8 and 148 ± 10 ergs cm.⁻², respectively.

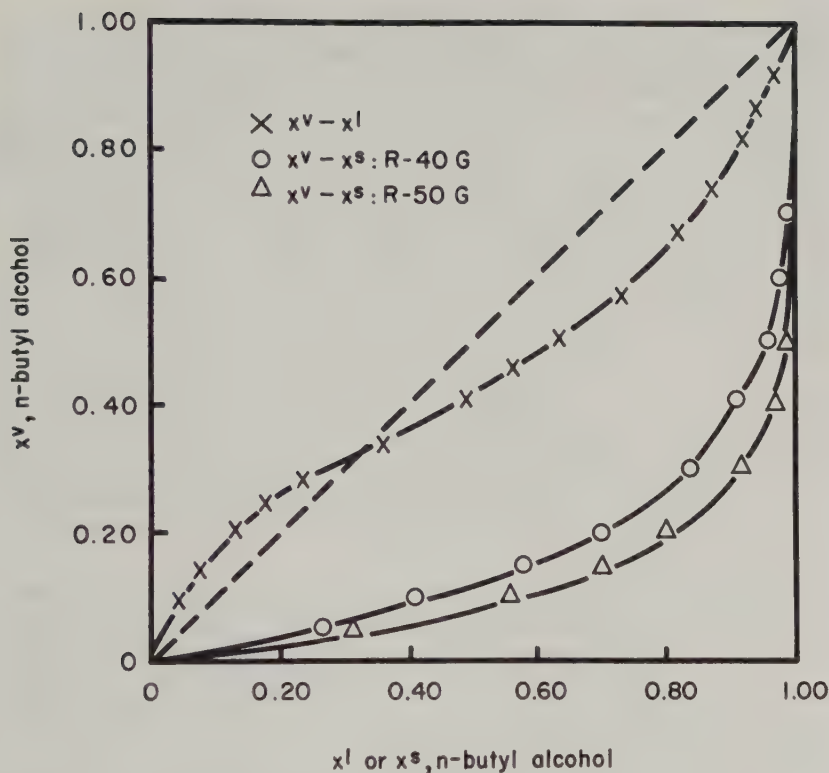


FIG. 3. *n*-Butyl alcohol mole fractions of vapor vs. liquid and adsorbed by rutile powders.

sumption is (*b*) that the adsorbed molecules of butyl alcohol and toluene form a monolayer. Monolayer adsorption has been observed to take place on carbon blacks, alumina, and silica powders from various organics (15, 19-21).

The mole fraction adsorption isotherms (Fig. 2) reveal that powder R-50G adsorbs proportionally more alcohol from the binary solutions than powder R-40G. The significance of preferential adsorption can be elucidated by comparing the vapor mole fractions of *n*-butyl alcohol (x^v) which do not depart significantly from ideality with those of the corresponding mole fractions of *n*-butyl alcohol in the binary solutions (x^l) and adsorbed on the surfaces (x^s) (Fig. 3). Firstly, one should note that at $0 < x^l < 0.33$, $x^v > x^l$ and that at $x^l > 0.33$, $x^l > x^v$. Secondly, the x^v - x^s curves are sharply displaced to the right of the x^v - x^l curve showing very distinctly the strong preferential adsorption of *n*-butyl alcohol by the TiO_2 powders. The displacements also show that this preferential adsorption is stronger in R-50G than in R-40G (Fig. 3).

Since the rutile surfaces have electrostatic fields (Table III) which interact with the *n*-butyl alcohol dipoles, it is expected that these molecules should be adsorbed on rutile surfaces preferentially over the slightly polar toluene molecules and in proportion to the magnitude of the surface electrostatic fields. The intensity of adsorption is proportional to force per unit of charge; therefore, as is shown in Figs. 2 and 3, it follows that powder R-50G adsorbs proportionally more butyl alcohol than powder R-40G.

Moreover, since the net heat of adsorption $H_a = \int_0^\theta (H_{av} - H_v) d\theta$ is related to the heat of immersion H_i by the equation

$$H_i = H_{lv} + \int_0^\theta (H_{av} - H_v) d\theta,$$

where H_{lv} is the surface enthalpy of the immersing liquid, H_{av} and H_v are its heats of vapor adsorption and condensation, respectively, and θ is the extent of coverage of the solid surface by the adsorbed layer, one can readily see that the net heat of adsorption increases linearly with the dipole moment of the immersing liquids and that the H_a - μ lines have essentially the same slopes as the H_e - μ lines.

The heats of adsorption, H_a , are actually measurements of the overall interaction of the surface with the adsorbed layer; therefore, the higher these values, the stronger should be the forces which hold the adsorbed layer onto the surfaces. This corroborative evidence substantiates the significance of preferential adsorption of a highly polar phase from binary solutions containing a slightly polar phase.

These results show that the preferential adsorption of rutile powders for polar molecules from binary solutions containing slightly polar molecules depends on the strengths of the surface electrostatic fields. The significant difference in these surface parameters is attributed to the difference in surface composition of the two powders. The activated samples of R-40G have essentially oxide surfaces with negligible hydration, whereas the activated samples of R-50G have hydroxylated surfaces because of the coverage of the oxide surfaces with silica and alumina hydrate. The elucidation of this problem is the subject of a separate investigation.

SUMMARY

The heats of emersion of two rutile, titanium dioxide powders which differ in surface composition have been measured in a series of *n*-butane derivatives with various dipole moments. An analysis of the straight line plots of heats of emersion against dipole moments show that the slopes of these lines are related to the electrostatic field strengths of the surfaces. By estimating the average areas of coverage of the *n*-butyl molecules, the surface electrostatic field intensities have been calculated. The values are 2.00×10^5 e.s.u.-cm.⁻² for R-40G and 3.18×10^5 e.s.u.-cm.⁻² for R-50G.

The binary adsorption isotherms obtained by equilibrating samples of these rutile powders with solutions of *n*-butyl alcohol and toluene covering the concentration range of zero to unity mole fraction, were used to actually derive the mole fraction adsorption isotherms. The mole fraction distributions of *n*-butyl alcohol and toluene in the adsorbed layer reveal that the molecular ratios of *n*-butyl alcohol to toluene are higher for R-50G than for R-40G throughout the whole concentration range.

It has been established that the adsorption selectivity of rutile for polar molecules depends on the electrostatic field strengths of the solid surfaces. The significant differences in these surface parameters are attributed to differences in composition of the rutile surfaces resulting from alumina hydrate and silica treatment of one of the samples.

ACKNOWLEDGMENT

The author wishes to thank Drs. B. H. Perkins and W. J. Angulo for their constructive criticisms during the preparation of the manuscript.

REFERENCES

1. HARKINS, W. D., AND DAHLSTROM, R., *Ind. Eng. Chem.* **22**, 897 (1930).
2. ZETTEMAYER, A. C., YOUNG, G. J., CHESSICK, J. J., AND HEALEY, F. H., *J. Phys. Chem.* **57**, 649 (1953).
3. BARTELL, F. E., AND SUGGIT, M. R., *J. Phys. Chem.* **58**, 36 (1954).
4. HARKINS, W. D., "The Physical Chemistry of Surface Films," pp. 210, 268. Reinhold, New York, 1952.
5. HARKINS, W. D., AND JURA, G., *J. Am. Chem. Soc.* **66**, 919 (1944).
6. HEALEY, F. H., CHESSICK, N. J., ZETTEMAYER, A. C., AND YOUNG, G. J., *J. Phys. Chem.* **58**, 887 (1954).
7. WOLF, K. L., AND GROSS, W. J., *Z. physik. Chem.* **14B**, 305 (1931).
8. HOJENDAHL, R., Thesis, Copenhagen, 1928.
9. WEISSBERGER, A., "Physical Methods in Organic Chemistry," Vol. 2, p. 1614. Interscience, New York, 1949.
10. DENNIS, K. S., PACE, E., AND BAUGHMAN, C. S., *J. Am. Chem. Soc.* **75**, 3269 (1953).
11. BOYD, G. E., AND HARKINS, W. D., *J. Am. Chem. Soc.* **64**, 1190 (1942).
12. GUGGENHEIM, E. A., AND ADAM, N. K., *Proc. Roy. Soc. (London)* **139A**, 218 (1933).
13. OSTWALD, W., AND DE IZAGUIRRE, R., *Kolloid-Z.* **30**, 279 (1922).
14. CRAIG, R. C., VAN VOORHIS, J. J., AND BARTELL, G. E., *J. Phys. Chem.* **30**, 1230 (1956).
15. KISIELEV, A. V., KHOPINA, V. V., AND ELTEKOV, A., *Izvest. Akad. Nauk S.S.S.R.* **6**, 664 (1958).
16. BRUNAUER, S., EMMETT, P. H., AND TELLER, E., *J. Am. Chem. Soc.* **60**, 309 (1938).
17. DRAIN, C. E., AND MORRISON, J. A., *Trans. Faraday Soc.* **48**, 316 (1952).
18. ZARKISOV, E. S., *Zhurn. Fiz. Khim.* **28**, 627 (1954).
19. KISIELEV, A. V., "Adsorption," *Akad. Nauk S.S.S.R.* (1959).
20. ELTON, G. A. H., *J. Chem. Soc.* **1951**, 2958.
21. KIPLING, J. J., AND TESTER, D. A., *J. Chem. Soc.* **1952**, 4123.

THE APPROACH OF GAS BUBBLES TO A GAS/LIQUID INTERFACE¹

R. S. Allan, G. E. Charles, and S. G. Mason

*Physical Chemistry Division, Pulp & Paper Research Institute of Canada, and
Department of Chemistry, McGill University, Montreal, Canada*

Received September 13, 1960; revised November 10, 1960

List of Symbols

- b = radius of bubble (Phase 1).
- c = radius of bulge created in a flat interface by a spherical bubble (Phase 1).
- c' = radius of circle of minimum separation.
- $f(h)$ = fraction of bubbles which have coalesced at or above a Phase 2 film thickness h .
- $f(\tau)$ = fraction of bubbles which have coalesced before time τ .
- g = acceleration due to gravity.
- h = Phase 2 film thickness.
- $\bar{h}, h_{1/2}$ = film thickness at $\bar{\tau}, \tau_{1/2}$, respectively.
- n = refractive index of Phase 2.
- p = η_1/η_2 = viscosity ratio.
- t = time.
- $u_{\text{exptl.}}$ = rate of bubble rise (measured).
- u_{fluid} = theoretical rate of rise of fluid sphere with internal circulation.
- u_{Stokes} = Stokes sedimentation velocity of solid sphere.
- γ = surface tension.
- λ_0, λ = wavelength of monochromatic light in air and Phase 2, respectively.
- η_1, η_2 = viscosity of Phase 1 (internal) and Phase 2 (external), respectively.
- $\Delta\rho$ = $\rho_2 - \rho_1$ = density difference of Phases 2 (external) and 1 (internal).
- τ = rest-time.
- $\bar{\tau}, \tau_{1/2}$ = mean and median rest-times.

ABSTRACT

The approach of nitrogen bubbles to the free surface of aqueous glycerol solutions and polyglycol oils was investigated using interference rings and interference colors to estimate the thickness of the liquid films. The rate of approach in close proximity to the liquid surface was found to decrease rapidly with decreasing separation. The

¹ This work was conducted with financial assistance from the Defence Research Board of Canada, DRB Grant 9510-05.

intervening liquid film deformed with progressive thinning and, eventually, was thinnest around a ring at a distance c' from the center. Analysis showed that this occurred where the upper surface started to bulge. The rate of film thinning increased with decreasing film viscosity and showed good agreement with a theoretical equation previously derived. The rupture of the intervening liquid film occurred over a range of film thicknesses in any given system, in many cases at values $< 900 \text{ \AA}$.

The effect of an added surfactant was to decrease the rate of film thinning at comparable thicknesses, increase the mean rest-time, and lead to thinner films at rupture than in the case of the pure system.

INTRODUCTION

It has been shown (1-7) that when a fluid drop (Phase 1) of density ρ_1 immersed in a liquid (Phase 2) of density ρ_2 rises ($\rho_1 < \rho_2$) or falls ($\rho_1 > \rho_2$) gently onto the interface separating Phases 1 and 2, it "rests" at the interface before coalescing with the over- or underlying phase.

For a given system, it is found that the rest-time τ of a series of identical drops defined as the interval between the arrival of the drop and its coalescence, has a distribution of values about a mean value $\bar{\tau}$.

Early investigators (8-12) attributed this temporary stability to the presence of a residual film of Phase 2 liquid between the drop and the interface which thins until it suddenly ruptures and coalescence occurs. The variation in τ is believed (2, 7) to result from a variation from drop to drop in the film thickness existing at rupture.

This investigation deals with the approach of gas bubbles to a gas/liquid interface using interference rings from monochromatic light and interference colors from white light as a means of estimating the thickness of the liquid films. Similar techniques have been used by others (13-18) under somewhat simpler conditions. In the present work, these methods were adapted to measure the rate of approach of bubbles to the interface, the shape of the intervening liquid film, and its thickness at rupture. The influence of added emulsifiers was also studied.

EXPERIMENTAL PART

1. Methods

A Reichert Zetopan research microscope with incident illuminator was used to observe the bubbles. The condenser carrier of the microscope was fitted with a specially constructed holder which accommodated a jacketed Pyrex cell in which the liquid under study was placed. The cell (*A*) is illustrated schematically in Fig. 1. The bubble-forming tip (*B*), connected to a gas cylinder through a three-way stopcock (not shown), was introduced in the liquid through the small opening (*C*) at the bottom of the cell. The end of the tip was maintained approximately 3 to 4 cm. below the surface (*D*). The opening at the top of the cell was large enough to accommodate the microscope objective (*E*) which could be focused on the liquid surface.

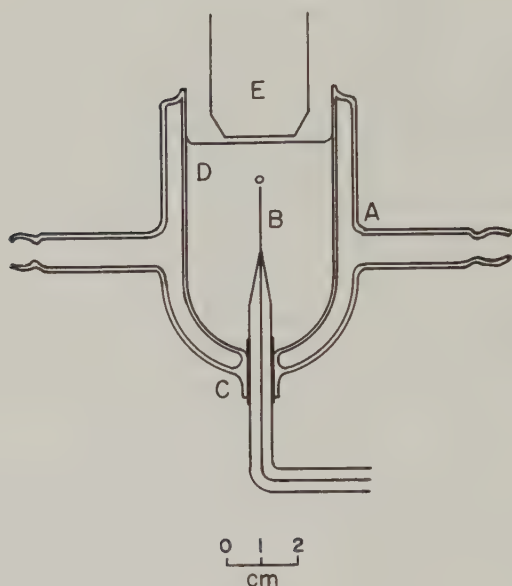


FIG. 1. Jacketed cell for gas bubbles. *A*—cell. *B*—capillary tip. *C*—opening. *D*—liquid surface. *E*—microscope objective with epi-illumination.

The liquid was protected from the atmosphere by means of a latex rubber sleeve fitted over the top of the cell and the microscope objective. The temperature in the cell was maintained at $20^{\circ} \pm 0.01^{\circ}\text{C}$. by circulating water through the jacket from a constant-temperature bath. A minimum of 1 hour was allowed to establish temperature equilibrium before each experiment.

Small bubbles were used to minimize spherical distortion. The tips employed were constructed from 0.3 mm. Pyrex capillary tubing which was heated and pulled out to hairline dimensions. Single bubbles as small as $150\ \mu$ in diameter were formed by venting the gas pressure in the capillary through the three-way stopcock immediately after bubble release. In most of the experiments, $570\ \mu$ diameter bubbles were used; the bubble size was measured by means of a graticule in the microscope eyepiece.

The monochromatic light ($\lambda_0 = 5460\ \text{\AA}$.) was from a high-intensity mercury-vapor lamp² using a No. 77A Wratten filter. Incident white light was provided by the built-in low-voltage tungsten illuminator of the microscope.

A 16 mm. high-speed Fastax (Model WF-3) cine-camera³ with a 35.6 mm.

² HBO-109, G. W. Gates & Co., Long Island, New York.

³ Wollensak Optical Co., Rochester, New York.

lens was positioned to view the field through one side of the binocular viewer of the microscope; the other side was used for visual observations.

As a bubble approached the surface, it was observed to give a constant changing pattern of Newton's rings in monochromatic light. Preliminary experiments with water revealed that the events occurred too rapidly to photograph them at the level of illumination available. By using polyglycol oils and aqueous glycerol solutions the rate of change of the interference pattern was decreased sufficiently by the increase in viscosity to be photographed.

When photographing the rings, the camera was started 1 to 2 sec. before the first appearance of the interference pattern in order to photograph at a maximum film speed of approximately 500 pictures/sec. The film speed was registered directly on the film by the built-in timing light operated at 100 impulses/sec. from a crystal-controlled pulse generator. The film thinning data were obtained by projecting the photographic film at a known magnification.

When viewed in incident white light, a changing pattern of interference colors was observed which corresponded to changing thicknesses of the intervening film. From the color pattern, the order of interference and approximate film thickness were estimated by use of the standard interference color tables (19). It was found that below the third order of interference colors (*ca.* 5000 Å.) the rate of drainage had slowed sufficiently to allow visual observations. A tape recorder was used for verbal recording of the observations, and the time between successive color changes was subsequently obtained from the playback.

The distribution of τ and the film thickness at rupture for each system were determined for at least 25 bubbles. The time interval between the arrival and the bursting of a bubble at the liquid surface was measured using a stop watch and viewing through the microscope.

Surface tension measurements were made using a ring tensiometer.

2. Materials

Glycerol (A.C.S. grade) and aqueous solutions containing 91 % and 85 % glycerol by weight, all three having approximately the same surface tension (Table I), were employed. In addition, mixtures of polyglycols⁴ having approximately the same viscosities as the glycerol solutions were used as liquids. The refractive index, n , of the liquid was determined using an Abbé refractometer, and the wavelength λ in the liquid film was found from the relationship, $\lambda = \lambda_0/n$. Likewise the thickness of the film corresponding to a given interference color was found by dividing the values for thin layers of air ($n = 1$) by the appropriate n .

⁴ Union Carbide UCON 50 HB Nos. 55, 260, and 5100.

TABLE I
Data for Rising Nitrogen Bubbles
 Temperature = 20°C.
 Diameter = 0.057 cm. (in glycerol solutions)
 = 0.055 cm. (in UCON oil mixtures)

Liquid	n	γ (dynes/cm.)	ρ_2 (g./c.c.)	η_2^b (poise)	c' exptl. (microns)	c calc. (microns)	$u_{\text{exptl.}}$ (cm./sec.)	u_{Stokes} (cm./sec.)	$\frac{u_{\text{exptl.}}}{u_{\text{Stokes}}}$
Aqueous glycerols no emulsifier									
97%	1.4668	63.6	1.2535	8.05	29.4	29.1	0.0372	0.0260	1.43
91	1.4592	64.1	1.2367	2.65	29.7	28.8	0.107	0.0778	1.38
85	1.4510	64.5	1.2221	1.15			0.236	0.177	1.33
Aqueous glycerols with emulsi- fier									
91 + 0.0025% ^a	1.4595	61.5	1.2371	2.75	30.6	29.3	0.0720	0.0752	0.96
91 + 0.025% ^a	1.4595	52.0	1.2362	2.61	29.4	31.9	0.0750	0.0791	0.95
UCON oil mix- tures									
1	1.4568	35.3	1.0447	8.02	32.0	33.4	0.0228	0.0219	1.04
2	1.4553	34.5	1.0378	2.63	28.1	30.0	0.0600	0.0552	1.08
3	1.4530	32.0	1.0295	1.13	35.2	36.0	0.180	0.172	1.05

Mean $c'/c = 0.98 \pm 0.04$.

^a Tween 20.

^b For aqueous glycerol solutions, obtained from viscosity-density tables.
 For UCON oil mixtures, measured on Epprecht-Rheometer.

Tween-20 (polyoxyethylene sorbitan monolaurate)⁵ an oil-in-water emulsifier, was dissolved in the aqueous glycerol in some experiments.

Nitrogen bubbles were used in all cases.

RESULTS AND DISCUSSION

1. Shape of Liquid Film

The variation in thickness and shape of the intervening film during the approach of a bubble to the liquid surface as shown by the high-speed cinefilms of the Newton's rings is illustrated in Fig. 2 and is typical of all the systems examined.

Initially, as the bubble approached the surface, each successive dark ring started as a dark spot at the center of the ring pattern and then moved radially outwards, indicating that the minimum separation was at the center (Fig. 2a). The rate of ring formation decreased rapidly, and the diameter of the initial central dark spot increased with time. These observa-

⁵ Atlas Powder Co.

tions indicate that during this period the liquid thinned at a progressively decreasing rate and became more uniform in thickness at the center.

As thinning proceeded, a time was reached when a change in the ring pattern was observed. Each new ring then formed initially at a radial dis-

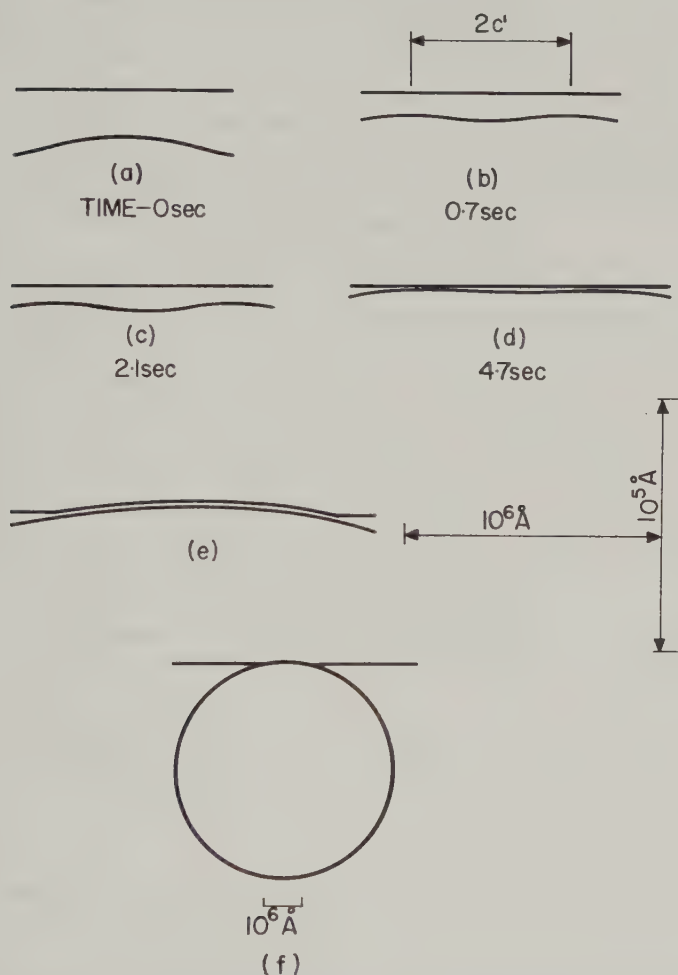


FIG. 2. Variation of the intervening liquid film during the approach of a nitrogen bubble (0.059 cm. diameter) to the surface of a 91% glycerol in water solution at different times before bursting. The data were obtained from high-speed cine-photographs of the Newton's interference rings, with the order of interference being determined from the interference colors. (a) Minimum separation at the center. (b) Minimum separation at radius c' . (c) Film is thicker at center than at the circle of minimum separation. (d) Difference in the thickness between the center and peripheral minimum separation decreased after bulk movement of liquid trapped at the center. (e) Probable profile of liquid film in view of surface deformation of the liquid. (f) Whole bubble at the interface. Parts (a) to (e) are drawn to the same scale.

tance c' from the center and split into two rings, with one moving outwards, as before, and the other inwards. This indicated that the thinnest part of the film was no longer at the center but along the circle of radius c' (Fig. 2*b*). Similar observations were made by Derjaguin and Kussakov (13) and others (14, 15) for gas bubbles approaching a horizontal solid surface, although the reasons for this behavior are not understood; it is possible that the development of this ring of minimum film thickness is analogous to the development of Plateau's borders in foams (18). Observations in incident white light showed that the ring c' was first developed in the third to sixth order of interference colors, i.e., when the film was 0.3 to 1.2 μ thick.

Following this, it was observed that thinning occurred at a greater rate at c' than at the center where the liquid was temporarily immobilized (Fig. 2*c*). This was indicated by the formation and the coexistence of as many as four rings (or colors) between the center and c' , with practically no change occurring in the pattern at the center. The radius c' tended to increase slightly as thinning proceeded, but the change was within experimental error. Eventually the inner rings became elliptical in shape and moved together in the direction of their major axes until they disappeared from the ring pattern, indicating a bulk movement of the liquid. This generally occurred at a film thickness of about 1500 Å. After this, thinning at the center occurred at approximately the same rate as at the periphery with occasional high spots in the center. The film was therefore more uniform in thickness (Fig. 2*d*). When the first-order white was reached, thinning continued from the edges with grey, then black areas slowly forming around the edges in a scalloped pattern. With the less viscous media investigated, there was also a great deal of movement within the liquid film as grey and black areas swirled around.

In Fig. 2 (*a* to *d*), the liquid surface is drawn flat. However, since the surface was deformable, it was, in fact, lifted by the buoyant force of the bubble. This probably accounts for the bulk movement of the trapped liquid (Fig. 2*c*), since, as the liquid was raised, an unstable condition arose owing to gravity.

On the assumption that the bubble (radius b) remains spherical and creates a bulge (radius c) in the flat interface, then at static equilibrium the buoyant force of the bubble is equal to the downward component of the force due to surface tension. This yields the equation

$$c = b^2 \left[\frac{2(\Delta\rho)g}{3\gamma} \right]^{1/2}, \quad [1]$$

where $\Delta\rho$ is the density difference of Phases 1 and 2, γ the surface tension, and g the acceleration due to gravity.

Equation [1] is identical with the relationship derived (13) for a deform-

able drop at a rigid plane, where it was assumed that the drop makes contact with the surface over a flat disc of radius c (7).

The experimental values of c' showed excellent agreement with values of c calculated from Eq. [1], as shown in Table I. We may assume therefore that the point of minimum thickness occurs where the upper surface starts to bulge. Thus, the final profile of the adjacent surfaces near the center of a bubble at the interface is as illustrated in Fig. 2e. Figure 2f shows (to scale) the whole bubble at the interface.

Although these experiments were limited to gas bubbles at a liquid interface, it is believed that the phenomena illustrated in Fig. 2 and described above also occur when a liquid drop approaches a liquid/liquid interface.

2. Thinning of the Liquid Film

Since the time interval between successive frames of the cine pictures was accurately known, it was possible to measure the change of the liquid film thickness with time at a given point. For convenience, the point of

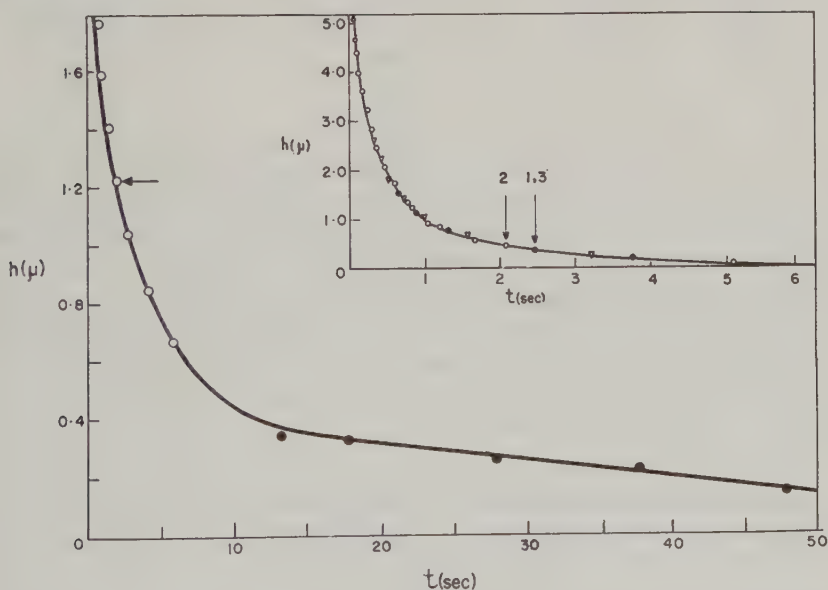


FIG. 3 (a)

FIG. 3. (a) h versus t for a nitrogen bubble (diam. = 0.057 cm.) rising through 97% glycerol. Inset: curves for three identical bubbles (No. 1 to 3, diam. = 0.049 cm.) in 97% glycerol were superimposed to show the reproducibility of the h versus t curve. (b) Effect of viscosity on h - t curve for nitrogen bubbles (diameter = 0.055 cm.) rising through UCON oil mixtures. Curves 1, 2, 3 correspond to η_2 of 8.02, 2.63, and 1.13 poise, respectively. The open points are for monochromatic light and the closed are for incident white light. In all curves the arrow represents the point at which the minimum thickness moved from the center to c' .

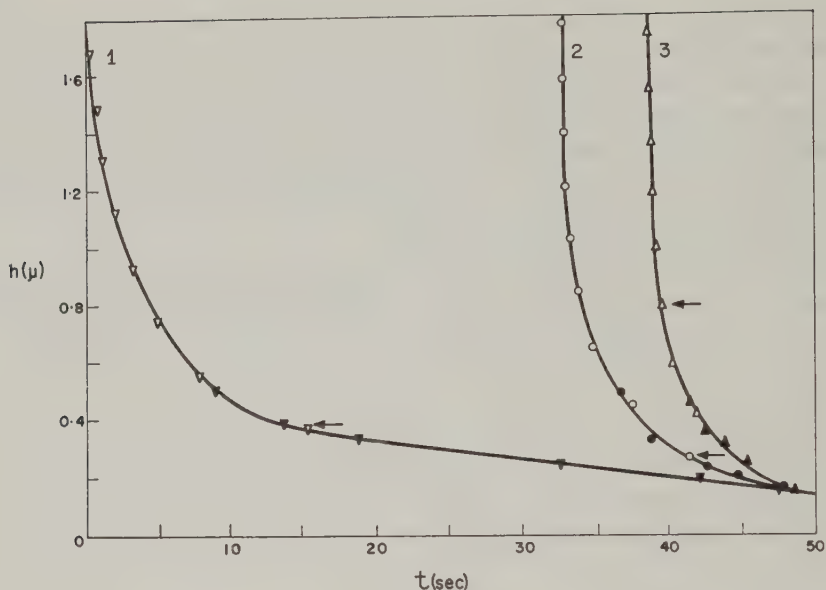


FIG. 3 (b)

minimum separation was chosen and the time intervals between the initial appearance of successive rings at that point were recorded. Initially, when the minimum separation was at the center, the time interval was that between the first appearance of two consecutive black spots.

Clearly, each interval represents an optical path difference of one wavelength λ and, hence, a change of $\lambda/2$ in the film thickness h at the reference point. It was thus possible to obtain directly the change in relative h with time t from the cine-film, where t was measured from an arbitrarily chosen frame on the cine-film.

A typical plot of h versus t is given in Fig. 3a (open points). The h - t plot constructed from the changing interference colors exhibited in white light (closed points) was superimposed to give absolute values of the thickness at each successive interference ring. The curve based on interference colors represents the average of 10 to 15 bubbles and also represents the minimum separation at any time. The first appearance of rings at c' as described above is indicated by the arrow.

In the inset of Fig. 3a, plots obtained with monochromatic light for three identical bubbles in glycerol were superimposed by shifting the time axes to show the reproducibility of the h - t curve. It will be noted that in two cases the times of appearance of the ring coincided, and in the third it was within 0.5 sec. of the other two.

Similar curves were obtained with the two other aqueous glycerol systems

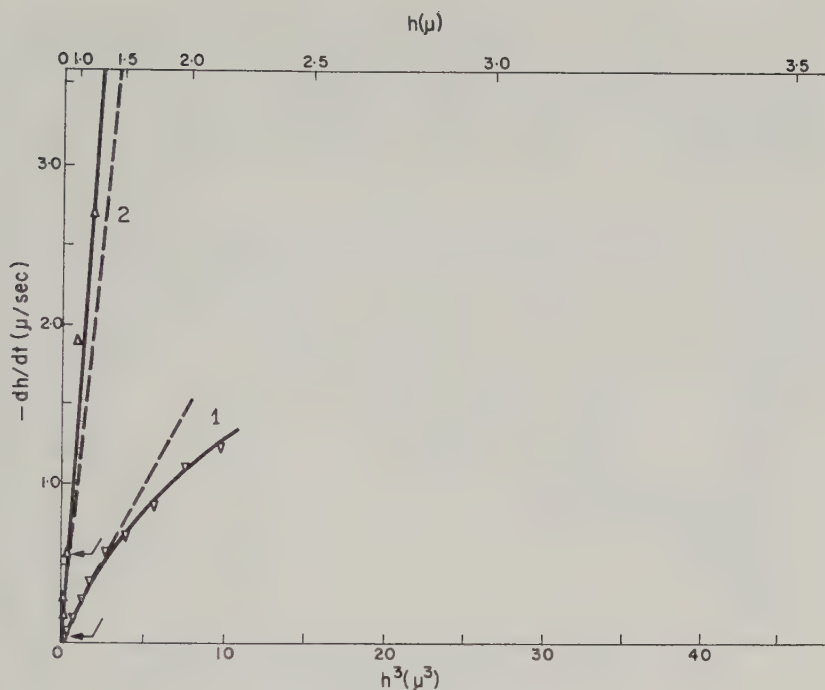


FIG. 4 (a)

FIG. 4. (a) Effect of viscosity on dh/dt versus h^3 curve for nitrogen bubbles (diameter = 0.055 cm.) in UCON oil mixtures. Curves 1 and 2 represent 8.02 and 1.13 poise oils, respectively. The dotted lines represent the theoretical values for a parallel-disc approach (Eq. [2]) corresponding to $\gamma = 34$ dynes/cm. (b) Plot of dh/dt versus h^3 for nitrogen bubbles (diam. = 0.057 cm.) in 91% glycerol in water solutions containing surfactant. Curves 1, 2, and 3 represent 0, 0.0025%, and 0.025% Tween-20, respectively. The dotted line represents the theoretical values for a parallel-disc approach corresponding to $\gamma = 64$ dynes/cm. As in Fig. 3 (a) and (b), the arrow represents the point at which the minimum thickness moved from the center to c' .

examined without emulsifier. The effect of viscosity on the rate of rise of a nitrogen bubble in UCON oils is illustrated in Fig. 3b. As might be expected from the fact that γ was approximately constant for the three systems, the rate of thinning at any given thickness increased as η_2 decreased.

This is shown more clearly in Fig. 4a. For a parallel-disc approach or the approach of a rigid sphere to a deformable interface which can resist a shear stress, Charles and Mason (7) give the following relationship

$$-\frac{dh}{dt} = \left[\frac{2\gamma^2}{\eta_2(\Delta\rho)gb^5} \right] h^3, \quad [2]$$

where η_2 is the viscosity of the liquid film.*

* ADDED IN PROOF: Recent experiments by D. M MacKay using a range of bubble sizes in glycerine have shown good agreement with Eq. [2].

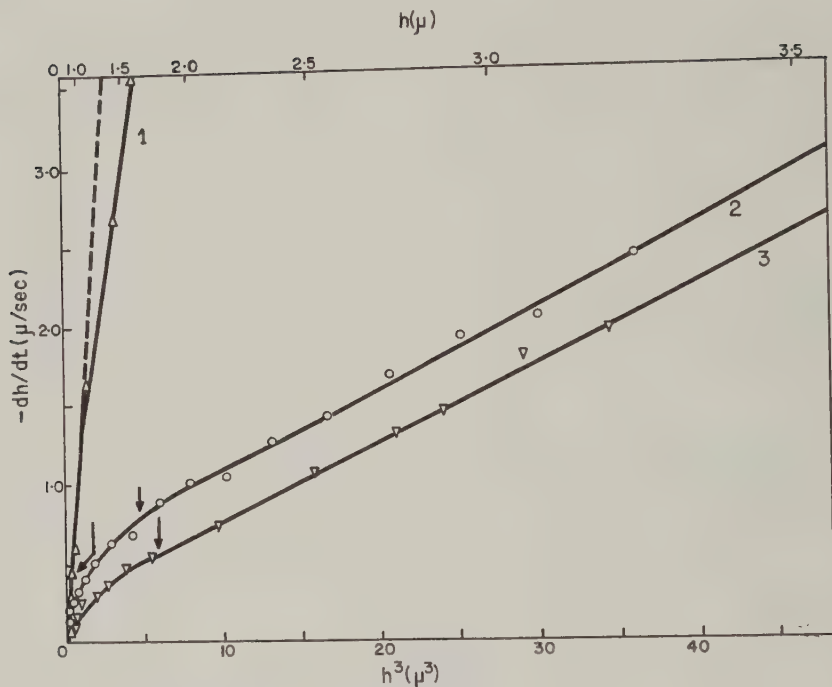


FIG. 4 (b)

A plot of $-dh/dt$ versus h^3 should thus yield a straight line passing through the origin, the slope of which is inversely proportional to the Phase 2 viscosity. This is evident from Fig. 4a and Table II. The agreement between the experimental slope and the theoretical slope calculated from Eq. [2] is considered to be very good, although it must be borne in mind that the data are not sufficiently sensitive to afford a rigorous test of the theory.

The mean rate of bubble rise at a point 2 to 3 cm. from the interface was measured using a cathetometer and stop watch. The experimental values ($u_{\text{exptl.}}$) are shown in Table I together with the calculated Stokes velocities for rigid spheres of the same diameter (u_{Stokes}). The latter values were corrected for the influence of the walls and top of the cell on velocity (20). It can be seen that the ratio of the measured velocity to the corresponding Stokes velocity is about 1.4 for the pure aqueous glycerol solutions and close to unity for the UCON oil mixtures.

Hadamard (21) gives the following relationship for the ratio of the velocity of a fluid sphere having fully developed internal circulation to that of a solid sphere of the same diameter and density:

$$\frac{u_{\text{fluid}}}{u_{\text{Stokes}}} = \frac{p + 1}{p + \frac{2}{3}}, \quad [3]$$

where p is the ratio of viscosity of the fluid drop to that of the medium. For the present case, $p = 0$ and hence $u_{\text{fluid}}/u_{\text{Stokes}} = 1.5$.

The values of $u_{\text{exptl.}}/u_{\text{Stokes}}$ obtained here for the pure glycerol solutions are slightly less than predicted by Eq. [3], and indicate some inhibition of internal circulation by the bubble interface, similar to that observed in a

TABLE II

Effect of Viscosity on Rate of Film Thinning for Nitrogen Bubbles in UCON Oils
Same conditions as in Table I

UCON oil mixture	η_2 (poise)	Exptl. slope ^a	Theor. slope ^b	Exptl. slope
				Theor. slope
1	8.02	0.19	0.192	1.00
2	2.63	0.65	0.735	0.89
3	1.13	1.35	1.02	1.32
				Mean 1.07

^a Fig. 4a.

^b Calculated from Eq. [2] assuming a parallel-disc approach.

TABLE III

Film Thickness at Rupture for Bursting Nitrogen Bubbles
Same conditions as in Table I

Liquid	Rest-time (sec.)		(1 - f(h)) from interference colors							$\bar{h}_{\text{ca.10.}}^b$	$h_{1/2b}$
	$\bar{\tau}$	$\tau_{1/2}$	900 A.	1230 A.	1370 A.	2100 A.	2430 A.	3120 A.	3590 A.	(A.)	(A.)
Aqueous glycerols no emulsifier											
97%	340	340	1.00							570	570
91	18.1	18.3	0.92	0.92	1.00					1400	1390
85	14.9	11.6	0.78	0.90	0.93	0.96	0.96	0.96	1.00	1010	1140
Aqueous glycerols with emulsi- fier											
91 + 0.0025% ^a	28.0	22.6	0.73	0.76	0.93	0.96	1.00			1200	1330
91 + 0.025% ^a	>360	>360	1.00							<390	<390
UCON oil mix- tures											
1	>360	>360	1.00							<850	<850
2	69.1	65.3	1.00							1000	1020
3	40.0	39.0	1.00							1100	1120

^a Tween 20.

^b Calculated from $\bar{\tau}$ and $\tau_{1/2}$ using equation for approach of rigid parallel plates (7).

velocity gradient (22). The data for the UCON oils indicate complete suppression of internal circulation.

3. Film Thickness at Rupture

It was found that in most cases, the film thinned to the grey or black stage ($h < 900$ Å.) below the limit of resolution of the interference-color method. A fraction of bubbles in glycerol solutions, which increased as η_2 decreased, burst at film thicknesses within the first and second order of colors. All films were found to thin below 4000 Å. before rupture. The results are summarized in Table III where $(1 - f(h))$ represents the fraction of bubbles examined which coalesced at or below a film thickness h corresponding to the position of minimum separation.

The measured distribution of rest-times τ for aqueous glycerol solutions is shown in Fig. 5 and is similar to that observed in liquid/liquid systems (1-7). The mean and median film thickness at rupture calculated from the

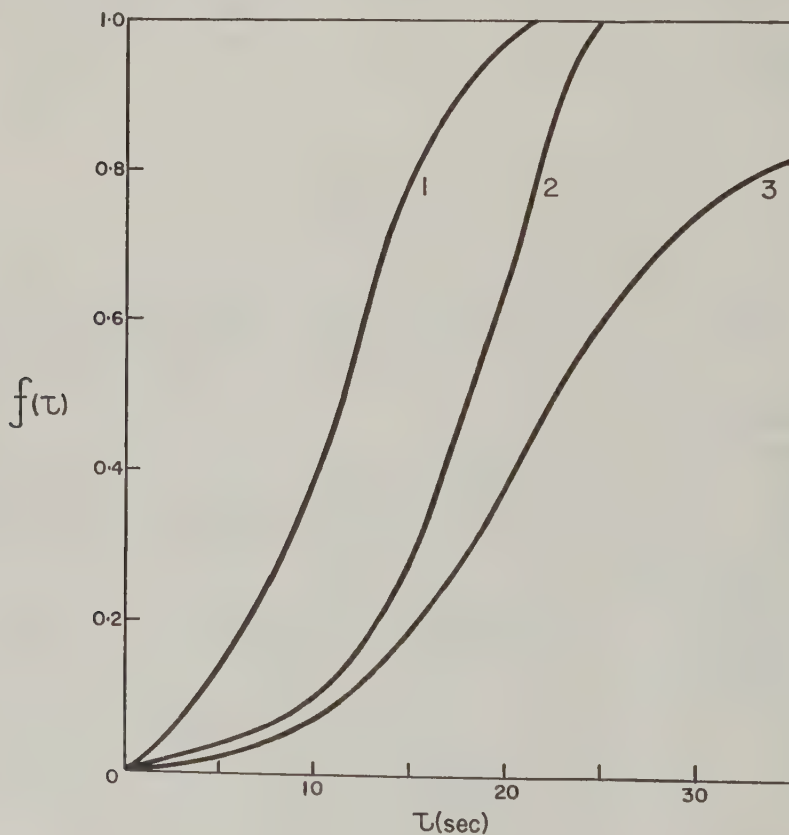


FIG. 5. Integral distribution of τ for nitrogen bubbles (diam. = 0.057 cm.). Curves 1 and 2 are for 85% and 91% glycerol in water solutions, respectively. Curve 3 is for 91% glycerol in water solution containing 0.0025% Tween-20.

corresponding rest-times ($\bar{\tau}$ and $\tau_{1/2}$) assuming a parallel-disc approach (7) are recorded in Table III. The values of $h_{1/2}$ obtained are somewhat higher than the optical measurements; this is to be expected since the theory assumes that the interfaces are rigid and may therefore predict rates of drainage in the emulsifier-free systems which are too low (7). Inspection of the data showed that (1) in a given glycerol solution, an increase in τ corresponded to a decrease in h at rupture, thus directly confirming earlier conclusions (2, 7); (2) the bubble stability measured by $\bar{\tau}$ or $\tau_{1/2}$ increased with increasing η_2 ; and (3) \bar{h} (from optical measurements) at rupture decreased with increasing η_2 . Similar results were obtained with the UCON oil mixtures.

4. Effect of Surfactants

The effect of an added surfactant on the rate of rise of a gas bubble in 91% glycerol is shown in Fig. 6 and on the increase in $\bar{\tau}$ in Table III. It will

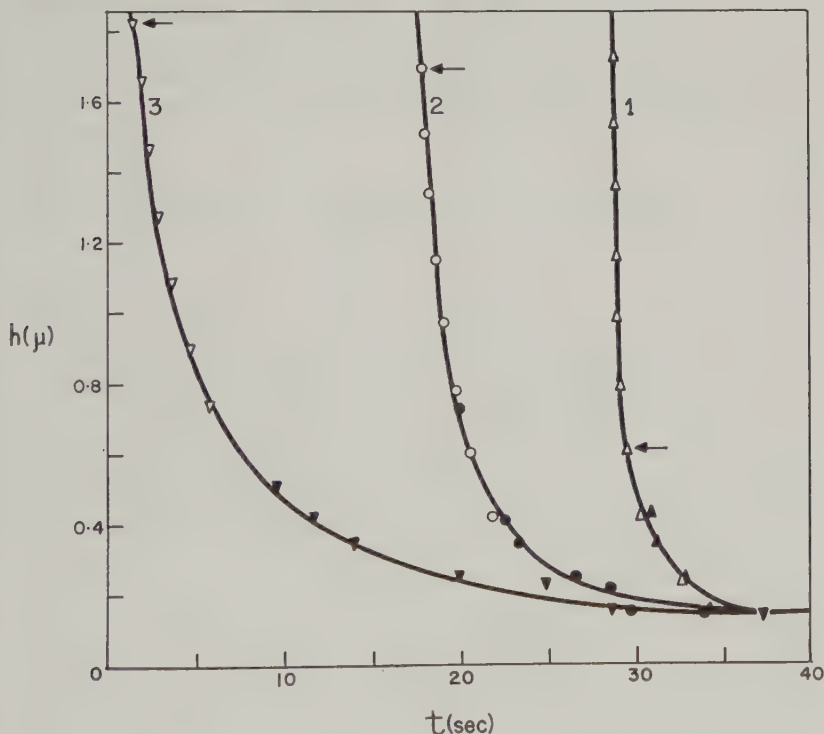


FIG. 6. Effect of surfactant on h - t curve for nitrogen bubbles (diam. = 0.057 cm.) in 91% glycerol/water solutions. Curves 1, 2, and 3 correspond to 0, 0.0025%, and 0.025% Tween-20, respectively. The open points are for monochromatic light while the closed are for incident white light. The arrow represents the point at which the minimum thickness moved from the center to c' . The origins of time were adjusted to make the curves intersect at a common point.

be noted that the rate of film thinning at comparable film thicknesses decreases markedly with the addition of even a small amount of surfactant. This is shown more clearly in Fig. 4b, where the rate of film thinning, $-dh/dt$, is plotted against h^3 . It is seen that both with and without the emulsifier at thicknesses below the initial formation of a ring, the slopes tend to approach the theoretical value given by Eq. [2] (Fig. 4b). Unfortunately, no surfactants were found which were soluble in UCON oils.

The velocity of the rising bubble a long way from the surface when surfactant was present in glycerol is shown in Table I. The ratio of measured velocity to Stokes velocity is approximately 1.0. It is apparent that the surfactant suppressed internal circulation in the rising gas bubble (22, 23), causing it to behave like a rigid sphere. This suggests that the reduction in the rate of film thinning with the emulsifier present (Fig. 4b) resulted not only from the reduction in γ (Eq. [2]) but also from the interface acting as an elastic membrane which is capable of resisting shear stresses as assumed in the theory (7), although it is deformed by normal stresses in accordance with Eq. [1]. This is possible by establishing gradients in surface pressure as discussed elsewhere (22, 23). It is possible that the UCON oil mixtures, which can be used as defoamers and demulsifiers, contained surfactants. This would explain the behaviour observed in the present work.

It is proposed to extend these experiments to the cases of a liquid drop approaching liquid/liquid and liquid/solid interfaces.

REFERENCES

1. COCKBAIN, E. G., AND MCROBERTS, T. S., *J. Colloid Sci.* **8**, 440 (1953).
2. GILLESPIE, T., AND RIDEAL, E. K., *Trans. Faraday Soc.* **52**, 173 (1956).
3. ELTON, G. A. H., AND PICKNETT, R. G., Proceedings of the 2nd International Congress of Surface Activity, Vol. 1, p. 287. Butterworths, London, 1957.
4. PICKNETT, R. G., Ph.D. Thesis, University of London, London, 1957.
5. WATANABE, T., AND KUSUI, M., *Bull. Chem. Soc. Japan* **31**, 236 (1958).
6. NIELSON, L. E., WALL, R., AND ADAMS, G., *J. Colloid Sci.* **13**, 441 (1958).
7. CHARLES, G. E., AND MASON, S. G., *J. Colloid Sci.* **15**, 236 (1960).
8. REYNOLDS, O., *Chem. News* **44**, 211 (1881).
9. GOSSART, E., *Ann. chim. et phys.* (5) **4**, 391 (1895).
10. REHBINDER, P. A., AND WENSTROM, E. K., *Kolloid-Z.* **53**, 145 (1930).
11. MAHAJAN, L. D., *Kolloid-Z.* **65**, 20 (1933).
12. MAHAJAN, L. D., *Kolloid-Z.* **69**, 16 (1934).
13. DERJAGUIN, B. V., AND KUSSAKOV, M., *Acta Physicochim. U.R.S.S.* **10**, 25 (1939).
14. ELTON, G. A. H., *Proc. Roy. Soc. (London)* **A194**, 275 (1948).
15. EVANS, L. F., *Ind. Eng. Chem.* **46**, 2420 (1954).
16. SHELUDKO, A., *Kolloid-Z.* **155**, 39 (1957).
17. VAN DEN TEMPEL, M., *J. Colloid Sci.* **13**, 125 (1958).
18. MYSELS, K. J., SHINODA, K., AND FRANKEL, S., "Soap Films." Pergamon Press, New York, 1959.

19. REINOLD, A. W., AND RÜCKER, A. W., *Phil. Trans. Roy. Soc.* **177**, 627, London, 1887. See also Lawrence, A.C.S., Soap Films, p. 137. G. Bell and Sons Ltd., London, 1929.
20. DANIELS, F., MATHEWS, J. H., WILLIAMS, J. W., AND STAFF, "Experimental Physical Chemistry," 4th ed. McGraw-Hill, New York, 1949.
21. HADAMARD, M. J., *Comptes rend.* **152**, 1735 (1911).
22. RUMSCHEIDT, F., AND MASON, S. G., *J. Colloid Sci.*, in press. (1961).
23. LINTON, M., AND SUTHERLAND, K. I., Proceedings of the 2nd International Congress of Surface Activity, Vol. 1, p. 494. Butterworths, London, 1957.

DYNAMIC MECHANICAL PROPERTIES AND CREEP OF POLY-2-ETHYL BUTYL METHACRYLATE¹

Theodore P. Yin² and John D. Ferry

Department of Chemistry, University of Wisconsin, Madison, Wisconsin

Received July 26, 1960, revised November 15, 1960

INTRODUCTION

Measurements of time-dependent mechanical properties have previously been made in this laboratory on six *n*-alkyl methacrylate polymers, with alkyl groups ranging from 2 to 22 carbon atoms in length (1), in a cooperative investigation with the Feltman Research and Engineering Laboratories, Picatinny Arsenal. The results have been analyzed in terms of the temperature dependence of the relaxation times using the WLF equation; the monomeric friction coefficient and its relation to free volume; and the average spacing between entanglement coupling points and its dependence on temperature. One polymer with a branched side group has now been chosen for a similar investigation to compare with the above series—poly-2-ethyl butyl methacrylate, the ester group of which has the same molecular weight as that of the *n*-hexyl (2) but the same length as that of the *n*-butyl (3).

MATERIALS AND METHODS

The synthesis and fractionation of the polymer were carried out at Picatinny Arsenal (4), and the weight-average molecular weight was determined there to be 2.20×10^6 . The density was 1.040 at 25°C., measured pycnometrically, and the refractive index was 1.477 at 25°C. The thermal expansion coefficient was estimated from pycnometric measurements as $6.0 \times 10^{-4} \text{ deg.}^{-1}$.

The glass transition temperature was determined refractometrically, following the method of Jenckel and Heusch (5) as described in a previous publication (6), to be 11°C.

Measurements of the complex shear compliance ($J^* = J' - iJ''$) were made between 24 and 3600 cycles/sec. with the Fitzgerald Transducer Apparatus (7). Three pairs of samples were used, detailed descriptions of which follow.

¹ Part XXXIII of a series on Mechanical Properties of Substances of High Molecular Weight.

² Present address: E. I. du Pont de Nemours and Company, Wilmington, Delaware.

Samples 125, approximate dimensions $\frac{5}{16}$ in. diameter by $\frac{3}{16}$ in. thick, were compressed about 5%, and the sample coefficient was 4.58 cm. at room temperature. Measurements were made at temperatures in the sequence of approximately 50°, 54°, 60°, 65°, 70°, 75°, 80°, 85°, 50°, 45°, 40°, 35°, 30°, 26°, and 20°C. (The exact temperatures are given in the legend of Fig. 2.) After 85°, the samples experienced a sequence of temperatures up to 111°, being mounted in the apparatus together with samples 126 described below. The two runs at 45° agreed well.

Samples 126, approximate dimensions $1\frac{1}{16}$ in. by $\frac{3}{32}$ in., were compressed about 5%, and the sample coefficient was 21.4 cm. at 25°C. Measurements were made at approximately 50°, 60°, 70°, 80°, 85°, 90°, 95°, 101°, 106°, 111°, 80°, and 75°C.; the two runs at 80° agreed well. At overlapping temperatures, the results of samples 125 and 126 agreed closely, and no empirical corrections were applied to the data.

Samples 127, approximate dimensions $1\frac{1}{16}$ in. by $\frac{1}{32}$ in., were compressed slightly and the sample coefficient was 73.9 cm. at 25°C. Measurements were made at approximately 111°, 121°, 132°, 141°, 151°, 101°, and 106°C., followed by a check run at 111° which agreed with the initial results. The values of J' and J'' were about 5% higher than those from Samples 126 at overlapping temperatures; they were accordingly corrected by an empirical factor of 0.95, since the sample coefficient is more difficult to specify precisely for very thin samples.

At lower frequencies, between 0.05 and 1.6 cycles/sec., measurements were made with the torsion pendulum of Plazek, Vrancken, and Berge (8). Two samples were used, one each of the pairs 125 and 126 previously studied in the Fitzgerald Apparatus. The former was measured at approximately 90°, 80°, 75°, 70°, 65°, and 60°; the latter at 70°, 75°, 80°, 85°, 90°, 95°, 101°, 106°, 111°, 121°, 70°, 132°, 141°, 151°, and 90°. The check runs at 70° and 90° agreed well with the earlier ones. The temperatures were all chosen to match exactly those used in the transducer measurements, and their precise values appear in the legend of Fig. 2. The nominal sample coefficient was always calculated from the sample height as measured *in situ* and the volume (mass/density), assuming cylindrical shape.

These samples, having been further compressed by mounting in the torsion pendulum, bulged laterally to some degree, so that the calculation on the basis of cylindrical shape could not be expected to be exactly correct. At overlapping temperatures, the magnitudes of G' (or those of J' and J'' when the latter were calculated from the primary measurements of G' and $\tan \delta$) agreed for the two samples after G' for the thicker one was multiplied by an empirical correction factor of 1.065. But further correction was necessary to bring the results into accord with the transducer data.

The comparison of data from the two instruments could not be made directly, since there was a gap between the two frequency ranges, but only after temperature reduction. For this purpose, the torsion pendulum data

and the Fitzgerald transducer data were reduced separately with the a_T factor calculated from the WLF equation and the f -factor associated with entanglement coupling as will be described below, to give composite curves for J' and J'' . On the reduced curves, both J' and J'' as derived from the Fitzgerald transducer were smaller by a factor of 0.63. Though this discrepancy is rather large, the transducer data were taken as correct in view of their excellent internal consistency and the fact that the effective sample coefficient in the torsion pendulum, involving the fourth power of the sample radius, is especially sensitive to bulging or other shape irregularities. A similar situation was encountered previously with poly-*n*-octyl methacrylate (9). The torsion pendulum data for J' and J'' were accordingly all multiplied by a factor of 0.63.

Finally, measurements of creep and creep recovery were made in the torsion pendulum on a sample of intermediate thickness (original dimensions $1\frac{1}{16}$ in. by $\frac{3}{32}$ in.), at 101°, 121°, 141°, and 151°. Since this sample was further distorted by a third compression in remounting, its nominal sample coefficient was also in doubt. The magnitude of the creep compliance, $J(t)$, was compared with that derived from the dynamic transducer data by the approximation calculation of Ninomiya and Ferry (10). From the comparison it was evident that the creep compliances based on the nominal sample coefficient required multiplying by the rather severe correction factor of 0.40. This factor was confirmed by a few dynamic measurements on the same sample while mounted for the creep measurements. Although the torque exerted by the torsion wire decreased slightly during a creep run, this change was less than 1% and introduced no perceptible errors in either creep or recovery data.

RESULTS

The creep data are plotted with logarithmic scales in Fig. 1. To save space, the dynamic data are not shown before temperature reduction; superficially, they resemble those presented previously for other members of the methacrylate series.

For reduction to a standard temperature, 100°C. was chosen as the reference, T_0 . The transducer data in the range from 60° to 106° and the torsion pendulum data from 60° to 80° provided values of the shift factor a_T which fitted the usual empirical equation (11)

$$\log a_T = -c_1^0(T - T_0)/(c_2^0 + T - T_0), \quad [1]$$

with $c_1^0 = 11.58$ and $c_2^0 = 208.9$. (Below 60°, the original curves were too flat for adequate estimations of $\Delta \log a_T$ from adjacent temperatures, whereas above 106° the original curves were not parallel owing to the appearance of an entanglement anomaly.)

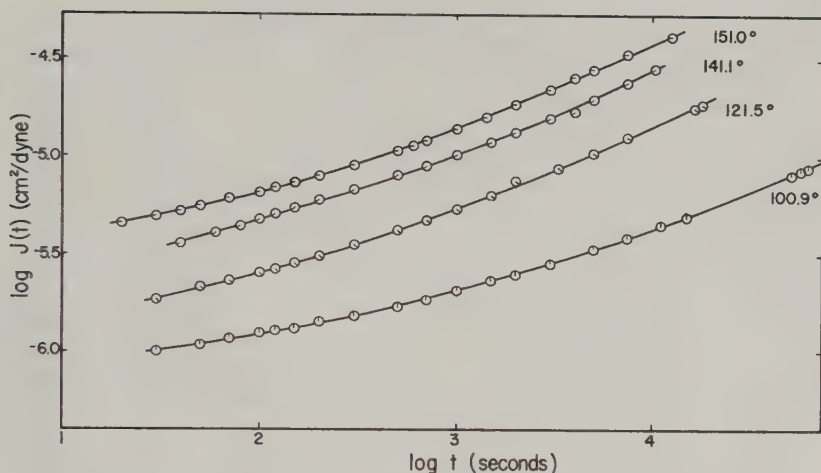


FIG. 1. Creep compliance plotted logarithmically at 4 temperatures.

Reduced plots for J_p' and J_p'' , using a_T values calculated from Eq. [1], are shown in Figs. 2 and 3. The superposition is very good except for the anomaly near the maximum in J'' which in several other methacrylates (9) has been attributed to temperature dependence of the spacing between coupling entanglements. The procedure used previously for resolving this anomaly (9) was successful, involving plotting $J_p'f$ and $J_p''f$ against $\omega a_T/f^2$, where f is the ratio of the number of entanglements per cubic centimeter at the temperature of measurement to that at T_0 . It may be remarked that the form of this reduction, originally proposed on the basis of molecular theories for cross-linked networks, is also consistent with the theory for entanglement networks recently introduced by Marvin (12). For poly-2-ethyl butyl methacrylate, the temperature variation of f follows a van't Hoff type of relation with $\Delta H = 4.4$ kcal./mole.

Values of J' and J'' in the vicinity of the anomaly are plotted in Figs. 4 and 5 after reduction for the temperature dependence of both a_T and f . Most of the data now fall satisfactorily on the two composite curves. In the transition zone, the f -reduction can be and has been ignored (9), because it shifts points in the direction of the curve itself, and at high frequencies the values of J' and J'' must become independent of the spacing between linkage points. Interpolated logarithmic values of J' and J'' in the transition zone from Figs. 2 and 3 and the plateau zone from Figs. 4 and 5 are given in Table I.

Since the creep measurements correspond to the plateau and terminal zones, they are subject to reduction for both a_T and f . The corresponding reduced plot is $J(t)f$ against tf^2/a_T , and this does provide excellent superposition, as shown in Fig. 6, further confirming the choice of the coefficients

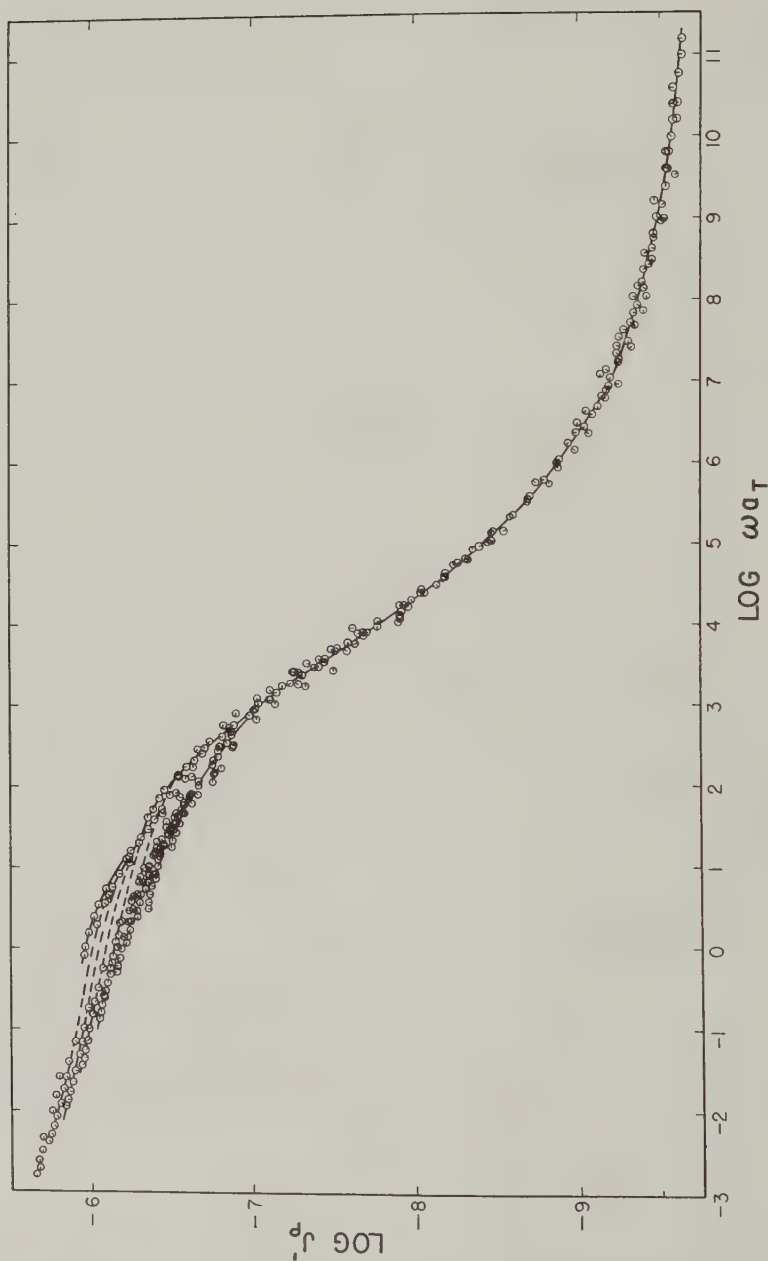


FIG. 2. Real part of complex compliance plotted logarithmically after reduction with shift factor a_T . Pip up at right, 20.0°C., successive 45° rotations clockwise correspond to 25.6°, 30.2°, 35.5°, 40.3°, 45.1°, 49.6°, 54.5°, 59.5°, 64.7°, 70.1°, 75.0°, 80.0°, 85.0°, 90.2°, 95.3°, 100.9°, 106.2°, 110.9°, 121.5°, 131.7°, 141.1°, and 151.0°C.

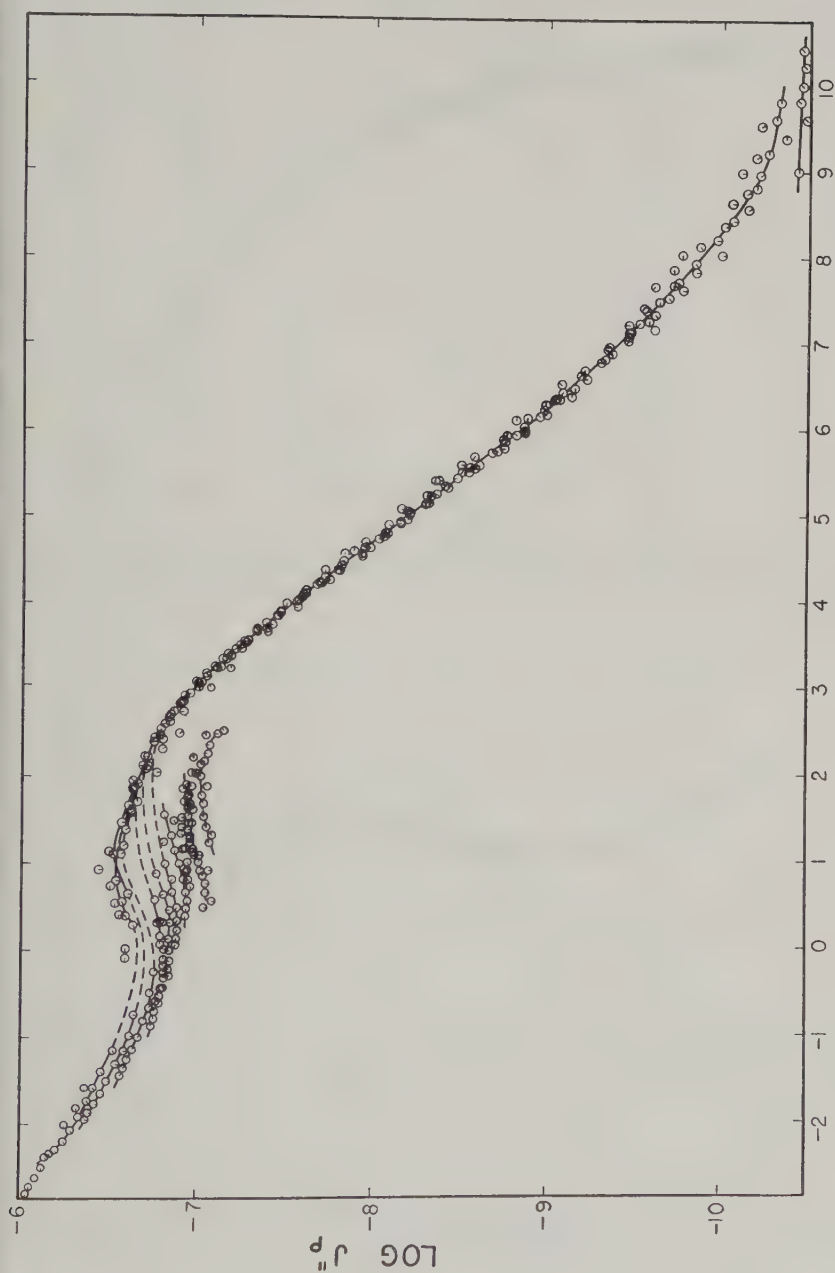


Fig. 3. Imaginary part of complex compliance plotted as in Fig. 1.

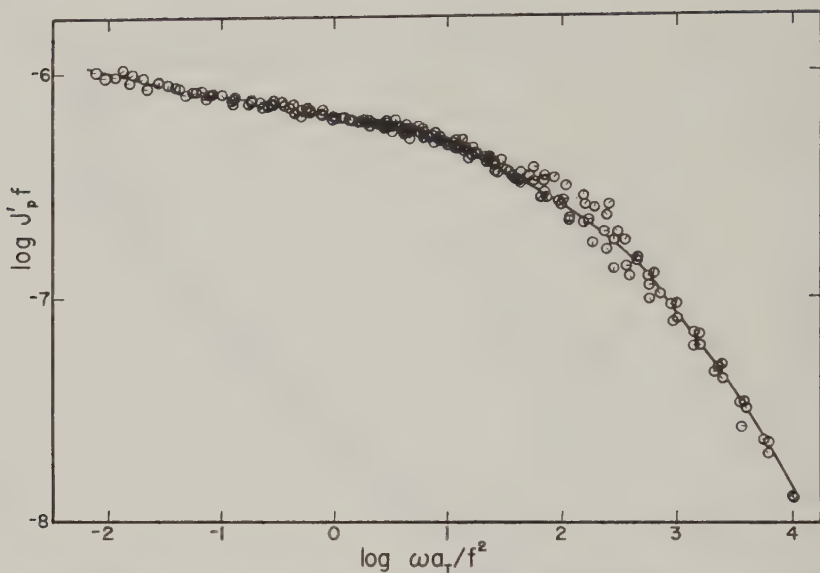


FIG. 4. Real part of complex compliance in plateau zone reduced for temperature variation of both a_T and f . Temperature key same as in Fig. 2, ranging from 95.3° to 151.0°C.

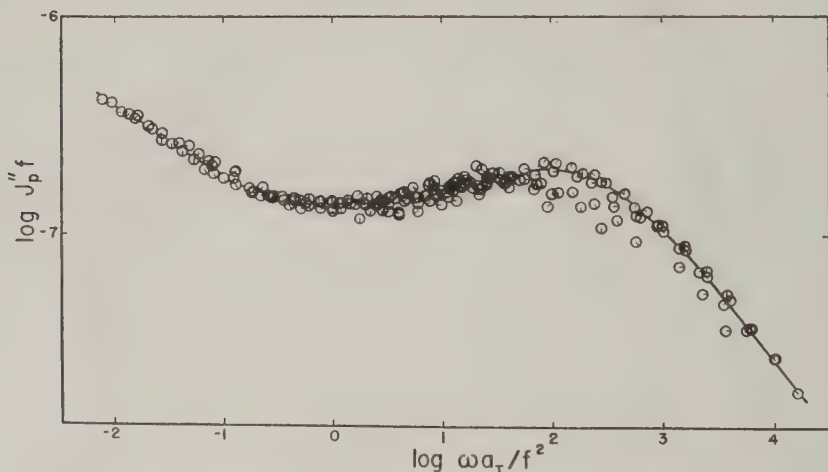


FIG. 5. Imaginary part of complex compliance reduced and plotted as in Fig. 4.

in Eq. [1] and the value of ΔH . Figure 6 includes also some points calculated from creep recovery, according to the equation

$$J(t) = J_r(t) + J(t - \theta), \quad [2]$$

where θ is the time of load removal and $J_r(t)$ is the creep compliance measured during recovery at a time t elapsed since the load was first applied.

TABLE I

Interpolated Values of J' , J'' , and $J(t)$ Reduced to 100°C. for Temperature Dependence of Both a_T and f

Log ω	Log J'	Log J''	Log ω	Log J'	Log J''	Log t	Log $J(t)$
-2.0	-5.97	-6.40	4.5	-8.13	-7.84	1.0	-6.52
-1.5	-6.05	-6.57	5.0	-8.43	-8.18	1.5	-6.33
-1.0	-6.10	-6.73	5.5	-8.68	-8.50	2.0	-6.09
-0.5	-6.15	-6.83	6.0	-8.89	-8.85	2.5	-5.83
0	-6.19	-6.87	6.5	-9.06	-9.13	3.0	-5.45
0.5	-6.23	-6.85	7.0	-9.22	-9.41	3.5	-5.10
1.0	-6.31	-6.80	7.5	-9.30	-9.64	4.0	-4.62
1.5	-6.43	-6.74	8.0	-9.37	-9.87	4.5	-4.12
2.0	-6.58	-6.70	8.5	-9.43	-10.07		
2.5	-6.77	-6.77	9.0	-9.48	-10.23		
3.0	-7.06	-6.97	9.5	-9.53	-10.30		
3.5	-7.41	-7.24	10.0	-9.57	-10.33		
4.0	-7.79	-7.55	10.5	-9.60			
			11.0	-9.62			

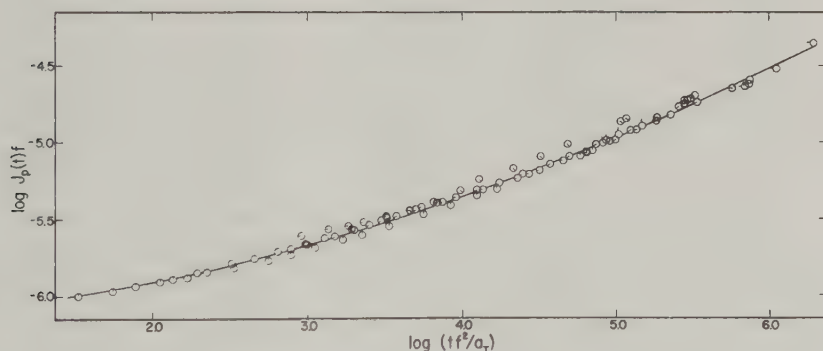


FIG. 6. Creep compliance reduced for temperature variation of both a_T and f . Points with external tags calculated from creep recovery measurements by Eq. [2].

Where this calculation overlaps the part of the curve directly measured, it provides a test of the Boltzmann superposition principle, and beyond this it gives an extension of $J(t)$ to times somewhat longer than the duration of the direct measurements. Values of $\log J(t)$ interpolated from Fig. 6 are also included in Table I.

RELAXATION AND RETARDATION SPECTRA

From the data of Table I, the retardation spectrum L was calculated using several approximation methods, chosen in accordance with previous experience with poly-*n*-octyl methacrylate (9): the Williams-Ferry method (13) for J' and J'' over most of the range, the Schwarzl-Staverman (14) and Fujita (15) methods for J' and J'' in the regions of greatest change in

TABLE II
Retardation and Relaxation Spectra Reduced to 100°C. for Temperature Dependence of Both a_T and f

Log τ_p	Log L_p (cm. ² /dyne)		Log H_p (dyne/cm. ²)	
	From J'	From J''	From G'	From G''
-11.0	-10.99			
-10.5	-10.94		8.19	8.56
-10.0	-10.83		8.46	8.57
-9.5	-10.60	-10.54	8.52	8.54
-9.0	-10.41	-10.47	8.47	8.51
-8.5	-10.30	-10.39	8.56	8.53
-8.0	-10.36	-10.20	8.63	8.61
-7.5	-10.16	-10.10	8.62	8.66
-7.0	-9.84	-9.77	8.68	8.69
-6.5	-9.56	-9.55	8.51	8.57
-6.0	-9.40	-9.35	8.27	8.34
-5.5	-9.09	-8.98	7.92	7.95
-5.0	-8.79	-8.69	7.58	7.65
-4.5	-8.38	-8.27	7.24	7.29
-4.0	-8.01	-8.00	6.81	6.89
-3.5	-7.64	-7.65	6.51	6.62
-3.0	-7.31	-7.26	6.24 ^a	6.30 ^b
-2.5	-7.06	-6.98	5.80 ^a	6.09 ^b
-2.0	-7.12	-6.92	5.55 ^a	5.91 ^b
-1.5	-6.99	-6.93	5.43 ^a	5.65 ^b
-1.0	-7.11 ^a	-7.05 ^b	5.32 ^a	5.40 ^b
-0.5	-7.36 ^a	-7.11 ^b	5.15 ^a	5.26 ^b
0	-7.33 ^a	-7.15 ^b	4.86 ^a	5.21 ^b
+0.5	-7.23 ^a	-7.13 ^b	5.07 ^a	5.19 ^b
+1.0	-7.16 ^a	-7.04 ^b	5.19 ^a	5.23 ^b
+1.5	-7.02 ^a	-6.87 ^b	5.28 ^a	5.25 ^b
+2.0	-6.75	-6.64	5.20	5.30

TABLE II—CONTINUED

Log τ_p	Log L_p from creep	Log τ_p	Log H_p from creep
1.2	-7.02	1.5	5.29
1.7	-6.86	2.0	5.28
2.2	-6.65	2.5	5.18
2.7	-6.42	3.0	5.10
3.2	-6.27	3.5	5.01
3.7	-6.07	4.0	4.84
4.2	-5.85	4.5	4.70
4.7	-5.66	5.0	4.51
5.2	-5.40	5.5	4.27
5.7	-5.17	6.0	4.05
		6.3	3.90

^a From Schwarzl-Staverman approximation (14).

^b From Fujita approximation (15).

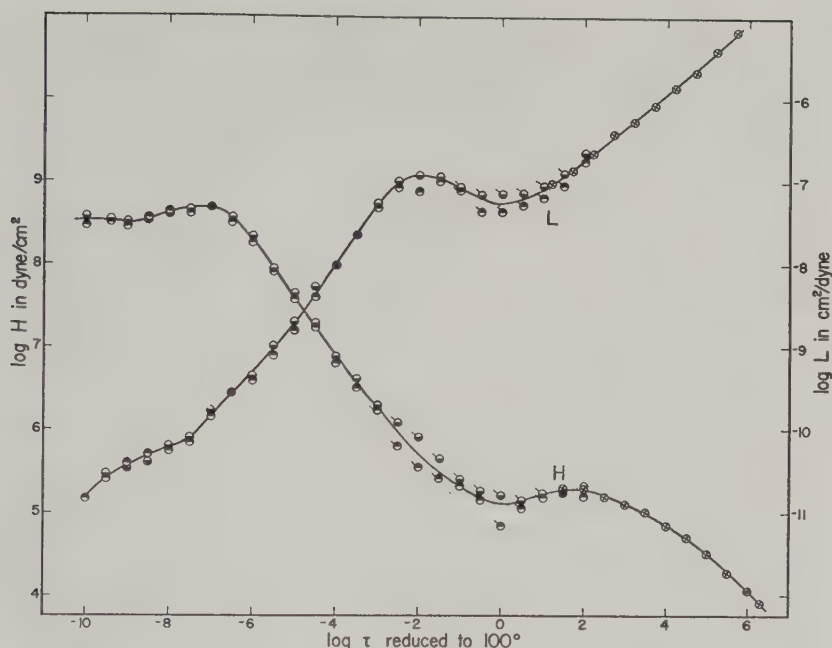


FIG. 7. Retardation spectrum (L) and relaxation spectrum (H). Points with tags from Schwarzl-Staverman and Fujita approximations. Top half black, from G' or J' ; bottom black, from G'' or J'' ; crossed circles, from creep.

curvature, and the modified Schwarzl-Staverman method (16), which does not require specification of the steady-flow viscosity, for creep.

The values of J' and J'' were also converted to the modulus components G' and G'' by the usual formulas, and $J(t)$ was converted to the relaxation modulus $G(t)$ by the approximation quoted by Smith (17). From these moduli, the relaxation spectrum H was calculated using the various approximation methods corresponding to those described in the preceding paragraph. The two spectra are listed in Table II and plotted in Fig. 7. The agreement between calculations from real and imaginary components is quite good except near the minimum in L and the bottom of the transition zone in H . The calculations from the transient functions also agree very well where they overlap. The spectra fully cover the transition (from glass-like to rubberlike consistency) and plateau zones of the time scale.

DISCUSSION

Interest in these results centers primarily in their comparison with those of two members of the n -alkyl methacrylate polymer series, the n -butyl and n -hexyl, which have the same side chain length and side chain molecular weight, respectively, as the 2-ethyl butyl polymer. The most important parameters are listed in Table III.

TABLE III
Comparison of Parameters for the 2-Ethyl Butyl Polymer and for Two Similar Polymers
with Linear Side Groups

	<i>n</i> -Butyl	2-Ethyl butyl	<i>n</i> -Hexyl
<i>v</i> at 100° C.	0.996	1.006	1.042
<i>T</i> _g	27°	11°	-5°
<i>f</i> _g	0.026	0.021	0.025
$\alpha_f \times 10^4$	2.6	1.8	1.9
log ζ_0 at 100°	-3.51	-3.69	-5.21
log ζ_0 at <i>T</i> _g	3.74	4.79	2.63
<i>Z</i> _e from <i>J</i> ^{''} _m at 100°	92	115	180
<i>Z</i> _e from ω_m at 100°	160	178	270
<i>Z</i> _e from Δ at 100°	—	83	—
ΔH for <i>f</i> -shift, kcal.	2.3	4.4	2.3

Parameters Associated with Free Volume

The specific volume (*v*) of the branched polymer at 100°C. is intermediate between those of the two linear polymers, but closer to that of the butyl. Its glass transition temperature is exactly the mean of the other two.

From the coefficients of Eq. [1] and *T*_g, the fractional free volume at *T*_g (*f*_g) and its thermal expansion coefficient relative to the total volume (α_f) can be calculated by the usual formulas (11). As Table III shows, *f*_g for the branched polymer is slightly lower than for either of the others, indicating perhaps that the branched side chains require slightly less free volume for the motions by which volume changes are accomplished. The value of α_f is nearly the same as that of the *n*-hexyl polymer.

The Transition Zone

The location of the transition between rubberlike and glasslike consistency may be characterized by the monomeric friction coefficient, ζ_0 , calculated as usual by applying the Rouse theory to the region of the relaxation spectrum where the slope (with logarithmic scales) has the theoretical value of $-\frac{1}{2}$ (18). For this purpose, the root-mean-square end-to-end separation per square root of the number of monomer units, *a*, is taken as 6.5 Å. from dilute solution measurements in a Θ -solvent (4). At 100°C., log $\zeta_0 = -3.69$, very close to that of the *n*-butyl polymer (Table III). Thus the ethyl branch on the side group has comparatively little influence on the local mobility of the chain backbone when the temperature is far above *T*_g.

The relation of the monomeric friction coefficient to free volume in the *n*-alkyl methacrylate series of polymers has been considered in treatments from this laboratory (19) and by Fujita and Kishimoto (20). In the latter, it is predicted that $1/\Delta \log a^2 \zeta_0$ should be a linear function of $1/\Delta \alpha \Delta T_g$, pro-

vided the effect of varying side group length reflects differences in free volume alone. Here $\Delta \log a^2 \zeta_0$ is the difference between $\log a^2 \zeta_0$ for a given member of the homologous series and for a particular member chosen as reference, when compared at the glass transition temperature of the latter; ΔT_g is the corresponding difference between glass transition temperatures; and $\Delta \alpha$ may be identified with α_f . In Fig. 8, the open circles, reproduced from a previous paper (21), conform to this prediction. Here the reference polymer is the ethyl methacrylate, with $T_g = 62^\circ\text{C}$., and an average value of $2.4 \times 10^{-4} \text{ deg}^{-1}$ is taken for $\Delta \alpha$. However, the black circle representing the 2-ethyl butyl polymer falls above the line. Thus the friction coefficient for the branched side group is somewhat larger than would be expected on the basis of free volume alone.

It is also of interest to compare the monomeric friction coefficients of the different polymers each at its own T_g . For the 2-ethyl butyl methacrylate, $\log \zeta_0$ at T_g is 4.79, calculated by reduction with Eq. [1]. Table III shows that it is actually higher than that of either of the n -alkyl analogs. This may be associated with the fact that f_g is slightly less for the branched polymer; at any rate, the presence of the ethyl branch diminishes the mobility by a factor of 10 when the n -butyl and the 2-ethyl butyl polymers are compared in this manner.

The characteristics of the chain backbone motions are reflected in the detailed shape of the relaxation spectrum in the transition zone. For compari-

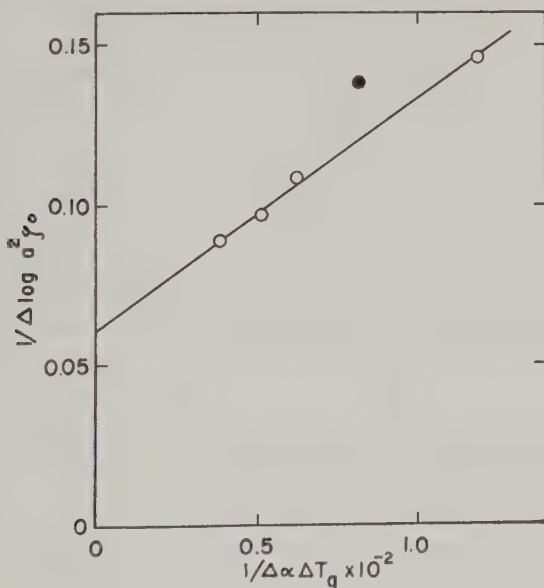


FIG. 8. Fujita-Kishimoto plot for methacrylate polymers. Open circles, left to right: n -dodecyl, n -octyl, n -hexyl, n -butyl; black circle, 2-ethyl butyl.

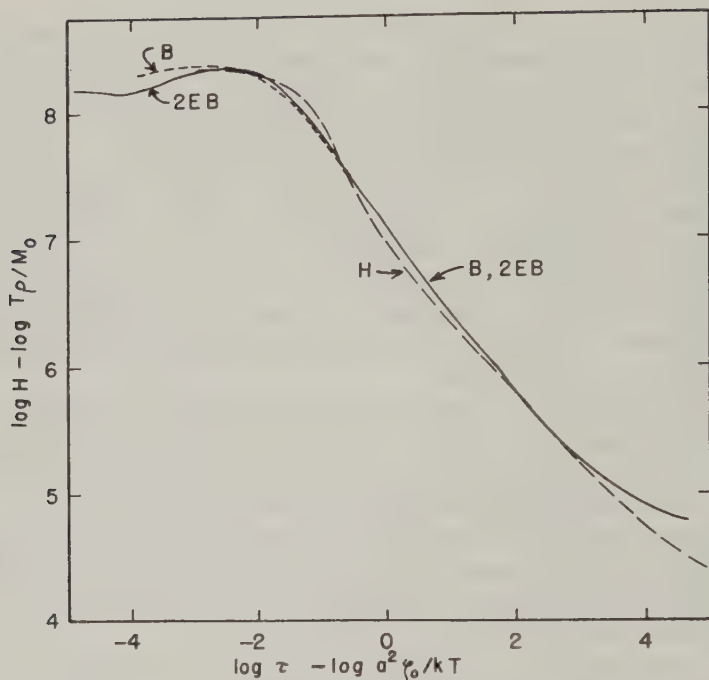


FIG. 9. Relaxation spectra of the *n*-butyl (B), *n*-hexyl (H), and 2-ethyl butyl (2EB) polymers reduced to corresponding states as described in the text.

sons, it is convenient to reduce to corresponding states (22) by plotting the logarithms of $HM_0/\rho T'$ vs. $\tau kT/a^2 \zeta_0$. (The abscissa is dimensionless, and the ordinate is dimensionless except for a factor of R .) Here ρ is the density and M_0 is the monomer molecular weight. As shown in Fig. 9, the relaxation spectra for the *n*-butyl and 2-ethyl butyl polymers when plotted in this manner coincide throughout the entire transition zone except for a slight divergence to the left of the maximum at the entrance to the glassy zone. Thus the cooperative chain motions responsible for mechanical response appear to be of identical character. The spectrum for the *n*-hexyl polymer deviates slightly from the other two.

The Retardation Spectrum and Entanglements

A similar reduction of the retardation spectra to corresponding states (22) is shown in Fig. 10. Here again the spectra for the *n*-butyl and 2-ethyl butyl polymers very nearly coincide, through the maximum which reflects the entanglement network. It is qualitatively evident that the entanglement coupling spacings for these two are closely similar. The maximum for the *n*-hexyl polymer is higher and appears to the right on the time scale, corresponding to a broader spacing between entanglements.

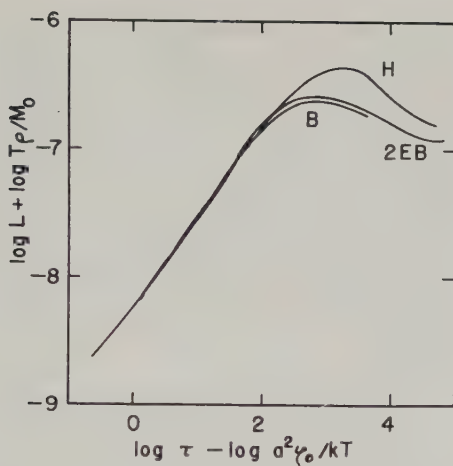


FIG. 10. Retardation spectra reduced to corresponding states as in Fig. 9.

The degree of polymerization between entanglement coupling points, Z_e , can be estimated from the present data in three ways: from the spacing Δ between the limbs of the relaxation spectrum in the transition and terminal zones where the slopes are $-\frac{1}{2}$ (or the corresponding spacing for the retardation spectrum between limbs with slope $\frac{1}{2}$); from the height of the maximum in J'' ; and from the location of the maximum in J'' on the frequency scale, ω_m . The last two calculations are based on the theory of Marvin (12). The appropriate formulas are (9, 12, 22):

$$\log Z_e = \log (M/2M_0) - \Delta/2.4 \quad [3]$$

$$Z_e = J_m'' \rho RT / 0.32 M_0 \quad [4]$$

$$Z_e = (48 kT / a^2 \zeta_0 \omega_m)^{1/2} \quad [5]$$

For the 2-ethyl butyl polymer, $\Delta = 4.53$, $\log J_m'' = -6.69$, and $\log \omega_m = 1.95$ at 100°C . The values of $\log Z_e$ obtained from these are included in Table III. The calculations from the different sources agree in order of magnitude; that from ω_m is larger, and it may reflect an average which weights the longer species in a distribution of entanglement lengths. Again the 2-ethyl butyl resembles the *n*-butyl much more closely than the *n*-hexyl; the ethyl branch increases the average spacing between entanglements only slightly.

In a comparison of the maxima of the retardation spectra (to which the average molecular weight between entanglements should be proportional) for undiluted *n*-alkyl methacrylate polymers and solutions of poly-*n*-butyl methacrylate, it was concluded (1) that the entanglement spacings were increased by dilution of the polymer chain backbones to about the same

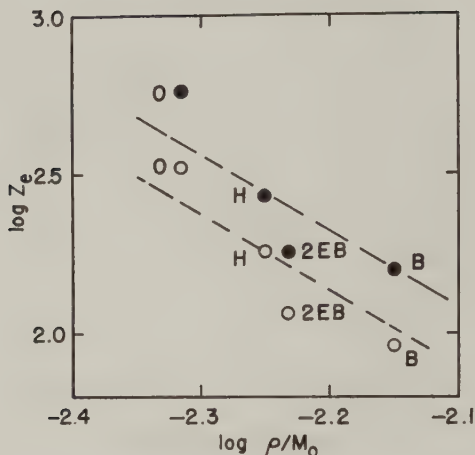


Fig. 11. Degree of polymerization between entanglement points plotted logarithmically against moles monomer units per cubic centimeter. Open circles, from J_m'' ; black circles, from ω_m ; O is *n*-octyl; other identifications as in Fig. 9.

extent whether the dilution was by solvent molecules or increasingly large side groups; since L_{\max} was proportional to $(\rho/M_0)^{3.4}$ —or $(c/M_0)^{3.4}$ for solutions, where c is concentration in grams per cubic centimeter— Z_e should be proportional to $(\rho/M_0)^{2.4}$. A logarithmic test plot for this relation is given in Fig. 11, where the open circles are calculated from J_m'' and the black circles from ω_m . The points for the 2-ethyl butyl polymer, as expected, are out of line; the concentration of monomer units per cubic centimeter, ρ/M_0 , is close to that for the hexyl, but the entanglement spacing is close to that of the butyl.

Table III also includes a comparison of the apparent heats of dissociation of entanglement points, ΔH . The value for the 2-ethyl butyl polymer is somewhat higher than the others, but no significance can be attached to this difference until the nature of the entanglement coupling is better understood.

SUMMARY

The real (J') and imaginary (J'') components of the complex compliance have been measured between 0.05 and 3600 cycles/sec. in the temperature range from 20° to 151°C. for a fractionated poly-2-ethyl butyl methacrylate with molecular weight 2.20×10^6 . The creep compliance, $J(t)$, and creep recovery were measured from 101° to 151°. The glass transition temperature was determined to be 11°C. The method of reduced variables gave superposed curves in the transition zone with shift factors following the WLF form of equation; the WLF parameters were $f_g = 0.021$, $\alpha_f = 1.8 \times 10^{-4} \text{ deg.}^{-1}$. In the plateau zone (including the creep) an additional f -reduction for temperature dependence of entanglement was necessary,

with $\Delta H = 4.4$ kcal. The retardation and relaxation spectra were calculated; the latter is almost identical in shape throughout with that of the *n*-butyl polymer. The logarithm of the monomeric friction coefficient is -3.69 at 100°C . and 4.79 at T_g . The average degree of polymerization between the entanglement coupling points is calculated to be 83, 115, and 178, respectively, from the plateau in the spectra, from the height of the maximum in J'' , and from the position of the latter on the frequency scale. In general, the viscoelastic behavior of the 2-ethyl butyl polymer resembles that of the *n*-butyl much more closely than that of the *n*-hexyl which has the same side chain molecular weight.

ACKNOWLEDGMENTS

This work was sponsored and supported in part by the Office of Ordnance Research, U. S. Army. It was also supported in part by the Research Committee of the Graduate School of the University of Wisconsin from funds supplied by the Wisconsin Alumni Research Foundation. We are much indebted to Mrs. W. C. Frazier and Mrs. A. Rossol for help with the calculations, and to Drs. S. E. Lovell and D. J. Plazek for valuable advice.

REFERENCES

1. SAUNDERS, P. R., AND FERRY, J. D., *J. Colloid Sci.* **14**, 239 (1959).
2. CHILD, W. C., JR., AND FERRY, J. D., *J. Colloid Sci.* **12**, 389 (1957).
3. CHILD, W. C., JR., AND FERRY, J. D., *J. Colloid Sci.* **12**, 327 (1957).
4. DIDOT, F. E., CHINAI, S. N., AND LEVI, D. W., *J. Polymer Sci.* **43**, 557 (1960).
5. JENCKEL, E., AND HEUSCH, R., *Kolloid-Z.* **130**, 89 (1953).
6. SAUNDERS, P. R., STERN, D. M., KURATH, S. F., SAKOONKIM, C., AND FERRY, J. D., *J. Colloid Sci.* **14**, 222 (1959).
7. FITZGERALD, E. R., *J. Chem. Phys.* **27**, 1180 (1957).
8. PLAZEK, D. J., VRANCKEN, M. N., AND BERGE, J. W., *Trans. Soc. Rheol.* **2**, 39 (1958).
9. BERGE, J. W., SAUNDERS, P. R., AND FERRY, J. D., *J. Colloid Sci.* **14**, 135 (1959).
10. NINOMIYA, K., AND FERRY, J. D., *J. Colloid Sci.* **14**, 36 (1959).
11. WILLIAMS, M. L., LANDEL, R. F., AND FERRY, J. D., *J. Am. Chem. Soc.* **77**, 3701 (1955).
12. MARVIN, R. S., in J. T. BERGEN, ed., "Viscoelasticity—Phenomenological Aspects," p. 27. Academic Press, New York, 1960; and personal communication.
13. WILLIAMS, M. L., AND FERRY, J. D., *J. Polymer Sci.* **11**, 169 (1953).
14. SCHWARZL, F., AND STAVERMAN, A. J., in H. STUART, ed., "Die Physik der Hochpolymeren," Vol. 4, p. 44. Springer, Berlin, 1956.
15. FUJITA, H., *J. Appl. Phys.* **29**, 943 (1958).
16. LEADERMAN, H., in F. EIRICH, ed., "Rheology," Vol. 2, p. 49. Academic Press, New York, 1958.
17. SMITH, T. L., *Trans. Soc. Rheol.* **2**, 39 (1958).
18. FERRY, J. D., AND LANDEL, R. F., *Kolloid-Z.* **148**, 1 (1956).
19. DANNHAUSER, W., CHILD, W. C., JR., AND FERRY, J. D., *J. Colloid Sci.* **13**, 103 (1958).
20. FUJITA, H., AND KISHIMOTO, A., *J. Colloid Sci.* **13**, 418 (1958).
21. KURATH, S. F., YIN, T. P., BERGE, J. W., AND FERRY, J. D., *J. Colloid Sci.* **14**, 147 (1959).
22. FERRY, J. D., "The Viscoelastic Properties of Polymers," Wiley, New York, 1961.

THE MORPHOLOGY OF THERMALLY GRAPHITIZED P-33 CARBON BLACK IN RELATION TO ITS ADSORBENT UNIFORMITY

Donald Graham and Walter S. Kay

*Organic Chemicals Department, E. I. Du Pont de Nemours and
Company, Wilmington, Delaware*

Received October 20, 1960

ABSTRACT

Electronmicrographs of thermally graphitized P-33 carbon black indicate that the particles are predominantly doubly truncated polygonal bipyramids. The previously determined concentration of strong adsorption sites is an order of magnitude too small to cover the intersections of the individual planes in the surface, supporting the earlier suggestion of Kmetko that these planes are joined to each other by valence bonds.

DISCUSSION

Thermal graphitization of carbon blacks in the absence of air has provided a series of solid adsorbents of high surface uniformity (1, 2).

The energetic uniformity of the surface (as evidenced in adsorption data) and the planarity of the surfaces (as indicated by electronmicrographic profiles) increases with particle size. The compromise between surface area and surface uniformity which seems to be proving most useful in adsorption research is the P-33 carbon black,¹ graphitized in the absence of air at 2700°–3000°C. This product has a surface area of 12.5 m.²/g., and average crystallite dimensions $L_a = 120$ A. and $L_c = 142$ A. The "c" spacing is 6.84 A. (1, 2).

The extent of heterogeneity (or concentration of strong adsorption sites) as indicated by data for adsorption of nitrogen or argon is only about 0.1% of the total surface (3).

X-ray studies of ungraphitized P-33 indicate that there is some stacking of the graphite planes but without orientation about the layer normal (4) ("turbostratic structure").

Dark-field electron microscopy has shown that the small crystallites which make up the "spherical" particles of ungraphitized P-33 (or at least those crystallites near the surface) are probably oriented with the basal planes parallel to the surface (5).

¹ Produced by Thermatomic Carbon Company, Sterlington, Louisiana.



FIG. 1. Electronmicrograph of graphitized P-33 carbon black.



FIG. 2. 3/1 shadowed electronmicrograph of graphitized P-33.

When heated to 2700°–3000°C. in the absence of air, the basal planes are extended converting the originally "spherical" particles to polyhedra. Formvar replicas were used to obtain information regarding the gross morphology of these particles and although results were negative for graphitized P-33, some significant views of the larger particles of graphitized Thermax carbon black were obtained (6). The results were interpreted

as indicating that these particles were polyhedra bounded by hexagons and pentagons. It was further concluded that each face was valence bonded to its neighbor making the individual particle a closed system.

More recent and more sharply detailed electronmicrographs of thermally graphitized Thermax carbon black (7) serve to correct the earlier model, showing the particles to be principally truncated polygonal bipyramids.

To obtain comparable information regarding the form of graphitized P-33 particles, electronmicrographs at $15,500\times$ magnification (direct) were made. (The original sample of Polley, Schaeffer, and Smith (1) was used, obtained through the courtesy of Mr. W. D. Schaeffer, then of the Godfrey L. Cabot Co. of Boston, Massachusetts.) The pictures show the polygonal outline of the particles and diffraction effects also bring out the individual faces with unexpected clarity (Fig. 1). Each particle, as viewed from above, is represented by a central polygon (usually of six or eight sides) surrounded by trapezoids. Shadowed electronmicrographs (Fig. 2) indicate that the depth of the particles is roughly comparable with the width. It is therefore concluded that the individual particles are (as in the case of graphitized Thermax) doubly truncated polygonal (principally hexagonal and octagonal) bipyramids.

If these particles were polycrystals with pyramidal crystallites converging at the center, it would be expected that the intersections of the surface planes would constitute strong adsorption sites representing approximately 1% of the total surface. The previously measured concentration of strong sites, about one tenth of this quantity, supports the suggestion of Kmetko that the adjacent faces are valence bonded to each other.

REFERENCES

1. POLLEY, M. H., SCHAEFFER, W. D., AND SMITH, W. R., *J. Phys. Chem.* **57**, 469 (1953).
2. SCHAEFFER, W. D., SMITH, W. R., AND POLLEY, M. H., *Ind. Eng. Chem.* **45**, 1721 (1953).
3. GRAHAM, D., *J. Phys. Chem.* **61**, 1310 (1957).
4. BISCOE, J., AND WARREN, B. E., *J. Appl. Phys.* **13**, 364 (1942).
5. HALL, C. E., *J. Appl. Phys.* **19** (No. 3), 271 (1948).
6. KMETKO, E. A., Proceedings of the First and Second Conferences on Carbon P-21, Univ. of Buffalo, Buffalo, N. Y., 1956.
7. KURODA, H., AND AKAMATU, H., *Bull. Chem. Soc. Japan* **32**, 142 (1959).

LETTERS TO THE EDITOR

MODELS OF A LIQUID DROP APPROACHING AN INTERFACE

In their paper, "The Coalescence of Liquid Drops with Flat Liquid/Liquid Interfaces," Charles and Mason (1) discuss two models for the rate of thinning of the intervening film. These are (I) the spherical-planar approach where neither the drop nor the plane deforms and (II) the parallel-disk approach where the drop flattens until its weight is supported by its internal pressure (see Fig. 1). Model II might be termed a uniform-film model. The two other uniform-film models shown in Fig. 1 have been mentioned by other workers (2, 3).

The equations describing Model III, the approach of a sphere to a deformable interface, were derived by Nielsen (2) but are complicated by the part of the drop which lies below the interface. The force balance in this case gives

$$m \left(1 + \frac{2\sigma m}{(\rho_1 - \rho_2)gb^3} - \frac{m^2}{3b^2} \right) = \frac{2\sigma}{(\rho_1 - \rho_2)gb} - \frac{2b}{3}, \quad [1]$$

where m is the distance from the center of the drop to the plane of the interface, b , the drop radius, σ , the surface tension, ρ_1 and ρ_2 , densities, and g , the gravitational constant. The time, $t_{1,2}$, required to thin to a given film thickness, h_2 , is based on parallel disks of area equal to the spherical segments:

$$t_{1,2} = \frac{9\eta_2 b^2(b-m)^2}{(2b^3 + 3b^2m - m^3)(\rho_1 - \rho_2)gh_2^2}, \quad [2]$$

where η_2 is the continuous phase viscosity. This is the simplified equation where the initial separation, h_1 , is much greater than h_2 .

Equations [1] and [2] must be solved simultaneously. This was done numerically; the results are shown in Fig. 2 in terms of dimensionless groups. The relative equilibrium deformation is only a function of the dimensionless group

$$\pi_5 = \frac{\sigma}{b^2(\rho_1 - \rho_2)g}. \quad [3]$$

As seen in Fig. 2, the results with small deformations approach those for Model II as given by Charles and Mason's (1) Eq. [21]. (This equation can also be simply derived for Model III by not correcting for the weight of the drop below the plane of the interface.)

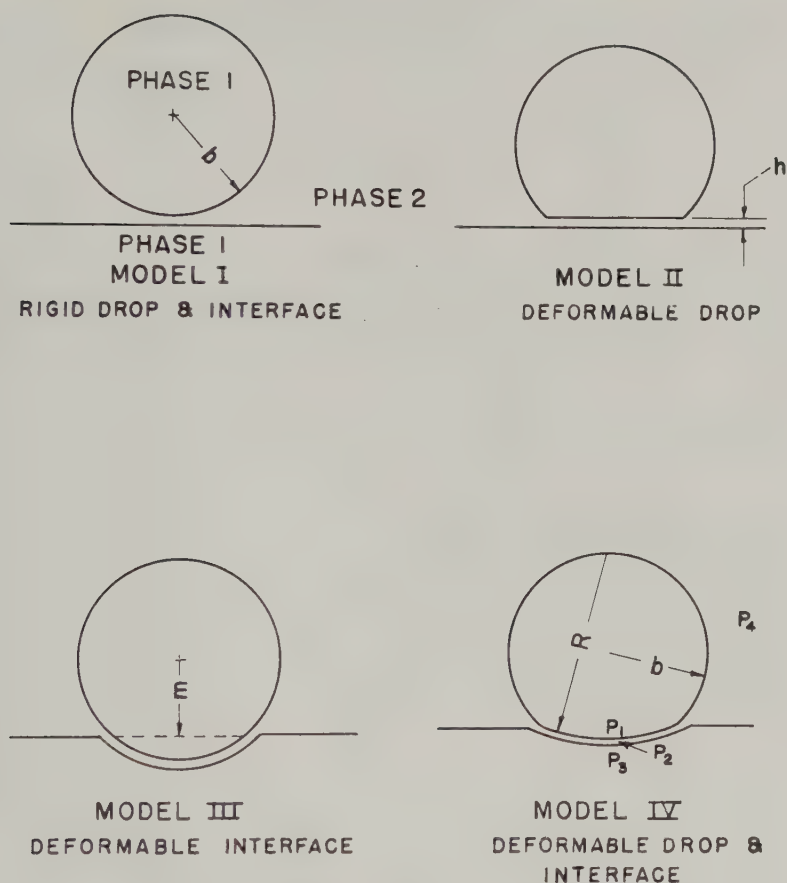


FIG. 1. Models of a fluid drop on a flat interface.

A more general model would have a constant but arbitrary radius of curvature, R , at the surface of contact. Models II and III will be limiting cases where $R = \infty$ and $R = b$, respectively. If one assumes small spherical deformations and equal interfacial tensions on both sides of the film,

$$P_1 - P_2 = \frac{2\sigma}{R} = P_2 - P_3, \quad [4]$$

where P_1 is the pressure inside the drop, P_2 , at the center of the film, and P_3 , in the bulk phase below the film (see Fig. 1). There is no pressure drop across the flat interface. Neglecting hydrostatic head (i.e., a sufficiently small drop), $P_1 - P_3$ is equal to the pressure drop across the free drop surface.

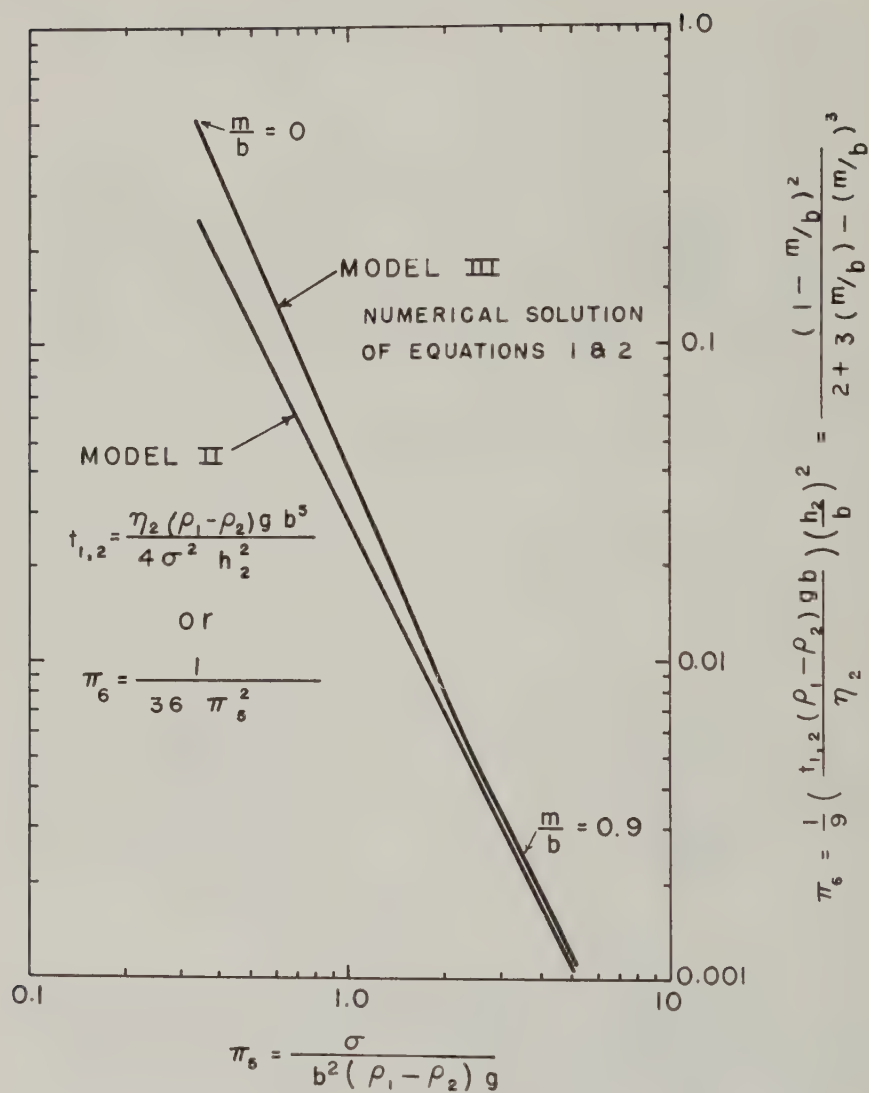


FIG. 2. Relation of system parameters, deformation, film thickness, and time.

Thus

$$P_1 - P_3 = 2 \frac{(2\sigma)}{(R)} = \frac{2\sigma}{b}, \quad [5]$$

$$R = 2b. \quad [6]$$

This is Model IV.

Model IV would seem the most realistic of the uniform-film models. It was one of the cases arbitrarily selected by Elton and Picknett (3). If one again neglects the weight correction for the part of the drop below the interface (i.e., small deformation), one can derive the approximate equation

$$t_{1,2} = \frac{\eta_2(\rho_1 - \rho_2)gb^5}{i\sigma^2h_2^2}, \quad [7]$$

where $i = 1$. The equation for Model II(Charles and Mason's Eq. [21]) and the approximate equation for Model III are the same as [7] except that $i = 4$; the area required to support the drop is only half as much in these cases. (See Elton and Picknett (3) for plots of both cases.)

It should be noted that all uniform film models predict the approach time increases as b^5 and also *increases* with *increasing* density difference. The latter, rather surprising result is the effect of the increased area which overcomes the direct effect of the increased force.

As Charles and Mason (1) point out, the effect of radius on mean rest time is less than b^5 ; Nielsen, Wall, and Adams (4) show that rest time decreases with increased force. These effects suggest that with small radii and small deformations, Model I may be a better approximation. Here times decrease with increasing radius and increasing density difference (Charles and Mason's (1) Eq. [24]). Intermediate radii would then require a mixed model.

Another failure of all uniform-film models can be seen from further consideration of the effect of film pressure on the curvature of the deformable interfaces. Since the pressure in the flowing film must drop in the direction of flow, going from a maximum at the axis to the bulk pressure at the edge, the two principal radii of curvature must vary and the film thickness can no longer be uniform. Specifically, the radii of the drop interface at the edge of the film may be equal to the undeformed drop curvature ($R = b$) and will tend to increase as one moves to the axis of the drop. (More precisely, the sum of the reciprocals of the two principal radii will decrease as the axis is approached.) In easily deformable drops, the radii might become infinite and even negative as the axis is approached, offering an explanation for the observations of Derjaguin and Kussakov (5) where the thinnest part of the film is around an annulus, not at the center. The descriptive differential equations for the more realistic model are complex and have not, as yet, been solved. The problem of relating the film thickness to the probability of film rupture also remains.

I would like to thank Dr. S. G. Mason for his encouragement and for his comments on this letter.

REFERENCES

1. CHARLES, G. E., AND MASON, S. G., "The Coalescence of Liquid Drops with Flat Liquid/Liquid Interfaces," *J. Colloid Sci.* **15**, 236 (1960).
2. NIELSEN, L. E., unpublished derivation.
3. ELTON, G. A. H., AND PICKNETT, R. G., Proceedings of the 2nd International Congress of Surface Activity, Vol. 1, p. 287. Butterworths, London, 1957.
4. NIELSEN, L. E., WALL, R., AND ADAMS, G., *J. Colloid Sci.* **13**, 441 (1958).
5. DERJAGUIN, B. V., AND KUSSAKOV, M., *Acta Physicochim. U.R.S.S.* **10**, 25 (1939).

Plastics Division,
Monsanto Chemical Company,
Springfield, Massachusetts

D. C. CHAPPELEAR

Received January 13, 1961

THE DIELECTRIC CONSTANT IN THE EQUATIONS OF ELECTROKINETICS

The continued use of the dielectric constant in the equations of electrokinetics indicates that currently accepted concepts relating to electrical units have not been introduced into this field. For example, Smoluchowski's equation for the electrophoretic mobility, U ($\text{cm.}^2 \text{ statvolt}^{-1} \text{ sec.}^{-1}$), of a particle moving with velocity, v (cm. sec.^{-1}), under a potential gradient, X (statvolt cm.^{-1}), is usually stated in the form:

$$U = \frac{v}{X} = \frac{D\zeta}{4\pi\eta},$$

where ζ is the electrokinetic potential (statvolt), η is the viscosity of the medium (poise = $\text{gram cm.}^{-1} \text{ sec.}^{-1}$), and D is the dielectric constant. It is clear from the units stated that the factor $D/4\pi$ must have units $\text{gram cm. sec.}^{-2} \text{ statvolt}^{-2}$ or (e.s.u. of charge) $^2 \text{ gram}^{-1} \text{ cm.}^{-3} \text{ sec.}^2$. Guggenheim (1) has suggested that these units be assigned to the factor 4π since he defines D as a dimensionless ratio. Wood (2) has criticised this proposal and has assigned the necessary units to D . The dielectric constant can, however, be defined *only* as a dimensionless comparison ratio.

The earlier solution to this difficulty regarded the ratio $D/4\pi$ as dimensionless, implying that the e.s.u. of charge had dimensions $M^{1/2} L^{3/2} T^{-1}$. Several workers (1, 3) have argued strongly against this artificial reduction in the number of dimensions for electrical quantities from four to three. The introduction of the concept of the "permittivity of free space" enables a satisfactory four-dimensional system to be developed.

The fundamental equation for the force, f (dynes = $\text{gram cm. sec.}^{-2}$), between two charges q_1, q_2 (statcoulomb) separated a distance d (cm.) in a

medium of permittivity K is:

$$f = \frac{q_1 q_2}{K d^2}.$$

The dimensions of K are thus identical with those of the factor $D/4\pi$. The statcoulomb or e.s.u. of charge is defined by assigning the value $K = K_0 = 1 \text{ statcoulomb}^2 \text{ gram}^{-1} \text{ cm.}^{-3} \text{ sec.}^2$ to the permittivity of free space. The dielectric constant D is defined as K/K_0 (or some equivalent comparison ratio) and in the three-dimensional system, since K and K_0 are arbitrarily considered dimensionless, K and D become identical. To preserve the four dimensions it is necessary only to reintroduce K , with appropriate dimensions, in place of D .

This same problem was discussed briefly by Grahame (4) in connection with the theory of electrocapillarity, and a similar solution was offered. The pertinence of Grahame's discussion to the theory of electrokinetics, however, does not seem to have been generally recognized.

Guggenheim (1) has pointed out that only in those cases where K/K_0 is constant should it be called the dielectric *constant*. It has been suggested (5) that this may not be the case in colloidal systems, and this constitutes another argument in favor of the use of K . A permittivity which varies with field strength does not present the contradiction in terms of the system currently in use.

A further improvement may be made by introducing the M.K.S. system of units in accordance with the recommendations of the International Union of Pure and Applied Chemistry (1958) (6). In the "rationalized" (7) version of this system Smoluchowski's equation becomes $U = K\zeta/\eta$, where U is in meter² volt⁻¹ sec.⁻¹, ζ is in volts, and η is in kg. meter⁻¹ sec.⁻¹. Here K is the absolute permittivity = DK_0 where $K_0 = 10^7/4\pi c^2 \text{ coulomb}^2 \text{ kg.}^{-1} \text{ meter}^{-3} \text{ sec.}^2$ (or farad meter⁻¹); c = velocity of electromagnetic waves *in vacuo* $\doteq 3 \times 10^8 \text{ meter sec.}^{-1}$.

The customary practice of recording ζ in volts rather than statvolts would facilitate the introduction of the M.K.S. system with its greater consistency.

I wish to thank Professor A. E. Alexander for his guidance and encouragement in this work.

REFERENCES

1. GUGGENHEIM, E. A., *Trans. Faraday Soc.* **36**(1), 139 (1940).
2. WOOD, L. A., *J. Am. Chem. Soc.* **68**, 432 (1946).
3. JAUNCEY, G. E. M., AND LANGSDORF, A. S., "M.K.S. Units and Dimensions," p. 20. Macmillan, New York, 1940.
4. GRAHAME, D. C., *Chem. Revs.* **41**, 441 (1947).
5. ROBINSON, L. B., *J. Chem. Phys.* **14**, 721 (1946).
- BOLT, G. H., *J. Colloid Sci.* **10**, 206 (1955).

- KITCHENER, J. A., AND HAYDON, D. A., Report of discussion on "Electrical Double Layer in Colloid Science." *Nature* **183**, 78 (1959).
6. Commission on Symbols and Terminology, Section of Physical Chemistry, I.U.P.A.C., Copenhagen, 1958.
7. MARRIOTT, H., AND CULLEN, A. L., *Proc. Inst. Elec. Engrs. (London)* **97**(1), 245 (1950).

*Division of Soils,
C. S. I. R. O.,
Canberra,
Australia*

R. J. HUNTER

Received November 15, 1960

STREAMING POTENTIAL AND TURBULENCE

We have measured E/P and E/v relationships for two Pyrex glass capillaries and found definite indications of a change in slope when the Reynolds number is approximately 2000. These results contrast with those of Bocquet, Sliepcevich, and Bohr (1) and also with those of Rutgers, de Smet, and de Moyer (2) using aqueous solutions, although the latter authors detected a strong turbulence effect when using a benzene solution of Zn-di-*i*-propyl-salicylate.

Streaming potential measurements were carried out on two Pyrex capillaries, capillary I having $l = 33.3$ cm., $r = 0.057$ cm., and capillary II having $l = 24.5$ cm., $r = 0.104$ cm.; with these dimensions the factor by which the fluid velocity must be multiplied to give Reynolds number is 12.5 for I and 23.3 for II. The capillaries were cleaned with hot chromic acid, washed with conductivity water, and dried for 5 hours at 200°C . before measurements. The streaming measurements were carried out using an experimental setup similar to that used by Bocquet *et al.* with compressed nitrogen as the driving force and a Keithley Model 600 electrometer for the potential measurements. The electrodes consisted of $\frac{1}{8}$ inch internal diameter silver tubes appropriately treated internally to form Ag-AgCl electrodes; these tubes were $\frac{3}{4}$ inch long and of the same external diameter as the Pyrex tubes to which they were butted and affixed with an external seal of Tygon tubing. The fluid flow rates were of course actually measured and converted to linear velocities from the capillary dimensions. The results shown in Figs. 1 and 2 are for twice distilled water of conductivity 2.8×10^{-6} ohm $^{-1}$ cm. $^{-1}$ in the case of capillary I (second distillation from alkaline permanganate), and once distilled water of conductivity 8.6×10^{-6} for capillary II.

Calculation of the zeta potential by the Helmholtz-Smoluchowski equation from the slopes of each portion of the E/P curve of capillary I gives

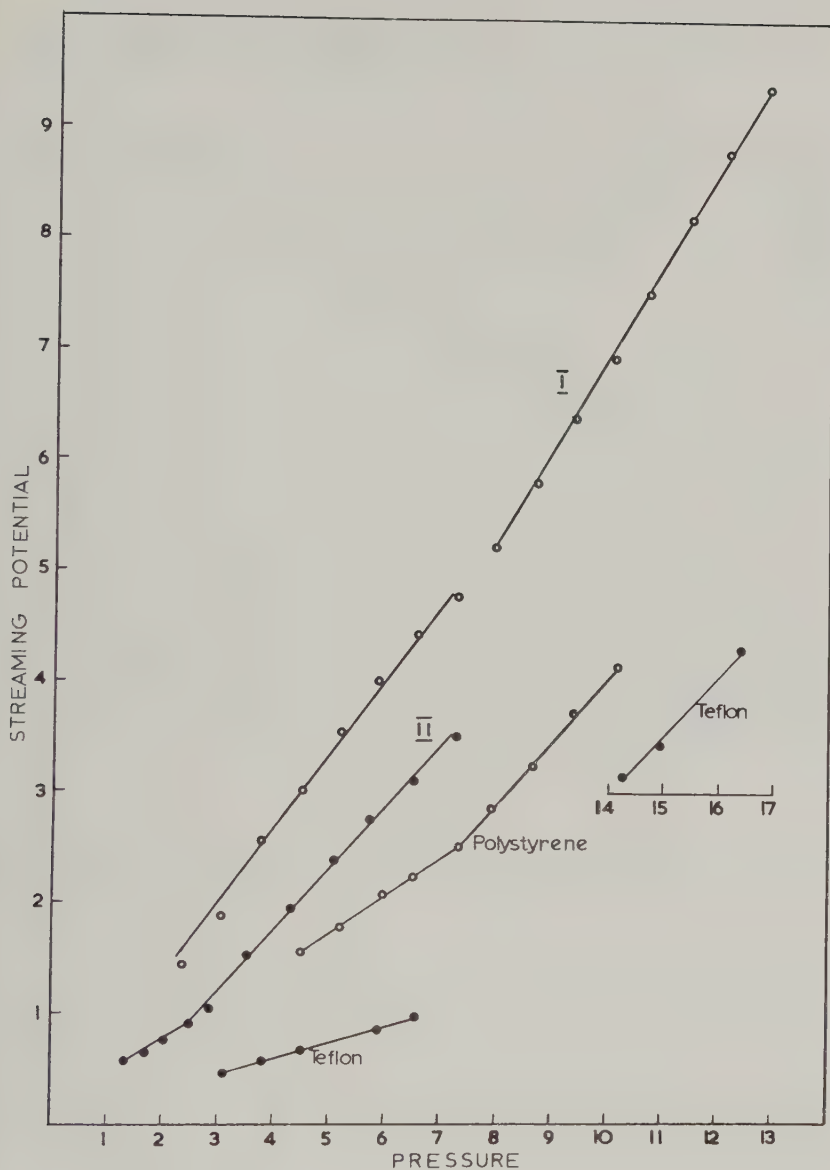


FIG. 1. Streaming potential (volts) versus pressure (cm. Hg).

184 mv. (in good agreement with published values) for the laminar portion and 248 mv. for the turbulent part. Some further results obtained from packings of Teflon chips and Polystyrene beads and (once) distilled water are also shown.

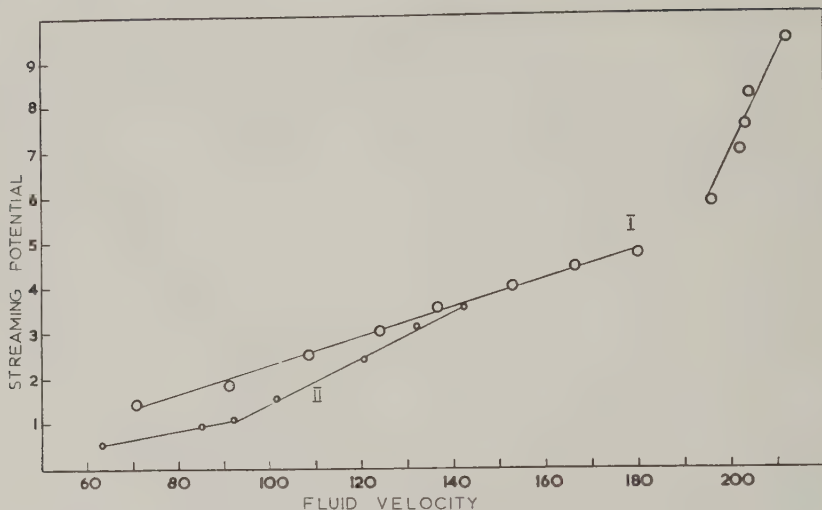


FIG. 2. Streaming potential (volts) versus fluid velocity (cm./sec.).

As a corollary to this study we suggest that the simple experimental arrangement of tubular electrodes fitted to Pyrex tubing provides a convenient surface-active contaminant tester in different distilled waters of similar conductivity. Thus we could calculate $\zeta = 2.9$ mv. for demineralized water of conductivity 2.73×10^{-6} as opposed to the $\zeta = 184$ mv. for the twice distilled water of conductivity 2.8×10^{-6} .

ACKNOWLEDGMENT

This work was financially assisted by a contract from the Chemical Warfare Laboratories, Army Chemical Center, Maryland.

REFERENCES

1. BOCQUET, P. E., SLIEPCEVICH, C. M., AND BOHR, D. F., *Ind. Eng. Chem.* **48**, 197 (1956).
2. RUTGERS, A. H., DE SMET, M., AND DE MOYER, G., *Experientia* **12**, 371 (1956).

Department of Mining
and Metallurgical Engineering,
University of Illinois,
Urbana, Illinois

P. R. STEWART¹
N. STREET²

Received December 2, 1960

¹ Now with Shell Oil Company, Houston 1, Texas.

² Now with Commonwealth Research Station, Merbein, Victoria, Australia.

COMMENT ON THE PAPER "STUDY OF WETTABILITY OF POLYMERS BY SLIDING OF WATER DROPS"

BY KOJI KAWASAKI

In the October 1960 issue of this *Journal*, Koji Kawasaki reported on the sliding of water drops on polymer surfaces (1). In order to explain the experimental results, some relations were given between the mass of the drop (m) and the angle of tilt (α) of the polymer plate at which the drop begins to roll down. Relations were also given for the dependence of m , α , and the width (d) of the drop on the surface tension (σ_{lg}) of the liquid and the advancing and receding contact angles (θ_a and θ_r), respectively, at the head and the tail of the drop at the moment of the "tearing off."

1. In reference to the work of Uriu *et al.* (2), the author gives a linear relation between $\sin \alpha$ and m for the case that $m \geq m_{crit.}$, the latter being the mass of a drop which adheres, without sliding, to the *vertical* plate ($\alpha = 90^\circ$). It can be seen, however (see Fig. 2 in reference 1), that deviations from linearity occur also for $m \geq m_{crit.}$. A better approximation to the experimental results has been given in our earlier work (3) on the sliding of drops of dilute aqueous solutions on paraffin surfaces in the form

$$\sin \alpha = km^{-n}. \quad [1]$$

Here k and n are constants and n has values between 0 and 1. The constant k is obviously equal to $m_{crit.}^n$, and Eq. [1] can therefore be written as

$$\sin \alpha = (m_{crit.}/m)^n. \quad [1a]$$

The plot of $\log \sin \alpha$ versus $\log m$ gives excellent straight lines both for paraffin (3) and polymer surfaces (4), the slope of these straight lines being, regardless of the nature of the surface, $-2/3$, i.e., the exponent n in Eq. [1] is equal to $2/3$ (see Fig. 1).

It can be shown as follows that this is in accord with theory. For *small* water drops the quotient m/r^3 (r being the radius of the circle-shaped contact line between air, drop, and solid and equal to $d/2$), is to a first approximation a function only of the equilibrium contact angle.¹ Thus

$$m/r^3 = k_\theta (\approx \text{constant}). \quad [2]$$

On the other hand, it was shown in earlier work (5) that the relation

$$mg \sin \alpha / 2r\pi = k_\alpha \quad [3]$$

¹ The strongly valid relation between m/r^3 and drop dimensions is more complicated (see, for example, in J. J. Bikerman, "Surface Chemistry," Academic Press, New York, 1958, p. 343). A very simple approximation is recently given by K. Weber (Diploma work, Dresden, 1960).

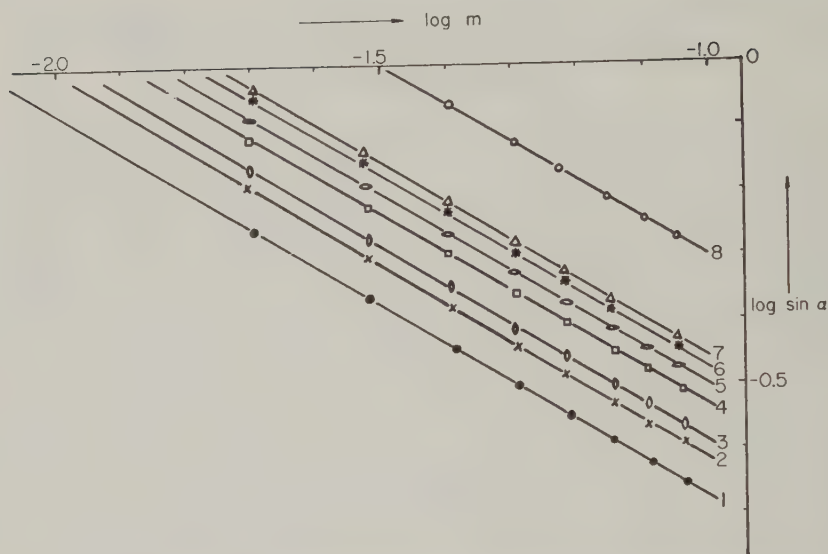


FIG. 1. The $\log \sin \alpha \sim \log m$ relation for the sliding of water drops on low energy surfaces (the author's data). (1) Paraffin; (2) and (4) polyvinyl chloride A and B; (3) polyethylene; (5) and (7) polystyrene A and B; (6) polymethyl methacrylate; (8) polyvinyl acetate.

is also valid. Here g is acceleration due to gravity and k_α is, for a given liquid-solid pair, a constant number ("tearing-off constant," "*Abreisskonstante*" (6)).

From Eq. [2] it follows that

$$r = k_\theta^{-1/3} m^{1/3} \quad [2a]$$

(see also (7)), and from [2a] and [3] it follows that

$$\sin \alpha = (2\pi k_\alpha / k_\theta^{1/3} g) m^{-2/3}. \quad [3a]$$

Equation [3a] is identical with Eq. [1] and the comparison shows that

$$k = 2\pi k_\alpha / k_\theta^{1/3} g = m_{\text{crit.}}^n$$

and

$$n = 2/3,$$

which is in full accord with the experiment.

Recently, we found that the directly measured values of $m_{\text{crit.}}$ correspond not only with those determined graphically from the $\log \sin \alpha \sim \log m$ relation (4) but also with those observed on transferring the drop from one horizontal plate to another horizontal plate ("*Umhaftung*" (8)).

2. The relation

$$mg \sin \alpha = d\sigma_{ig} (\cos \theta_r - \cos \theta_a) \quad [4]$$

(see Eq. [5] in (1)) was first derived in our cited work (3). However, recent work shows that in Eq. [4] a correction must be considered because of the surface pressure of the adsorbed film in the case of drops of aqueous solutions of surface-active agents on paraffin and polymer surfaces (6). It may even be possible to calculate the film pressure of the adsorbed molecules from the difference of the measured and the theoretical value of the "tearing off-constant" k_α (9).

REFERENCES

1. KAWASAKI, K., *J. Colloid Sci.* **15**, 402 (1960).
2. URIU, T., *et al.*, *J. Chem. Soc. Japan (Ind. Chem. Sect.)* **62**, 862 (1959).
3. BUZÁGH, A., AND WOLFRAM, E., *Kolloid-Z.* **157**, 50 (1958); WOLFRAM, E., *Magyar Kém. Folyóirat* **64**, 258 (1958).
4. WOLFRAM, E., AND WEBER, K., to be published.
5. BUZÁGH, A., AND WOLFRAM, E., *Kolloid-Z.* **149**, 125 (1956); BIKERMAN, J. J., *J. Colloid Sci.* **5**, 349 (1950).
6. WOLFRAM, E., Paper (Nr. 64, Sect. B) presented at the 3rd International Congress on Surface Activity in Cologne, September, 1960, in press.
7. NEUDERT, W., *Kolloid-Z.* **118**, 113 (1950); *ibid.* **126**, 104 (1952).
8. WOLFRAM, E., *Kolloid-Z.* **173**, 73 (1960).
9. WOLFRAM, E., unpublished work.

*Institute of Colloid Chemistry
and Colloid Technology of The
University, Budapest, Hungary
and*

*Institute of Colloid Chemistry,
Technische Hochschule Dresden,
Germany*

Received December 27, 1960

ERVIN WOLFRAM

Advances in PROTEIN CHEMISTRY

Edited by: C. B. ANFENSEN, JR., M. L. ANSON,
KENNETH BAILEY, and JOHN T. EDSALL

VOLUME 15

1960, 447 pp., illus., \$13.00

CONTENTS:

Protamines

By KURT FELIX, *Institut für Vegetative Physiologie, Frankfurt, Germany*

Osmotic Pressure

By D. W. KUPKE, *School of Medicine, University of Virginia, Charlottesville*

Protein Malnutrition in Man

By J. CRAVIOTO, *Hospital Infantil de México*, J. C. WATERLOW, and M. L. STEPHEN, *University College of the West Indies, Jamaica*

Reactive Sites and Biological Transport

By HALVOR N. CHRISTENSEN, *The University of Michigan, Ann Arbor*

Crystallized Enzymes from the Myogen of Rabbit Skeletal Muscle

By R. CZOK and TH. BÜCHER, *Philipps-Universität, Marburg, Germany*

AUTHOR INDEX—SUBJECT INDEX.

Previously published:

Vols. 1-7, 1944-1952, each \$10.00

Vols. 8-9, 1953-1954, each \$10.50

Vol. 10, 1955, \$10.00

Vols. 11-12, 1956-1957, each \$14.00

Vol. 13, 1958, 525 pp., illus., \$13.80

Vol. 14, 1959, 447 pp., illus., \$13.00

Reviews:

"No serious student of protein chemistry can afford to deny himself ready access to this work."

—*Archives of Biochemistry and Biophysics*

"This addition to the well-known series on 'Advances' contains seven articles, each written by masters well versed in the difficult art of weaving together several hundred disconnected papers into a readable whole."

—*Nature*



ACADEMIC PRESS

New York and London

111 Fifth Avenue, New York 3 17 Old Queen Street, London, S.W. 1

2nd Edition

Name Reactions in Organic Chemistry

By ALEXANDER R. SURREY

Sterling-Winthrop Research Institute, Rensselaer, New York

April 1961, 278 pp., illus., approx. \$3

Review of first edition:

‘It is rare to find a short book in chemistry that contains clear, concise, and accurate data that at the same time may be considered comprehensive in its treatment of the subject under consideration. Surrey’s book has succeeded in this unusual task and may be considered a baby, one-volume edition of the ‘Organic Reaction’ series. The author has briefly summarized the principal reactions for more than 100 name reactions, of which only about 40 have heretofore been treated. . . .

“The choice of name reactions covers the whole field of organic chemistry, and the main types are selected in order to give the maximum amount of information. Reaction mechanisms are used wherever possible, and the treatment combines classic synthetic organic chemistry with modern concepts in an authoritative and readable manner. Each name reaction is described and illustrated, and the side reactions are discussed. If rearrangements may take place under slightly different conditions, they are also described. References follow each name reaction, so that it is easy to go immediately to the literature for the reaction under consideration. . . .

“The subject index (14 pages) is very complete and has been carefully compiled. It has been set up as a preparation index that leads immediately to the reaction mechanism postulated (proved in many cases) and to a quick summary of the topic. . . . Similar work in other fields would be welcome.”

—Scientific Monthly

Detailed table of contents available upon request



ACADEMIC PRESS *New York and London*

111 Fifth Avenue, New York 3

17 Old Queen Street, London, S.

THE ISOIONIC POINT OF SILVER IODIDE SOLS AND SILVER BROMIDE AND BROMIODIDE EMULSIONS¹

A. H. Herz and J. O. Helling

Research Laboratories, Eastman Kodak Company, Rochester, New York

Received November 2, 1960

ABSTRACT

The isoionic points (IP) of silver bromide and iodide dispersions were measured in the presence of surface-active materials by means of the desorption of silver or halide ions on digestion, as a function of initial pAg of the dispersion. Anionic materials increased adsorption of silver ions and decreased that of halide, so that the pAg of the IP was increased. Conversely, cationic surfactants and polyethylene oxide lowered the IP. Silver bromide and bromiodide gelatin emulsions changed their IP as a function of pH in accordance with the ionization of gelatin.

The maximum amount of bromide ions desorbed on digestion of a silver bromide emulsion was about 1 milliequivalent per mole of silver bromide, corresponding to an original bromide coverage of approximately one tenth of the surface. Desorption of bromide was observed even when the surface area, as measured by dye adsorption, remained unchanged.

INTRODUCTION

The isoionic point (IP) of a silver halide suspension is defined by that pAg at which neither excess halide nor excess silver ions are adsorbed at the silver halide surface. If a silver salt does not exhibit a preference for adsorbing either of its lattice ions from aqueous solution, then its isoionic point and equivalence potential will be identical.

Actually, silver bromide, and particularly silver iodide sols, have been known for many years to show greater adsorptive affinity for their halide constituents than for silver ions. Thus by extrapolation of Owen and Brinkley's data (1), the solubility product of silver iodide at 23°C. is $10^{-16.2}$; this corresponds to the equivalence potential $pI = pAg = 8.1$. Yet, in various investigations (2), including this one, the IP of silver iodide at room temperature was found to be located at approximately pAg 6.0. This difference between the isoionic point and the equivalence potential of silver iodide is an indication of preferential iodide adsorption. Quantitatively, the difference in these constants means that, in order to reach the isoionic point where as many silver as iodide ions are adsorbed, the solu-

¹ Communication No. 2128 from the Kodak Research Laboratories.

tion in equilibrium with silver iodide must contain about 10^4 times more silver than iodide ions.

For determining the isoionic point, a procedure due to Kolthoff and Lingane (3) was employed because their method appeared likely to be applicable to silver bromide and bromoidiodide gelatin emulsions for which such data have not previously been reported. Essentially this method consists in the preparation of silver halide suspensions at various initial pAg values and observing the change of pAg upon digestion. No assumptions are required other than that an increase of silver-ion activity (lower pAg) after aging indicates desorption of excess silver ions and, conversely, that a decrease in silver-ion activity (higher pAg) is evidence for desorption of excess halide. That pAg of the silver halide system which does not change, but remains constant during aging, corresponds to the isoionic point of the system.

DESORPTION EXPERIMENTS WITH SILVER IODIDE SOLS

In agreement with the observations of Kolthoff and Lingane (3), it was found necessary to employ drastic digestion conditions to bring about appreciable desorption of silver or iodide ions from silver iodide sols. In general, the experiments were carried out with 0.01 mole of sol at pH 5.6 (acetate buffer) or pH 7.8 (borax buffer) in a volume of 125 ml. In each experiment, sols were adjusted at 23°C., to initial pAg values covering the range of about pAg 4 to 8.5. The electrode assembly consisted of a silver/silver iodide indicator electrode and a calomel reference electrode with a salt bridge suitably connected to a Beckman Model G pH meter. After the sols had been digested in closed, agitated flasks for about 15 hours at 90°C., the samples were cooled to 23°C., and from the measured pAg change the equivalents of excess silver or iodide ions which had been desorbed could be calculated. In their determinations, Kolthoff and Lingane equated loss of silver ions, i.e., increase of pAg on digestion, directly with gain of iodide ions.² In our calculations, the appropriate solubility product was introduced ($10^{-16.2}$ and $10^{-12.3}$ at 23°C. for AgI and AgBr, respectively) on the grounds that any halide entering solution must meet the requirements imposed by the solubility-product relationship. The actual calculations were simple. If there was an increase in pAg upon digestion, the solubility product of silver iodide was introduced to convert the observed pAg change into a pI change. This transformation allowed the determination of $\Delta [I^-]$, the increase in iodide concentration in moles per liter, from which the number of moles desorbed in the experiment could be obtained directly. If pAg decreased on digestion, the number of excess silver ions was determined in a similar fashion. The appropriate calcula-

² In a different experimental procedure not involving digestion, these authors employed precision titrations to measure adsorption of lattice ions on AgI.

TABLE I^a*Microequivalents Iodide Desorbed from Silver Iodide*

0.01 mole AgI in about 0.14 l. Arrow indicates change after digestion near 90°C.

pAg → pAg	pI → pI		[I ⁻] → [I ⁻] (moles/l.)		$\Delta[I^-]$ (moles/l.)	μ equiv. iodide desorbed from 0.01 mole AgI/0.14 l.	
						Recalcd. values	K. + L. (3) values
6.12 6.6	10.08	9.60	8.3×10^{-11}	2.5×10^{-10}	1.67×10^{-10}	2.3×10^{-5}	7×10^{-2}
6.15 6.58	10.05	9.62	8.9×10^{-11}	2.4×10^{-10}	1.51×10^{-10}	2.1×10^{-5}	9×10^{-2}
6.40 8.19	9.8	8.01	1.6×10^{-10}	9.7×10^{-9}	9.55×10^{-9}	1.3×10^{-3}	5×10^{-2}

^a The pAg changes on which these sample calculations are based were originally reported by Kolthoff and Lingane (3).

tions for some pAg changes on digestion of silver iodide are illustrated in Table I. Also shown in Table I are the desorbed iodide equivalents as given by Kolthoff and Lingane, as well as the corresponding values recalculated from the same data by the indicated procedure. Evidently, the recalculated values are consistent with the theoretical expectation that (in the given range) more iodide should be desorbed from a system at high pAg than from one at low pAg.

In order to make the desorption data unambiguous, it was necessary to show that neither silver nor iodide ions were lost by chemical or physical reactions during the digestion procedure. Control experiments with small amounts of silver or iodide ions in the absence of silver iodide showed that the digestion process caused no substantial change in the concentration of these potential-determining ions. Unless otherwise stated, no interference with these ions was observed in the presence of the compounds discussed in the following sections.

Once the equivalents of desorbed silver and iodide ions had been determined, they were plotted against the pAg value at which the digestion process had been initiated. The intersection of the curve thus obtained with the line of zero desorption indicated the position of the isoionic point. A representative plot based on an experiment with silver iodide in acetate buffer is shown in Fig. 1. From this curve it is apparent that, under the given conditions and in the absence of other compounds, the isoionic point was located at pAg 6.6. Since compounds which are adsorbed to silver halides might influence the adsorption of one or both of the lattice ions, experiments were continued in the presence of some such materials. Their effects on the isoionic point of silver iodide, which are summarized in Table II, may be interpreted as follows:

Gelatin. Lime-processed gelatin interfered seriously in these experiments.

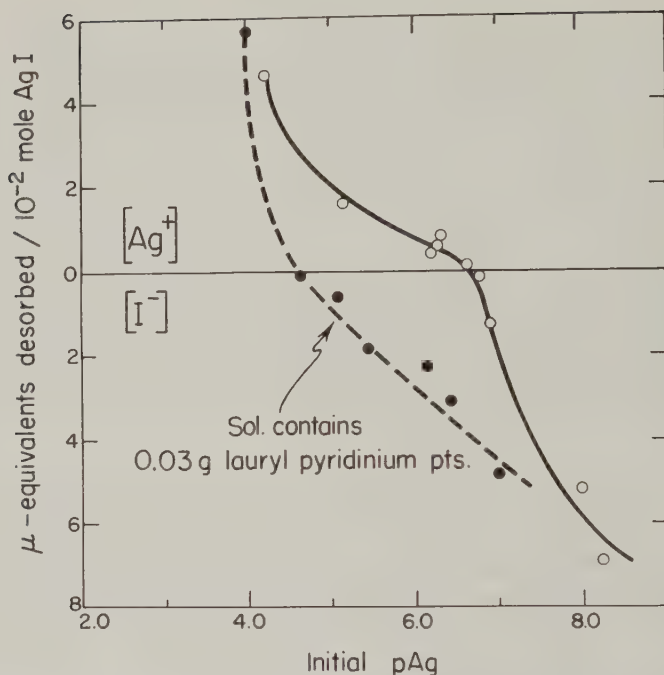


FIG. 1. Desorption of lattice ions from AgI sol. 0.01 mole AgI in 125 ml., pH 5.6; about 15 hours digestion at 90°C.; pAg determinations at 23°C.

TABLE II
Isoionic Points of Silver Iodide at 23°C.

Compounds added per mole AgI	pH	Buffer salts	IP pAg \pm 0.2
Buffer salts	6.7	Bicarbonate	6.0
	7.8	Borax	6.0
	5.6	Acetate	6.6
100 g. Cd(NO ₃) ₂ ·4H ₂ O	5.6	Acetate	6.7
0.6 g. Alkanol B	7.8	Borax	7.6
0.9 g. Decyl trimethylammonium pts.	7.8	Borax	5.3
0.3 g. Lauryl pyridinium pts.	7.8	Borax	5.6
3.0 g. Lauryl pyridinium pts.	5.6	Acetate	4.6
0.8 g. Carbowax—1000	5.6	Acetate	4.9
3.0 g. Carbowax—1000	5.6	Acetate	4.4

With as little as 20 g. of gelatin per mole of silver iodide, reduction of silver ions occurred at pH 5.6 under the required drastic digestion conditions. Furthermore, above the expected isoionic point, in the region of pAg 8–9, the change of iodide concentration on digestion was too small for mean-

ingful evaluation. As has been previously noted in related silver halide systems (4), gelatin appears to have inhibited the grain growth of silver iodide which was obvious in the absence of this colloid.

Salts. The effect of various electrolytes has not been specifically evaluated, although polyvalent ions like La^{+3} or Th^{+4} would be expected to change the isoionic point in the same direction as would surface-active quaternary salts. According to Overbeek and Kruyt (2), 1 *M* KNO_3 had a negligible effect. Similarly, it was found in these experiments that cadmium nitrate at 100 g. per mole of silver iodide caused no appreciable change in the isoionic point. On the other hand, it is known (5) that solvents such as acetone which can alter the hydration shell of ions may produce very substantial changes in this value.

pH. Over the range pH 6.7–7.3, the isoionic point of silver iodide remained constant at pAg 6.0. It is probable that the higher value obtained at pH 5.6, in acetate buffer, was not related to the hydrogen-ion concentration but is an indication of specific adsorption of acetate ions. Evidence for such an effect was first reported by Beekley and Taylor (6a) and has been confirmed by Kellermann and Lange (6b). The last-named authors have shown that, with silver iodide sols in the region pH 2–7, hydrogen-ion concentration has no influence on the adsorption of iodide or silver ions but that acetate promotes adsorption of silver ions.

Anionic Surfactants. The suggestion that acetate ion was responsible for the increased isoionic point was further supported by the observation that Alkanol B (a tri-isopropyl naphthalene sulfonate) and sodium laurate (7a) similarly increased the isoionic point of silver iodide. These facts show that anions which can be adsorbed on silver iodide may increase its isoionic point by enhancing the adsorption of silver ions or by competing with adsorption of iodide.

Cationic Surfactants. In contradistinction to anionic surfactants, cationic compounds exemplified by lauryl pyridinium *p*-toluenesulfonate strongly depressed the isoionic point of silver iodide. This behavior is considered to indicate that, with adsorption of the organic cation, the capacity of the silver salt for binding iodide anions is increased or, what is equivalent in the present context, its adsorptive capacity for silver ions is diminished.

A similar effect (7b) on the position of the isoionic point of silver sulfide has been caused by an adsorbed ammonium salt. Hence, in general, one may expect a depression of the isoionic point of silver salts upon preferential adsorption of cations. This conclusion, it may be added, does not constitute disagreement with the observation that adsorbed cations increase the isoelectric point of silver halides as determined by electrokinetic (zeta-) potential measurements (8). Electrokinetic data, it must be remembered, relate to charge and charge density of particles, whereas the elec-

trochemical method, with which we are concerned here, measures the relative silver and halide adsorption, irrespective of the charge of the silver halide.

Nonionic Surfactants. The observation that polyethylene oxide (Carbowax—1000) decreased the isoionic point of silver iodide, suggests that upon adsorption on the silver salt, the nonionic ether acquires a positive charge. This pseudo-cationic character of the polyethylene oxide, which is presumably caused by formation of oxonium ions (9) involving silver-oxygen bonds, makes it probable that polyethylene glycols also increase the zeta-potential of silver halide.

DESORPTION EXPERIMENTS WITH SILVER BROMIDE EMULSIONS

Various attempts in the past to determine electrokinetic (zeta-) potentials and the isoionic point of silver halides in the presence of gelatin (8, 10) have failed because of the overriding effect of the gelatin charge. Thus, LuValle's data (8) showed that in acidic media where the gelatin had a net positive charge, silver bromide retained a positive zeta-potential, regardless of the bromide concentration, whereas at pH 9.5, where gelatin was anionic, the zeta-potential remained negative even at low pAg.

Such difficulties were not encountered in the present desorption procedure. Excess bromide or silver ions could be desorbed from the silver bromide surface regardless of the presence and charge of gelatin. Furthermore, under the mild digestion conditions which were employed with the silver bromide emulsions, the number of silver or bromide ions reacting irreversibly with gelatin could be neglected for the present purpose. Thus in the absence of emulsion grains, a 0.8% gelatin solution, adjusted with silver nitrate to about pAg 6.0 in the range pH 5.6–10.5, generally changed by less than 0.2 pAg unit during 15 hours digestion at 40°C. Under the same conditions, the bromide concentration of a gelatin control solution remained essentially constant.

The majority of experiments were carried out with the fine-grained Emulsion A because it desorbed excess lattice ions readily (*cf.* Table III for a description of Emulsions A and B). The desorption procedure and calculations were analogous to those used with silver iodide sols. Samples of 0.01 mole of silver halide emulsion in about 120 ml. were adjusted to cover the appropriate pAg range and were agitated in closed flasks for 15 hours at 40°C. before their pAg change was measured. Except where 40°C. determinations were indicated, all pAg measurements were carried out with silver/silver bromide electrodes at 23°C. Although simple inspection of the observed pAg changes may suffice for an approximation of the isoionic point, it will be seen that more information becomes available from a quantitative evaluation of desorption data. A typical desorption curve obtained with Emulsion A in the region of pAg 5–8 is reproduced

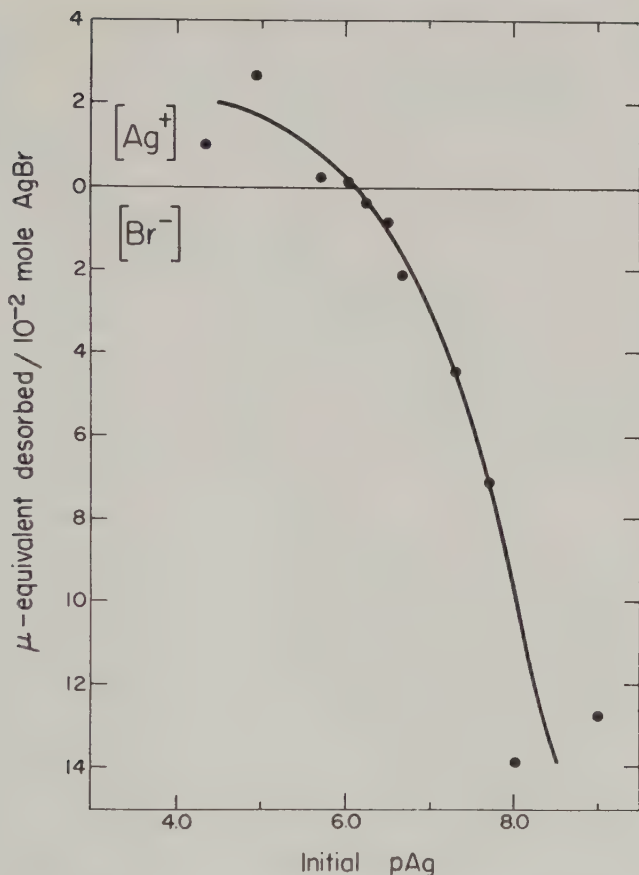


FIG. 2. Desorption of lattice ions from AgBr-gelatin Emulsion A. 0.01 mole AgBr in 120 ml. 0.8% gelatin, pH 5.6; about 15 hours digestion at 40°C.; pAg determinations at 23°C.

in Fig. 2. Although it is possible to obtain desorption data on the bromide emulsions at pAg above 8, the results are less reproducible, since in the concentrated halide solutions corresponding to high pAg values, it becomes more difficult to measure small changes in halide concentration. At any rate, the curve of Fig. 2 shows that at pH 5.6 (23°C.), the isoionic point of the silver bromide emulsion is located near pAg 6.0. Below this pAg, excess silver ions were adsorbed, while above it, excess bromide was bound to the emulsion grains.

Although variations of gelatin concentration, digestion temperature, and emulsion-precipitation conditions had no substantial influence on the isoionic point of silver bromide emulsions, its value turned out to be highly

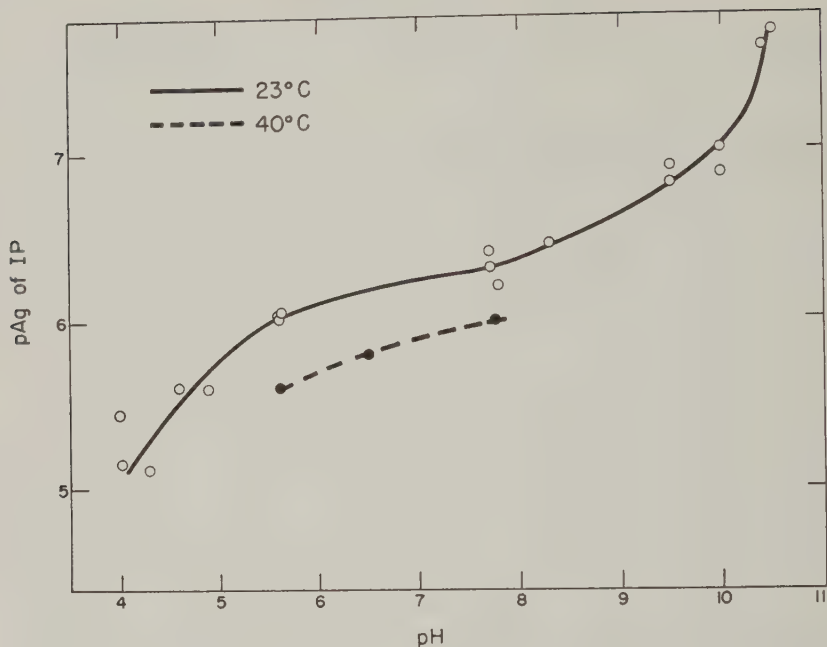


FIG. 3. Dependence on pH of the IP of AgBr-gelatin Emulsion A. Digestion at 40°C.; pAg determinations at 23° and 40°C.

pH-dependent, as shown in Fig. 3. As also shown in this figure, a variation of temperature from 23° to 40°C. lowered the isoionic point of Emulsion A under various pH conditions by 0.3–0.4 pAg unit. Since this difference agreed with the change of the equivalence potential of silver bromide at these temperatures,³ it appears that the relative adsorption of lattice ions was not affected by the given change of temperature.

DESORPTION EXPERIMENTS WITH SILVER BROMIODIDE EMULSIONS

Exploratory experiments readily indicated that, in contradistinction to silver bromide emulsions, bromiodides resisted the desorption of excess lattice ions on digestion. This may have been a manifestation of their relatively slow rate of Ostwald ripening. Although both ripening and desorption of excess halide or silver ions could be accelerated by increasing the temperature, digestion conditions above 60°C. were avoided because of the danger of causing reduction of silver ions. For this reason, the bromiodide emulsions were digested at 40°C. (15 hours), although relatively few excess ions were desorbed under these conditions. The majority of experiments were carried out with an unwashed, very-fine-grained emulsion

³ From Owen and Brinkley (1): at 23°C. $pBr = pAg = 6.15$. At 40°C. $pBr = pAg = 5.80$.

containing 5 mole % iodide and 50 g. of lime-processed gelatin per mole of silver halide. The isoionic point of this emulsion turned out to be substantially the same as that of the bromide Emulsion A. As determined at 23°C., the isoionic point of the bromiodide emulsion increased from pAg 5.8 \pm 0.2 at pH 5.6 to pAg 6.8 \pm 0.2 at pH 10.0.

DESORPTION AND SURFACE-AREA CHANGES IN EMULSIONS

Under the drastic digestion conditions required to bring about desorption of excess lattice ions from silver iodide sols, it was observed that the particle size increased by a factor of ten or more. However, during the experiments with silver bromide-gelatin emulsions, it was noted that desorption of excess bromide ions was not necessarily accompanied by a decrease in the microscopic surface area of the grains. This surface area was determined from the adsorption of 1,1'-diethyl-2,2'-cyanine, which is known to form a close-packed monolayer on silver halide surfaces requiring an area of 79 Å.² per dye ion (11).

The surface areas thus obtained for Emulsions A and B are shown in Table III. Examination of the data makes it apparent that Emulsion B desorbed bromide ions without measurable change in its surface area. Furthermore, the results indicate that in the range of pAg 6.0–6.5, Emulsions A and B desorbed the same number of bromide ions, although the emulsions varied by a factor greater than three in surface area as well as in surface-area changes caused by the desorption process.

TABLE III

Desorption of Lattice Ions from AgBr-Gelatin Emulsions

0.01 mole AgBr in 120 ml. of 0.8% gelatin, pH 5.6. Approx. 15 hours digestion at 40°C. pAg determinations at 23°C.

Emulsion	pAg		Microequiv. ions desorbed from 0.01 mole AgBr	Specific area ^a in cm. ² /g. silver	
	before	after digestion		before	after digestion
A	5.30	4.93	0.82 Ag ⁺	128 \times 10 ³	89 \times 10 ³
	6.28	6.98	0.46 Br ⁻	128 \times 10 ³	89 \times 10 ³
	6.49	7.22	0.82 Br ⁻	—	—
B	6.30	6.95	0.41 Br ⁻	38 \times 10 ³	38 \times 10 ³
	6.48	7.13	0.63 Br ⁻	38 \times 10 ³	38 \times 10 ³
	6.50	7.22	0.82 Br ⁻	38 \times 10 ³	38 \times 10 ³

^a Determined by adsorption isotherm of 1,1'-diethyl-2,2'-cyanine.

Emulsion A: Unwashed AgBr emulsion precipitated at 23°C. 100 g. lime-processed gelatin per mole AgBr.

Emulsion B: Washed AgBr emulsion precipitated at 60°C. 100 g. lime-processed gelatin per mole AgBr.

DISCUSSION

It is known that in the absence of gelatin, adsorption of lattice ions on silver halide sols is not influenced by hydrogen-ion concentration over a wide pH range (6b). Hence, it appears that the pH-dependence of the IP of silver bromide and bromiodide gelatin emulsions can be related to changes of the sign and density of ionic charges of gelatin. The observation that the isoionic point of silver bromide emulsions was low in acidic media, but high at elevated pH values, can be interpreted by the same reasoning that was used to explain the change of the isoionic point of silver iodide in the presence of adsorbable cations and anions. At low pH, the positively charged gelatin enhanced adsorption of halide (or diminished adsorption of silver ions) and thus depressed the isoionic point. On the other hand, in the pH range where gelatin became increasingly negatively charged and behaved like an adsorbed anion, the adsorption of silver ions was promoted, with a consequent elevation of the isoionic point. This effect is particularly obvious at the high pH prevailing under most photographic development conditions; there the isoionic point was located considerably above the equivalence potential of silver bromide.

It may be noted that removal of desorbed silver ions by reaction with gelatin (12) or some other compound could not cause an elevation of the IP. For example, if the same number of halide and silver ions are desorbed but the latter are reduced, the result would be an apparent diminution of the isoionic point.

According to these interpretations one might expect that the lime-processed gelatin at pH 4.9, where it is electrically neutral, should exhibit a minimum effect on the adsorption of halide and silver ions. Indeed, this appeared to be the case; as shown in Fig. 3, the isoionic point of silver bromide emulsions at pH 4.9 was located near pAg 5.6. This value is in agreement with the isoelectric point of silver bromide sols in the absence of gelatin, which has been variously reported (8, 13, 14) between pAg 5.2 and pAg 5.8.

As illustrated by the data of Table III, the number of bromide ions desorbed from silver bromide can be independent of its surface area. This fact supports the view that bromide is adsorbed at specific sites (13-15) such as lattice imperfections or crystal edges and corners. Furthermore, since with Emulsion B, bromide desorption was not accompanied by area changes, as determined by separate dye coverage measurements, it appears the bromide and dye ions were adsorbed at different surface sites.

In addition to deductions concerning adsorption sites, the data permit quantitative conclusions on bromide coverage of the silver bromide emulsion grains. Thus from Fig. 2 it can be seen that near pAg 8, at least 1.4 milliequivalents bromide had been adsorbed per mole of silver bromide

emulsion at pH 5.6. On the basis of the surface area of this emulsion ($128 \times 10^3 \text{ cm.}^2$ per gram of silver) and using 15 \AA^2 as the average area of ion-sites encountered on octahedral and cubic silver bromide faces, this corresponds to coverage of a tenth of the surface ion sites by bromide ions. For Emulsion B, which desorbed up to 0.13 milliequivalent bromide per mole of silver bromide, this coverage involved about 3% of the surface. Bromide coverages of the same magnitude were obtained by Boyer, Cappelaere, and Pouradier with silver bromide sols in the absence of gelatin (15). Hence, it appears that under the given pH conditions, this colloid has only a minor influence on bromide coverage of silver bromide grains.

REFERENCES

1. OWEN, B. S., AND BRINKLEY, S. R., *J. Am. Chem. Soc.* **60**, 2233 (1938).
2. OVERBEEK, J. T., in H. KRUYT, ed., "Colloid Science," Vol. 1, p. 161. Elsevier, Amsterdam, 1952.
3. KOLTHOFF, I. M., AND LINGANE, J. J., *J. Am. Chem. Soc.* **58**, 1528 (1936).
4. AMMANN-BRASS, H., *Chimia (Switz.)* **10**, 173 (1956).
5. MACKOR, E. L., *Rec. trav. chim.* **70**, 742 (1951).
6. (a) BEEKLEY, J. S., AND TAYLOR, H. S., *J. Phys. Chem.* **29**, 942 (1925).
(b) KELLERMANN, A., AND LANGE, E., *Kolloid-Z.* **88**, 341 (1939).
7. (a) BERGNA, H. E., AND DE BRUYN, P. L., Abst. of papers presented in the Division of Colloid Chemistry at meeting of The American Chemical Society, Miami, April, 1957, pp. 61-71.
(b) IWASAKI, I., AND DE BRUYN, P. L., *ibid.*
8. LUVALLE, J. E., AND JACKSON, J. M., *J. Phys. Chem.* **61**, 1216 (1957).
9. WURZSCHMITT, B., *Z. anal. Chem.* **130**, 105 (1949/50).
10. AMELINA, K. S., *J. Phys. Chem. (U.S.S.R.)* **11**, 818 (1938).
11. WEST, W., CARROLL, B. H., AND WHITCOMB, D., *Ann. N. Y. Acad. Sci.* **58**, 893 (1954).
12. MEES, C. E. K., "The Theory of the Photographic Process," revised ed., p. 59. Macmillan Co., New York, 1954.
13. BASINSKI, A., *Rec. trav. chim.* **59**, 331 (1940); **60**, 267 (1941).
14. DAVIES, K. N., AND HOLLIDAY, A. K., *Trans. Faraday Soc.* **48**, 1061 (1952).
15. BOYER, S., CAPPELAERE, J., AND POURADIER, J., *J. chim. phys.* **56**, 495 (1959).

PARTICLE MOTIONS IN SHEARED SUSPENSIONS XI. INTERNAL CIRCULATION IN FLUID DROPLETS (EXPERIMENTAL)¹

F. D. Rumscheidt² and S. G. Mason

*Physical Chemistry Division, Pulp and Paper Research Institute of Canada,
and Department of Chemistry, McGill University, Montreal, Canada*

Received June 7, 1960; revised September 28, 1960

List of Symbols

a, b	= diameter and radius of undistorted drops.
c	= surface concentration.
f_s, f_n	= shear stress and normal stress at interface.
F_s	= total shear force per unit width in Z-direction per quadrant.
G	= velocity gradient.
h	= streamline constnt (y —coordinate of streamline when $x \rightarrow \infty$).
k_1, k_2	= streamline constant inside drop for plane hyperbolic flow and laminar shear flow, respectively.
m	= circulation number = $T_c G / 4\pi$.
m_0	= circulation number at interface.
p	= viscosity ratio η/η_0 .
$P(r), Q(r)$	= functions of r (Eq. [12]).
r	= radius vector measured from origin of coordinate system.
R	= r/b .
t	= time.
T_c, T_0	= mean period of circulation inside drop and at interface.
u, v, w	= velocity components in laminar shear flow.
u', v', w'	= velocity components in plane hyperbolic flow.
x, y, z	= coordinates for laminar shear.
x', y', z'	= coordinates for plane hyperbolic flow.
γ	= interfacial tension.
ϵ	= function of p and b (Eq. [9]).
η, η_0	= viscosity of disperse and continuous phases.

¹ Conducted with financial assistance from the Defence Research Board of Canada, DRB Grant 9510-05.

² Holder of the Spruce Falls Power and Paper Company Limited Fellowship during the academic year 1959/60.

κ	= compressibility of interfacial film.
σ'	= 2-dimensional dilatational viscosity of interfacial film.
π	= surface pressure.
$\tau'(\phi),$ $\tau_0(\phi), \tau(\phi),$ $\tau_i(\phi)$	$\left. \vphantom{\begin{matrix} \tau'(\phi), \\ \tau_0(\phi), \tau(\phi), \\ \tau_i(\phi) \end{matrix}} \right\} = \begin{cases} \text{time of passage along a streamline between } 0 \text{ and } \phi \text{ for} \\ \text{(i) undisturbed shear flow, (ii) on drop surface, (iii)} \\ \text{outside, and (iv) inside the drop in the equatorial plane.} \end{cases}$
ϕ	= polar coordinate angle measured from Y -axis.
ψ, ψ'	= stream functions for shear and hyperbolic flow.
ω, ω_0	= angular velocity ($d\phi/dt$); angular velocity of equator.

INTRODUCTION

In an earlier paper in this series (1), equations were derived for the streamlines inside a viscous fluid sphere suspended at the origin of an infinite body of an immiscible viscous liquid which is undergoing plane-hyperbolic deformation, using a set of equations for velocity components originally derived by Taylor (2) as part of a theory of viscosity of dilute emulsions. By means of a simple transformation, the same set of equations was used to determine the streamlines inside and outside a spherical drop undergoing laminar shear flow (1). Equations were also derived for the period of internal circulation along equatorial streamlines near the center and near the surface.

Experiments with liquid drops (diameter 100 to 200 μ) suspended in corn syrup indicated that internal circulation did not occur in shear flow until the velocity gradient was great enough to deform the drops from spheres into ellipsoids (3, 4). It was concluded from these experiments and from others on the coalescence of drops undergoing two-body collisions that internal circulation was inhibited by the growth of an interfacial film of surface-active impurities in the corn syrup.

Indirect evidence of internal circulation was obtained from careful measurements of the viscosity of dilute monodisperse emulsions (diameter 2.5 to 3.5 μ) (5). In a number of cases, excellent agreement with Taylor's equations was found; in other cases, the intrinsic viscosity was greater than predicted from the theory. It was concluded that Taylor's viscosity theory held except when a viscoelastic film of surface-active emulsifier which tended to inhibit circulation was formed at the interface.

In this paper, we describe an experimental study of circulation inside and outside fluid drops in both laminar-shear and plane-hyperbolic flow which confirms the theory outlined previously (1), and which demonstrates the sensitivity of the phenomena to the presence of surface-active components and impurities. In addition, a number of details of the theory have been expanded to facilitate analysis of the experimental data and to explain the inhibition of internal circulation by surface-active agents ac-

cumulating at the interfaces; these are presented in the Theoretical Part which follows.

The phenomena and principles involved are of interest in connection with the rheology and stability of emulsions and suspensions (4).

THEORETICAL PART

1. General

The equations describing plane-hyperbolic and laminar-shear deformation of the suspending fluid in the absence of any particles are as follows:

$$\begin{aligned} \text{hyperbolic flow} \quad \psi' &= \frac{G}{2} x'y'; & u' &= \frac{G}{2} x'; \\ & & v' &= -\frac{G}{2} y'; & w' &= 0; \end{aligned} \quad [1]$$

$$\text{shear flow} \quad \psi = \frac{Gy^2}{2}; \quad u = Gy; \quad v = 0; \quad w = 0; \quad [2]$$

where ψ is the stream function, u , v , and w are the velocities along the X , Y , and Z axes, and G is the rate of shear of the field defined by Eq. [2]. Equations for the velocity field inside and outside a fluid drop of radius b placed at the origin of the suspending liquid in both of the above types of flow have been given previously (1). In the theory presented below, consideration is limited to shear flow in the $z = 0$ plane.

2. Internal Streamlines

According to the theory (1), the streamlines in the equatorial plane inside the undeformed drop (i.e., $R \leq 1$) are given by the polar equation

$$[R^2 \cos 2\phi + (p + 1)]^3 [R^2 - 1]^2 = k_2. \quad [3]$$

Here $R = r/b$, (r, ϕ) are plane polar coordinates, $\phi = 0$ corresponds to the Y -axis, b is the drop radius, p is the viscosity ratio of the disperse phase to the continuous phase, and k_2 is a constant which describes a particular streamline; k_2 varies continuously from 0, the outermost streamline at the periphery of the drop, to $(p + 1)^3$ at the center. It follows from Eq. [3] that the streamlines are roughly elliptical in shape with the major axes along the Y -axis; in addition, when $p < \frac{1}{2}$ two pockets of fluid circulation exist close to the center of the drop.

The angular velocity along a particular streamline is given by the simple transformation equation

$$\frac{d\phi}{dt} = \omega = \frac{u}{r \cos \phi + \sin \phi \frac{dr}{d\phi}}; \quad [4a]$$

$$= \frac{-v}{r \sin \phi - \cos \phi \frac{dr}{d\phi}}; \quad [4b]$$

where u and v are given by

$$u = \frac{Gr \cos \phi}{4(p+1)} [R^2(5 - 4 \sin^2 \phi) + (2p - 1)]; \quad [5a]$$

$$v = \frac{Gr \sin \phi}{4(p+1)} [R^2(5 - 4 \cos^2 \phi) - (2p + 5)]. \quad [5b]$$

From Eqs. [3], [4a], and [5a] it is possible to calculate ω along various streamlines. Figure 1 shows calculated values of ω along various streamlines for $p = 1$. Along the streamlines near the outside of the drop, i.e., for low values of k_2 , the maximum angular velocity occurs at $\phi = 0$ and the minimum at $\phi = 90^\circ$; near the inside of the drop this is reversed; and

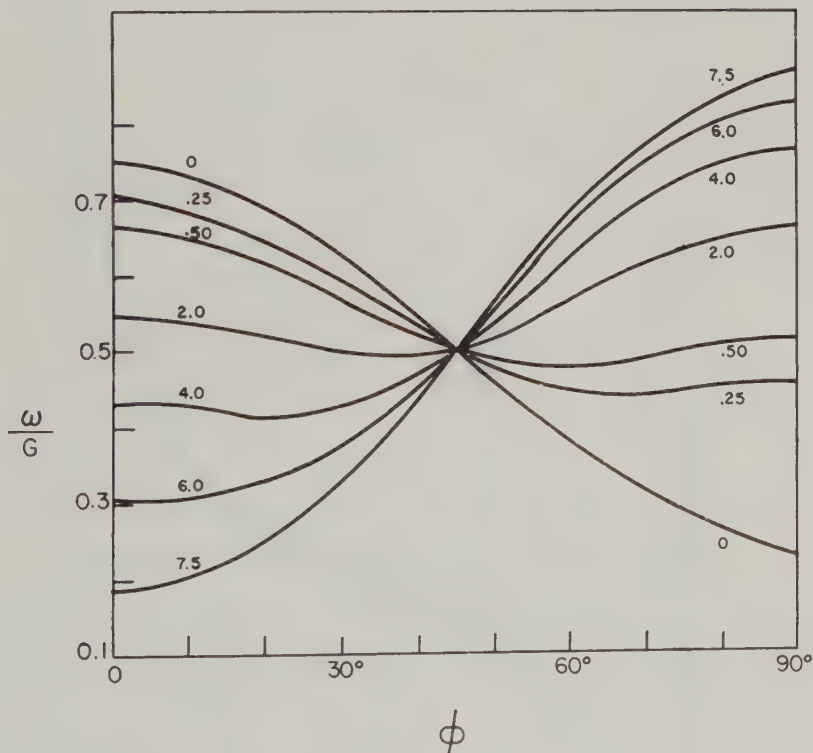


FIG. 1. Calculated angular velocities along streamlines inside a drop of viscosity ratio $p = 1$. The numbers designate values of the streamline constant k_2 ($= 0$ at interface). Note that all curves cross one another at $\omega/G = \frac{1}{2}$ and $\phi = 45^\circ$, as required by Eqs. [4] and [5].

at an intermediate streamline ($k_2 = 2.0$) it remains approximately constant.

The time of passage $\tau_i(\phi)$ along a streamline from 0 to ϕ and the period of circulation T_c around a complete streamline can be calculated from the relations

$$\tau_i(\phi) = \int_0^\phi \frac{d\phi}{\omega}; \quad [6a]$$

$$T_c = \tau_i(2\pi). \quad [6b]$$

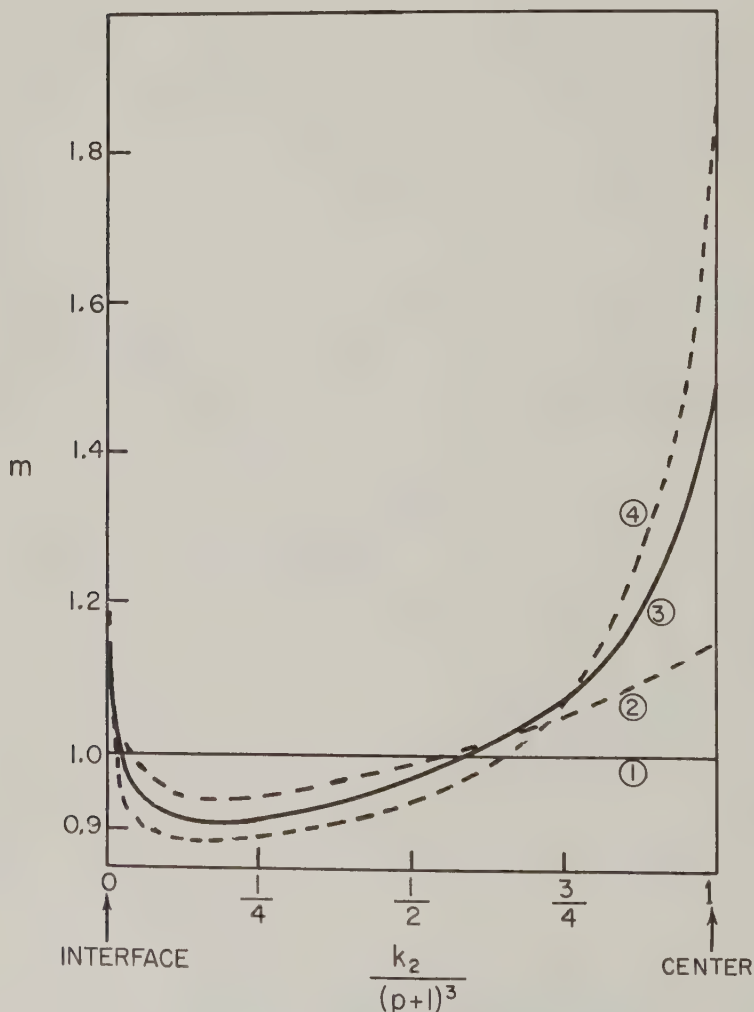


FIG. 2. Circulation number m along various streamlines for $p = \infty$ (curve 1), $p = 2$ (curve 2), $p = 1$ (curve 3), $p = \frac{3}{4}$ (curve 4). The broken lines are based on a limited number of calculations.

The latter quantity is most conveniently expressed as the circulation number $m_{k_2} = T_c G / 4\pi$. Equation [6] can be integrated analytically for the limiting streamlines $k_2 = 0$ and $(p + 1)^3$ to give the following (1):

$$m_0 = \frac{(p - 1)}{\sqrt{p(p + 2)}}; \quad [7]$$

and

$$m_{(p+1)^3} = \frac{2(p+1)}{\sqrt{(2p+5)(2p-1)}}. \quad [8]$$

Values of m for intermediate streamlines can be evaluated by numerical integration of Eq. [6], using the calculated values of ω . This has been done for $p = 0.75, 1$, and 2 with the results shown in Fig. 2; two stream-

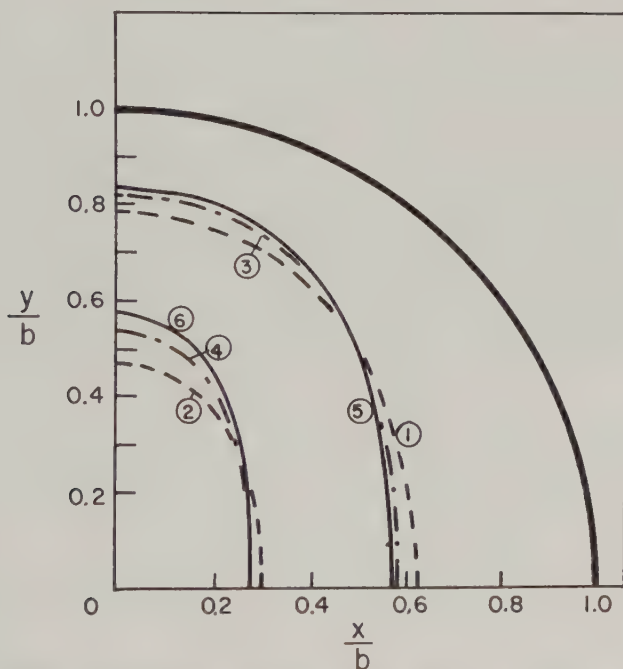


FIG. 3. Internal streamlines in a quadrant calculated from Eq. [3] for the following values:

Curve No.	p	k_2
1	2	6.75
2	2	20.25
3	1	2.00
4	1	6.00
5	$\frac{3}{4}$	1.34
6	$\frac{3}{4}$	4.02

Note that as p increases, the eccentricity of the streamline decreases.

TABLE I
Mean Speeds along Internal Streamlines
 Viscosity ratio $p = 1$

Streamline constant k_2	Relative mean speed
0	1.00
0.25	1.14
0.50	1.12
2.0	0.924
4.0	0.709
6.0	0.474
7.5	0.236

lines for each of these values of p calculated by means of Eq. [3] are plotted in Fig. 3 and show a trend of increasing eccentricity with decreasing p .

It should be noted from Fig. 2 that the circulation number decreases from the periphery until a minimum is reached in the vicinity of the streamline $k_2 = (p + 1)^{3/4}$, and then increases to a value greater than m_0 . A constant value of $m = 1$ indicates behavior as a rigid sphere ($p = \infty$). By means of the path length along a streamline as measured with a map reader, the mean linear speeds ($= \text{path length}/T_c$) around streamlines were calculated and found to be highest along an intermediate streamline between the periphery and the center of the drop. This is illustrated for $p = 1$ in Table I, taking the mean peripheral speed to be unity.

3. External Streamlines

The differential equation for streamlines in the $z = 0$ plane outside the sphere ($R > 1$) may be expressed in a form slightly different from that previously employed (*cf.* Eq. [19] of reference (1)):

$$\frac{d\phi}{dr} = \frac{\epsilon_1 \cos 2\phi + r^5 \cos^2 \phi}{(\epsilon_2 r + \epsilon_3 r^3 + r^6) \sin \phi \cos \phi} \quad [9]$$

where

$$\epsilon_1 = -\frac{pb^5}{2(p+1)}; \quad \epsilon_2 = \frac{3pb^5}{2(p+1)}; \quad \epsilon_3 = -\frac{(5p+2)b^3}{2(p+1)}.$$

By neglecting terms in $(b/r)^5$, Eq. [9] can be integrated to yield for the equation of each streamline

$$R = \left[\frac{h^3}{b^3 \cos^3 \phi} + \frac{5p+2}{2(p+1)} \right]^{1/3}, \quad [10]$$

where h is the streamline constant, the y -coordinate of the streamline when $x \rightarrow \infty$.

Equation [10] is exact only in the limiting case $p = 0$. Better numerical solutions can be derived by numerical integration, using the general solution for Eq. [9]

$$\cos 2\phi = \frac{\left[\int_{r_0}^r Q(r_1) \cdot \exp \left(\int_{r_0}^{r_1} P(r_2) dr_2 \right) \cdot dr_1 \right] + 1}{\exp \left(\int_{r_0}^r P(r_1) dr_1 \right)}, \quad [11]$$

where

$$Q(r) = \frac{-2r^5}{(\epsilon_2 r + \epsilon_3 r^3 + r^6)}; \quad [12a]$$

$$P(r) = \frac{2(2\epsilon_1 + r^3)}{(\epsilon_2 r + \epsilon_3 r^3 + r^6)}; \quad [12b]$$

and r_0 is the radius vector of the particular streamline at $\phi = 0$. Although the calculations are somewhat laborious, Eq. [11] can be integrated numerically for given values of r_0 and p .

Streamlines having identical values of r_0 for $p = 1$ and $p = \infty$ calculated from Eq. [11] are shown in Fig. 4, and from Eq. [10] for $p = 0$. It is seen that as predicted (1) from the approximate solution, the disturbance to a given streamline caused by the sphere is least when $p = 0$ and greatest when $p = \infty$. This behavior is reflected in the respective intrinsic viscosities (5). A streamline calculated from Eq. [10] for $p = \infty$ is shown for comparison in Fig. 4 and is seen to represent a greater disturbance than the exact solution.

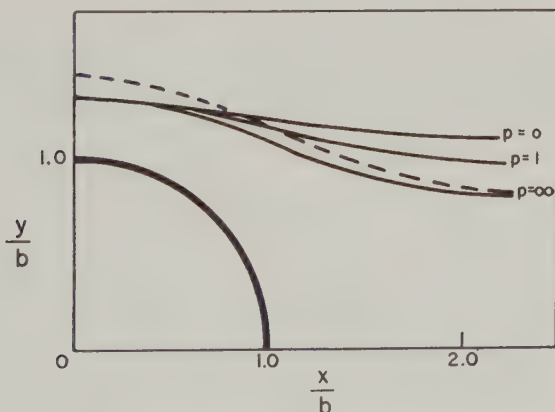


FIG. 4. Calculated external streamlines in a quadrant for $r_0/b = 1.30$ (solid lines). The broken curve is the approximate solution furnished by Eq. [10] for the same value of h as the streamline corresponding to $p = \infty$ by the exact method.

The time of passage $\tau'(\phi)$ between 0 and ϕ along a streamline when no particle is present is calculated directly from Eq. [2] to be

$$\begin{aligned}\tau'(\phi) &= \frac{r \sin \phi}{Gr \cos \phi} \\ &= \frac{\tan \phi}{G},\end{aligned}\quad [13]$$

which is independent of the streamline constant h . The corresponding time of passage $\tau(\phi)$ along an equatorial streamline around a drop may be calculated by means of Eqs. [4] using Eq. [9] and the following (1):

$$u = \frac{Gr \cos \phi}{(p+1)} \left[\frac{5}{2} \left(\frac{P}{R^2} - p - \frac{2}{5} \right) \frac{\sin^2 \phi}{R^3} - \frac{p}{2R^5} + p + 1 \right], \quad [14a]$$

$$v = \frac{Gr \sin \phi}{(p+1)} \left[\frac{5}{2} \left(\frac{p}{R^2} - p - \frac{2}{5} \right) \frac{\cos^2 \phi}{R^3} - \frac{p}{R^5} \right]; \quad [14b]$$

where $R \geq 1$.

When $p = 0$, Eq. [4] reduces to

$$\frac{d\phi}{dt} = G \cos^2 \phi \quad [15]$$

along all streamlines (including the surface of the drop) and integrates to the same as Eq. [13]. Rather remarkably, therefore, the time of passage should in this case be unaffected by the presence of a drop.

Equation [13] also applies for all values of p at infinite h .

When $h = 0$, corresponding to the drop interface, the following equation applies (1)

$$\frac{d\phi}{dt} = \frac{G}{2(p+1)} [p + 2 \cos^2 \phi]. \quad [16]$$

When p becomes infinite, Eq. [16] yields

$$\tau_0(\phi) = \frac{2\phi}{G}. \quad [17]$$

For finite non-zero values of p , Eq. [16] integrates to

$$\tau_0(\phi) = \frac{(p+1)}{G} \frac{2}{\sqrt{p(p+2)}} \tan^{-1} \left[\sqrt{\frac{p}{(p+2)}} \tan \phi \right]. \quad [18]$$

For intermediate streamlines, it is not possible to find an exact solution when $p > 0$. Taking the extreme case $p = \infty$, Eq. [4] reduces to

$$\frac{1}{G} \left(\frac{d\phi}{ds} \right) = \frac{(R^5 - \frac{1}{2}) - \frac{5}{2} \sin^2 \phi \cdot (R^2 - 1)}{R^5 \left[1 + \frac{\sin^2 \phi \cdot (R^5 - \frac{5}{2} R^2 + \frac{3}{2})}{\cos^2 \phi \cdot (R^5 - \frac{1}{2}) + \frac{1}{2} \sin^2 \phi} \right]}. \quad [19]$$

Equation [19] can be integrated numerically along a given streamline to yield $\tau(\phi)$ by inserting values of r calculated by means of Eq. [11]. A number of calculated values of $\tau(\phi)$ are given in Fig. 13.

It is interesting to note that it follows from Eqs. [4] and [16] that when $\phi = \pm 45^\circ$, $\omega = G/2$ for all values of p along all streamlines both inside and outside the drop. This general results (illustrated in Fig. 1) can undoubtedly be traced to the equivalence of irrotational hyperbolic flow and the rotational shear flow when the field described by Eq. [1] is rotated to yield that given by Eq. [2] (1).

4. Interfacial Stresses

It is useful to calculate the stresses generated by the fluid motion at the drop interface. The shear stress f_s at the equatorial interface is given by the simple equation for viscous drag

$$f_s = \eta_0 b \left(\frac{\partial \omega}{\partial r} \right)_{r=b} \quad [20]$$

For shear flow, the angular velocity gradient $(\partial \omega / \partial r)_\phi$ can be calculated directly from Eq. [5] using the general relation obtained by eliminating $(dr/d\phi)$ from Eqs. [4a] and [4b]

$$\omega = \frac{u \cos \phi}{r} - \frac{v \sin \phi}{r}$$

This yields

$$f_s = \frac{5}{2} \left(\frac{p}{p+1} \right) \cdot \eta_0 G \cos 2\phi. \quad [21]$$

The same result follows when $(\partial \omega / \partial r)_\phi$ is calculated from the velocity components outside the drop (Eq. [14])—a result which satisfies the boundary condition in Taylor's theory (2) that shear stresses are transmitted undiminished across the interface. Equation [21] can also be derived from Taylor's Eq. 16 by substituting

$$\phi' = \phi + \frac{\pi}{4}$$

where ϕ' is the corresponding angular coordinate in hyperbolic flow (1). In the latter flow system, f_s is given by substituting $(\sin 2\phi')$ for $(\cos 2\phi)$ in Eq. [21].

According to Taylor's Eq. 16 (2), the normal stress f_n acting radially outwards is

$$f_n = \frac{5}{2} \left(\frac{p + \frac{8}{5}}{p+1} \right) \eta_0 G \sin 2\phi. \quad [22]$$

For the limiting cases $p = \infty$, these equations reduce to

$$f_s = \frac{5}{2}\eta_0 G \cos 2\phi; \quad [23a]$$

$$f_n = \frac{5}{2}\eta_0 G \sin 2\phi. \quad [23b]$$

Equation [23b] is identical with that derived by Vand (6) for rigid spheres.

The significance of the shear stresses in connection with internal circulation is considered in the Discussion, and of the normal stresses in the following paper (7) dealing with drop deformation. In the experiments described below, gas bubbles and liquid drops suspended in a variety of liquids providing a range of p from 0 to 35 were studied in both hyperbolic and shear flow, with the main object of checking Eqs. [3], [6] to [8], [11], [15], and [17] to [19]. In addition, systematic studies were made of the inhibition of internal circulation by impurities and by added surfactants. The experiments were conducted at low values of Gb (<0.05 cm. sec.⁻¹) in order to avoid appreciable deformation of the drops (3, 7).

EXPERIMENTAL PART

1. Plane-Hyperbolic Flow

The experiments using hyperbolic flow were conducted in a "four-roller" apparatus similar to that of Taylor (8). It consisted essentially of four identical aluminum cylinders 5 cm. long mounted vertically at the corners of a square with a side length of 10 cm. as shown schematically in Fig. 5. The rollers were immersed in the suspending fluid contained in a shaped aluminum housing 5.5 cm. deep with a sealed-in plate glass bottom and a removable plate glass cover. The housing was bolted to the top plate which contained the roller mounts, a single chain driving all the rollers and a clutch on each roller.

The rollers were driven at identical speeds in the directions indicated in Fig. 5, i.e., adjacent pairs in opposite directions. By depressing a clutch, the corresponding roller could be brought immediately to rest. A thyrotron-controlled reversible variable-speed d.-c. motor was used to drive the rollers through a gear-reduction box. The speed of the rollers was measured on a self-timing tachometer. For the observation of drops a Zeiss stereomicroscope was mounted above the center of the field. A low-voltage microscope lamp could be arranged to provide either transmitted- or epi-illumination.

End effects resulting from the drag exerted by the bottom of the container were avoided in the same way as in the Couette apparatus mentioned below, by floating the viscous liquids used as continuous phases on a layer of an immiscible liquid of higher density and much lower viscosity.

The rollers were interchangeable and sets of various diameters were available depending on the range of G desired. For the present investigation diameters of 2.30 and 4.00 cm. were used. Following the method used

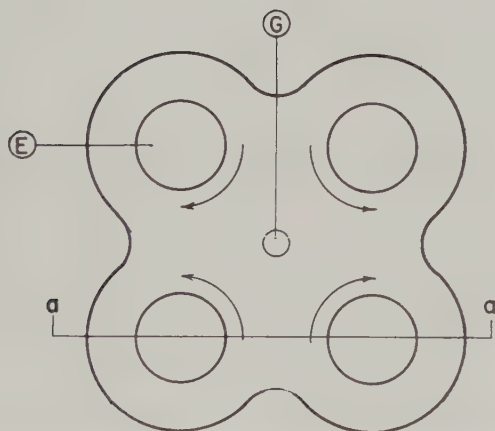
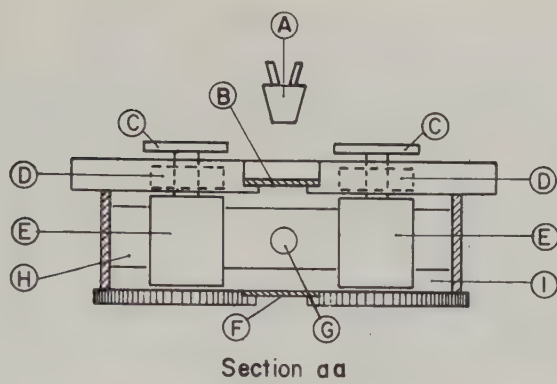


FIG. 5. Vertical section and plan view of the four-roller apparatus (schematic).

- | | |
|--------------------------------------|-----------------------------|
| <i>A</i> —stereo microscope | <i>F</i> —glass insert |
| <i>B</i> —glass cover | <i>G</i> —suspended drop |
| <i>C</i> —clutch | <i>H</i> —suspending medium |
| <i>D</i> —clutch and drive mechanism | <i>I</i> —floating liquid |
| <i>E</i> —roller | |

by Taylor (8), the resulting hyperbolic field was calibrated by timing the passage of tracer particles along various rectangular-hyperbolic paths. The following values of G for the field defined by Eq. [1] near the origin were found:

$$\begin{aligned}
 G &= 20 \times 10^{-3} \text{ N sec.}^{-1} \text{ for 4.00 cm. diam. rollers,} \\
 &= 7.9 \times 10^{-3} \text{ N sec.}^{-1} \text{ for 2.30 cm. diam. rollers;}
 \end{aligned}$$

where N is the speed of the rollers in r.p.m. The range of N available was from 0 to 130 r.p.m.

Single drops, usually between 500 and 1500 μ in diameter, were introduced into the apparatus through the open top by direct injection from a syringe through a hypodermic needle. At the end of an experiment the drops were removed to avoid contamination.

After the apparatus was started the drop was manoeuvred into the center of the field by manipulation of the clutches on the rollers. However, since the central position was inherently unstable, it was necessary to operate the clutches intermittently in order to maintain the drop in the center. Because of this instability, the apparatus could be used only for qualitative observations of internal circulation.

2. Laminar Shear Flow

The Couette apparatus previously (9) described was used to observe particles along the Z -axis of the field of laminar shear flow defined by Eq. [2]. In the initial experiments, the range of shear rates G available at the stationary layer was 0 to 10 sec^{-1} ; by changing the reduction gears, this was reduced to 0 to 3 sec^{-1} .

Qualitative observations of the pattern of internal and external streamlines of drops were made from still photomicrographs taken with a 35-mm. Robot Royal automatic camera mounted on a Zeiss stereomicroscope. Quantitative measurements of periods of circulation and details of streamlines were made cine-photomicrographically, using a Bolex Paillard H16 (16-mm.) camera operated at 8 frames per second. The camera was mounted on the Couette apparatus and a combination of a 75-mm. Berthiot lens (with extension rings) and a beam splitter provided sufficient magnification to dispense with the microscope.

Vertical illumination was usually used, making it possible to observe movements of tracer particles inside the drop and to obtain an indication of their depth. Whereas transmitted light gave better definition of the interface along the equatorial ($z = 0$) plane, it failed to provide a sense of depth and, because of refractive index differences across the interface, obscured the regions just inside the drop.

For accurate time measurements, a Robot electronic timer was used to mark the cine-film at known intervals of time. The duration of recorded events could then be found by a simple count of these marks along the film. The developed film was projected on a screen, and the events under study were traced on paper in a frame by frame analysis. With this combination of photomicroscopy and film projection, magnifications up to 400 \times were obtained.

A single drop was generally used. Drops were removed at the end of each experiment to avoid contamination of the suspending medium.

Both sets of apparatus were operated in a room maintained at $20^\circ \pm 1^\circ\text{C}$.

3. Materials

The following liquids were used as continuous phases:

1. Silicone oil 5000 (Dow Corning fluid 200); $\eta = 52.6$ p., $\rho = 0.975$ gm./c.c. at 20°C . This was used for most of the experiments.
2. Household corn syrup; $\eta = 91$ p., $\rho = 1.38$ g./c.c.
3. Glycerol; $\eta = 9.4$ p., $\rho = 1.26$ g./c.c.
4. Polyglycol, Ucon oil 50HB5100 (Union Carbide); $\eta = 31$ p., $\rho = 1.065$ g./c.c.; water soluble.
5. Castor oil Pale 4 (Baker Castor Oil Co., New York); $\eta = 60$ p., $\rho = 0.993$.

Liquids 1 and 5 were floated on water with sugar added to increase ρ sufficiently to insure flat interfaces. Liquids 2 and 3 were floated on carbon tetrachloride, and liquid 4 on ethylene glycol.

The following liquids were used as dispersed phases:

1. Oxidized castor oils Pale 4 (as above), and No. 300 (Baker); $\eta = 34$ p., $\rho = 0.98$ g./c.c.
2. Cyclohexanol phthalate (designated as CHP); $\eta = 230$ p., $\rho = 1.08$ g./c.c.
3. Silicone oils 1, 100, and 1000 (Dow Corning fluid 200); $\eta = 0.01$, 1.0, and 10 p., $\rho = 0.818$, 0.970, and 0.973 g./c.c., respectively.
4. Polyglycol Ucon LB 1715 (Union Carbide); $\eta = 8$ p., $\rho = 1.003$ g./c.c.; water insoluble.

Other liquids used were water, ethylene glycol, methanol, ethanol, propanol, glycerol, and several hydrocarbon oils. In addition, solid polystyrene spheres ($b = 500 \mu$) were used. All liquids used with the exception of CHP showed Newtonian behavior.

To follow the course of streamlines, various small tracer particles were used, including aluminum flakes, Celite powder, and solid and hollow glass spheres (Eccospheres, Emerson and Cuming Inc., Canton, Mass). Great difficulty was experienced in getting tracer particles to adhere to the drop interface in order to measure m_0 . The only particles found suitable for this purpose were of water-wetted Celite when silicone oils were used as suspending medium and aqueous solutions as drops. When sedimentation was critical, as in liquids of low viscosity, the hollow glass spheres were particularly useful; since they had a wide range of densities, it was possible to match the density of the suspending liquid by simple sedimentation. Water was found to emulsify readily in droplets of diameter 3 to 50μ when introduced into both Pale 4 and Ucon oils; these emulsions were useful for observing circulation in drops in the four-roller apparatus.

RESULTS

1. General Observations of Internal Circulation

a. Hyperbolic Flow. When internal circulation occurred, the characteristic quadrant pattern of streamlines predicted for the $z = 0$ plane (1)

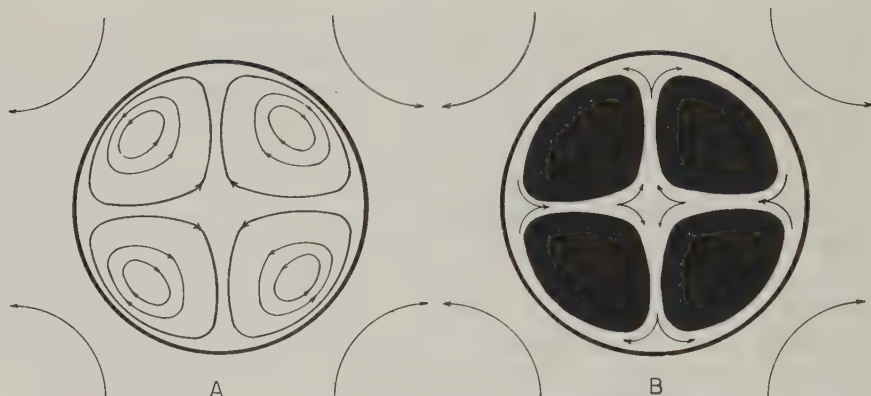


FIG. 6. Internal quadrant pattern observed in hyperbolic flow. The paths of individual tracer particles are shown on the left and are in qualitative agreement with the theory. The pattern developed by emulsified water drops is shown on the right; the light portion indicates regions containing no emulsion droplets.

was readily observed throughout the drop, particularly when the stereomicroscope was used for viewing. Single aluminum flakes could be seen clearly to move along streamlines as illustrated in Fig. 6a. The pattern was revealed strikingly by coarse emulsified water droplets in Pale 4 and in Ucon oil drops; after a short time the emulsion droplets became concentrated into four quadrants clearly separated from one another by two droplet-free layers along the $x' = 0$ and $y' = 0$ planes, and a layer near the surface as shown in Fig. 6b. The quadrant patterns could be seen throughout the height (i.e., along the Z-axis) of the drop. The droplet-free layers are believed to come from the high-velocity peripheral zone near the drop interface which is depleted of droplet centers from the layer within one droplet radius of the wall. The effect is thus analogous to the "axial concentration" of particles in a suspension undergoing laminar flow through a narrow tube (10).

Numerous experiments were conducted, using a variety of liquid/liquid systems at values of G sufficiently low ($< 0.3 \text{ sec.}^{-1}$) to avoid appreciable deformation of the drops. Since the experiments were qualitative in nature, the results are presented in summary form.

The rate of circulation at a given G invariably decreased progressively with the age of the drop and often ceased completely. The time interval during which circulation could be observed tended to increase with increasing p and decreasing G . It could also be substantially increased by reducing contamination of the drops. This was done by rigorous cleaning (including extraction for 48 hrs. with water in a Soxhlet extractor) of the hypodermic needles and glass syringes from which the drops were released. In this way, the elapsed time before circulation was arrested in water drops suspended

in silicone oil at $G = 0.2 \text{ sec.}^{-1}$ was increased from 2 to 30 min. Similar results were found with other liquids suspended in silicone oil, Ucon oil, and castor oil.

Once circulation had stopped, it could be re-established by increasing G ; and the smaller the drop, the greater the G required.

These observations confirm the earlier conclusions (3, 4) concerning the inhibitory effect on internal circulation when surface-active impurities accumulate at the interface. This was corroborated by observing drops of CCl_4 and CHP; internal circulation stopped within seconds after the drops were introduced into corn syrup, which is believed to contain appreciable amounts of surface-active impurities. When the same drops were released into silicone oil, precautions being taken to avoid contamination, circulation was maintained for periods of at least 20 min. The same behavior was shown by CHP ($p = 35$), Pale 4 castor oil ($p = 7$), and silicone oil 100 ($p = 0.1$) in pure glycerol; however, on adding a surfactant (polyoxyethylene sorbitan monolaurate, nonionic) to the glycerol, the circulation was arrested in much the same way as in corn syrup.

Internal circulation was also observed in air bubbles containing NH_4Cl smoke and injected into silicone oil. The quadrant pattern was developed in about 1 sec. Owing to rapid flotation of the bubbles, however, observations could be made only for about 15 sec.

b. Shear Flow. As a result of continuous rotation in all parts of a drop for all p 's, it proved more difficult to follow internal circulation visually in shear flow than in hyperbolic flow, particularly at low G 's (0.03 to 0.1 sec.^{-1}) when the drops remained nearly spherical. When it occurred, it was possible, however, to detect qualitatively the variation of ω with ϕ shown in Fig. 1, viz., a minimum in ω at $\phi = 90^\circ$ and 270° and a maximum at $\phi = 0^\circ$ and 180° near the interface and vice versa near the center of the drop. The elliptical paths of particles inside the drop could be observed. The more complicated streamline patterns near the center of the drop predicted for $p < \frac{1}{2}$ were never seen possibly because of incomplete development of internal circulation. The trends illustrated in Fig. 2 and Table I were also observed; tracer particles just inside the drop interface completed a rotation more rapidly and moved at greater speeds than particles at the interface or near the center. The above observations were made in about 20 different liquid pairs, many of which involved silicone oil 5000 as the suspending medium, with rigorous cleaning of the syringes containing the droplets to be dispersed.

Indirect evidence of internal circulation in air bubbles dispersed in corn syrup was provided by observing carbon powder introduced inside the bubbles so that it settled on the interface near the bottom. The powder remained there as G was increased until a critical value was reached, after which the powder climbed up the interface and approached the equatorial

plane ($z = 0$); upon decreasing G the particles sedimented back to the bottom of the bubble. Observations on bubbles of different radius b indicated that the critical G varied inversely with b . According to the theory (1), the vertical component of velocity at the interface is

$$w = -\frac{G}{(p+1)} \frac{xyz}{b^2}, \quad [24]$$

when internal circulation occurs, but is otherwise zero. Thus the existence of non-zero w at the interface indicates internal transport.

When liquid drops were deformed appreciably by the gradient, internal circulation was invariably observed. A discussion of the behavior of deformed drops will be presented in another paper (7).

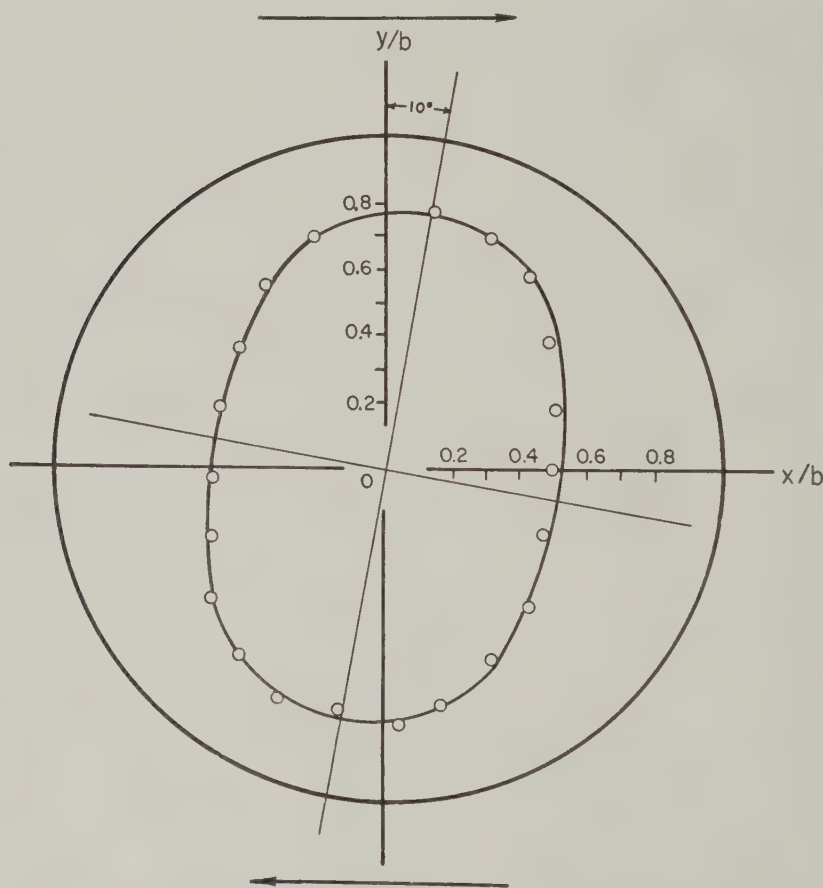


FIG. 7. Streamline inside a Pale 4 castor oil drop ($b = 700 \mu$) suspended in silicone oil 5000. The points are experimental values and the line is that calculated from Eq. [3] using $p = 1$ and $k_2 = 2.75$ and rotated clockwise 10° to allow for deformation at the $Gb(3 \times 10^{-3} \text{ cm. sec.}^{-1})$ used in the experiment.

2. Internal Streamlines

Quantitative measurements of internal streamlines in shear flow proved to be difficult to make, and were found possible only when aluminum flakes were used, since it was necessary to follow individually identifiable tracer particles over 360° rotations. This eliminated systems of low p for quantitative study since the tracer particles sedimented too rapidly. The most satisfactory system was castor oil in silicone oil ($p = 1.09$). Here it proved possible to obtain a cine-photographic record of elliptical streamlines in the equatorial plane; streamlines in nearby planes were similar in shape but decreased in eccentricity with distance from $z = 0$.

Figure 7 shows a comparison of an experimental streamline with that calculated from Eq. [3] using the value of k_2 giving the best fit. To obtain a proper fit, it was necessary to shift the major axis of the calculated streamline from $\phi = 0$ to $\phi = 10^\circ$; this was undoubtedly due to the small but calculable (3, 7) deformation of the drop along an angle $\phi = 48^\circ$ at the low Gb (3×10^{-3} cm. sec. $^{-1}$) used. Similar agreement with the theory was found for streamlines in 2 other drops. Values of $\tau_i(\phi)$ for the streamline shown in Fig. 7 were in excellent accord with the calculated values (Fig. 8, Curve 1); in addition, the measured and calculated (Fig. 2) values of m

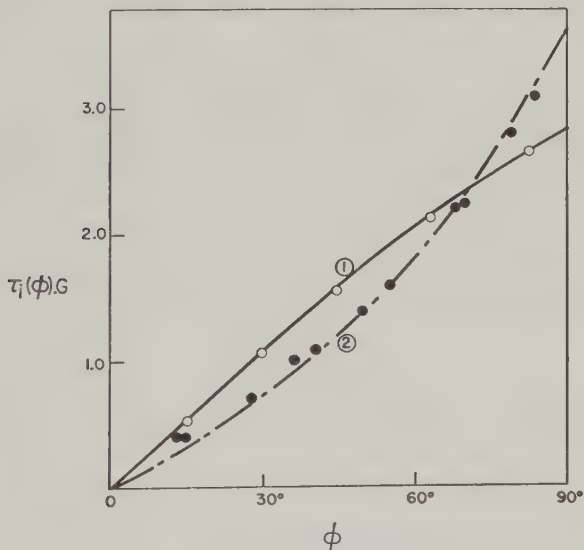


FIG. 8. Curve 1: $\tau_i(\phi)$ for the internal streamline shown in Fig. 7. Each point is the mean of four measured values, one from each quadrant. The curve corresponds to theoretical values calculated from Eq. [6a]. Curve 2: $\tau_o(\phi)$ for another Pale 4 castor oil drop suspended in silicone oil at $Gb = 3.7 \times 10^{-3}$ cm. sec. $^{-1}$. The points are experimental values and the curve is calculated from Eq. [18] for $p = 1.0$. In order to bring the points into coincidence with the respective theoretical curves, it was necessary to subtract 10° from the measured values of ϕ (cf. Fig. 7).

for this streamline were both 0.92, thus providing additional confirmation of details of the theory.

3. Measurement of m_0

Air Bubbles. Careful measurements of the period of peripheral rotation in the equatorial plane of a series of air bubbles ($b = 500$ to 1000μ , $p = 0$) in corn syrup over a range of G from 0.5 to 2.5 sec.^{-1} (which caused negligible deformation) yielded a mean value $m_0 = 1.11 \pm 0.02$ indicating some internal circulation. After aging for 24 hrs., the same system yielded $m_0 = 1.02 \pm .01$, showing that the circulation had practically stopped. This last value is in agreement with earlier (11) measurements. In other measurements on fresh systems, values of m_0 ranging from 1.2 to 1.7 were found.

Air bubbles suspended in "pure" liquids such as silicone oil, Ucon oil, and castor oil yielded values of m_0 from 1.5 to 2.3.

Ethylene Glycol and Glycerol Drops. Measurements of m_0 on 6 different drops of glycol of diameter 400 to 800μ in silicone oil ($p = 3.8 \times 10^{-3}$) yielded some scatter about a common straight line when the results were plotted against Gb as in Fig. 9. The extrapolated value of $m_0 = 1.50$ at $G = 0$ indicates appreciable circulation.

Glycerine/water drops containing 5%, 10% and 25% glycerine ($b = 250$ to 540μ , $p = 2 \times 10^{-4}$ to 0.15) also fell on a common straight line (Fig. 9) of much lower slope which extrapolated to $m_0 = 1$ at $G = 0$, indicating complete suppression of circulation.

Water Drops. The most complete measurements were made on drops of water in silicone oil ($p = 1.9 \times 10^{-4}$). Figure 10 shows a series of plots of m_0 against Gb for seven drops ($b = 295$ to 850μ), each of which yielded a different straight line of approximately the same slope with intercepts

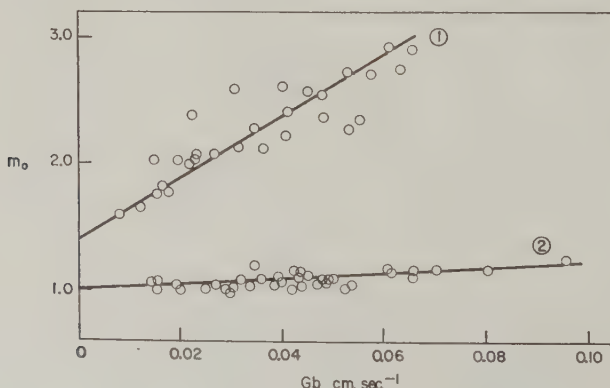


FIG. 9. Circulation number m_0 vs. Gb for ethylene glycol drops (upper line) and for aqueous glycerine drops (lower line) suspended in silicone oil.

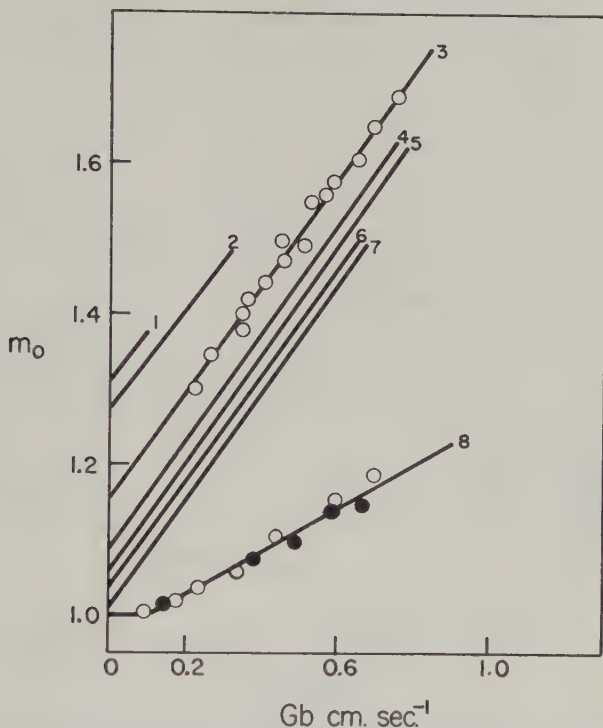


FIG. 10. Circulation number m_0 vs. Gb for water drops in silicone oil. Lines 1 to 7 correspond to water drops of radius 0.30, 0.37, 0.37, 0.40, 0.43, 0.49, and 0.54 mm., respectively. Line 8 is for 2 water drops each containing 0.05% G-3300 ionic surfactant.

varying from 1.01 to 1.31. The variation from drop to drop was undoubtedly due to traces of surface-active impurities; it is significant that the highest values of m_0 were obtained when the rigorous cleaning procedures described earlier were followed.

The pronounced effect of a surfactant in reducing circulation was shown by adding 0.05% of an anionic emulsifier (Atlas G 3300 propyl benzene amine sulfonate) to the water; m_0 showed a pronounced reproducible decrease (Fig. 10) at a given G to a value of unity below $Gb = 0.05 \text{ cm. sec}^{-1}$. The effect was demonstrated in another set of experiments. A drop of water (No. 1) was allowed to collide and coalesce with a drop (No. 2) of similar size ($b = 750 \mu$) containing 0.025% of Atlas G 3300 emulsifier. Coalescence of the colliding drops was induced by applying an electrostatic field of 1500 volts/cm. across the cylinders of the Couette apparatus (12). A third water drop (No. 3) containing CaCl_2 was allowed to coalesce with No. (1 + 2) so as to precipitate the emulsifier. Table II summarizes

TABLE II
Inhibition of Internal Circulation by a Surfactant

Drop	Gb , (cm./sec.)	m_0
1	85×10^{-4}	1.33
(1 + 2)	90×10^{-4}	1.05
(1 + 2) + 3	120×10^{-4}	1.21

Drop 1 = pure water, $b = 800 \mu$.

Drop 2 = 0.025% Atlas G3300; $b = 750 \mu$.

Drop 3 = 3% CaCl_2 ; $b = 720 \mu$.

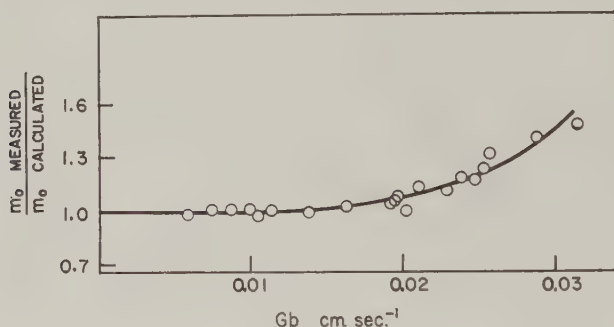


FIG. 11. Ratio of measured to calculated values of m_0 in Pale 4 castor oil drop suspended in silicone oil at various gradients. Four different drops were used ($b = 390$ to 1430μ) over a range of gradients. Calculated $m_0 = 1.154$ (Eq. [7]).

the m_0 values at approximately equal values of Gb : the existence of a minimum m_0 close to unity clearly demonstrates the inhibition of circulation present in the pure water by adding the emulsifier and its re-establishment by precipitating the emulsifier.

Castor Oil in Silicone Oil. Even when circulation did occur in the systems considered above, the value of m_0 was always less than the theoretical value given by Eq. [7]. As might be expected, however, agreement with the theory was found for the castor oil/silicone oil system ($p = 1.09$), confirming details of the theory of internal circulation (Figs. 7 and 8). Figure 11 shows that agreement with the theory was excellent up to $Gb = 0.02$ cm. sec.⁻¹, after which a positive deviation occurred. It is significant that Taylor's deformation equation (3, 8) also applied exactly up to this point and then deviated from the experimental values. The significance of this will be discussed elsewhere (7). Measured values of $\tau_0(\phi)$ at $Gb = 3.7 \times 10^{-3}$ cm. sec.⁻¹ have been plotted in Fig. 8, Curve 2; in order to bring the points into coincidence with the calculated curve, it was necessary to subtract 10° from the measured values of ϕ , the same shift

for the the internal streamlines noted in Fig. 7 and 8, Curve 2, for another drop at approximately the same value of Gb .

4. External Streamlines

Streamlines were determined from photomicrographs taken at known time intervals of the movement of small glass spheres (10 to 30 μ diam.) in the continuous phase. Figure 12 shows experimental points along a streamline in each of three systems ($p = 0, 1$, and ∞). It is seen that in each case there is good agreement with the streamline calculated for the corresponding p by numerical integration of Eq. [11]. In two of the cases, streamlines calculated for other values of p show significant differences from the experimental points, showing that the streamlines are sensitive to changes in p . The observations and calculations (see also Fig. 3) show clearly the increase in streamline distortion with increasing p predicted previously (1). A re-examination of the external streamline around a carbon tetrachloride drop in corn syrup (Fig. 7, Mason and Bartok (4)) has shown that it lay between those calculated for $p = 1$ and ∞ . Since

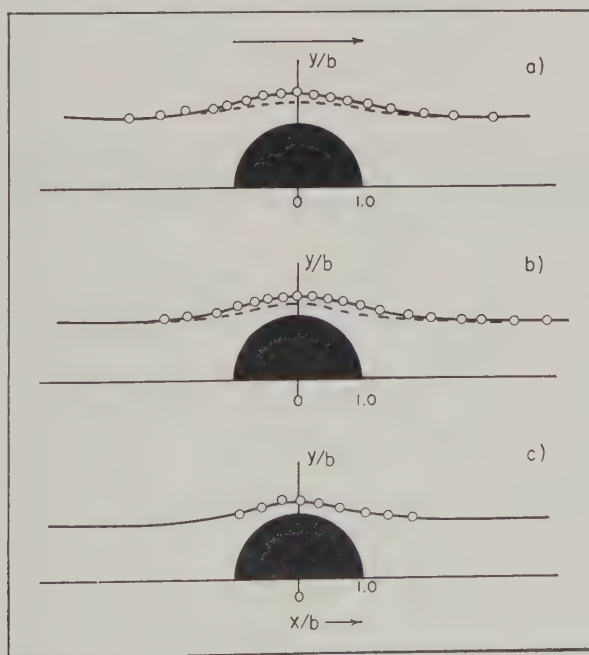


FIG. 12. Experimental points along external streamlines in shear flow: a). a poly-styrene sphere in silicone oil. The solid line is calculated for $p = \infty$ and the broken line for $p = 0$. b). Pale 4 castor oil in silicone oil. The solid line is calculated for $p = 1$ and the broken line for $p = 0$. c). Air in silicone oil. The solid line is calculated for $p = 0$.

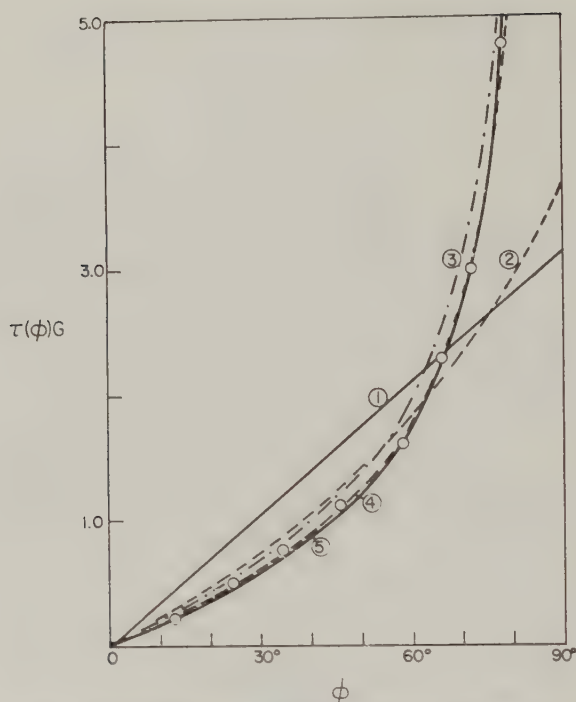


FIG. 13. Calculated and measured times of passage $\tau(\phi)$ along external and peripheral streamlines. The calculated lines have been checked experimentally for the cases indicated below, but for clarity the experimental points have been omitted except for Curve 5 (air bubble in silicone oil).

Curve	p	(h/b)	Equation used	Remarks
1	∞	0	[17]	Checked experimentally
2	1.0	0	[18]	Checked experimentally
3	∞	0.73	[19]	—
4	∞	1.1	[19]	Checked experimentally
5	∞	∞	[13]	Checked experimentally
5	0	0 to ∞	[13]	Checked experimentally for $h/b = 0.73$

the actual $p = 10^{-4}$, this may be considered to be evidence of a partial inhibition of internal circulation.

Times of passage $\tau(\phi)$ were measured in a number of cases and showed good agreement with Eqs. [17], [18], and [19]. The results are summarized in Fig. 13, where, to avoid confusion between the closely spaced curves, the experimental points have been omitted from all except that for an air bubble in silicone oil ($p = 0$, $h/b = 0.73$) which despite the low values of m_0 showed good agreement with the theory. However, it is evident from the narrow spread of curves that $\tau(\phi)$ along external streamlines is rather insensitive to changes in both p and h .

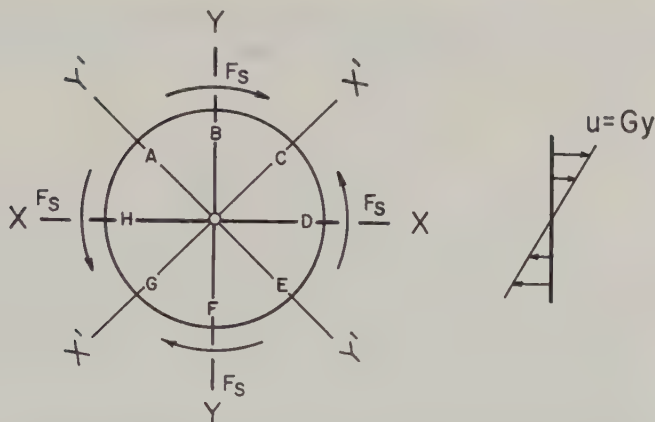


FIG. 14. Calculated distribution of shear forces (schematic) generated by the continuous phase at the surface of the drop. Points *A*, *C*, *E*, and *G* are points of zero shear stress and *B*, *D*, *F*, *H* are points of maximum shear stress

$$f_{s, \max} = \frac{5}{2}[p/(p+1)]\eta_0 G.$$

ψ_1 and ψ_2 are identical when the $X'Y'$ coordinate system is rotated in the clockwise direction at $\omega = G/2$ when in the position shown (1).

DISCUSSION

It is evident from the foregoing experiments that when internal circulation can occur in undeformed drops, the theory presented earlier (1) and amplified in the Theoretical Part is quantitatively confirmed in practically all details for shear flow, and qualitatively for hyperbolic flow. Because of the equivalence of the two at zero deformation (1, 2, 8), we may conclude that the theory holds exactly in both types of flow, provided that the shear stresses are transmitted undiminished across the drop interface. Of the systems examined, castor oil in silicone oil most closely met this condition.

Since the effects of deformation on these phenomena are to be discussed in another paper (7), it remains only to consider the mechanism of inhibition of internal circulation here. The present experiments confirm the earlier conclusion (3-5) that minute traces of surface-active substance whether deliberately added or present as adventitious impurities can arrest internal circulation just as in liquid drops sedimenting under gravity through another liquid (13-15).

The explanation can be found by considering the shear stresses at the drop surface following the procedure used by Linton and Sutherland (15) for sedimenting fluid drops. According to Eq. [21], $f_s = 0$ at $\phi = \pm 45^\circ$ and $\pm 135^\circ$; these points of zero shear stress (*A*, *C*, *E*, *G* in Fig. 14) define four quadrants, the direction of the stress being constant in a given quadrant and of maximum magnitude at its mid-point (*B*, *D*, *F*, *H* in Fig. 14).

The total shear force F_s acting per unit width (in Z -direction) in one of these quadrants is therefore given by

$$\begin{aligned} F_s &= \int_{-45^\circ}^{45^\circ} f_s b \, d\phi; \\ &= \frac{5}{2} \frac{p}{(p+1)} \eta_0 Gb. \end{aligned} \quad [25]$$

The direction of the shear force reverses between adjacent quadrants so that the net moment on the drop is zero—a necessary condition for equilibrium. When the internal circulation is unrestricted, as assumed in the theory, the shear forces are resisted by establishing the appropriate set of velocity gradients at the inside surface of the drop.

When internal circulation is *completely stopped*, however, the drop behaves as though $p = \infty$, so that

$$F_s' = \frac{5}{2} \eta_0 Gb. \quad [26]$$

This requires that a difference in surface tension $-\Delta\gamma = \gamma_c - \gamma_A = F_s'$ be established across each quadrant. This is possible if there is a surface-active agent present which renders the surface viscoelastic so that a corresponding difference in surface pressure $-\Delta\pi = \Delta\gamma$ is established. If, for simplicity, we neglect diffusion in and out of the interface (an assumption which has been shown reasonable in considerations of surface aging in the presence of surface-active agents (16)) so that the equation of continuity becomes

$$\omega_0(\phi) \cdot c(\phi) = \text{constant}, \quad [27]$$

where ω_0 is the peripheral angular velocity and c is the surface concentration, and if we assume linear viscoelasticity in the film, then we may write for a point moving on the periphery (using the Lagrangian system)

$$\pi = f(c) + \sigma' \left| \frac{d \ln c}{dt} \right|, \quad [28]$$

where σ' is an appropriate linear combination of the two-dimensional shear viscosity and of the area viscosity of the film (17, 18) and $f(c)$ is the purely elastic component of the surface pressure. Converting to a point of fixed coordinates (the Eulerian system), Eqs. [27] and [28] lead directly to

$$\Delta\pi = \frac{1}{\kappa} \Delta \ln c + \sigma' \Delta \left| \frac{d\omega}{d\phi} \right|, \quad [29]$$

where κ is the surface compressibility (18). Previously (5) we have calculated σ' from viscosity data by assuming a purely viscous film ($\kappa = \infty$), using a theory due to Oldroyd (18). For the present we consider the more

plausible case of a purely elastic film ($\sigma' = 0$); thus inhibition of circulation will occur when a compression of the film occurs over a quadrant such that

$$F'_s = \Delta\pi = \frac{1}{\kappa} \Delta \ln c. \quad [30]$$

Taking as a typical example of the present experiments, $b = 0.1$ cm., $\eta_0 = 50$ poises, $G = 0.1$ sec.⁻¹, we calculate from Eq. [26] that $-\Delta\gamma = \Delta\pi = 1.25$ dynes/cm., which is small. A reasonable value of κ for a condensed monolayer is 10^{-2} cm./dyne (17, 19), so that for the case we are considering $\Delta c/c = 1.25 \times 10^{-2}$. With reference to Fig. 14, this means that as an element of interface rotates from A to C , a linear compression of only 1.25% followed by the same expansion between C and E is sufficient to prevent internal circulation. This would be reflected by a change in $\omega_0(\phi)$ to satisfy Eq. [27] so that the angular velocity at points A and E would be 1.25% higher than at C and G . This minute deviation from $\omega = G/2$ for a rigid sphere would not be readily detected. It is not difficult to imagine how the rotation of the sphere could accommodate itself to produce the necessary changes in surface concentration. Taking representative values of molecular weight (300) and surface concentration for a condensed monolayer (10 \AA^2 per molecule) the amount of surface-active agent required at the interface of a drop ($b = 0.1$ cm.) is only 6×10^{-8} gm. It is thus clear why mere traces can have so profound an effect.

The calculated value of $\Delta\gamma$ for complete inhibition of circulation in the viscosity measurements on emulsions by Nawab and Mason (5) ($G = 5 \times 10^2$ sec.⁻¹, $b = 2\mu$, $\eta_0 = 10^{-2}$) is 2.5×10^{-3} . This is so small, indeed, that when circulation did occur, as indicated by partial or complete agreement with Taylor's viscosity equation (2), the emulsifier in the surface phase must have had a high κ and a low σ' . When the viscosities deviated from theory, values of σ' were calculated (5) by means of Oldroyd's theory (18) on the assumption that the film was purely viscous. Oldroyd's theory cannot be used, however, to calculate κ from the viscosity data for a purely elastic film; in fact, Oldroyd's theory predicts that when $\sigma' = 0$ and κ is finite the intrinsic viscosity at $G = 0$ is $\frac{5}{2}\zeta$, the value for rigid spheres, corresponding to a complete suppression of internal circulation. This implies that if κ is finite, the film must have a viscous component (or a non-zero relaxation time (18)) if the drops are to have internal circulation at low G 's; this is consistent with the ideas outlined above and embodied in Eqs. [26] and [29].

It is clear from these considerations why the behavior inside the drop is so highly sensitive to traces of surfactants present in either the drop or the suspending liquid which accumulate at the interface and render it viscoelastic.

The observations on decay of internal circulation (in the four-roller apparatus) can be explained in the same way. In these experiments, the surface-active impurities responsible were almost certainly dissolved in the drops. According to Eq. [3] (Bartok and Mason (1)), the velocity components u' , v' , w' at any point inside the drop, and thus the rate at which the surface-active impurities are convected to the interface, vary directly as $G/(p + 1)$; this is why the time elapsing before cessation of circulation increased with increasing p and decreasing G . Equation [25] and the subsequent discussion indicate why the G required to re-establish circulation increased with decreasing drop radius b .

Whereas surface-active agents can inhibit internal circulation, it does not necessarily follow that when they are rigorously excluded all inhibition ceases. This has been demonstrated only for the castor oil/silicone oil system in the present experiments; in all the other systems examined, m_0 was less than the theoretical value. If the interface in rigorously pure systems is viscoelastic as implied by Henniker (20), then some inhibition would be expected. This may account for the consistently low values of m_0 observed, especially with air bubbles.

SUMMARY

The circulation pattern inside fluid drops suspended in a liquid subjected to hyperbolic and to shear flow has been studied and compared with that predicted from a fluid mechanical theory which assumes that the drops remain spherical and that shear stresses are transmitted without diminution across the drop interface. Observations of liquid drops and air bubbles showed that the streamline pattern predicted for hyperbolic flow was established. The intensity of circulation in the drops was found to be decreased by impurities and added surface-active agents.

Details of streamlines inside and outside drops and periods of circulation have been determined for a variety of liquid pairs in laminar shear flow. Impurities and surface-active agents exercise a pronounced inhibitory effect and often completely prevent internal circulation. In several vigorously purified systems the extent of internal circulation was less than predicted, but one liquid pair was found in which the theory was followed in all measurable details.

It is shown theoretically that a viscoelastic film at the interface can reduce the shear stresses transmitted inside the drop and thus attenuate internal circulation. Calculations show that films due to surface-active materials of representative surface compressibilities are capable of completely suppressing internal circulation under the experimental conditions employed. Whereas the theory based on a nonviscous interface of zero elasticity, i.e., of constant surface tension, held for one vigorously purified system, disagreement with the theory in several others may have been due to interfacial viscosity.

REFERENCES

1. BARTOK, W., AND MASON, S. G., *J. Colloid Sci.* **13**, 293 (1958).
2. TAYLOR, G. I., *Proc. Roy. Soc. (London)* **138A**, 41 (1932).
3. BARTOK, W., AND MASON, S. G., *J. Colloid Sci.* **14**, 13 (1959).
4. MASON, S. G., AND BARTOK, W., in C. C. Mill, ed., "Rheology of Disperse Systems," p. 16 et seq. Pergamon Press, London, 1959.
5. NAWAB, M. A., AND MASON, S. G., *Trans. Faraday Soc.* **54**, 1712 (1958).
6. VAND, V., *J. Phys. Chem.* **52**, 277 (1948).
7. RUMSCHEIDT, F. D., AND MASON, S. G., *J. Colloid Sci.* **16**, 238 (1961).
8. TAYLOR, G. I., *Proc. Roy. Soc. (London)* **146A**, 501 (1934).
9. BARTOK, W., AND MASON, S. G., *J. Colloid Sci.* **12**, 243 (1957).
10. WHITMORE, R. L., in C. C. Mill, ed., "Rheology of Disperse Systems," p. 49 et seq. Pergamon Press, London, 1959.
11. MANLEY, R. ST. J., AND MASON, S. G., *Can. J. Chem.* **33**, 763 (1955).
12. CHARLES, G. E., AND MASON, S. G., *J. Colloid Sci.*, **15**, 236 (1960).
13. GARNER, F. H., AND SKELLAND, A. H. P., *Chem. Eng. Sci.* **4**, 149 (1955).
14. GARNER, F. H., AND HAYCOCK, P. J., *Proc. Roy. Soc. (London)* **252A**, 457 (1959).
15. LINTON, M., AND SUTHERLAND, K. L., Second International Congress on Surface Activity, Vol. 1, p. 494 et seq.
16. MOILLIET, J. L., AND COLLIE, B., "Surface Activity," p. 86 et seq. E. and F. N. Spons Ltd., London, 1951.
17. HARKINS, W. D., "The Physical Chemistry of Surface Films," p. 135. Reinhold Publishing Corp., New York, 1952.
18. OLDROYD, J. D., *Proc. Roy. Soc. (London)* **232A**, 567 (1955).
19. ROBERTSON, R. F., WINKLER, C. A., AND MASON, S. G., *Can. J. Chem.* **34**, 716 (1956).
20. HENNIKER, J. C., *Revs. Mod. Phys.* **21**, 322 (1949).

PARTICLE MOTIONS IN SHEARED SUSPENSIONS

XII. DEFORMATION AND BURST OF FLUID DROPS IN SHEAR AND HYPERBOLIC FLOW¹

F. D. Rumscheidt² and S. G. Mason

*Physical Chemistry Division, Pulp and Paper Research Institute of Canada,
and Department of Chemistry, McGill University, Montreal, Canada*

Received June 7, 1960

List of Symbols

b	= radius of undistorted drop.
b_1, b_2	= principal radii of curvature of interface.
B	= minor axis of deformed drop.
D	= deformation of drop = $(L - B)/(L + B)$.
D_B, D'	= deformation at burst; limiting deformation.
E, E_B	= ratio of viscous to surface tension forces = $(Gb\eta_0/\gamma)f(p)$; E at burst.
F, F_B	= $Gb\eta_0/\gamma$; F at burst.
$f(p)$	= $(19p + 16)/(16p + 16)$.
f_s, f_n	= shear and normal stresses at interface.
G, G_B	= velocity gradient; G at burst.
L	= major axis of deformed drop.
m_0, m_0'	= circulation number at interface; limiting value of m_0 .
p	= viscosity ratio = η/η_0 .
Δp	= pressure difference across drop interface.
r	= radius vector measured from origin of coordinate system.
S	= mean annular radius in Couette.
T_0	= mean period of circulation at drop interface.
u', v', w'	= velocity components in plane hyperbolic flow.
u, v, w	= velocity components in laminar shear flow.
x', y', z'	= coordinates for plane hyperbolic flow.
x, y, z	= coordinates for laminar flow.
γ	= interfacial tension.
δ	= angle between principal stress and radius vector.

¹ Conducted with financial assistance from the Defence Research Board of Canada, DRB Grant 9510-05.

² Holder of the Spruce Falls Power and Paper Company Limited Fellowship during the academic year 1959/60.

Δ	= radial separation in Class B-2 breakup.
η, η_0	= viscosity of disperse and continuous phases, respectively.
ϕ', ϕ	= polar angle measured from Y' and Y axis, respectively.
$\phi_m, \phi_{m,B}, \phi_{m,\infty}$	= orientation of the major axis of deformed drops: (i) below burst, (ii) at burst, (iii) beyond burst for class B-2 deformation.
ω, ω_0	= angular velocity ($d\phi/dt$); value at equatorial perimeter of drop.
$\Delta\omega_0$	= difference between maximum and minimum ω_0 for deformed drops.

INTRODUCTION

Previous papers in this series have described the rotation and deformation of threadlike particles (1-7) in laminar shear flow and the circulation currents inside fluid drops in shear and plane hyperbolic flows (8, 9). One investigation (10) dealt briefly with the deformation and breakup of fluid drops in shear flow. This paper describes a study of the deformation and breakup of fluid drops in both shear and hyperbolic flow which was undertaken to extend the earlier observations and those of Taylor (11).

The essential features of the relevant theories are described in the Theoretical Part which follows. The phenomena considered here are of interest in connection with the formation, stability, and the rheology of emulsions and suspensions.

THEORETICAL PART

1. General

As before (8, 9) the two fields of laminar flow used, when no particles are present, are described by

$$\text{hyperbolic flow} \quad u' = \frac{Gx'}{2}; \quad v' = -\frac{Gy'}{2}; \quad w' = 0; \quad [1]$$

$$\text{shear flow} \quad u = Gy; \quad v = 0; \quad w = 0; \quad [2]$$

where u, v, w are the velocity components along the X, Y , and Z axes and G is the rate of shear defined by Eq. [2]. The first field is irrotational and the second rotational (rotation = $G/2$). The two become identical (8, 14) when the X', Y' axes (a) lag by the angle $\pi/4$ behind the X, Y axes, and (b) are rotated clockwise at an angular velocity $G/2$ as shown in Fig. 1. In this case, the polar angles are related by

$$\phi' = \phi + \pi/4. \quad [3]$$

It should be noted that the rate of strain of a line in the XY plane in the fluid is $(G/2) \sin 2\phi$, corresponding to maximum rates of extension and contraction $G/2$ along the lines $\phi = \pm\pi/4$, respectively (Fig. 1).

Taylor (11) has pointed out that effects which depend on the instantaneous distribution of velocity and are not affected by rotation of the whole system will be identical in the two fields; this applies to internal circulation in undeformed fluid drops (9). However, effects which depend both on the instantaneous distribution and on the time sequence of distribution will be different. This occurs when fluid drops suffer large deformations (11).

2. Taylor's Deformation Equations

When a fluid drop is placed at the origin of either of the two fields of flow defined by Eqs. [1] and [2], the motion of the fluid in the neighborhood of the particle is disturbed (8, 9, 12). The disturbance generates a stress system which can be resolved into tangential and normal stresses acting at the drop interface (9, 12). The tangential stresses are assumed to be transmitted undiminished across the interface and thus establish a system of gradients inside the drop. The normal stresses, on the other hand, are discontinuous at the drop interface and generate a pressure difference across the interface given, in the equatorial plane, for nearly spherical drops by

$$\Delta p_G = -4G\eta_0 \left[\frac{19p + 16}{16p + 16} \right] \cos 2\phi', \quad [4]$$

where Δp is the pressure difference between the inside and the outside of the drop, p is the viscosity ratio of the disperse to the continuous phase, and η_0 the viscosity of the continuous phase. It should be noted that Δp_G is in

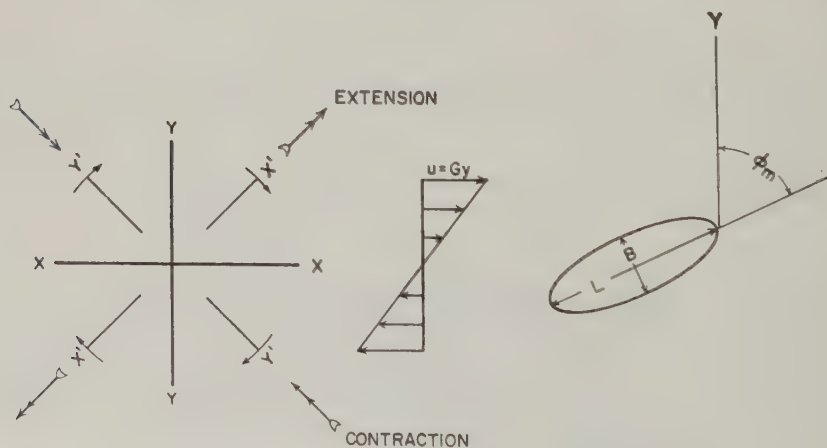


FIG. 1. Coordinate systems for hyperbolic (Eq. [1]) and shear flow (Eq. [2]). The two fields are equivalent when the $X'Y'$ axes are 45° behind XY axes and rotated clockwise at a rate $G/2$ as indicated on the left. The principal deformation axes are indicated by the double arrows. The parameters of a deformed fluid drop are shown on the right.

addition to the capillary pressure given by the Laplace equation

$$\Delta p_\gamma = \left[\frac{1}{b_1} + \frac{1}{b_2} \right] \gamma, \quad [5]$$

where γ is the interfacial tension, and b_1 and b_2 are the principal radii of curvature. For a truly spherical drop of radius b , $\Delta p_\gamma = 2\gamma/b$.

It should be noted that Δp_σ is maximum positive when $\phi' = \pi/2$ and negative when $\phi' = 0$, corresponding to the principal axes of distortion shown in Fig. 1. When Δp_σ is not zero, the drop is deformed in such a way that the stresses generated by flow are balanced by the interfacial tension, i.e., the curvature of the drop changes so as to satisfy the condition for equilibrium:

$$\Delta p = \Delta p_\sigma + \frac{2\gamma}{b}. \quad [6]$$

Taylor (11) showed that for small deformations this condition was satisfied when the equator of the drop assumed an ellipsoidal form given by the polar equation:

$$r(\phi') = b(1 - D \cos 2\phi'). \quad [7]$$

Here D is the deformation defined as

$$D = (L - B)/(L + B), \quad [8]$$

where L and B are, respectively, the length and breadth of the ellipsoid, and for small deformations is given by

$$D = Ff(p), \quad [9a]$$

$$= E; \quad [9b]$$

where E is the ratio of viscous to surface tension forces and

$$F = \frac{Gb\eta_0}{\gamma}; \quad f(p) = \frac{19p + 16}{16p + 16}; \quad \text{and} \quad E = Ff(p). \quad [9c]$$

It should be noted that $f(p)$ varies from unity to 1.187 as p varies between 0 and ∞ , and that $D = 0$ for a sphere.

Equations [4] to [7] should also apply to deformation in shear flow when $\sin 2\phi$ is substituted for $-\cos 2\phi'$, provided D is small so that rotation of the particle is slow enough to allow the particle sufficient time to accommodate its shape to the changing stresses. Under these circumstances the principal axis of the drop is at $\phi = \pi/4$, i.e., along the principal axis of elongation as in the case of hyperbolic flow. As the deformation increases, however, the lines of particles in the drop lying in this direction are continually being rotated towards $\phi = \pi/2$, where the rate of deformation is

zero. Owing to the finite rate of accommodation of the particle shape to the deforming stresses, the orientation ϕ_m of the principal axis of the particle increases beyond $\pi/4$ as G increases. This effect has been investigated theoretically by Cerf (13), who pointed out that alignment at $\phi_m = \pi/4$ arises from taking only first-order terms in G in the stress tensor. When second-order terms are taken into account

$$\phi_m = \frac{\pi}{4} + \left(1 + \frac{2p}{5}\right) E, \quad [10]$$

which, if Eq. [9] applies, can also be written as

$$\phi_m = \frac{\pi}{4} + \left(1 + \frac{2p}{5}\right) D. \quad [11]$$

It should be noted, however, that Eq. [10] can be valid only at lower values of E since $\phi_m \leq \pi/2$. Further, because of the irrotational nature of the hyperbolic flow, $\phi_m' = \pi/2$ for all values of E .

3. Deformation at Burst

Following the suggestion of Taylor (12), we may imagine that when the maximum value of Δp_G tending to disrupt the drop exceeds the force due to surface tension which tends to hold it together, the drop will burst. Assuming Eq. [4] to hold, and neglecting deviation from the spherical shape, this occurs when

$$4G\eta_0 f(p) > \frac{2\gamma}{b}. \quad [12]$$

If Eq. [9] still applies, the critical deformation above which the drop will burst, for both shear and hyperbolic flow, is thus given by

$$D_B = E_B = \frac{1}{2}. \quad [13]$$

A relation similar to Eq. [13] was mentioned incidentally by Taylor in a theoretical discussion of the viscosity of emulsions (12), but for reasons unknown was not employed in the subsequent investigation of the bursting of drops (11).

4. Shear Deformation at High p

Taylor (11) gives an approximate analysis of the special case in which p and $Gb\eta_0$ are so high that the surface tension forces opposing deformation are negligible compared with those due to viscosity. It follows from Taylor's equations that in hyperbolic flow under these circumstances the drop "bursts" at a rate of radial extension

$$\left(\frac{\partial r}{\partial t}\right)_{\phi'} = -\frac{5Gb}{2(2p+3)} \cos 2\phi'. \quad [14]$$

In shear flow the particle rotates and assumes a steady shape in space such that at a fixed ϕ the sum of the radial component of velocity due to rotation and that due to deformation (Eq. [14]) is zero. This condition is satisfied by the surface

$$r = b \left(1 - \frac{5}{2(2p+3)} \cos 2\phi \right), \quad [15]$$

corresponding to a limiting deformation which is independent of G given by

$$D' = \frac{5}{2(2p+3)} \quad [16]$$

and an orientation along the direction of flow ($\phi_m = \pi/2$).

It should be noted that the analysis is based on small values of D . Taylor made a further approximation to Eqs. [14] to [16] by substituting $5/4p$ for $5/2(2p+3)$.

5. Further Remarks

Taylor (11) observed that following the burst of a drop in hyperbolic flow, it was drawn into a thread which remained coherent as long as it was being extended, but which disintegrated rapidly when the motion of the field was arrested. A theoretical analysis of the mode of breakup of a thread by the growth of capillary disturbances under these circumstances was undertaken by Tomotika (14, 15). This is considered further in a forthcoming paper (16).

Taylor (11) obtained rough agreement with Eq. [9] for low values of D in both hyperbolic and shear flow for several values of p , but the precision of the data was limited by the approximate measurements of γ . Bartok and Mason (10) obtained linear variation of D with Gb for several systems but unfortunately γ was not known; an increase of ϕ_m with Gb was observed. Using data from one of Taylor's systems (11), Cerf (13) found approximate agreement with Eq. [10]. The mechanism of breakup of drops at high values of D was found to vary with p (10) and to be different for shear and hyperbolic flow (11). Taylor (11) found that at $p = 20$ in a shear field, a drop attained a constant shape, independent of G , with $\phi_m = \pi/2$ but D' was about three times greater than given by Eq. [16].

In the present investigation Eq. [9] has been tested for a number of systems having a wide range of p (0 to 30) of accurately known γ in the two types of flow. In addition, Eqs. [10], [13], [14], and [16] have been checked, and, in general, very satisfactory agreement with the theory outlined above has been obtained. Finally, systematic observations on the nature of breakup above D_B , of the effects of added surfactants and electrostatic fields, and of the rotational behavior of the deformed drops in shear have been made as an extension of the earlier work (9, 10).

TABLE I
Properties of Fluid Systems
 Temperature = 20°C.

System No.	Continuous phase	Poise	Dispersed phase	ρ	γ (dynes/cm.)	Interfacial tension method	Shear flow		Deformation class
							$\phi_{m,B}$ (deg.)	$\frac{d^2D}{d(Gb)^2}$	
1	Silicone oil 5000 ¹	52.6	Oronite ²	6.4	2.1	a, b, c		—	C
2			CHP ³	3.8	2.7	a, b		—	C
3			Pale 4 ⁴	1.0	4.8	a, b, c	77	+	B-1
4			LTC ⁵	0.65	2.2	a, b	73	+	B-1
5	Glycerol		Glycerol	0.14	24.5	a, c	75	+	B-1
6			Glycerol + 0.005% Tween 20 ⁶	0.14	13.5	c	60	+	B-1
7			Glycerol + 0.5% Tween 20	0.14	6.0	a, b, c	70	+	B-1
8	Terresso 52 ⁵		Dibutyl phthalate	0.03	1.4	a, b	76	—	B-1
9			Ethylene glycol	4×10^{-3}	2.5	a, b	72	—	A
10				4×10^{-3}	15.0	a, c	68	—	A
11	H ₂ O (distilled)		H ₂ O	2×10^{-4}	38	c	66	+	A
12			H ₂ O + 0.005% Tween 20 ⁶	2×10^{-4}	20	c	70	+	A
13			H ₂ O + 0.5% Tween 20	2×10^{-4}	6.6	c	67	—	A
14			Air	0	20.9	a, b, c	65	+	A

15	Pale 4 ⁴	60.0	Silicone oil 100 000 ¹	17		—	C
16			Silicone oil 30 000 ¹	6.0	6.0	—	C
17			Silicone oil 5000 ¹	1.0	4.8	76	B-1
18			Silicone oil 1000 ¹	0.19	4.5	64	A
19	Glycerol			0.14	10.4	62	A
20	Silicone oil 2 ¹			3×10^{-4}	2.7	67	A
21	Air			0	38.1	65	A
22	Glycerol	8	CHP ³	29	16.4	c	C
23			Pale 4 ⁴	7	10.4	c	C
24			Silicone oil 5000 ¹	7	25.0	a, c	C
25			Silicone oil 2 ¹	4×10^{-3}	26.3	c	A
26	Corn syrup	90	CHP ³	2.2	24	a, c	B-2
27			Silicone oil 10 000 ¹	1.1	38.7	c	B-2
28			Pale 4 ⁴	0.7	21	c	B-2
29			Pale 4 + .5% Span 85 ⁷	0.7	20	c	B-2
30			Carbon tetrachloride	1.3×10^{-4}	38	a, b	A

a = pendant drop shape; b = pendant drop volume; c = du Nouy ring tensiometer.

¹ Dow Corning fluid.

² Oronite Polybutene 24 (Diversified Research and Sales Ltd., Toronto).

³ Cyclohexanol phthalate.

⁴ Oxidized castor oil (Baker Castor Oil Co., New York).

⁵ Hydrocarbon oil (Imperial Oil Co. Ltd., Sarnia, Ont.).

⁶ Polyoxyethylene sorbitan monolaurate, O/W emulsifier (Atlas Powder Co., Brantford, Ont.).

⁷ Sorbitan tri-oleate, W/O emulsifier (Atlas Powder Co.).

EXPERIMENTAL PART

The experiments were conducted in the four-roller apparatus (9), which provided hyperbolic flow, and the Couette device (3), which provided shear flow; both were arranged for viewing along the Z-axis. Since a drop was inherently more stable in the Couette apparatus (9), this was used for most of the experiments. It was equipped with reversible direct-current motor drives (magnetic amplifier control) on vibration-free mounts and with additional reduction gears. These changes improved the control and the stability of the flow, and provided a range of G from 0.003 to 40 sec.⁻¹ at the stationary layer. Measurements could be made by using a stereo-microscope or the still and cine photo-micrographic methods previously described (9).

The viscosity of the liquids used was measured in a thermostated (20.00° ± .01°C.) rotational viscometer (Drage viscometer, A. G. Epprecht, Chemisches Institut, Zurich, Switzerland) at shear rates between 4 and 125 sec.⁻¹. Good agreement was found with falling ball measurements.

The interfacial tension in most systems was determined by the pendant drop and drop-volume methods. The drops were photographed with a 35-mm. still camera having a 75-mm. Berthiot lens and extension rings. Transmitted light gave sharp boundaries and magnifications of 100× could be used in the analysis. Additional values were obtained by the ring method with corrections suggested by Zuidema and Waters (17). Good agreement among the three methods was found, even though the measurements were often made difficult by high viscosities and low density differences of the two phases. Attempts to use the bubble pressure method which Taylor (11) employed and which is independent of the density were unsuccessful because of the high viscosity of the systems.

All the equipment was used in a room maintained at 20° ± 1°C.

The properties of the fluid systems used are listed in Table I. All the liquids were found to be Newtonian over the range of gradients employed in the viscosity measurements with the exception of Oronite and CHP, which were slightly viscoelastic. As before (9) great care was taken to prevent contamination of the drop interfaces by impurities, except when surfactants were added as in Systems 6, 7, 12, 13, and 29. Drops of diameters ranging from 500 to 2000 μ were used. System 3 was previously found to show internal circulation at low velocity gradients which was in excellent agreement with the theory based on unrestricted transmission of shear stresses across the interface; in many of the other systems, including all those below $p = 1$, there was some inhibition of internal circulation (9).

End effects (3) in the flow devices were avoided by floating the silicone oil 5000 and the Pale 4 used as continuous phases on water-glycerol mixtures of sufficiently high density to ensure flat interfaces; carbon tetrachloride was used with corn syrup, whereas no floating medium was required for the glycerol.

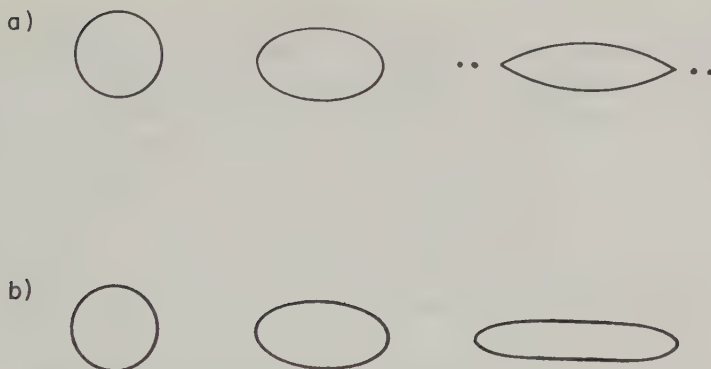


FIG. 2. Typical observations (traced from photographs) of deformation and burst of drops in plane hyperbolic flow. Part (a): Water drop (System 11, $p = 2 \times 10^{-4}$). After burst the drop formed unstable pointed ends from which small droplets were ejected. Part (b): Pale 4 castor oil (System 3, $p = 1.0$). After burst the drop became extended into a long cylindrical thread which eventually disintegrated. The major axis of each drop was along the X' -axis.

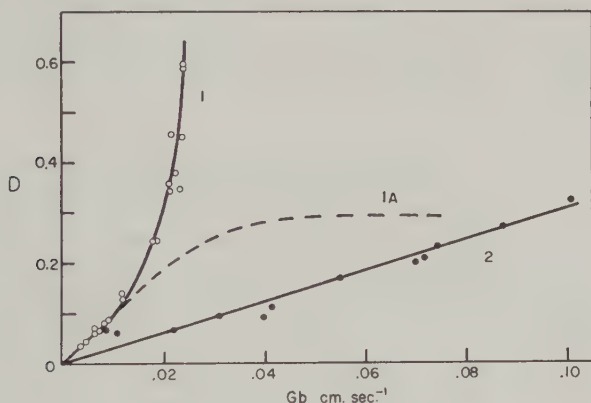


FIG. 3. Deformation in hyperbolic flow for Systems 16 and 3 (curves 1 and 2). At high values of D (not shown because of scale limitations) curve 2 had the same shape as curve 1. The broken line (1A) is for System 16 in shear flow.

RESULTS

1. Hyperbolic Flow

The general behavior of drops in the four-roller apparatus was as described by Taylor (11). A drop suspended in the middle of the field was distorted into a prolate spheroid oriented along the X' -axis, the deformation increasing with G until a sharply defined critical G_B was reached, above which the drop burst. When the drop drifted away from $x', y' = 0$ the deformation and pattern of burst tended to be unsymmetrical; in the

experiments described here, every effort was made to maintain the center of the drop at the origin. When $G > G_B$ and at low values of p (< 0.2 approximately), the ends of the particle drew out into sharp points from which fragments of disperse phase were released (Fig. 2a); after a time at a fixed G the particle reverted to a stable prolate spheroid as the result of the decrease in volume; on increasing G the axis ratio of the drop increased and the pointed ends developed again. When $p > 0.2$ and $G > G_B$, instead of developing pointed ends, the drop was pulled out into a thread (Fig. 2b) which increased in length until it reached a diameter of the order of 10 to 50 μ , when it disintegrated into fine droplets of 20 to 80 μ diameter; when the apparatus was stopped after the initial thread formation, the breakup began after a short time interval which seemed to be roughly inversely proportional to the interfacial tension. The thread became varicose and finally broke up into a series of regularly spaced droplets of uniform size, each pair being separated by three smaller satellite drops.

Quantitative measurements of D at various values of G up to the point of breakup were made on several systems in order to test Eqs. [9] and [13]. Figure 3 shows the linear variation of D with Gb in the early stages of deformation; the values of γ in Table II calculated from initial slope by means of Eq. [9] show excellent agreement with the directly measured values for Systems 3 and 16. At high values of D the D vs. Gb curved upwards until

TABLE II
Deformation in Hyperbolic Flow

System No. (and p)	γ (deformation) Eq. [9] (dynes/cm)	γ (deformation) γ (table I)	Measured D_B	Measured E_B	Drop shape at burst
3 (1.0)	4.8	1.00	0.50	0.22	Rounded ends
11 (2×10^{-4})	17.2	0.45	—	—	Pointed ends
16 (6.0)	7.5	1.20	0.45	0.26	Rounded ends

TABLE III
Radial Extension of Drop Interface in Hyperbolic Flow, System No. 16
 $p = 6.0$ $G = 0.19 \text{ sec.}^{-1}$ $l = 0.075 \text{ cm.}$

ϕ' (degrees)	$\left(\frac{\partial r}{\partial t}\right)\phi'$ (cm. sec. ⁻¹)	
	Measured	Calculated from Eq. [14]
0	-2.0×10^{-3}	-2.4×10^{-3}
45	0	0
90	$+2.2 \times 10^{-3}$	$+2.4 \times 10^{-3}$

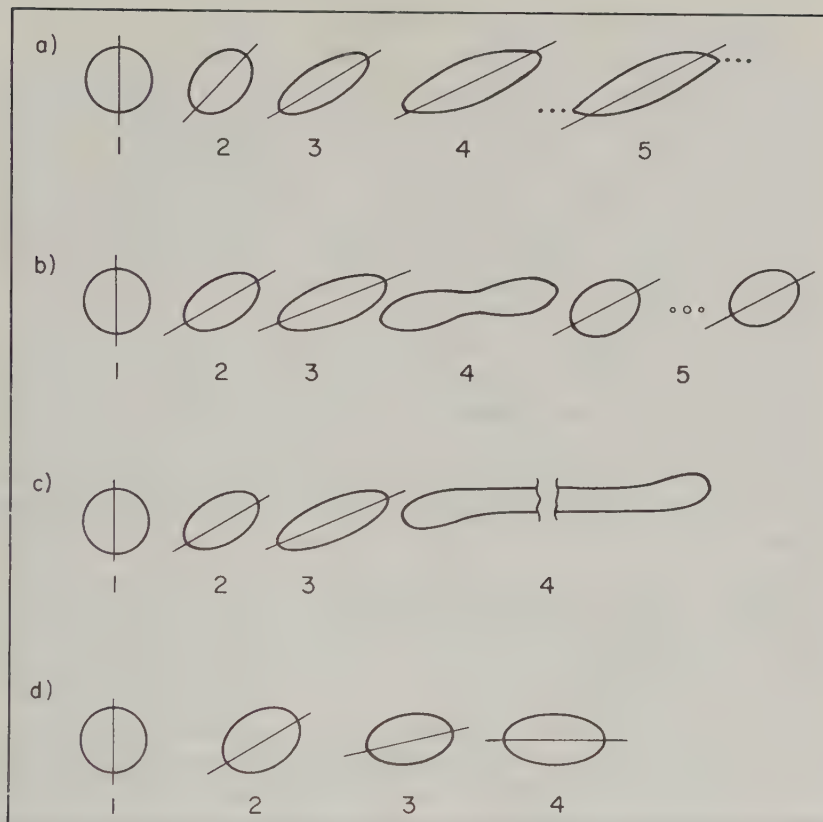


FIG. 4. Tracings from photographs of drops in shear flow showing the change in D , ϕ_m with increasing G up to breakup. (a) Class A deformation (System 11, $p = 2 \times 10^{-4}$). (b) Class B-1 deformation (System 3, $p = 1.0$). The neck formed (picture 4) disintegrated into three satellite droplets. (c) Class B-2 deformation (System 28, $p = 0.7$). Drops were drawn out into long cylindrical threads (picture 4). (d) Class C deformation (System 16, $p = 6.0$). No burst was observed.

the drop burst; measured values of D_B (Table II) were reasonably close to the predicted value $\frac{1}{2}$ (Eq. [13]), whereas values of E_B were low because of deviation from Eq. [9] in this region.

With water in silicone oil (System 11) it was not possible to measure D_B accurately enough owing to instability of the drop in the flow field at the high values of G required by the high interfacial tension. The value of γ calculated from D showed a marked deviation from the directly measured value, for reasons which will be discussed later.

The measured initial rate of radial extension in a system having a high p (No. 16) showed good agreement with Eq. [14] at $\phi' = 0$, $\pi/4$, and $\pi/2$ (Table III).

2. Shear Flow

a). *General Observations.* Except for several details, the general behavior for shear flow was as previously reported (10, 11) and as predicted by the theory. At low gradients, a drop was deformed into a prolate spheroid initially aligned at $\phi_m = \pi/4$, with both D and ϕ_m increasing with G . Tracer particles inside the drop indicated that internal circulation along approximately elliptical paths invariably occurred inside deformed drops (9, 10).

As the deformation increased, four distinct modes of behavior were observed which depended mainly upon p . These are illustrated in Fig. 4 and are described as follows.

(i) *Class A.* The behavior was similar to that of drops of low p in hyperbolic flow, except for the modifications imposed by the rotation. When $G \geq G_B$, the drop assumed a sigmoidal shape (Fig. 4a) at $\phi_m > \pi/4$ with pointed ends from which fragments of liquid of 50μ diameter were released. After a time the drop volume and hence Gb were reduced until the stable spheroidal shape was re-established. On increasing G again the process was repeated. The transition from rounded to pointed ends on increasing G was sudden.

(ii) *Class B-1.* At G_B the central portion of the drop suddenly started to extend into a cylinder which then formed a neck in the middle. The neck progressively thinned until two identical daughter drops and three satellite droplets (10) were created (Fig. 4b).

(iii) *Class B-2.* This was a variation of Class B-1 in which, when $G \geq G_B$, the drop became extended into a long thread which increased progressively in length until it broke up into a large number of fine droplets. This class (Fig. 4c) was similar in appearance to that for a drop of high p in hyperbolic flow described above.

(iv) *Class C.* This occurred at high values of p and as predicted by Taylor's theory (Eqs. [15] and [16]). As G was increased, the ellipsoidal drop reached an upper limit of deformation at which $\phi_m = \pi/2$ (Fig. 4d). This deformation was maintained until the upper limit of G of the apparatus (40 sec.⁻¹) without any sign of disintegration of the drop.

All three classes of deformation, except B-2, have been previously observed in shear flow (10, 11). They are considered below in greater detail.

b). *Variation of D .* The variation of D with G was measured for the thirty systems listed in Table I. Figure 5 shows typical examples of the increase in deformation with Gb . At low values of D , the variation was linear as in hyperbolic flow (Fig. 3). As illustrated in Fig. 6, values of interfacial tension calculated from the initial slope of the deformation curve using Eq. [9] showed good agreement with the directly measured values, except for the nine systems indicated. Systems 6 and 12 (both containing an emulsifier) showed the spread in γ calculated from deformation of individual drops indicated by the vertical bars in Fig. 6; otherwise the deformation

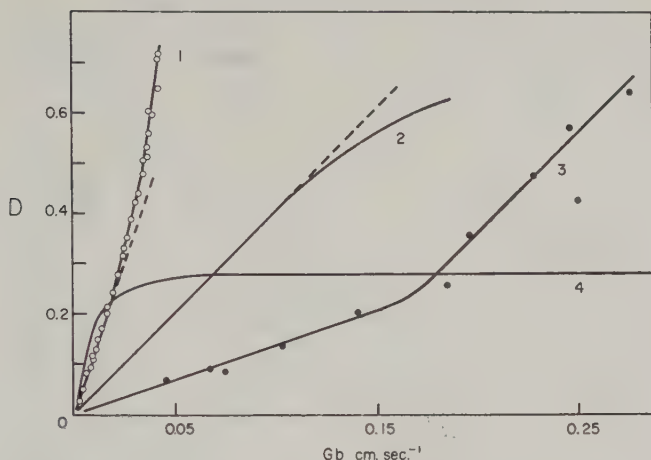


FIG. 5. Typical curves for deformation in shear flow illustrating Class A (curves 2 and 3, Systems 10 and 14), Class B-1 (curve 1, System 3), and Class C (curve 4, System 1).

data on different drops in a given system were reproducible. Omitting the nine systems for reasons which are discussed later, the mean value γ (deformation)/ γ (measured) = $1.01 \pm .13$; this is considered to be excellent confirmation of Eq. [9].

As D increased, there was deviation from Eq. [9] as indicated in Fig. 5; this deviation was sometimes positive (curving upwards) and sometimes negative (curving downwards). The penultimate column of Table I indicates the type of deviation observed in shear flow. In hyperbolic flow the deviation was invariably positive (Fig. 3). In shear flow, the deviation was negative at high values of p (>2), but otherwise no systematic correlation of the deviation with system properties could be made. The deformation in System 16 is seen in Fig. 3 to be identical in shear and hyperbolic flow at low values of G but to show opposite deviations at high values. This is to be expected from Taylor's theory for high values of p .

c). *Variation of ϕ_m* . The angle of alignment was measured by projecting the image of the drop onto a rectangular coordinate system which was rotated until the coordinate axes were judged visually to coincide with the main axes of symmetry of the particle. With Class A drops at high D (pictures 4 and 5 of Fig. 4a) the principal axis of symmetry was taken for the main body of the drop without regard for the pointed ends, which were about 5° beyond ϕ_m . To check the accuracy of this method, the parameters in the general equation of a conic section were computed from measured coordinates and ϕ_m was calculated; the angles so obtained agreed with the directly measured values within 2° except at low values of D when $\phi_m < 48^\circ$.

The variation of ϕ_m with Gb is illustrated in Fig. 7 for three systems in-

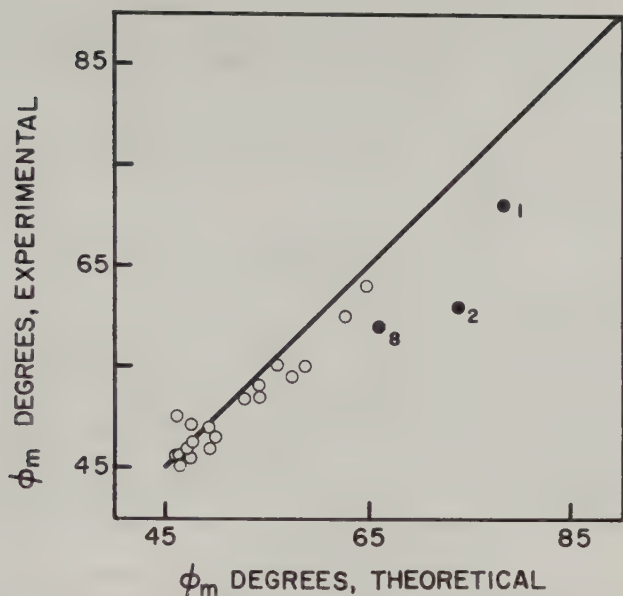


FIG. 8. Comparison of measured ϕ_m at $Gb = 10^{-2}$ cm. sec. $^{-1}$ with values calculated from Eq. [10] for 24 of the systems listed in Table I. The mean ϕ_m (experimental) / ϕ_m (theoretical) = 0.97 ± 0.05 — a good check of Cerf's theory (13).

cluding one of high p ($=6.4$) in which ϕ_m approached $\pi/2$. It is seen that in the linear range, the experimental points are in excellent agreement with Eq. [10] when the measured values of γ , η_0 , and p are used to calculate E . As expected, experimental points fall below values from Eq. [10] at high Gb .

Values of ϕ_m were measured for the twenty-two systems listed in Table I for which + or - designations are given for $d^2D/d(Gb)^2$ in addition to Systems 19 and 21; measurements in the remaining systems were not possible because of rapid sedimentation, low optical contrast across the particle interface, and other experimental difficulties. As a further check of the theory interpolated experimental values of ϕ_m corresponding to a fixed value of $Gb = 10^{-2}$ cm. sec. $^{-1}$ have been plotted (Fig. 8) against the values calculated from Eq. [10] using the values of γ and η_0 from Table I. Except for three systems the agreement is excellent; two of the exceptions have p 's so high that the deviation from Eq. [10] is already significant at the value of Gb used for the comparison (Fig. 7, curve 1), and the third (System No. 8) has a γ so low that it can be appreciably in error.

d). *Rotation of Drops.* Forgacs and Mason (6) showed that the period of rotation of a variety of drops was influenced by deformation. For liquid drops the circulation number of the equatorial interface, defined as

$$m_0 = \frac{T_0 G}{4\pi}, \quad [17]$$

where T_0 is the period of rotation, decreased with increasing G (6, 9, 10). According to the theory presented before, at $D = 0$ and for fully developed internal circulation, the angular velocity of the equator is

$$\omega_0(\phi) = \frac{G}{2(p+1)} (p + 2 \cos^2 \phi), \quad [18]$$

and the circulation number

$$m_0 = \frac{(p+1)}{\sqrt{p(p+2)}}. \quad [19]$$

The variation of m_0 with D for the three classes of deformation is illustrated in Fig. 9. In System 3 ($p = 1.0$), the only system known to be in complete accord with Eqs. [18] and [19], m_0 remained constant at the theoretical value of 1.15 up to $D = 0.2$, the limit of validity of Taylor's deformation (Fig. 5, line 1), and then increased. A linear increase of m_0 was shown in System No. 11 ($p = 2 \times 10^{-4}$), in which internal circulation was shown to be inhibited by traces of impurity (9). At high values of p ($= 6.0$, System

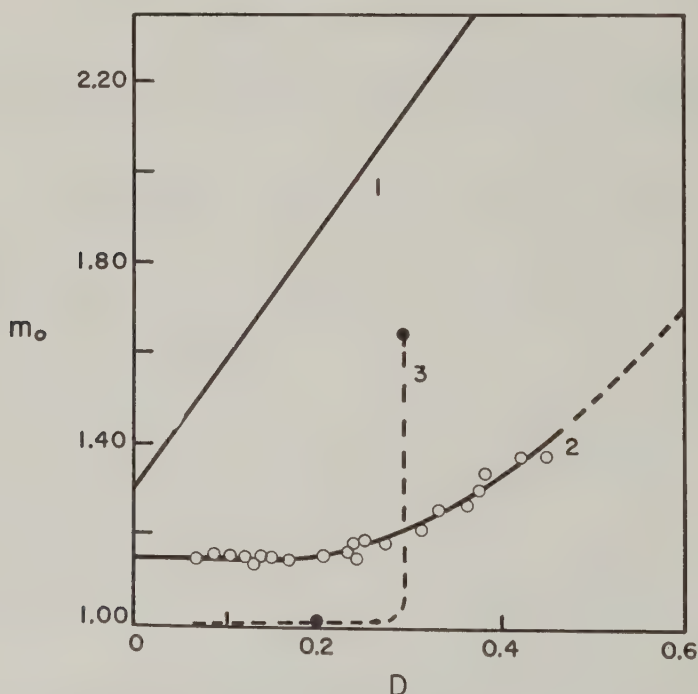


FIG. 9. Variation of circulation number m_0 with D for System 11 (line 1, Class A, theoretical $m_0 = 50$), System 3 (line 2, Class B, theoretical $m_0 = 1.15$), and System 16 (line 3, Class C, theoretical $m_0 = 1.01$). Note that m_0 in System 11 is much smaller than the theoretical value.

16), m_0 remained close to the theoretical value of 1.01 and then suddenly increased to limiting values $m_0' = 1.65$ and $D' = 0.29$, both of which were independent of G . The sudden increase in m_0 is probably related to the leveling off in ϕ_m (at $\pi/2$) and D in systems of high p at increasing Gb (Fig. 7, line 1, and Fig. 5, line 4). Since m_0 increased with deformation with fully developed internal circulation (System 3), some of the increase in m_0 observed in Systems 11 and 16 can be attributed to the deformation itself; the remainder can be attributed to the onset of internal circulation in the deformed drop.

A number of observations were made of the variation of $\omega_0(\phi)$ in deformed drops used in measuring m_0 . Plots of $\omega_0(\phi)/G$ against ϕ showed the periodic variation indicated by Eq. [18]. Owing to the deformation, however, the maximum and minimum values were shifted from the theoretical values $\phi = 0, 90^\circ$, respectively; the measured positions are summarized in Table IV. According to Eq. [18] the difference between the maximum and minimum ω_0 is

$$\Delta\omega_0 = \frac{G}{(p+1)}. \quad [20]$$

In Fig. 10 values of $\Delta\omega_0$ (measured)/ $\Delta\omega_0$ (theoretical) have been plotted against D . In two of the systems the ratio increased with increasing D , and in all three it extrapolated to the theoretical value of $D = 0$.

The phenomena involved here are complex and not understood, but are briefly summarized as follows:

1. At low p (Class A) and when internal circulation was partially inhibited, the angles of ω_{\max} and ω_{\min} were shifted 10° to the left of the theoretical. When the deformation approached D_B (Fig. 4a, picture 4) the position of ω_{\max} moved 10° to the right but that of ω_{\min} remained unchanged.

2. At intermediate p (Class B) the positions were initially 10° to the right, but as the deformation started to increase a shift of 10° to the left occurred which persisted until burst.

TABLE IV
Effect of Deformation on $\omega_0(\phi)$

System No.	p	D	ϕ (degrees)	$\phi(\omega_{\max})$ (degrees)	$\phi(\omega_{\min})$ (degrees)
11 (Class A)	2×10^{-4}	0.01-0.4	45-60	-10	80
		0.54	65	+10	80
3 (Class B)	1.0	0.0-0.1	45	+10	100
		0.2-0.58	60-76	-10	80
16 (Class C)	17	0.29	90	+10	100

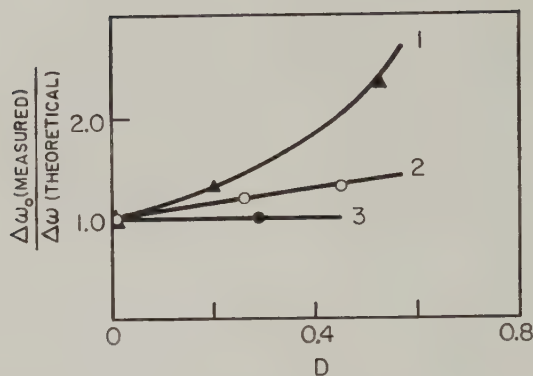


FIG. 10. Comparison of measured and calculated (Eq. [20]) values of $\Delta\omega_0$ for Systems 11, 3, and 16 (lines 1, 2, 3, respectively).

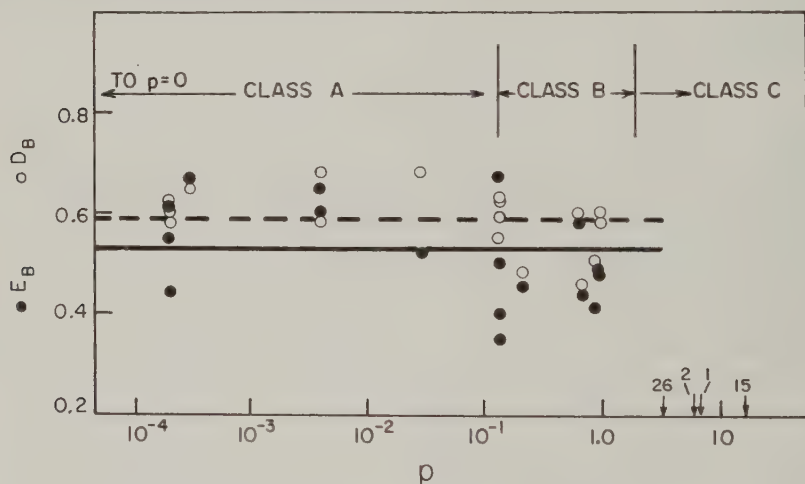


FIG. 11. Measured values of D_B (open circles) and E_B (solid circles) for Class A and B deformation. The mean value of D_B is given by the broken line, the solid line is for the mean E_B . The values of p exhibiting Class C deformation are shown by the arrows and are identified by the System number.

3. At high p (Class C) the shift was 10° to the right at D' , thus probably extending over the whole range of D .

Tracer particles inside the deformed drops moved in elliptical streamlines with the major axis near $\phi = +10^\circ$ (9). This occurred in all Class A and B deformations except close to D_B , when the streamlines tended to parallel the outer contour of the drop. In Class C deformation, the elliptical internal streamlines started to follow the outer contours of the drop at early stages of the deformation and at the limiting D' were oriented at $\phi = \pi/2$.

e). *Bursting of Drops.* The class of deformation was observed for all the systems and is listed in the last column of Table I. In addition, values of D_B , E_B , and $\phi_{m,B}$ were determined for Classes A, B-1, and B-2. Since there were experimental difficulties in measuring the exact value of G_B for each system, the data show an unavoidable scatter. Nevertheless, a reasonably systematic pattern of behavior has been revealed.

In Fig. 11, values of D_B and E_B are shown plotted against $\log p$. The value of D_B was determined directly, whereas E_B was calculated from G_B by means of Eq. [9] from the values of γ given in Table I, except with Systems 6, 11, and 12, and γ calculated from the initial deformation was used. The mean experimental values and standard deviations for the series are

$$\bar{D}_B = 0.59 \pm 0.06;$$

$$\bar{E}_B = 0.52 \pm 0.10.$$

The difference between the two means arises from deviations from Eq. [9b] at high values of deformation. However, the agreement with Eq. [13], especially in the cases of E_B , is considered to be good.

The three classes of deformation are also indicated in Fig. 11 and are seen to be related to p although there are no sharp boundaries between them. Class A extended from $p = 0$ to $p = 0.19$ (System 18), Class B (including B-2) from $p = 0.03$ (System 8) to $p = 2.2$ (System 26), and Class C behavior, in which there was no breakup, occurred at $p = 3.8$ (System 2) and up. The transition observed in hyperbolic flow from pointed to rounded drop ends (Fig. 2) is almost certainly the same transition as that from Class A to B and in the same range of p .

Values of $\phi_{m,B}$ have been tabulated in Table I. Although there is considerable scatter, an analysis shows that $\phi_{m,B}$ follows a significantly increasing trend with increasing p , and that $\phi_{m,B} < 70^\circ$ for Class A deformation, and $> 70^\circ$ for Class B.

In a given system the class of deformation was independent of drop size, and as may be expected from what has been discussed above $G_B b$ was independent of b .

As indicated earlier, Class B-2 appeared to be a special case of B-1, in which the rate of growth of the disturbance leading to neck formation and then breakup was so low that appreciable extension of the drop into a thread occurred. This behavior was observed when corn syrup was used as the suspending medium at values of p which with other continuous media would yield Class B-1. When the shear rate was set 10% or more above G_B so that the rate of drop extension was increased, Systems 3, 4, and 8 which normally showed Class B-1 breakup could be stretched into threads which disintegrated rapidly into three or more droplets.

In Systems 27 and 28 the threads developed by the gradient had bulbous

ends and could be extended until they passed two or three times around the annulus, corresponding to lengths of 75 to 200 cm. and diameters of 50 to 150 μ , before disintegrating into droplets of diameter 60 and 250 μ . After extension, the orientation angle of the thread increased progressively above the initial value and could be calculated from the relation

$$\tan \phi_{m,\infty} = \frac{2\pi S}{\Delta}, \quad [21]$$

where Δ is the radial separation occurring during one revolution of the thread around the annulus, and S is the mean annular radius. In both systems, just before disintegration of the drop, $\phi_{m,\infty} = 89^\circ 47'$.

However, breakup in both systems could be made to occur before this extension was reached by stopping the apparatus or reducing G below G_B . At $G = 0$ the thread disintegrated rapidly into more or less uniform drops, as was observed in the four-roller apparatus. When $0 < G < G_B$ the thread tended to break up just before each bulbous end (picture 4 of Fig. 4c); this developed a new bulbous end and the process was repeated, releasing one droplet at a time from both ends.

f). Deformation at High p . The limiting deformation D' occurring at high values of p and Gb is illustrated in Figs. 3 and 5 for Systems 16 and 1, respectively. Table V lists the measured values of D' for the four systems showing Class C behavior (Table I). The values are 25% to 75% greater than calculated from Eq. [16]. The agreement is considered to be good, however, since very small values of D' are assumed in the theory, and agreement is much better than that found by Taylor (11).

Limiting values of the circulation number m_0' are included in Table V for two systems, and as before (Fig. 9) are greater than given by the theoretical equation for an undeformed drop with fully developed internal circulation (Eq. [19]). At these high p 's, the theoretical m_0 is almost unity, the value for a rigid sphere (1).

Several experiments were conducted with SAIB (sucrose acetate isobutyrate from Eastman Chemical Products, Kingsport, Tennessee), which appeared to be Newtonian and of viscosity about 10^5 poises. When released into silicone oil 5000 ($p = 2 \times 10^4$ approximately), nearly spherical drops rotated like rigid bodies. When pulled out into threads and then immersed in the medium they tended to develop helical and coiled rotational orbits in the same way as flexible elastomer filaments (6). In this system η was so high that the drops never had sufficient time to enable the interfacial tension to bring the drop into an equilibrium configuration.

Striking transient effects could be observed at lower p , e.g., in Systems 15 and 16 when a high Gb (> 0.1 cm. sec. $^{-1}$) was suddenly applied to a spherical drop. Initially, the drop was deformed and then rotated to $\phi_m > 90^\circ$; in this unstable position the drop underwent a damped oscillation about $\phi_m = 90^\circ$, until it assumed the equilibrium position.

TABLE V
Limiting Deformation and Circulation at High p

System No.	p	Measured D'	$\frac{D' \text{ (measured)}}{D' \text{ (Eq. [16])}}$	m_0'	m_0 Eq. [19]
2	3.8	0.38	1.60		
16	6.0	0.29	1.75	1.65	1.01
1	6.4	0.28	1.75		
15	17	0.085	1.25	1.12	1.00

TABLE VI

Effect of an Electrostatic Field on Shear Deformation

Water in silicone oil 5000 + 0.25% G 3300 Emulsifier,^a $Gb = 9.0 \times 10^{-2}$ cm. sec.⁻¹

	0 volts/cm.	400 volts/cm.
D	0.244	0.345
L/B	1.65	2.08
ϕ_m (degrees)	55	48

^a Atlas Powder Company.

g). Effect of an Electrostatic Field. A few experiments were conducted on the effect of an electrostatic field applied across the Couette (i.e., along the Y -axis), as an extension of the technique used to promote coalescence of colliding drops (9).

With Systems 3 and 11 no changes in D or ϕ_m upon application of fields up to 1000 volts/cm. were observed, but marked changes were produced when an emulsifier which reduced γ was present. One characteristic set of data is given in Table VI for water drops containing an anionic emulsifier. The electrical field caused a marked increase in D and a decrease in ϕ_m , undoubtedly owing to the added component of tensile stress along the Y -axis generated by the induced electrical charge on the drop. The existence of this force was demonstrated as $G = 0$ when the drop became appreciably deformed with $\phi_m = 0$.

DISCUSSION

These experiments have confirmed most of the details of the theory outlined in the Theoretical Part and specifically Eqs. [9], [10], [13], [14], and [16]. The accord is better than might be expected since the theory is based on small values of D . Agreement with Eq. [9] was much better than found by Taylor (11). It is believed that his discrepancies were due to the inaccuracy of the bubble-pressure method for measuring γ in viscous systems.

The theory assumes unrestricted transmission of the shear stress across the drop interface. It is significant that this assumption is probably invalid in the nine systems which deviated from Eq. [9] (Fig. 6 and Table II), since

it has been shown that circulation inside the drops in these systems can be inhibited. It has been demonstrated that an interfacial film of a surface-active substance (present in corn syrup and in the systems containing emulsifiers) is capable of resisting a shear stress at the interface by establishing a gradient in surface pressure. Shear stresses can also be resisted by air and water bubbles (Systems 11, 14, and 21), but it is not known whether or not this is due to traces of contamination (9).

Assuming complete inhibition of internal circulation so that the system behaves as though $p = \infty$, the normal and tangential stresses on the outside equator of a drop at low D are (9):

$$f_n = \frac{5}{2}\eta_0 G \sin 2\phi; \quad [22]$$

$$f_s = \frac{5}{2}\eta_0 G \cos 2\phi. \quad [23]$$

The total stress f is therefore

$$f = \frac{5}{2}\eta_0 G, \quad [24]$$

acting at an angle δ to the normal given by

$$\tan \delta = \cot 2\phi. \quad [25]$$

If f_s is borne by the interface, the total deforming stress f is thus greater than assumed in the theory except at $\phi = \pm\pi/4$, where it is the same. The value of D should therefore be greater than given by Eq. [9], and γ calculated from the deformation should be too small; this deviation is shown by seven of the nine systems in shear flow (Fig. 6) and the water drops (System 11) in hyperbolic flow (Table II).

As will be shown (16), Tomotika's theory (14, 15) of the rate of growth of capillary disturbances in liquid threads, also based on the assumption of complete transmission of shear stress across the interface, applies in systems in which internal circulation occurs but not in corn syrup media.

Emulsifiers, in addition to lowering γ and interfering with the transmission of shear stress, caused variations in the D vs. Gb curve from drop to drop especially at high deformations. They also caused the deformation of a drop at fixed G to increase with time; this behavior was probably associated with the decay in internal circulation observed under the same conditions (9), and was undoubtedly due to the accumulation at the interface of the surface-active material dissolved in the drop by diffusion and convection. In shear flow, drops showed no change in class of deformation or of D_B upon addition of emulsifiers. Breakup of threads at rest ($G = 0$) and in hyperbolic flow gave less uniform and larger drops when emulsifiers were present. It seems likely that the differences in behavior caused by adding emulsifiers were due to the formation of viscoelastic interfaces.

SUMMARY

The deformation, orientation, and burst of fluid drops suspended in a liquid subjected to both hyperbolic and shear flow have been measured for a large number of fluid pairs covering a wide range of viscosity ratio p . At low deformation excellent agreement with theoretical equations due to Taylor and Cerf was found. Three classes of drop behavior for large deformations in shear flow are described and are shown to depend upon p . Two of these classes lead to bursting of the drop in shear flow, and the third to an upper limit of deformation. The critical conditions of burst were shown to be in reasonable agreement with the theory. The effects of added emulsifiers and of electrostatic fields on the deformation have also been studied.

REFERENCES

1. TREVELYAN, B. J., AND MASON, S. G., *J. Colloid Sci.* **6**, 354 (1951).
2. MASON, S. G., AND MANLEY, R. ST. J., *Proc. Roy. Soc. (London)* **A238**, 117 (1956).
3. BARTOK, W., AND MASON, S. G., *J. Colloid Sci.* **12**, 243 (1957).
4. ARLOV, A. P., FORGACS, O. L., AND MASON, S. G., *Svensk Papperstidn.* **61**, 61 (1958).
5. FORGACS, O. L., AND MASON, S. G., *J. Colloid Sci.* **14**, 457 (1959).
6. FORGACS, O. L., AND MASON, S. G., *J. Colloid Sci.* **14**, 473 (1959).
7. MASON, S. G., AND BARTOK, W., in C. C. Mill, ed., "Rheology of Disperse Systems," p. 19 et seq. Pergamon Press, London, 1959.
8. BARTOK, W., AND MASON, S. G., *J. Colloid Sci.* **13**, 293 (1958).
9. RUMSCHEIDT, F. D., AND MASON, S. G., *J. Colloid Sci.* **16**, 210 (1961).
10. BARTOK, W., AND MASON, S. G., *J. Colloid Sci.* **14**, 13 (1959).
11. TAYLOR, G. I., *Proc. Roy. Soc. (London)* **A146**, 501 (1934).
12. TAYLOR, G. I., *Proc. Roy. Soc. (London)* **A138**, 41 (1932).
13. CERF, R., *J. chim. phys.* **48**, 59 (1951).
14. TOMOTIKA, S., *Proc. Roy. Soc. (London)* **A150**, 322 (1935).
15. TOMOTIKA, S., *Proc. Roy. Soc. (London)* **A153**, 302 (1936).
16. RUMSCHEIDT, F. D., AND MASON, S. G., forthcoming publication.
17. ZUIDEMA, H. H., AND WATERS, G. W., *Ind. Eng. Chem., Anal. Ed.* **13**, 312 (1941).

TENSILE STRESS RELAXATION BEHAVIOR OF METHYLMETHACRYLATE AND METHYL- ACRYLATE COPOLYMERS¹

Kiyohisa Fujino, Kazuo Senshu, and Hiromichi Kawai²

*Department of Textile Chemistry, Kyoto University, Kyoto, Japan, and
Department of Chemistry, University of Massachusetts, Amherst,
Massachusetts*

Received August 1, 1960

I. INTRODUCTION

As is well known, the linear viscoelastic behavior of materials has been systematically formulated by using Boltzmann's superposition principle (1), a mathematical expression of the "Law of Causality," to relate stress, strain, and time, assuming that the memory function in the superposition principle can be expressed in the form of the Laplace integral of a function of τ or λ , both of which are rates of memory disappearance and are called relaxation or retardation times. These functions of relaxation or retardation time are also called relaxation or retardation spectra, respectively (2).

The spectra, either of which can be inverted from the other (2), should be the most fundamental and characteristic functions, at least from a phenomenological point of view, for predicting the mechanical behavior of linear viscoelastic materials. They have the same importance as elastic modulus for Hookean elastic materials and viscosity coefficient for Newtonian viscous materials.

The relation between the relaxation spectrum and the molecular structure of materials has been studied by many workers experimentally (3) and theoretically (4). As far as amorphous polymers are concerned, the relaxation spectrum has been generalized to consist of at least three of the following characteristic portions: At shorter relaxation times, there exists a characteristic portion which has a close relation to the monomeric structure of a polymer, such as the nature of the side chain or side group, but for which a definite shape of its contribution to the spectrum has not been elucidated. The middle relaxation time range has a unique wedge-type

¹ A portion of this work is from the thesis of K. Senshu for the master's degree presented at the Department of Textile Chemistry, Kyoto University, Kyoto, Japan, on March 15, 1959.

² Present address, Department of Textile Chemistry, Kyoto University, Kyoto, Japan.

portion with a slope of $-\frac{1}{2}$ for almost every polymer, in which the intensity ranges from about 10^9 to 10^6 dynes/cm.². At longer relaxation times, a box-type portion having an almost constant intensity of about 10^6 dynes/cm.² appears the width of which increases as the D.P. of the polymer increases. The edge of the box at the longer time end becomes steeper as the D.P. distribution of the polymer becomes sharper.

Nevertheless, there are still many interesting problems not only in the wedge portion, which has been the one chiefly studied, but also in the other two portions, and further experimental data and a more refined theoretical analysis are needed.

In this paper, the stress relaxation behavior of methylmethacrylate and methylacrylate copolymers are studied in terms of the relaxation spectrum. The results not only confirm the well-known and generalized correlation between the spectrum and the molecular structure of amorphous polymers but also suggest some systematic changes of the spectrum with molecular structure. This paper is also presented as a preliminary step in a systematic investigation of the spectrum changes which occur on going from amorphous to crystalline polymer. The relaxation spectra of the crystalline polymer have been found to be quite different from those of the amorphous polymer, especially in the wedge and/or the box portions (5).

II. PREPARATION OF SAMPLE POLYMERS AND TEST SPECIMENS

Five copolymers of different mole ratios including polymethylmethacrylate (PMMA) and polymethylacrylate (PMA) as the extremes were prepared using a solution polymerization method under the conditions which are shown in Table I. It is believed that these conditions were mild enough to obtain linear polymers.

Since the determination of the mole ratios of MMA to MA in their copolymers by means of an ordinary chemical analysis is generally difficult, an infrared absorption method using a characteristic band of the methyl group at 1140 to 1160 cm.⁻¹ was used. The results obtained are shown in Table II, together with other physical properties such as density and intrinsic viscosity. The density was measured at 25°C. by the flotation method in carbon disulfide and *n*-heptane mixtures. The intrinsic viscosity was measured at 25°C. in benzene.

The degrees of polymerization, \bar{P}_n , of the two polymers PMMA and PMA were estimated from their intrinsic viscosities in chloroform and acetone,³ with the results that $\bar{P}_n = 7300$ for PMMA and 3700 for PMA. The polymer samples obtained are designated as PMMA, MM-M2, MM-M3, MM-M4, and PMA in the order of increasing mole ratio of methylacrylate.

³ The equations used are PMA-acetone at 20°C. (6a), $\bar{P}_n = \{\text{antilog } ([\eta]/0.239) - 1\} \times 2000$; PMMA-chloroform at 20°C. (6b), $\bar{P}_n = ([\eta] - 0.0095)/0.47 \times 10^{-4}$.

TABLE I
Polymerization Condition of the Copolymers

Specifi- cation	Monomer charge ratio (moles)	Catalyzer	Polymerization medium	Temperature time	Con- version (wt. %)
PMMA	100/0	B.P.O. 0.020 mole/l.* commonly	methanol 11.1 water 24.9 mole/l.* commonly	65°C. 2 hrs. commonly	70>
MM-M2	66/34				30>
MM-M3	36/64				30>
MM-M4	17/83				30>
PMA	0/100				70>

* For whole system.

TABLE II
Composition, Density, and Intrinsic Viscosity of the Copolymers

Specification	Mole ratio (MMA/MA)	Density (g./c.c. at 25° C.)	Intrinsic viscosity (l./g. in benzen 25 °C.)
PMMA	100/0	1.216	0.153
MM-M2	75/25	1.212	0.158
MM-M3	61/39	1.209	0.157
MM-M4	42/58	1.207	0.336
PMA	0/100	—	0.369

The polymers were cast into thin films from 0.05 to 0.5 mm. thick by pouring their acetone solutions on a glass plate floating on mercury, followed by gradual evaporation in a desiccator for about a week. The films thus obtained were swollen in distilled water, stripped off the glass plate, and dried in air. The films were then cut into test specimens about 5 cm. long and 1.0 to 6.5 mm. wide. It was necessary to cut glassy polymers such as PMMA on a hot plate (80°C. for PMMA) in order to avoid cracking.

The test specimens thus prepared were dried again in a vacuum oven at 50°C. for more than a week, and stored in a P₂O₅ vacuum desiccator until used.

Before the measurement of stress relaxation, the test specimen was hung freely from an upper jaw of the stress measurement apparatus and was annealed at a desired temperature (from 100°C. for PMA to 180°C. for PMMA) for 10 min. Then it was cooled gradually down to a temperature of measurement in an oven attached to the apparatus.

The annealing was necessary to avoid scattering of the results, especially for glassy state measurements, because the mechanical properties of these

polymers are very sensitive to thermal history as well as moisture content, as demonstrated by Tobolsky and his co-workers for PMMA (7a, b).

III. APPARATUS AND PROCEDURE

Two sets of a chainomatic balance type auto-recording relaxometer which are essentially the same as that used by Fujita and Ninomiya (8, 9) and for which some details will be described in a following paper, were used. One of these was a high-capacity type for glassy and transition region measurements; the other was a light-capacity type for rubbery and flow region measurements. The supports for these balance arms were agate

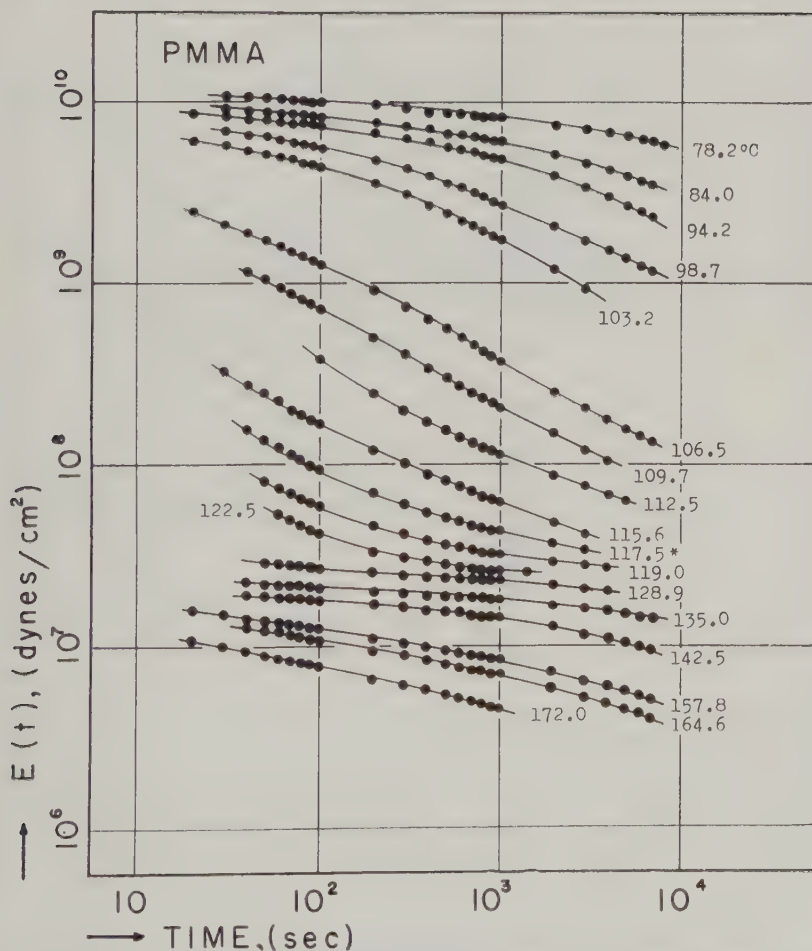


FIG. 1. Stress relaxation of polymethylmethacrylate shown by relaxation modulus, $E(t)$ vs. time, t (seconds) at various temperatures.

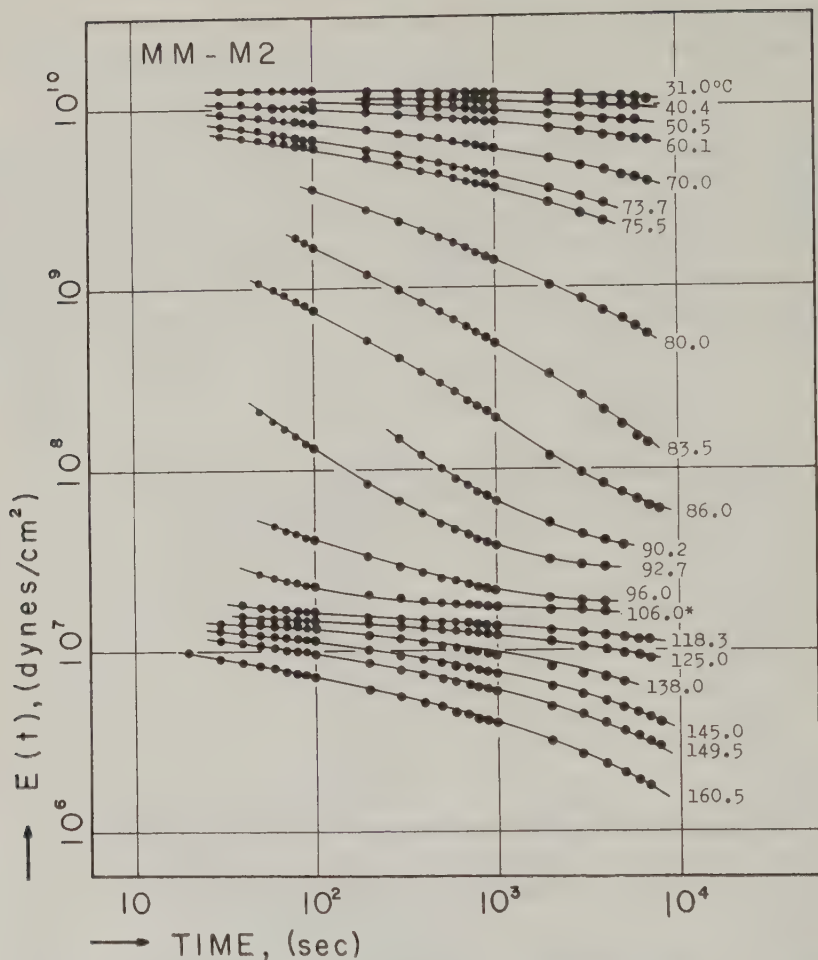


FIG. 2. Stress relaxation of 75/25-MMA/MA copolymer shown by relaxation modulus, $E(t)$ vs. time, t (seconds) at various temperatures.

knife edges and steel plates for the former and a pin-pivot of steel needle and agate pivot for the latter.

The temperature oven was a double-shielded type. The temperature of the outer oven was always kept about 5°C. lower than that of the inner oven, and the accuracy of the inner oven was $\pm 0.1^\circ\text{C}$. at any measuring temperature. An excess of P_2O_5 powder was used to reduce humidity in the inner oven.

An initial tensile strain was applied to the sample by means of a micro-screw attached to the lower jaw of the apparatus. The magnitude of tensile strain was less than 1.1 % for the glassy state, less than 3.0 % for the transi-

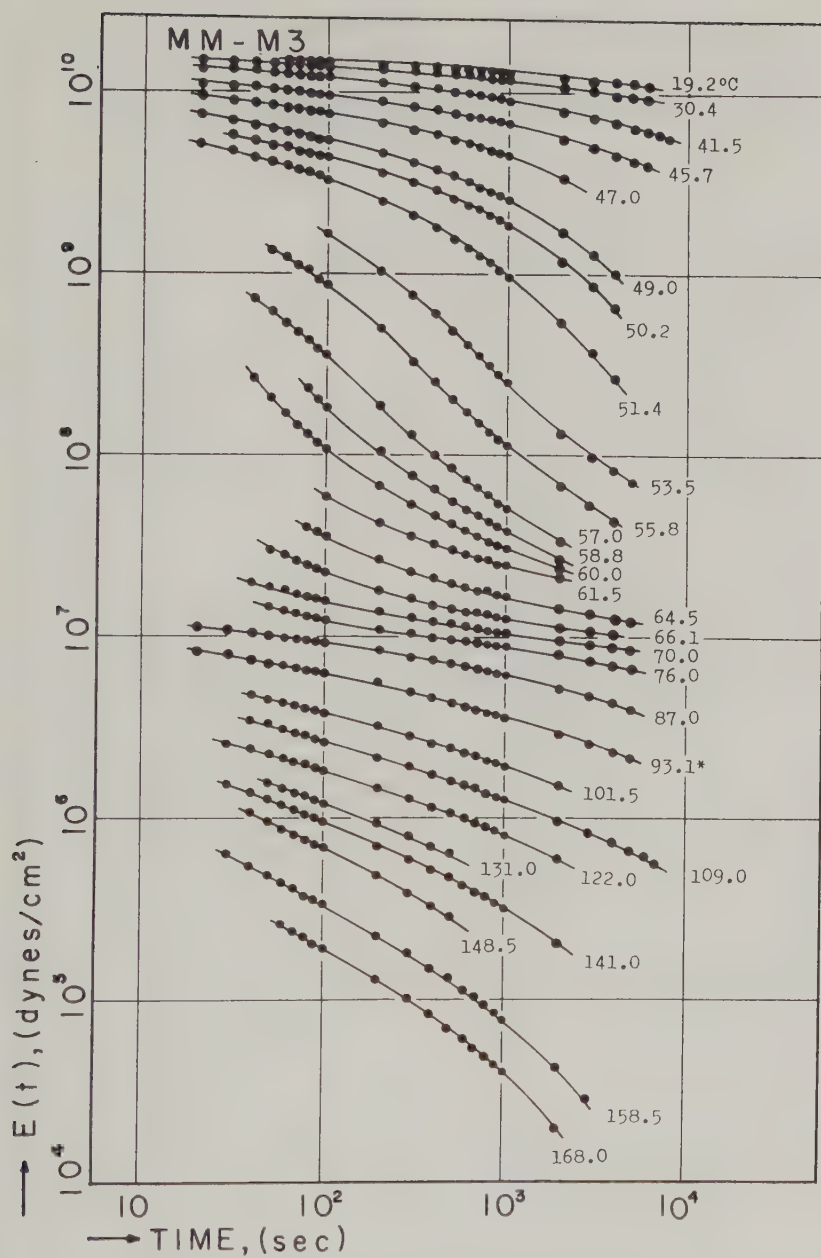


FIG. 3. Stress relaxation of 61/39-MMA/MA copolymer shown by relaxation modulus, $E(t)$ vs. time, t (seconds) at various temperatures.

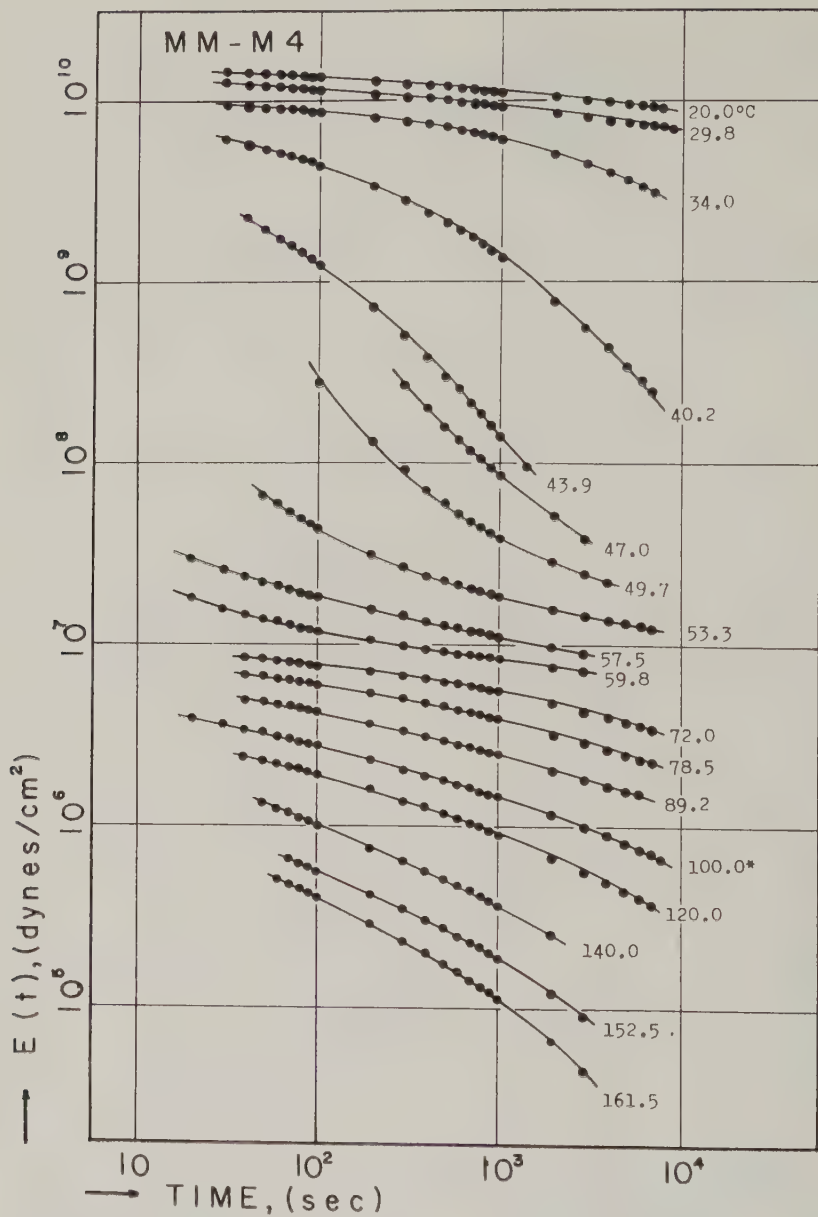


FIG. 4. Stress relaxation of 42/58-MMA/MA copolymer shown by relaxation modulus, $E(t)$ vs. time, t (seconds) at various temperatures.

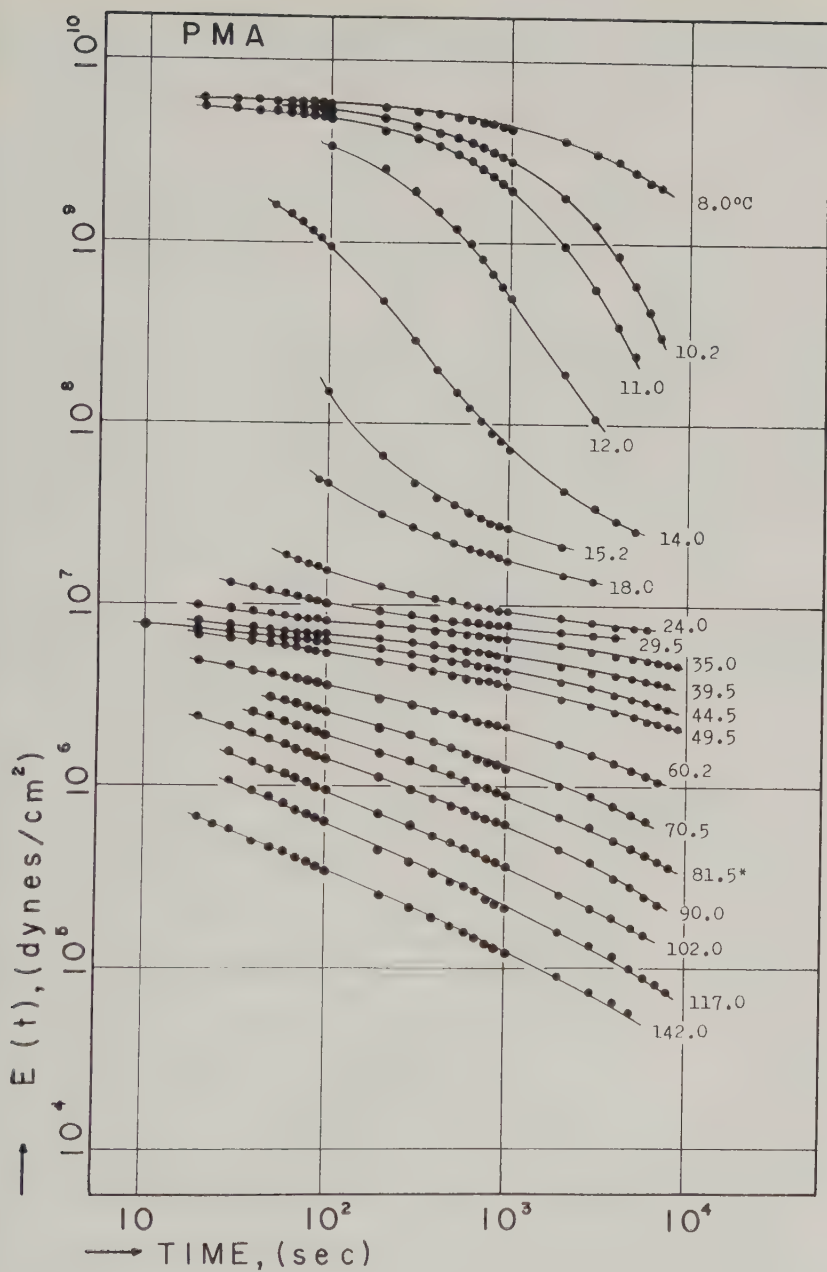


FIG. 5. Stress relaxation of polymethylacrylate shown by relaxation modulus, $E(t)$ vs. time, t (seconds) at various temperatures.

tion state, less than 10% for the rubbery state, and less than 15% for the flow state for all polymers. These magnitudes seemed to be sufficient to insure that the measurements were within the limits of linear mechanical behavior.

IV. RESULTS

Figures 1 to 5 show results obtained for the five polymers; the relaxation modulus $E(t)$ in dynes/cm.² is plotted against time (seconds) double-logarithmically at various temperatures ranging from room temperature up to about 170°C.

It is seen that these polymers resemble each other in relaxation behavior and that this behavior is typical of amorphous linear polymers (non-crosslinked); with increasing temperature, the relaxation modulus decreases from the glassy value of about 10^{10} dynes/cm.² to the rubbery value of about 10^7 dynes/cm.², passing through a transition region where the modulus decreases sharply within a rather narrow temperature interval. The rubbery region is followed by a flow region where the modulus decreases sharply again. It is observed that the transition region appears at lower temperatures as the mole ratio of methylaerylate increases.

In order to make the discussion more quantitative, it is convenient to compose a so-called master curve (10) of stress relaxation from the original data by using the "reduced variables method" (11). For every polymer

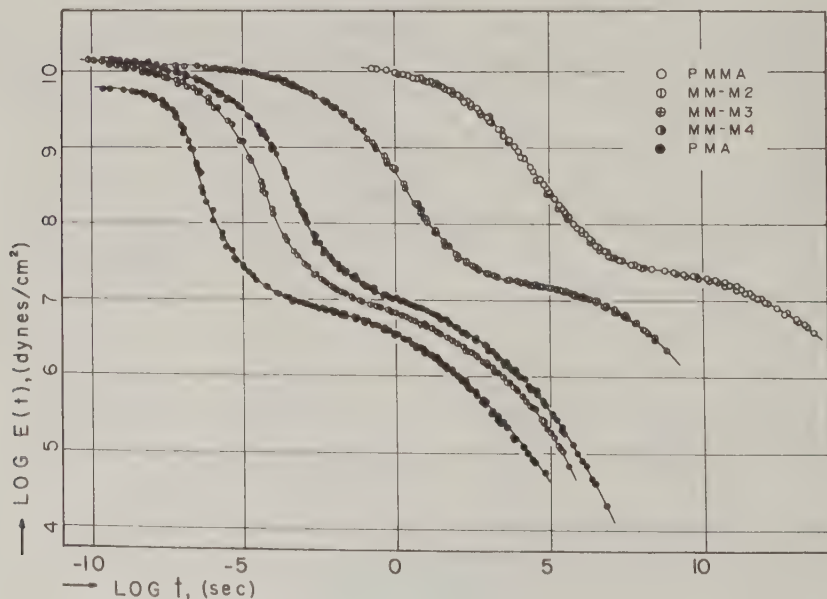


FIG. 6. Comparison of master curves of the copolymers, further shifted to 100°C.

studied it was fairly easy to compose such a master curve,⁴ i.e., to superpose the relaxation curve at one temperature to another by sliding the curve along the time axis.

At first, a reference temperature T_0 was chosen arbitrarily about the middle of the temperature interval for each polymer. The temperature T_0 is shown by the symbol* in Figs. 1 to 5: 117.5°, 106.0°, 93.1°, 100.0°, and 81.5°C. for the polymers in order from PMMA to PMA. Relaxation curves at various temperatures were shifted to the curve at the reference temperature along the time axis until they made a smooth composite curve, a "master curve." The master curve at the reference temperature was further shifted to a particular temperature, 100.0°C., by using a method discussed later and was compared with each of the others in Fig. 6.

It is seen that the position and the shape of the master curves so obtained change systematically with increasing mole ratio of methylacrylate; that is, the position is shifted to shorter times and the transition from glassy to rubbery state occurs more sharply.

V. DISCUSSION

Composition of the Master Curve

The logarithm of the amount of shift of a given relaxation curve along the time axis, i.e., the shift factor a_T , (12), was plotted against temperature, and the resulting curve was found to coincide well with the W.L.F. equation (13) except at lower temperature. The equation is:

$$\log a_{T_0}(T) = \frac{-c_1 c_2 (T - T_0)}{(c_2 + T - T_s)(c_2 + T_0 - T_s)}, \quad [1]$$

where a_{T_0} is the shift factor obtained when T_0 in °K. is taken as the reference temperature; c_1 and c_2 are constants of 8.86 and 101.6, respectively; T_s is the distinctive temperature and T is the measuring temperature, both in °K. The value of T_s was found by a trial-and-error method to be 429°, 395°, 368°, 357°, and 326°K. for the polymers in order from PMMA to PMA.

By using these values of T_s , the shift factor with T_s as the new reference temperature, i.e., $\log a_{T_s}(T)$, can be calculated from

$$\log a_{T_s}(T) = \log a_{T_0}(T) + \log a_{T_0}(T_s), \quad [2]$$

where the first term on the right-hand side can be determined experimentally and the second term is calculated by substituting T_s for T in Eq. [1].

In Fig. 7, $\log a_{T_s}(T)$ is plotted against $(T - T_s)$. The results coincide quite well with the W.L.F. equation shown by the solid line over the

⁴ A correction for thermal expansion and for temperature dependency of elastic modulus due to rubber elasticity was neglected, assuming $T_p/T_0\rho_0$ to be unity.

temperature ranges studied except at lower temperatures than -50°K . in $(T - T_s)$, where the experimental data appear to have an inflection point. Such a deviation from the W.L.F. equation in the lower temperature range has been noted previously for other amorphous polymers (14).

Strictly speaking, the reduced variables method, that is, the time-temperature superposition hypothesis, is valid only for a system in which all the relaxation processes have the same apparent activation energy not only in magnitude but also in their temperature dependency (15). This suggests the reason why the superposition hypothesis should not be extended from the transition region to other regions—glassy region or the rubbery region. The nature of the relaxation process of these other regions should be quite different from its character in the transition region. The difference is especially marked between the glassy and the transition regions.

Some experiments have shown that the activation energy of the relaxation process in the glassy region is quite small compared with that in the transition region (16–18). The process in the glassy region might be due

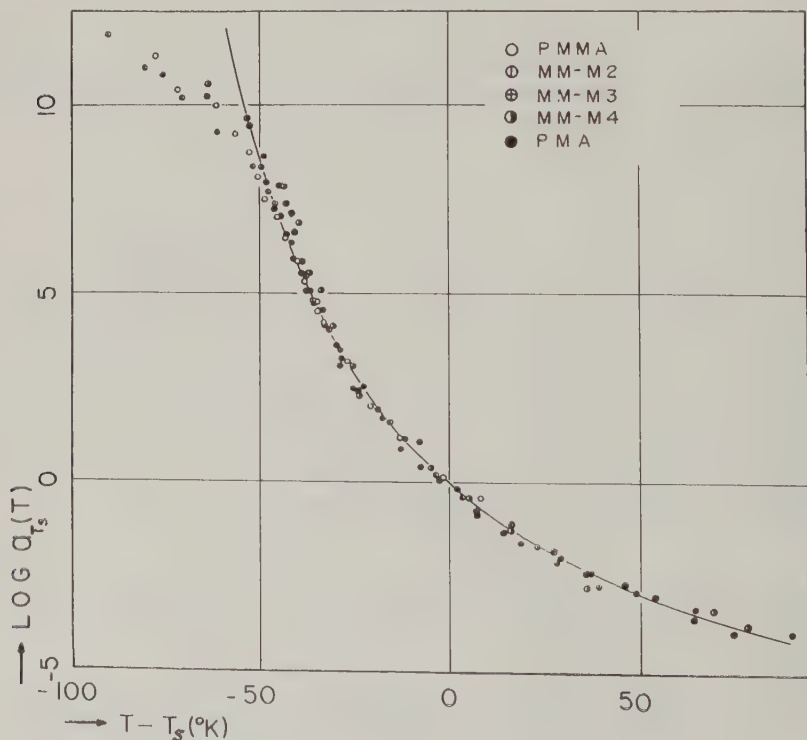


FIG. 7. Check of fitting of the data to the W.L.F. equation between shift factor a_T and $T - T_s$, where the equation is shown by solid line.

to a thermal motion of the localized small portions in the chain molecule, whereas the process in the transition region has been postulated to be due to a cooperative segmental diffusion in the molecule. Some attempts have also been made to separate these two relaxation processes for polymethylmethacrylate by Iwayanagi *et al.* (19) and for the polymethacrylate series by Ferry *et al.* (18).

Consequently, it is rather reasonable that the shift factor $\log a_{T_s}(T)$ diverges at lower temperatures from the W.L.F. equation, which has empirically validated the time-temperature superposition hypothesis, at least within the temperature range of $T_s \pm 50^\circ\text{K.}$ for linear amorphous polymers, even if the procedure of the superposition, i.e., shifting relaxation curves along the time axis and composing a master curve, is applied smoothly.

A similar consideration should hold for superposing the relaxation curves in the zone between the transition and the rubbery regions (15). The relaxation process in the rubbery region might be characterized by an intermolecular relaxation due to loosening of some type of intermolecular junctions, whereas that in the glassy or in the transition region is of an intramolecular nature. The temperature range of $T_s + 50^\circ\text{K.}$ in the W.L.F. equation covers the range from the transition to the rubbery region for most linear amorphous polymers. The validity of the equation for the superposition in this temperature range, which has been insured by only an experimental agreement between the relaxation spectra of polyisobutylene, one of which was obtained from Philippoff's absolute measurement (20) of dynamic modulus from transition to rubbery region at a fixed temperature and the others of which were obtained from Ferry's (21) and Tobolsky's (22) measurements by means of the reduced variables method mainly in transition and rubbery region, respectively, might deny the consideration as above.

The validity of the equation for the superposition in this temperature range seems to hold for materials in which intermolecular junctions are only mechanical entanglements between chain molecules, and it is hoped to test the validity rigorously for many kinds of polymers including even crystalline polymers, taking into account the details of the nature of intermolecular junctions. In this connection it is of significance to note that there have been some systematic failures of the reduced variables method in the boundary between the transition and the rubbery regions for some polymethacrylates (23). There have also been some difficulties in superposing mechanical data in the rubbery region for polymethylmethacrylate (7b) and Buna-N vulcanizate (24). Moreover, it was almost hopeless to obtain the superposition of the data for crystalline polymers (25); however, an interesting modification of the reduced variables method for

TABLE III
Comparison of Characteristic Temperatures of the Copolymers

Specification	Reference temp. $T_0(^{\circ}\text{K.})$	Distinctive temp. $T_s(^{\circ}\text{K.})$	Glass tran. temp. from max. of act. eneg. $T_d(^{\circ}\text{K.})$	Glass tran. temp. from G-T eq. $T_g(^{\circ}\text{K.})$	$T_s - T_d$	Shift factor to 100°C., $\log a_{373}(T_0)$
PMMA	390.5	429	390	390	39	-3.79
MM-M2	379	395	357	359	38	-0.79
MM-M3	366	368	322	342	46	+0.56
MM-M4	373	357	319	320	38	0.00
PMA	354.5	326	285	285	41	+0.86

these polymers has been proposed by Nagamatsu *et al.* (26), taking into account the variation of the degree of crystallinity with temperature.

As described above, the master curves in Fig. 6 were further shifted to 100°C. from their respective reference temperatures T_0 . In this procedure the shift factor $\log a_{373}(T_0)$ is easily calculated for MM-M2 to PMA by using Eq. [1]. However, for PMMA the temperature 100°C. (373°K.) is beyond the limit of Eq. [1] (i.e., the difference between 373°K. and T_s (429°K.) is -56°K.). Therefore the shift factor $\log a_{373}(T_0)$ for this polymer is determined from the following equation, which holds similarly as in the case of Eq. [2],

$$\log a_{373}(T_0) = \log a_{T_s}(T_0) + \log a_{373}(T_s). \quad [3]$$

The first term in the right-hand side of the equation can be calculated by using Eq. [1], and the second term is obtained from actual plots for PMMA in Fig. 7. The value of the total shift factor thus obtained is -3.79, and is considerably smaller than the value of -5.41 calculated by using Eq. [1]. In Table III, the shift factor $\log a_{373}(T_0)$, the reference temperature T_0 , and the distinctive temperature T_s are listed, together with other values which will be discussed later.

Apparent Activation Energy of the Relaxation Process and Relation between Glass Transition Temperature and Mole Ratio of the Copolymers

On the assumption that the stress relaxation phenomena can be treated as a rate process, an activation energy of the process, ΔH_a , can be calculated from the data of the shift factor a_T by the equation:

$$\begin{aligned} \Delta H_a &= 2.303 R d \log a_T / d (1/T); \\ &= -2.303 R T^2 d \log a_T / d T. \end{aligned} \quad [4]$$

The values of ΔH_a calculated for the present five polymers are plotted in Fig. 8 against the reciprocal of the absolute temperature. The activation

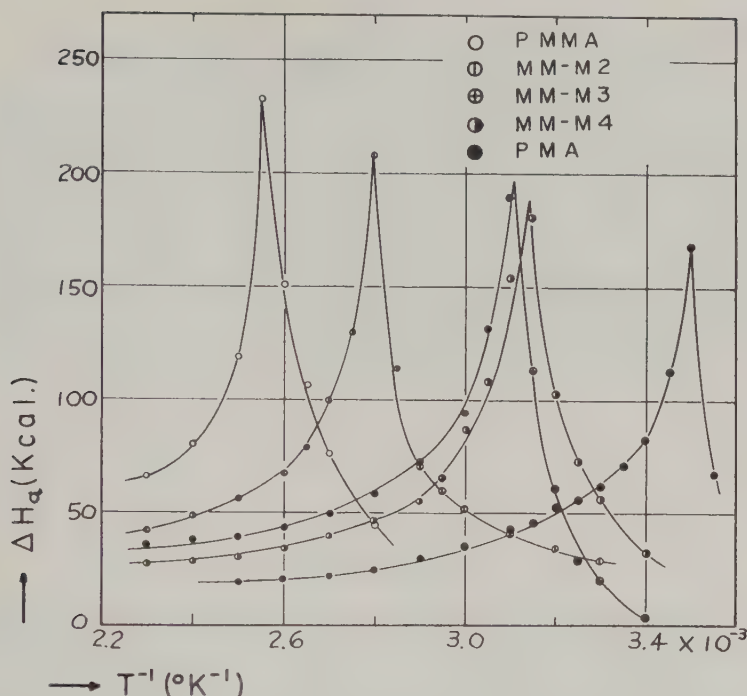


FIG. 8. Temperature dependency of apparent activation energy for relaxation process, ΔH_a .

energy is not independent of temperature; it has a sharp maximum at a temperature corresponding to the inflection point found in Fig. 7 near -50°K . in $(T - T_g)$.

The temperature, T_d , at which the apparent activation energy ΔH_a attains a maximum may be a point where the true activation energy, if defined, changes in a sharp stepwise fashion, suggesting that the mode of molecular motion changes suddenly at this temperature. Hence the temperature T_d may be closely related to the glass transition temperature T_g . The values of T_d for the respective polymers are given in Table III.

As shown in Table III and Fig. 8, the temperature T_d and the maximum activation energy $(\Delta H_a)_{\max.}$ increase systematically with increasing mole ratio of methylmethacrylate. If T_d is closely related to T_g (14), this correlation suggests that the chain stiffness against segmental motion increases with increasing mole ratio of methylmethacrylate which might be more rigid than methylacrylate (16, 17) owing to the existence of the α -methyl group.

Catsiff and Tobolsky presented an empirical equation relating T_d to $(\Delta H_a)_{\max.}$, which reads (22)

$$(\Delta H_a)_{\max.} = KT_d^2. \quad [5]$$

This form is also obtained from Eq. [4], i.e.,

$$(\Delta H_a)_{\max.} = -2.303 RT_d^2 (d \log a_T/dT)_{T_d} \equiv KT_d^2.$$

It was reported for several amorphous polymers that K is a constant ranging from 1.5 to 2.0×10^{-3} . The values of K calculated for the copolymers are shown in Table IV, together with the corresponding maximum activation energies $(\Delta H_a)_{\max.}$. These values of K are reasonable when compared with other literature values (9, 22, 27). The magnitude of $(\Delta H_a)_{\max.}$ of PMMA, for example, is rather close to the values of 260 kcal. and 280 kcal. given by Bueche (27) and Iwayanagi (28), respectively.

Gordon and Taylor have presented an equation (29) relating the glass transition temperature T_g to the mole ratio in a copolymer; i.e.,

$$C_2 = \frac{\theta - \theta_1}{k(\theta_2 - \theta) + (\theta - \theta_1)},$$

where

$$k = \frac{\beta_{R_2} - \beta_{G_2}}{\beta_{R_1} - \beta_{G_1}}. \quad [6]$$

Here C_2 is the weight fraction of the second component in the copolymer, θ is the glass transition temperature of the copolymer and θ_1 and θ_2 are the glass transition temperatures of the pure polymers, respectively. β_{R_i} and β_{G_i} are the volume expansion coefficients in the rubbery and glassy states of the pure polymer ($i = 1, 2$).

The value of k was taken as 0.87 from the literature (30), θ_1 and θ_2 as 285° and 390°K. from T_d of this work, and C_2 from the results of infrared analysis shown in Table I. Then the glass transition temperature T_g is calculated by using Eq. [6] and is shown in the fifth column of Table III.

The values of T_s and T_d and T_g thus calculated are illustrated in Fig. 9 as a function of the mole fraction of MMA, in which dot, circle, and cross marks correspond to T_s , T_d , and T_g , respectively. The literature values of T_s and T_g for PMA and PMMA collected by Williams (31) are also illustrated in Fig. 9 by squares and by triangles, respectively.

TABLE IV
Maximum Activation Energy $(\Delta H_a)_{\max}$ and Value of K

Specification	$(\Delta H_a)_{\max}$ (kcal./mole)	K
PMMA	233	1.53×10^{-3}
MM-M2	208	1.63×10^{-3}
MM-M3	190	1.83×10^{-3}
MM-M4	181	1.78×10^{-3}
PMA	169	2.08×10^{-3}

The values of T_s for PMMA and PMA obtained in this work agree fairly well with these literature values. The value of T_s increases with increasing mole ratio of MMA in a quadratic fashion. Whereas the values of T_d for PMMA and PMA are about 10°C. higher than the reported values of T_g obtained from thermal volume expansion measurements, the values of T_g for the copolymers predicted from the Gordon and Taylor equation by using T_d of PMA and PMMA in this work as θ_1 and θ_2 show good agreement with the T_d values for the copolymers except for the case of MM-M3.

It is not unusual, as far as experimental results are concerned, that T_d is always somewhat higher than T_g obtained by some static methods such

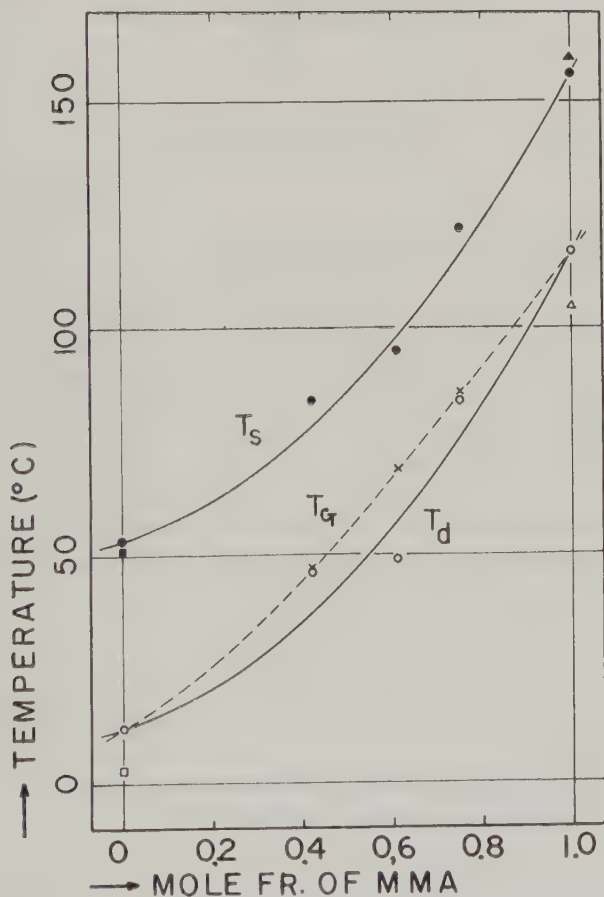


FIG. 9. Mole fraction dependency of characteristic temperatures, T_s , T_d , and T_g of the copolymers. Dots and circles are T_s and T_d in this work. Cross marks are T_g predicted by the Gordon-Taylor equation from T_d values in this work. Triangles are T_s and T_g for PMMA by Bischoff and Fox and squares are T_s and T_g for PMA by Williams and Jenkel.

as dilatometry. But the large discrepancy for MM-M3 found above is probably due to an overestimation of the MMA fraction in the infrared analysis.⁶ If this is the case, the experimental results indicated by the solid lines in Fig. 9 may be redrawn somewhat straighter, by neglecting the points for MM-M3.

Relaxation Spectrum

The relaxation spectra of the respective polymers were deduced from the master curves at 100°C. by using Schwarzl and Staverman's first approximation method (32):

$$H(\tau) = - \left. \frac{dE(t)}{d(\ln t)} \right|_{t=\tau}$$

or

$$= -E(t) \left. \frac{d(\ln E(t))}{d(\ln t)} \right|_{t=\tau}, \quad [7]$$

where $H(\tau)$ is the relaxation spectrum in terms of the logarithmic relaxation time. The results are shown in Fig. 10.

Generally speaking, the shape of the relaxation spectra obtained agrees well with those of well-known amorphous linear polymers (33). It consists of at least three characteristic portions, a high-intensity plateau, a $-\frac{1}{2}$ slope wedge, and a low intensity plateau. As far as the shape and the position of the wedge portions for PMMA and PMA are concerned, they agree fairly with those from the literature (7, 28, 34, 35)⁶ in spite of probable differences in the preparation of test specimens and in experimental conditions. The slope of the wedge agrees with a theoretical value $-\frac{1}{2}$ only at the skirt of the wedge except for PMMA. This discrepancy will be discussed later. The gradual decrease of the intensity at the end portion of the low plateau, which was not observed for PMMA and MM-M2 owing to the limitation of the measuring temperature, may be ascribed to the broad distribution of molecular weights in the unfractionated polymer samples used in this investigation (9, 36).

In comparing relaxation spectra, the following three systematic features may be noted:

1. The relative position along the relaxation time axis is shifted to longer times with increasing mole ratio of MMA.

⁵ The mole ratio of MM-M3 was recalculated as 56:44, using monomer reactivity ratios of 0.144 (MA) and 1.145 (MMA) which were estimated from the monomer charging ratio and the mole ratio of yield copolymer shown in Tables I and II except for MM-M3.

⁶ The average slope of the wedge of PMA in the literature is somewhat less steep than that obtained here.

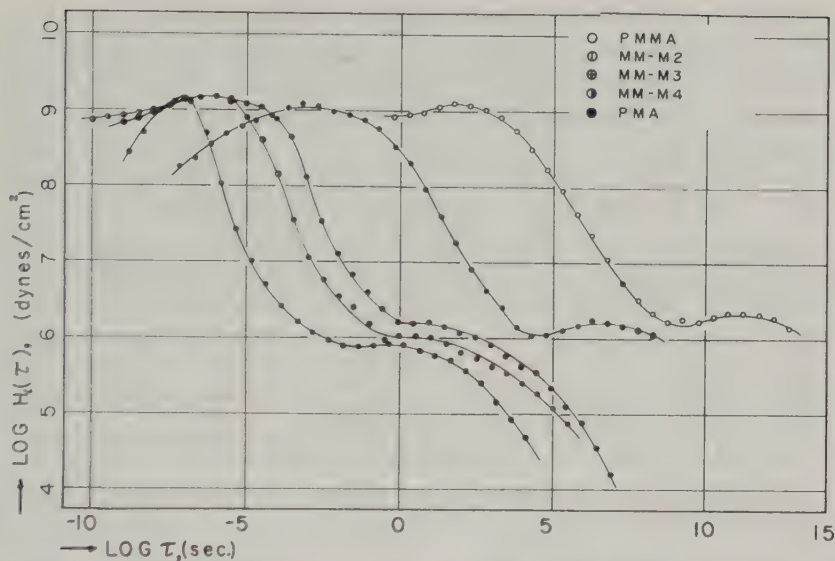


FIG. 10. Relaxation spectra obtained by using Schwarzl and Staverman's first approximation method from the master curves of respective polymers at 100°C. shown in Fig. 6.

2. The average slope of the wedge portion decreases and approaches the theoretical value of $-\frac{1}{2}$ with increasing mole ratio of MMA.

3. The height of the lower plateau portion, i.e., the so-called box portion, increases with increasing mole ratio of MMA.

The first feature (1) has also been found for the master curves and is closely related to the glass transition temperature of the polymers; that is, the higher the glass transition temperature, the more the relaxation spectrum shifts to the longer time side. This might be interpreted in terms of increasing chain stiffness due to increasing mole ratio of MMA; in other words, in terms of the increasing monomeric friction coefficient, ζ_0 , in the Rouse theory (4a). The same tendency has been observed by Catsiff and Tobolsky for a series of copolymers of styrene and butadiene (37).

Concerning feature (2), Ferry (38) has pointed out that the departure from theory of the spectrum intensity, especially near the top of the wedge, seems to be related to the chemical structure of the monomeric unit of the polymer. The discrepancy may also be explained, as by Zimm (4d, 39), in terms of the change of hydrodynamic interaction. The softer the chain backbone, the steeper becomes the average slope of the wedge portion. According to Kurata's calculation (40), the slope of the wedge for a polymer with a stiff chain such as cellulose is -0.5 (free draining case), while the slope for a polymer with a soft chain, such as a vinyl, is -0.66 (non-free draining case).

It must be remembered again that the reduced variables method to obtain a master curve is valid only for a system for which all relaxation processes have the same activation energy not only in magnitude but also in their temperature dependency. Therefore, it is of questionable validity to extend the method to the boundary between the glassy and the transition regions, for the relaxation processes are quite different for the two regions—even if a smooth master curve can be determined in the boundary zone. The upper part of the wedge portion in the spectrum corresponds more or less to this boundary region and probably consists of at least two quite different relaxation processes. Consequently, the shape of the relaxation spectrum in this portion is not a unique one, being dependent on temperature. On the basis of these considerations feature (2) seems to be indefinite. Whereas some hopeful attack on these obscurities has been continued by Ferry *et al.* and by Iwayanagi *et al.* as mentioned above, the most reliable way must be to adopt some absolute means for measurements of dynamic properties in this boundary region and to compare the results at several different temperatures, completely avoiding the hypothesis of time-temperature superposition.

Regarding the lower plateau, the so-called box portion, some articles (9, 36) have related the width of the box to the molecular weight of the polymer and the shape of the longer time end to the molecular weight distribution; however, no article has interpreted the height of the box in terms of molecular theory. Thus, the explanation of feature (3) seems to be quite difficult owing to the present lack of an adequate theory which is appropriate for the shape of the box portion.

However, we tend to believe that feature (3) is due to a different nature of entanglement or of interaction between polymer chains and not to molecular weight difference alone. In a forthcoming paper some experimental results will be shown, which indicate the effects of acetylation (3 to 100 mole %) of polyvinyl alcohol upon the shape of the relaxation spectrum; the degrees of polymerization of the samples used were hardly changed. The effect is, however, more distinctive not only in decreasing the height of the box but also in increasing the slope of the wedge, approaching the theoretical value $-1/2$.

VI. SUMMARY

1. The stress relaxation curves of methylmethacrylate-methylacrylate copolymers including polymethylmethacrylate and polymethylacrylate as extremes studied at various temperatures. The so-called master curves were composed from stress relaxation curves without any difficulty. The relation between the "shift factor" a_T and temperature agreed well with the W.L.F. equation within the temperature range of $\pm 50^\circ\text{K}$. about T_s , a distinctive temperature.

2. The apparent activation energy of the relaxation process ΔH_a which was obtained by differentiating the logarithm of the shift factor a_T with respect to the reciprocal of absolute temperature, showed a maximum value at a particular temperature T_d . The values of $(\Delta H_a)_{\max.}$ and the temperature T_d increased with increasing mole ratio of MMA. The relation between T_d and the mole ratio of the copolymers agreed well with that predicted by the Gordon-Taylor equation.

3. The shapes of relaxation spectra for the polymers studied were similar and were typical of an amorphous polymer. The position along the relaxation time axis at a particular temperature was consistent with existing literature data.

The following three systematic features were obtained with increasing mole ratio of MMA:

a. The relative position of the spectrum along the time axis shifted to longer times.

b. The average slope of the wedge portion decreased and approached the theoretical value $-\frac{1}{2}$.

c. The intensity of the lower plateau portion increased.

ACKNOWLEDGMENTS

The authors are indebted to Prof. R. S. Stein, Department of Chemistry, University of Massachusetts, Dr. M. Kurata, Department of Chemistry, Massachusetts Institute of Technology, Dr. H. Fujita, Department of Fisheries, Kyoto University, and Dr. H. Leaderman, National Bureau of Standards, who read the manuscript and offered valuable comments and suggestions for improvement.

The polymerization of the polymer sample used was kindly conducted by Dr. K. Uno and Mr. N. Takahashi, Department of Textile Chemistry, Kyoto University, and the infrared analysis was carried out by Dr. E. Nagai, Governmental Industrial Research Institute, Osaka, Japan.

REFERENCES

1. BOLTZMANN, L., *Pogg. Ann. Physik* **7**, 624 (1876).
2. GROSS, B., "Mathematical Structure of the Theories of Viscoelasticity." Hermann et Cie, Paris, 1953.
3. FERRY, J. D., in H. A. Stuart, ed., "Die Physik der Hochpolymeren," Vol. 4, p. 373. Springer, Berlin, 1957. TOBOLSKY, A. V., "Rheology," Vol. 2, p. 63. Academic Press, New York, 1957.
- 4(a). ROUSE, R. E., *J. Chem. Phys.* **21**, 1271 (1953). (b). BUECHE, F., *J. Chem. Phys.* **22**, 603 (1954). (c). NAKADA, O., *J. Phys. Soc. Japan* **10**, 804 (1955). (d). ZIMM, B. H., *J. Chem. Phys.* **24**, 269 (1956). (e). YAMAMOTO, M., *J. Phys. Soc. Japan* **11**, 413 (1956); **12**, 1148 (1957).
5. FUJINO, K., KAWAI, H., HORINO, T., AND MIYAMOTO, K., *Textile Research J.* **25**, 722, (1955); **26**, 852, (1956). TOKITA, N., *J. Polymer Sci.* **20**, 515 (1956). NAGAMATZU, K., YOSHITOMI, T., AND TAKEMOTO, T., *J. Polymer Sci.* **27**, 335 (1958); *J. Colloid Sci.* **13**, 257 (1958).
- 6(a). SAKURADA, I., "Introduction to High-polymer Chemistry," p. 196. Kobunshi

- Kagaku Kyokai, Kyoto, 1948. (b). SAKURADA, I., *J. Soc. Polymer Sci. Japan* **2**, 253 (1945).
- 7(a). McLOUGHLIN, J. R., AND TOBOLSKY, A. V., *J. Polymer Sci.* **7**, 658 (1951). (b). McLOUGHLIN, J. R., AND TOBOLSKY, A. V., *J. Colloid Sci.* **7**, 555 (1952).
8. NINOMIYA, K., KISHIMOTO, A., AND FUJITA, H., *J. Soc. Polymer Sci. Japan* **14**, 504 (1957).
9. NINOMIYA, K., AND FUJITA, H., *J. Colloid Sci.* **12**, 204 (1957).
10. BISCHOFF, J., CATSIFF, E., AND TOBOLSKY, A. V., *J. Am. Chem. Soc.* **74**, 3378 (1952).
11. LEADERMAN, H., "Elastic and Creep Properties of Filamentous Materials." The Textile Foundation Inc., Washington, D. C., 1943. MARVIN, R. S., FITZGERALD, E. R., AND FERRY, J. D., *J. Appl. Phys.* **21**, 197 (1950). FERRY, J. D., AND FITZGERALD, E. R., *J. Colloid Sci.* **8**, 224 (1953). CATSIFF, E., AND TOBOLSKY, A. V., *J. Colloid Sci.* **10**, 375 (1955). SCHWARZL, F., AND STAVERMAN, A. J., *J. Appl. Phys.* **23**, 838 (1952).
12. FERRY, J. D., *J. Am. Chem. Soc.* **72**, 3746 (1950).
13. WILLIAMS, M. L., LANDEL, R. F., AND FERRY, J. D., *J. Am. Chem. Soc.* **77**, 3701 (1955).
14. TOBOLSKY, A. V., *J. Appl. Phys.* **27**, 673 (1956).
15. NAKADA, O., *J. Phys. Soc. Japan* **12**, 1218 (1958).
16. HOFF, E. A. W., ROBINSON, D. W., AND WILLBURN, A. H., *J. Polymer Sci.* **15**, 161 (1955).
17. HEIJBOER, J., *Kolloid-Z.* **148**, 36 (1956); *Proc. 2nd Intern. Congr. Rheology*, p. 123. Butterworth, London, 1954. IWAYANAGI, S., AND HIDESHIMA, T., *J. Phys. Soc. Japan* **8**, 368 (1953).
18. FERRY, J. D., CHILD, W. C., ZAND, R., STERN, D. M., WILLIAMS, M. L., AND LANDEL, R. F., *J. Colloid Sci.* **12**, 53 (1957). CHILD, W. C., AND FERRY, J. D., *J. Colloid Sci.* **12**, 327 (1957). CHILD, W. C., AND FERRY, J. D., *J. Colloid Sci.* **12**, 389 (1957). DANNHAUSER, W., CHILD, W. C., AND FERRY, J. D., *J. Colloid Sci.* **13**, 103 (1958).
19. SATO, K., NAKANE, H., HIDESHIMA, T., AND IWAYANAGI, S., *J. Phys. Soc. Japan* **9**, 413 (1954). HIDESHIMA, T., AND IWAYANAGI, S., *J. Japan. Soc. Testing Material* **6**, 219 (1957).
20. PHILIPPOFF, W., *J. Appl. Phys.* **24**, 685 (1953).
21. FERRY, J. D., *et al.*, *J. Appl. Phys.* **24**, 650, 911 (1953).
22. CATSIFF, E., AND TOBOLSKY, A. V., *J. Colloid Sci.* **10**, 375 (1955).
23. BERGE, J. W., SAUNDERS, P. R., AND FERRY, J. D., *J. Colloid Sci.* **14**, 135 (1959). CHILD, W. C., AND FERRY, J. D., *J. Colloid Sci.* **12**, 389 (1957).
24. HUTTON, A. Q., AND NOLLE, A. W., *J. Appl. Phys.* **25**, 350 (1954).
25. TOBOLSKY, A. V., AND McLOUGHLIN, J. R., *J. Phys. Chem.* **59**, 989 (1955). CATSIFF, E., TOBOLSKY, A. V., AND OFFENBACH, J., *J. Colloid Sci.* **11**, 48 (1956).
26. TAKEMURA, T., *J. Polymer Sci.* **38**, 471 (1959). NAGAMATSU, K., TAKEMURA, T., TOSHITOMI, T., AND TAKETOMI, T., *J. Polymer Sci.* **33**, 515 (1958).
27. BUECHE, F., *J. Appl. Phys.* **26**, 738 (1955).
28. HIDESHIMA, M., NAKANE, H., AND IWAYANAGI, S., *Repts. Sci. Research Inst. Japan* **32**, 111, 140 (1956).
29. GORDON, M., AND TAYLOR, J. S., *J. Appl. Chem.* **2**, 495 (1952).
30. RYUM, S. K., *J. Soc. Polymer Sci. Japan* **15**, 18 (1958).
31. WILLIAMS, M. L., *J. Phys. Chem.* **59**, 95 (1955).
32. SCHWARZL, F., AND STAVERMAN, A. J., *Physica* **18**, 791 (1952); *Appl. Sci. Research A4*, 127 (1953).

33. FERRY, J. D., AND NINOMIYA K., in J. T. Bergen, ed., "Comparison of Viscoelastic Behavior in Seven Typical Polymer Systems, Viscoelasticity: Phenomenological Aspects." Academic Press, New York, 1960.
34. BROWN, G. M., AND TOBOLSKY, A. V., *J. Polymer Sci.* **6**, 165 (1951).
35. WILLIAMS, M. L., AND FERRY, J. D., *J. Colloid Sci.* **10**, 474 (1955).
36. MARK, H., AND TOBOLSKY, A. V., "Physical Chemistry of High Polymer System," p. 344. Interscience, New York, 1950. ANDREWS, R. D., HOFMAN-BANG, N., AND TOBOLSKY, A. V., *J. Polymer Sci.*, **3**, 669 (1948). TOBOLSKY, A. V., AND McLOUGHLIN, J. R., *J. Polymer Sci.* **8**, 543 (1952).
37. CATSIFF, E., AND TOBOLSKY, A. V., *J. Appl. Phys.* **25**, 1092 (1954).
38. FERRY, J. D., "Die Physik der Hochpolymeren," Vol. 4, p. 407. Springer, Berlin, 1956.
39. ZIMM, B. H., ROE, G. M., AND EPSTEIN, L. F., *J. Chem. Phys.* **24**, 279 (1956).
40. Private communication from Dr. Michio Kurata, Department of Chemistry Massachusetts Institute of Technology, Cambridge, Mass.

MECHANICAL PROPERTIES OF PLASTIC-DISPERSE SYSTEMS AT VERY SMALL DEFORMATIONS

M. Van den Tempel

Unilever Research Laboratory, Vlaardingen, Netherlands

Received August 2, 1960; revised November 15, 1960

ABSTRACT

A system containing flocculated solid particles in a liquid shows viscoelastic behavior at very small deformations. A model is described by means of which the elastic modulus of the system can be correlated with the forces acting between the particles. It is assumed that these forces are due to van der Waals-London attraction, and their contribution to the modulus is calculated. A method is indicated which allows the contribution of the van der Waals-London forces to the modulus of the material to be measured under specified conditions. Experiments on materials containing fat crystals in oil show agreement between predicted and experimental values for this contribution, if it is assumed that the solid particles in the aggregate approach each other to a distance of about 10 Å.

The energy content of the van der Waals-London bonds in these materials has been estimated from measurements of their rate of breaking in creep experiments, i.e., under the influence of a constant, low shearing stress. The energy content of about 40 kT -units is in satisfactory agreement with the results of stiffness measurements.

List of Symbols

- A = Hamaker's constant determining van der Waals-London attraction (erg).
 B_2 = Abbreviation defined in Eq. [16].
 D = Average particle diameter (cm.).
 ΔF_i = Free energy of activation for breaking a bond of type i .
 f_i = Average force exerted on bond of type i .
 G = Shear modulus (dynes/cm.²).
 g_i = Stiffness of interparticle bond (dynes/cm.).
 H = Average interparticle distance (cm.).
 h = Planck's constant.
 k = Boltzmann's constant.
 M_i = Contribution of bonds of type i to shear modulus (dynes/cm.²).
 N_i = Number of bonds of type i in cross section normal to the direction of the stress (cm.⁻²).
 n_i = Number of bonds of type i per cm. in direction of stress.

- p = Number of solid particles per cm.³ of material.
 S = Stress (dynes/cm.²).
 T = Absolute temperature.
 t = Time.
 γ = Shear.
 ϵ = Elongation.
 λ_i = Maximum elongation of a single bond of type i .
 τ = Relaxation time.
 ϕ = Volume fraction occupied by solid.

Subscript 0 refers to $t = 0$.

1 refers to primary (irreversible) bonds.

2 refers to secondary (reversible) bonds.

A material containing flocculated solid particles of colloidal dimensions, imbedded in a liquid, may possess rigidity or plasticity. At very small deformations, such plastic disperse systems show viscoelastic properties resembling those of certain polymers, but in which elasticity is not of an entropic nature. It is generally accepted that the elastic properties of these systems are due to the presence of a three-dimensional network of solid particles, formed by flocculation or aggregation of the dispersed particles under conditions where attraction prevails. In nonpolar liquids the most generally occurring type of interaction between dispersed particles is the van der Waals-London attraction. It is a purpose of this paper to investigate in how far van der Waals-London forces between the dispersed particles may contribute to the rigidity. The contribution of this interaction to the strength of a typical plastic disperse system was discussed by Bradley (1), who did, however, not take into account that the dispersed particles are in a flocculated state.

NETWORK STRUCTURE

If only attractive forces between the particles are operative so long as they are not in actual physical contact, a flocculate will be formed in which the particles are arranged in such a way that their average mutual distance is as small as possible. On the other hand, the flocculate continues to take up the entire available space in the types of material considered here. An arrangement of particles which meets these two requirements is obtained by considering the flocculate as an assembly of chains, each chain consisting of a linear array of particles placed very close together. The chains are branched and interlinked to form the strong three-dimensional network, the voids of which are filled with liquid.

In a sample containing p particles per cm.³ an average particle diameter D is defined by:

$$\pi D^3 p = 6\phi, \quad [1]$$

where ϕ is the volume-fraction occupied by the solid. If the mutual distance between neighboring particles in a chain is negligible with respect to D , the total length of all the chains present in a cube of 1 cm.³ is $pD = 6\phi/\pi D^2$. In the simple model considered here, this total chain length is made up of straight chains oriented in three mutually perpendicular directions in the cube. In that case, one-third of the total chain length represents the number of chains that can support stresses in a given direction. A cross section cuts, therefore, through $2\phi/\pi D^2$ chains per square centimeter of its area, and these are the chains which transmit forces from one part of the sample to the other.

FORCES BETWEEN PARTICLES

The mechanical properties of this system should be investigated under such conditions, that no appreciable breakdown occurs before and during a measurement, i.e., at very low stress and strain values. Under these conditions the elastic properties are predominant, and this means that a large proportion of the interparticle bonds remains unbroken during the experiment (2). Part of the deformation is due to stretching of unbroken bonds, and another part to breaking of bonds followed by their re-formation after suitable reorientation of the particles involved. Bonds which remain intact during a measurement are called "primary" bonds. The interparticle bonds which may break and re-form during an experiment are called "secondary" bonds, and it will be assumed that these are due to van der Waals-London attraction between neighboring particles.

No specific assumptions need be introduced at this stage regarding the nature of the unbroken (primary) bonds. In many cases they may consist of relatively strong van der Waals-London bonds between favorably oriented particles. The presence of a different kind of interparticle bond has, however, been recognized in several types of plastic disperse systems (3). Both in plastic fats and in dispersions of metal soaps in oil, part of the hardness is irreversibly lost by working, and this part of the hardness is attributed to the presence of irreversible bonds which have been formed during precipitation of the solid from its solution. Still other types of primary bonds may be formed during deformation of the sample, by mechanical entanglement of parts of the network moving relative to one another. The latter type of bond is operative only if the deformation is continued in the original direction, and consequently gives rise to anisotropic shear hardening.

The essential feature of all these primary bonds is that their restoration after breaking requires much more time than is available in an experiment, and that their stiffness and energy content are larger than those of (reversible) secondary bonds between similar particles.

The contribution of the secondary bonds to the modulus of the material

can be measured if this contribution is sufficiently large and if irreversible breakdown of interparticle bonds is prevented. Essentially, the method consists of measurements of the strain both before and after complete relaxation of the secondary bonds, under the influence of a constant stress. If it can be shown that during relaxation of the secondary bonds no irreversible breakdown of bonds has occurred, the difference between the modulus values before and after relaxation represents the contribution of the secondary bonds.

The modulus due to van der Waals-London attraction between the particles in the model network described above will now be calculated. Since the attractive forces between colloidal particles are acting only over distances comparable with the dimensions of the particles, only nearest-neighbor interactions will be taken into account.

VAN DER WAALS-LONDON ATTRACTION

The magnitude of the van der Waals-London attraction between closely spaced particles is well known if the particles have a simple shape and orientation (4). The interaction energy between two spheres of diameter D at a distance $H \ll D$ between the surfaces is $(AD/12H)$, where A is a constant depending on the polarizabilities of the atoms present. The value of this constant for the system considered here is estimated in the Appendix. Similarly, the interaction energy between two parallel thick plates at a mutual distance H is $A/12\pi H^2$ per square centimeter of surface area. For cubes of edge-length D , whose edges are parallel, the energy is $AD^2/12\pi H^2$ if the line connecting the centers is perpendicular to the opposing faces and the separation is small compared with D .

For cubes which are oriented otherwise, and for anisometric particles, no general expression for the magnitude of the attraction can be given, but a detailed investigation of several typical cases (5) has shown that the magnitude of the interaction is generally intermediate between that for spheres and for cubes. This result suggests that an average value of the interaction energy between particles of various shapes and orientations may be obtained by considering the attraction as intermediate between that for spheres and for well-oriented cubes, i.e.,

$$\Delta F = \frac{AD^{1.5}}{12H^{1.5}} \quad [2]$$

The attractive force between consecutive particles in a chain is then:

$$\text{Force} = -\frac{AD^{1.5}}{8H^{2.5}} \quad [3]$$

and the magnitude of the stress transmitted through 1 cm.² of a cross

section is obtained by multiplying the force [3] in each chain by the number of chains:

$$S = \frac{A\phi}{4\pi D^{0.5}H^{2.5}}. \quad [4]$$

The modulus of the network model is obtained by considering the effect of a deformation on the interparticle distance H . In an unstrained condition, the average distance between the surfaces of neighboring particles in a chain is H_0 , and as a result of uniform stretching this distance increases to H . Since the particles themselves are undeformable, the relative extension of the sample is:

$$\epsilon = (H - H_0)/D. \quad [5]$$

Measurements on materials of this type should be carried out in simple shear in order to avoid the occurrence of liquid movement with respect to the solid framework. The shear γ which corresponds to the extension ϵ is:

$$\gamma = 2(H - H_0)/D. \quad [6]$$

The shear modulus of the unstrained network is:

$$G_0 = \frac{1}{3} \left(\frac{dS}{d\epsilon} \right)_{H_0} = \frac{2}{3} \left(\frac{dS}{d\gamma} \right)_{H_0} = \frac{2}{3} \left(\frac{dS}{dH} \right)_{H_0} \cdot \frac{dH}{d\gamma} = \frac{D}{3} \left(\frac{dS}{dH} \right)_{H_0}, \quad [7]$$

where S has been used as a tensile stress throughout. Combination of Eqs. [4] and [7] results in:

$$G_0 = \frac{5A\phi D^{0.5}}{24\pi H_0^{3.5}}. \quad [8]$$

Inspection of Eq. [4] clearly shows the nonlinearity of the mechanical behavior, and also a continuous drop in stress on increasing strain. This is to be expected in a model where the increasing distance between the particles results in a diminishing attractive force, and it explains the low tensile strength of samples in which coherence is due only to van der Waals-London forces between solid particles imbedded in a liquid. Coherence in shear is due to rapid re-formation of broken bonds after suitable rearrangement of the particles involved. This is essentially the phenomenon we wish to investigate.

The initial shear modulus should be proportional to the volume-fraction of solid and should not be very sensitive to variations in particle size. This may seem somewhat unexpected, as it is generally held that the "strength" and stiffness of these materials are very sensitive to variations in particle size and concentration. These conclusions have, however, been obtained from experiments at much larger deformations. The behavior at sufficiently small deformations depends mainly on the average interparticle distance, for which no separate measuring method is available.

The modulus of plastic disperse systems is frequently in the same range as that of rubberlike materials, i.e., of the order of 10^6 or 10^7 dynes/cm.². Insertion of these values in Eq. [8] shows that the average interparticle distance H_0 should have a value between about 10 and 20 Å. in systems containing particles of colloidal dimensions in amounts of 10% to 30%.

BREAKING OF BONDS

The behavior of materials containing both primary and secondary bonds has already been discussed from the point of view of reaction rate theory (6). It is assumed that the number of bonds cut by a cross section is made up of N_1 primary bonds and N_2 secondary bonds per square centimeter. The total stress S , normal to the cross section considered, is distributed over the chains in such a way that:

$$S = S_1 + S_2 = f_1 N_1 + f_2 N_2, \quad [9]$$

where f_1 represents the mean force exerted on a primary bond and f_2 that on a secondary bond. The mean free energy of activation for breaking primary and secondary bonds is ΔF_1 and ΔF_2 , respectively, and the distance over which the particles must be moved apart to break the bonds is λ_1 and λ_2 . The rate of breaking of the bonds is then given by absolute reaction rate theory as:

$$-\frac{1}{N_i} \frac{dN_i}{dt} = 2 \frac{kT}{h} \exp \left(-\frac{\Delta F_i}{kT} \right) \sinh \left(\frac{f_i \lambda_i}{kT} \right). \quad (i = 1, 2) \quad [10]$$

In this equation, k and h represent the constants of Boltzmann and Planck, respectively, and the term kT/h is an elementary frequency of about 10^{13} sec.⁻¹.

The rate of strain is governed by the sum of two contributions, the first of which is determined by the rate at which the unbroken bonds are stretched, and the second by the rate at which bonds are broken. The first contribution is found by considering that an infinitesimal increase of the stress on an unbroken bond causes it to stretch further by an amount proportional to the increase of the stress. Together with Eq. [10] this gives:

$$\dot{\gamma}_i = \frac{n_i}{g_i} \frac{df_i}{dt} + 2n_i \lambda_i \frac{kT}{h} \exp \left(-\frac{\Delta F_i}{kT} \right) \sinh \left(\frac{f_i \lambda_i}{kT} \right), \quad (i = 1, 2) \quad [11]$$

where it has been assumed that the strain increases by an amount λ_i whenever a bond of type i is broken. The number of bonds of type i per centimeter chain length in the direction of the stress has been called n_i , and g_i measures the stiffness of the bonds of type i . The stiffness of the secondary bonds (g_2) depends on the particle separation as expressed in Eq. [3], but an average value may be used for the large number of secondary

bonds present in unit area of a cross section, and this average value remains practically constant during a deformation.

Experiments are carried out under such conditions that no primary bonds are broken, which is expressed by the vanishing of the second term in Eq. [11] for $i = 1$. So long as coherence in the sample is maintained, the stress is distributed over primary and secondary bonds in such a way that the rate of strain is the same for each:

$$\dot{\gamma} = \dot{\gamma}_1 = \dot{\gamma}_2. \quad [12]$$

Under these conditions, Eq. [11] is written as:

$$\frac{n_1}{g_1} \frac{df_1}{dt} = \frac{n_2}{g_2} \frac{df_2}{dt} + 2n_2\lambda_2 \frac{kT}{h} \exp\left(-\frac{\Delta F_2}{kT}\right) \sinh\left(\frac{f_2\lambda_2}{kT}\right). \quad [13]$$

In a creep experiment, at constant stress, Eq. [9] shows that:

$$\frac{df_1}{dt} = -\frac{N_2}{N_1} \frac{df_2}{dt}. \quad [14]$$

Elimination of f_1 from [13] and [14] and integration results in:

$$\tanh\left(\frac{f_2\lambda_2}{2kT}\right) = \tanh\left(\frac{f_2^0\lambda_2}{2kT}\right) \exp\left(-\frac{gB_2\lambda_2 t}{kT}\right), \quad [15]$$

where the following abbreviations have been introduced:

$$B_2 = 2n_2\lambda_2 \frac{kT}{h} \exp\left(-\frac{\Delta F_2}{kT}\right); \quad [16]$$

$$\frac{1}{g} = \left(\frac{n_1}{g_1 N_1} + \frac{n_2}{g_2 N_2}\right) N_2. \quad [17]$$

The mean force on a secondary bond immediately after the application of the load is f_2^0 , and Eq. [15] shows how this mean force decreases with time. In general, $f_2^0\lambda_2 \gg 2kT$, and therefore $\tanh(f_2^0\lambda_2/2kT) \cong 1$. So long as $f_2\lambda_2 > kT$, Eq. [15] is adequately approximated by:

$$\frac{\lambda_2 f_2}{kT} = -\ln\left(\frac{gB_2\lambda_2 t}{2kT}\right) = -\ln(t/\tau) \quad [18]$$

The "relaxation" time $\tau = 2kT/gB_2\lambda_2$ indicates the time required to make the secondary bonds completely stress-free, if this relaxation should proceed indefinitely according to Eq. [18]. It is noteworthy that stress-relaxation does not proceed in accordance with a Maxwell-mechanism but according to Trouton-Rankine.

The stress supported by the primary bonds can now be found at any time by subtracting the stress on the secondary bonds from the constant total stress. The relation between deformation and time is then obtained as:

$$\begin{aligned}\gamma = \gamma_1 &= \frac{n_1}{g_1} f_1 = \frac{n_1}{g_1} \left(\frac{S}{N_1} - f_2 \frac{N_2}{N_1} \right) \\ &= \left(\frac{S}{M_1} - \frac{N_2 k T}{M_1 \lambda_2} \ln \tau \right) + \frac{N_2 k T}{M_1 \lambda_2} \ln t;\end{aligned}\quad [19]$$

where $M_1 = N_1 g_1 / n_1$. According to this equation the creep curve should be straight in a semi-logarithmic plot so long as the sample remains coherent and no primary bonds are broken. The first part of Eq. [19] represents the rapid elastic deformation, and the factor before $\ln t$ is the slope of the creep curve in a semi-logarithmic plot. It is of interest to note that this slope should be independent of the stress. Measurements on identical samples with different values of the shearing stress should result in parallel creep curves in the semi-logarithmic plot, whereas breakdown of primary bonds in one of the measurements results in a reduction of M_1 and a strongly increased slope. This provides a method for selecting measurements in which no breakdown of primary bonds has occurred.

If two measurements carried out on the same or identical samples with stress values S and S' have resulted in semi-logarithmic creep curves of the same slope, the contribution of the primary bonds to the modulus may be obtained from the nonlinearity of the rapid elastic deformation. Application of Eq. [19] to the results of these measurements, and comparing the deformations after an arbitrarily selected time, gives:

$$M_1 = \frac{S - S'}{\gamma - \gamma'}.\quad [20]$$

Insertion of this value of M_1 in Eq. [19] representing the experimental results allows the determination of τ and of N_2/λ_2 .

The meaning of M_1 can be found by considering the deformation of the sample at $t = 0$, when the load has already been applied but no secondary bonds have yet been broken. Application of Eqs. [9] and [11] under these conditions shows that:

$$G = \frac{S}{\gamma_0} = \frac{g_1 N_1}{n_1} + \frac{g_2 N_2}{n_2} = M_1 + M_2.\quad [21]$$

After complete relaxation of the secondary bonds, i.e., at $t = \tau$, the modulus is identical with M_1 . It follows that M_i represents the contribution of each type of bond to the modulus of the sample, and in particular that M_2 may be identified with G_0 of Eq. [8]. Similarly, ΔF_2 may be identified with the bond energy as given in Eq. [2].

If M_1 is known from Eq. [20] a value for M_2 can be obtained if a reasonable estimate can be made of the modulus G as defined in Eq. [21]. Experimental determination of this modulus is not easily accomplished, but its value may be roughly estimated from the deformation occurring imme-

diately after the load has been applied, with a velocity so large that it cannot be measured by the recording apparatus used. In the present investigation, application of the load took about 2 seconds and the value of the modulus G was obtained from the deformation after about 5 to 6 seconds.

Further progress can now be made by assuming that the number of primary bonds is only a small fraction of the number of secondary bonds in the network. In view of the approximations which have already been introduced, this seems a reasonable assumption in the kinds of material investigated here. In this case:

$$N_2 = \frac{2\phi}{\pi D^2} \quad \text{and} \quad n_2 = 1/D. \quad [22]$$

A sufficient number of relations between the measured parameters M_1 , M_2 , N_2/λ_2 , and τ , and the unknown parameters D , H , and λ_2 is now available to calculate the latter. A convenient method consists of selecting an arbitrary value of λ_2 and calculating N_2 from the known value of N_2/λ_2 . A first approximation of D and n_2 is thereupon obtained by inserting this value of N_2 in Eq. [22]. Application of Eqs. [17] and [16] results in a value for ΔF_2 , which is used together with the known value of $M_2 = G_0$ in Eqs. [2] and [8] to obtain approximations of D and H . This improved value of D is again used in Eq. [22] to obtain improved values for N_2 and, therefore, λ_2 , and the whole calculation is repeated with this improved value of λ_2 . Generally, the second approximation results already in a self-consistent system of parameters.

EXPERIMENTAL PART

Materials

The samples investigated consisted of 25% (w/w) of glyceryl tristearate (m.p. 71°–72°C.) in either groundnut oil or a paraffin oil. At temperatures in excess of its melting point, the tristearate is completely miscible with the oil whereas its solubility can be neglected at room temperature. The volume-fraction of solid phase is found from the known densities of the components; the values are 0.221 in paraffin oil and 0.228 in groundnut oil.

Particle size can be varied over a wide range by varying the rate of crystallization. Samples containing submicroscopic crystals were obtained if the hot solution was crystallized within a few seconds by spreading it in a thin layer on a cooled metal surface. Much larger crystals of fairly uniform size and shape could be formed by slow cooling. The consistency of the products varied between that of a soft, plastic paste and a hard, brittle solid, depending on the temperature of nucleation and the amount of working after crystallization had been completed. However, only those samples in which a considerable fraction of the stiffness was due to secondary bonds could be used in the present investigation, which was, therefore, restricted to products containing particles in the smaller size range.

The samples had been stored for at least 24 hours at room temperature before the measurements were carried out at 22°C.

Creep Experiments

In the creep experiments, a hollow cylinder of the material was subjected to torsion by applying a couple to the upper surface while keeping the lower surface stationary (7). The inner radius of the cylinder was 2 cm., wall thickness 1 cm., height between 3 and 4 cm. The forces were transmitted to the sample by means of ruffled metal disks contacting the upper and lower surfaces of the cylinder. Each disk contained 15 sharp ridges of 3 mm. height in a radial arrangement. Effective height of the sample was measured between the edges of the ridges. Rotation of the upper surface was measured by means of an optical lever, the moving light beam of which actuated a recorder pen placed at a suitable distance. Shear in the sample did never exceed about 0.5%, whereas changes in shear of 0.005% could be measured.

RESULTS AND DISCUSSION

The creep curves obtained with one sample have been recorded in Fig. 1 as a typical sample. Removal of the load after 7 min. in the first measurement results in recovery which becomes practically complete after sufficiently long time. A second measurement was carried out on the same sample, using a higher stress value, after recovery had been allowed to proceed for 1 hour. Figure 2 shows the same results in a semi-logarithmic plot. It is observed that the first measurement results in a straight line, whereas the initial part of the second measurement is on a straight line parallel to the first one. The suddenly increasing slope of the second curve after about 3 min. is attributed to breaking of irreversible bonds (7).

The parallelism of the semi-logarithmic creep curves is held to mean that

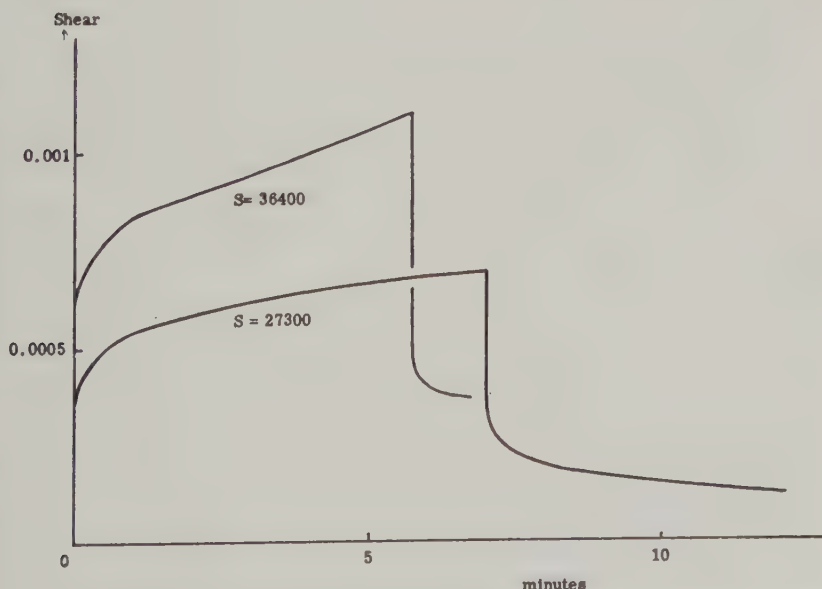


FIG. 1. Creep and recovery of sample no. V with two values of the shearing stress.

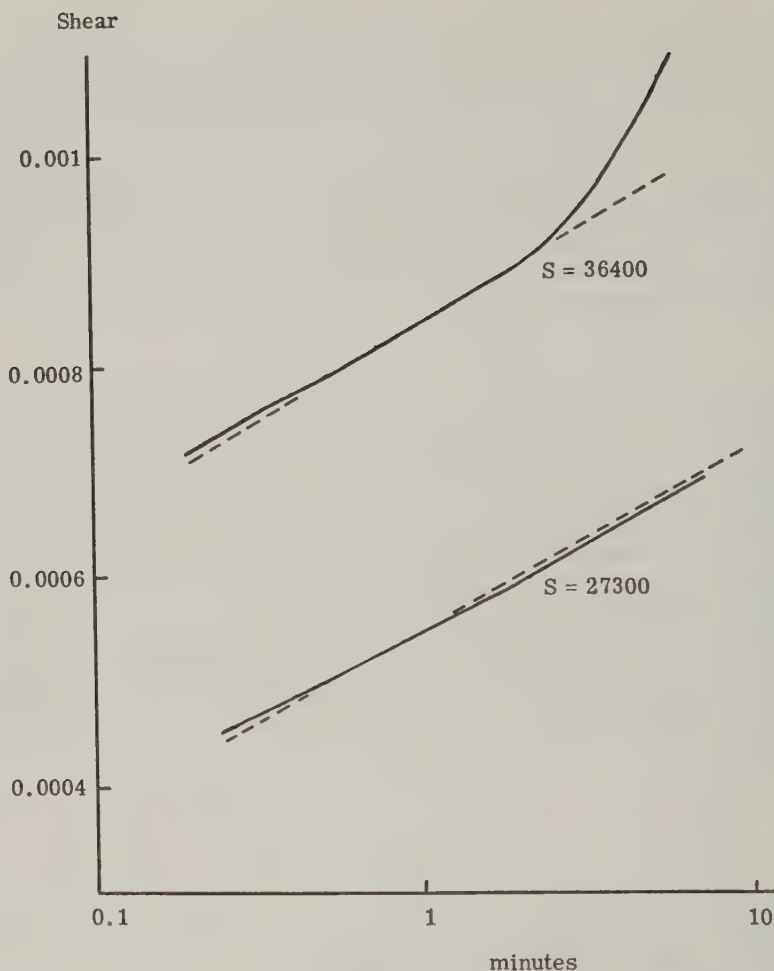


FIG. 2. Same as Fig. 1 on semi-logarithmic scale. Dotted lines represent average slope used in calculation.

no bonds have been broken irreversibly, and the results of these measurements may be used in the theory. A large number of samples has been investigated, but only a relatively small number gave results to which the theory can be applied. This is undoubtedly due to the restricted range of stress values that can be used in this kind of investigation: the stress must be sufficiently high to allow the strain to be measured accurately, but not so high that irreversible breaking of bonds occurs already in the first few minutes of a measurement. The results of measurements on five different samples have been collected in the table, together with the structural parameters calculated from these results.

TABLE I
Results of Creep Measurements

Sample no.	I	II	III	IV	V
Liquid phase	Paraffin oil		Groundnut oil		
Nucl. temp. (°C.)	35	12	30	20	12
$S \times 10^{-3}$	4.66	4.55	4.55	27.3	27.3
$\gamma \times 10^3$ (1 min.)	0.62	1.03	0.310	0.334	0.548
slope $\times 10^3$	0.41	0.62	0.125	0.066	0.175
$G \times 10^{-6}$	12.2	11.3	33.1	103	65
$S' \times 10^{-3}$	9.3	6.37	9.1	36.4	36.4
$\gamma' \times 10^3$ (1 min.)	1.18	1.50	0.489	0.490	0.842
slope $\times 10^3$	0.41	0.57	0.130	0.055	0.184
$M_1 \times 10^{-6}$	8.35	3.9	25.4	62	31
$M_2 \times 10^{-6}$	3.85	7.4	7.7	41	34
τ (sec.)	42	101	5.5	2400	4660
F_2/kT	38.2	40.4	37.9	46.2	45.6
$H_0 \times 10^8$	13.0	10.5	10.4	6.1	6.5
$D \times 10^6$	4.2	3.6	3.4	2.2	2.4

The contribution of the van der Waals-London forces to the modulus has been determined as the difference between the two measured quantities G and M_1 , both of which, however, are not easily accessible to accurate measurement. The values of M_2 occurring in the table should, therefore, be regarded as rough estimates only, and no great precision is claimed for the values of the structural parameters derived therefrom.

The important parameters in this table are the (effective) average particle diameter, D , and the average bond energy ΔF_2 . No independent and reliable method for measuring particle size in this type of systems is at present available. Comparison of the values obtained in the different samples shows that there is a definite tendency to produce smaller particles at lower crystallization temperatures. Moreover, the particles obtained in groundnut oil are always smaller than those obtained in paraffin oil, under the same conditions. Verification of the latter result must await the development of other methods for measuring particle size in these systems.

More interesting conclusions may be drawn from the values of H_0 found in these samples. On the one hand, it has been shown that the shear modulus of plastic disperse systems may be explained solely from van der Waals-London attraction between solid particles if the interparticle distance is about 10 Å., for a large range of particle sizes and concentrations. On the other hand, the rate of breaking of the interparticle bonds under the influence of a stress has been found to correspond with a bond energy of roughly 40 kT -units, and this again requires an interparticle distance of

about 10 Å. if these bonds are due to van der Waals-London attraction between solid particles. It is concluded that a considerable part of the stiffness of these plastic-disperse systems can be explained as the result of van der Waals-London attraction between the dispersed particles.

APPENDIX

The absolute magnitude of the van der Waals-London attraction between closely spaced particles is proportional to (4):

$$A = \pi^2(q_s^2\xi_s + q_L^2\xi_L - 2q_sq_L\xi_{sL}),$$

where q is the number of atoms per cubic centimeter, ξ is a parameter depending mainly on the polarizabilities of the atoms concerned, the subscript S refers to the solid and L to the liquid. If each of the phases contains several different atoms, the summation must be carried out over each of the atomic species in one of the phases with each atomic species in the other phase. As, however, the value of ξ is not accurately known, it is generally sufficient to use a kind of average value for the atoms present in each of the phases. In the present investigation, the solid and liquid phase had a very similar composition, and it will be assumed that the value of ξ in both phases is the same. In this case the van der Waals-London interaction is due solely to the density difference between solid and liquid phases, which is about 10% and corresponds with a value of $(q_s - q_L)$ of about 10^{22} atoms per cubic centimeter.

An estimate of ξ may be made by using the formula proposed by Slater and Kirkwood (8), which results in values of the order of 10^{-58} erg cm.⁶ for the atoms used in this investigation. It follows that the constant A to be used in Eqs. [2] and [8] has a value of about 10^{-13} erg.

The use of the more complicated expression, containing the interaction of each of the atomic species separately, would result in a value for A of 2.5×10^{-13} erg. The increased accuracy is only apparent, as a number of estimates must be made in evaluating the several ξ 's occurring in the complete summation. A value of $A = 10^{-13}$ erg has been used in all the calculations.

REFERENCES

1. BRADLEY, R. S., *J. Colloid Sci.* **11**, 237 (1956).
2. EFREMOV, I. F., AND NERPIN, S. V., *Colloid J. (U.S.S.R.)* **19**, 759 (1957).
3. MIKHAILOV, N. V., AND REBINDER, P. A., *Colloid J. (U.S.S.R.)* **17**, 99 (1955).
4. HAMAKER, H. C., *Physica* **4**, 1058 (1937).
5. VOLD, M. J., *J. Colloid Sci.* **9**, 451 (1954).
6. TOBOLSKY, A., AND EYRING, H., *J. Chem. Phys.* **11**, 125 (1943).
7. VAN DEN TEMPEL, M., *Rheologica Acta* **1**, 115 (1958).
8. SLATER, J. C., AND KIRKWOOD, J. G., *Phys. Rev.* **37**, 682 (1931).

MACROSCOPIC PROPERTIES AND MICROSCOPIC STRUCTURE IN PAPER

Morton Litt¹

*Chemistry Department, State College of Forestry at Syracuse University,
Syracuse, New York*

Received September 6, 1960; revised November 3, 1960

ABSTRACT

A theory of paper elasticity was developed considering that paper fibers were flat ribbons joined to many other fibers by hydrogen bonds. When paper was stressed, the force was equalized for each interfiber bond without regard for the orientation of the fiber, and the fiber segments between bonds were distorted in the direction of the force. An analysis of literature experimental results shows that this theory can explain Young's modulus for paper. The theory was tentatively extended to discuss Poisson's ratio and, qualitatively, plastic flow behavior.

INTRODUCTION

Paper has been the object of many attempts to predict its physical properties either from its microscopic structure or in terms of some idealized model. The earlier work is reviewed by Rance (1). A recent attempt based on an idealized model has been made by Nissan (2). The recent work and thought has been well summarized by Van Den Akker (3). The following paper is an attempt to derive some properties of paper from the properties of its microscopic constituents, pulp fibers, and a consideration of the ways in which they interact. A similar synthesis using most of the assumptions presented in this paper was recently published (4).

GENERAL DISCUSSION

The arrangement and bonding of fibers are postulated to be as described by Van Den Akker (3). One can consider paper handsheets as an assemblage of fibers the axes of which are randomly oriented in the plane of the surfaces and which are bonded together (with hydrogen bonds) over a greater or lesser area wherever they are in contact. Thus any one fiber will be bonded to a great many others. It is also assumed that the fibers in the final dried sheet will be collapsed ribbons and that the wide portion of the collapsed fiber will be parallel to the plane of the sheet, as this is its most

¹ Present address: Central Research Laboratory, Allied Chemical Corporation, Morristown, New Jersey.

stable position. Wet pressing of the sheet will probably collapse the fibers in such an orientation also. Photomicrographs of cross sections of paper tend to confirm these suppositions (5).

The picture of paper presented therefore is a network of ribbonlike fibers the axes of which are randomly oriented in, and whose wide surfaces are parallel to, the plane of the paper surface; the fibers are well bonded at many points. The next question that arises is: when such a network is stressed, where is the energy stored? Is it mainly the interfiber bonds or is it the fibers themselves? A small calculation will show that if the complete surface of the fibers were bonded, the energy which could be stored by the hydrogen bonds would be of the order of 100 ergs/cm^2 . The actual energies involved are a factor of 10^5 higher. This means that essentially all the energy is stored by stressing the fiber. The deformation of the network before the point of plastic flow is then due to a distortion of the fiber segments between interfiber bonds, while the bonds remain unchanged. Van Den Akker (3) has shown that the interfiber bonds cannot stretch nor the interfiber angles change without breaking the bond. Any distortion at the bond small enough to keep the hydrogen bonds intact is too small to affect the orientation of the fibers and thus need not be considered.

THEORETICAL MODEL FOR PAPER

One can consider paper, therefore, as being, ideally, a two-dimensional network of flat fiber segments linked together by hydrogen bonding. If the orientation of the fiber axes are within 10° to 20° to the paper plane, the third dimension need not be considered for a discussion of paper strength in the x and y directions. The segment can be replaced, for the treatment, by a rectangular rod crossed and linked at a fixed, but arbitrary, angle to two other rods, one at each end. If there are many interfiber bonds per fiber, the unbonded ends of the fiber constitute only a small part of its length, and may be neglected for the treatment of preplastic flow properties. It is also assumed that the force extending the segment is identical for each segment, regardless of its orientation. This should be true as an average, though some segments will be stressed more than others. (It seems that in a highly cross-linked network the average elongation per segment should be constant, rather than the average force; this is indeed the hypothesis made by Onogi and Sasaguri (4) and is the only point where they differed from the present work. There are arguments against this, however, and one of the best is that there is no agreement with experimental results using this assumption.) It is also assumed that there is no built-in stress in the network, as happens when paper is dried under tension. This would cause some segments to be under tension while others are compressed, and on the whole will change Young's modulus and the shape of the stress-strain curve.

Although the fibers are closely linked together, the bonding is so irregular

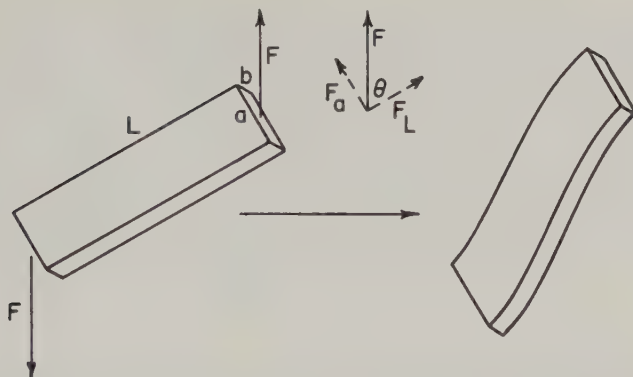


FIG. 1. Distortion of fiber segment upon straining exaggerated for demonstration purposes.

that if one follows any one series of fibers and interfiber bonds to form a closed loop, it may contain many segments, and the whole loop can form an irregular polygon. Under such conditions if a force is applied to the polygon, the fiber segments should distribute the force equally, as they can respond almost independently. If the polygons are so small that triangles or quadrilaterals are formed, then the distortions for the polygons as a whole should be calculated. This has been neglected in the present treatment.

For small distortions of a segment, we can resolve the force into two components, one parallel and the other perpendicular to the fiber axis and assume each acts independently. The parallel force will extend the fiber, while the force perpendicular to the axis will cause a shear distortion. This last is complicated by the requirement that the segment ends are bound to other fibers and must maintain their relative orientations to the force. The total distortion of the fiber will be the resultant of these motions, as illustrated in Fig. 1, and when integrated around all orientations of the fiber to the force, will give the average extension of a segment for a given force. The work per segment can then be found by integrating the force times the elongation in the direction of the force.

MATHEMATICAL TREATMENT OF YOUNG'S MODULUS

Consider a fiber segment of width, a , thickness, b , and length, L , being stressed by a force at an arbitrary angle θ , to the fiber axis. The force can be resolved into two vectors, one in the direction of the fiber axis \mathbf{F}_L , and one perpendicular to the axis, \mathbf{F}_a . For small extensions, where Hooke's law is followed, it can be assumed that the fiber will respond to each force independently and the elongation will be the vector sum of \mathbf{s}_a , the distortion perpendicular to the axis, and \mathbf{S}_L , the distortion parallel to the axis.

$$\text{Shear Distortion } \mathbf{s}_a = \frac{\mathbf{F}_a L^3}{a^3 b E};$$

$$\text{Axial Extension } \mathbf{s}_L = \frac{\mathbf{F}_L L}{ab E}.$$

Here E is Young's modulus for the fiber. It is the same for both types of elongation because the shear distortion can be considered as a stretching of half the fiber with compression of the other half. The elongation, \mathbf{s} , is thus:

$$\mathbf{s} = \mathbf{s}_a + \mathbf{s}_L = \frac{L}{Eab} \left(\frac{\mathbf{F}_a L^2}{a^2} + \mathbf{F}_L \right); \quad [1]$$

and the work done would be then

$$W = \int_0^s \mathbf{F} \cdot d\mathbf{s} = \frac{L}{2 Eab} \left(\frac{F_a^2 L^2}{a^2} + F_L^2 \right), \quad [2]$$

or in terms of the angle between the fiber axis and the force,

$$W = \frac{L}{2 Eab} F^2 \left(\frac{L^2}{a^2} \sin^2 \theta + \cos^2 \theta \right). \quad [3]$$

Since the force per fiber segment has been postulated to be constant, Eq. [3] can be integrated over all fiber orientations to obtain the average work per fiber segment.

$$\begin{aligned} W_{\text{avg.}} &= \frac{L}{2 Eab} F^2 \frac{2}{\pi} \int_0^{\pi/2} \left(\frac{L^2}{a^2} \sin^2 \theta + \cos^2 \theta \right) d\theta \\ &= \frac{L}{4 Eab} F^2 \left(\frac{L^2}{a^2} + 1 \right). \end{aligned} \quad [4]$$

The average distortion of the fiber in the direction of the force, s_{\parallel} , is shown in Eq. [5].

$$s_{\parallel} = \frac{2}{\pi} \int_0^{\pi/2} \frac{\mathbf{F} \cdot \mathbf{s}}{F} d\theta = \frac{FL}{2 Eab} \left(\frac{L^2}{a^2} + 1 \right). \quad [5]$$

Combining Eqs. [4] and [5] to eliminate F , we arrive at an expression for the average work per segment in terms of the average distortion, Eq. [6].

$$W_{\text{avg.}} = (Eab/L) s_{\parallel}^2 [(L^2/a^2) + 1]^{-1}. \quad [6]$$

In a paper of apparent density, d , and where the fibers have a density, δ , the number of segments per unit volume, n , is:

$$n = d/abL\delta, \quad [7]$$

and the average work per unit volume of paper is then

$$n W_{\text{avg.}} = (Ed/\delta) (s_{\parallel}^2/L^2) [(L^2/a^2) + 1]^{-1}. \quad [8]$$

Equation [8] expresses the work expended in reversibly stretching a unit volume of paper in terms of fiber properties. These must be replaced by macroscopic properties before the equation is useful. The relative elongation of the paper, ϵ , in microscopic quantities is the average distortion of the fiber in the direction of the force, s_{\parallel} , divided by the average projection of the fiber length in the direction of the force, L' .

$$L' = \frac{2}{\pi} \int_0^{\pi/2} L \cos \theta d\theta = \frac{2}{\pi} L,$$

$$s_{\parallel}/L = \frac{2\epsilon}{\pi}$$

The density of the fiber, δ , can be taken to be that of cellulose, or approximately 1.56 g./c.c. Young's modulus for single, delignified, fibers of Douglas-fir, cypress, and white spruce at 72°F. and 50% R.H. was recently investigated (6). In all cases, the earlywood fibers had lower Young's moduli than the latewood fibers by a factor of 1.5 to 2.5, but the average moduli for the different species were almost identical. The average combined modulus was $28 \pm 5 \times 10^{10}$ dynes/cm.². It was also shown that the fibers followed Hooke's law to greater than 1% extension.

Equation [8] can now be written as:

$$nW_{\text{avg.}} = \frac{Ed\epsilon^2}{1.56(\pi/2)^2[(L^2/a^2) + 1]}, \quad [9]$$

and Young's modulus for the paper, Y , is then

$$Y = \frac{d(nW_{\text{avg.}})}{\epsilon d\epsilon} = \frac{Ed}{1.93[(L^2/a^2) + 1]}. \quad [10]$$

COMPARISON OF THEORY WITH EXPERIMENT

The one term that cannot be replaced is L^2/a^2 . This is a measure of the increase in interfiber contacts (decrease of L) and is a function of the paper density; at present there is no published work on the subject. Relationships can be found by rearranging Eq. [10] to obtain values for L^2/a^2 , on the assumption that it follows an equation of the type $L^2/a^2 = K/d^k$.

$$\log \left(\frac{Ed}{1.93 Y} - 1 \right) = \log K - k \log d. \quad [11]$$

This was done using the data relating Y and d of Clark (7) for values of E of 25 and 30×10^{10} dynes/cm.². The following equations were obtained:

$$E = 30 \times 10^{10} \text{ dynes/cm.}^2; \quad Y = 30 d / 1.93 (1.0/d^{1.5} + 1) \cdot 10^{10} \text{ dynes/cm.}^2 \quad [12a]$$

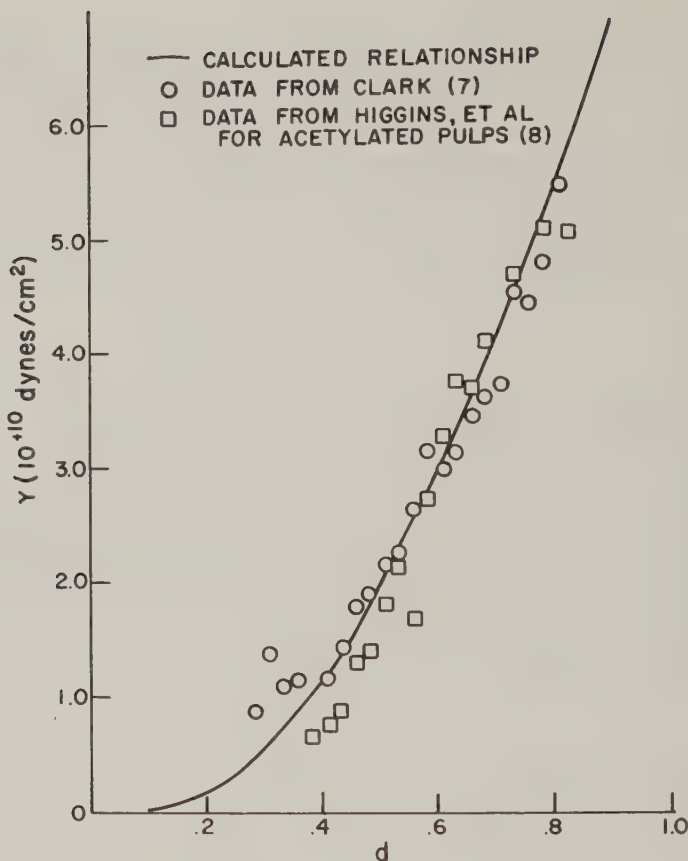


FIG. 2. Comparison of experimental results with Eq. [12a].

$$E = 25 \times 10^{10} \text{ dynes/cm.}^2; \quad Y = 25d/1.93 (.75/d^{1.67} + 1) \cdot 10^{10} \text{ dynes/cm.}^2 \quad [12b]$$

The correspondence between Clark's (7) and Higgins' (8) data and Eq. [12a] is shown in Fig. 2. Higgins' data for a series of partially acetylated pulps fell on the curve above $d = 0.5$, which includes the better beaten, less acetylated material. It can be seen that the semi-theoretical curve fits the experimental points quite well. Below $d = 0.4$, Young's modulus no longer falls on the curve for the cellulose handsheets. This is understandable in view of the model used. Low densities in paper are achieved by low wet pressures and very mild beating. This treatment does not damage the fiber structure much and many fibers would still be cylindrical rather than flattened. Such fibers have a much higher bending modulus and raise the paper modulus accordingly.

The argument will be considerably strengthened if it can be shown that the ratio L/a is meaningful in the density range where the equations are valid. Using the values in Eq. [12a] or [12b],

$$L/a = 1.0/d^{0.75} \quad [13a]$$

and

$$L/a = 0.87/d^{0.83}. \quad [13b]$$

In the range of densities from 0.4 to 0.8, the two ratios differ by less than 10 %. They go from about 2 at $d = 0.4$ to about 1.1 at $d = 0.8$. This is a reasonable figure. At $d = 0.4$, about one-quarter of the volume around a fiber is occupied by other fibers, and therefore about one-quarter of its surface area should be in contact with these fibers. Since bonds are formed on two sides, the ratio L/a should average about 2. As the density increases, bonds become harder to form because of interference from previously formed bonds. Also the thickness of the fiber, b , enters into the estimate of L/a , making L larger, since many times one measures the length between bond centers through the fiber as well as along it. These considerations make the value of L/a at $d = 0.8$ found from Eqs. [13a] and [13b] quite reasonable. A more exact relationship must await better data.

Another factor neglected in this treatment, because the data are not accurate enough to warrant it, is the matter of the density of an unbonded sheet. In such a handsheet, with an experimental density of about 0.1, $L/a = \infty$. This density, d_0 , may be subtracted from the apparent density in Eq. [11] and new constants can be calculated. However, this introduces a new curve-fitting parameter, d_0 , and I wanted as few as possible in the derivation. The experimental d_0 will be larger than a theoretical d_0 because the latter would refer to a sheet of paper composed of fibers of almost infinite length.

An experiment which would help determine the validity of the foregoing derivation would be to make handsheets out of earlywood fibers only, which are more flexible and seem to have less scatter for Young's modulus, E , and cross-sectional area (6) than do latewood fibers. If papers are made with apparent densities over the widest range possible, and density, Young's modulus, and Poisson's ratio in the x, y direction are very carefully measured (Poisson's ratio will be discussed later), it should be possible to prove or disprove the theory. Microscopic data on the length of fiber segments between bonds and fiber shapes would also be valuable as a direct confirmation of the hypothesized values shown in Eqs. [13a] and [13b]. Of course, E for the fibers must also be measured very carefully.

APPLICATION TO PAPER WITH MACHINE DIRECTION

The above theory is applicable to anisotropic paper if the change in distribution of fibers is taken into account. In machine-made paper, fibers

tend to be aligned in the machine direction, and will therefore require more work for a given elongation in the machine direction than in the cross direction where they can bend easily. The following adaption of Eqs. [3] and [5] can be used.

$$W_{\text{avg.}} = \frac{L}{2 Eab} F^2 \frac{1}{\pi} \int_{-\pi/2}^{+\pi/2} \left(\frac{L^2}{a^2} \sin^2 \theta + \cos^2 \theta \right) G(c, \theta, \phi) d\theta \quad [14]$$

and

$$s_{\parallel} = \frac{1}{\pi} \int_{-\pi/2}^{+\pi/2} \frac{\mathbf{F} \cdot \mathbf{s}}{F} G(c, \theta, \phi) d\theta. \quad [15]$$

The function, $G(c, \theta)$, is a description of the relative amount of fiber orientation, and ϕ is the angle of the stretching force to the machine direction; such a function could have a form of the type:

$$G(c, \theta, \phi) = c \cos^2(\theta + \phi) + (2 - c) \sin^2(\theta + \phi). \quad [16]$$

The value, c , represents the relative increase in the fraction of fibers with axes in the machine direction over the average in all directions. When $c = 1$, there is no orientation, and $G(1, \theta, \phi) \equiv 1$. The distribution function should be chosen to correspond to the experimentally observed distribution, but whatever type is used must become independent of angle when $c = 1$. When Eqs. [14] and [15] are integrated and F is eliminated between them, as before, we can obtain the average work done on a single segment. The development proceeds as outlined in the previous sections on two-dimensionally isotropic paper, except that L' , the average length of the segment in the direction of the force, which is needed to find the relative elongation $\epsilon = s_{\parallel}/L'$, must be derived by the integration shown in Eq. [17].

$$L' = \frac{1}{\pi} \int_{-\pi/2}^{+\pi/2} L \cos \theta G(c, \theta, \phi) d\theta. \quad [17]$$

Young's modulus for paper with machine direction, when the paper is stressed at an angle ϕ to that direction, is then

$$Y = \frac{d(nW_{\text{avg.}}(\phi))}{\epsilon(\phi) d\epsilon(\phi)}, \quad [18]$$

since when Eq. [14], [15], and [17] are integrated, they remain functions of ϕ .

BEHAVIOR IN THE PLASTIC FLOW REGION

Although paper behavior beyond the yield point cannot be described quantitatively at present by the theory, some portion of the behavior can be treated, and a qualitative description ventured. Many people (1, 3) have held that plastic flow is due to interfiber bond breaking, and this view is accepted here. It is also postulated that the interfiber bonds hold as well

as they do because the only force on them is shear force, and all the hydrogen bonds would have to be broken at once to break a bond (9).

Also, since there must be some variation of stress in the bonds, it is reasonable to suppose that the bonds under the greatest stress, where the fiber segments have the greatest strain, will be the ones to break first. When the bond breaks, the fiber segments held by the bond relax, and the stress must be taken up by the neighboring fiber segments and bonds. This causes the bond breaking to propagate along the paper and the process appears macroscopically as the formation of strain lines (10). The fibers along a strain line are stretched during the process and thus the paper lengthens. However, the force necessary to break more interfiber bonds will not change much and thus the stress-strain curve in the plastic flow region will have a low slope up to several per cent extension. The widening of the strain lines as the stress continues indicates that interfiber bonds are broken successively on the same fibers. Eventually, the end of the fiber will be reached and the fiber will be partly removed from the network. If this happens to enough fibers in any area, the rest cannot take the load and the paper tears. This can explain qualitatively the dependence of tensile and bursting strength on fiber length. It is probable that some of the fibers will break in stress but, of course, once the rupture starts propagating, many fibers will tear before their interfiber bonds can be broken.

As the bond-free portion of the fiber lengthens, it will twist appreciably to align itself with the force. Thus, more work is necessary to stretch a long segment to a given elongation than is calculated from the equations, and the approximations initially presented break down.

SEMI-QUANTITATIVE APPLICATION OF THEORY BEYOND THE YIELD POINT

Some work has been done recently relating to the energy lost when paper is stretched past the yield point to the increase in unbonded area as measured by light scattering (11). The change in scattering in a paper handsheet was correlated with the irreversible work done during a stretching cycle. The hypothesis was made that the increase in measured scattering area was equal to the area of interfiber hydrogen bonds broken during the stretching process; the work lost per unit area of bonds broken during the stretching process was then found to be 2.5×10^5 ergs/cm.² for spruce handsheets. Nordmann considers that the energy was stored in the interfiber hydrogen bonds and lost when the bonds were broken. However, to obtain reasonable energy values one must assume that the bonded area is at least 10^3 greater than the optically measured area. Since even the nitrogen adsorption area is nowhere near this figure, there is a discrepancy between his results and conclusions.

Nordmann's data can be considered on the model presented in this paper, and more reasonable conclusions are reached. Two extreme

hypotheses may be considered. Either the work stored per fiber segment reaches a certain constant value before the interfiber bond breaks, or the force per unit area of bond at the interfiber bond must reach a certain value. Each of these hypotheses predicts an amount of work lost of the magnitude which Nordmann finds, but they say different things about the change in the point of initiation of nonreversible elongation with density.

When an interfiber bond breaks, fresh nonbonded area on two fibers is formed which is approximately equal, optically, to $2a^2$, where a is the width of the fiber. The four fiber segments stressed by the bond are now two much more relaxed segments. If the neighboring bonds still hold, the stress will be distributed among them, and the released energy will be mainly transformed into heat. Therefore the work lost is the energy stored in four segments of length L minus the energy stored in two segments of length $2L$. Equation [6] may be adapted to find the work lost per unit area of surface formed by dividing the work lost, ΔW , by $2a^2$, the surface formed, to obtain Eq. [19].

$$\frac{\Delta W}{2a^2} = \frac{E\epsilon^2 b}{2} \left(\frac{2}{\pi}\right)^2 \frac{L}{a} \frac{4}{1 + (L^2/a^2)} - \frac{E\epsilon^2 b}{2} \left(\frac{2}{\pi}\right)^2 \frac{2L}{a} \frac{2}{1 + 4(L^2/a^2)}. \quad [19]$$

Substituting $L/a = 1.0/d^{3/4}$, one obtains

$$\Delta W/2a^2 = [2Eb(2/\pi)^2]/(d^{3/4})\{[1/(d^{3/2}) + 1]^{-1} - [4/(d^{3/2}) + 1]^{-1}\}\epsilon^2. \quad [20]$$

Equation [20] is almost independent of density in the region $0.4 < d < 0.8$, for any given ϵ , and can be simplified to

$$\Delta W/2a^2 \cong 0.24 Eb\epsilon^2. \quad [21]$$

Equation [21] holds for both hypotheses presented at the beginning of this section, and it is seen that work necessary to break interfiber bonds should be directly proportional to the fiber thickness, b . For birch and spruce woods, b is 17 and 25 μ , respectively ($5b$), and Nordmann found "rupture energies" of 1.9 and 2.6×10^5 ergs/cm.² for handsheets made from these woods. For these papers, the correspondence between fiber thickness and $\Delta W/2a^2$ is very close.

In the first case, where bond rupture depends on work stored in the segments, since $\Delta W/2a^2$ is directly proportional to ϵ^2 for any paper, plastic flow should start at about the same elongation for paper of all densities. All the terms in Eq. [21] can be estimated, so we can obtain tentative values for $\Delta W/2a^2$ and compare them with Nordmann's. Reasonable values for E and b are: $E = 30 \times 10^{10}$ dynes/cm.², and $b = 25 \times 10^{-4}$ cm. (5). Substituting into Eq. [21] we find

$$\Delta W/2a^2 \cong 18 \times 10^7 \epsilon^2 \text{ ergs/cm.}^2.$$

With a reasonable value for the elongation of about 0.02, considering that

the most strained bonds will break first and that plastic flow starts at an elongation of about 0.006, one finds

$$\Delta W/2a^2 \cong 7 \times 10^4 \text{ ergs/cm.}^2.$$

Nordmann's value of $2.5 \times 10^5 \text{ ergs/cm.}^2$ can be obtained if $\epsilon = 3.6\%$. This is somewhat higher than expected, but it is in reasonable agreement considering the type of measurements and the approximations involved, not only in the theory, but in considering that $2a^2$ represents the increase in optically measured area. If the optical increase is smaller than the loss in bonded area, because the fibers remain close to each other, the value found must be higher than that calculated.

The preceding treatment assumed that an interfiber bond would break after the fiber segments stored a given amount of energy. The alternate hypothesis is that the interfiber bond will break when the force at the bond per unit area of bond reached a certain value. This value may be found solving for ϵ in Eq. [5], considering $F/2a^2$ constant and substituting in Eq. [21]. One then obtains Eq. [22]:

$$\Delta W/2a^2 \cong 0.24(F/2a^2)^2[(L^2/a^2) + 1]^2 a^2/bE. \quad [22]$$

The value of $F/2a^2$ can be calculated from Eq. [5] if a given elongation and density are assumed. For $d = 0.7$ and $\epsilon = 0.02$, $F/2a^2 = 6.7 \times 10^8 \text{ dynes/cm.}^2$. The value of $\Delta W/2a^2$ will then range from $\sim 3 \times 10^5$ to $\sim 5 \times 10^4 \text{ ergs/cm.}^2$ as the paper density goes from 0.4 to 0.8. The average elongation at which plastic flow begins should then decrease by a factor of about 2 as the density increases from 0.4 to 0.8. (This assumes that $a/b \cong 3.5$ and $a \cong 70 \times 10^{-4} \text{ cm.}$ (5b), which are the values for the fibers used by Nordmann.) Since there was no mention of change in interfiber bond rupture energy for handsheets made from spruce and birch pulps with various degrees of beating, which presumably produces papers of different densities, the work lost upon rupture per segment cannot depend so markedly on the density, though the hypothesis just presented seems to be reasonable.

A possible explanation of this is found when the paper structure is examined. In a loose paper, the interfiber bonds are far apart and may follow the second hypothesis, but in the range of investigation, $0.4 < d < 0.8$, the bonds are so close and the fibers so interwoven that they buttress each other and thus can take higher forces at the bonds. The buttressing would then depend on the distance between interfiber bonds and be greater at higher densities. Also, the bond quality may improve with beating to produce stronger interfiber bonds.

POISSON'S RATIO

Since the third dimension has been neglected in this treatment, Poisson's ratio, the ratio of the relative change in width to the relative change in

length of the paper, $(\Delta y/y)/(\Delta x/x)$, can be calculated from the average deformation of the web parallel to the force and the average deformation of the web perpendicular to the force. This reduces to the ratio of average segment distortion parallel to the force, s_{\parallel} , and the average segment distortion perpendicular to the force, s_{\perp} .

$$s_{\perp} = \frac{2}{\pi} \int_0^{\pi/2} \left| \frac{\mathbf{F} \times \mathbf{s}}{F} \right| d\theta = \frac{FL}{\pi Eab} \left(\frac{L^2}{a^2} - 1 \right). \quad [23]$$

$$\text{Poisson's ratio} = s_{\perp}/s_{\parallel} = \frac{2}{\pi} \cdot \frac{(L^2/a^2) - 1}{(L^2/a^2) + 1}. \quad [24]$$

It is proportional to density only. An approximate graph of its value relative to density is shown in Fig. 3. At the point where $L^2/a^2 = 1$, Poisson's ratio is zero, and for denser papers it becomes negative. This is reasonable, because very short segments at an angle to the applied force would elongate rather than deform. The elongation has an outward component perpendicular to the force and the paper expands.

The third dimension of paper has been deliberately neglected, although it can be included. It has been shown that the fiber axes in paper are aligned at small angles only to the paper surface (12). The change in Poisson's ratio due to including the third dimension will then be negligible except at very high densities, where the fiber segments are small and the orientation is more random. Any fiber the axis of which is not completely parallel to the surface will have a component of its distortion in the z direction. Poisson's ratio in the x - z plane should be relatively small but essentially proportional to that shown in Fig. 3, slightly positive at low, and slightly negative at high, densities.

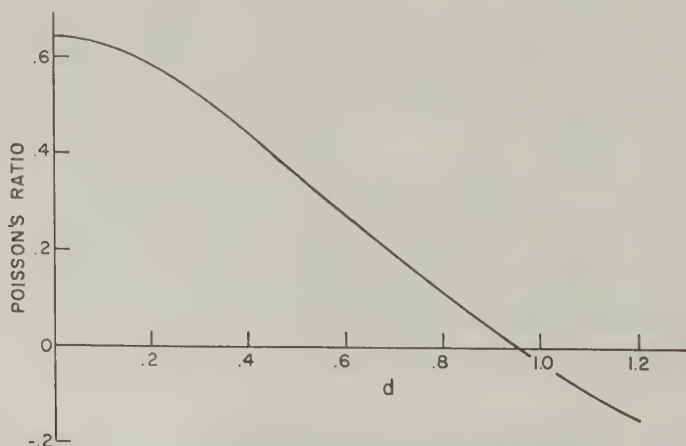


FIG. 3. Variation of Poisson's ratio with paper density.

CONCLUSIONS

A theory relating certain properties of paper to the properties of its constituent fibers and their interactions has been developed. The theory postulates that, within certain limits, Young's modulus and Poisson's ratio for two-dimensionally isotropic paper should be dependent only upon Young's modulus of the fiber and paper density. The prediction with regard to Young's modulus was tested and found to hold within the large uncertainties of the data. The theory was then developed to cover paper with machine direction.

Some aspects of behavior after the yield point are mentioned, but the interpretations are speculative and need more data before they can be tested.

The present theory can easily be generalized to cover all types of fiber orientations within paper and applied to any material composed of matted fibers. If the actual distortions of fiber segments are computed (which will be necessary if nonwoven fabrics are considered), the theory can be extended to cover large elongations, when they are reversible.

Some complications deserve to be mentioned. First, as the paper density increases, the segment orientations depart from the paper plane and become more random. This was not included in the simple theory and limits its predictions to paper densities below 0.8 or 0.9. Second and more seriously, as the interfiber bonds increase in number, the approximation of the fiber segment as a rectangular rod becomes less accurate and again limits the prediction at high densities. These objections may be overcome by using experimental data to determine the correct relationships. Third, the theory assumes that all the fibers have the same width and thickness. The predictions seem to hold if the fibers are not too unhomogeneous, that is if one species only is used, but if widely differing fibers are blended to make paper the simple theory will probably fail.

It is necessary to re-emphasize, along with many other investigators, that the most important factor determining paper strength is its density. When ultimate strength properties are to be considered the ratio of the fiber length to width is also important (rather than the length itself), as this determines the number of interfiber bondings per fiber at a given density. With these two terms, Young's modulus for the fibers, and a knowledge of fiber orientations, it may be possible to derive quantitatively the plastic flow behavior once the qualitative picture is known accurately, but the derivation will probably be quite difficult.

Many thanks are due to the faculty of the Pulp and Paper Department of the New York State College of Forestry and to Dr. J. J. Hermans for their cooperation, interest, and discussions. I would also like to thank Dr. J. A. Van Den Akker for helpful criticisms of the manuscript.

REFERENCES

1. RANCE, H. F., in R. Meredith, ed., "Mechanical Properties of Wood and Paper." Interscience Publishers, New York, 1953.
2. NISSAN, A. H., *Trans. Faraday Soc.*, **53**, 700-709 (1957); *Tappi* **41**, No. 3, 131 (1958).
3. VAN DEN AKKER, J. A., *Tappi* **49**, No. 12, 940 (1959).
4. ONOGI, S., AND SASAGURI, K., *Tappi (Japan)* **11**, No. 4, 233 (1957).
5. (a) MARTON, R., *Tappi* **42**, No. 12, 948 (1959); (b) private communication.
6. JAYNE, B. A., *Tappi* **42**, No. 6, 461 (1959).
7. CLARK, P. C., M.S. Thesis, State University College of Forestry at Syracuse University, Syracuse, New York (1959).
8. HIGGINS, H. G., MCKENZIE, A. W., AND HARRINGTON, K. J., *Tappi* **41**, No. 5, 193 (1958).
9. CAMPBELL, W. BOYD, *Tappi* **42**, No. 12, 999 (1959).
10. MEREDITH, R., "Mechanical Properties of Wood and Paper," pp. 188 ff. Interscience Publishers, New York, 1953.
11. NORDMANN, L. S., "Fundamentals of Papermaking Fibers," p. 333. Technical Section of British Paper and Board Makers Association, 1958.
12. AALTIO, E. A., AND HERMANS, J. J., *Tappi* **42**, No. 12, 1002 (1959).

BOOK REVIEWS

Saline Water Conversion [Library of Congress 60-53480] Advances in Chemistry. Series Number 27 Special Issue Sales American Chemical Society, Washington, D. C., 1960.

Potable water is the most essential and exotic liquid that exists on this planet—all life is dependent upon it—the importance of water is recognized only when the spigot runs dry. If water is not in the tap, it must be in the reservoir; if not in sight, it must be just over the horizon; or if the fields are parched, the rains are sure to come. *This is a common delusion which should be corrected*, because the lack of fresh water may be of national importance in the near future.

These sentences are from the introduction to a monograph summarizing the scientific and engineering researches that have been conducted upon saline water conversion by the U. S. Department of the Interior since the initiation of their program in 1952.

Other branches of the U. S. Government, notably the U. S. Public Health Service, are emphasizing the contiguous problems of the recovery of water from all types of polluted sources for the rapidly expanding American industry. They claim the problem is already of national importance at the present time and will become critical within a decade.

This monograph is restricted to papers dealing with a thorough investigation not only of the thermodynamic limitations and engineering evaluation of the obvious methods of distillation and solar evaporation of sea water but also of the feasibility of other methods of low cost. Of these, one of the most interesting is the separation achieved by adaptations of conventional freezing techniques.

A further proposal involves the flash evaporation of a volatile and immiscible hydrocarbon, such as butane, in direct contact with sea water to cause part of the water to freeze. Theoretically, freezing has several inherent advantages over conventional distillation processes, for example, the lesser tendency toward scaling and corrosion because of the low operating temperatures and the lower energy requirements as compared to the evaporation of sea water. A pilot plant employing freezing has been in operation at Syracuse, New York, since 1959 and is now being moved to a seashore location for further operational testing.

Evaporation is, of course, treated in great detail, but there are interesting chapters on "Ammonium Salts Ion Exchange," "Osmosis through a Vapor Gap Supported by Capillarity," and several chapters on "Porous Electrodes" and "Ion Exchange Membranes."

Unfortunately, no mention is made of current methods of prevention of evaporation of the water after it is in storage reservoirs, for example, by monolayers. It is equally important to prevent evaporation as it is to separate the water from the sea or other brackish sources.

The scientist will be interested in learning what short times have elapsed, since his visionary ideas were suggested, before engineering research and pilot plants have come into operation.

This monograph is a "must" for engineers interested in all forms of water recovery, saline or otherwise.

VICTOR K. LA MER, New York, New York

The Nucleic Acids. Vol. III. Edited by ERWIN CHARGAFF and J. M. DAVIDSON. Academic Press Inc., New York 3, New York, 1960. 588 pp. Price \$18.

To this reviewer, whose knowledge of the nucleic acids was neither exhaustive nor, on opening this volume, up-to-date, this third volume of the Nucleic Acids series has provided considerably more interest than did the earlier two volumes. Since the publication of the latter, the ties between nucleic acid chemistry and many of the great themes of biology (genetics, metabolism, protein synthesis, immunological specificity, and functional cellular organization) have been established more securely than seemed possible five years ago. The progress made earlier in understanding the structure of the nucleotides and nucleic acids has touched off a vigorous, highly diversified round of discoveries in biochemistry, bacteriology, virology, genetics, and studies of metabolism—and these, in turn, have created new problems and new subjects of inquiry for students of nucleic acids. This interplay is now at its height—the process is at least as intense as any that occurred in the most active periods in the development of protein chemistry. Full participation in it cannot be achieved by reading a single volume, but the present volume provides a rich sample, characterized by the timeliness and discrimination which can be provided only by contributors who are themselves importantly engaged in the nucleic acid adventure.

The foregoing should not leave the impression that strictly chemical or physico-chemical aspects of the nucleic acids are absent. The first two chapters, by C. L. Sadron (Strasburg) and by Dr. Shugar (Warsaw), respectively, deal with nucleic acids as macromolecules and with their photochemistry. In the first, both light-scattering and “hydrodynamic” methods are examined critically, and the probability of fragmentation during extraction is stressed; the second includes a treatment of hyperchromaticity and its bearing on structure, as well as on the correspondence between light absorption and photolysis, and such biological effects as mutation, and inactivation or reactivation of viruses, phages, and transforming DNAs. A lengthy paper by H. G. Khorana (ex-Vancouver, now Madison) on “Chemical and Enzymatic Synthesis of Polynucleotides” follows, and marks a transition to the stronger biochemical or biological orientation of the remainder. “The Biosynthesis of Purine Nucleotides” by J. M. Buchanan (Cambridge, Mass.) reviews “the major lines of evidence upon which the current formulations of the reactions of purine synthesis *de novo* are based,” ranging from isotopic experiments with the intact animal or isolated enzyme systems to the use of microbial mutants and antimetabolites. These are followed by: “The Chemistry of the Nucleic Acids of Micro-organisms” by A. W. Belozерky and A. S. Spirin (Moscow), in which the relation of nucleic acid content to the dynamics of protein synthesis, and discussion of species specificity, are found; “The Nucleic Acids of the Bacterial Viruses” by R. L. Sinsheimer (Pasadena), which treats function in viral infection and replication at least as fully as the structures of the nucleic acids involved, drawing on radiobiological and genetic experiments as well as on biochemical results; “The Ribonucleic Acids of Viruses” by H. Schuster (Tübingen), with large emphasis on TMV, but with material on animal viruses included as well—size, structure, infectivity, susceptibility to chemically induced mutation, interaction with host, and reconstitution are among the topics included; “Relationship of Nucleic Acid and Protein Synthesis in Studies of Cell-Free Systems,” by M. B. Hoaglund (Boston), and “Biosynthesis of Proteins in Intact Bacterial Cells” by G. F. Gros (Paris) between them provide a stimulating and lively description of an extremely active field which may illuminate protein chemistry as much as nucleic acid chemistry; “Agents Which Influence Nucleic Acid Metabolism,” by R. E. Handschumaker and A. D. Welch (New Haven) includes details of “the facility with which bacterial and neoplastic populations of cells become im-

mune to the action of most of the compounds" (antimetabolites) which block known reactions or sequences of reactions in nucleotide synthesis; and finally, "The Effect of Radiations on Nucleic Acid Metabolism," by L. G. Lajtha (Oxford), which relates the effects to the genetic, cytological, and selectively lethal effects on living systems.

JACINTO STEINHARDT, Cambridge, Massachusetts

Organic Coating Technology. By HENRY FLEMING PAYNE, Professor in charge of Organic Coating Research and Technology, University of Florida. John Wiley and Sons Inc. New York, London, 1961. Volume II, 730 pp. Price \$17.50.

This volume covers the chemistry, physics, and technology of pigments and pigmented organic coatings. It complements Volume I, which deals with the polymers comprising binders or paint vehicles. In the first chapter the factors which govern the appearance of a dry film and the viscosity of a fluid paint are discussed. The next six chapters cover the chemistry and manufacture of common pigments and extenders. These are followed by a chapter on formulation and production of pigmented coatings of various types including milling equipment and properties conferred on the coating by pigment and binder. Other subjects covered are surface preparation before painting, metal cleaning, and anodizing treatments, and discussions of three standard classifications of finishes—Architectural, Industrial, and Corrosion Resistant Finishes.

Each chapter has a long list of references. The text material is replete with illustrations. The index is good. Theories are well illustrated with examples.

The style tends to be informal. With the skill of a good teacher the author distills the meaning out of dry theoretical work and presents it in a comprehensible fashion. The book will be regarded by some as too "easy," but this reviewer finds this quality rare, difficult to attain, and hard to overdo.

The volume is of use to beginning technologists in organic coatings but will not be considered sufficiently profound by highly specialized technologists in any one field. Such a specialist will, however, find plenty to satisfy him in the sections of the book with which he is less familiar and he will find the references useful.

SEYMORE HOCHBERG, Philadelphia, Pennsylvania

ANNOUNCEMENT

In order to permit rapid publication of the increasing number of manuscripts that have been accepted by the *Journal of Colloid Science*, Volume **17**, 1962, will be published in 9 issues instead of 6. The number of pages to be published will be increased from 600 to 900. The months of publication will be:

January, February, March, April, June, August, September, October, December.

CONTACT ANGLES OF LIQUIDS AT DEFORMABLE SOLID SURFACES

G. R. Lester

*Imperial Chemical Industries Limited, Dyestuffs Division, Hexagon House,
Blackley, Manchester, 9*

Received December 2, 1960

ABSTRACT

The relation between the contact angles and the interfacial tensions for a liquid droplet resting on a solid surface is examined. Neumann's triangle of forces is valid, in principle, for contact angles on solids, liquids, or gels so long as an equilibrium configuration is possible. If the solid is nondeformable, Neumann's triangle of forces is equivalent to Young's equation. Only in the case of nondeformable solid surfaces is Young's equation applicable, since the interfacial boundary does not remain planar in other cases.

If a solid has a deformability within a certain range, the experimentally measured angles will be neither the angles in Young's equation nor those in Neumann's triangle. This is illustrated by an analysis of the nature of the deformation produced in the solid surface for an assumed stress distribution. Whereas the magnitude of the deformation may be infinitesimal, this is not true of the curvature as the three-phase boundary is approached. Neumann's condition is, therefore, of a largely formal character since it relates to angles which have no assignable significance. Criteria which define the limitations of Young's equation and Neumann's triangle are derived.

INTRODUCTION

The validity of Young's equation for contact angles (1) has recently been examined from several standpoints. This equation relates the contact angle to the interfacial surface tensions as follows:

$$\cos \theta = \frac{\gamma_{13} - \gamma_{23}}{\gamma_{12}}.$$

Bikerman (2) has expressed the view that the theoretical foundation for the relation is at least dubious, whereas Johnson (3) has claimed that the correct application of thermodynamical principles can avoid such difficulties in theoretical interpretation. Gravitational effects have received some consideration by Pethica and Pethica (4), who suggest that these can render the relation invalid. At the same time no calculations appear to have been made in which the deformability of the solid surface is explicitly included, although Bikerman has emphasized that vertical components of surface tension should cause some distortion in the surface and that it is

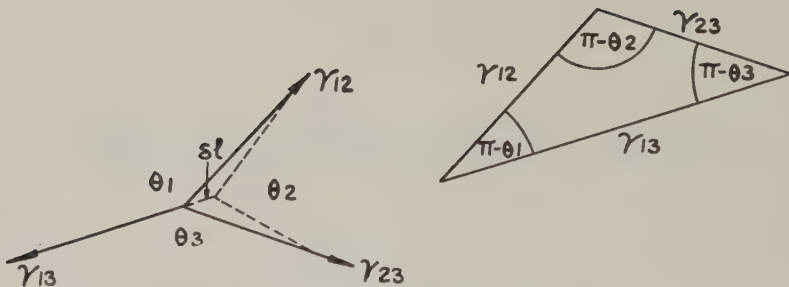


FIG. 1. Neumann's triangle.

misleading to ignore this effect. In the present paper an attempt is made to assess the importance of this contribution, and it is concluded that Young's equation is inapplicable when the deformability of the surface becomes appreciable, as might be the case with certain types of gel and with highly deformable membranes.

THE CONCEPT OF SURFACE TENSION AND THE TRIANGLE OF FORCES

The triangle of forces for surface tensions was apparently first enunciated by Neumann (5) and has come to be known as Neumann's triangle. That this condition must always be satisfied at any three-phase boundary which is capable of an equilibrium form follows directly from the definition of interfacial tension. We shall show that the validity of Neumann's condition for equilibrium is never in question in principle; what is questionable is whether or not angles determined experimentally have, or are ever likely to have, any resemblance whatsoever to those implied in the enunciation of this condition.

So-called proofs of Neumann's triangle have appeared elsewhere, and for our purpose lengthy discussion is not required. We shall omit gravitational forces which only complicate the argument without making any material difference, as R. E. Johnson (3) has shown. Consider an interface perpendicular to the plane of the paper and extending to a depth h . A plane cross section of the interfacial region has the form shown in Fig. 1. The interfacial tensions are defined by:

$$\gamma_{ij} = \left(\frac{\partial F}{\partial S_{ij}} \right)_{T, V, n_r},$$

where F = Helmholtz Free Energy, S_{ij} = interfacial area for media i and j , T = temperature, V = volume, n_r = molar concentration of the r^{th} component present in these media. That is to say,

$$\gamma_{ij} = \lim_{(\delta S_{ij} \rightarrow 0)} \frac{\delta F}{\delta S_{ij}}$$

and must not be confused with specific free-energy quantities such as F/S_{ij} . Now

$$\delta S_{13} = h\delta l; \quad \delta S_{12} = h \cos \theta_1 \delta l; \quad \delta S_{23} = h \cos \theta_3 \delta l.$$

According to the stationary free-energy condition, the equilibrium configuration (if it exists at all) must satisfy:

$$\delta(S_{13}\gamma_{13} + S_{12}\gamma_{12} + S_{23}\gamma_{23}) = 0,$$

whence

$$\gamma_{13} + \gamma_{12} \cos \theta_1 + \gamma_{23} \cos \theta_3 = 0.$$

Since we are at liberty to take δl along any interfacial boundary (or for that matter in any arbitrarily chosen direction), we also have:

$$\gamma_{12} + \gamma_{23} \cos \theta_2 + \gamma_{13} \cos \theta_1 = 0;$$

$$\gamma_{23} + \gamma_{13} \cos \theta_3 + \gamma_{12} \cos \theta_2 = 0;$$

and the conditions imply

$$\frac{\gamma_{23}}{\sin \theta_1} = \frac{\gamma_{13}}{\sin \theta_2} = \frac{\gamma_{12}}{\sin \theta_3},$$

as is otherwise obvious from the triangle of forces.

Now all this is demonstrably true if one knows how to measure the angles θ_1 , θ_2 , θ_3 , but we shall show that this possibility depends largely on the nature of the solid surface. Any such measurement involves an assumption that the limit of a convergent sequence of values may be derived by extrapolation from observations in the region of the interfacial boundary, as this is approached. That such an assumption is implicitly involved does not appear to have been sufficiently recognized previously, and, in our view, most of the difficulties concerning Young's equation stem essentially from this. We shall show, by an approximate calculation of the shape of the deformed surface, that the radius of curvature of the solid boundary very close to the interfacial zone is comparable in order of magnitude with the thickness of the surface layer in this region. Since this may in some cases be measured in molecular diameters, the contact angles are varying so rapidly in this zone that no certain meaning can be assigned to the limiting values implied by Neumann's triangle.

THE STRESS DISTRIBUTION

Consider a drop of liquid at rest on a deformable solid surface. There will exist a certain stress distribution over the area of contact such that the resultant force (with the neglect of gravitational force) vanishes. That the resultant force on the surface vanishes is clear from two considerations.

Firstly, the law of action and reaction shows that there is an equal force on the drop in the opposite direction to that on the surface and since the drop is at rest the resultant force on this must vanish; secondly, the pressure over the external surface of the drop and of the uncovered solid surface is everywhere atmospheric, as it would be over the whole of the solid surface if the drop were removed. The presence of the drop cannot therefore affect the resultant force on the surface but only the distribution of stress.

Now the pressure inside the drop (P) exceeds the external pressure by $2\gamma_{12}/R$, where R = the radius of curvature of its liquid-air boundary and γ_{12} = the interfacial tension. At the external boundary of the liquid there cannot be a pressure discontinuity; hence the pressure at the external surface is atmospheric pressure, taken to be the zero level of pressure measurements, and attains $2\gamma_{12}/R$ inside the drop but outside the surface layer. Our conclusion that there is no resultant force on the solid boundary implies therefore that a negative stress must occur in the surface layer, of the appropriate magnitude to balance the downward force.

The actual distribution of stress in the boundary region is not known exactly but, for an order of magnitude calculation, it could be considered to vary linearly from the extremities of the region (of breadth t) and to attain a maximum of P^* at the center. For mathematical tractability we shall introduce the further simplification of an equivalent mean stress P^* acting vertically upwards on the solid boundary over a ring bounded by circles of radii a and $a + t/2$ (see Fig. 2).

By resolving forces

$$\frac{t}{2} 2\pi a P^* = \pi a^2 P$$

$$\text{i.e., } P^* = \left(\frac{a}{t}\right) P = \frac{P}{\xi},$$

$$\text{where } \xi = \frac{t}{a}.$$

SURFACE DEFORMATION

The shape of the solid surface under the drop may now be calculated with these assumptions. For a constant pressure P over a circle of radius a applied to a semi-infinite solid, Sneddon (6) has given the displacement in the form:

$$y(r) = \frac{2(1 - \nu^2)Pa}{E} \int_0^\infty \frac{J_0(\xi r) J_1(\xi a)}{\xi} d\xi,$$

where E and ν are the Young's modulus and Poisson's ratio for the solid and J_0 , J_1 refer to Bessel functions of order zero and order one, respectively.

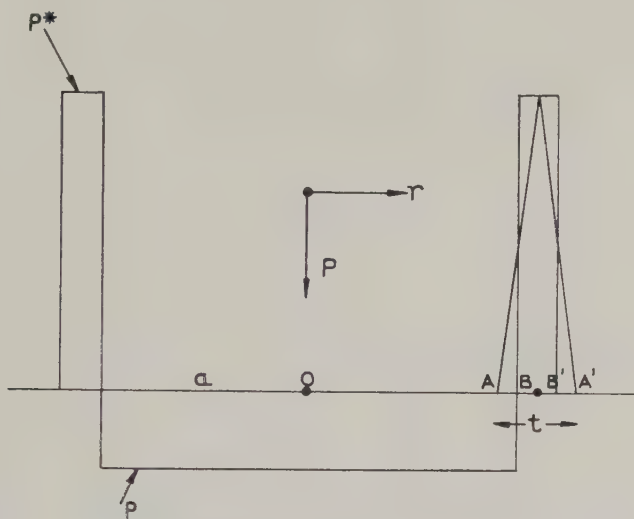


FIG. 2. The stress distribution at the surface.

Now this integral may be expressed in terms of hypergeometric functions (7):

$$\int_0^\infty \frac{J_0(\xi r) J_1(\xi a)}{\xi} d\xi = {}_2F_1\left(\frac{1}{2}, -\frac{1}{2}, 1; r^2/a^2\right), \quad (r < a);$$

$$= \frac{a}{2r} \cdot {}_2F_1\left(\frac{1}{2}, \frac{1}{2}, 2; a^2/r^2\right), \quad (r > a).$$

It is readily shown that ${}_2F_1\left(\frac{1}{2}, -\frac{1}{2}, 1; k^2\right) = \frac{2}{\pi} E(k)$, where $E(k)$ is the elliptic integral of the second kind. Similarly (see appendix),

$${}_2F_1\left(\frac{1}{2}, \frac{1}{2}, 2; k^2\right) = \frac{4}{\pi k^2} \int_0^k k K(k) dk = \frac{2}{\pi} G(k) \quad (\text{say}),$$

where $K(k)$ is the elliptic integral of the first kind.

Now let us calculate the displacement at $r = a + \beta t$ for a uniform pressure $P + P^*$ over a circle of radius a and a uniform stress $-P^*$ over a circle of radius $(a + t/2)$. By the principle of superposition, valid for linear elasticity, this system is equivalent to the one assumed by us.

$$\frac{1}{2} y(\beta) = A(P + P^*) \left[\frac{a^2}{(a + \beta t)} \right] G \left[\frac{a}{(a + \beta t)} \right]$$

$$- AP^* \frac{(a + t/2)^2}{(a + \beta t)} G \left[\frac{(a + t/2)}{(a + \beta t)} \right]$$

where

$$G(k) = \frac{2}{k^2} \int_0^k kK(k)dk$$

and

$$A = \frac{(1 - \nu^2)}{\pi E}.$$

Therefore,

$$\begin{aligned} \frac{1}{2} y(\beta) = APa \left(1 + \frac{1}{\zeta}\right) (1 - \beta\zeta)G(1 - \beta\zeta) \\ - \frac{APa}{\zeta} (1 + \zeta - \beta\zeta)G(1 + \zeta/2 - \beta\zeta). \end{aligned}$$

Since $\zeta \ll 1$, we may write $G(1 + \zeta/2 - \beta\zeta) = G(1 + \zeta/4 - \beta\zeta) + \frac{1}{4}\zeta G'(1 + \zeta/4 - \beta\zeta)$ and then obtain $y(\beta) = -APaG'(1 + \zeta/4 - \beta\zeta)$.

This may be expressed in terms of the ordinary elliptic integrals for

$$G'(k) = \frac{-4}{k^3} \int_0^k kK(k) dk + \frac{2K}{k} = \frac{2(K - G)}{k}$$

and

$$G(k) = \frac{2}{k^2} [E - (1 - k^2)K],$$

whence

$$G'(k) = \frac{2}{k^3} [(2 - k^2)K - 2E].$$

As $k \rightarrow 1$, $E \rightarrow 1$ but K tends to infinity logarithmically such that

$$K(k) \rightarrow \log_e \frac{4}{\sqrt{1 - k^2}}$$

and $y(\beta) \rightarrow APa \log_e (\beta - \frac{1}{4})\zeta$ for small ζ . This expression defines the shape of the deformed surface at the common boundary of the three phases and may be used to derive the equation for equilibrium. In an exactly similar way, at the internal boundary (point A in Fig. 2), the surface deformation is given by:

$$\frac{y(\beta)}{4APa} = \left(1 + \frac{1}{\zeta}\right) E(1 - \beta\zeta) - \frac{1}{\zeta} E \left(1 - \frac{1}{2}\zeta - \beta\zeta\right),$$

putting $r = a - \beta t$. Hence $y(\beta) \rightarrow APa \log_e (\beta + \frac{1}{4})\zeta$, but in this case $\beta = \frac{1}{4}$, whereas, at the external point A' , $\beta = \frac{3}{4}$. The angles subtended

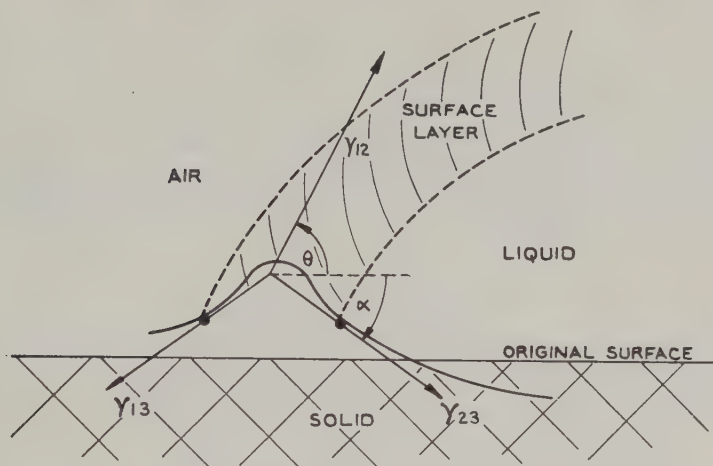


FIG. 3. Contact angles at a deformable surface.

to the horizontal by the deformed surface are therefore equal and given by

$$\tan \alpha = \frac{dy}{dr} = \frac{dy}{d\beta} \bigg/ \frac{dr}{d\beta} = \frac{AP}{(\beta \pm 1/4)\xi}$$

so that $\alpha = \alpha' = \tan^{-1}(2AP/\xi)$.

Moreover the mean curvature of the deformed surface is given by $2 \sin \alpha/t$. Thus the curvature is considerable in the region of actual contact of the droplet, and erroneous conclusions in expressing the conditions for equilibrium must result from failure to recognize this departure from planarity.

CONDITIONS FOR EQUILIBRIUM

The configuration of the system in the region of the surface layer is shown in Fig. 3. No account is taken of the surface distortion in ordinary measurements since it is of submicroscopic dimensions like the boundary layer itself; nevertheless its curvature and the angles subtended to the horizontal need be by no means negligible. This appears to be the source of anomalies and discrepancies in conventional formulations of Young's equation.

We have seen that

$$\alpha = \tan^{-1} \frac{2AP}{\xi} = \tan^{-1} \left(\frac{4\gamma_{12}(1 - \nu^2)}{\pi \xi ER} \right)$$

where

$$A = \frac{1 - \nu^2}{\pi E}, \quad P = \frac{2\gamma_{12}}{R},$$

so that $\alpha \rightarrow 0$ for common solids with large modulus of elasticity. As we have already seen, the energy condition derived from virtual displacements can be expressed equivalently as a triangle of forces involving surface tensions:

$$\gamma_{12} \cos \theta = (\gamma_{13} - \gamma_{23}) \cos \alpha \quad [1]$$

$$\gamma_{12} \sin \theta = (\gamma_{13} + \gamma_{23}) \sin \alpha \quad [2]$$

where

$$\alpha = \tan^{-1} \frac{4\gamma_{12}(1 - \nu^2)}{\pi \zeta ER}. \quad [3]$$

Neumann's triangle of forces is therefore directly applicable to the contact angles at a deformable solid boundary, but only when the appropriate angles are properly identified. Since the surface is disturbed, Young's equation as ordinarily expressed amounts to an erroneous horizontal resolution of forces with an implicit assumption that the boundary remains plane however closely the contact region is approached. In fact, it never does remain absolutely plane and the deviations from planarity given by Eq. [3] are just sufficient to remove any anomaly in the equilibration of surface tensions. The component $\gamma_{12} \sin \theta$ is therefore not by any means an anomalous feature but is always precisely balanced according to Eq. [2].

The use of Young's equation in its conventional form $\gamma_{12} \cos \theta = \gamma_{13} - \gamma_{23}$ implies that resolved components of the actual surface tensions appear on the right-hand side. Equivalently, this is not a physical equation involving true surface tensions and a real or observed contact angle, but is in the nature of a definition for a hypothetical angle θ , appropriate to a case where the solid surface is immobile.

The surface deformation is small only when the condition $\gamma_{12}/ER\zeta \ll 1$ is satisfied. On the assumption that the surface layer is several molecular diameters across (say 10 Å) and that a and R are of similar magnitude (true for a rigid surface where $a = R \sin \theta$), Young's equation will be valid provided γ_{12}/Et is small, where $t \approx 10^{-7}$ cm. Assuming a typical value for γ_{12} of 73 dynes/cm. (water and air value), it follows that discrepancies should begin to occur whenever the Young's modulus for the solid falls below about 10^{10} dynes/cm. For common solid materials with $E \approx 10^{12}$ dynes/cm. the effect is therefore negligible; whereas for rubber and certain gels it could be significant, though the latter will in many cases behave essentially as liquids from the present standpoint, since for these a typical value of Young's modulus is as low as 2×10^5 dynes/cm. (8).

DISCUSSION

The existence of the vertical stress component implies that a ridge or ripple should be produced in a surface of a sufficiently deformable character such as a gel or membrane. In the equation, $\gamma_{12} \cos \theta = (\gamma_{13} - \gamma_{23}) \cos \alpha$, θ is the apparent contact angle, measured with respect to the horizontal. If the surface were immobile, the contact angle with respect to the horizontal (θ_0) would satisfy

$$\cos \theta_0 = \frac{\gamma_{13} - \gamma_{23}}{\gamma_{12}}.$$

Then θ_0 is merely a defined angle and may be used as such, for example, in thermodynamical calculations, so long as it is not confused with θ (measured contact angle with respect to the horizontal plane) or even $(\theta + \alpha)$ (actual contact angle between liquid and solid surface). It will be noticed that θ (supposed less than 90°) always exceeds θ_0 since $\cos \alpha \leq 1$, whereas θ is itself always exceeded by the true contact angle $\theta_t = \theta + \alpha$; that is,

$$\theta_0 \leq \theta \leq \theta_t.$$

Whilst our discussion of the deformation in the solid surface was primarily illustrative and only a first approximation, it is interesting to enquire whether the surface layer thickness t used in this calculation may be related in some way to surface layer dimensions measured by other techniques. It is often supposed that this layer is only a few molecules in extent (9). Certain investigators, however, have claimed that interfacial layers may extend to considerably greater depths. Jura, for example (10), quotes surface layers of 4 molecules range for van der Waals' interactions and 30 molecules for ionic solids; Bakker (11) suggests that these layers may be several millimicrons across, and others have claimed that they can even approach microscopic dimensions. The order of magnitude which one assigns to t in our calculation will clearly be important in assessing the significance of the associated deformation. An attempt has been made by Bakker (12) to relate the capillary layer thickness (t) to radial and transverse pressure components for liquids in the form

$$t = \frac{\gamma}{(p_N - \bar{p}_T)},$$

where p_N = the vapor pressure and \bar{p}_T = the mean transverse stress through the capillary layer. In some cases the transverse component becomes negative in sign, and in our calculation the origin of the negative stress P^* may perhaps be interpreted in this way. The nature of the stress distribution in proximity to phase boundaries has been discussed further by Green (13), who has emphasized that pressure is neither isotropic nor homogeneous under such conditions. For a more detailed study of contact angles and their

dependence on stress distributions within surface layers, the fundamental approach of Green might be used with advantage.

It has been argued by Johnson (3) that Young's equation is necessarily valid if suitably defined surface tensions are used, and that such confusion as may have arisen is due to a misconception in their replacement by specific surface free energies. This view is no doubt correct if Young's equation is generalized to include Neumann's triangle of forces in the case where the solid is appreciably deformable, but no question of definitions alone can alter the fact that in this situation the horizontal tensions do not remain collinear. If surface curvature is large in the region of the interfacial boundary it is almost impossible to conceive of any experimental technique for measuring these angles, for they may vary considerably over a submicroscopic region. Thus, it may be said that Neumann's triangle is always valid in principle, but in application its validity is very problematical in many cases where a solid or gel-like boundary is involved. It becomes therefore largely a matter of taste whether one assigns any validity to the equations in such cases. For if it is, in the nature of things, almost impossible to relate the condition to measurable magnitudes, it would probably be justifiable to claim that its validity in principle is of no real significance. The situation for Young's equation is more clear-cut. For nonrigid solid boundaries, neither in principle nor in fact is the condition meaningful, for the enunciation of the equation is itself based on a misconception that the surface is planar no matter how closely the interfacial boundary is approached.

In conclusion, it may be said that Young's equation is incorrect unless surface deformation is virtually absent. Neumann's triangle, on the other hand, is still valid provided the contact angles can be properly identified, but this may be difficult since the surface curvature occurs within a region of similar dimensions to that of the surface layer. The additional relation involving an elastic modulus and the zone thickness shows how the amplitude of the ripple in the surface depends upon these factors. Whether or not a meaningful interpretation can be attributed to curvatures of a surface in a region of molecular dimensions is perhaps doubtful, but this feature serves only to emphasize the limitations of the concept of surface tension when applied to solids.

There are good reasons, both theoretical and practical, for wishing to understand the proper basis of Young's equation. Its application has been so wide in colloid chemistry that it is particularly desirable that its true theoretical validity should be well understood and the discrepancies suggested can be of much more than academic interest. The processing of textile fibers is an obvious example where deformability may be important, particularly as the outermost layers may be in the state of a quasi-gel.

Thanks are due to the referee of this *Journal* for suggesting a number of clarifications and improvements in the presentation of this paper.

APPENDIX

Let

$$f(z) = {}_2F_1\left(\frac{1}{2}, \frac{1}{2}, 2; z\right) = 1 + \left(\frac{1}{2}\right)^2 \frac{z}{2} \\ + \left(\frac{1 \cdot 3}{2 \cdot 4}\right)^2 z^2/3 + \left(\frac{1 \cdot 3 \cdot 5}{2 \cdot 4 \cdot 6}\right)^2 \frac{z^3}{4} + \dots$$

Then

$$\frac{d}{dz} [zf(z)] = 1 + \left(\frac{1}{2}\right)^2 z + \left(\frac{1 \cdot 3}{2 \cdot 4}\right)^2 z^2 + \left(\frac{1 \cdot 3 \cdot 5}{2 \cdot 4 \cdot 6}\right)^2 z^3 + \dots \\ = {}_2F_1\left(\frac{1}{2}, \frac{1}{2}, 1; z\right); \\ = \frac{2}{\pi} K(\sqrt{z}).$$

Therefore

$$f(z) = \frac{2}{\pi z} \int_0^z K(\sqrt{z}) dz.$$

Put

$$z = k^2$$

so that

$$f(k^2) = \frac{4}{\pi k^2} \int_0^k K(k) k dk.$$

Now let

$$f(k^2) = {}_2F_1(1/2, 1/2, 2; k^2) = \frac{2}{\pi} G(k).$$

Then

$$G(k) = \frac{2}{k^2} \int_0^k K(k) k dk.$$

The expression for $y(r)$ is then

$$y(r) = \frac{(1 - \nu^2)Pa^2}{Er} {}_2F_1\left(\frac{1}{2}, \frac{1}{2}, 2; a^2/r^2\right) \quad (r > a) \\ = \frac{2(1 - \nu^2)Pa^2}{\pi Er} G(a/r).$$

REFERENCES

1. YOUNG, T., *Phil. Trans. Roy. Soc.* **84** (1805).
2. BIKERMAN, J. J., *Proc. 2nd Intern. Congr. on Surface Activity* **III**, 125 (1957).
3. JOHNSON, R. E., *J. Phys. Chem.* **63**, 1655 (1959).
4. PETHICA, B. A., AND PETHICA, T. J. P., *Proc. 2nd Intern. Congr. on Surface Activity* **III**, 131 (1957).
5. NEUMANN, F., "Vorlesungen über die Theorie der Capillarität." Teubner, Leipzig, 1894.
6. SNEDDON, I. N., "Fourier Transforms," p. 528. McGraw-Hill, London, 1951.
7. WATSON, G. N., "Bessel Functions," 2nd ed., p. 401. Cambridge University Press, 1944.
8. SAUNDERS, P. R., AND WARD, A. G., *Proc. 2nd Intern. Congr. on Rheology*, p. 284 (1954).
9. ADAM, N. K., "The Physics and Chemistry of Surfaces," 3rd ed., p. 4. Oxford University Press, London, 1941.
10. JURA, G., *J. Phys. & Colloid Chem.* **63**, 40 (1948).
11. BAKKER, G., *Z. physik. Chem.* **93**, 171 (1919).
12. BAKKER, G., *Z. physik. Chem.* **104**, 10 (1923).
13. GREEN, H. S., "The Molecular Theory of Fluids." North-Holland Publishing Co., Amsterdam, 1952.

SOME HYDRODYNAMIC PROPERTIES OF NEUTRAL SUSPENSIONS OF CELLULOSE CRYSTALLITES AS RELATED TO SIZE AND SHAPE¹

R. H. Marchessault, F. F. Morehead, and M. Joan Koch

*American Viscose Corporation, Research and Development Division,
Marcus Hook, Pennsylvania*

Received July 8, 1960; revised December 27, 1960

ABSTRACT

Viscosity, flow birefringence, and sedimentation measurements are reported for suspensions of crystalline cellulose particles which were obtained by the hydrolysis of native celluloses with strong sulfuric acid (955 g./l. 24 hours, 40°C.). The hydrodynamic behavior of the particles was typical of rigid rods. The length of the equivalent prolate ellipsoid was much greater for suspensions made from bacterial cellulose than from ramie. In both cases, however, the hydrodynamic unit is an aggregate of microfibrillar fragments.

Ultrasonic treatment of the suspensions from ramie fibers caused a marked reduction in the average length of the equivalent ellipsoid. The observed hydrodynamic properties after this treatment could be directly correlated with the size and length distribution of particles in the suspension as viewed in the electron microscope. The lateral dimensions of the latter particles indicate that they are derived by transverse cleavage of the microfibrils; hence a true suspension of cellulose crystallites was obtained.

The possibility of using these suspensions as model systems of rigid rods for hydrodynamic studies is discussed.

I. INTRODUCTION

One of the characteristic properties of cellulose as it occurs in nature is its fibrillar structure. Sufficient evidence (1) has accumulated concerning this morphological feature, which occurs also in oriented regenerated cellulose, that it can be considered as a natural consequence of the strong crystallizing tendencies of the cellulose molecule. However, even the smallest fibrils (the so-called micellar strings, about 100-150 Å wide) are most probably supercrystalline units: accordingly to study the crystalline entities various hydrolytic treatments have been used to break down the fibrillar structure to small rodlike colloidal particles which are usually equated with the x-ray crystallites of polymer structure. The aim of the present communication is to show by means of well-established methods of colloid

¹ Presented at the "Symposium on Macromolecules in Solutions," 137th American Chemical Society Meeting, Cleveland, 1960.

chemistry that the elongated colloidal particles, which result from the hydrolysis of cellulose with strong sulfuric acid, behave as rigid particles whose size and shape in an aqueous suspension closely approximate those observed in the electron microscope after drying.

The foregoing objectives are of particular interest to the cellulose chemist. However, when it was discovered quite early in the course of this work that these particles do behave as rigid rods, evaluation of their colloidal properties was extended to establish whether or not these easily prepared suspensions might not serve as a model system of rigid rods.

Prior hydrodynamic measurements on colloidal dispersions of crystalline cellulose were made by Ranby (2), who determined the sedimentation constant. He concluded that the sedimenting unit appeared to be an aggregate of the basic particle visible in the electron microscope. It should be noted that this author used an ultrasound treatment on the suspension before observation in the electron microscope.

More recently flow birefringence studies on a similar dispersion were made by McLennan and Mason (3). Their work also indicated that the hydrodynamic unit is considerably greater than the basic cellulose "micelle" reported by Ranby (2).

Both of these studies were made on dispersions prepared by treating cotton or regenerated cellulose with 2.5 *N* H₂SO₄. Since recent work (4) has shown that a more particulate dispersion is obtained by the hydrolysis method of Mukherjee and Woods (5), the present study was concentrated on colloidal dispersions of ramie cellulose prepared by this technique.

II. EXPERIMENTAL

A. Sample Preparation

Stable colloidal dispersions of cellulose were prepared by hydrolysis with strong sulfuric acid according to a previously described method (5). For native cellulose the acid strength was 955 g./l.; 20 g. of air-dried cellulose was immersed in 250 ml. of acid at 40°C. for 24 hours. A temperature of 30°C. was used for mercerized native cellulose. The samples were washed free of acid by centrifugation until complete dispersion had occurred (somewhere in the pH range of 1 to 3), after which the combined suspension was dialyzed against "Permutit water" (contains only sodium ions) until neutrality.

In some cases the dispersions were kept as separate fractions according to the pH at which peptization occurred. The principal difference observed between these fractions was in the viscosity behavior. Thus, the initial fractions in the case of a cotton linters sample, which was broken into 9 fractions, had lower reduced specific viscosities over a given range of shear rates than the final and largest fraction that was chosen for study in this investigation. However, the fractionation was poorly reproducible and

seemed to be dependent on the amount of agitation during hydrolysis. In another case a ramie sample which had been mercerized prior to hydrolysis yielded only one fraction. Since mercerization may be considered to make the structure more accessible, this may indicate that fractionation is simply related to the heterogeneity of the hydrolysis. It can be reasonably assumed that the peptizing action arises from repulsive forces inside the hydrocellulose which come into play as the pH increases. The fractionation is the result of a balance between cohesional intermolecular forces and repulsive peptizing forces in the hydrocellulose as the pH increases.

The repulsive forces could arise from the ionization of sulfate half esters which are produced when strong sulfuric acid reacts with an alcohol. Analysis of the hydrocellulose constituting the neutral suspension, after freeze-drying, always showed about 1% to 2% sulfur. Sulfur analysis of the neutral dispersion prepared according to Ranby (2) showed only 0.013% sulfur.

A preliminary electrophoresis study showed that the particles obtained by the strong sulfuric acid method were negatively charged, just as Ranby (2) had observed for his preparations.

As mentioned above, this study was focused on the colloidal dispersions made from native bleached ramie (99% alpha cellulose). Dispersions were also prepared starting from: bleached mercerized ramie, cotton linters, dissolving grade pulps, and bacterial cellulose. The latter was kindly supplied by Prof. B. G. Ranby and was purified according to his published procedure (6).

B. Viscosity

Viscosity measurements were made over a wide range of shear rates on neutral aqueous suspensions of ramie crystallites. The solutions of various concentrations were prepared by diluting a stock solution the solids content of which was measured by drying to constant weight.

A multibulb Ubbelohde viscometer (7) was used to cover the shear range from 2000 to about 300 sec^{-1} . The calculation of the maximum shearing stress, τ , and the nominal rate of shear, D , at the capillary wall from the dimensions of the instrument has been described previously (8).

A viscometer similar to the one described recently by Hermans and Hermans (9) was designed to cover the range of shear from 100 to 10 sec^{-1} . The all-glass instrument, which was of the suspended-level type, is shown in Fig. 1.

Operating procedure for the low-shear viscometer involves the determination of h_{∞} (cf. Fig. 1), the equilibrium height of the meniscus in the measuring tube. It was assumed that this value was the same for the suspension as for water, the solvent. A dynamic method involving the use of a digital computer provided the value of h_{∞} giving the best straight-line fit for a plot

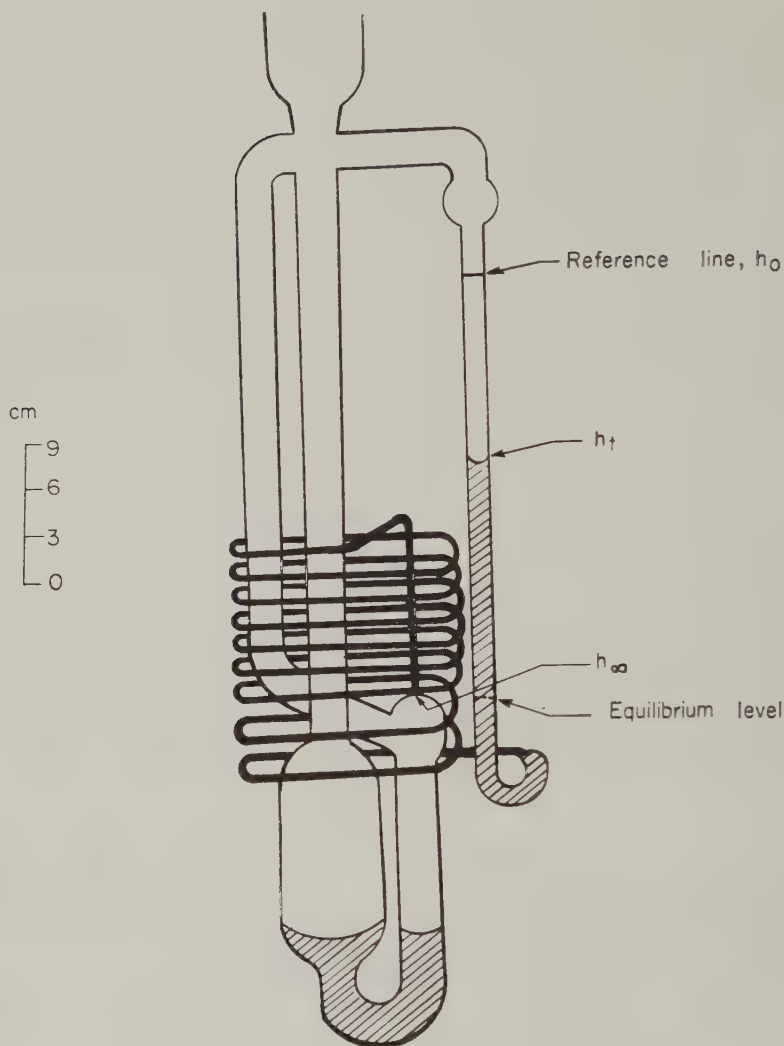


FIG. 1. Sketch of low shear viscometer.

of $\log (h_t - h_\infty)$ vs. t when the flowing liquid was water. The h_t values were obtained by means of a cathetometer (readable to ± 0.005 cm.) which was focused on the measuring tube of the viscometer when the latter was inside a constant-temperature bath. A special holder ensured reproducibility of position and verticality of the measuring tube inside the bath. Since all h_t values could be referred to a fixed mark h_0 on the measuring tube the computed h_∞ was converted to an instrument constant. For water $(h_0 - h_\infty) = 23.896$ cm. The same value was assumed to be valid for the suspensions.

The value of h_∞ derived from the computer was not identical with the value obtained by direct measurement 24 hours after flow was started. On the few occasions where comparisons were made the computer value was found to be several hundredths of a centimeter higher than the value obtained by direct measurement, 24 hours after flow was started. The exact reason for this discrepancy was not established, but it does illustrate an important source of error when viscosity data are collected at very low pressure heads. Ideally a viscometer should have dimensions such that $(h_t - h_\infty)$ for the smallest shear stresses does not change significantly with slight variations in h_∞ . In the present study the lowest Δh values were about 0.200 cm.

Two separate methods of evaluating η_{sp} were used. First of all, for each concentration the corresponding t and Δh , i.e., $(h_t - h_\infty)$ values were fitted to a second-degree equation of the form

$$t = b_0 + b_1 \ln \Delta h + b_2 (\ln \Delta h)^2, \quad [1]$$

and the slope $dt/d(\ln \Delta h)$ at each point was derived directly from the computer program. It has been shown (9) that the viscosity of a non-Newtonian solution η_τ at a given maximum shear stress τ is related to the viscosity of the Newtonian solvent, η_0 , by the relation

$$\frac{\eta_\tau}{\eta_0} = \frac{(d \ln \Delta h / dt)_\tau}{(d \ln \Delta h / dt)_0}. \quad [2]$$

A second method of analyzing the data involved expanded plots of $\ln \Delta h$ vs. t for solvent and suspension from which t_∞ and t_0 values corresponding to various Δh 's were read off. From these the specific viscosity and shear stress were computed. The same method could be used by programming a digital computer to yield t values corresponding to a certain $\ln \Delta h$ by interpolation of the experimental data. This method is equivalent to a hypothetical division of the measuring capillary into a series of bulbs with a determination of the corresponding viscosity increment in each.

C. Flow Birefringence

Since the ramie suspensions show very strong birefringence, they were studied at a single concentration in the range of 0.01 g./dl. which gave readings almost identical with those which would be obtained if concentration dependence were considered. Measurements were made with a Rao Instrument, Model 4-B, that has been described previously (10). Unfiltered light was used for the measurements so that average wavelength was about 500 $m\mu$.

D. Sedimentation and Partial Specific Volume

Sedimentation analysis was performed in an oil-driven Svedberg-type ultracentrifuge at the Biochemical Research Foundation, Wilmington,

Delaware, through the courtesy of Mrs. Laura Krejci. Speeds of about 15,000 r.p.m. were used, and polydispersity was evidenced by the widening of the sedimentation boundary in all cases. Measurements were also made using a Spinco Model E ultracentrifuge at speeds in the range of 10,000 r.p.m. It was found that at concentrations below 0.1 g./100 ml. the concentration dependence of sedimentation was not an important factor. All measurements were at 25°C.

The partial specific volume of a neutral suspension of ramie crystallites was determined in the usual way by measuring the density at several concentrations. A value of 0.669 ml. g.⁻¹ was obtained which is several per cent more than the specific volume of the dry particles. Assumedly, this is due to surface hydration, since it is well known that the cellulose crystal does not take up water.

E. Ultrasound Treatment

A "Hypersonic Generator" (Model BU-204) was used as a source of ultrasonic waves. The ramie suspension at the concentration desired for the subsequent measurement was treated for 30 minutes by immersing a tightly stoppered test tube, 40 mm. in diameter, containing 50 ml. of suspension to a depth of 1 inch in the activated oil bath. Although the oil was water-cooled the temperature rose to about 50°C. during the treatment. A frequency of 750 kc. was used.

III. RESULTS

A. Particle and Molecular Size

Electron micrographs of the various preparations were identical to those reported by Mukherjee and Woods (5). A typical electron micrograph which was obtained from a dilute suspension of hydrolyzed mercerized ramie is shown in Fig. 2. It should be noted that this sample was given an ultrasound treatment prior to drying on an electron microscope sample grid. It was found that this treatment considerably reduced the degree of aggregation visible in the electron microscope. It was originally thought that this aggregation was largely a drying artifact. It will be shown below, however, that this is probably not true and that Fig. 2 represents a better state of dispersion than actually existed in the unirradiated suspension. However, even after ultrasound treatment, electron micrographs of bacterial cellulose always showed a high degree of aggregation (*cf.* Fig. 3).

Preparations from various cellulose samples differed mainly with respect to particle size as observed after ultrasound treatment.

A length distribution study was made from electron micrographs of a cotton linters suspension. Seventy particles were involved in the counting and the lengths were distributed about a number-average length (\bar{L}_n) of 1200 Å. Since the cellulose molecules are arranged with their chain axes



FIG. 2. Cellulose crystallites from the hydrolysis of mercerized ramie fibers with H_2SO_4 at 30°C . for 24 hours; treated with ultrasound ($\times 37,500$).

parallel to the long axis of the particle (5) a one-to-one correlation should exist between the number-average degree of polymerization of the crystallites and their average length. (This hypothesis is conditional on all particles having roughly the same cross-sectional dimensions.) The number-average degree of polymerization measured on a nitrated sample of the same cotton linters hydrolysis residue yielded a value of 120, and the weight-average degree of polymerization derived from the intrinsic viscosity was 246. Since the length of a glucose residue in crystalline cellulose is 5.15 Å, there is a clear discrepancy between the measured length of the molecules and that expected if they traveled uninterruptedly the length of the crystallite. This implies that there is probably a goodly number of chain breaks within the crystallites. It is noteworthy that milder hydrolysis conditions appear to yield better agreement between the average crystallite length and the number-average degree of polymerization (2).



FIG. 3. Cellulose crystallites from hydrolysis of bacterial cellulose with H_2SO_4 at 40°C . for 24 hours; treated with ultrasound ($\times 12,500$).

The effect of ultrasound on the degree of polymerization of the crystallites was studied by measuring the viscosity in cupriethylenediamine (11) before and after treatment for a suspension of ramie crystallites. The same value for the degree of polymerization was found before and after treatment. Clearly ultrasonic vibration merely effects a deaggregation of side-by-side hydrogen-bonded particles but does not cause breakdown in the primary valence structure of the cellulose within the crystallites. The nature of this side-by-side particle aggregation is evident in Figs. 2 and 3. The fact that these aggregates can withstand both the solvating action of the strong sulfuric acid and the ultrasound treatment suggests that something

akin to a crystallization phenomenon occurs between these adjacent crystallites.²

Of the fibrous samples whose hydrolytic residues were examined in the electron microscope ramie had the greatest average particle length: 2000 Å; whereas the particles from cotton linters were some 900 Å shorter. In the bacterial cellulose preparations one frequently encountered individual particles which were 5000 Å in length whereas the average length of the visible single particles was 4000 Å. Wood pulps yielded electron micrographs with particles comparable in length to cotton but with much accompanying debris and ill-defined material.

On the question of width-to-thickness ratio of the ramie particles it was found as reported by Mukherjee and Woods (5) that the particles are wider than they are thick. This was deduced from the width of the metal shadow. Precise measurements were made by allowing a dilute suspension to dry down on a freshly cleaned glass slide which was then metal shadowed with platinum. The 30-mil platinum wire was wrapped around a heated tungsten filament over a 1-inch length so as to provide, in effect, a slit source. The plate was then dipped in a nitrocellulose solution and the sample stripped off. The sample was mounted in the electron microscope with the nitrocellulose side to the electron beam and the image formed was due entirely to the metal cast. Figure 2 was prepared in this way. Results of such measurements on samples from bleached and mercerized ramie gave an average width-to-thickness ratio of about 3, although it should be emphasized that there actually was a wide distribution of ratios (5.7 to 1.9). For the various suspensions the average width was 150 to 160 Å and the average thickness was 40 to 50 Å.

B. Hydrodynamic Measurements

The viscosity data from the "low shear" viscometer are shown in Fig. 5 as plots of $\ln \Delta h$ vs. t at the various concentrations. Also included in Fig. 5 is the Huggins plot for the suspensions at zero shear as calculated from the slopes of these lines. The linearity of course implies that the non-Newtonian behavior in this range of shearing stresses was negligible. This fact tended to make the second-degree curve fitting method superfluous in this particular case, although it could be useful when there is more non-Newtonian behavior, bearing in mind what was said above about h_{∞} .

Application of the second method for evaluating the viscosity data as

² This lateral accretion of the microfibrillar fragments may account for the fact that the widths of the crystallites were distributed about an average value of 150 Å which is considerably more than the average width of the microfibrils as reported by Ranby (17). Another explanation for the discrepancy is that entanglement of the microfibrils does not allow them to be preferentially on their widest face as are the crystallites.

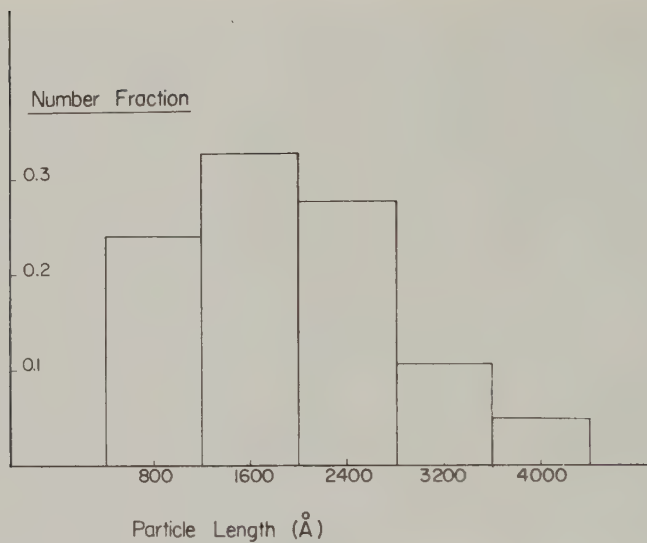


FIG. 4. Histogram distribution plot of particle lengths of ultrasound-treated ramie crystallites.

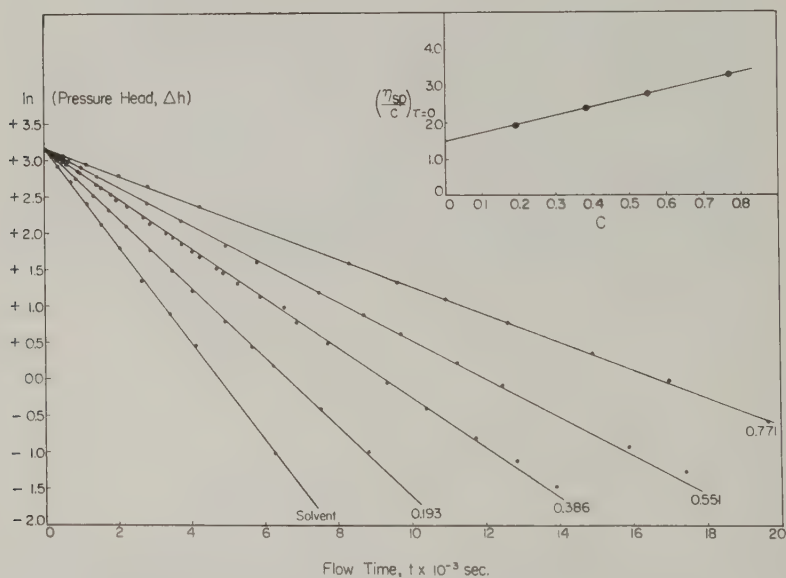


FIG. 5. Natural logarithm of the hydrostatic pressure head in the low shear viscometer versus flow time for ramie suspension in "low shear" viscometer.

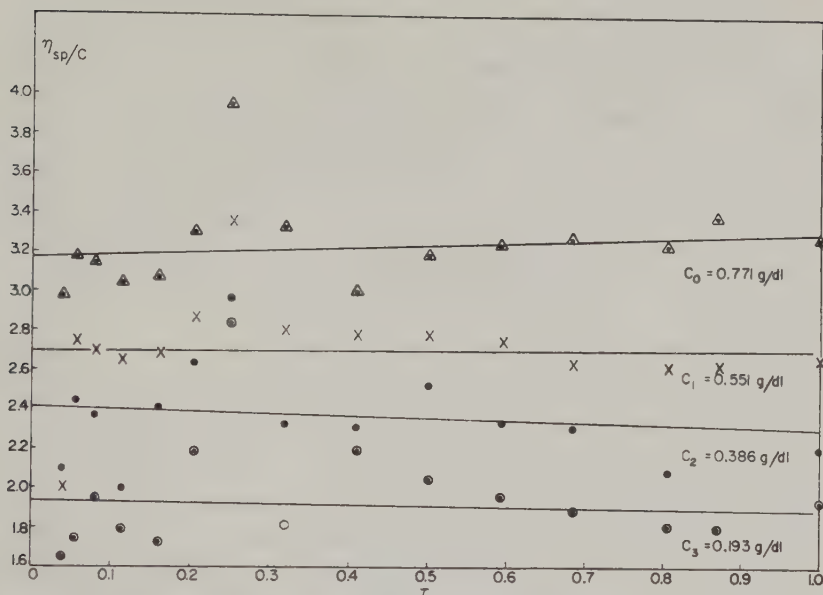


FIG. 6. Reduced specific viscosity versus shearing stress τ in dynes, cm^{-2} , for ramie suspensions. The straight lines are based on a "least squares" analysis of the data.

outlined above confirmed the essentially Newtonian character of the suspensions over the entire range of shear stresses. Despite the scatter of the points as shown in Fig. 6 (in part due to the interpolation technique), it is evident that η_{sp}/c for each concentration is essentially constant. The "least squares" line is drawn through each set of points.

Combination of the data from the "low" and "high" shear stress viscometers leads to the composite curve shown in Fig. 7. The break in the line is the dividing point between the data collected in the two viscometers. The large decrease in viscosity at relatively low rates of shear is characteristic of rigid particles with a small rotational diffusion constant. Unfortunately the range of the two viscometers did not overlap, but from the known rotational diffusion constant it can readily be shown (8) that the pronounced drop in viscosity is at the expected rate of shear.

It must be remembered, however, that the excellent dispersion shown in Fig. 2 is in part due to the effect of the ultrasound treatment. That this is so, is shown by the pronounced drop in viscosity for the ultrasound-treated sample in Fig. 7. The viscosity measurements from which this curve was derived were somewhat erratic (most probably because of some reaggregation process). Measurements were made only in the high-shear viscometer where several measurements could be conveniently made over a short

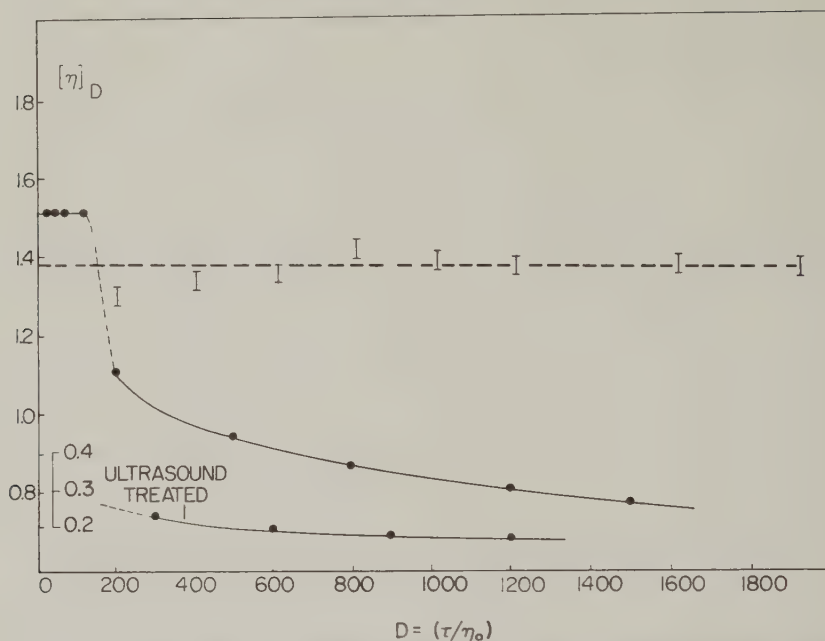


FIG. 7. Intrinsic viscosity versus nominal rate of shear for ramie suspension before and after ultrasound treatment. The calculated values of $[\eta]_D/F(\chi)_{a,p}$ are shown as bars.

period of time. Accordingly, only an approximate correlation can be made between observed particle size and viscosity. The viscosity average length at zero shear can be derived from the equation (12)

$$[\eta]_{D=0} = \frac{N \nu V_e}{100 M};$$

or

$$[\eta]_{D=0} M = 4\pi N/300 (a^3)(\nu/p^2);$$

where M is the molecular weight, a is the length of the major semi-axis, and ν is a function of axial ratio p . The factor (ν/p^2) is rather insensitive to axial ratio; accordingly a value of 25 based on the electron micrographs was selected. A weight-average molecular weight of 16.5 million was computed from the distribution shown in Fig. 3; it was assumed that all particles had the same cross section and $[\eta]_{D=0}$ was taken as 0.34 dl. g.⁻¹. The calculated semimajor axis of the equivalent ellipsoid was found to be 1450 Å, which is some 30% more than the average length from the electron micrographs. The somewhat greater length of the equivalent ellipsoid is of the same order of magnitude as was observed (19) recently in the case of tobacco mosaic

virus where an accurate molecular weight and narrow size distribution was available. It was suggested then that the discrepancy appears to be related to the inability of the ellipsoidal model to represent a cylinder accurately.

The effect of ultrasound treatment is demonstrated also in Fig. 8, where the extinction angle is plotted against the quantity $D\eta_0/T$. The full curve through the points for the irradiated sample was calculated taking the polydispersity shown in Fig. 4 into account according to Eq. [4]:

$$\tan 2\chi = \frac{\sum_i c_i f_i \sin 2\chi_i}{\sum_i c_i f_i \cos 2\chi_i} \quad [4]$$

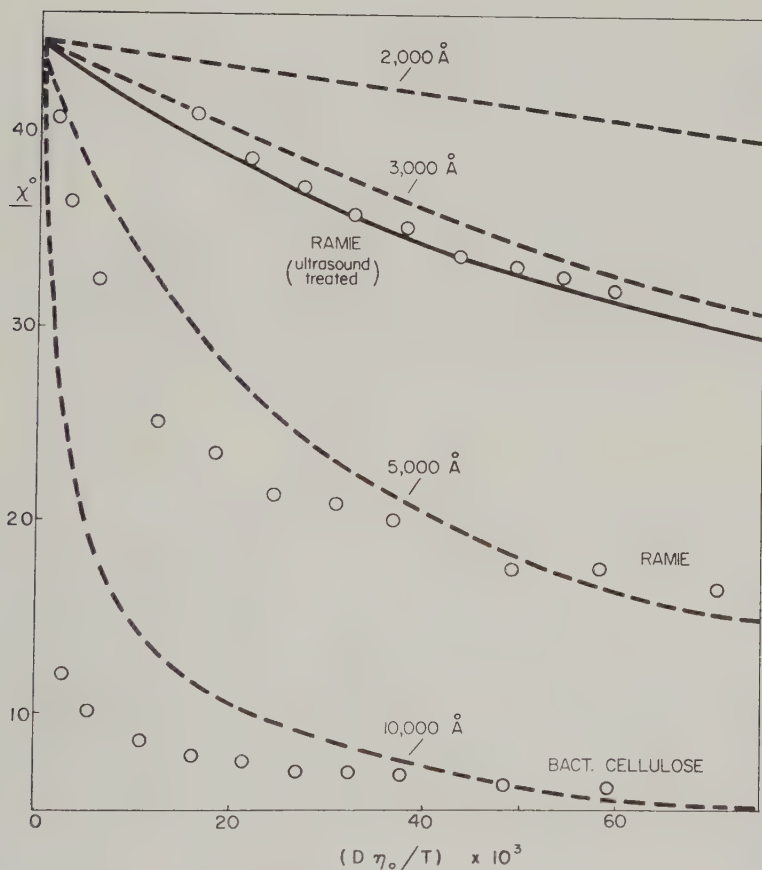


FIG. 8. Extinction angle plotted against the quantity $(D\eta_0/T) \times 10^3$ for ramie bacterial cellulose and ultrasound-treated ramie suspensions. The full line for the ultrasound treated ramie suspensions is the theoretical curve for the length distribution in Fig. 4, and the broken lines are for monodisperse systems.

TABLE I
Apparent Lengths of Prolate Ellipsoids

D (sec ⁻¹)	$L(A)$ (from χ)	$L(A)$ (from $[\eta]$)
0	—	—
50	7000	8900
100	6640	8240
200	6500	—
300	6300	7900
600	5900	6880
1000	5410	6600
1500	5200	—

where c_i and f_i are the volume fraction and orientation factor of the i th component, respectively. The relative values of c_i were obtained from the histogram plot (assuming cross-sectional area was constant) while f_i and χ_i corresponding to L_i at a given $D\eta_0/T$ were obtained from the tables (13). Similar agreement between theory and observation has been reported (3) for an unirradiated suspension of cotton crystallites.

The large initial decrease in χ in Fig. 8 for the non-ultrasound treated suspension parallels the viscosity behavior at low shear. Since both intrinsic viscosity and extinction angle are a function of parameter $\alpha (=D/\theta)$, where θ is the rotary diffusion constant of the solute, combination of the measurements leads to a function (14)

$$F(\chi_D) = \frac{[\eta]D}{[\eta]_{D=0}}, \quad [5]$$

with α and p (axial ratio) as parameters. Using the published conversion factors one can derive the value of $[\eta]_{D=0}$ corresponding to $[\eta]_D$. Obviously the factors for oblate and prolate ellipsoids differ significantly, and the very fact can be used to draw some conclusion as to which model is applicable. With the proper model, $[\eta]_{D=0}$ corresponding to any $[\eta]_D$ should be invariant. This is shown by the dotted line through the bars (p was assumed to be 50) in Fig. 7 which leads to an extrapolated $[\eta]_{D=0}$ which is about 10 % less than the viscosity value. The oblate model gives a still lower line, from which it is concluded that the prolate model applies in this case. Points at very low shear stresses were ignored because of the different average values which intrinsic viscosity and flow birefringence would yield in the low shear range (15).

The relation between non-Newtonian viscosity and extinction angle for the non-ultrasound treated suspension is further illustrated by the data in Table I, which compares the apparent lengths derived from the two measurements. The differences between the two sets of data may possibly be

due to errors in determining the intrinsic viscosity at zero shear as described above.

The relatively small χ values for the bacterial cellulose crystallite samples, included in Fig. 8, testify to the fact that the numerous aggregates visible even in the electron micrographs of the ultrasound-treated sample are primary in nature and hydrodynamically they behave as single units. For this reason the lengths derived from flow birefringence are much greater than the average length of 4050 Å of the clearly discernible single particles in electron micrographs such as Fig. 3. The higher state of primary aggregation is almost certainly related to the higher crystallinity of this sample compared to ramie.

IV. SEDIMENTATION

Sedimentation constants were measured for an ultrasound-treated suspension of ramie crystallites (2 hours after treatment) and one which was not treated. The values obtained were 174 s and 397 s, respectively. This difference in sedimentation constant was reflected in the differences in the turbidity of the two suspensions, the ultrasound-treated sample being visibly clearer. Likewise, the spreading of the sedimentation boundary was less for the latter, indicating a narrower distribution of particle sizes. Just as the viscosity behavior of the ultrasound-treated sample suggested a certain instability immediately after treatment, the sedimentation constant showed about a 15 % increase over a period of 4 days; this must be indicative of some reaggregation as a function of time.

An estimate of the short semiaxis b of the equivalent ellipsoid can be derived from the equation:

$$s = 0.222 \frac{(1 - \bar{V}\rho)}{\bar{V}\eta_0} b^2 \ln \left(\frac{2a}{b} \right), \quad [6]$$

where ρ is the solvent density, \bar{V} is the partial specific volume, a is the long semiaxis, b is the short semiaxis, and η_0 is the solvent viscosity. If a/b is taken as 25, the quantity $2b$ is found equal to 114 Å, which is 14 % greater than the average value of the width and thickness $(150 + 50)/2$ from the electron micrographs. When combined with the axial ratio of 25 this yields a length of 2850 Å for the ellipsoid, in good agreement with the viscosity length.

Strictly speaking Eq. [6] is incorrect since it should involve the volume of the equivalent ellipsoid V_e rather than \bar{V} . The magnitude of the error in b due to this substitution should be very small in the present case, where the particles are rigid and impermeable to solvent. A precise value for V_e requires (18) an accurate determination of molecular weight, which was lacking in the present case. That our calculated value of 16.5 million is a

reasonable approximation, however, can be shown by combining s and $[\eta]_{D=0}$ to compute (18) a molecular weight of 19 million.

A similar combination of $[\eta]_{D=0}$ and s for the untreated suspensions ($a/b = 60$) gives a molecular weight of 110 million. This suggests that the aggregates in the unirradiated suspensions are made up of five or six of the single particles in Fig. 2.

The sedimentation constants were measured also for two untreated fractions of cotton linters crystallites. Fraction 9 (the final and largest) had a sedimentation constant of 450 s , whereas fraction 7 had a value of 160 s . This suggests that the shorter and/or the less aggregated particles peptize first. It is noteworthy that Ranby (2) reported a value of 500–700 s for an ultrasound-treated suspension prepared from a "high alpha" pulp according to his method of hydrolysis. This serves to emphasize that each method of hydrolysis produces its own characteristic state of dispersion and that the Mukherjee-Woods method gives a superior breakdown into elementary particles.

V. DISCUSSION

From the foregoing data the following conclusions can be made: (a) crystallite suspensions prepared according to the method of Mukherjee and Woods show hydrodynamic properties characteristic of rigid elongated particles; (b) ultrasound treatment of suspensions prepared from cotton linters or ramie fibers (and indeed probably any fibrous cellulose) causes considerable breakdown of the spindle-like aggregates into shorter particles whose lateral dimensions indicate that they were derived by transverse cleavage of the microfibrillar fragments.

Thus only after ultrasound treatment do the so-called cellulose micelle, visible in the electron microscope, and the hydrodynamic unit coincide. This system would appear to be quite satisfactory as a model system of rigid rods since it is considerably easier to prepare than tobacco mosaic virus. However it has the disadvantage of being polydisperse ($M_w/M_n \sim 1.2$ to 1.3). A suitable method for measuring molecular weight has yet to be worked out since our first attempts at light scattering in buffered system resulted in aggregation. One property of the cellulose crystallite system which is unique is its high positive birefringence which is useful for testing the Peterlin Stuart expression for birefringence of a flowing suspension.

From the measured birefringence of a flowing suspension the Peterlin Stuart theory allows calculation of the principal refractive indices of the moving particles. The birefringence, $\Delta\eta$, for the ultrasound-treated ramie crystallites at $D = 2244 \text{ sec}^{-1}$ was 96.3×10^{-8} for light whose $\lambda_{av.} = 500 \text{ m}\mu$. It was found, using the theory of Peterlin and Stuart, the measured $(d\eta/dc)_{546} = 0.148 \text{ ml. g}^{-1}$, and the approximation for elongated particles, that $\eta_1 = 1.59$ and $\eta_2 = 1.55$. For a completely crystalline native

TABLE II

Particle Dimensions and Results of Hydrodynamic Measurements for Ultrasound-Treated Ramie Crystallites at 30°C.

Electron microscopy	Viscosity
$\bar{L}_w = 2400 \text{ \AA}$, $\bar{L}_n = 2000 \text{ \AA}$ $\bar{M}_w = 16 \times 10^6$, $\bar{M}_n = 13 \times 10^6$ Width: 150 \AA ; thickness: 50 \AA	$[\eta]_{D=0} \simeq 0.34$ $L_e = 2850 \text{ \AA}$
Flow birefringence	Sedimentation
$[\eta\phi/T]_{D=0} = 15 \times 10^{-3}$ $L = 3500 \text{ \AA}$ $n_1 = 1.59$; $n_2 = 1.55$	$s = 190 \times 10^{-13}$ Diameter: 114 \AA

cellulose fiber, Hermans (16) has computed the values 1.613 and 1.543. The agreement between these two determinations could perhaps be improved by a more refined optical system on the Rao apparatus. Nevertheless, the result clearly indicates that the crystallites are directly related to the fiber crystallites and are flowing with their fiber axis along the streamlines. Further evidence of this fact was obtained by means of x-ray diffraction on a concentrated suspension of the crystallites. The pattern of native cellulose was clearly discernible.

A summary of the hydrodynamic data and the various dimensional factors for the ultrasound-treated ramie crystallites are contained in Table II.

The dimensions of the equivalent ellipsoid for the non-ultrasound treated ramie suggest that about five or more of the individual particles shown in Fig. 2 are aggregated side by side to yield a stable rodlike particle. This material is likewise suitable as a model system of rigid rods. Although harder to characterize by electron microscopy they are more stable and show more striking non-Newtonian behavior than their ultrasound-treated counterparts. The same high birefringence is present but these particles are too large to test the theory of Peterlin and Stuart.

REFERENCES

1. "The general discussion on cellulose," *Svensk Papperstidn.* **57**, 9 (1954).
2. RANBY, B. G., *Discussions Faraday Soc.* **No. 11**, 158 (1951).
3. MCLENNAN, D. F., AND MASON, S. G., *Can. J. Chem.* **37**, 1788 (1959).
4. "Summarized proceeding on electron microscopy conference," *Brit. J. Appl. Phys.* **8**, 1 (1957).
5. MUKHERJEE, S. M., AND WOODS, H. J., *Biochim. et Biophys. Acta* **10**, 499 (1953).
6. RANBY, B. G., *Arkiv Kemi* **4**, 249 (1952).
7. SCHURZ, J., AND IMMERGUT, E. H., *J. Polymer Sci.* **9**, 279 (1952).
8. YANG, J. T., *J. Am. Chem. Soc.* **80**, 1783 (1958).
9. HERMANS, J. AND HERMANS, J. J., *Koninkl. Ned. Akad. Wetenschap. Proc.* **61B**, 324 (1958).

10. EDSALL, J. T., RICH, A., AND GOLDSTEIN, M., *Rev. Sci. Instr.* **23**, 695 (1956).
11. BATTISTA, O. A., *Ind. Eng. Chem., Anal. Ed.* **16**, 351 (1954).
12. SIMHA, R., *J. Phys. Chem.* **44**, 25 (1940).
13. SCHERAGA, H. A., EDSALL, J. T., AND GADD, J. O., *J. Chem. Phys.* **19**, 1101 (1951).
14. YANG, J. T., *J. Phys. Chem.* **62**, 894 (1958).
15. GOLDSTEIN, M., AND REICHMAN, M. E., *J. Am. Chem. Soc.* **76**, 3357 (1954).
16. HERMANS, P. H., "The Physics and Chemistry of Cellulose Fibers," p. 236. Elsevier, New York, 1949.
17. RÅNBY, B. G., Doctoral Dissertation, University of Uppsala, Uppsala, Sweden, 1952.
18. SCHERAGA, H. A., AND MANDELKERN, L., *J. Am. Chem. Soc.* **75**, 179 (1953).
19. BOEDTKER, H., AND SIMMONS, N. S., *J. Am. Chem. Soc.* **80**, 2550 (1958).

SOME HYDRODYNAMIC PROPERTIES OF RAMIE CRYSTALLITES IN PHOSPHATE BUFFER¹

R. H. Marchessault, M. Joan Koch, and J. T. Yang

*Research and Development Division, American Viscose Corporation,
Marcus Hook, Pennsylvania*

Received July 8, 1960; revised October 10, 1960

ABSTRACT

The hydrodynamic properties of a suspension of cellulose crystallites in 0.01 *M* phosphate buffer were studied by a combination of flow birefringence, viscosity, and light-scattering techniques. The hydrodynamic behavior of the crystallites in this medium was typical of polydisperse oblate ellipsoids. Since the individual crystallites are rodlike in shape it was concluded that a side-by-side aggregate had occurred in the presence of buffer to form a disclike aggregate. Electron microscope observations supported this conclusion. The weight-average molecular weight of the aggregates was 200 millions, the diameter of the disc about 5000 Å, and the thickness 15 to 30 Å.

Ultracentrifugal analysis yielded a very narrow distribution of sedimentation constants which reflects the uniformity in thickness of the aggregates.

I. INTRODUCTION

In a previous report (1) it was concluded that the ramie particles derived from the hydrolysis procedure of Mukherjee and Woods (2) do not exist in suspension as the free individual particles which are observed in the electron microscope. It appeared that a considerable amount of primary aggregation (deriving from the fiber morphology) is present in the starting suspension. This aggregation could be considerably reduced by ultrasonic irradiation.

The present report focuses on the colloidal properties of dilute suspensions of ramie particles in a 0.01 *M* phosphate buffer. This solvent was chosen in order to minimize concentration effects in the light-scattering measurements. At the same time flow-birefringence viscosity and sedimentation data were recorded for the suspension in the same solvent in order to compare the derived size parameters. It will be shown that considerable secondary aggregation takes place even in this solvent of low ionic strength and the resulting aggregates behave as oblate ellipsoids. The

¹ Presented at the "Symposium on Macromolecules in Solution," 137th American Chemical Society Meeting, Cleveland, 1960.

flocculating effect of electrolytes on colloidal suspensions of cellulose has been reported previously (3).

II. EXPERIMENTAL

A. Preparation of Ramie Crystallites

Colloidal suspensions of ramie crystallites were prepared by the method of Mukherjee and Woods (2) and have been described in the previous report (1).

Unless otherwise stated, all solutions were made up by diluting the aqueous suspensions with an equal volume of 0.02 *M* phosphate buffer and allowing at least one day at room temperature (25°C.) before use. Subsequent dilutions were made with 0.01 *M* phosphate buffer (0.01 *M* KH_2PO_4 plus 0.01 *M* Na_2HPO_4 ; pH = 6.7; ionic strength = 0.04).

B. Concentration Determinations

The concentration of the neutral aqueous stock solution was determined by drying and weighing, whereas that in buffers was derived from the refractive index increment.

C. Clarification of Solutions

Significant sedimentation loss during centrifugation was detected. Virtually all solids could be sedimented by centrifugation at 31000 *g* for more than 30 minutes. As a compromise all solutions were centrifuged in a Servall type SS-1 superspeed angle centrifuge for exactly 30 minutes at 8600 *g*. The centrifuge came to a dead stop in about 8 to 9 minutes without braking. From refractive increment measurements the loss was found to be 21 %.

D. Flow Birefringence

The extinction angles, χ , and birefringence, Δn , were measured on a Rao Instrument, Model 4-B, that has been described previously (4).

E. Intrinsic Viscosity

Viscosities of ramie suspensions were measured in specially designed multigradient Ubbelohde-type viscometers. Calculations of the maximum shearing stress, τ , and nominal rate of shear, D , at the capillary wall have been described elsewhere (5). The values of τ with water were 3.30, 6.49, 10.0, and 12.0 dynes per cm^2 , respectively.

F. Light Scattering

Angular scattering measurements at 546 $\text{m}\mu$ were made in a Brice-Speiser Photometer, Universal 1000 Series, using a special thin-walled cylindrical cell (Phoenix Instrument Company). Clean solvent was obtained by filtra-

tion through an ultrafine sintered glass filter, whereas solutions were clarified by centrifugation in a Servall centrifuge as mentioned earlier.

G. Refractive Index Increment

The specific refractive index increment, dn/dc , was determined with a Brice-Speiser differential refractometer. The value of dn/dc for ramie crystallites both in water and in phosphate buffer was found to be 0.148 ml. g.⁻¹ at 546 m μ .

H. Ultracentrifuge Analysis

Sedimentation analysis was performed in a Spinco ultracentrifuge at the State College of Forestry, Syracuse, New York, through the courtesy of Professor J. J. Hermans, Director of the Cellulose Research Institute.

III. RESULTS

A. Effect of Electrolytes on the Ramie Suspensions

Preliminary study of the effect of phosphate buffer on the viscosity of ramie suspensions has revealed a gradual increase in viscosity (about 10 %) for the first 10 hours or so after mixing the aqueous suspensions with equal volume of 0.02 *M* phosphate buffer—a fact indicative of some size and/or shape change of the particles in the presence of electrolyte. The same effect was also detected in the flow birefringence studies, where the extinction angle at a given rate of shear was smaller in the presence of phosphate buffer than without. For this reason all experimental measurements on buffered ramie suspensions were always made one or two days after mixing with buffer.

B. Electron Microscope Observations

Although previous studies (1, 2) clearly indicate that the basic particle in these suspensions is elongated and tabular, it is obvious from hydrodynamic observations on the neutral suspensions that the average size of the flowing unit is considerably greater. From the electron micrographs on systems containing the 0.01 *M* phosphate buffer it appears that still further aggregation occurs in this medium, compared to the unbuffered system. The electron micrograph in Fig. 1 suggests, however, that this secondary aggregation involves side-by-side aggregation of the particles so that their hydrodynamic behavior approaches that of flat discs. Ultrasonic irradiation of these suspensions according to a previously described procedure (1) resulted in the usual dispersion of single rodlike components (1, 2).

C. Flow Birefringence

The ramie suspensions exhibit very strong birefringence and therefore can be studied at very low concentrations. The concentration dependence

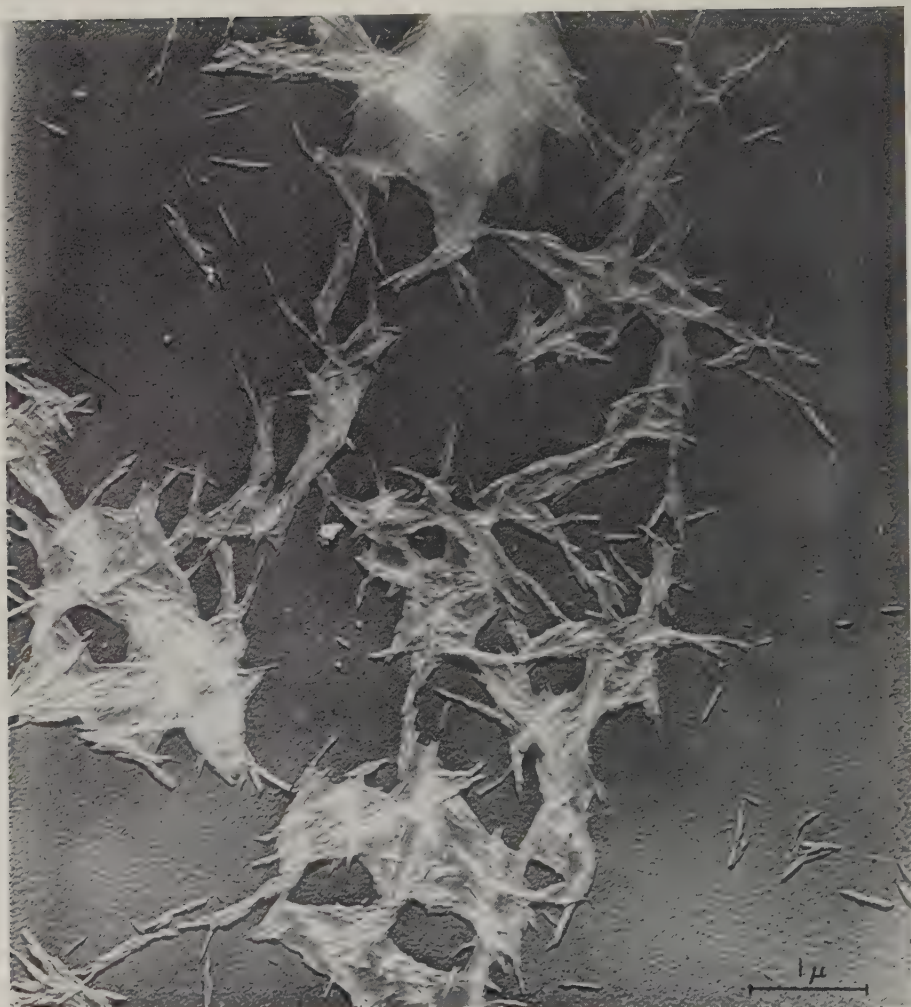


FIG. 1. Electron micrograph of ramie crystallites from 0.01 *M* phosphate buffer. Samples were not dispersed by any vibratory procedure. $\times 25,000$.

of both the extinction angle, χ , and the birefringence increment, Δn , became insignificant under these conditions. However, in order to minimize any experimental errors, we have intentionally employed higher concentrations and determined the intrinsic extinction angle, χ_0 , by means of the relation (4)

$$\cot 2\chi = \cot 2\chi_0 + KC$$

at constant rates of shear, where C is the concentration and K is a constant at each rate of shear. The results for ramie suspensions in 0.01 *M* phosphate

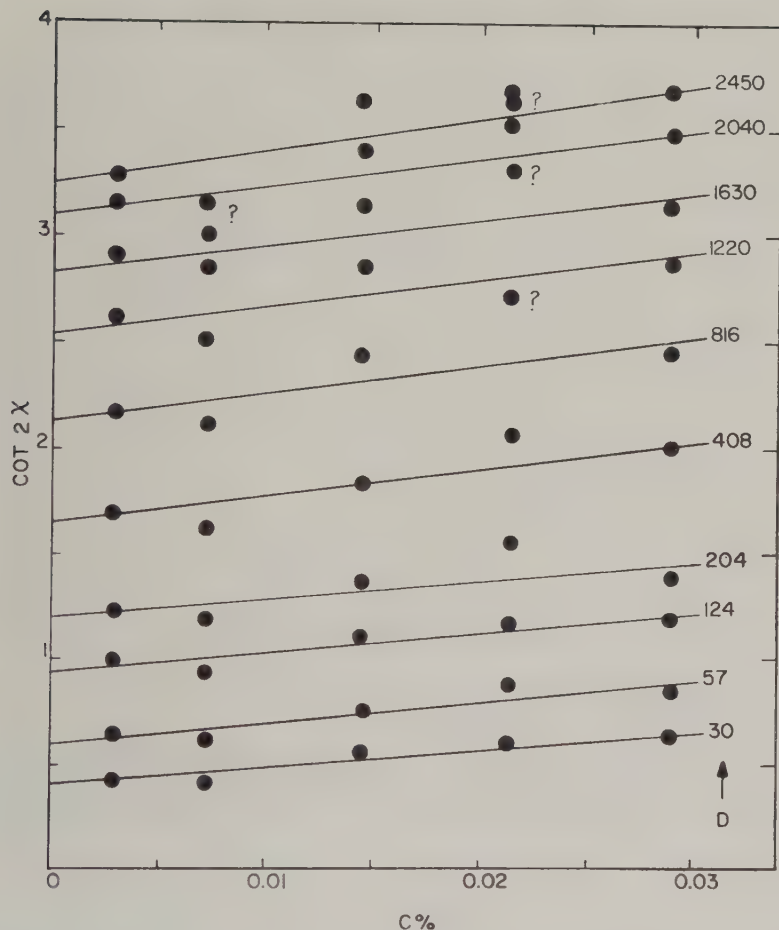


FIG. 2. Extinction angle from flow birefringence measurements plotted as $\cot 2\chi$ vs. concentration.

buffer are plotted in Fig. 2, and the intrinsic χ_0 values are shown in Fig. 3. Also included in the figure are the birefringence increments, $\Delta n/c$, as a function of the rates of shear. Owing to the inherent imperfection in the optical arrangement of the Rao instrument, it is very difficult to obtain precise Δn values and plot them in a manner similar to Fig. 2. However, the shape of the $\Delta n/c$ curve clearly indicates that these aggregates are rigid particles. It is noteworthy also that the "leveling off" intrinsic birefringence for the buffered suspension has the same sign (positive) but greater magnitude than for the unbuffered (1). Since the form birefringence of discs is always negative, this fact suggests that aggregation in the presence of buffers involves a parallel alignment of the particles into an oblong disc

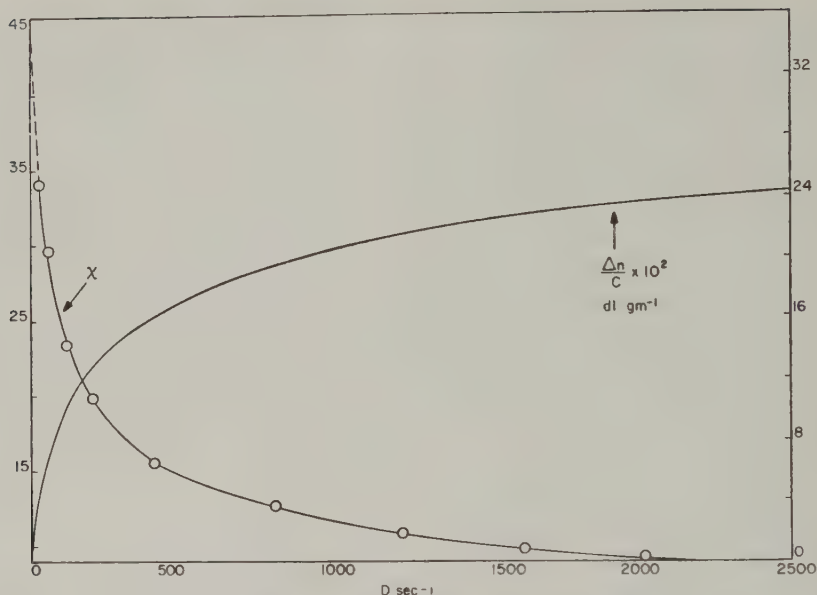


FIG. 3. Intrinsic χ_0 values and birefringence increments, $\Delta n/c$, vs. rate of shear

(cf. Fig. 9). For a random aggregation of particles into a disclike structure a negative birefringence would be predicted.

From the extinction angle data it is also possible to calculate the linear dimensions of the crystallites, provided the correct model is chosen and a rough estimate of the axial ratio is available. This will be done in a later section.

D. Intrinsic Viscosity

Figure 4 shows the shear dependence of the reduced viscosities, η_{sp}/c , at three concentrations. Here τ is the maximum shearing stress at the wall of the capillary and η_0 the solvent viscosity. The pronounced non-Newtonian behavior of these particles in the observed range of shear stresses made it very difficult to extrapolate the data to zero shear. By the use of a previously described method (6) it was possible to determine the intrinsic viscosity at zero shear by making use of flow birefringence data. The results of this computation are also shown in Fig. 4, where the vertical bars represent the ratio of $[\eta]_\tau/F(\chi)$ at each shear used. The ratio is a constant when the correct model is chosen since the relation

$$\frac{[\eta]_\tau}{[\eta]_{\tau=0}} = F(\chi)\alpha, p$$

is different for the oblate and prolate models. Here α is defined as the ratio of the rate of shear, D , to the rotary diffusion constant, θ , and p is the

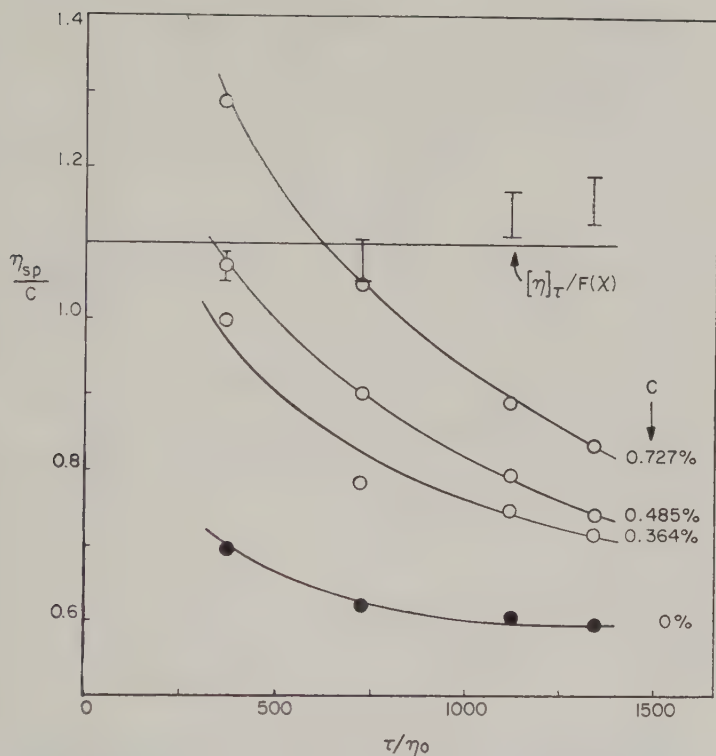


Fig. 4. Reduced viscosity vs. rate of shear at various concentrations. The bars represent the ratio $[\eta]_T/F(X)$.

axial ratio, which becomes an insignificant parameter for highly asymmetric particles. In the present case the oblate model yields roughly a horizontal line, whereas the prolate model results in a relatively steep line with positive slope not shown in Fig. 4. The intrinsic viscosity at zero shear by this extrapolation technique is 1.1 dl./g. The scattering of the vertical bars is attributed to experimental errors, and in all cases the deviations from the horizontal line are less than 5%.

Figure 4 is a good illustration of the impossibility of extrapolating intrinsic viscosities to zero shear when experimental points at low rates of shear are not available. Various extrapolation methods have been proposed among which plots of relative viscosity or its logarithm versus rate of shear appear to be most popular. In Fig. 5 it is shown that neither plot yields a straight line in the present case. The extrapolated curves (dotted lines) are quite arbitrary and involve appreciable error. On the other hand, if straight lines were drawn through the points, the resulting intrinsic viscosities are not in agreement. These remarks are by way of emphasizing the uncertainties which can arise in such extrapolations.

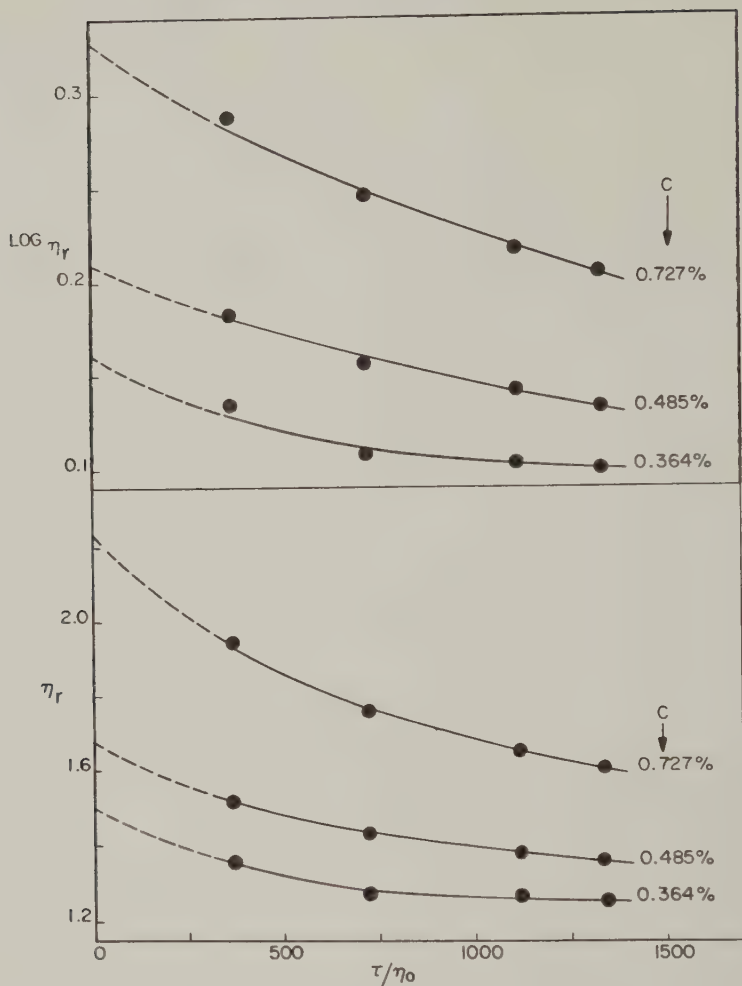


FIG. 5. Relative viscosity, η_r , vs. rate of shear on rectangular coordinate and semi-log scale for different concentrations.

By assuming an equivalent oblate model having a large axial ratio (> 10), the apparent diameter of the aggregates at various rates of shear can be calculated from both the ratios of $[\eta]_\tau/[\eta]_{\tau=0}$ and the extinction angles, χ , using the well-known Perrin equations (7). The results are listed in Table I. Polydispersity of the particles is reflected in the variation of the apparent diameter with rate of shear. The apparent diameters as calculated from both the intrinsic viscosity and flow birefringence are in fair agreement. Strictly speaking, the two methods give different average values for a polydisperse system. The viscosity measurements would be expected to

TABLE I
Apparent Diameters of Equivalent Oblate Ellipsoids

Rate of shear (sec ⁻¹)	Apparent diameter (Å)	
	From flow birefringence	From viscosity
31	6560	—
57	6150	—
122	5790	—
204	5400	—
369	—	5320
408	5120	—
726	—	4340
816	4720	—
1120	—	3890
1220	—	—
1340	—	3770
1630	4520	—
2040	4460	—
2450	4330	—

give a somewhat larger diameter (8) at a given rate of shear; this is not the case in Table I mainly owing to unavoidable experimental errors.

E. Light Scattering

The Zimm-type light scattering envelopes for the crystalline suspension are plotted in Fig. 6. Lack of theoretical treatment for disclike particles makes it impossible to compare the experimental curves with the theoretical values. Consequently, we have only calculated the diameter for a disc from the radius of gyration, noting that for a circular disc the diameter is $2\sqrt{2}$ times the radius of gyration. The intrinsic dissymmetry, $[Z]$ ($=Z_{c=0}$), was determined by plotting $1/[Z - 1]$ against the concentration and extrapolating it to zero concentration. All the pertinent data are listed in Table II.

When colloidal particles possess optical and shape anisotropy, depolarization of the scattered light can occur; this must then be taken into account before the molecular weight is computed. To do so the scattering of a 0.001% solution was compared with that of a Ludox suspension having approximately the same turbidity, using vertically polarized light. Figure 7 shows the reduced intensities at low scattering angles as obtained with the polarizer (in front of the phototube) parallel (H_v) and perpendicular (V_v) to the incident vertically polarized beam. It has been found (9) that a straight line resulted when the reciprocals of H_v or V_v were plotted against $\sin^2(\theta/2)$ for low angles. Thus, the depolarization factor, $\rho_v = H_v/V_v$, was calculated from the intercepts at zero angle. Similar calculations were also

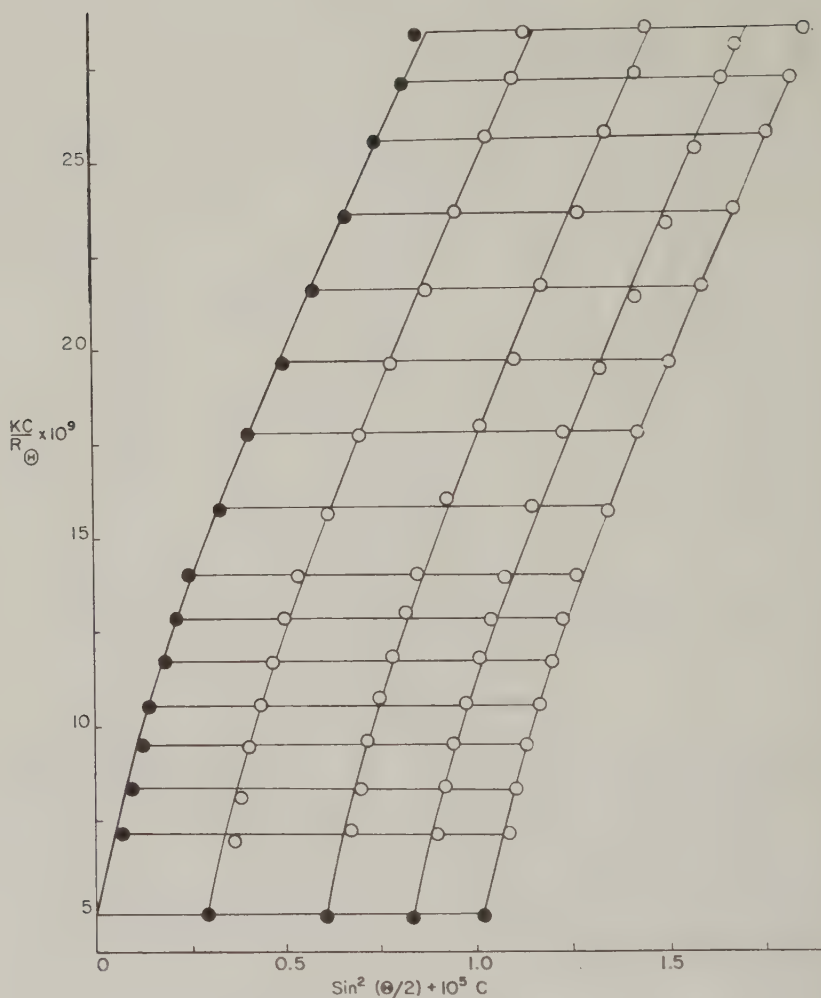


FIG. 6. Zimm plot for buffered suspension of ramie crystallites.

carried out for the isotropic Ludox suspension which was used to correct the inherent instrument errors. Strictly speaking, the ρ_v values should be extrapolated further to zero concentration. However, the error involved in the use of a finite concentration should be quite small (9). The true ρ_v , which is the apparent ρ_v for ramie (0.020) minus that for Ludox (0.005) (background correction), was about 0.015. If we use the Cabannes' formula: $(3 + 3\rho_v) / (3 - 4\rho_v)$ (10), which in the present case was equal to 1.036, the molecular weight as determined from the Zimm plot should be reduced by 3.6%, which is well within the experimental error. (Strictly speaking,

TABLE II

Summary of Molecular and Hydrodynamic Properties of Ramie Crystallites

Molecular weight, M_w	200×10^6
Radius of gyration, r_z	1710 Å
Diameter from light scattering	4800 Å
Intrinsic dissymmetry	2.79
Intrinsic viscosity at zero shear	1.10
$\eta_0\theta/T$ from flow birefringence	0.0003 ($D \rightarrow 0$)
	0.0013 ($D = 2500$)

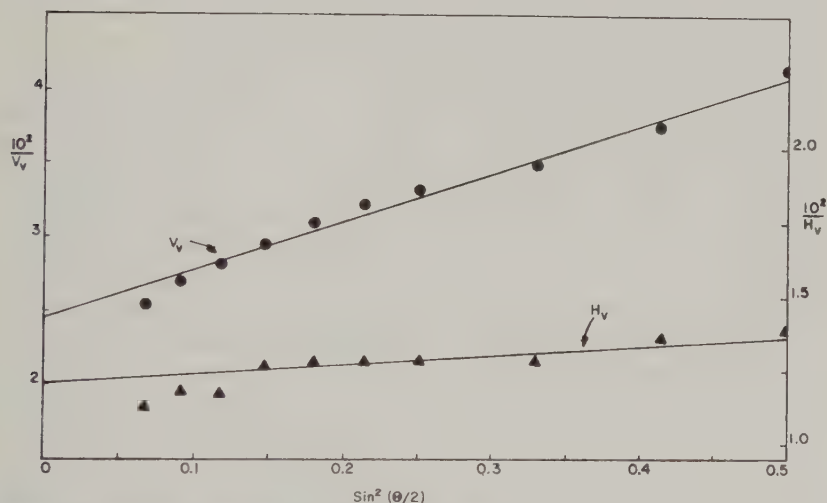


FIG. 7. Reduced intensities for vertically (V_v) and horizontally (H_v) polarized light scattered by dilute buffered suspension of ramie crystallites.

Cabannes' formula is applied only to R_{90} values.) Thus, the depolarization factor was not significant in the case of ramie suspensions.

For very turbid systems such as the one in question the particle size and molecular weight can also be determined by the "absorption-extrapolation" light-scattering method (11), in which turbidity measurements are made as a function of wavelength with a spectrophotometer such as the Beckman Model DU. We have also determined the molecular weight of the buffered ramie suspension by this method, and the result was in reasonable agreement with that derived from the Zimm plot in Fig. 6.

F. Sedimentation

The sedimentation of the ramie crystallites in 0.01 *M* buffer was studied at concentrations of 0.146, 0.073, and 0.049 g./100 ml. The rotational speed was 4000 r.p.m. and the acceleration 1.21×10^6 c.g.s. units. The

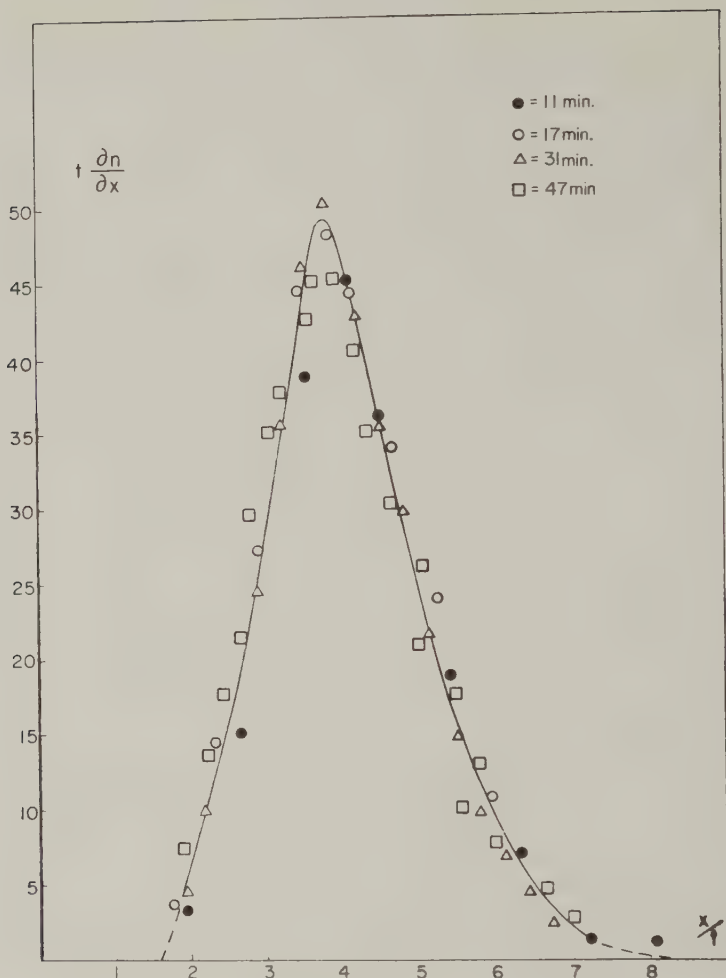


FIG. 8. Distribution of sedimentation constants. The ordinate is equivalent to $c(s)$; and the abscissa represents the sedimentation constant s . Units are arbitrary, $c = 0.073\%$. ● = 11 min.; ○ = 17 min.; △ = 31 min.; □ = 47 min.

velocity of the peak in the diagram was found to be constant at concentrations below 0.07 g./100 ml., being 1.10×10^{-4} cm./sec. From which

$$s = \frac{dx/dt}{\omega^2 x} = \frac{1.10 \times 10^{-4}}{1.21 \times 10^6} = 907 \times 10^{-13} \text{ in c.g.s. units.}$$

It should be noted that this measurement, unfortunately, was performed on a suspension which had been prepared two months prior rather than a few days as was usually the case. It will be seen below that continuous aggregation appears to have occurred over this period.

An interesting feature of the sedimentation data brought to our attention by Prof. Hermans was the unusually sharp distribution of sedimentation constants. Thus for a concentration of 0.073 % a plot of tdn/dx vs. x/t as shown in Fig. 8 is equivalent with the distribution curve $c(s)$ versus sedimentation constant s (12). It is seen that the width at the half maximum height extends over no more than a twofold range of s values. This observation probably reflects the insensitivity of the sedimentation constant to the diameter of the sedimenting discs (13) and suggests a uniformity in the thickness of the proposed aggregates, since it is the mass per unit area which is important in this case.

IV. DISCUSSION

By comparison with the hydrodynamic data for the unbuffered suspensions it is obvious that aggregation, which will be referred to as "secondary," has occurred as a result of the added buffer. The extent of aggregation depended on the amount of added electrolyte. The surprising feature of the foregoing data is that the aggregates behave as oblate rather than prolate ellipsoids, the shape characteristic of the particles in the unbuffered system. The electron micrograph shown in Fig. 1, although taken under poor conditions (buffer was present), nevertheless seems to support the idea of flat "tactoid shape" aggregates as idealized in Fig. 9. About twenty particles with average length of about 1500 Å and average diameters of 100 Å would make up the dimensions shown in Table II. The corresponding particle weight would likewise agree with that derived from light scattering and, as will be shown below, so does that calculated from the hydrodynamic properties. The idea of an ordered aggregate, as proposed here, is entirely in agreement with thermodynamic requirements for the crystallization of rigid particles (14).

It is customary to estimate the axial ratio of ellipsoids from the intrinsic

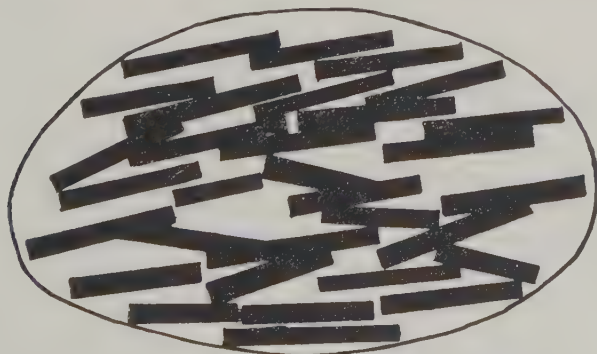


Fig. 9. Idealized tactoid which apparently constitutes the flowing unit in the buffered suspension.

viscosity by means of the equation

$$[\eta] = \frac{\bar{v}\nu}{100}, \quad [1]$$

where $[\eta]$ is in dl. per gram, \bar{v} is the partial specific volume of the particles, and ν is a function of axial ratio which has been tabulated by Simha (15). By taking $\bar{v} = 0.66$ (the partial specific volume of the crystallites (1)) and assuming no hydration, $\nu = 167$, which corresponded to an axial ratio of about 250 for oblate ellipsoids. For diameters in the range of 4000 to 7000 Å (Table I) this yielded a thickness of about 15 to 30 Å, which is of the right order of magnitude (1, 2) for a one-layer aggregate.

A somewhat different treatment of the hydrodynamic data involves the recent hypothesis of equivalent ellipsoids. In principle, by combining intrinsic viscosity with sedimentation-diffusion or flow birefringence it is possible to solve simultaneously for the two unknowns: the equivalent hydrodynamic volume and the axial ratio, without additional assumptions. Thus Scheraga and Mandelkern (16) have derived a delta-function:

$$\delta \equiv \frac{600}{NK} \left(\frac{\eta_0 \theta}{T} \right) [\eta] M = J\nu. \quad [2]$$

Here N = Avogadro's number, k = the Boltzmann constant, η_0 = solvent viscosity, θ = rotary diffusion constant, T = absolute temperature, $[\eta]$ = intrinsic viscosity, M = molecular weight. The quantity $J\nu$ depends only on the axial ratio, p , and its values have been tabulated (16). In principle one can determine the axial ratio unambiguously. Unfortunately, the δ values are extremely insensitive to the variation of axial ratio. For example, for oblate ellipsoids, $\delta = 2.50$ at $p = 1$ and $\delta = 1.60$ at $p = 300$. Consequently, because of the insensitiveness of δ with respect to p it is more practical to use Eq. [2] for the determination of the molecular weight of macromolecules by estimating an axial ratio from the intrinsic viscosity. In the case of ramie, $\delta = 1.60$ ($p = 250$), $[\eta] = 1.10$, and $\eta_0\theta/T = 0.00094$ (for a diameter of 4800 Å from light scattering), which in turn gave a molecular weight value of 200 millions.

It should be noted that the foregoing agreement is probably better than what might normally be expected since the diameter of a disc, as determined from light scattering, is not a weight-average value. Strictly speaking Eq. [2] is applicable only to a monodisperse system because $\eta_0\theta/T$ as determined either by non-Newtonian viscosity or flow birefringence is not well defined in a polydisperse system. In fact, it decreases rapidly with increasing rate of shear owing to the fact that $\eta_0\theta/T$ is inversely proportional to the cube of the particle length or diameter and the latter varies with the applied shear. At present there is no available hydrodynamic method for the determination of the weight-average value of $\eta_0\theta/T$ for a macromolecule

at zero shear. Consequently, any error involved in the determination of the apparent particle length or diameter will cause roughly three times as large an error in the estimated $\eta_0\theta/T$ value. The resultant effect on the molecular weight of the particle calculated from Eq. [2] can be illustrated as follows: if the diameter of the aggregate were taken as 4000, 4500, 5000, and 5500 Å instead of 4800 Å, the corresponding molecular weights would be 125, 178, 243, and 325 millions, respectively. The method can give only an approximate estimate of the molecular weight in a polydisperse system.

It is interesting to apply the equivalent ellipsoid method to the combined sedimentation-viscosity data. In this case a beta-function has been defined (16):

$$\beta = \frac{Ns[\eta]^{1/3}\eta_0}{M^{2/3}(1 - \bar{v}\rho)}, \quad [3]$$

where ρ is the density of the solution and the other terms have the same meaning as above. For oblate ellipsoids of axial ratio 250, $\beta = 2.15 \times 10^6$. Solving for M a value of 7×10^8 is obtained, which is 3.5 times greater than that derived from light scattering. The most likely explanation for this discrepancy is that continued aggregation took place during the two-month storage period at 7°C. between the viscosity and the ultracentrifuge measurements. (All other measurements were made a few days after mixing with buffer.) After a period of six months storage at room temperature, it was observed that the buffered suspensions were completely sedimented.

ACKNOWLEDGMENTS

The authors are most grateful for the interest shown in this work by Professor J. J. Hermans and the assistance of A. M. Rýke. Fig. 1 was provided by Mr. F. F. Morehead.

REFERENCES

1. MARCHESSAULT, R. H., MOREHEAD, F. F., AND KOCH, M. JOAN, *J. Coll. Sci.* **16**, 327 (1961).
2. MUKHERJEE, S. M., AND WOODS, H. J., *Biochim. et Biophys. Acta* **10**, 499 (1953).
3. RÂNBY, B. G., *Discussions Faraday Soc.* No. **11**, 158 (1951).
4. EDSALL, J. T., RICH, A., AND GOLDSTEIN, M., *Rev. Sci. Instr.* **23**, 695 (1952); *J. Am. Chem. Soc.* **80**, 5139 (1958).
5. YANG, J. T., *J. Am. Chem. Soc.* **80**, 1783 (1958); *ibid.* **81**, 3902 (1959).
6. YANG, J. T., *J. Phys. Chem.* **62**, 894 (1958).
7. PERRIN, F., *J. Phys. Radium* **7**[5], 497 (1934).
8. YANG, J. T., Unpublished work.
9. DOTY, P., AND YANG, J. T., Manuscript in preparation.
10. CABANNES, J., AND ROCARD, Y., "La Diffusion Moleculaire de la Lumière." Les Presses Universitaires de Paris, 1929.
11. CASHIN, W. M., AND DEBYE, P., *Phys. Rev.* **75**, 1307A (1949); BILLMEYER, F. W., JR., *J. Am. Chem. Soc.* **76**, 4636 (1954).
12. HERMANS, J. J., AND RÝKE, A. M., *J. Colloid Sci.* **18**, 508 (1958).

13. SCHACHMAN, H. K., "Ultracentrifugation in Biochemistry," p. 245. Academic Press, New York, 1949.
14. FLORY, P. J., *Proc. Roy. Soc. (London)* **A234**, 60 (1956).
15. SIMHA, R., *J. Phys. Chem.* **44**, 25 (1940); MEHL, J. W., ONCLEY, J. L., AND SIMHA, R., *Science* **92**, 132 (1940).
16. SCHERAGA, H. A., AND MANDELKERN, L., *J. Am. Chem. Soc.* **75**, 179 (1953). Similar ideas were earlier advanced by C. Sadron; for a recent review, see SADRON, C., *Progr. Biophys. and Biophys. Chem.* **3**, 237 (1953), in particular, pp. 254-260, inclusive.

FILMS OF MIXED HORIZONTALLY AND VERTICALLY ORIENTED COMPOUNDS¹

Herman E. Ries, Jr., and Donald C. Walker

*Research and Development Department, American Oil Company,
Whiting, Indiana*

Received August 8, 1960; revised December 27, 1960

ABSTRACT

Knowledge of the interaction of horizontally and vertically oriented molecules at interfaces should prove valuable in many areas of surface chemistry. However, little is known about the structure and behavior of mixed films—particularly those in which the components differ widely in structure. Accordingly, we have studied a series of binary mixtures of a horizontally oriented polar polymer with seven different vertically oriented compounds. Observed effects were unexpected.

Pressure-area isotherms for the equiweight binary mixtures of horizontally oriented polyvinyl acetate and the vertically oriented compounds have an inflection point or plateau near the collapse pressure for the polymer alone. Polymer is presumably squeezed out of the monolayer at this pressure. Films of polyvinyl acetate with 1-octadecanol, methyl stearate, or cholesterol collapse near the maximum pressure for the stronger component. Films of the polymer with stearic, *n*-hexacosanoic, *n*-hexatriacontanoic, and 2-hydroxystearic acids collapse at pressures far greater than those for the components.

Electron micrographs of the mixed film of polyvinyl acetate and *n*-hexatriacontanoic acid, transferred from the film balance at low pressures, show wormlike islands of the acid that may reflect the geometry of the polymer molecules. As pressure rises, the islands increase in length and in number per unit area. At high pressures, above the collapse pressure for the polymer, characteristic amorphous masses appear that must be the polymer squeezed out of the monolayer.

INTRODUCTION

An understanding of the interaction of horizontally and vertically oriented molecules at interfaces should broaden the usefulness of many areas of surface chemistry. However, little is known about the structure of monomolecular films or monolayers—particularly those of mixtures. Selected aspects of certain mixed monolayers have received attention (1-7), but essentially no systematic work has been done with mixtures of components differing widely in structure.

Basic information is needed on molecular geometry and orientation,

¹ Presented in part before the Division of Colloid Chemistry at the 136th Meeting of the American Chemical Society, Atlantic City, September 14, 1959.

cohesion and adhesion, and the location and strength of polar groups. Pressure-area isotherms obtained on the film balance provide the cross-sectional area per molecule, film thickness, collapse pressure, and compressibility. Electron microscopy supplies additional details on film structure, changes on compression, and the nature of collapse; it relates the properties of films on liquids to those on solids. Combined film-balance and electron-microscope techniques have been used recently in our laboratory for the study of monolayers (8-10).

With remarkable results, these techniques have now been applied to binary mixtures of horizontally and vertically oriented compounds. The horizontally oriented component under study was polyvinyl acetate; its film properties are well-defined and highly reproducible (11). Seven vertically oriented compounds that differ in hydrocarbon geometry or polar group were used in binary mixtures with the polymer. Three of these were fatty acids that differ only in chain length: stearic (18 carbons), *n*-hexacosanoic (26 carbons), and *n*-hexatriacontanoic (36 carbons). A fourth, 2-hydroxystearic acid, has the same chain length as stearic acid but a stronger polar group. Methylstearate and *n*-octadecanol have the same chain length as stearic acid but weaker polar groups that differ in size. Cholesterol has a single hydroxy polar group but a much more complex and bulky hydrocarbon geometry than the simple *n*-octadecanol.

EXPERIMENTAL

Pressure-area isotherms were determined for the seven binary mixtures and their components. Samples of representative films, before and after collapse, were transferred from the film balance to solid supports and examined in the electron microscope. Basic apparatus and techniques have been described (7, 9, 12).

Materials

All film-forming materials were of the highest purity available. The polyvinyl acetate was prepared by R. A. Ahlbeck at the University of Michigan; it is an amorphous material of density 1.19 g./c.c. and it has a viscosity-average molecular weight of about one million. Special preparations of stearic acid, m.p. 69.61°C., and methylstearate, m.p. 37.70°C., were obtained from H. J. Harwood of the Research Division of Armour & Company; *n*-hexatriacontanoic acid (36 carbons), m.p. 99.46°C., was supplied by V. P. Kucski of the C. P. Hall Company; *n*-hexacosanoic acid (26 carbons) was supplied by R. J. Meyer of the University of Wisconsin; and 2-hydroxystearic acid was specially prepared by the Aldrich Chemical Company. The 1-octadecanol, Eastman Kodak white-label grade, was recrystallized by S. P. Malchick of our laboratory. Cholesterol was obtained from L. C. King of Northwestern University.

Volatile solvent for spreading the film-forming compounds was C.P. benzene twice distilled to remove nonvolatile impurities. Film-balance experiments with the benzene alone showed that remaining impurities were negligible. The two principal compounds of this study, polyvinyl acetate and *n*-hexatriacontanoic acid, are effectively insoluble in *n*-hexane.

Ion-exchange water used as the substrate in the trough had a pH of 6 and a specific conductivity of about 0.5 micromho. Careful preparation of the ion-exchange column and thorough testing of the water surface on the film balance insured freedom from significant capillary-active contamination. Recent experiments in our laboratory on water distilled twice in quartz agree with work performed on the ion-exchange water, although under some conditions others have observed differences (13).

Film-Balance Measurements

The film balance used consists essentially of a long shallow trough that contains water on which the films are spread, a float and torsion-wire system for measuring surface pressure, and a large brass barrier for compressing the film (1, 2, 7). The apparatus is housed in a double-walled cabinet; pressure and area adjustments, as well as transfer of film samples, are made with the cabinet closed. The entire apparatus stands on a 3000-pound concrete base, which reduces vibration and improves reproducibility—particularly that of film collapse. A glass weighing pipet (7) is used for spreading the film-forming materials dissolved in a few drops of volatile solvent.

Extreme care was taken to prevent contamination. Before each experiment, all parts of the film balance that come in contact with water were thoroughly cleaned. Teflon-coated troughs were cleaned in a vapor degreaser constructed for the purpose (12). Wax-coated troughs were cleaned by removing the high-melting paraffin wax and recoating. After the trough was filled with deionized water, the water surface was swept many times with small barriers and the film was spread. The area of the film was reduced in small decrements, and surface pressures were read—usually at intervals of 2 minutes. The film was compressed to collapse, as indicated by a constant or falling pressure.

For this series of experiments, temperature differences between 24° and 26°C. had little effect on the films studied. During individual experiments at 25° ± 1°C., temperature rarely varied more than 0.1°C.

Electron Microscopy

Electron micrographs were obtained with an RCA Type EMU electron microscope. Standard 200-mesh screens, 1/8 inch in diameter, were covered with a thin sheet of collodion. Monolayer samples were transferred directly to the collodion-covered supports; the samples were then shadowcast with

gold-palladium alloy at an angle of about 15° and in the direction indicated by the arrows on the micrographs. Shadows appear as light areas. The monolayers under study are not visible without shadowcasting because their density to the electron beam is not sufficient.

Although several transfer techniques (9) have given similar results in our laboratory, the vertical-plate technique was used for most transfers of monolayer samples. In this technique, electron-microscope screens are sandwiched between a small glass plate and the collodion film. A deep well built into the shallow trough near the float is large enough to accommodate several plates, each of which holds six rows of four screens. A low-pitch vertical screw with a variable-speed motor drive raises the plate slowly and smoothly through the monolayer, as in the Langmuir-Blodgett method for transferring films to solid surfaces (14). Constant pressure is maintained by another motor drive that moves the main barrier and reduces the surface area; representative transfer is thus approached.

One source of strain in transfer is evaporation of the thin film of water from between the monolayer and the collodion. This strain is believed to be minor, because evaporation is slow and especially because most of the water probably escapes through holes in the collodion. Our experiments with a horizontal-plate technique, in which the collodion contacts the monolayer directly, indicate that the water film in vertical-plate transfer does not interfere.

Monolayer distribution in the micrographs may not warrant quantitative treatment (9). Strains that occur in transfer may disturb the samples. However, four widely different transfer techniques reproduce the main features of the micrographs. Despite difficulties, the sequence of micrographs undoubtedly parallels a similar sequence of changes during compression of the film on water.

PRESSURE-AREA ISOTHERMS

In Fig. 1, pressure-area isotherms are shown for stearic acid and polyvinyl acetate, for duplicates of their equiweight mixture, and for a calculated average based on simple additivity of areas. For the mixture, reproducibility is excellent—as has also been shown for the individual components.

The isotherm for the monolayer of stearic acid alone (7) gives an extrapolated area of 0.43 square meters per milligram ($\text{m}^2/\text{mg.}$) or 20 square Angstroms (\AA^2) per molecule. The monolayer has a thickness of about 25 \AA , a collapse pressure of 42 dynes per centimeter, and a compressibility of 0.0019. Compressibility is the change in area with pressure:

$$\frac{a_0 - a_1}{a_0 f_1},$$

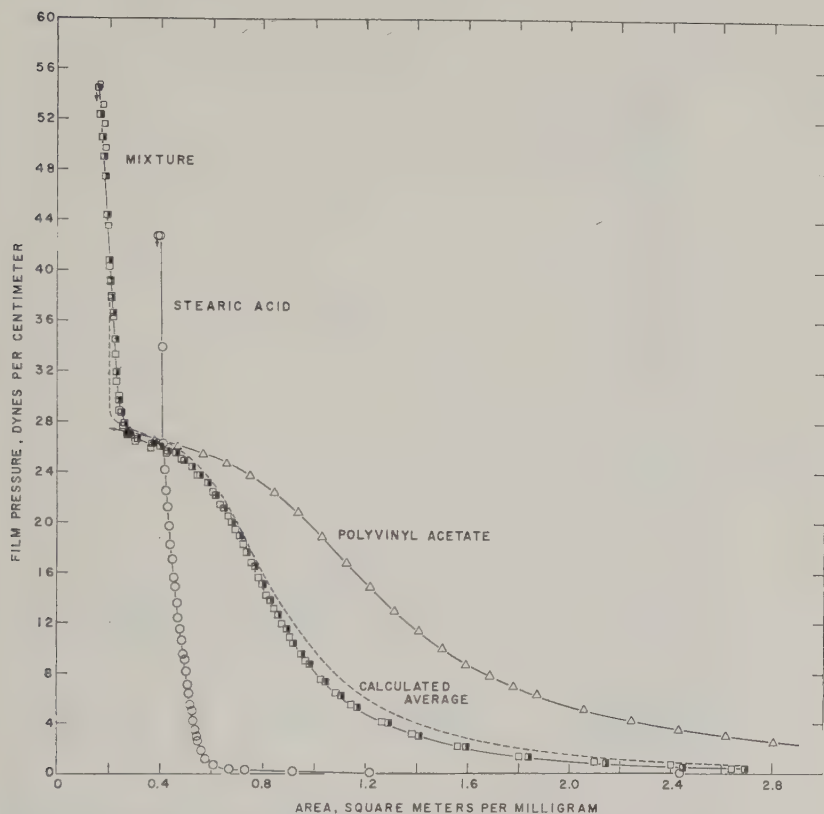


FIG. 1. Pressure-area isotherms for stearic acid, polyvinyl acetate, and an equilibrium mixture.

where a_0 is the extrapolated area at zero pressure and a_1 is a smaller area at pressure f_1 . Compression-expansion isotherms for stearic acid normally show marked hysteresis.

The isotherm for polyvinyl acetate gives an extrapolated area of 1.9 m.²/mg. or 27 Å² per monomer unit (15–19). This area corresponds to a film thickness of about 5 Å, which establishes horizontal orientation for the polymer molecules. Schematic drawings of the polymer and the stearic acid molecules at a water-air interface are shown in Fig. 2. Compressibility of the polymer film is 0.0252. Collapse occurs gradually at about 25 dynes/cm.—a high pressure for a film of horizontally oriented molecules.

The film of polyvinyl acetate shows no hysteresis on compression and expansion; moreover, the response to compression and expansion is *unusually rapid*. Complete compression and complete expansion can be performed within a few minutes, with all points falling on the equilibrium isotherm as

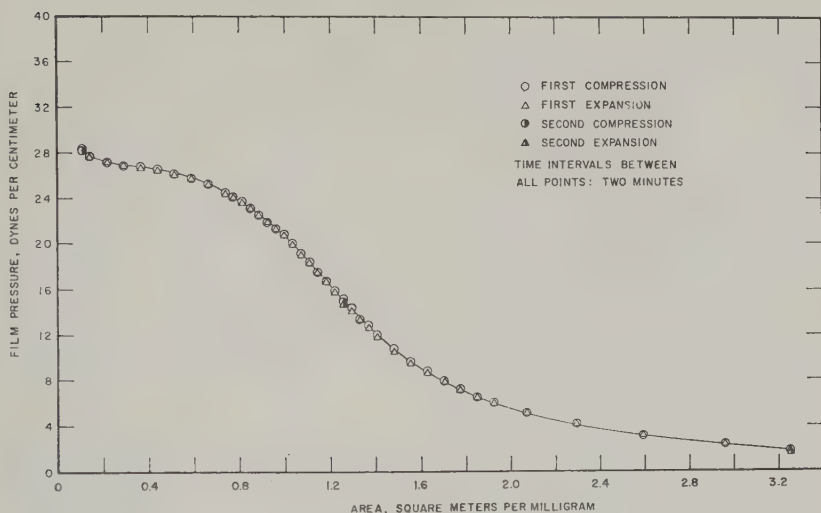


FIG. 3. Compression-expansion isotherms for polyvinyl acetate.

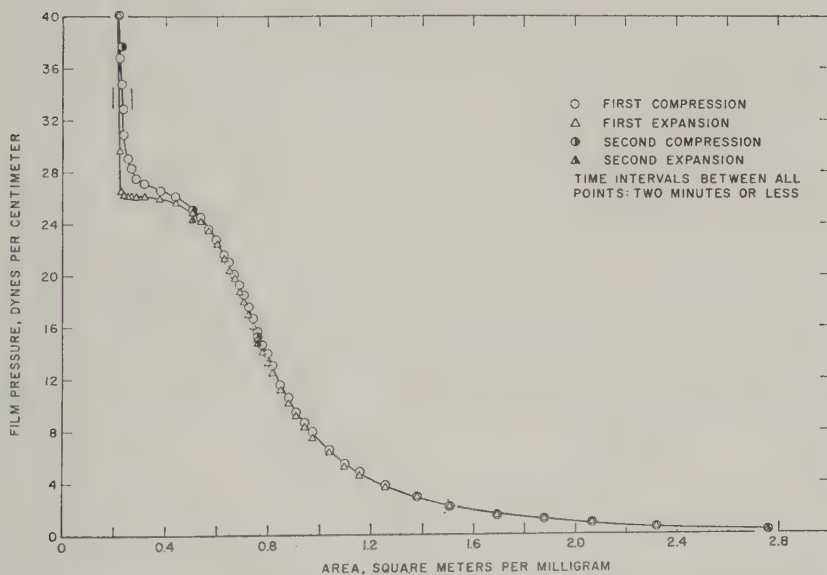


FIG. 4. Compression-expansion isotherms for an equiweight mixture of stearic acid and polyvinyl acetate.

acetate facilitates reversibility; monolayers of stearic acid alone normally expand extremely slowly. The reversibility of the mixed film precludes the possibility that significant chemical change takes place during the compression.

TABLE I
Collapse Pressures for Equiweight Binary Mixtures and Components
 (Dynes per cm.)

	Alone	Mixed with PVAc
Polyvinyl acetate (PVAc)	23	—
Stearic acid	42	55
<i>n</i> -Hexacosanoic acid	58	68
<i>n</i> -Hexatriacontanoic acid	58	70
2-Hydroxystearic acid	57	69
Methyl stearate	36	41
1-Octadecanol	42	39
Cholesterol	42	38

Films of binary mixtures of the polymer with other long-chain acids also give high collapse pressures as listed in Table I. A detailed study was made on the equiweight mixture of polyvinyl acetate and *n*-hexatriacontanoic acid; as apparent in Fig. 5, the contour of the isotherm is similar to that for the mixture with stearic acid. Equiweight binary mixtures of polyvinyl acetate with *n*-hexacosanoic and 2-hydroxystearic acids give similar results, including high collapse pressures. However, binary mixtures of the polymer with 1-octadecanol, methyl stearate, and cholesterol give collapse pressures close to those obtained without the polymer.

Isotherms for all mixtures studied have plateaus near 25 dynes/cm.; at this pressure polymer is presumably squeezed out of the mixed monolayers. With the four acids, however, enough polymer may remain to maintain a polymer monolayer under or intimately associated with the carboxyl groups. Stability may result from hydrogen bonding between free carboxyl groups and acetate groups. Film structure may be tantamount to a fatty-acid monolayer on top of a polyvinyl acetate monolayer. The polar, bulky, amorphous polymer may interfere with the folding and structured collapse of the fatty-acid layer (9). Interaction of the acetate groups of the polymer with hydroxyl and other ester groups appears slight.

ELECTRON MICROGRAPHS

Electron-microscope studies have already provided much information on the structure and behavior of monolayers of vertically oriented molecules (9, 10, 21). Because horizontally oriented polyvinyl acetate is beyond the limit of resolution of the electron microscope, direct observation of the polymer monolayer is precluded. Electron micrographs of the mixed films transferred at low pressures show only the vertically oriented component. However, micrographs of samples transferred at high surface pressures clearly show large bulbous masses that must be bulk polymer squeezed out of the monolayer.

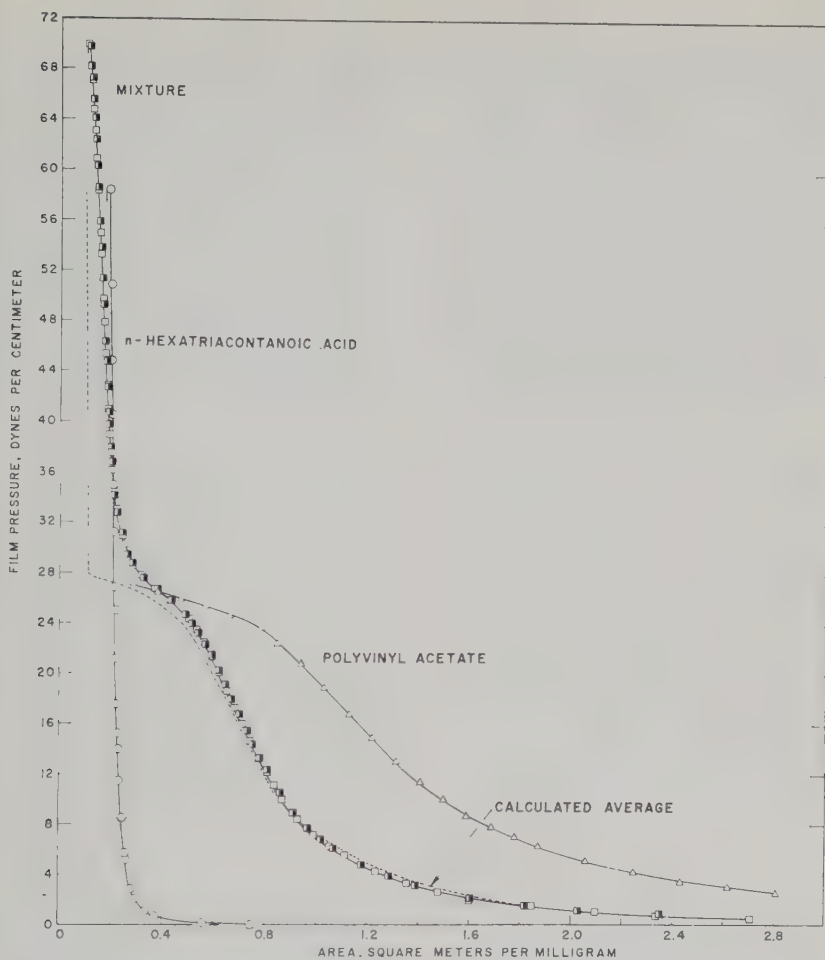


FIG. 5. Pressure-area isotherms for *n*-hexatriacontanoic acid, polyvinyl acetate, and an equiweight mixture.

In preliminary studies, film samples of the equiweight mixture of stearic acid and polyvinyl acetate were transferred at 30 dynes/cm., and after collapse as shown in Fig. 6. At 30 dynes/cm., which is above the plateau region where the polymer film presumably collapses, amorphous bulbous masses of the polymer are apparent. These masses are unlike anything observed before in our laboratory and are presumably characteristic of the out-squeezed polymer. A representative sample transferred after final collapse of the mixed film shows thin platelet or ribbon-like structures in addition to the thick amorphous masses. Such platelets are typical collapse structures of the long-chain fatty acids (9).

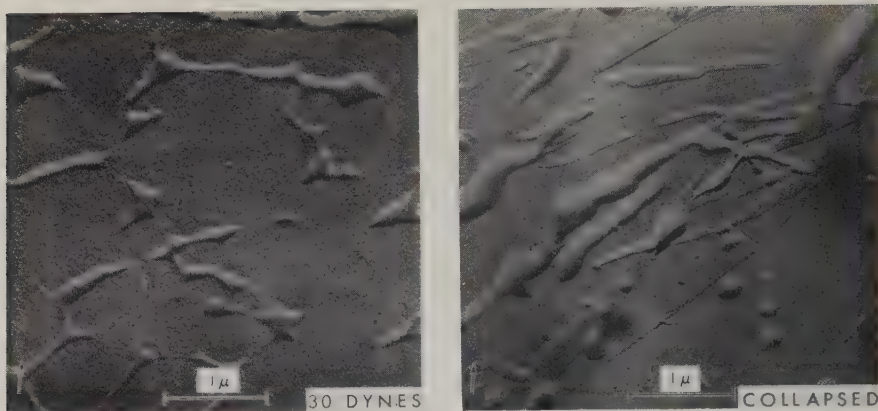


FIG. 6. Electron micrographs of equiweight mixture of stearic acid and polyvinyl acetate.

Films of an equiweight mixture of *n*-hexatriacontanoic acid and polyvinyl acetate have been examined in more detail. The length and vertical orientation of the longer hydrocarbon chain greatly facilitate electron-microscope study.

For comparison, micrographs of samples of *n*-hexatriacontanoic acid alone are shown in Fig. 7. At 15 dynes/cm., the monolayer islands are irregular in size and shape. At 20 dynes/cm., the monolayer becomes the continuous phase; the "bare" portions are now discontinuous. The ratio of covered to uncovered area increases at 25 dynes/cm., as one would expect. At 40 dynes/cm., large homogeneous areas of continuous monolayer are observed. After collapse, long, thin platelets appear; they are about 100 Å or two molecules thick, and they rest on a continuous monolayer substrate (9).

Micrographs of the mixed film of *n*-hexatriacontanoic acid and polyvinyl acetate transferred at six different pressures are shown in Fig. 8. Again, the monolayer structure of the polymer can not be seen, but the visible geometry of the acid portion may well reflect the structure and behavior of the polymer.

At low pressures, few typical islands of the acid are found, but many long structures are observed that are narrow, flat, and curved. At 5 dynes/cm., such wormlike monolayer islands are widely separated, presumably by the invisible intervening polymer. These curving structures may reflect the geometry of the linear polymer alongside or beneath the fatty acid. As surface pressure rises, the islands increase in length and number per unit area, but maintain their wormlike structure. Such longer structures are shown at 10 dynes/cm. At 25 dynes/cm., consolidation is apparent in the

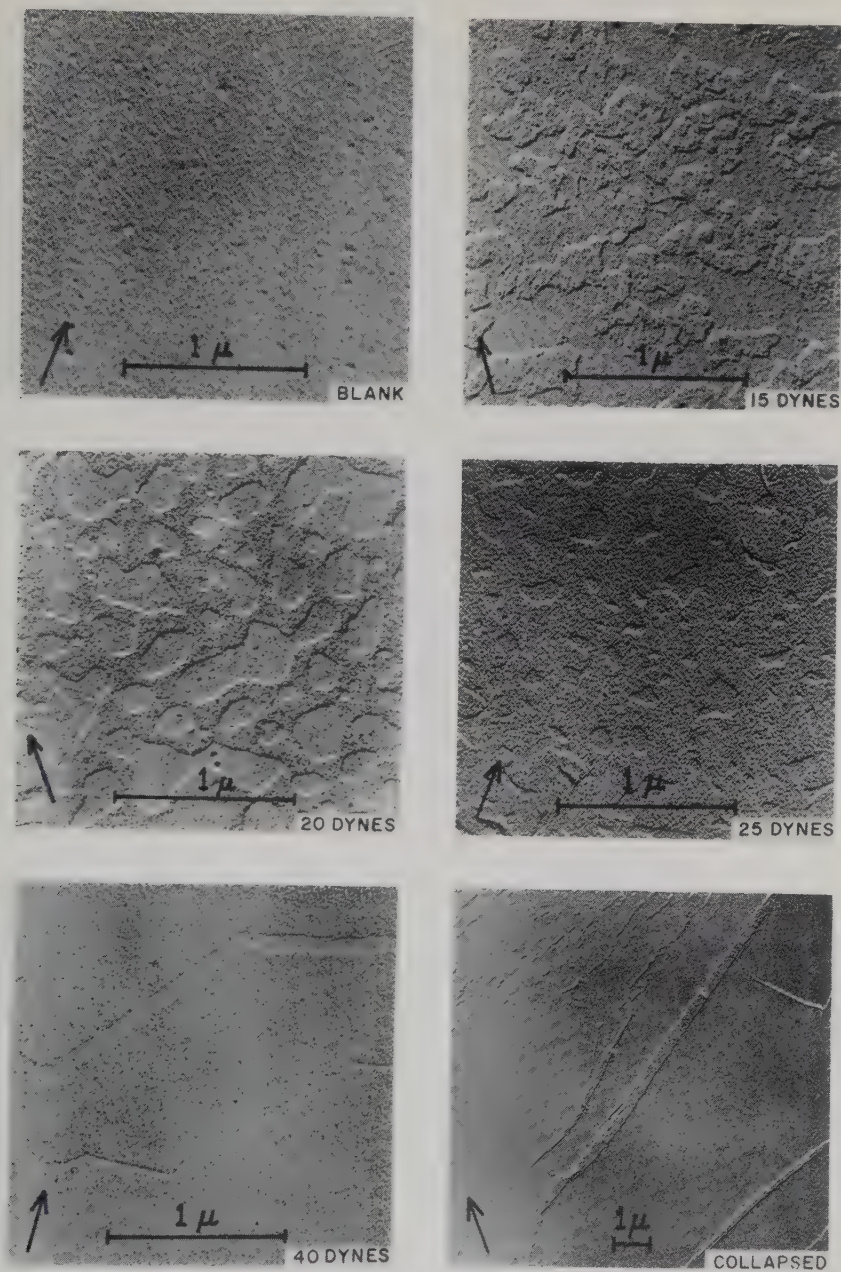


FIG. 7. Electron micrographs of monolayers of *n*-hexatriacontanoic acid.

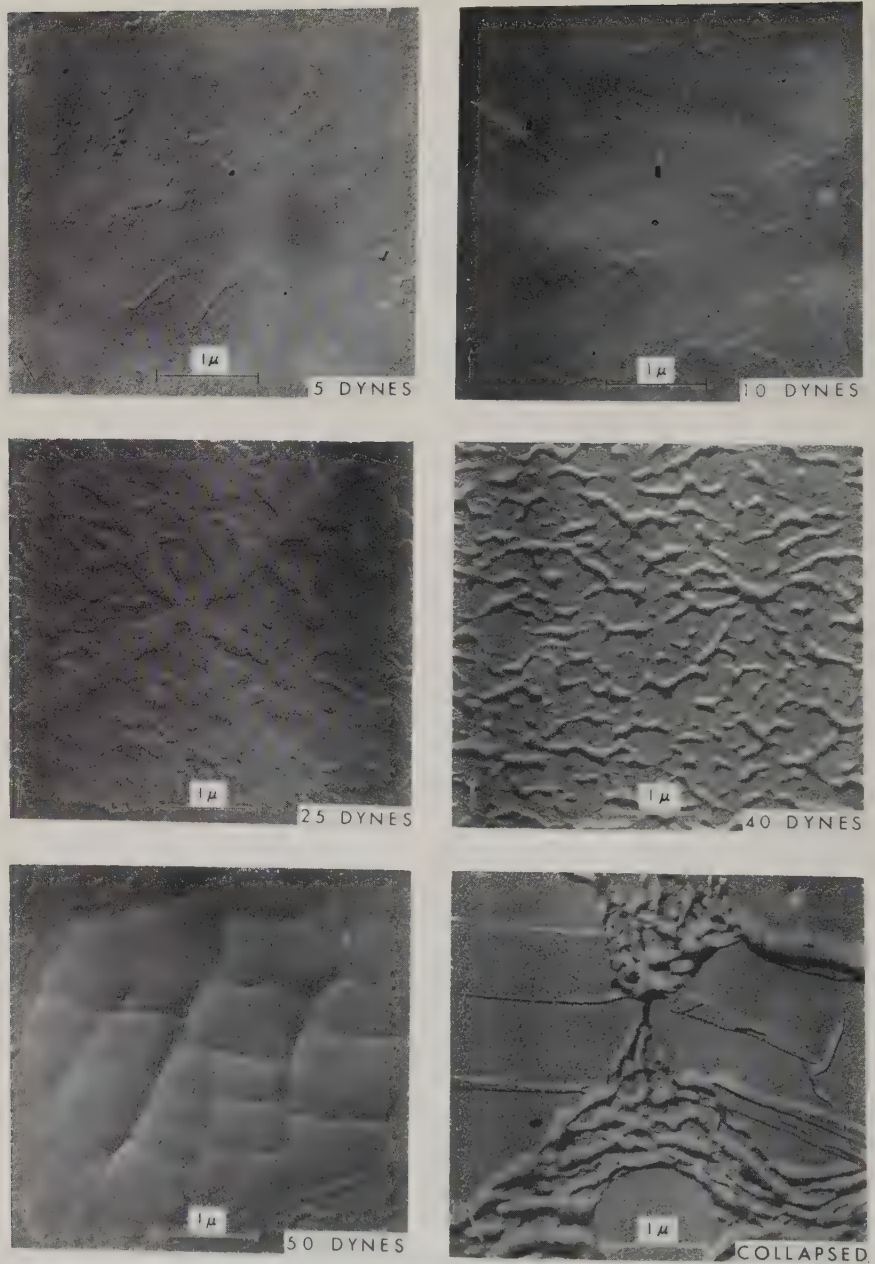


FIG. 8. Electron micrographs of equiweight mixture of *n*-hexatriacontanoic acid and polyvinyl acetate.

large center cross; the smooth curving contours of its branches are characteristic of the mixture and widely different from those of the acid alone.

At higher pressures, above the collapse pressure for polyvinyl acetate alone but below that for the mixture, amorphous bulbous masses again appear. At 40 dynes/cm., these masses are densely packed. In many cases, a monolayer of the acid apparently covers these outcroppings. Also, quilt-like structures are found in which the polymer appears to push up from below; cracking at the seams of the quilt is seen at 50 dynes/cm. After final collapse, platelet structures typical of the collapsed film of the acid are observed, in addition to the large masses of the polymer.

The micrographs of Fig. 8 apparently reflect the long narrow curving geometry of the polymer. They show that close packing of the fatty-acid islands is postponed in the presence of the polymer. Above the collapse pressure for the polymer alone, outqueezing of polymer from the monolayer is clearly demonstrated. Because the polymer is polar, bulky, and amorphous, it may postpone and interfere with the consolidation, folding, and structured collapse of the fatty-acid layer.

CONCLUSION

The study of mixed monolayers by combined film-balance and electron-microscope techniques has revealed unexpected properties for mixtures of vertically and horizontally oriented components. Many related mixtures now warrant detailed examination. An understanding of the interaction between large and small molecules of various orientations in thin films should prove valuable, not only in research on fatty-acid type molecules and polymers but also in many broad areas of surface chemistry.

ACKNOWLEDGMENTS

The authors are grateful to R. A. Ahlbeck, R. L. Burwell, and W. A. Kimball for helpful suggestions, and to Joseph Gabor, Bernard Girman, and Norman Isaacs for valuable assistance in the experimental work.

REFERENCES

1. ADAM, N. K., "The Physics and Chemistry of Surfaces," 3rd ed. Oxford University Press, Oxford, 1941.
2. HARKINS, W. D., "The Physical Chemistry of Surface Films." Reinhold Publishing Corporation, New York, 1952.
3. SCHULMAN, J. H., AND RIDEAL, E. K., *Proc. Roy. Soc. (London)* **B122**, 29 (1937).
4. GODDARD, E. D., AND SCHULMAN, J. H., *J. Colloid Sci.* **8**, 309, 329 (1953).
5. SHERESHEFSKY, J. L., AND WALL, A. A., *J. Am. Chem. Soc.* **66**, 1072 (1944).
6. SOBOTKA, H., AND ROSENBERG, S., *J. Colloid Sci.* **5**, 581 (1950).
7. RIES, H. E., JR., AND COOK, H. D., *J. Colloid Sci.* **9**, 535 (1954).
8. RIES, H. E., JR., AND KIMBALL, W. A., *J. Phys. Chem.* **59**, 94 (1955).
9. RIES, H. E., JR., AND KIMBALL, W. A., "Proceedings of the Second International

- Congress on Surface Activity," Vol. 1, p. 75. Butterworths Scientific Publications, London, 1957.
10. RIES, H. E., JR., AND KIMBALL, W. A., *Nature* **181**, 901 (1958).
 11. RIES, H. E., JR., AHLBECK, R. A., AND GABOR, J., *J. Colloid Sci.* **14**, 354 (1959).
 12. COOK, H. D., AND RIES, H. E., JR., *J. Phys. Chem.* **60**, 1533 (1956).
 13. GAINES, G. L., JR., *J. Phys. Chem.* **63**, 1322 (1959).
 14. BLODGETT, K. B., AND LANGMUIR, I., *Phys. Rev.* **51**, 964 (1937).
 15. CRISP, D. J., *J. Colloid Sci.* **1**, 49 (1946).
 16. BENSON, G. C., AND MCINTOSH, R. L., *J. Colloid Sci.* **3**, 323 (1948).
 17. HOTTA, H., *J. Colloid Sci.* **9**, 504 (1954).
 18. LLOPIS, J., AND REBOLLO, D. V., *J. Colloid Sci.* **11**, 543 (1956).
 19. SCHICK, M. J., *J. Polymer Sci.* **25**, 465 (1957).
 20. COOK, H. D., AND RIES, H. E., JR., *J. Am. Chem. Soc.* **81**, 501 (1959).
 21. RIES, H. E., JR., COOK, H. D., AND LOANE, C. M., "Symposium on Steam Turbine Oils," p. 55. Special Technical Publication No. 211, American Society for Testing Materials, Philadelphia, Pennsylvania, 1957.

DEVELOPMENT OF CHARGE IN LOW CONDUCTIVITY LIQUIDS FLOWING PAST SURFACES: A THEORY OF THE PHENOMENON IN TUBES

Jerome Gavis and Ihor Koszman

*Department of Chemical Engineering, The Johns Hopkins University,
Baltimore 18, Maryland*

Received September 6, 1960

ABSTRACT

The phenomenon of charge generation in low conductivity liquids as they flow past surfaces is described. A brief review and critique of theories previously proposed to explain the observations is given. A new, general formulation which may be particularized to specific situations is developed for the phenomenon in tubes. The equations developed are solved for the special case of uniform velocity profile and the solution is compared with previous theories. It is shown to be the same as the solution for very low conductivity and agrees in form with reported experimental observations. Several predictions are able to be made for higher conductivities from the equations, and these are shown to agree with observation.

Several electrokinetic phenomena at solid-liquid interfaces with relative motion between the phases have been extensively studied and are comparatively well understood. Summaries of the experimental observations and the theories of electroosmosis, electrophoresis, and the streaming potential in systems where the liquid phase is relatively conductive and of high dielectric constant, such as a dilute aqueous solution of an electrolyte, may be obtained in the standard references (1, 2).

An electrokinetic effect less extensively studied, for which there has been no adequate theoretical explanation, is the generation of charge in low conductivity, low dielectric constant liquids, such as hydrocarbons, when they flow past solid surfaces. The effects of charge generation in pipes and pipelines carrying petroleum products have been thought responsible for many otherwise unexplainable explosions and fires in refineries and tankers. Further investigation of this phenomenon is thus important not only in order to gain further insight into the structure of natural phenomena but also in technical applications where understanding may lead to methods of control with resulting saving of life and property.

A. THE PHENOMENON

When a liquid of low conductivity flows in a tube there appear in the liquid free electric charges, positive or negative depending upon the par-

ticular situation, which are carried along by the liquid. Simultaneously, charges of opposite sign appear on the surface. When the liquid is run into a storage tank the charges will accumulate and may raise the potential in the tank to a high enough level to cause spark discharge. Should the volatility of the liquid be in the correct range to provide an explosive mixture with the air above it an explosion and fire can occur. How the charges, once generated, accumulate and cause trouble will not be discussed here. A review of fundamentals and a description of an experimental program which explored the processes of charge accumulation and discharge has been given by Klinkenberg and van der Minne (3), together with graphic descriptions of how explosions occur when petroleum products are piped into tanks.

The charge generation or "electrification" effect appears to have been recognized as long ago as 1913, when Dolezalek (4) described the electrification of benzene and ether in metal pipes. Since then reports on observations and studies of the phenomenon have been published by Russig (5), Brüninghaus (6), Nitka (7), Mackeown and Wouk (8), Ernsberger (9), Keller and Hoelscher (10), Hampel and Luther (11), Rutgers, de Smet, and de Myer (12), Klinkenberg and van der Minne (3), and Boumans (13).

Unfortunately there is much disagreement among the various investigators concerning the observations. This was caused by failure to recognize the difficulties inherent in obtaining good electrokinetic data by some of the investigators. Others failed to define their systems adequately.

On the other hand, one may extract from all or most of the work reported a common core of observations upon which to base a description of the phenomenon:

1. A pure liquid, presumably of zero conductivity, will not electrify. Addition of solutes which increase the conductivity of a liquid induces charge generation so that the generation rate appears to increase with increasing conductivity. At some conductivity, however, the generation rate reaches a maximum and then decreases so that no electrification at all is noticed with such relatively highly conducting liquids as "conductivity water." The chemical nature of the solute may affect the generation rate, but not appreciably (5, 6, 9, 11, 13).

2. Flow of the liquid against a surface is necessary. In laminar flow the rate of charge generation is comparatively small; it is larger for turbulent flow. In tubes the rate depends upon flow velocity, in some cases approximately proportionally, in others to the one and one-half power or to the square power, and in still others in a more complicated manner (3, 4, 6, 7, 8, 10, 12, 13).

3. The nature of the surface affects the generation rate. Metals give the highest rate, with comparatively small differences between different metals. Electrification in glass, plastic, and rubber tubes occurs also. With respect to the small currents observed these act as conductors. In plastic

tubes, at least, it has been demonstrated that there is a change in the tube surface and in the liquid composition associated with charge generation. The sign of the charge may be positive or negative, depending upon the nature of the impurities in the liquid and the nature of the surface (4, 6, 8, 10, 13).

4. The generation rate in tubes depends upon tube length proportionally at most, with decreasing dependence as length becomes larger. The rate finally becomes independent of length for long tubes (3, 7, 8, 9, 13).

5. Charge may be generated continuously. There is one report of decrease of generation rate with time which is probably a transient effect, since the times for the experiments were comparatively short, and another where a true transient is superimposed on the steady generation (3, 6, 9, 13).

6. In this summary no magnitudes have been given since direct comparison between various authors cannot be made. To give the reader some feeling for the magnitudes involved, however, the conductivities where generation has been reported ranged from 10^{-10} to $10^{-15} \Omega^{-1} \text{ cm.}^{-1}$. Above about $10^{-12} \Omega^{-1} \text{ cm.}^{-1}$ the rate began to decrease until at about $10^{-9} \Omega^{-1} \text{ cm.}^{-1}$ the rate became immeasurably small. The currents measured from tube to ground were of the order of 10^{-9} to 10^{-14} ampere, and the charge densities in the liquid 10^{-5} to 10^{-12} coulomb/cm³. The potentials built up on receivers were as much as 2000 volts. Tube diameters ranged from a millimeter to several inches, lengths from a few centimeters to 20 feet or more, flow conditions from laminar to turbulent at Reynolds numbers as high as 30,000.

B. EARLIER THEORIES

The first attempt to explain electrification was made by Cooper (14), who invoked the classical theory of the streaming potential, applying it directly to hydrocarbon electrification both in laminar (15) and in turbulent flow (16, 17) in tubes. Cooper, however, did not consider the large effect decrease in conductivity has on diffusing the charge distribution in the electric double layer. His theory is strictly applicable to higher conductivity liquids than most hydrocarbon solutions, therefore.

This was recognized by Rutgers, de Smet, and de Myer (12). They determined experimentally that in liquids the conductivity of which was about $10^{-12} \Omega^{-1} \text{ cm.}^{-1}$ the charge distribution extended far enough from the tube wall to be influenced by turbulence. Boumans (18) discussed the effects of conductivity and turbulence. Although he made several rather arbitrary assumptions, apparently conditioned by a knowledge of what the results should be, he extended Cooper's theory to low conductivities.

The theories based on the classical double layer, however, are at variance with observation. First, these theories allow for no dependence of charge generation rate on tube length. Second, if the double-layer zeta potential is assumed to increase with ion concentration and thus with conductivity,

these theories predict only an increase in generation rate with conductivity. How the generation rate goes through a maximum and then decreases with increasing conductivity is not explained. The fact that the theories, except that of Boumans, predict proportionality of generation rate to flow velocity whereas dependences up to the square of the flow velocity have been reported may also be cited. Finally, the classical double-layer theories are inconsistent with the observation that charge may be generated continuously. In these theories the ionic charge in the double-layer distribution is sheared away by the flowing fluid and collects in a receiving vessel. Since only a small quantity of charge is needed to raise the vessel's potential considerably one aspect of the phenomenon is explained. But once the ionic charge has been removed generation should cease.

This was realized by Boumans, who introduced a "wall current," i.e., charge which entered the fluid from the wall, as an appendage to his theory. The nature of the wall current was not specified nor were the effects of this current calculated beyond a rough approximation. Hydrodynamic entrance effects and a relaxation effect in which the time to form a double-layer distribution was compared to the residence time of the fluid in the tube were invoked also to explain length dependence. But these were not quantified, and no scheme for quantifying them was presented.

In a theory attributed to G. Schön by Hampel and Luther (11) and described by Klinkenberg and van der Minne (3) the double-layer concept was not used. A wall current of unspecified origin but constant along the length of the tube supplied the charge. Because of the conductivity, however small, there would be a drift of ionic charge back to the wall under the influence of the radial field of the charge. These would discharge in an unspecified manner, constituting a relaxation current. The relaxation current would increase with increasing charge density and therefore with position downstream but would decrease with increased velocity. The net current, therefore, would depend upon axial position and velocity. With the further assumption of highly turbulent flow and uniform radial charge distribution integration of the expression for the net current with respect to tube length yielded an expression for the charge generation rate in terms of the wall current. The wall current was likened to a mass transfer process at high Schmidt number across the laminar sublayer. But only velocity, radius, and length dependence could be obtained since only proportionality of the wall current to length, to radius, and to the inverse seven-eighths power of velocity could be extracted from the analogy.

The length and velocity dependences of the charge generation rate given by Schön's theory are reasonable when compared with observation. The ideas of a wall current tempered by a relaxation current affording continuous charge generation are certainly reasonable guesses. But the unspecified nature of these currents, the arbitrary assumption of uniform charge den-

sity and uniform velocity profile, and the absence of any device for extending the theory beyond the limitations these impose leave the theory unsatisfying and incomplete.

C. DEVELOPMENT OF PRESENT THEORY

The system of units which will be employed is a rationalized one. With time expressed in seconds and lengths in centimeters the introduction of the permittivity of free space, $\epsilon_0 = 8.854 \times 10^{-14}$ farads/cm., allows the use of ordinary units for electrical quantities. The relative dielectric constant, ϵ , is dimensionless; potential, ψ , has the units volts; current, J , amperes; resistance, Ω , ohms; current density, j , amperes/cm.²; conductivity, κ , ohm⁻¹ cm.⁻¹, and resistivity, ρ , its reciprocal. Concentration, C , which may be substituted for activity in the dilute solutions under consideration, is expressed in moles/cm.³; the relationship between ionic concentration and charge density is given by the Faraday number, $F = 96,500$ coulombs/mole, for a univalent ion or by zF , where z is the ionic valence, for polyvalent ions. The diffusivity, D , has the units cm.²/sec.; the gas constant, R , is 8.32 volt-coulombs/°K.-mole.

It will be assumed for simplicity that the valencies of the positive and negative ions are the same, and:

$$|z_+| = |z_-| = z; \quad C_+ + C_- \cong 2C. \quad [1a, b]$$

In hydrocarbons ionic solutes act as weak electrolytes (19, 22). Because of the small quantities of charge moved it will be assumed that the total ionic concentration is constant and that the dissociation constant of the solute is constant. To obtain an idea of the ionic concentrations involved, for a conductivity of 10^{-12} Ω^{-1} cm.⁻¹, for example, and assuming an ionic mobility of 5×10^{-4} cm.²/volt-sec. for univalent ions the concentration may be calculated from Eq. [4] to be 4×10^{-14} moles/cm.³, equivalent to 2×10^{-10} coulombs/cm.³ each of positive and negative charge.

Several well-known electrokinetic relationships will be written down for later reference. The relaxation time of an electrolyte solution is defined as:

$$\tau \equiv \epsilon\epsilon_0/\kappa. \quad [2]$$

The conductivity of an ion is related to its mobility and diffusivity by:

$$\kappa_{\pm} = C_{\pm} z_{\pm} \mu_{\pm} F = C_{\pm} z_{\pm}^2 F^2 D / RT, \quad [3a, b]$$

where μ_{\pm} is the ionic mobility. The total conductivity is:

$$\kappa = \kappa_+ + \kappa_- = (C_+ D_+ + C_- D_-) z^2 F^2 / RT = 2C z^2 F^2 D / RT, \quad [4]$$

if the diffusivity of the positive and negative ions may be assumed approximately equal. The distance over which the double-layer potential or charge distribution in a liquid decreases to $1/e$ of its value at a surface is

often termed the double-layer thickness, δ :

$$\delta = \left(\frac{RT\epsilon\epsilon_0}{2CF^2z^2} \right)^{1/2} = (D\tau)^{1/2}. \quad [5a, b]$$

In a moving liquid transport of charge occurs by three mechanisms: diffusion, conduction, and convection. This may be written:

$$\mathbf{j}_{\pm} = \mp D_{\pm} z F \nabla C_{\pm} \mp \kappa_{\pm} \nabla \psi \pm \mathbf{v} F C_{\pm} z, \quad [6]$$

where \mathbf{v} is the local velocity, generally a function of position.

1. The Original Charge Distribution

At the interface between a solid and a liquid containing dissolved ions adsorption of ions of one sign or the other will give rise to a potential difference across the interface. In the simplest situation this would cause a double layer of charge to appear in the liquid at the interface with charges of opposite sign to those adsorbed. Because of random thermal motion the charges on the liquid side will tend to be spread out into the liquid, however. The model adopted here is that of Gouy (20) and Chapman (21) and is adequate for present purposes. In solutions of moderate to high conductivity the diffuse double layer extends, with sharply decreasing concentration gradient, only of the order of molecular dimensions into the liquid. In very low conductivity solutions, however, its extent will be macroscopic and the gradient flat.

After the double layer has formed at a surface it may be considered in an equilibrium condition in which conduction of ions in the potential field near the surface is balanced by a counter diffusion down the ionic concentration gradient thus set up. There is no net current and in a stationary liquid Eq. [6] becomes, with Eq. [3b]:

$$zF\nabla C_{\pm} = \mp (z^2 F^2 C_{\pm} / RT) \nabla \psi \quad [7a, b]$$

If the adsorbed charge is considered negative then the net positive charge density in the liquid is:

$$\nabla q = -(2Cz^2 F^2 / RT) \nabla \psi, \quad [8]$$

where:

$$q = (C_+ - C_-) z F. \quad [9]$$

Poisson's equation affords another relation between q and ψ :

$$\nabla^2 \psi = -q / \epsilon\epsilon_0. \quad [10]$$

When ψ is eliminated between Eqs. [8] and [10] an equation for q as a function of position only results. With Eq. [5A]

$$\nabla^2 q = q / \delta^2 \quad [11]$$

In cylindrical coordinates, for tubes:

$$\frac{1}{r} \frac{d}{dr} \left(r \frac{dq}{dr} \right) - \frac{q}{\delta^2} = 0. \quad [12]$$

The solution of Eq. [12] which is symmetrical about the axis gives q as a function of r :

$$\frac{q}{q_0} = \frac{I_0 \left(\frac{r/a}{\delta/a} \right)}{I_0 \left(\frac{1}{\delta/a} \right)}, \quad [13a]$$

where q_0 is the charge density at radius a , the wall. The value of q_0 may be found by solving Eqs. [8] and [10] for ψ and evaluating $\nabla^2 \psi$ at a , but it is not needed here. I_0 is the modified Bessel function of the first kind of order zero.

Equation [13] may be written:

$$\frac{q}{q_{av.}} = \frac{a}{2\delta} I_0 \left(\frac{r/a}{\delta/a} \right) / I_1 \left(\frac{1}{\delta/a} \right) \quad [13b]$$

where:

$$q_{av.} = \frac{2}{a^2} \int_0^a q r \, dr = q_0 \frac{2\delta}{a} I_1 \left(\frac{1}{\delta/a} \right) / I_0 \left(\frac{1}{\delta/a} \right).$$

Figure 1 is a plot of $q/q_{av.}$ against r/a for three values of δ/a . For $\delta/a > 5$ the charge distribution may be considered uniform. The conductivity at which this will be so depends upon the liquid and upon the tube diameter. For example, with heptane, $\epsilon = 2$, in a 1 mm. I.D. tube, a uniform distribution will occur, according to Eqs. [5b] and [2], with $D \sim 10^{-5} \text{ cm.}^2/\text{sec.}$, for $\kappa \sim 7 \times 10^{-18} \Omega^{-1} \text{ cm.}^{-1}$. For a 1-cm. tube a uniform distribution will occur for $\kappa = 7 \times 10^{-20} \Omega^{-1} \text{ cm.}^{-1}$.

The ratio of the integral of the right-hand side of Eq. [13] over the tube cross section between 0 and $0.99 a$ to the integral between 0 and a will give the fraction of charge contained within the fluid up to a distance of 1 % of a from the tube wall. The results of such a calculation are plotted in Fig. 2 against δ/a . It is to be noted that even in such nonuniform distributions as that for $\delta/a = 0.5$ the charge contained in the central 99 % of the tube diameter is less than 1 % smaller than the maximum possible 98 %.

2. Flow Superimposed on a Half Electrode in a Low Conductivity Liquid

The solid-liquid interfacial system just described is equivalent to a half electrode. Consider now that another solid phase onto which positive ions adsorb is immersed in the liquid. A double-layer distribution opposite in

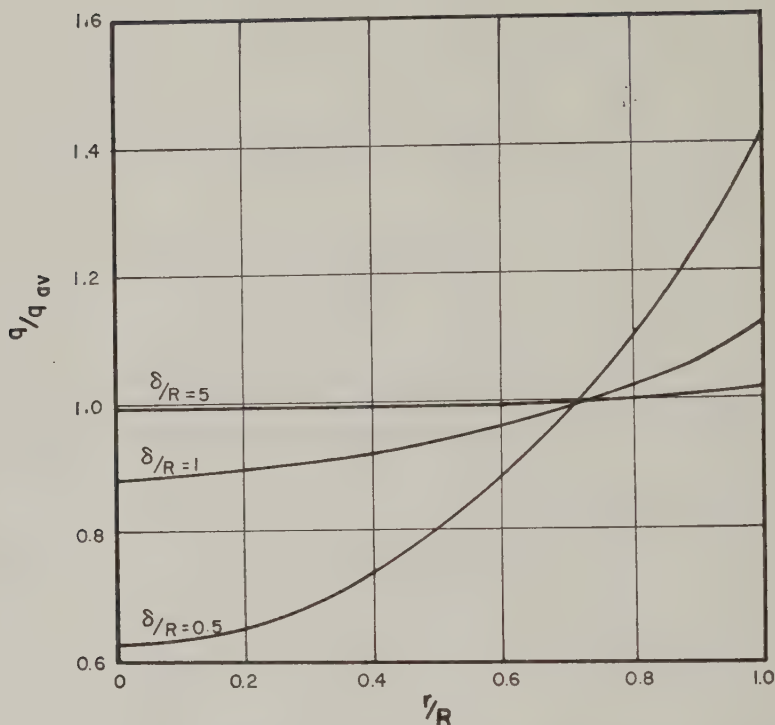


FIG. 1. Charge distribution in low-conductivity liquids in tubes. Curves are applicable to fluids at rest and to fluids moving with uniform velocity profile in long tubes.

sign to that near the first interface will form about the second. Its charge density, however, will differ from that near the first depending upon the differences in potential across the individual interfaces. If the two half electrodes are electrically connected, current will flow in the external circuit and ionic migration will occur: negative ions toward the first electrode, positive toward the second. If polarization may be neglected for the moment, a potential difference appears between the electrodes equal to the algebraic sum of the original interfacial potentials. It is not necessary that the solid phases be metallic so long as they are not perfect insulators, for under the potential difference set up a current will flow, however small, depending upon the resistivity of the electrode materials. Obviously this current will be greater with better conductors, but because of polarization it will not be larger by as much as the ratio of the conductivities. What is being described is a cell reaction. It may be inferred from the well-known electrolytic oxidation-reduction reactions of organic compounds in nonaqueous media (23) that cell reactions of this type are possible in hydrocarbon solution although they do not appear to have been studied yet. It is not neces-

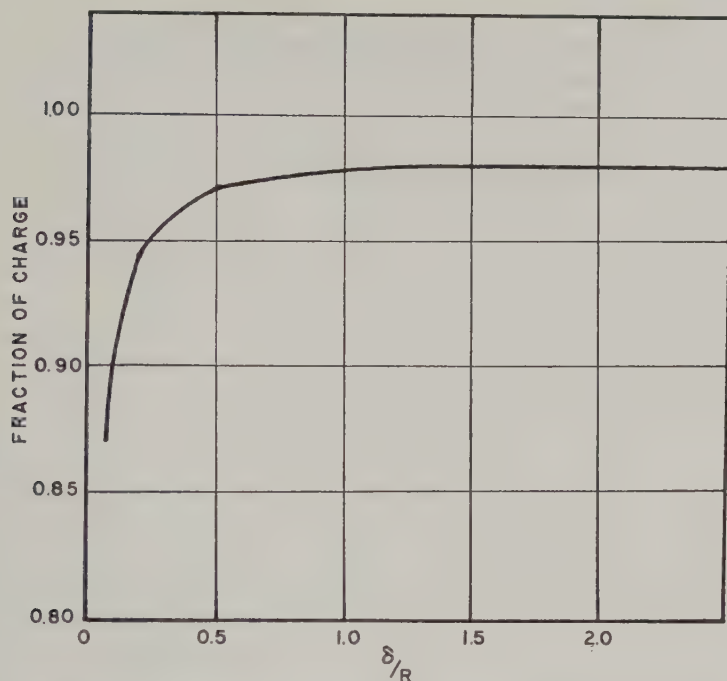


FIG. 2. Fraction of charge in low-conductivity liquids within 99% of tube diameter. Curves are applicable to fluids at rest and to fluids moving with uniform velocity profile in long tubes.

sary for what follows to describe any particular reaction: electrode oxidation-reduction of organic compounds in hydrocarbon solution is postulated as a basic process in the electrification phenomenon. That this is reasonable may be determined by how well the theory based upon it is able to describe the observed phenomena.

At finite current polarization will raise the potential differences across the interfaces, decrease the effective potential difference between the electrodes, and limit the current able to be drawn. Of the three types of polarization, ohmic, activation, and concentration, only the last will be considered. This is because at very low current densities ohmic polarization will be small, and, because electrification is known to be very velocity dependent, concentration polarization will be large compared with activation polarization.

In concentration polarization diffusion to the surfaces cannot maintain a sufficient supply of ions to be discharged at an arbitrarily large current density. The limiting current would be that at which the concentration of ions discharging at the wall is zero, but in a cell from which current is drawn the steady-state concentration is greater than zero and the current is lower

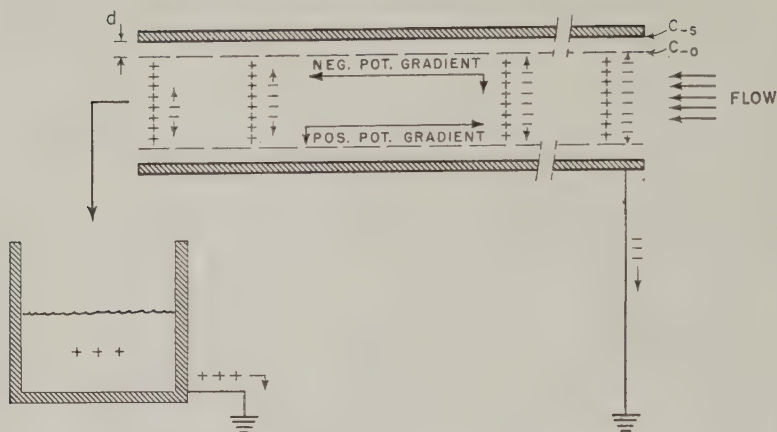


FIG. 3. Schematic representation of charge generating process in tubes.

than the limiting current. The distance over which the concentration changes from C_0 in the liquid bulk to C_s at the surface is known as the diffusion layer thickness, d . Agitation of the liquid decreases d . For high Schmidt number fluids, i.e., liquids, d will be somewhat smaller than the laminar sublayer thickness if turbulent flow exists around the electrode. In the absence of turbulence d will be somewhat smaller than the Prandtl velocity boundary layer thickness. In both cases d may be estimated (24-26).

If negative ions are considered discharged at the surface, the surface current flux may be shown to be (24):

$$j_s = - \frac{DzF}{dn_+} (C_{-0} - C_{-s}). \quad [14]$$

where n_+ is the transference number of the positive ions. The actual cell potential, ψ_s , is given by:

$$\psi_s - \psi^0 = (RT/zF) \ln C_{-s}, \quad [15]$$

where ψ^0 is the cell potential for unit concentration. The cell will adjust itself such that j_s will be a maximum consistent with Eqs. [14, 15]. The value of ψ_s will then be zero and C_{-s} becomes:

$$C_{-s} = \exp (-zF\psi^0/RT). \quad [16]$$

The exponential is understood to be multiplied by unit concentration so that the equation is dimensionally correct.

Now consider a half electrode consisting of a grounded tube through which a low conductivity liquid electrolyte may flow into a grounded re-

ceiver isolated from the tube, as illustrated in Fig. 3. Before flow begins let the ionic charge distribution in the liquid in the tube be positive. It need not be uniform radially. If fresh, uncharged liquid is admitted to the tube it will displace the positive ions and transport them into the receiver. From the start of the flow there will be a concentration gradient of positive ions down the tube which will arise originally because of the finite time it takes to move all the ions the entire length of the tube. It is easily shown by means of Poisson's Eq. [10] that this would result in a negative potential gradient downstream so that the entrance region is positive relative to the exit region. The adsorbed negative ions near the entrance will discharge under the influence of the gradient in the same way as corresponding ions in a half cell will discharge when another half electrode is connected. Negative ions from the solution will continuously diffuse to the surface to discharge and maintain the current. At annular tube elements downstream there will always be maintained, in steady flow, a concentration of excess positive ions which have come from elements upstream. The presence of the positive ions progressively decreases the rate of discharge of negative ions in succeeding elements while the concentration of excess positive ions increases asymptotically to a limit which will be calculated in the next section. This is a form of polarization.

Concentration polarization must be included, however. In laminar flow this will occur across a now somewhat indeterminate diffusion layer since a true boundary layer exists only near the entrance of a tube, but in turbulent flow the diffusion layer may be estimated as before. The equations describing polarization here are similar to Eqs. [14], [15], [16] except that the presence of excess positive ions gives rise to a field which alters j_s . The field at the tube wall may be expressed, for example, in the form of an integral of the excess positive ions over the tube cross section at any axial position if the axial field is considered small compared with the radial field. Since the field affects both positive and negative ions alike, the decrease in j_s may be written as the product of the total conductivity and the field. The equivalent of Eq. [14a] for this situation would be:

$$j_s = - \frac{D_z F}{dn_{\mp}} (C_{-0} - C_{-s}) + \frac{\kappa}{a\epsilon\epsilon_0} \int_0^a q(x,r)r dr, \quad [17]$$

where $q(x, r)$ represents the charge density of the excess positive ions.

It is to be noted that ψ^0 becomes an absolute half-electrode potential in this situation because the circuit is completed without the intervention of another half electrode. Because absolute half-electrode potentials are unobtainable, estimates may be made for them by using corresponding zeta potentials. Unless electrification is found to be appreciably dependent upon ψ^0 through C_{-s} , however, this point will prove of little difficulty.

3. The Charge Distribution with Superimposed Flow

In a flowing liquid in which charge is transported, Eq. [6] becomes:

$$\mathbf{j}_{\pm} = \mp D_z F \nabla C_{\pm} \mp \kappa \nabla \psi \pm \mathbf{v} F z C_{\pm} \quad [18a, b]$$

from which:

$$\mathbf{j} = \mathbf{j}_+ + \mathbf{j}_- = -D \nabla q - \kappa \nabla \psi + \mathbf{v} q, \quad [19]$$

where approximate equality of D_+ and D_- is assumed again. In the steady state the divergence of \mathbf{j} , or of its time average, vanishes for laminar and for turbulent flow, respectively. Equation [19] may then be transformed by the use of Eqs. [1] and [10] and conservation of matter for incompressible fluids to:

$$\nabla \cdot \nabla q - \nabla \cdot (D \nabla q) + q/\tau = 0. \quad [20]$$

For turbulent flow \mathbf{v} and q represent time averaged quantities. The turbulent flux components have been incorporated into the diffusivity to give an effective diffusivity, the sum of the molecular and the "eddy" diffusivities, which is a function of r (25). Then, if diffusion in the axial direction may be neglected with respect to convection, Eq. [20] may be written for turbulent flow in cylindrical tubes as:

$$v(r) \frac{\partial q}{\partial x} - \frac{1}{r} \frac{\partial}{\partial r} \left[r D(r) \frac{\partial q}{\partial r} \right] + \frac{q}{\tau} = 0. \quad [21a]$$

For laminar flow the diffusivity is the constant molecular diffusivity. In fully developed laminar flow in tubes v is quadratic in r . Equation [20] now becomes, if axial diffusion is neglected:

$$2v_{av} \left[1 - \left(\frac{r}{a} \right)^2 \right] \frac{\partial q}{\partial x} - \frac{D}{r} \frac{\partial}{\partial r} \left(r \frac{\partial q}{\partial r} \right) + \frac{q}{\tau} = 0. \quad [21b]$$

These are generalizations of Eq. [12] to include axial dependence and convection. Their solutions describe all the possible charge distributions for laminar or turbulent flow in tubes. Conditions imposed on the boundaries of the tube determine the particular forms of the distributions. For the electrification problem the condition at the tube wall is that relation which describes the loss of negative charge at the surface, or, equivalently, the gain of positive charge by the fluid. This is expressed with the help of Eq. [6]:

$$-D_+ \frac{dq}{dr} \Big|_{x,a} - \kappa \frac{d\psi}{dr} \Big|_{x,a} = j_s. \quad [22]$$

But the second term on the left of Eq. [22] is the same product of conductivity and field (equal to the negative of the potential gradient) by which j_s was diminished because of the excess of positive ions. When Eq. [22]

is compared with, say, Eq. [17] and equality of the ionic diffusivities is assumed once more:

$$D \frac{dq}{dr} \Big|_{x,a} = \frac{zFD}{dn_+} (C_{-0} - C_{-s}) = \text{constant.} \quad [23]$$

The condition at the tube entrance will be taken to be:

$$q|_{0,r} = 0, \quad [24]$$

i.e., the entering fluid will be assumed uncharged. In addition all applicable solutions of Eqs. [21] must be symmetrical about the tube axis.

Equations [21a, b] with conditions [23] and [24] constitute a general formulation of the electrification phenomenon in tubes. From them the correct charge distribution in the fluid may be found as a function of radial and axial position. The development forms a complete theory of the phenomenon.

The solution of the system of Eqs. [21a] or [21b], [23], and [24], however, presents formidable difficulties in real flows. Although D is constant in laminar flow, v is quadratic in r . In turbulent flow both D and v are complicated functions of r not expressible in terms of simple functions. Approximate forms for D and v in turbulent flow obtained by graphical integration have been given by Deissler (26). Although Deissler's expression for D was derived for a situation where q/τ was not present in the diffusion equation [20], it may be used here, at least as a first approximation, since expressions which include the possible influence of q/τ are unavailable. In addition, flow in the entrance region of the tube, both in laminar and in turbulent flow, is very complicated. In real flows, therefore, the equations, although linear, appear with nonconstant coefficients. Because to solve the equations numerical or graphical methods would be required this will not be attempted here.

A simple case, easily solved, is that for v and D independent of r . Although it will not describe the charge distributions correctly, the solution in terms of well-known functions will nevertheless afford some insight into the essential nature of the charge distribution without unusual expenditure of effort. In this case one may obtain by standard means:

$$q = \frac{zF(C_{-0} - C_{-s})\delta}{dn_+} \left[\frac{I_0\left(\frac{r/a}{\delta/a}\right)}{I_1\left(\frac{1}{\delta/a}\right)} - \frac{2a}{\delta} \sum_{n=0}^{\infty} \frac{J_0\left(\frac{\alpha_n r}{a}\right) \cdot \exp - \left(\frac{1}{v\tau} + \frac{\alpha_n^2 D}{a^2 v}\right)x}{(\alpha_n^2 - a^2/\delta^2)J_0(\alpha_n)} \right], \quad [25]$$

where α_n is the n^{th} zero of the first-order Bessel Function of the first kind, $J_1(\alpha)$, with $\alpha_0 = 0$ and $J_0(\alpha_0) = 1$.

For long tubes it is easily shown that Eq. [25] may be transformed into an equation identical with Eq. [13b] with q_{av} here given by:

$$q_{av} = 2zF(C_{-0} - C_{-s})\delta^2/a \, dn_+.$$

The distribution for long tubes is identical in form to the distribution which occurs in the absence of flow. Figures 1 and 2 may, therefore, be taken over directly in this case.

4. The Charge Generation Rate

The rate at which charge leaves the tube entrained in the liquid is the electrification rate or total charge generation rate. It is given by:

$$J = 2\pi \int_0^a r q(L, r) v(r) \, dr \quad [26]$$

where L is the length of the tube.

In the particular case of v and D independent of r substitution of Eq. [25] for q and integration yields:

$$J = 2\pi av\tau \frac{zF(C_{-0} - C_{-s})D}{dn_+} \left[1 - \exp\left(-\frac{L}{v\tau}\right) \right]. \quad [27]$$

In fact, this equation may easily be obtained by direct integration of Eq. [20] with respect to r for v independent of r regardless of the form of D . This is similar in form to the equation developed by Schön (11). The unspecified wall current introduced by Schön, however, is described explicitly in Eq. [27] as a diffusion current which arises because of concentration polarization at an electrode. Except for this Schön's theory may be obtained as a special case of the general theory developed here.

For $L \gg v\tau$ the exponential vanishes, J is independent of L ; for $L \ll v\tau$ the factor in the brackets becomes $L/v\tau$ and J is proportional to L . At intermediate values of L intermediate dependence of J upon L is exhibited. This agrees with observation.

Unless C_{-s} is nearly as large as C_{-0} , $(C_{-0} - C_{-s})$ is practically proportional to κ (Eq. [3a]); τ is inversely proportional to κ (Eq. [2]). Therefore for $L \gg v\tau$, J is independent of κ ; and for $L \ll v\tau$, it is proportional to κ . The latter case is in agreement with observation. The former case does not agree with observation for small τ , but the opposite situation, very large L and large τ , seems not to have been investigated.

The comparatively small effect that the nature of the ionic solute and the material of which the tube wall is made have on the rate of charge generation is accounted for by the presence of C_{-s} which is determined by the chemical properties of the system through ψ^0 (Eq. [16]). Unless C_{-s} is very close to C_{-0} in value, it will have but little influence on J . But if it is close to C_{-0} , J will become small and very dependent upon ψ^0 . Apparently

$C_{-5} \ll C_{-0}$, since electrification has been found to depend but slightly upon surface or solute materials. Electrification is then diffusion rather than kinetically controlled.

Although Eq. [27] was not directly derived for turbulent flow, if the dependence of d on the inverse $7/8$ ths power of v for turbulent flow (26) is inserted into Eq. [27] J will vary with the $17/8$ ths power of v for $L \gg v\tau$ and with the $7/8$ ths power for $L \ll v\tau$. For intermediate values of L the dependences will be more complicated than simple power dependence. Since velocity dependences between first and second power have been noted this is in fair agreement with observation.

5. Discussion

If the radial charge distribution is uniform, the second term in Eqs. [21] vanishes, and the boundary condition [23] becomes a constant generation term. Equations [21] may then be integrated subject to condition [24] directly to Eq. [27] regardless of the form of v . Therefore, it is to be expected that Eq. [27] is a fair representation of the electrification phenomenon for those situations where the charge distribution may be considered uniform provided $v(r)$ is replaced by the proper average velocity. This is borne out by the fact that for large δ/a , for which this would be true, τ would be large and $L \ll v\tau$. It has already been noted that Eq. [27] agrees with observation for this situation.

Although it would be necessary to solve the equations using the correct form for $v(r)$ in order to compare the theory with observation at higher conductivities, it is possible to make some statements without the necessity for doing so. It has already been mentioned that turbulence influences the charge distribution. Its influence may be incorporated into the value of δ , however. This will spread out but not otherwise alter the distribution at a given conductivity (18). Therefore, in turbulent flow the conductivity at which a uniform distribution will occur may be higher than in a stationary fluid, although for a given value of δ/a Figs. 1 and 2 are still applicable. The effect is to extend the utility of Eq. [27] to higher conductivities.

Actually, in turbulent flow Eq. [27] should remain approximately applicable even beyond the point at which the charge remains uniform ($\delta/a \sim 5$), for, as Fig. 2 indicates, when the distribution is becoming nonuniform an overwhelming fraction of the charge may still be found in the central portion where the velocity profile is comparatively flat.

Upon direct integration of Eq. [20] in cylindrical coordinates with respect to r there results:

$$\frac{\partial}{\partial x} \int_0^a vrq \, dr - aD \left. \frac{\partial q}{\partial r} \right|_{a,x} + \frac{1}{\tau} \int_0^a rq \, dr = 0. \quad [28]$$

If the equation is divided by $2/a^2$ the last term becomes \bar{q} , the average charge density, divided by τ ; and if the second term is replaced by Eq. [23]:

$$\frac{2}{a^2} \frac{\partial}{\partial x} \int_0^a v r q \, dr - \frac{2DzF(C_{-0} - C_{-s})}{a d n_+} + \frac{\bar{q}}{\tau} = 0. \quad [29]$$

Without actually performing the integration in Eq. [29] it is possible to find some value of v , say \bar{v} , such that at constant overall rate of fluid flow:

$$\frac{2}{a^2} \frac{\partial}{\partial x} \int_0^a v r q \, dr = \bar{v} \frac{2}{a^2} \frac{\partial}{\partial x} \int_0^a r q \, dr = \bar{v} \frac{\partial \bar{q}}{\partial x}. \quad [30]$$

Then Eq. [29] may be integrated with respect to x between $x = 0$ where $q = 0$ and $x = L$ to give:

$$\bar{q} = \frac{2\tau DzF(C_{-0} - C_{-s})}{a d n_+} \left[1 - \exp\left(-\frac{L}{\bar{v}\tau}\right) \right]. \quad [31]$$

By Eq. [26] J is:

$$J = 2\pi a \bar{v} \tau \frac{DzF(C_{-0} - C_{-s})}{d n_+} \left[1 - \exp\left(-\frac{L}{\bar{v}\tau}\right) \right]. \quad [32]$$

Now, as the conductivity increases and the charge distribution becomes more and more concentrated near the tube walls where v is smallest, the value of the integral in Eq. [30] becomes smaller and the value of \bar{v} decreases. Thus the exponential term in Eq. [32] becomes less important, J becomes independent of L , and since J is proportional to \bar{v} it decreases as the conductivity increases. Since at much lower conductivities J increases with conductivity a maximum will occur in the conductivity dependence of J . As the flow rate is increased, moreover, v remains large closer and closer to the wall. Therefore \bar{v} will become larger, but it will do so more quickly than the change in d with flow rate, because q is a rapidly changing function of d close to the wall. Since d varies as the inverse $7/8$ ths power of flow rate it is to be expected that J will vary with flow rate to a power greater than $13/4$ ths.

The theory then is able to account correctly for the electrification phenomenon at very low conductivity and to indicate the form of the phenomenon at higher conductivities without undue expenditure of effort. Upon comparison of the form with observation it is seen that the predictions of a maximum in the generation rate-conductivity relationships and dependence upon at least the $13/4$ ths power of flow rate are in accord with observation.

Before quantitative statements may be made, however, it will be necessary to examine in detail the solutions of Eqs. [21] for real flows. This forms part of a continuing research effort. In addition it is difficult with the available data to do more than compare the forms of any equations developed with observation. An experimental program with the purpose of illustrating and corroborating the points made here has been conducted as part of the present research effort. Its results will be submitted in the near future.

ACKNOWLEDGMENT

The authors wish to thank the American Petroleum Institute for the continued support under Static Research Project S-2 which made this work possible.

REFERENCES

1. KRUYT, H. R., "Colloid Science," Vol. 1. Elsevier, Amsterdam, 1952.
2. KORTUM, G., AND BOCKRIS, J. O., "Electrochemistry," Vol. 2. Elsevier, Amsterdam, 1951.
3. KLINKENBERG, A., AND VAN DER MINNE, J. L., "Electrostatics in the Petroleum Industry." Elsevier, Amsterdam, 1958.
4. DOLEZALEK, F., *Chem. Ind.* **36**, 33 (1913).
5. RUSSIG, F., *Chem. Ind.* **36**, 62 (1913).
6. BRÜNINGHAUS, L., *J. phys. radium* **VII** **1**, 11 (1930).
7. NITKA, H., *Chem. Fabrik* **14**, 211 (1941).
8. MACKEOWN, S. S., AND WOUK, V., *Ind. Eng. Chem.* **34**, 659 (1942).
9. ERNSBERGER, F. M., *J. Appl. Phys.* **27**, 418 (1956).
10. KELLER, H. N., AND HOELSCHER, H. E., *Ind. Eng. Chem.* **49**, 1433 (1942).
11. HAMPEL, B. AND LUTHER, H., *Chem. Ins. Tech.* **29**, 323 (1947).
12. RUTGERS, A. J., DE SMET, M., AND DE MYER, G., *Trans. Faraday Soc.* **53**, 393 (1957).
13. BOUMANS, A. A., *Physica* **23**, 1038, 1047 (1957).
14. COOPER, W. F., *Brit. J. Appl. Phys.* **4** (Suppl. 2), 511 (1953).
15. HELMHOLTZ, H., *Ann. Physik* **243**, 337 (1879).
16. REICHARDT, H., *Z. physik. Chem.* **A174**: 15 (1935).
17. BOCQUET, P. E., SLIEPCEVICH, C. M., AND BOHR, D. F., *Ind. Eng. Chem.* **48**, 197 (1956).
18. BOUMANS, A. A., loc. cit., pp. 1007, 1027.
19. GEMANT, A., *Appl. Sci. Research* **A6**, 1 (1955).
20. GOUY, G., *Ann. phys.* [9] **7**, 129 (1917).
21. CHAPMAN, D. L., *Phil Mag.* [6] **25**, 475 (1913).
22. WALDEN, P., "Salts, Acids and Bases." McGraw-Hill, New York (1929).
23. PAGE, J. E., *Quart. Revs. (London)* **6**, 262 (1952).
24. LEVICH, P., *Discussions Faraday Soc.* **1**, 37 (1947).
25. LIN, C. S., MOULTON, R. W., AND PUTNAM, G. L., *Ind. Eng. Chem.* **45**, 636 (1953).
26. DEISSLER, R. G., NACA Report 1210 (1955).

THE INTERACTION OF AMYLOPECTIN WITH CETYLPYRIDINIUM CHLORIDE¹

Myer M. Fishman and Isaac Freund²

Department of Chemistry, City College of New York, New York 31, New York

Received October 18, 1960

ABSTRACT

The complex which is formed between amylopectin and cetylpyridinium chloride (CPC) in dilute aqueous NaOH is indicated by a turbidity, measured spectrophotometrically. No significant turbidity is apparent in the absence of any of the components. Aggregation of the complex is dependent on the relative concentrations of polysaccharide and surfactant and the absolute concentration of NaOH. A simple analytical expression relating these concentrations is derived from the experimental data, on the basis of which accurate qualitative and quantitative predictions are made and verified.

On the basis of the suggestion that the active form of the surfactant is the micelle, the critical micelle concentration of CPC is calculated as a function of electrolyte concentration. Within experimental error, agreement is obtained with recent literature values.

The aggregated complex is pictured as consisting of a matrix of negatively charged amylopectin molecules, cross-linked by positively charged CPC micelles.

INTRODUCTION

In recent years, many investigators have been concerned with the interaction of macromolecules with long-chain surfactants. In particular, the marked affinity of proteins for these compounds has led to numerous studies on the binding of both cationic and anionic surfactants (1, 2), but there have been few investigations on similar reactions with polysaccharides.

Scott (3) has demonstrated that the quaternary ammonium compound cetylpyridinium chloride reacts with sulfated polysaccharides to produce insoluble precipitates, with stoichiometric binding of the CPC. Ehrenpreis and Fishman (4) have compared the binding of monoquaternary and diquaternary ammonium compounds to chondroitin sulfate, an acid mucopolysaccharide which has bifunctional charges on the repeating unit. Stoichiometric complexes were formed with binding ratios of 2/1 (with CPC) and 1/1 (with curare).

¹ Presented in part at the 138th meeting of the American Chemical Society, New York City, Sept. 12-16, 1960.

² Present address: Department of Chemistry, Columbia University, New York.

The interaction of neutral polysaccharides with cationic surfactants in alkaline media represents a comparatively unstudied area in which there are many interesting problems. Barker *et al.* (5) have reported the precipitation of neutral polysaccharides with cetyltrimethylammonium bromide (CTAB) both in borate buffer and in 0.1 *N* NaOH. The reaction in borate buffer was assumed to be precipitation of the polysaccharide-borate complex. Palmstierna (6), too, has reported the precipitation of starch with CPC in KOH. Fishman and Miller (7) described some preliminary studies in which they compared the interaction of CTAB with amylose, the linear fraction, and with amylopectin, the branched fraction of corn starch, in weakly alkaline solution. In these systems, the stoichiometry is complex and the mechanism of binding is obscure.

In any study which involves aqueous alkaline solutions, one must always consider the possibility of either degradation or structural changes in the carbohydrates. In our work, no effort was made to exclude oxygen, although it is in the presence of oxygen that carbohydrates will undergo their greatest changes. However, Stacy *et al.* (8) have shown that amylopectin, dispersed in 1 *N* alkali, shows very little change over a 24-hour period. Therefore, it would not appear that the significance of our results would be affected by the contact of amylopectin with 0.1 *N* alkali, for time intervals up to 30 minutes.

It is the purpose of this communication to extend our earlier studies on some of the physicochemical properties of amylopectin-surfactant complexes in alkaline solution, but using CPC instead of CTAB. It was also intended that these results would provide a more quantitative relationship between the reactants and might determine whether the reaction involves the binding of surfactant monomers and/or micelles.

EXPERIMENTAL

The amylopectin (NURD-148SP) was supplied by the Northern Utilization Research Division of the U. S. Department of Agriculture, Peoria, Illinois. It had been fractionated from corn starch by the Schoch butanol procedure (9). All solutions were prepared in distilled water, in concentrations of 1 mg./ml., by heating to near boiling for 30 minutes. An initial rapid heating of the solution produced convection currents which prevented adhesion of the amylopectin, either to the bottom or to the sides of the beaker.

The cetylpyridinium chloride was purchased from the K & K Laboratories, Jamaica, New York, and was used as received. It dissolved readily in water but was warmed to insure completeness of solution. Anacker (10) has shown that under ordinary conditions CPC exists as a monohydrate, $\text{CPC} \cdot \text{H}_2\text{O}$. Therefore, unless otherwise indicated, concentrations will refer to that of the monohydrate.

All reactions were run at a total volume of 20 ml.; individual reactants

were varied and adjusted to keep the volume constant. The order of addition of the reagents was amylopectin, H_2O , NaOH , and CPC, but changing the order of addition did not alter the results.

Turbidities were determined with the aid of a Model B Beckman spectrophotometer. For these purposes, the turbidity (τ) is defined in a manner analogous to absorbancy or optical density and is not to be confused with the usual light-scattering turbidity. Heller and Tabibian (11) have discussed the sources of error involved in the use of unmodified commercial instruments for the measurement of turbidity, but in this investigation relative changes in turbidity were more important than precise turbidity values.

Readings were taken 10 ± 0.5 minutes following the addition of CPC, so as to allow time for the system to reach a steady state. This time interval represented a plateau region, although the turbidity was never really constant with time. Changes after this period were generally small.

The temperature was generally ambient room temperature which varied between 20°C . and 25°C . Throughout this temperature range, turbidity measurements were in good agreement within the precision of the measurements. However, in order to prevent decomposition of CPC in solutions of NaOH with concentrations greater than $0.050\text{ }N$, the temperature of such solutions was kept close to 20°C . Fresh solutions of CPC and amylopectin were prepared daily and the agreement between results obtained on different days was as good as duplicates obtained on the same day. The overall precision was estimated at better than 3%.

Qualitative, but direct, measurements of changes in particle size were made by a modification of the Mie theory (12-14), the principle of which is based on a decrease of a wavelength exponent n , with increasing particle diameter, in the formal equation

$$\tau = k\lambda^{-n}, \quad [1]$$

where τ is the turbidity, λ , the wavelength of light, and k , a constant for a given system. To a first approximation, n is independent of λ and probably only slightly dependent on concentration. Straight lines were obtained by plotting $\log 1/\tau$ vs. $\log \lambda$ over the wavelength range 400-600 $\text{m}\mu$. The slopes of the lines were taken to be the values of n .

RESULTS AND DISCUSSION

The results of our studies are summarized in Figs. 1-7. For the sake of conciseness, experimental data, empirical correlations, and theoretical interpretations will be discussed simultaneously.

In Fig. 1, the turbidity is plotted for increasing concentrations of CPC, at various concentrations of amylopectin, in $0.050\text{ }N$ NaOH . Similar results were obtained for other concentrations of NaOH . (It should be

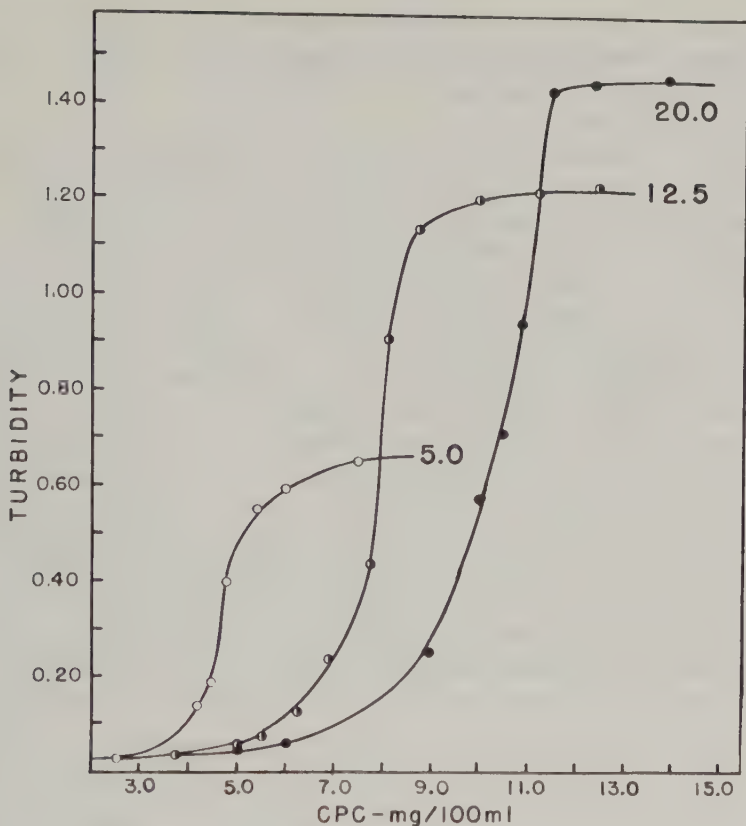


FIG. 1. Turbidity vs. CPC for amylopectin concentrations of 5.0, 12.5, and 20.0 mg./100 ml., in 0.050 *N* NaOH.

pointed out that the indicated concentrations in this and subsequent figures are the initial and not the equilibrium concentrations.) At low concentrations of CPC, the turbidity is also low, but it rises rapidly once the concentration of surfactant has exceeded a certain value. The amount of CPC required to produce this rapid rise in turbidity increases in a regular manner with an increase in the concentration of amylopectin.

In the absence of NaOH, there is no apparent binding of CPC to amylopectin. The introduction of NaOH imparts a negative charge to the amylopectin, presumably through one or more of its hydroxyl groups, and with the addition of a cationic surfactant, e.g., CPC, a complex is formed due to the ionic attraction between its positive charges and the negatively charged amylopectin. This is marked by an increase in turbidity. However, the large and rapid increases in turbidity are interpreted as being due to an aggregation of the complex, which occurs once

a sufficient amount of CPC has been bound to the amylopectin. At high concentrations of CPC, although more of the surfactant may be bound, the turbidity reaches a plateau and there is no significant increase in particle size.

In Fig. 2, the turbidity is plotted for increasing concentrations of amylopectin in 0.050 *N* NaOH, at various concentrations of CPC. Comparable results were obtained at other concentrations of NaOH. The initial rapid increase in turbidity is due to the fact that with an excess of CPC, both the number and size of the aggregates increase as the amylopectin concentration increases. In addition, in this region, the curves are virtually tangent because the amount of amylopectin is the same. As the concentration of amylopectin is further increased, the number of aggregates will also increase but their average size may decrease because a given amount of CPC is spread over a larger number of amylopectin particles. The net result is a slower rate of increase of turbidity. The point is finally reached where the critical amount of CPC is no longer available, aggregation fails to occur, and the turbidity drops precipitously. At high concentrations of amylopectin, the bound molecules of CPC are spread so diffusely that they have a negligible effect in terms of aggregation.

In Fig. 3, the dependence of turbidity on the concentration of NaOH is shown for various combinations of amylopectin and CPC (see Table I). In the absence of a large excess of CPC, the NaOH can be increased to a

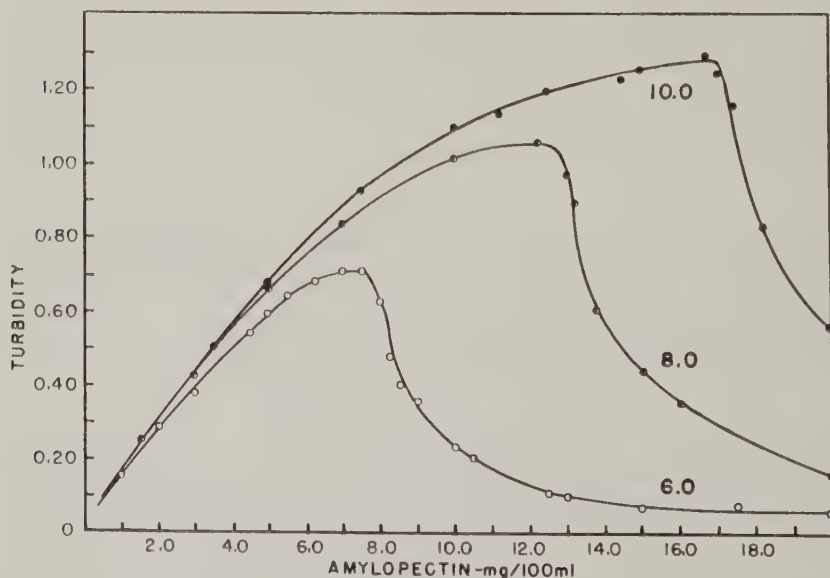


Fig. 2. Turbidity vs. amylopectin for CPC concentrations of 6.0, 8.0, and 10.0 mg./100 ml., in 0.050 *N* NaOH.

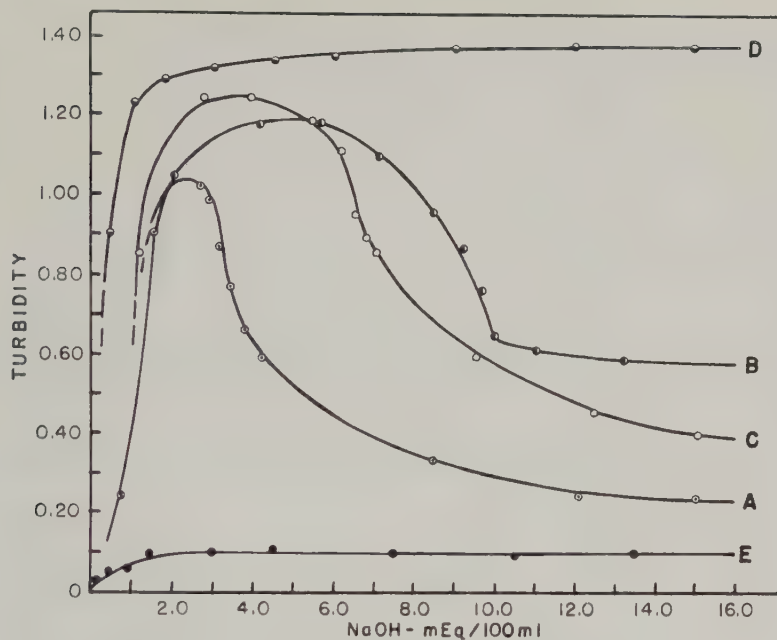


FIG. 3. Turbidity vs. NaOH. The concentrations of amylopectin and CPC for the various curves are given in Table I.

TABLE I

Comparison between Calculated (Eq. [4]) and Experimental Values for Critical Concentration of NaOH

Fig. 3 curve	Amylopectin (mg./100 ml.)	CPC (mg./100 ml.)	NaOH (meq./100 ml.)	
			Calculated	Experimental
A	16.2	9.0	3.52	3.3
B	13.0	9.0	9.79	9.8
C	16.2	10.0	6.62	6.5
D	16.2	15.3	∞	*
E	13.0	6.2	-1.03	*

* Qualitative agreement.

point where the charge density on the amylopectin is high enough so that there is an insufficient amount of CPC to produce aggregation and there is a rapid decrease in particle size. This is evident in curves A, B, and C. The initial rapid increase in turbidity is due to the fact that it takes only a comparatively small amount of NaOH to effect complex formation.

The turbidity results given in Figs. 1-3 were very much dependent on a variety of factors which contribute to light-scattering behavior, e.g.,

particle size, particle shape, charge, concentration of the scattering unit, and degree of interaction with solvent. Therefore it appeared that the n values (Eq. [1]), which as a first approximation are primarily dependent on particle size, would qualitatively aid in the interpretation of the turbidity curves. In Fig. 4, n values for a series of typical curves are plotted as a function of concentration of reactants. The complexity of the systems precludes a rigorous application of the Mie theory but the data are in complete agreement with the picture of aggregation-disaggregation of the complex over wide ranges of concentration. From these results it becomes apparent that a criterion for aggregation is that a certain number of molecules of CPC must be bound per molecule of amylopectin; an increase in the number of amylopectin units should require a concomitant increase in the number of CPC molecules. Further, at some critical concentration of CPC there is a balance between repulsion and attraction, a point below which no significant aggregation will occur, whereas above it, the process will be quite rapid.

This conclusion can be tested experimentally by plotting the concentration of amylopectin against the critical concentration of CPC required to produce aggregation; the result might be a straight line passing through the origin. In order to do this, the experimental curves of Fig. 1 were approximated by the solid curve in Fig. 5a. The dashed curve in Fig. 5a is an idealization of the change in turbidity, with the maximum corresponding to the point of inflection. It is apparent that the point of maximum rate of aggregation on the solid curve, the point of inflection, corresponds to the critical concentration of CPC. Figure 6 is a graph of amylopectin vs. CPC, determined at the appropriate points of inflection. The open symbols were obtained from graphs similar to Fig. 1, but at various concentrations of NaOH. As expected, for a given concentra-

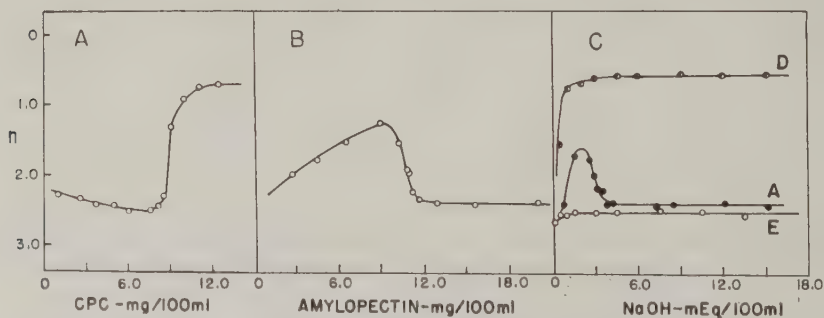


FIG. 4. Determination of changes in particle size, n (Eq. [1]) vs. concentration; the ordinate is inverted to give a qualitative measure of particle size. A. n vs. CPC, at amylopectin concentration of 15.0 mg./100 ml., in 0.050 N NaOH. B. n vs. amylopectin, at CPC concentration of 8.0 mg./100 ml., in 0.100 N NaOH. C. n vs. NaOH. The letters refer to the corresponding turbidity curves in Fig. 3.

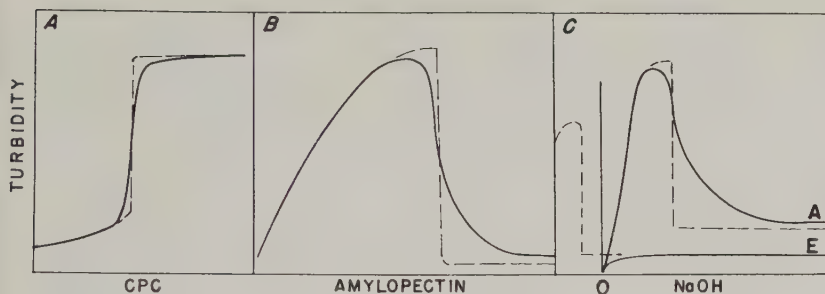


FIG. 5. Idealization of turbidity vs. concentration graphs. The solid curve approximates the experimental one; the broken curve is an idealization. (A) Turbidity vs. CPC. (B) Turbidity vs. amylopectin. (C) Turbidity vs. NaOH.

tion of NaOH, the points lie on a straight line, which, however, does not pass through the origin. It is also evident that with an increase in the concentration of NaOH, for a fixed amount of amylopectin, i.e., an increase in the charge density on the amylopectin, more CPC is required before aggregation will occur.

In a similar manner, one can determine from Fig. 2 the critical ratio of CPC to amylopectin required for aggregation. The idealization of Fig. 2 is shown in Fig. 5b, and the point of inflection (the point of maximum rate of decrease in particle size) is used to evaluate the critical ratio. These points, taken from a family of graphs similar to Fig. 2, appear as the closed symbols in Fig. 6. It is evident that these values are in excellent agreement with those from Fig. 1.

The lines in Fig. 6 do not pass through the origin as predicted, indicating that the lower threshold level of CPC is of particular importance, but do pass close to a point whose coordinates may be designated as A_0 and C_0 . This is useful in that the equation of any line may be represented by

$$\frac{A - A_0}{C - C_0} = s(N), \quad [2]$$

where A is the concentration of amylopectin in mg./100 ml., C is the concentration of CPC in mg./100 ml., and $s(N)$ is the slope of the line as a function of N , the concentration of NaOH in meq./100 ml.

Inasmuch as three values of $s(N)$ are available, there are many three-parameter equations which will fit the data. The particular form

$$s(N) = a + \frac{b}{N + c} \quad [3]$$

was chosen because it yields finite values for $s(N)$ at both zero and infinite concentrations of NaOH, and physically, one would expect that the slope should indeed be finite at both zero and infinite concentrations of NaOH. Such a choice increases the probability that the equation should be valid

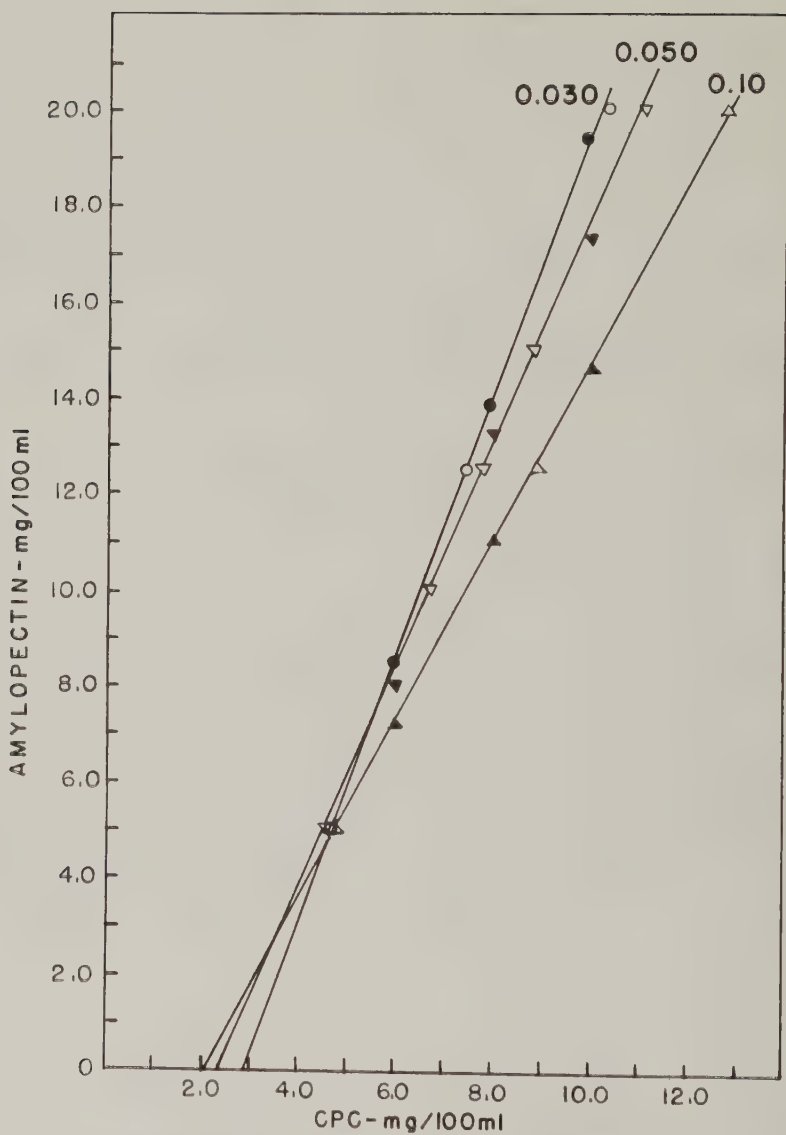


FIG. 6. Amylopectin vs. CPC for NaOH concentrations of 0.030, 0.050, and 0.100 *N*. The open symbols are taken from the points of inflection of graphs of turbidity vs. CPC. The closed symbols are taken from the points of inflection of graphs of turbidity vs. amylopectin.

for fairly large extrapolations. For these experiments, a least squares analysis of the data gives the following:

$$\frac{A - 4.83}{C - 4.61} = 1.066 + \frac{10.51}{N + 3.42} \quad [4]$$

This equation thus furnishes us with the means for determining the concentration of any one component required to initiate aggregation when the other two are known. The experimental data given by curves *A*, *B*, and *C* in Fig. 3 were used to evaluate the critical concentration of NaOH (see curve *A*, Fig. 5c) and compared with the values calculated from Eq. [4] (Table I). Inasmuch as the points which were chosen to establish Eq. [4] are only approximate, and the experimental uncertainty is ± 0.2 concentration unit, the agreement appears to be quite good.

Essentially, $s(N)$ represents the amount of amylopectin that can be aggregated by a unit amount of CPC, at a given concentration of NaOH. Thus, as the concentration of NaOH approaches zero, and no reaction occurs, a certain amount of CPC must be bound in order to overcome even the minimal repulsion between the dispersed amylopectin particles, before aggregation will occur. This results in a slope with some relatively large but finite value. On the other hand, as the concentration of NaOH approaches infinity, the charge density on the amylopectin approaches a maximum but finite value. Consequently, only a finite amount of CPC is required to effect aggregation, and the slope approaches a comparatively small, but non-zero, value.

It is apparent that there are combinations of amylopectin and CPC, calculable from Eq. [4], for which the points of inflection on the graphs of turbidity vs. NaOH concentration should lie either at zero or negative concentrations, or at infinity. The experimental evidence is indicated by curves *D* and *E* in Fig. 3. (Corresponding n values are shown in Fig. 4c, and an idealization of curve *E* is shown in Fig. 5c.)

In a physical sense, curve *E* (Fig. 3) indicates that for a finite concentration of NaOH, aggregation will not occur because the critical ratio of CPC to amylopectin is never attained. However, curve *D* indicates that with a large excess of CPC, disaggregation can occur only with an extremely large excess of NaOH.

We should now like to reconsider Fig. 6 and the reason why the lines do not pass through the origin. It has already been noted that the graphs were plotted using the total initial concentration of CPC. However, as the concentration of a surfactant in solution increases, there is an abrupt change from the simple monomeric state to a polymeric or micellar state, the point of change being referred to as the critical micelle concentration (c.m.c.). Thus, CPC exists in solution both as single ions and micellar ions and it might be expected that only one of these forms would be effective in the aggregation process. If this is so, then the data should be graphed, using the active form of CPC.

On the basis of light-scattering studies, a number of investigators have indicated that the c.m.c. decreases with increasing concentration of neutral electrolyte (15). It has also been demonstrated that a number of univalent electrolytes have a comparable effect on the lowering of the c.m.c. (16).

Therefore, if we assume that a similar effect occurs in the presence of NaOH, an examination of the data (comparable to Fig. 1) reveals that the turbidity does not begin to rise appreciably until the concentration of CPC exceeds the c.m.c. A precise determination of this point is difficult because the change in slope is gradual. However, when the attempt is made, the results are in surprisingly good agreement with the measured values for the c.m.c. (10).

It is accepted, to a first approximation, that in a solution of a surfactant above its c.m.c., the concentration of monomer remains fairly constant and is equal to the c.m.c., whereas the remainder of the surfactant exists as micelles (17). Therefore, if the points at which the straight lines in Fig. 6 cross the abscissa are assumed to be the c.m.c.'s of CPC, at the various electrolyte concentrations, then one can replot the data in terms of micelle concentration, i.e., the total concentration of CPC minus the c.m.c. These lines will now all pass through the origin. This suggests that it is the micellar form of the surfactant which is involved in complex formation and also acts as the cross-link between amylopectin chains in

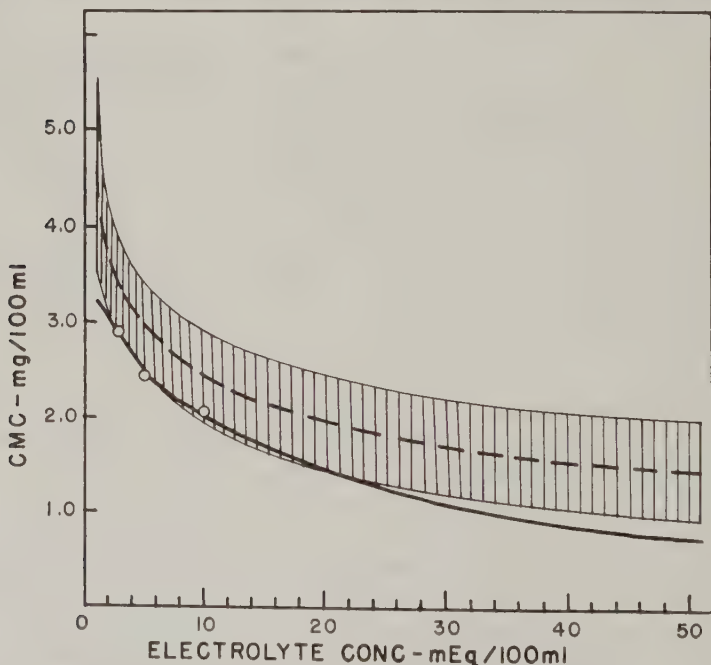


Fig. 7. Critical micelle concentration vs. electrolyte concentration. The broken curve is a graph of the equation: $\log (\text{c.m.c.} \times 10^5) = 2.04 - 0.292 \log (\text{Cl}^- \times 10^5)$, as given by Anacker (10). The width of the band corresponds to the standard deviations of the values calculated from the equation. The circles are the intercepts along the abscissa of the lines in Fig. 6. The solid curve was calculated from Eq. [6].

the aggregation process, rather than linkages through the hydrophobic portions of the quaternary ion as was suggested in an earlier paper (7).

The thought of surfactant micelles being bound to macromolecules has been proposed by a number of investigators (18-20). The validity of this assumption with regard to this work was tested by comparing our values for the c.m.c. with measured values, and for this, we selected some of the recent light-scattering data of Anacker (10). This comparison is shown in Fig. 7, where the broken curve represents Anacker's data, the width of the band corresponding to the standard deviation. The circles are the intercepts in Fig. 6 and the solid curve is based on calculations made with the aid of Eq. [3] and [4], where the c.m.c. is the intercept of the line along the abscissa, i.e., at $A = 0$, $C = \text{c.m.c.}$, and

$$\text{c.m.c.} = C_0 - \frac{A_0(N + c)}{a(N + c) + b}; \quad [5]$$

$$= 4.61 - \frac{4.51N + 15.3}{N + 13.3}. \quad [6]$$

Thus, one can calculate the c.m.c. at concentrations of NaOH both above and below those given in Fig. 6. Within experimental error, the agreement appears good, except at low concentrations of electrolyte, where the c.m.c. rises very rapidly. In part, this may be due to the fact that Eq. [6] covers a region in which there are only small changes of c.m.c. with electrolyte. However, preliminary measurements on glycogen appear to give good agreement in the low concentration region also. The results of these studies together with extensive salt studies will be reported at a later date.

CONCLUSIONS

The results of this investigation have demonstrated that in alkaline solution, amylopectin forms a complex with cetylpyridinium chloride. Aggregation of the complex occurs when critical amounts of CPC are bound and these in turn are dependent on the concentration of NaOH. The structure of the aggregates is pictured as a matrix of negatively charged particles of amylopectin cross-linked by positively charged CPC micelles.

ACKNOWLEDGMENTS

The authors wish to express their appreciation to the Corn Industries Research Foundation for its financial support and to the National Science Foundation for a grant to one of us (I.F.) as part of the Undergraduate Research Participation Program.

REFERENCES

1. PUTNAM, F., *Advances in Protein Chem.* **4**, 80 (1948).
2. YANG, J. T., AND FOSTER, J. F., *J. Am. Chem. Soc.* **75**, 5560 (1953).

3. SCOTT, J. E., *Biochim. et Biophys. Acta* **18**, 428 (1955).
4. EHRENPREIS, S., AND FISHMAN, M. M., Abstracts 135th Meeting, American Chemical Society, 7D (1959); *Biochim. et Biophys. Acta* **44**, 577 (1960).
5. BARKER, S. A., STACEY, M., AND ZWEIFEL, G., *Chemistry & Industry* **1957**, 330.
6. PALMSTIERNA, H., SCOTT, J. E., AND GARDELL, S., *Acta Chem. Scand.* **11**, 1792 (1957).
7. FISHMAN, M. M., AND MILLER, R. S., *J. Colloid Sci.* **15**, 232 (1960).
8. STACY, C. J., FOSTER, J. F., AND ERLANDER, S. R., *Makromol. Chem.* **17**, 181 (1956).
9. SCHOCH, T. J., *Advances in Carbohydrate Chem.* **1**, 247 (1945).
10. ANACKER, E. W., *J. Phys. Chem.* **62**, 41 (1958).
11. HELLER, W., AND TABIBIAN, R. M., *J. Colloid Sci.* **12**, 25 (1957).
12. MIE, G., *Ann. phys.* **25**, 377 (1908).
13. HELLER, W., AND VASSY, E., *J. Chem. Phys.* **14**, 565 (1946).
14. LA MER, V. K., *J. Phys. & Colloid Chem.* **52**, 65 (1948).
15. See for review: FISHMAN, M. M., "Light Scattering by Colloidal Systems." Technical Service Laboratories, River Edge, New Jersey, 1957.
16. CORRIN, M. L., AND HARKINS, W. D., *J. Am. Chem. Soc.* **69**, 683 (1947).
17. PHILLIPS, J. N., *Trans. Faraday Soc.* **51**, 561 (1955).
18. DERVICHIAN, D. G., *Discussions Faraday Soc.* **6**, 7 (1949).
19. HARRAP, B. S., AND SCHULMAN, J. H., *Discussions Faraday Soc.* **13**, 197 (1953).
20. BLEI, I., *J. Colloid Sci.* **14**, 358 (1959).

ON THE VARIATION OF ELECTRICAL RESISTANCE OF A POLYMER AS A FUNCTION OF THE EXTENT AND NATURE OF SORBED WATER

Koji Kawasaki

Electrotechnical Laboratory, Nagata-cho, Chiyoda-ku, Tokyo, Japan

Received November 1, 1960; revised received January 10, 1961

I. INTRODUCTION

The adsorption of water vapor on the surface of solids, such as insulating materials for electrical use, usually causes a considerable change in the surface conduction current. In order to discuss the mechanism of this effect of water vapor on the surface conduction, it is important to find out what is the carrier for conduction current along the adsorbed water layer. We have previously studied the mechanism of the variation of ionic conduction current along the surface of such solids as, glass and porcelain, with the adsorption of water vapor, and the change of the nature of the adsorbed layer (1). In the present paper, the relations between sorption of water vapor by polymers and electric resistance are further considered.

II. THE RELATIONS BETWEEN THE CONDUCTION CURRENT AND THE SORPTION OF WATER VAPOR

In general, the variation of the conduction current along the polymer film by the sorption of water vapor may be expressed by

$$\log i/i_0 = \beta m, \quad [1]$$

where i and i_0 are the intensities of current through the sample, sorbed and unsorbed, respectively; m is the moisture content in weight per cent and β is a constant of proportionality. When the moisture content is small, the variation of conduction current by the sorption of water vapor follows Eq. [1] as shown in Fig. 1 (2).

If the moisture content is large the variation of conduction current does not follow Eq. [1], as shown in Figs. 2 and 3. Rather Eq. [1] is an approximation of the range where the moisture content m , is less than a certain critical value characteristic of the material used, and as m increases above the critical value this linearity between $\log i/i_0$ and m ceases to hold, and the conduction current (i) increases linearly with m in good accordance

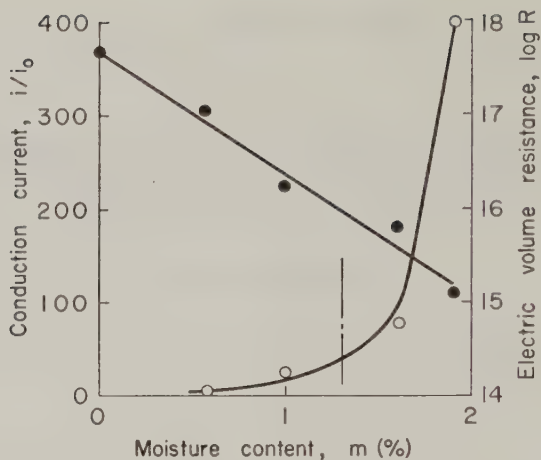


FIG. 1. Electrical current and resistance versus moisture content for polymethylmethacrylate. From the data of R. Kawai. \circ — i/i_0 ; \bullet — $\log R$.

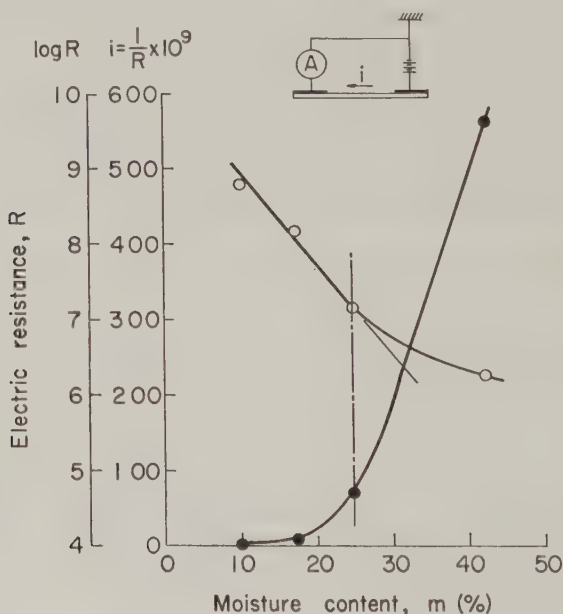


FIG. 2. Electrical current and resistance versus moisture content for a film of polyvinyl alcohol. \circ — i ; \bullet — $\log R$.

with the following expression:

$$i/i_0 = 1 + \alpha m, \quad [2]$$

where α is a constant.

From the results shown in Fig. 2 the critical value of m is about 25 for

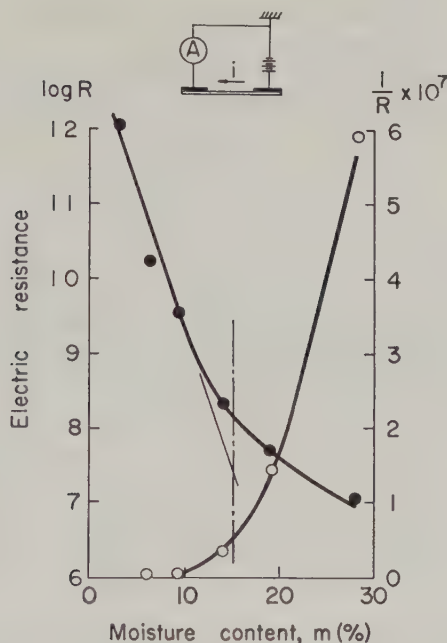


FIG. 3. Electrical current and resistance versus moisture content for a film of gel cellophane. ○— i ; ●— $\log R$.

polyvinyl alcohol film and about 15 for gel cellophane film. The deviation from Eq. [1] may be considered as due to the change of the nature of the sorbed water, namely, from localized water to mobile water.

The sorption isotherms for polymers were determined gravimetrically by suspending the sample from the end of a sensitive quartz spring in an all-glass vacuum vessel and measuring the spring elongation using a cathetometer. The variation of direct current by the sorption was measured with a galvanometer by the method previously reported (3).

III. ON THE PHASE OF THE SORBED WATER AND DOLE'S THEORY OF THE SORPTION ISOTHERM

From a theoretical point of view, there are two important regions in the adsorption isotherm. One of these regions is at very low pressures, at which the first few layers are formed, and the other is at very high pressures where the transition takes place from localized to mobile adsorption.

The physical difference between these two regions lies in the binding forces involved. At low vapor pressures, the forces between sorbed molecules and the adsorbent dominate the process, whereas at nearly saturated vapor pressure the forces between the water molecules become governing. When the amount of sorbed water is very large, sorbed molecules in the

upper strata are not affected by the fine structure of the adsorbent, and they are in a liquid-like state.

Dole (4) has generalized Hill's treatment to include variable heats of sorption in different layers. He has derived the following general isotherm:

$$\frac{m}{m_0} = x \left(\frac{\phi'}{\phi} \right) \quad [3]$$

$$\phi = 1 + C_1 x + C_1 C_2 x^2 + C_1 C_2 C_3 x^3 + \cdots, \quad [4]$$

where m is the moisture content (g./g.) in per cent, m_0 is the moisture content corresponding to a monolayer, x is the relative vapor pressure, ϕ' is the first derivative of ϕ with respect to x , and the constants C_1 , C_2 , etc., are the ratios of the internal partition functions of the sorbed molecules

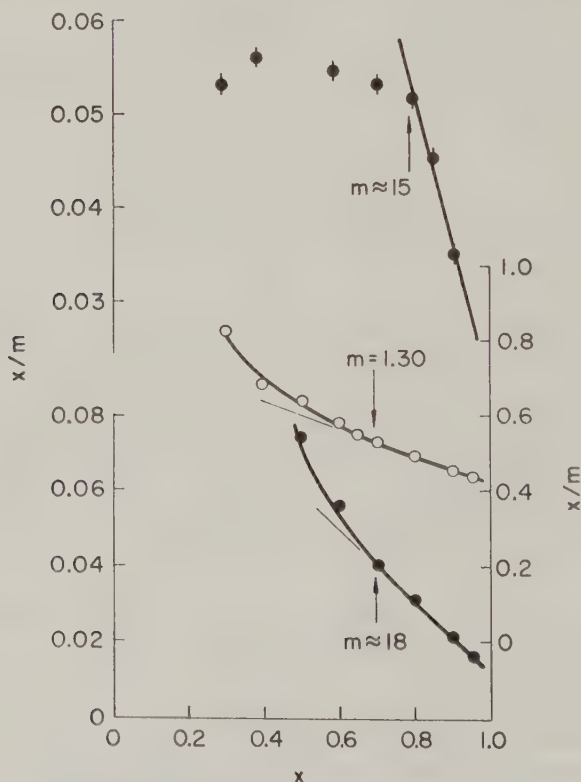


FIG. 4. Comparison of Dole's sorption isotherm (Eq. [5]) with the experimental data on isotherms for some polymers. ●—Polyvinyl alcohol, $k = 0.90$ (left ordinate); ●—Gel cellophane, $k = 0.88$ (left ordinate); ○—Polymethyl methacrylate, $k = 0.47$ (right ordinate).

in the first, second, etc., layers to the partition function of the molecule in the pure liquid.

If all C_1 are equal to $1/k$, it follows that:

$$\frac{x}{m} = \frac{1}{km_0} - \frac{x}{m_0}. \quad [5]$$

If the C constants are all unity, Eq. [5] becomes

$$\frac{x}{m} = \frac{1}{m_0} - \frac{x}{m_0}. \quad [6]$$

Equation [5] is considered to be a modified Raoult's law.

We shall assume that the limiting slope as x goes to unity represents the modified Raoult's law slope. Results on the sorption of water vapor for polyvinyl alcohol film, gel cellophane film, and a plate of polymethyl methacrylate are shown as a plot of x/m versus x in Fig. 4. The water sorption isotherms at high humidity show the linearity of x/m in m predicted in Eq. [5], and k is nearly equal to unity for polyvinyl alcohol and gel cellophane, but k for polymethyl methacrylate is considerably less than unity. Further the region where Eq. [5] holds is the region where Eq. [1] no longer holds.

The number of sorbed water molecules per structural unit of polymer, \bar{a} , may easily be calculated from the moisture content. Furthermore, if the number of hydrophilic sites in the basic unit, γ , is known, the number of sorbed water molecules per sorption site, (a), is obtained from $\bar{a} = \gamma a$. Values are readily calculated for adsorbents of known chemical constitution.

Values of \bar{a} and a for the various polymers are given in Table I for the critical value of m corresponding to the deviation of Eq. [5] from Eq. [1]. From this table it is found that the critical moisture content, in the region

TABLE I
Calculated Adsorption Characteristics

Substance	Cry- stal- linity	From Dole's Eq. [5]				From Eq. [1]			
		M_{ca}	\bar{a}	γ	a	M_{ci}	\bar{a}	γ	a
Polyvinyl alco- hol	≈ 25	18	0.6	1	0.6	25	0.8	1	0.8
Gel cellophane	35	15	1.8			10 ~ 15	1.1 ~ 1.8		
Polymethyl methacrylate		1.3	0.07	1	0.07				

M_{ca} : lower limit of moisture content at which Eq. [5] holds.

M_{ci} : upper limit of moisture content at which Eq. [1] holds.

where Eq. [1] ceases to hold and Eq. [5] holds with $k = 1$, corresponds to sorption when a is nearly equal to unity. However for materials in which a is considerably less than unity, Eq. [1] holds for high humidity.

The author is indebted to Mr. Y. Sekita for his measurements of sorption isotherms and to Mr. K. Kanou for his measurements of electrical properties.

REFERENCES

1. KAWASAKI, K., *J. Appl. Phys. Japan* **27**, 216 (1958).
2. KAWAI, R., Articles in Commemoration of the 10th Anniversary of the Founding of the Hitachi Central Research Laboratory, pp. 5-15, 1952.
3. KAWASAKI, K., AND KANOU, K., *Bull. Electrotech. Lab. (Tokyo)* **17**, 241 (1953).
4. DOLE, M., *J. Chem. Phys.* **16**, 25 (1948); *Annals N. Y. Acad. Sci.* **51**, 705 (1949).
DOLE, M., AND FALLER, L., *J. Am. Chem. Soc.* **72**, 414 (1950).

TENSILE STRESS RELAXATION BEHAVIOR OF PARTLY TO COMPLETELY ACETYLATED POLYVINYL ALCOHOL POLYMERS

Kiyohisa Fujino, Tuneso Horino,¹ Kihachiro Miyamoto, and
Hiromichi Kawai²

*Department of Textile Chemistry, Kyoto University, Kyoto, Japan, and Department of
Chemistry, University of Massachusetts, Amherst, Massachusetts*

Received November 2, 1960; revised received December 27, 1960

INTRODUCTION

In the previous paper of this series (1) the stress relaxation behavior of the copolymers of methylmethacrylate and methylacrylate, including polymethylmethacrylate and polymethylacrylate as the extremes, were studied at various temperatures. The results were discussed in terms of the relaxation spectrum, which was obtained from the so-called master relaxation curve composed of relaxation curves at various temperatures. The hypothesis of time-temperature superposition was employed in deriving the master relaxation curve.

The conclusion was drawn that with increasing mole ratio of methylmethacrylate in the copolymer; the stiffer the chain backbone, the less steep the average slope of the wedge portion of the spectrum approaching the theoretical value of $-1/2$, and the higher the intensity of the lower plateau portion of the spectrum (the so-called box-type portion).

These regular spectrum changes shown by amorphous polymers with variation of molecular structure are also interesting in relation to preliminary results in a systematic investigation of the spectrum changes which occur on going from an amorphous to a crystalline polymer. The relaxation spectrum of a crystalline polymer has been found to be quite different from that of an amorphous polymer, especially at the wedge and/or the box portions (2). Generally, the relaxation spectrum of a crystalline polymer has been found to be characterized by a less steep wedge and higher intensity box portions than that of an amorphous polymer. The result is a flatter relaxation spectrum as a whole for a crystalline polymer.

¹ Present address, Department of Textile Engineering, Art Industry and Textile College of Kyoto, Kyoto, Japan.

² Present address, Department of Textile Chemistry, Kyoto University, Kyoto, Japan.

TABLE I
Acetylation Condition of Polyvinyl Alcohol

Specification	Reagent (moles) ^a	Medium (moles) ^a	Catalyzer (mole/l.) ^b	Temp. (°C.)	Time (hours)
PVOH	—	—	—	—	—
PVAc-3	Acetic acid, 1.0	Water, 18.0	Hydrochloric acid, ^c 0.67	60	70
PVAc-15	Acetic acid, 2.7	Water, 14.7	Hydrochloric acid, 0.67	60	70
PVAc-40	Acetic acid, 5.0	Water, 6.5	Hydrochloric acid, 0.67	60	70
PVAc	Acetic anhydride, 1.6	Pyridine, 3.6	Hydrochloric acid, 0.67	80	70

^a For one mole pf PVOH.^b For whole system.^c Neutralized by sodium acetate and removed by dialysis under running water.

In the present paper the effects of acetylation of polyvinyl alcohol (ranging from 3 to 100 mole % acetate) upon the relaxation spectrum were studied as one of a series of systematic investigations of the spectrum changes which occur on going from a completely amorphous to a quasi-crystalline polymer.

PREPARATION OF SAMPLE POLYMERS AND TEST SPECIMENS

The sample polymers were prepared by acetylation from a purified polyvinyl alcohol (D.P. 1600) obtained by complete saponification of polyvinyl acetate. The conditions used (3) are shown in Table I.³ The degree of acetylation was determined by chemical analysis for the acetyl group and is shown in Table II, together with other characteristics such as the density and the X-ray diffraction diagram.

The sample polymers were cast into thin films about 0.2 mm. thick by pouring 10% aqueous solutions (acetone solution in the case of PVAc) onto a glass plate floating on mercury and then by drying gradually under room conditions. Polyvinyl acetate films were also leached by dipping in running water in order to extract residual acetone and were then dried in air. The films thus formed were cut into test specimens about 1 to 7 mm. wide and 60 mm. long. They were dried again in a vacuum desiccator with P₂O₅ for more than 2 weeks until used.

The X-ray diffraction diagrams of the polymers are briefly shown in Table II. The analysis was given by Fujimoto and Hirabayashi (4). The X-ray diagrams of partly acetylated polyvinyl alcohol up to 3 mole % still show crystalline features that are essentially the same as those of the

³ The molecular weight distribution of the polyvinyl alcohol and of its acetylated polymers seems to be very broad owing to a higher than 90% conversion in the polymerization of the original polyvinyl acetate before saponification.

TABLE II

Degree of Acetylation, Density, and X-Ray Diffraction Diagram of the Polymers

Specification	Degree of acetylation (mole %)	Density ^a (g./c.c.)	X-ray diffraction diagram
PVOH	0.3	1.284 (1.300) ^b	Fairly sharp rings
PVAc-3	3.0	1.274	Somewhat diffuse, essentially same as above except considerably diffuse ring of R_3
PVAc-15	14.0	1.236	A very broad and diffuse ring corresponding to R_3 of PVOH
PVAc-40	40.0	1.209	A very broad and diffuse ring corresponding to R_2 of PVAc
PVAc	100.0	1.176	A couple of diffuse rings

^a Measured at 30.0°C. by flotation method in mixtures of benzene and carbon-tetrachloride.

^b After annealing at 180°C. for 10 min.

air-dried polyvinyl alcohol cast from solution, except for a somewhat diffuse ring corresponding to R_3 of the PVA diagram. With increasing degree of acetylation up to 15 mole %, the diagrams indicate a gradual change from crystallinity to a completely amorphous condition with a very wide and diffuse ring corresponding to R_3 of the PVA diagram. The diagram for 40 mole % acetylation also shows an amorphous condition with a very diffuse ring corresponding to R_2 of PVAc. The change of density due to acetylation mainly occurs up to 15 mole % acetylation as shown in Table II. This result may be additional support for the change of crystallinity.

APPARATUS AND PROCEDURE

Three sets of chainomatic balance type auto-recording relaxometer were used. They essentially follow the design of Ninomiya *et al.* (5). They have different capacities and sensitivities owing to differences in the moment of inertia of the balance arm and in the construction of the arm supporter. For the glassy and transition region measurements the heavy capacity relaxometer has an arm supporter of steel plate and an agate knife edge; for the rubbery region measurements a medium capacity one has a steel pin and an agate pivot; for the flow region an extremely light capacity one of light arm was used.

The relaxometer is divided into two parts, Fig. 1, one of which consists of a balance, sample straining mechanism, and double-shielded type temperature oven. The other part is a stress recorder consisting of a recording drum and a pen. The drum can be driven at two different constant speeds for quick and slow recordings and the pen is driven by a series motor governed by an electric contact attached to the balance arm in such a way as to go

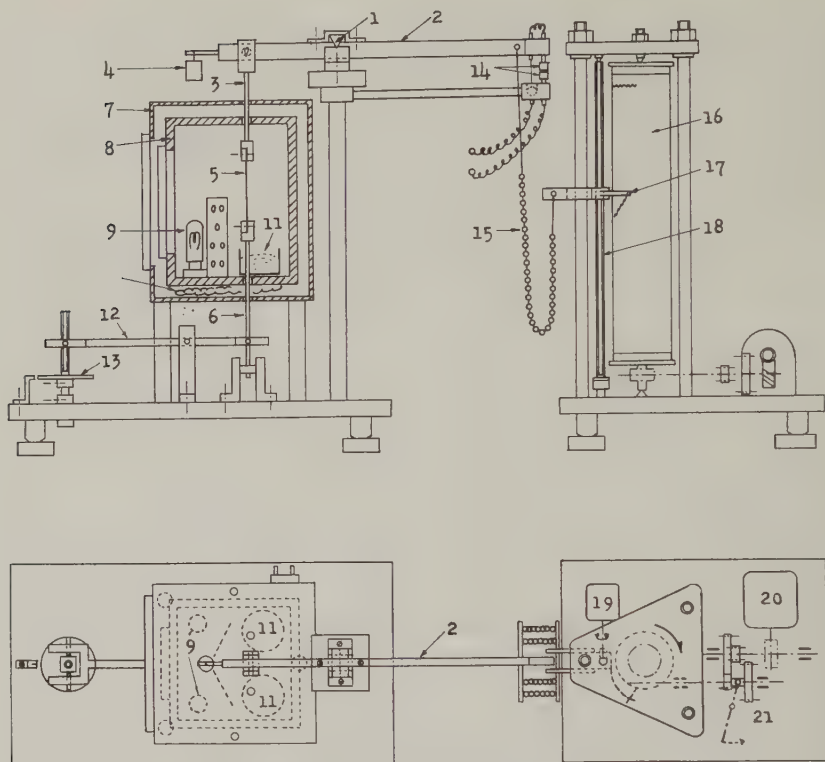


FIG. 1. Front and top views of the chainomatic balance type auto-recording relaxometer used. 1—Balance arm supporter; 2—balance arm; 3—upper jaw; 4—counter weight; 5—sample specimen; 6—lower jaw; 7—outer oven; 8—inner oven; 9—projector bulb as heat source for the inner oven; 10—Nichrome wire as heat source for the outer oven; 11— P_2O_5 powder for reducing humidity in the inner oven; 12—connecting lever between the lower jaw and the micro-screw; 13—micro-screw for straining the sample specimen; 14—electric contacts; 15—balancing chain; 16—recording drum; 17—recording pen; 18—screw for driving the recording pen upwards and downwards; 19—series motor for the pen motion; 20—synchronous motor for driving the recording drum.

upward when the contact closes and downward when the contact opens. A balancing chain is attached at one end to the balance arm and at the other end to the pen, so that the pen always records a change of tensile stress in the sample. Several kinds of balancing chain, with linear density ranges from 0.18 to 27.5 g/cm., were used according to the range of tension measured.

The temperature of the outer oven was always kept about 5°C . lower than that of the inner oven and the temperature of the inner oven was kept within $\pm 0.1^\circ\text{C}$. over the range from room temperature to 170°C . The heat

source of the outer oven was the usual Nichrome wire controlled by a bimetallic thermo-regulator, while the inner oven was heated by two 100-watt projector bulbs controlled by a mercury type thermo-regulator, which reduced the time lag of operation successfully. An excess of P_2O_5 powder was used to reduce humidity in the inner oven.

It was necessary to reduce the chattering of the relay due to excessive vibration of the balance arm by adding a C-R circuit of a proper time constant to the control grid of the vacuum tube in the relay circuit, as shown in Fig. 2. Actually, the time constant could be varied from 0.3 to 1.2 sec. for charging and from 0.1 to 0.4 sec. for discharging by changing the capacity of the condenser in the C-R circuit from 2 to 8 μF .

Before measurement, the test specimen was hung freely from the upper jaw of the relaxometer within the inner oven and was annealed as follows: 190°C., 10 min. for PVOH; 150°C., 10 min. for PVAc-3; 150°C., 1 min. for PVAc-15 and 40; 70°C., 1 min. for PVAc. The annealing temperature was taken as somewhat higher than the highest measuring temperature for each polymer. After annealing the sample was cooled gradually to the temperature for relaxation measurements.

The annealing was necessary to reduce scattering of the results due to differences in thermal history of the test specimens, not only for crystalline

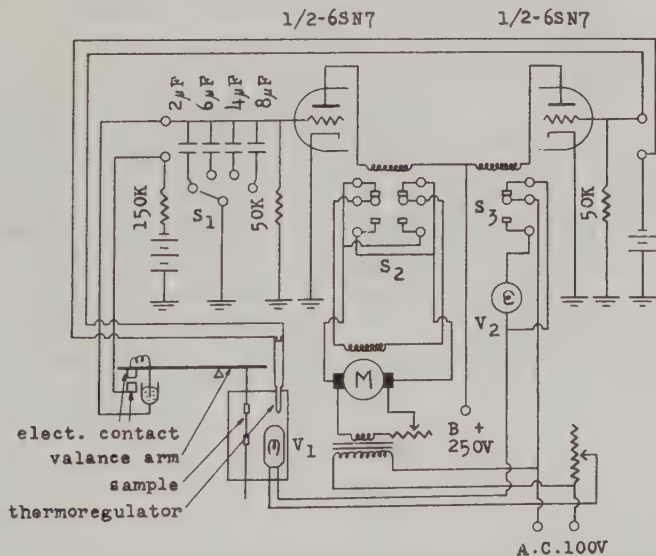


FIG. 2. Schematic diagram of the relay circuits controlling the recording pen motion and the temperature of the inner oven. V_1 = 100-w. projector bulb as heat source; V_2 —ballast tube; S_1 —1-pole 4-position rotary switch; S_2 —2-pole 2-position relay switch; S_3 —1-pole 2-position relay switch; M —series motor.

polymers such as PVOH but also for amorphous polymers such as PVAc. The annealing, of course, increased the density of the PVOH sample from 1.284 to 1.300 as well as the sharpness of the X-ray diffraction diagram. As calculated from the densities of the amorphous and crystalline phases of PVOH proposed by Sakurada *et al.* as 1.269 and 1.345, respectively, at 25°C. (6), the degree of crystallinity of the PVOH increased from 20% to 42%. However, for the other polymer samples there were seldom changes in density and in the X-ray diffraction diagram due to annealing (7).

An initial tensile strain was applied by the lower jaw of the relaxometer which was connected by a lever to a micrometer as shown in Fig. 1. The tensile strain was kept within 1.1% for glassy state measurements for every polymer sample; within 1.5% for the temperature range higher than the glassy state for PVOH and PVAc-3; 1.5% to 3.0% for transition region measurements, 5% to 10% for rubbery region measurements, and 10% to 15% for flow region measurements for the other three polymers. The levels of strain corresponded to linear viscoelastic behavior.

RESULTS AND DISCUSSION

The stress-relaxation behavior versus time is plotted in Figs. 3 to 7 as a function of temperature, where the stress is normalized by the relaxation

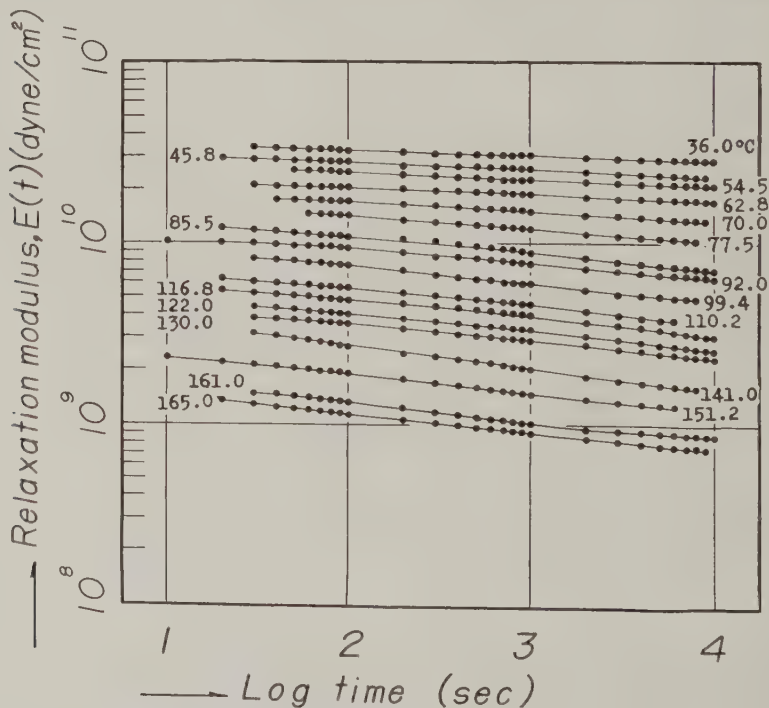


FIG. 3. Stress relaxation of PVOH shown by relaxation modulus, $E(t)$ vs. time t (sec.) at various temperatures.

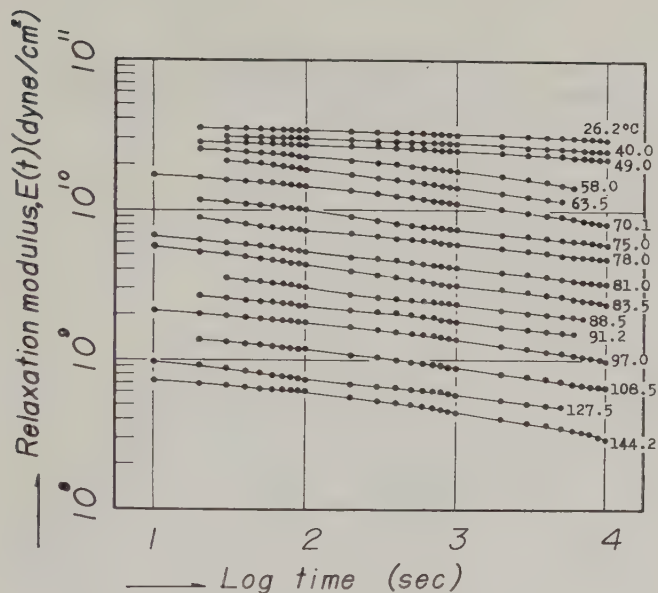


FIG. 4. Stress relaxation of PVAc-3 shown by relaxation modulus, $E(t)$ vs. time t (sec.) at various temperatures.

modulus function $E(t)$ in dynes/cm.², i.e., the stress divided by a given strain.

With increasing degree of acetylation, it is obvious that the relaxation modulus decreases remarkably with increase of temperature, showing a distinct transition from glassy to rubbery states as well as a flow region at high temperature. The behavior is typical of a linear amorphous polymer (non-crosslinked). The transition region also appears at a lower temperature with increasing degree of acetylation. However, for polymers with less than 15 mole % acetylation, the relaxation modulus does not decrease so much with increase of temperature and also does not show any discrete transition region nor any flow region, at least within the temperature range measured.

In order to compare the results for different polymers, the so-called master curve of stress relaxation was composed, at a reference temperature of 75°C., from the relaxation curves at various temperatures on the basis of the hypothesis of time-temperature superposition (8), an actual procedure of which will be discussed later. While the hypothesis was used it is recognized that its validity is still a matter of discussion for amorphous polymers and especially for crystalline polymers. (Nagamatzu *et al.* (2) and (9)).

For the crystalline polymers of PVOH to PVAc-3, it was assumed that within the temperature range corresponding to the glass transition region for amorphous polymers any structural change, such as crystallization or decrystallization, does not occur (10) and the hypothesis of time-temperature superposition is still valid.

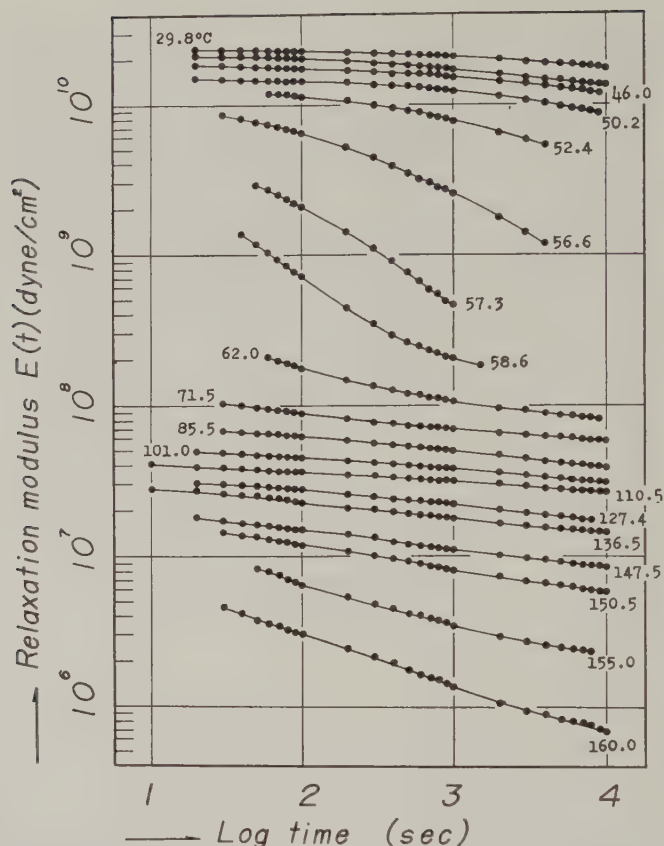


FIG. 5. Stress relaxation of PVAc-15 shown by relaxation modulus, $E(t)$ vs. time t (sec.) at various temperatures.

The glass transition temperatures (primary) of PVOH and PVAc-3 were determined as 90° and 82°C ., respectively, with an apparatus which measures the dynamic modulus as a function of temperature at a given constant frequency in the millicycle range (about 1.5×10^{-3} c.p.s.) by means of the hysteresis loop method (11). The results are shown in Figs. 8 and 9, where dots and half-dots are the real part of the dynamic modulus and of the mechanical loss tangent, respectively, and the circles are re-plotted from the stress relaxation moduli at 1000 sec. in Figs. 3 and 4. For the PVOH there are two small dispersions at about 90° and 130°C ., the former of which is considered as a dispersion due to segmental diffusion in the amorphous phase (12-14), i.e., the glass transition temperature (primary); the latter, however, has not been explained in terms of a molecular process although it may arise from a transition due to a structural change in the crystalline phase (15, 16). For the PVAc-3 there is a discrete dispersion at 82°C .,

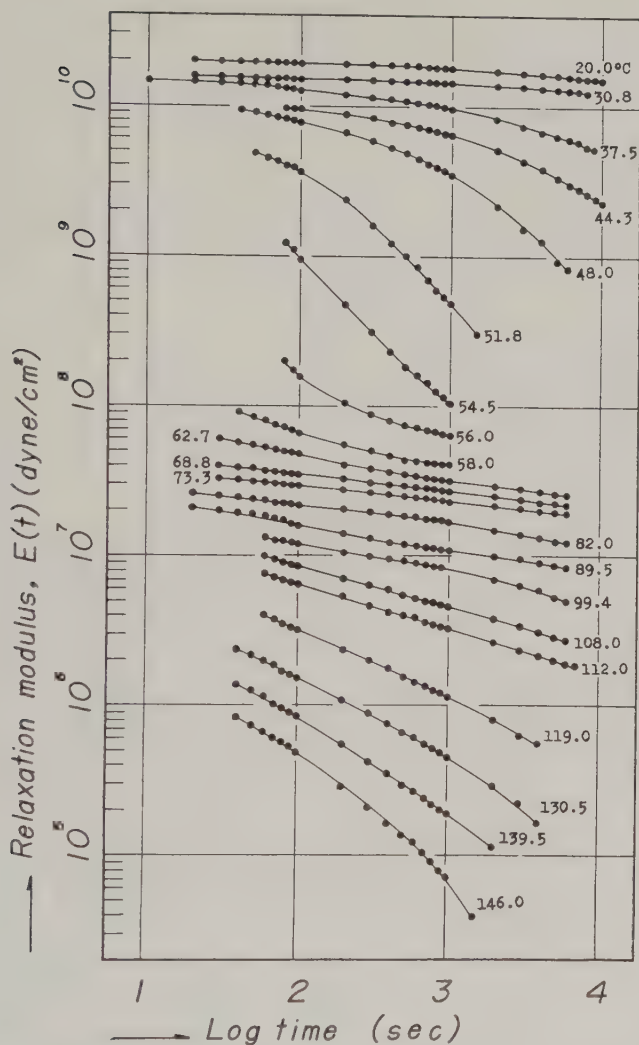


FIG. 6. Stress relaxation of PVAc-40 shown by relaxation modulus, $E(t)$ vs. time t (sec.) at various temperatures.

which corresponds to the glass transition temperature. Consequently, the glass transition regions of PVOH and PVAc-3 were assumed to be about 60° to 110°C. and about 60° to 120°C., respectively, where the hypothesis of time-temperature superposition is still valid.

For the amorphous polymers from PVAc-15 to PVAc, it was also assumed that the hypothesis of time-temperature superposition is valid for the whole temperature range covered; the validity of this assumption is, however, somewhat doubtful and will be discussed later.

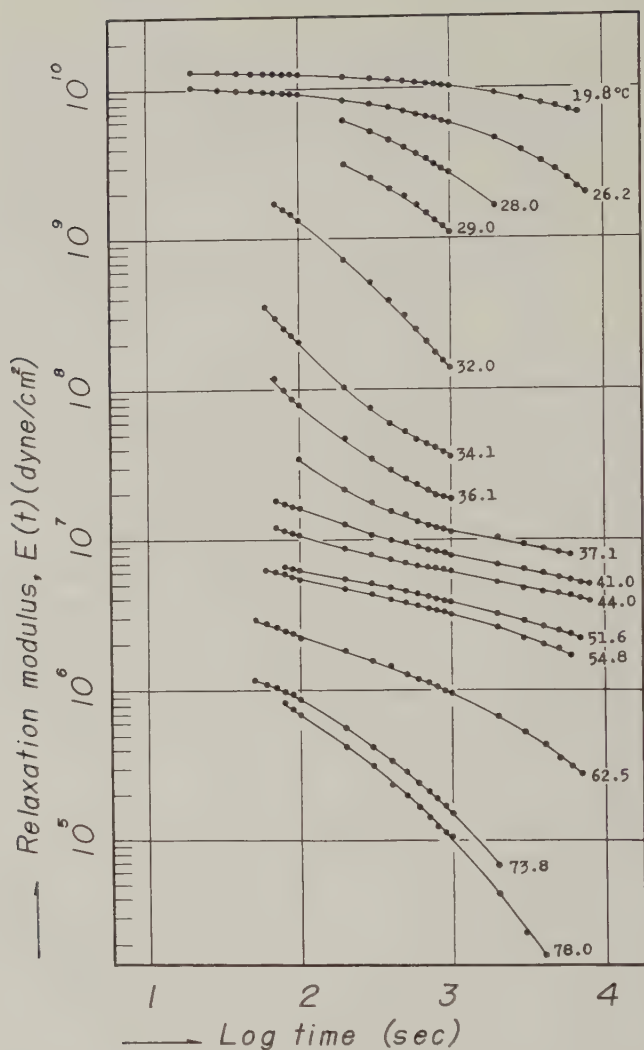


FIG. 7. Stress relaxation of PVAc shown by relaxation modulus, $E(t)$ vs. time t (sec.) at various temperatures.

Figure 10 shows the master relaxation curves reduced to 75°C. on the basis of the assumptions mentioned above, where the usual correction (17) for thermal expansion and for the temperature dependency of the elastic modulus due to rubber elasticity was neglected, assuming, $T\rho/T_0\rho_0$ to be unity.

Actually the procedure of superposition, i.e., composing the master curve, was quite easy for PVAc; somewhat difficult for the rubbery and flow regions of PVAc-40; and so difficult for the flow region of PVAc-15

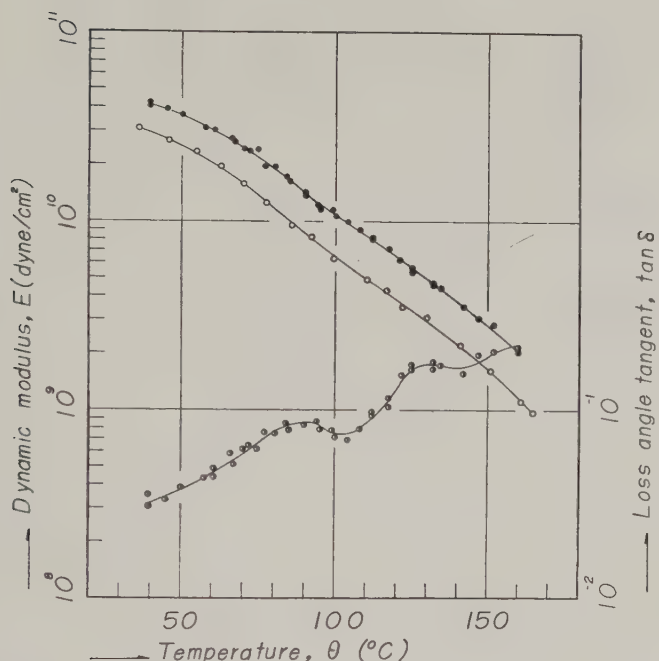


FIG. 8. Temperature dependency of dynamic modulus, $E(\omega)$, shown by dots, and loss angle tangent, $\tan \delta(\omega)$, shown by half-dots for PVOH at a particular frequency of 1.5×10^{-3} c.p.s., where open circles correspond to relaxation modulus $E(t)$ at 1×10^3 sec.

that the region was neglected.⁴ For PVAc-3 the procedure was rather easy, whereas for PVOH it was somewhat arbitrary.

The master relaxation curve of PVAc shows a typical shape for linear amorphous polymers and has four characteristic regions; a glassy state at a relaxation modulus of about 10^{10} dynes/cm.²; a transition region with steep decrease of the modulus from glassy to rubbery values; a rubbery state with a modulus of about 10^7 dynes/cm.²; and a flow region where the modulus decreases steeply again. With decreasing degree of acetylation, the master curve not only shifts to longer times but also loses the discrete transition and the flow regions and approaches a monotonic decrease of relaxation modulus.

An activation energy of the relaxation process, ΔH_n , can be calculated

⁴ The difficulty of the superposition in the rubbery region can be reduced to some extent by a correction proposed by Saunders *et al.* (*J. Colloid Sci.* **14**, 222 (1959)) assuming an effective dissociation of entanglement coupling points with increasing temperature; however, the difficulty in the flow region, especially for PVAc-15, cannot be reduced by the correction which may be invalid in the region, essentially. The details will be discussed in a following paper.

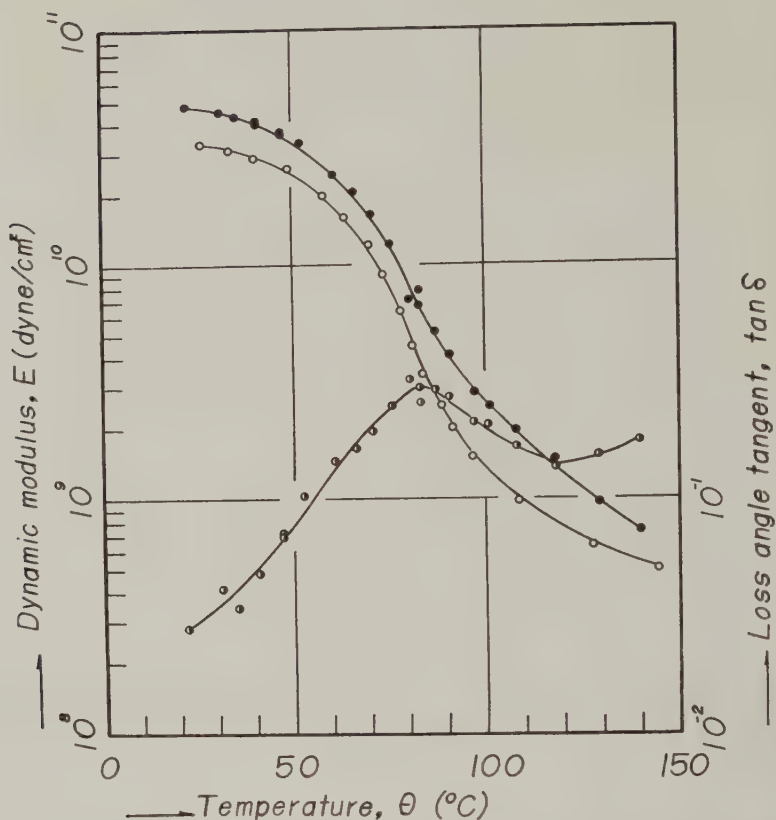


FIG. 9. Temperature dependency of dynamic modulus, $E(\omega)$, shown by dots and loss angle tangent, $\tan \delta(\omega)$, shown by half-dots for PVAc-3 at a particular frequency of 1.5×10^{-3} c.p.s., where open circles correspond to relaxation modulus $E(t)$ at 1×10^3 sec.

by using the so-called shift factor a_T as follows;

$$\Delta H_a = 2.303R \frac{d \log a_{T_0}}{d \left(\frac{1}{T} \right)}, \quad [1]$$

where a_{T_0} is the shift factor with respect to the reference temperature of 75°C., i.e., the amount of shift along the time axis applied to any relaxation curve at a certain temperature to make it conform with the master relaxation curve at the reference temperature of 75°C.; R is the gas constant; and T is the measurement temperature (°K.) of the original relaxation curve.

The results are shown in Fig. 11, where the PVOH result was neglected owing to arbitrariness in deciding the master curve. The activation energy

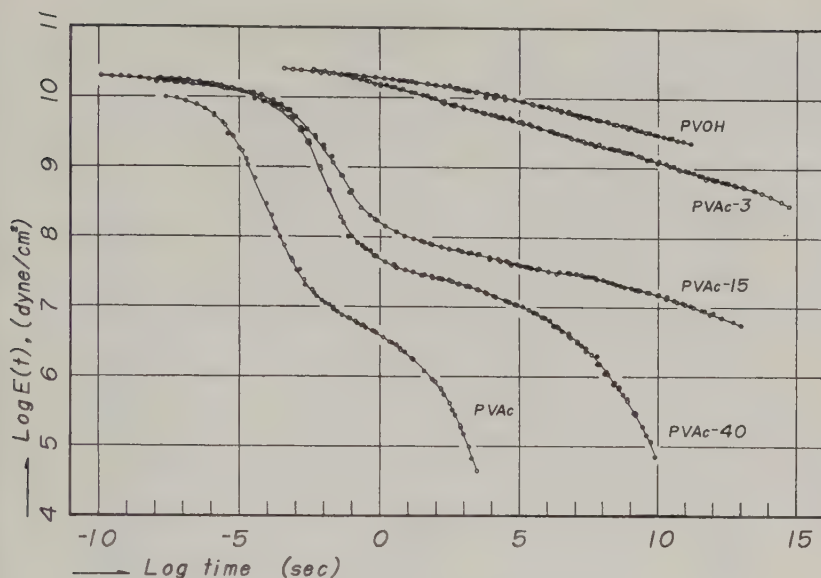


FIG. 10. Master relaxation curves reduced to 75°C.

of the relaxation process is not independent of temperature, having a sharp maximum at a particular temperature T_0 which has been closely related to the glass transition temperature (18). The particular temperature T_0 and the maximum apparent activation energy at the temperature are tabulated in Table III. The temperature T_0 as well as the maximum apparent activation energy $(\Delta H_a)_{\max.}$ increases with decreasing degree of acetylation.

Figure 12 compares the shift factors, a_T , determined as above with those predicted by the W.L.F. equation (13) within the temperature range higher than the glass transition temperature. The equation is

$$\log a_{T_0} = -\frac{C_1^0(T - T_0)}{(C_2^0 + T - T_0)}, \quad [2]$$

where C_1^0 and C_2^0 are constants with respect to T_0 . The equation can be reformed as follows:

$$\frac{(T - T_0)}{\log a_{T_0}} = -\left(\frac{C_2^0}{C_1^0}\right) + \frac{(T - T_0)}{C_1^0}, \quad [2']$$

which is applicable for checking the agreement by means of a linear relationship between $(T - T_0)/\log a_{T_0}$ and $T - T_0$.

As shown in the figure, the linear relationship holds fairly well for PVAc-3 and PVAc over the temperature range higher than T_0 , whereas the relationship does not hold for PVAc-15 and 40 having two or three inflexion

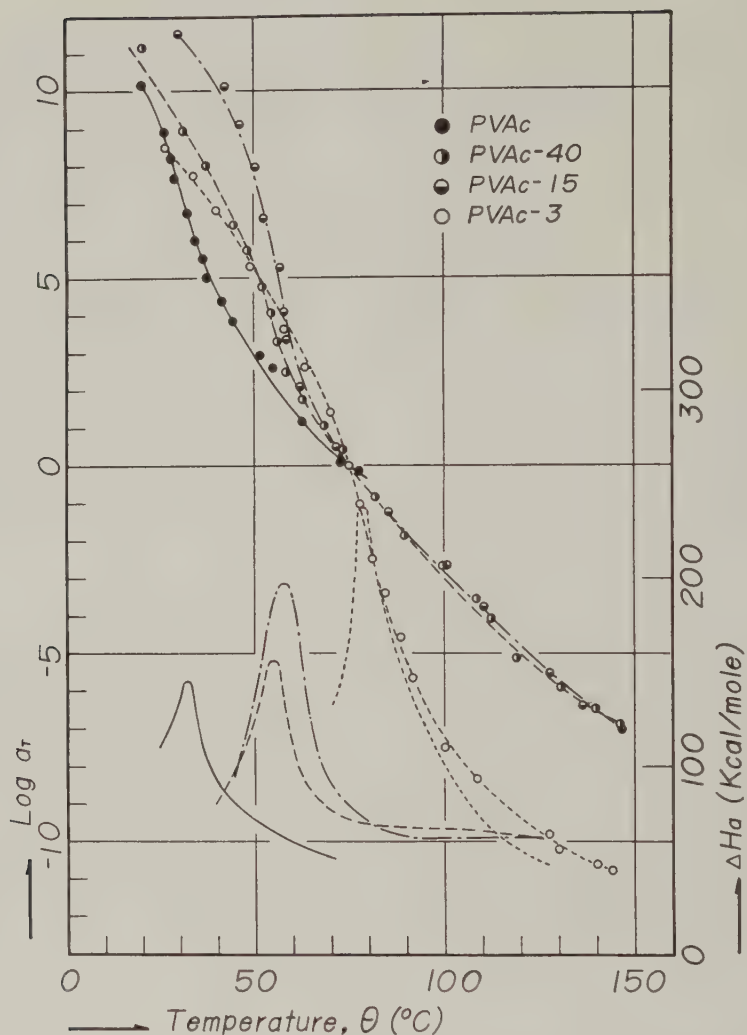


FIG. 11. Temperature dependency of shift factor, a_T and apparent activation energy for the relaxation process, ΔH_a .

points. Here, the reference temperature T_0 was chosen arbitrarily about the middle of measurements, about 50°K . higher than T_g , i.e., 400° , 380° , 371° , and 349°K . for PVAc-3, PVAc-15, PVAc-40, and PVAc, respectively.

In other words, the temperature dependence of a_T agrees well with that predicted from the W.L.F. equation for PVAc and PVAc-3 over quite a wide temperature range, as for other typical amorphous polymers for which the temperature range has been observed to extend from T_g to T_g plus

TABLE III
The Temperature at Maximum Activation Energy and the Value of the Energy

Specification	Temperature at max. activation energy T_g ($^{\circ}\text{K}$)	Max. activation energy (kcal./mole)
PVOH	(363) ^a	—
PVAc-3	352 (355) ^a	238
PVAc-15	331	198
PVAc-40	328	156
PVAc	305	145

^a Temperature at maximum loss angle tangent, $(\tan \delta)_{\max}$ in Figs. 8 and 9.

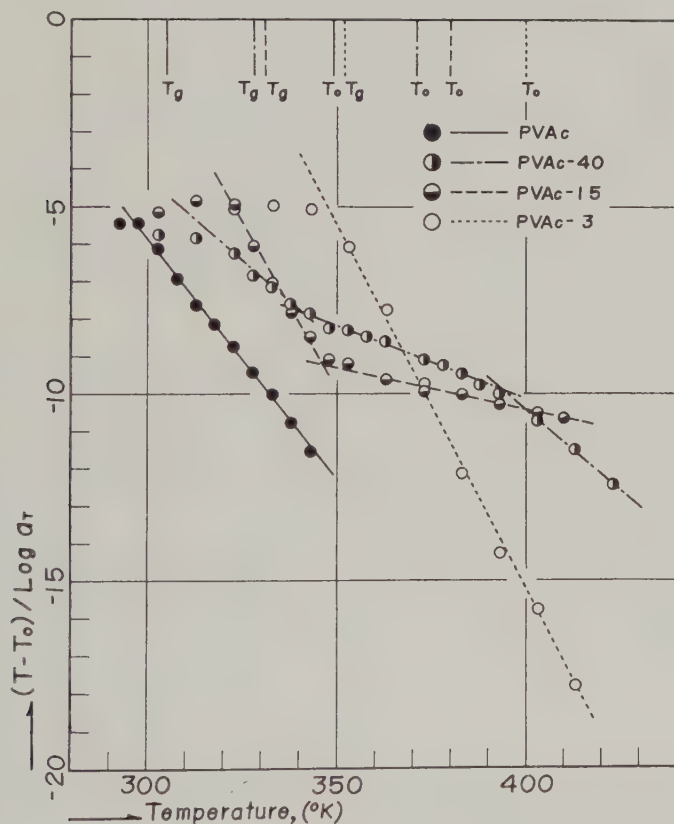


FIG. 12. Check of the temperature dependency of α_T with the predictions of the W. L. F. equation.

about 100°K . (13). But for PVAc-15 and 40, the temperature dependence can be presented by a combination of two or three of the W.L.F. equations for which the temperature ranges are relatively narrow, corresponding, at least qualitatively, to the transition and the rubbery regions for PVAc-15

and the transition, the rubbery, and the flow regions for PVAc-40, respectively.

The constants C_1^0 and C_2^0 can be evaluated from the slope of the linear relationship and from the extrapolated intercept of $(T - T_0)/\log a_T$ at $T = T_0$ in Fig. 12. They are shown in Table IV with respect to the reference temperature, together with other physical constants, the fractional free volume f_g at the glass transition temperature T_g , and the thermal expansion coefficient α_f , which can be obtained by using the following equation (13):

$$\log a_T = -\frac{1}{2.303f_g} \frac{T - T_g}{\frac{f_g}{\alpha_f} + T - T_g}, \quad [2'']$$

where the value of the glass transition temperature was temporarily adopted from T_g obtained in this experiment as the particular temperature at the maximum activation energy listed in Table III. It is difficult to find any systematic changes in f_g and α_f with changing degree of acetylation. However the values of f_g obtained from the first segment in the straight-line relationship, which corresponds to the transition region, are rather close to the theoretical values of 0.025 (13) and of 0.02 to 0.03 (19) and to other experimental values (20, 21).

It is noteworthy that the temperature dependency of a_T agrees well with that predicted from the W.L.F. equation within the temperature range of the glass transition region of such a quasi-crystalline polymers as PVAc-3, whereas the equation holds only within rather narrow temperature ranges for such amorphous polymers as PVAc-15 and 40. The anomaly found for the PVAc-15 and 40 may suggest some complex phase structures in the polymers when compared with other completely amorphous polymers, even if the former are amorphous polymers from the X-ray crystallographic point of view.

Figure 13 shows the relaxation spectra of the polyvinyl alcohol polymers, determined from the master curves at the reference temperature of 75°C.

TABLE IV

The Constants C_1^0 and C_2^0 at the Reference Temperature T_0 , the Fractional Free Volume f_g at T_g and the Thermal Expansion Coefficient α_f

	PVAc 3	PVAc-15			PVAc-40			PVAc
C_1^0	5.12	5.57	45.4	11.2	25.6	11.6	7.73	
C_2^0	77.9	85.0	454	118	230	92.1	94.1	
$T_0(^{\circ}\text{K.})$	400	380	380	371	371	371	349	
$f_g \times 10^2$	3.25	3.29	0.852	2.45	1.37	1.99	2.98	
$\alpha_f \times 10^4$	10.8	9.16	0.187	3.26	7.34	4.05	5.96	

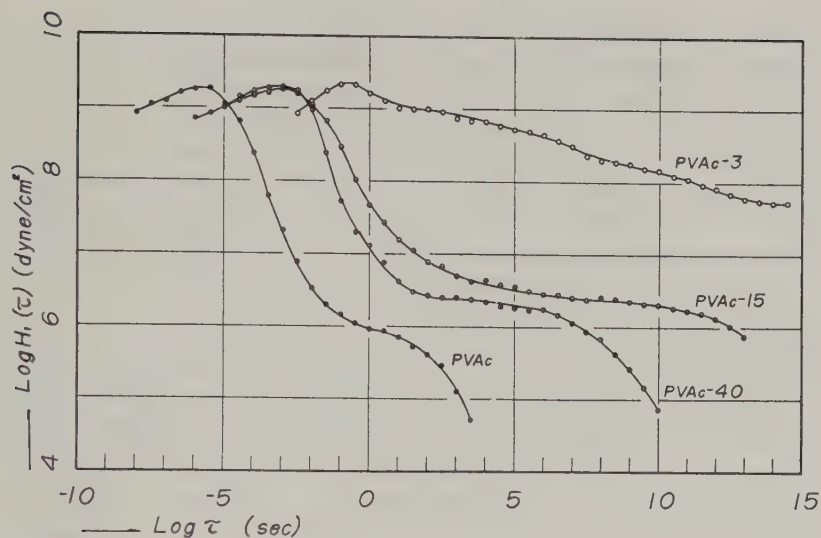


FIG. 13. Relaxation spectra obtained, by Schwarzl and Staverman's first approximation method, from the master curves reduced to 75°C. and shown in Fig. 10.

shown in Fig. 10 by using Schwarzl-Staverman's first approximation method (22).

The shape and the relative position of the relaxation spectra of PVAc agree fairly well with those in the literature (23). There are three distinctive portions: a higher intensity plateau of about 10^9 dynes/cm.² at shorter times; the well-known wedge type portion with a slope of $-\frac{1}{2}$ in the middle time range; and a lower intensity plateau of about 10^6 dynes/cm.², called the box-type portion, at longer times. With decreasing degree of acetylation, the spectrum not only shifts to longer times but also changes shape, the slope of the wedge portion decreasing and the height as well as the width of the box portion increasing. The result is a flatter and broader spectrum tending to lose a discrete wedge portion.

The change in the box portion in going from PVAc to PVAc-15, especially the change of the width, would seem to be due to a change in degree of polymerization caused by the acetylation; however, the conditions of acetylation shown in Table I are too mild to decrease the degree of polymerization (24). Therefore, the change in the spectrum may be due to some other reasons, such as a change in the nature of the interaction between chain molecules.

The results could also be considered to demonstrate a systematic change in the relaxation spectrum—from the well-known shape for completely amorphous polymers to a flatter curve for crystalline polymers—if the as-

sumptions adopted here for composing the master curve, that is, the hypothesis of time-temperature superposition, are strictly valid.

In discussing the hypothesis it is worth saying that it is valid only for a system in which all the relaxation processes have activation energies of the same magnitude and also of the same temperature dependency. This restriction should distinguish the higher plateau from the wedge portions and these in turn from the lower plateau portions in the relaxation spectrum even for completely amorphous polymers, because the corresponding relaxation processes should be different from one another. Moreover, the anomalous temperature dependence of a_T for PVAc-15 and 40, which shows a revolt from a single W.L.F. equation, may suggest that the relaxation process in the wedge portion is different from that in the lower plateau portions of PVAc-15, and for PVAc-40 there are differences among the wedge portion, the lower plateau, and its end portions (flow region). In other words, there is no guarantee that the shape of relaxation spectrum obtained here is a unique one independent of the reference temperature, especially at the boundaries between the different portions in the spectrum, even if the procedure of composing the master curve is carried out smoothly.

Unfortunately, there is no method of checking the validity of the hypothesis, at present, except for the painful and laborious work of comparing absolute measurements of dynamic properties over a wide time scale at various temperatures. However, the results obtained here may demonstrate a systematic change of relaxation spectrum on going from a completely amorphous polymer to a quasi-crystalline polymer, at least qualitatively, in spite of some obscurities at the boundaries between the different portions in the spectrum.

SUMMARY

The stress relaxation behavior of partly to completely acetylated polyvinyl alcohol polymers was studied as one of a series of systematic investigations of the relaxation spectrum changes which occur on going from a quasi-crystalline to a completely amorphous polymer.

The relaxation spectrum was determined from a so-called master relaxation curve composed of relaxation curves at various temperatures, mainly within the temperature range of the glass transition region, on the basis of the hypothesis of time-temperature superposition.

The procedure of superposition became somewhat difficult with decreasing degree of acetylation, and the agreement of the procedure with the W.L.F. equation was limited to rather narrower temperature ranges than for completely amorphous polymers.

With decreasing degree of acetylation of the polymers, the following systematic changes were observed;

1. The activation energy of the relaxation process was not independent

of temperature, showing a sharp maximum at a particular temperature T_g for each polymer. The temperature T_g and the apparent maximum activation energy $(\Delta H_a)_{\max.}$ at that temperature increase together.

2. The relaxation spectrum at a reference temperature of 75°C. not only shifted to longer times but also changed shape systematically, the slope of the wedge portion decreasing, and the height as well as the width of the box portion increasing. A flatter and broader spectrum resulted with loss of a discrete wedge portion.

ACKNOWLEDGMENTS

The authors are indebted to Prof. R. S. Stein, Department of Chemistry, University of Massachusetts, and Prof. J. D. Ferry, Department of Chemistry, University of Wisconsin, for their valuable suggestions and discussion.

The acetylation and chemical analysis of the polymers were conducted by Mr. F. Fujimoto, Department of Textile Chemistry, Kyoto University, Japan.

REFERENCES

1. FUJINO, K., SENSU, K., AND KAWAI, H., *J. Colloid Sci.* **16**, 262 (1961).
2. FUJINO, K., KAWAI, H., HORINO, T., AND MIYAMOTO, K., *Textile Research J.* **25**, 722 (1955); *ibid.* **26**, 852 (1956). TOKITA, N., *J. Polymer. Sci.* **20**, 515 (1956). NAGAMATZU, K., YOSHITOMI, T., TAKEMOTO, T., AND TAKEMURA, T., *J. Polymer Sci.* **27**, 335 (1958); *ibid.* **33**, 515 (1958); *J. Colloid Sci.* **13**, 257 (1958); *ibid.* **14**, 377 (1959).
3. FUJIMOTO, F., AND HIRABAYASHI, K., *Bull. Inst. Chem. Research, Kyoto Univ.* **24**, 92 (1951).
4. FUJIMOTO, F., AND HIRABAYASHI, K., Unpublished data.
5. NINOMIYA, K., KISHIMOTO, A., AND FUJITA, H., *J. Soc. Polymer. Sci. Japan* **14**, 504 (1957).
6. SAKURADA, I., NUKUSHINA, K., AND SONE, Y., *J. Soc. Polymer. Sci. Japan* **12**, 506, 517 (1955).
7. OZAWA, T., AND MATZUNAGA, T., *J. Soc. Polymer Sci. Japan* **7**, 248 (1950).
8. LEADERMAN, H., "Elastic and Creep Properties of Filamentous Materials." The Textile Foundation Inc., Washington, D. C., 1943. NAKADA, O., *J. Phys. Soc. Japan* **12**, 1218 (1958).
9. TOBOLSKY, A. V., MCLOUGHLIN, J. R., *J. Phys. Chem.* **59**, 989 (1955). CATSIF, E., TOBOLSKY, A. V., AND OFFENBACH, J., *J. Colloid Sci.* **11**, 48 (1956).
10. SAKURADA, I., NUKUSHINA, K., AND ORIDO, Z., *J. Soc. Polymer Sci. Japan* **16**, 587, 593 (1959); *ibid.* **17**, 13 (1960).
11. FUJINO, K., MIYAMOTO, K., HORINO, T., AND KAWAI, H., *J. Soc. Polymer Sci. Japan* **15**, 713 (1958).
12. JENKEL, E., *Kolloid-Z.* **100**, 163 (1942).
13. YANO, Y., *J. Chem. Soc. Japan* **73**, 708 (1952).
14. TOKITA, N., AND KAWAI, H., *J. Phys. Soc. Japan* **6**, 367 (1951).
15. NAGAI, E., by I. SAKURADA, ed., in "Polyvinyl Alcohol," p. 252. Society of Polymer Science, Japan, Tokyo, 1955.
16. NOHARA, S., *J. Soc. Polymer Sci. Japan* **15**, 105 (1958).
17. FERRY, J. D., *J. Am. Chem. Soc.* **72**, 3476 (1950).
18. TOBOLSKY, A. V., *J. Appl. Phys.* **27**, 673 (1956).
19. HIRAI, N., *J. Chem. Soc. Japan* **75**, 683 (1954).

20. FERRY, J. D., AND LANDEL, R. F., *Kolloid-Z.* **148**, 1 (1956).
21. FERRY, J. D., *et al.*, *J. Colloid Sci.* **12**, 53 (1957); *ibid.* **12**, 327 (1957); *ibid.* **12**, 389 (1957); *ibid.* **13**, 103 (1958); *ibid.* **14**, 147 (1959).
22. SCHWARZL, F., AND STAVERMAN, A. J., *Physica* **18**, 791 (1952); *Appl. Sci. Research* **A4**, 127 (1953).
23. NINOMIYA, K., AND FUJITA, H., *J. Colloid Sci.* **12**, 204 (1957).
24. NAKAJIMA, A., *J. Soc. Polymer Sci. Japan* **7**, 57 (1950).

ANALYSIS OF THE CONE-PLATE VISCOMETER

John C. Slattery

*Department of Chemical Engineering, Northwestern University, Evanston, Illinois**Received July 18, 1960; revised received December 27, 1960*

ABSTRACT

In order that there be only one non-zero component of the stress tensor for a non-Newtonian fluid in a cone-plate viscometer, inertial forces must be neglected with respect to viscous forces in the equation of motion. This is justified when the angle between the cone and plate is very small.

INTRODUCTION

Until recently only two geometries were commonly used in the study of non-Newtonian fluids (1): tangential flow between concentric, rotating cylinders and flow through a cylindrical tube. Recently a third geometry has been employed, flow between a rotating cone and a plate (2-10). With the latter to good approximation the entire sample is subjected to a uniform shearing stress; we wish to examine the nature of this approximation.

By the definition of an inelastic non-Newtonian fluid (11, page 225), the stress tensor (momentum flux tensor) τ_{ij} is a function of the rate-of-deformation tensor d_{ij} alone; for an incompressible fluid (11, page 228)¹:

$$\tau_{ij} = -G_1 d_{ij} - G_2 \sum_k d_{ik} d_{kj}; \quad [1]$$

$$G_\gamma = \sum_{m,n} G_{\gamma mn} [II]^m [III]^n; \quad [2]$$

$$II = \sum_{i,j} d_{ij} d_{ji}, \quad III = \sum_{i,j,k} d_{ij} d_{jk} d_{ki}. \quad [3]$$

In rectangular Cartesian coordinates,

$$d_{ij} = 1/2 \left[\frac{\partial v_i}{\partial x_j} + \frac{\partial v_j}{\partial x_i} \right]. \quad [4]$$

The coefficients $G_{\gamma mn}$ are independent of d_{ij} . For Newtonian fluids,

$$G_1 = 2\mu; \quad G_2 = 0. \quad [5]$$

DIMENSIONAL ANALYSIS CONSIDERATIONS

A cone-plate viscometer usually consists of a stationary plate and rotating cone, as suggested in Fig. 1. Let us consider the steady-state flow of an

¹ By d_{ij} and τ_{ij} we mean the physical components of these tensors (12).

incompressible, non-Newtonian fluid; we shall assume for the moment that

$$G_2 = 0; \quad III \equiv 0. \quad [6, 7]$$

The equation of motion in rectangular coordinates may then be made dimensionless to obtain

$$\frac{\partial v_i^*}{\partial t^*} + \sum_j v_j^* \frac{\partial v_i^*}{\partial x_j^*} = - \frac{\partial p^*}{\partial x_i^*} + \sum_{j,m} \frac{1}{Re_m} \frac{\partial}{\partial x_j^*} [(II)^m d_{ij}]. \quad [8]$$

$$Re_m = \frac{\rho(R \cos \Theta)^{2m+1} (\Omega R \sin \Theta)^{-2m+1}}{G_{1m0}} \quad [9]$$

$$v_i^* = \frac{v_i}{\Omega R \sin \Theta}; \quad p^* = \frac{p}{(\Omega R \sin \Theta)^2}; \quad [10]$$

$$x_i^* = \frac{x_i}{R \cos \Theta}; \quad t^* = \frac{t(\Omega R \sin \Theta)}{R \cos \Theta}.$$

For

$$Re_m \ll 1$$

the inertial forces may be neglected with respect to the viscous forces; Eq. [10] requires Θ approach $\pi/2$ to satisfy this condition. Note that this does not limit the solution to very low angular velocities as previously suggested² (9).

Solution of Equations of Motion Omitting Inertial Terms

Let us solve the equations of motion in spherical coordinates, dropping the inertial terms. We shall also neglect "edge effects," which McKennell reports to be small when the angle between the cone and plate is small (7). We shall attempt to find a solution by assuming Eq. [6] (not Eq. [7]) and

$$v_r = v_\theta = 0, \quad p = p(r, \theta). \quad [11, 11a]$$

Then from the equation of continuity (13, page 83)

$$v_\varphi = v_\varphi(r, \theta). \quad [12]$$

The equations of motion become with the above assumptions and neglecting external forces (13):

$$\frac{\partial p}{\partial r} = 0 \quad [13]$$

$$\frac{\partial p}{\partial \theta} = 0 \quad [14]$$

² This is analogous to the treatment of the slider bearing (14, page 87).

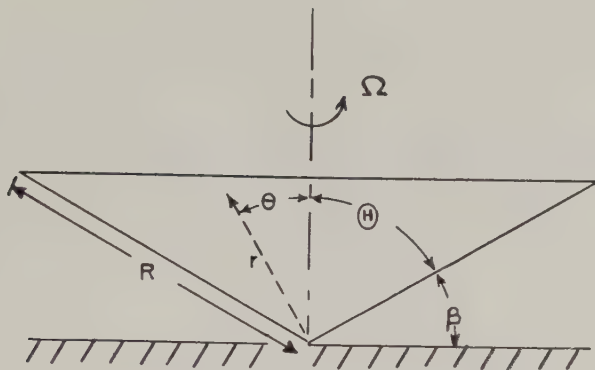


FIG. 1. Cone-plate viscometer.

$$\frac{1}{r} \frac{\partial}{\partial r} (r^2 \tau_{r\varphi}) + \frac{\partial \tau_{\theta\varphi}}{\partial \theta} + \tau_{r\varphi} + 2\tau_{\theta\varphi} \cot \theta = 0. \quad [15]$$

With Eqs. [11] and [12] the non-zero components of the rate-of-deformation tensor become

$$d_{r\varphi} = \frac{1}{2} \left[r \frac{\partial}{\partial r} \left[\frac{v_\varphi}{r} \right] \right]; \quad [16]$$

$$d_{\theta\varphi} = \frac{1}{2} \left[\frac{\sin \theta}{r} \frac{\partial}{\partial \theta} \left[\frac{v_\varphi}{\sin \theta} \right] \right]. \quad [17]$$

The boundary conditions are

$$\theta = \Theta: v_\varphi = \Omega r \sin \Theta; \quad [18]$$

$$\theta = \frac{\pi}{2}: v_\varphi = 0; \quad [19]$$

$$r = 0: v_\varphi = 0. \quad [20]$$

Equations [18] and [20] suggest a solution of the form³

$$v_\varphi = r f(\theta). \quad [21]$$

With this assumption and Eq. [6] we have

$$III \equiv 0, \quad \tau_{r\varphi} \equiv 0, \quad \tau_{\theta\varphi} = -G_1 d_{\theta\varphi}. \quad [22a, b, c]$$

Then Eq. [15] becomes

$$\frac{1}{r} \frac{d\tau_{\theta\varphi}}{d\theta} - \frac{2 \cot \theta}{r} \tau_{\theta\varphi} = 0; \quad [23]$$

³ For the flow of a Newtonian fluid in a cone-plate viscometer, it is necessary to assume only that the variables are separable (15, 16).

or

$$\tau_{\theta\varphi} = \frac{C_1}{\sin^2 \theta}, \quad [24]$$

where C_1 is a constant. Combining Eqs. [17], [22c], and [24] and solving with the boundary conditions Eqs. [18] and [19], we get

$$C_1 = \frac{\frac{1}{2}\Omega}{\int_{\theta}^{\pi/2} \frac{d\theta}{G_1 \sin^3 \theta}}; \quad [25]$$

$$v_{\varphi} = \frac{r\Omega \sin \theta \int_{\theta}^{\pi/2} \frac{d\theta}{G_1 \sin^3 \theta}}{\int_{\theta}^{\pi/2} \frac{d\theta}{G_1 \sin^3 \theta}}. \quad [26]$$

Equation [26] satisfies the differential equation representing the combination of Eqs. [15], [16], [17], and [22]; it also satisfies the boundary conditions, Eqs. [18], [19], and [20]. Therefore the assumptions of Eq. [11] are justified when the inertial terms may be neglected in the equations of motion.⁴

COMMENTS REGARDING THE INERTIAL TERMS

If we assume Eq. [11] but do not drop the inertial terms, Eq. [15] is unchanged, but Eqs. [13] and [14] become (13):

$$\frac{\partial p}{\partial r} = \rho \frac{v_{\varphi}^2}{r}; \quad [27]$$

$$\frac{\partial p}{\partial \theta} = \rho v_{\varphi}^2 \cot \theta. \quad [28]$$

Equation [26] of course satisfies Eq. [15], but it does not satisfy Eqs. [27] and [28], since they require that

$$\frac{\partial^2 p}{\partial \theta \partial r} = \frac{2\rho v_{\varphi}}{r} \frac{\partial v_{\varphi}}{\partial \theta} = 2\rho v_{\varphi} \cot \theta \frac{\partial v_{\varphi}}{\partial r} = \frac{\partial^2 p}{\partial r \partial \theta};$$

or that

$$\frac{\partial v_{\varphi}}{\partial \theta} = r \cot \theta \frac{\partial v_{\varphi}}{\partial r}. \quad [29]$$

We may conclude that, if the complete equations of motion are to be solved, Eq. [11] cannot be valid. The necessity for dropping the inertial terms from the equation of motion has been mentioned previously (4, 17).

⁴ This argument assumes that Eq. [26] represents a unique solution of Eq. [15] with the boundary conditions Eqs. [18], [19], and [20].

DEDUCTION OF RHEOGRAM FROM CONE-PLATE DATA

The torque, T , which must be exerted upon the cone to maintain rotation at a constant speed, Ω , is given by

$$\begin{aligned} T &= \int_0^R \tau_{\theta\varphi|\theta=\Theta} 2\pi(r \sin \Theta)^2 dr; \\ &= \tau_{\theta\varphi|\theta=\Theta} [\frac{2}{3} \pi R^3 \sin^2 \Theta]. \end{aligned} \quad [30]$$

Upon rearrangement,

$$\tau_{\theta\varphi|\theta=\Theta} = \frac{3}{2} \frac{T}{\pi R^3 \sin^2 \Theta}. \quad [31]$$

From Eqs. [24] and [25] we obtain

$$\tau_{\theta\varphi|\theta=\Theta} = \frac{1}{2} \frac{\Omega}{\sin^2 \Theta \int_{\Theta}^{\pi/2} \frac{d\theta}{G_1 \sin^3 \theta}}. \quad [32]$$

If $\tau_{\theta\varphi|\theta=\Theta}$ is eliminated between Eqs. [31] and [32] and the result is differentiated with respect to Θ holding the quantity $[T/\pi R^3]$ constant,

$$\frac{1}{2} \sin \Theta \left[\frac{\partial \Omega}{\partial \Theta} \right]_{\frac{T}{\pi R^3}} = - \frac{3}{2} \frac{T}{\pi R^3} \frac{1}{G_1 \sin^2 \Theta}. \quad [33]$$

For a particular value of Θ , say A , Eqs. [22], [31], and [33] may be combined to give

$$d_{\theta\varphi|\theta=A} = \frac{1}{2} \sin A \left[\frac{\partial \Omega}{\partial \Theta} \right]_{\frac{T}{\pi R^3}} \bigg|_{\theta=A}. \quad [34]$$

The corresponding $\tau_{\theta\varphi|\theta=A}$ may be obtained from Eq. [31]. Equations [31] and [34] might be used to analyze data from a cone-plate viscometer to obtain a plot of the rate of deformation ($d_{\theta\varphi}$) versus the shear stress ($\tau_{\theta\varphi}$); this curve is sometimes called the rheogram.

Fortunately Eq. [34] can be further simplified without appreciable loss in accuracy. We have assumed that Θ is very close to $\pi/2$; then from Eq. [24] $\tau_{\theta\varphi}$ is very nearly a constant throughout the entire gap between the cone and the plate. Equations [2] and [22] may be combined to show that $d_{\theta\varphi}$ and G_1 must be nearly constant as well from Eq. [32]

$$d_{\theta\varphi|\theta=\Theta} = \frac{\tau_{\theta\varphi|\theta=\Theta}}{-G_1} = \frac{\Omega}{\cos \Theta - \sin^2 \Theta \log \left[\tan \frac{\Theta}{2} \right]} \approx \frac{\Omega}{2\beta}. \quad [35]$$

Equations [35] may then be used to construct a rheogram from experimental data. Equations [31] and [35] have been given previously (9, 10, 17)

in discussions pertaining to Newtonian fluids, Eq. [5]. McKennel (7) has applied Eqs. [31] and [35] to non-Newtonian fluids as well.

SUMMARY

1. In the analysis of the cone-plate viscometer for a non-Newtonian fluid it is assumed that v_φ is the only non-zero component of velocity. This assumption is valid only when the inertial terms are not included in the equation of motion; the inertial terms may be neglected as the angle between the cone and the plate approaches zero, even though the angular velocity may be large.

2. With the above assumptions, Eq. [34] gives an expression for the rate of deformation, $d_{\theta\varphi}$, evaluated at the surface of the cone in terms of experimental data; the stress was not assumed to be uniform throughout the sample in deriving this result. The shear stress, $\tau_{\theta\varphi}$, at the cone surface is given by Eq. [31].

3. For the very small angle between the cone and plate required for the neglect of the inertial terms, the stress is nearly independent of position and the usual expressions for the rate of deformation are obtained, Eqs. [35].

ACKNOWLEDGMENTS

The author profited a great deal from discussion on this subject with R. B. Bird, R. M. Turian, and E. N. Lightfoot of the University of Wisconsin and with A. G. Fredrickson of the University of Minnesota.

List of Symbols

A	= Particular value of Θ .
C_1	= Constant.
d_{ij}	= Physical component of rate of deformation tensor (12).
$G_{\gamma mn}$	= Constant in expansion of G_γ .
G_γ	= Scalar function of rate of deformation tensor d_{ij} .
P	= Pressure.
r	= Spherical coordinate.
R	= Slant height of cone.
Re_m	= Modified Reynolds grouping.
t	= Time.
T	= Torque which must be exerted on the cone to maintain constant Ω .
v_i	= Physical component of velocity vector (12).
x_i	= Rectangular coordinate.
β	= Angle between cone and plate.
θ	= Spherical coordinate.
Θ	= Value of θ locating the surface of the cone.
φ	= Spherical coordinate.
ρ	= Density.

- τ_{ij} = Physical component of stress tensor (momentum flux tensor) (12).
 Ω = Angular velocity of cone.

REFERENCES

1. REINER, M., "Deformation, Strain and Flow." Interscience, New York, (1960).
2. HIGGINBOTHAM, R. S., *J. Sci. Instr.* **27**, 139 (1950).
3. HIGGINBOTHAM, R. S., AND BENBOW, J. J., *J. Sci. Instr.* **29**, 221 (1952).
4. MARKOVITZ, J., ELYASH, L. J., PADDEN, F. J., AND DEWITT, T. W., *J. Colloid Sci.* **10**, 165 (1955).
5. McKENNEL, R., *Proc. 2nd Intern. Congr. on Rheology*, p. 350 (1953).
6. McKENNEL, R., *Kolloid-Z.* **145**, 114 (1956).
7. McKENNEL, R., *Anal. Chem.* **28**, 1710 (1956).
8. PIPER, G. H., and SCOTT, I. R., *J. Sci. Instr.* **22**, 206 (1945).
9. SCHWABEN, R., AND UMSTÄTTER, H., *Konstruktion* **5**, 79 (1953).
10. SCHWABEN, R., AND UMSTÄTTER, H., *Konstruktion* **6**, 233 (1954).
11. TRUESDELL, C., *J. Rational Mech. Anal.* **1**, 125 (1952).
12. TRUESDELL, C., *Z. angew. Math. Mech.* **33**, 345 (1953).
13. BIRD, R. B., STEWART, W. E., AND LIGHTFOOT, E. N., "Transport Phenomena." Wiley, New York, (1960).
14. SCHLICHTING, H., "Boundary Layer Theory." McGraw-Hill, New York, (1955).
15. FREDERICKSON, A. G., Ph.D. Thesis, University of Wisconsin, Madison, Wisconsin, 1959.
16. SLATTERY, J. C., Ph.D. Thesis, University of Wisconsin, Madison, Wisconsin, 1959.
17. MOONEY, M., AND EWART, R. H., *Physics* **5**, 350 (1934).

EQUILIBRIUM BETWEEN SOLID AND COLLOIDAL FERRIC OXIDE

Stephen Schulman, Gene Pontrelli,¹ and Frank Brescia

The Chemistry Department, The City College of New York, New York, New York

Received February 27, 1961

A saturated solution is characterized by the existence of a dynamic equilibrium between the solid and dissolved phases. For example, when solid ferric oxide containing radioactive iron 59 is added to a saturated solution of nonradioactive ferric oxide, the radioactivity immediately passes into the solution. The purpose of this note is to report the results of an attempt to detect a dynamic equilibrium between solid ferric oxide and a ferric oxide colloidal solution.

The procedure used involved the detection of an exchange reaction between the dispersed and nondispersed phases. In a set of experiments, radioactive solid ferric oxide was added to a nonradioactive ferric oxide colloidal solution. The mixture was stirred intermittently for varying periods of time, after which the solid and colloidal solution were separated by centrifugation and the supernatant colloidal solution was tested for radioactivity. If the colloidal solution becomes radioactive, it may be concluded that exchange occurs and that therefore an equilibrium exists.

The radiation was measured with a Tracer Laboratory TGC-5 self-quenching dip tube connected to a Nuclear-Chicago Scaler (Model 183). Each sample counted was placed in a 10-ml. blood plasma tube, with constant cylindrical geometry maintained during the counting process. An open counting system was used (1). The "expected" deviation was calculated from the square root of the number of counts and the counting time in minutes (2). Measurements of pH were made with a Coleman pH Electrometer, Model 20.

A labile form of ferric oxide was prepared as follows: at room temperature, very dilute ammonia water (1-30) was added to 100 ml. $2.21 \times 10^{-3} M$ $FeCl_3$ forming a colloidal solution of ferric oxide; the colloidal solution stood at room temperature for 24 hours after which the pH remained constant at 2.42. The colloidal solution was then dialyzed against running water until broken and the gelatinous solid separated by centrifugation.

¹ Present address: Department of Chemistry, University of Wisconsin, Madison, Wisconsin. This work was carried out while a senior Honors student at the City College.

To prepare radioactive solid ferric oxide, 59-ferric chloride, a beta-ray emitter, was added to the ferric chloride solution.

When the solid so prepared is brought into contact with a saturated solution of ferric oxide in hydrochloric acid at 28.0°C., pH 2.42, the solution becomes radioactive, reaching a maximum within 24 hours; see Table I. The quantity of hydrous oxide is expressed in terms of Fe_2O_3 . If, however, the hydrous oxide is dehydrated at 60°C., a comparatively refractory solid oxide is obtained. Under the same conditions, the saturated solution of ferric oxide showed after 43 days a gross activity of 170 ± 1 c.p.m. against a background of 156 ± 1 c.p.m.

The procedure given above was also used to prepare colloidal solutions of ferric oxide. This preparation yields a colloidal state containing 93 % of the ferric iron. This value was ascertained by precipitating 25 ml. of radioactive colloidal solution of known activity with 3 drops of 0.1 *M* sodium sulfate and counting the supernatant liquid and the precipitate. In those measurements, the activity of the supernatant liquid and the recovered precipitate equaled the original activity to within 0.5 %. However, when 1:4 ammonia water is added to 3.43×10^{-2} *M* ferric chloride to the point where an additional drop would yield a precipitate of ferric hydroxide, the resultant colloidal solution contains 71 % of the ferric iron in the colloidal state and the solution pH is 3.27.

At the pH of the colloidal solutions used, the hydrous ferric oxide is relatively insoluble; hydrochloric acid, pH 2.42, showed after 122 days an activity of 83 ± 0 c.p.m., corrected for background. However, at these pH, a large portion of the hydrous ferric oxide passes spontaneously into the colloidal state. A blank consisting of radioactive hydrous ferric oxide in contact with hydrochloric acid was therefore also run with the experiments in which radioactive hydrous ferric oxide was brought into contact with colloidal solutions of ferric oxide.

TABLE I

Activity of Saturated Solution of Ferric Oxide in Hydrochloric Acid after Contact with Radioactive Solid Hydrous Ferric Oxide at 28.0°C.

Volume of solution = 25.0 ml.; pH = 2.42; mg. Fe_2O_3 = 16.5; activity of Fe_2O_3 sample = $11,000 \pm 19$ c.p.m.; background = 108 ± 1 c.p.m.

Time (hours)	Gross count of 10 ml. solution (c.p.m.)	
	Solution I	Solution II
0	108 ± 1	108 ± 1
1	853 ± 6	508 ± 5
3	977 ± 7	898 ± 6
24	1630 ± 7	1613 ± 7
28	1626 ± 7	1616 ± 7

The results are summarized in Table II; the counts, corrected for background, were made after separation of hydrous ferric oxide from the colloidal solution and from the hydrochloric acid blank solution. These results show that the hydrous ferric oxide does not exchange with colloidal ferric oxide under these conditions in 122 days.

Since these experiments show that no exchange occurs, it is concluded that no dynamic equilibrium exists between solid ferric oxide and its corresponding colloiddally dispersed particle in the sense that an equilibrium exists between solid ferric oxide and its true solution.

Also, the ferric iron originally present in true solution in the colloidal solution becomes radioactive through exchange with the solid ferric oxide. It therefore appears that the colloidal ferric oxide under these conditions

TABLE II

Activity of Colloidal Ferric Oxide Solution and of Hydrochloric Acid after Contact with Solid Radioactive Hydrous Ferric Oxide; Volume of Solution 25.0 ml.

	Colloidal solution		HCl blank	Colloidal solution		HCl blank
	I	II		III	IV	
pH	2.42	2.42	2.42	2.42	2.42	2.42
mg. radioactive Fe_2O_3	16.5	16.5	16.5	60	60	60
Net activity of Fe_2O_3 sample	608 \pm 3	598 \pm 3	605 \pm 3	12530 \pm 13	12520 \pm 13	12540 \pm 13
Contact time, days	41	41	41	122	122	122
Stirring time, days	18	18	18	48	48	48
Net count of 10 ml. solution, c.p.m.	222 \pm 1	218 \pm 1	230 \pm 1	4745 \pm 5	4740 \pm 5	4749 \pm 5
	Colloidal solution		HCl blank	Colloidal solution		HCl blank
	V	VI		VII	VIII	
pH	3.27	3.27	3.27	3.27	3.27	3.27
mg. radioactive Fe_2O_3	16.5	16.5	16.5	16.5	16.5	16.5
Net activity of Fe_2O_3 sample	11052 \pm 19	10868 \pm 19	10859 \pm 19	4580 \pm 11	4590 \pm 11	4590 \pm 11
Contact time, days	37	37	37	101	101	101
Stirring time, days	19	19	19	42	42	42
Net count of 10 ml. solution, c.p.m.	4160 \pm 8	4160 \pm 8	4160 \pm 8	1730 \pm 4	1731 \pm 4	1731 \pm 4

does not exchange with the dissolved ferric iron. Further experiments to detect exchange between iron III in true solution and colloidal ferric oxide are in progress.

These results agree with the conclusion (3) that ferric ion does not exchange with iron III complex ions. They are also in agreement with the accepted description of hydrophobic sols (4).

Support from the National Science Foundation under its Undergraduate Research Participation Program is gratefully acknowledged.

REFERENCES

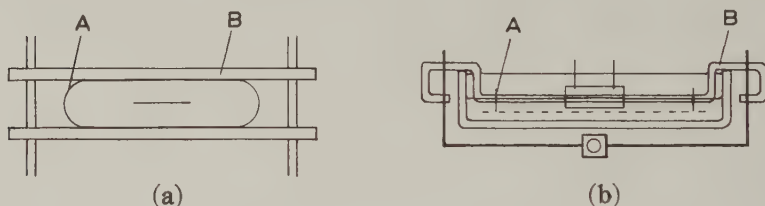
1. BLEULER, E., AND GOLDSMITH, G., "Experimental Nucleonics," pp. 16-33, 49-54. Rinehart, New York, 1952.
2. FRIEDLANDER, G., AND KENNEDY, J., "Nuclear and Radiochemistry," pp. 252-261. Wiley, New York, 1956.
3. MARTELL, A. E., AND CALVIN, M., "Chemistry of the Metal Chelate Compounds," pp. 225-227. Prentice-Hall, New York, 1952.
4. ZETTLEMOYER, A. E., *Ann. Rev. Phys. Chem.* **9**, 440 (1958).

LETTER TO THE EDITOR

**AN ALTERNATIVE METHOD FOR THE COMPRESSION
OF SURFACE FILMS**

Some of the difficulties usually experienced in the study of films at the air/water and oil/water interfaces have been overcome by enclosing the film in a flexible ring. Leakage past the barriers and overflow of the trough at high pressures are then eliminated, whilst compression of a film at the oil/water interface is made possible.

For use at the air/water interface (Fig. 1a), the ring *A* was constructed



from a strip of 0.025 cm. gauge "Astralon" rigid polyvinyl chloride sheet, the ends being heat-sealed. The ring was compressed between barriers *B*, film pressure being measured by the dipping plate method. For the oil/water interface (Fig. 1b), the barriers *B* were made of glass tubing. The ring, in this case, was constructed of mica, the ends being cemented with "Araldite." A compound of known pressure-area relationships was used for calibration purposes.

The authors wish to express their indebtedness to Professor A. E. Alexander for many helpful discussions and to the C.S.I.R.O. for research studentships.

*Department of Physical Chemistry
The University of Sydney,
Sydney, Australia*

J. H. BROOKS AND F. MACRITCHIE

Received April 12, 1961

Name Reactions in Organic Chemistry

By ALEXANDER R. SURREY

Sterling-Winthrop Research Institute, Rensselaer, New York

April 1961, 278 pp., illus., approx. \$5.50

Review of first edition:

‘It is rare to find a short book in chemistry that contains clear, concise, and accurate data that at the same time may be considered comprehensive in its treatment of the subject under consideration. Surrey’s book has succeeded in this unusual task and may be considered a baby, one-volume edition of the ‘Organic Reaction’ series. The author has briefly summarized the principal reactions for more than 100 name reactions, of which only about 40 have heretofore been treated. . . .

“The choice of name reactions covers the whole field of organic chemistry, and the main types are selected in order to give the maximum amount of information. Reaction mechanisms are used wherever possible, and the treatment combines classic synthetic organic chemistry with modern concepts in an authoritative and readable manner. Each name reaction is described and illustrated, and the side reactions are discussed. If rearrangements may take place under slightly different conditions, they are also described. References follow each name reaction, so that it is easy to go immediately to the literature for the reaction under consideration. . . .

“The subject index (14 pages) is very complete and has been carefully compiled. It has been set up as a preparation index that leads immediately to the reaction mechanism postulated (proved in many cases) and to a quick summary of the topic. . . . Similar work in other fields would be welcome.”

—*Scientific Monthly*

Detailed table of contents available upon request



ACADEMIC PRESS *New York and London*

111 Fifth Avenue, New York 3

17 Old Queen Street, London, S.W.1

Announcing a new serial publication...

Advances in IMMUNOLOGY

Edited by

W. M. TALIAFERRO
*Argonne National Laboratories,
Illinois*

J. H. HUMPHREY
*National Institute for
Medical Research, London*

VOLUME 1

July 1961, about 450 pp., approx. \$13.50

Contents

Delayed Hypersensitivity to Simple Protein Antigens

*By P. G. H. GELL, University of Birmingham, England and
B. BENACERRAF, New York University School of Medicine,
New York*

The Antigenic Structure of Tumors

By P. A. GORER, Guy's Hospital, London

Duration of Immunity in Virus Diseases

*By J. H. HALE, General Hospital,
Newcastle upon Tyne, England*

Transplantation Immunity and Tolerance

*By M. HÁSEK, A. LENGEROVA, and T. HRABA,
Czechoslovak Academy of Sciences, Prague*

Functions of the Complement System

*By ABRAHAM G. OSLER, The Johns Hopkins University
School of Medicine and School of Hygiene and
Public Health, Baltimore, Maryland*

Immunologic Tolerance of Non-Living Antigens

*By RICHARD T. SMITH, University of Florida College of
Medicine, Gainesville*

In Vitro Studies of the Antibody Response

*By ABRAM B. STAVITSKY, Western Reserve University
School of Medicine, Cleveland, Ohio*

Fate and Biological Action of Antigen-Antibody Complexes

*By WILLIAM O. WEIGLE, University of Pittsburgh School
of Medicine, Pennsylvania*

AUTHOR INDEX — SUBJECT INDEX.



ACADEMIC PRESS New York and London

111 Fifth Avenue, New York 3, N.Y.

17 Old Queen Street, London, S.W. 1

THE VAPOR PRESSURES OF ETHANOL-WATER SOLUTIONS OF DETERGENTS

B. D. Flockhart

Department of Chemistry, The Queen's University, Belfast 9, Northern Ireland

Received July 29, 1960; revised received December 27, 1960

ABSTRACT

The vapor pressures of ethanol-water solutions containing, separately, sodium dodecyl sulfate and sodium tetrapropylene benzene sulfonate have been measured over a wide range of detergent concentration and at temperatures between 20° and 50°C. The results show clearly that there is strong interaction between detergent and alcohol which is sufficient to overshadow the effects of detergent-water interaction so that the total vapor pressure is lowered. This is in contrast with simple strong electrolytes which raise the vapor pressure. As the concentration of either detergent or alcohol is raised or the temperature is lowered, these primary effects become less overwhelming. In the extreme case of low temperature, high alcohol concentration, and high detergent concentration, the vapor pressure begins to increase. These findings are discussed in terms of the distribution of alcohol between an aqueous and a detergent micelle phase.

INTRODUCTION

A significant property of aqueous solutions of detergents is their ability to dissolve organic compounds which are only slightly soluble in water. This solubility, designated as solubilization, involves the presence of colloidal micelles which incorporate within themselves the otherwise difficultly soluble material. Many cases of solubilization can be described quantitatively as a partition of the solute between two immiscible phases (1).

Water-soluble polar compounds are thought to be taken up on the exterior of the micelles. But the distribution of the polar compound between detergent and water is not known. A reasonably exact determination of the distribution of a volatile, nonionic polar compound would require partial vapor pressure measurements on dilute detergent solutions and the ability to distinguish quantitatively the effects of various interactions. Because of the very small pressure differences involved, these measurements cannot be made with sufficient accuracy to give meaning to the results. However, the addition of detergents to water is known to lower the vapor pressure by only a small amount (2). Useful information about the distribution between water and micelles of a compound, completely

miscible with water, might therefore be obtained from total vapor pressure measurements.

The present paper reports measurements of the vapor pressure of ethanol-water solutions which contain, separately, sodium dodecyl sulfate and sodium tetrapropylene benzene sulfonate. Dinonyl phthalate was used as manometer liquid. This greatly facilitated the determination of small changes in pressure. The results are discussed in terms of the distribution of ethanol between an aqueous and a detergent micelle phase.

EXPERIMENTAL

The sodium dodecyl sulfate has been described previously (3). In some measurements a sample of sodium dodecyl sulfate kindly supplied by Unilever Ltd., Port Sunlight, was used. This material gave identical vapor pressure readings. Thomas Hedley & Co., Newcastle upon Tyne, kindly provided the sodium tetrapropylene benzene sulfonate. This was prepared by direct sulfonation of tetrapropylene benzene with SO_3 . It had an apparent average molecular weight of 360 by the titrimetric method based on cetyl pyridinium bromide and of 340 by the benzidine complex method (4). The theoretical molecular weight is 348.5. Absolute alcohol was used without further purification. Distilled water from the laboratory supply was passed through an ion-exchange column before use.

All solutions were prepared by weight. Detergent concentrations are expressed in moles per 1000 g. of solvent. Solvent mixtures are recorded in terms of percentage of ethanol by weight. The exact values are given in the legends. In the text these mixtures will be referred to by the nearest whole number in the percentage of ethanol.

Figure 1 shows the design of the vapor pressure apparatus. The side arms of the center tap were bent so as to bring the tapered tubes together. Dinonyl phthalate (for gas chromatography) was used in the manometer. Prior to introduction of the test liquids, it was deaerated by multiple freeze-evacuate-thaw cycles. The same procedure was used for the test liquids. During this operation the stirrer bobs were kept in the neck of the tapered tubes. Before introducing the test liquids the system was filled with nitrogen to avoid ingress of carbon dioxide.

The vapor pressure of each solution was determined at 5° intervals between 20° (or 25°) and 50°C. The initial vapor pressure reading at 20°C. was checked by performing a further freeze-evacuate-thaw cycle. On completion of the series of measurements, the apparatus was left for 24 hr., when the initial reading was rechecked. The change in pressure, always positive, averaged 0.25 mm. of dinonyl phthalate.

The manometer reading gives the difference in vapor pressure between the detergent solution and the reference solution. The latter was either

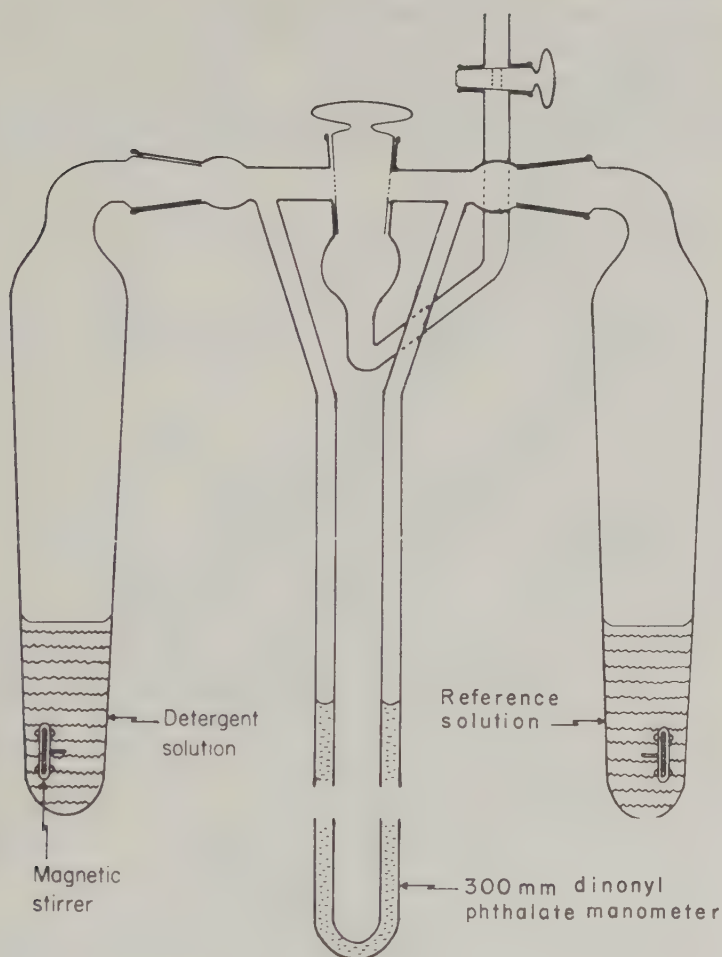


FIG. 1. Vapor pressure apparatus.

water, 15% ethanol, or 35% ethanol, these concentrations being chosen to make the differential pressures small. Values for the vapor pressure of these solutions were taken from reference 5. In the present paper, pressures are reported in millimeters of mercury at 0°C.

The apparatus was tested by measuring the vapor pressure of a series of ethanol-water solutions containing up to 45% of ethanol. The reference concentrations were those already stated. Agreement with the literature values was within 2% for the solutions of higher ethanol content. For solutions of low ethanol content the observed pressures were below the recorded figures, sometimes by as much as 4% at temperatures over 30°C.

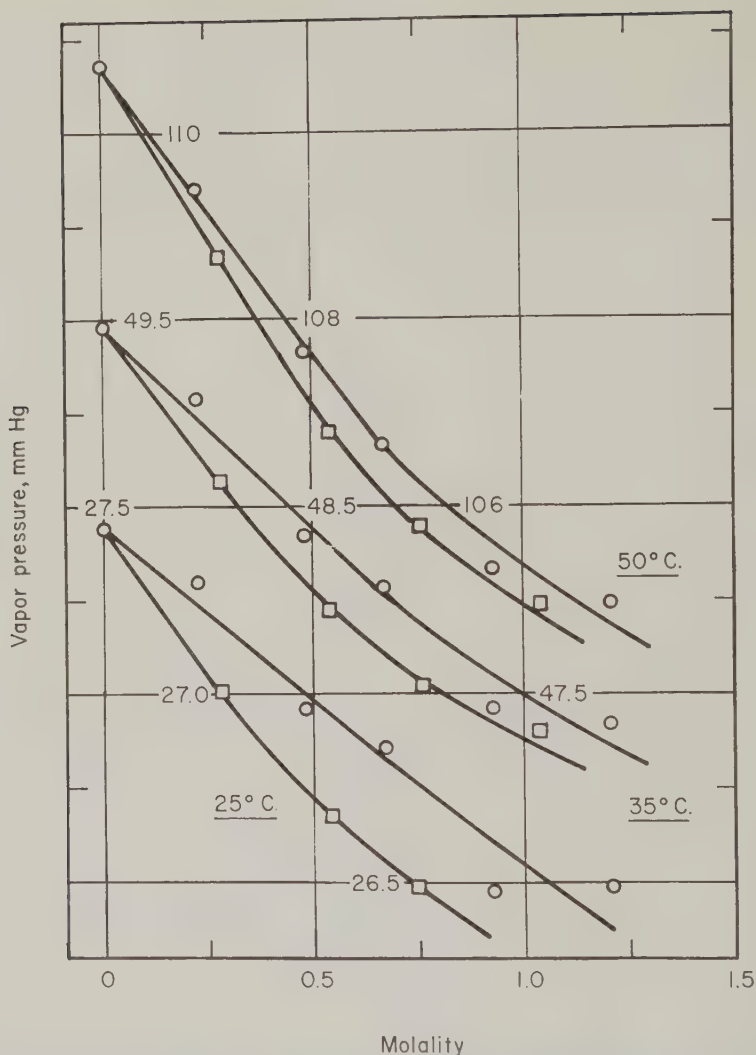


FIG. 2. Vapor pressure as a function of detergent concentration for sodium dodecyl sulfate (○) and sodium tetrapropylene benzene sulfonate (□) in 5.03% ethanol.

RESULTS

Figures 2 to 5 show the vapor pressure-concentration curves for sodium dodecyl sulfate and sodium tetrapropylene benzene sulfonate in 5%, 20%, and 45% ethanol at 25°, 35°, and 50°C. Measurements at 20°, 30°, 40°, and 45°C. are in agreement with these results.¹ The vapor pressure

¹ The complete vapor pressure data can be obtained from the Department of Chemistry, Queen's University.

decreases with increasing detergent concentration, the decrease usually being greater for sodium tetrapropylene benzene sulfonate. With 5% and 20% ethanol the vapor pressure falls less rapidly in the more concentrated detergent solutions. With 45% ethanol a minimum occurs in the vapor pressure-concentration plot for sodium dodecyl sulfate at temperatures under 35°C.

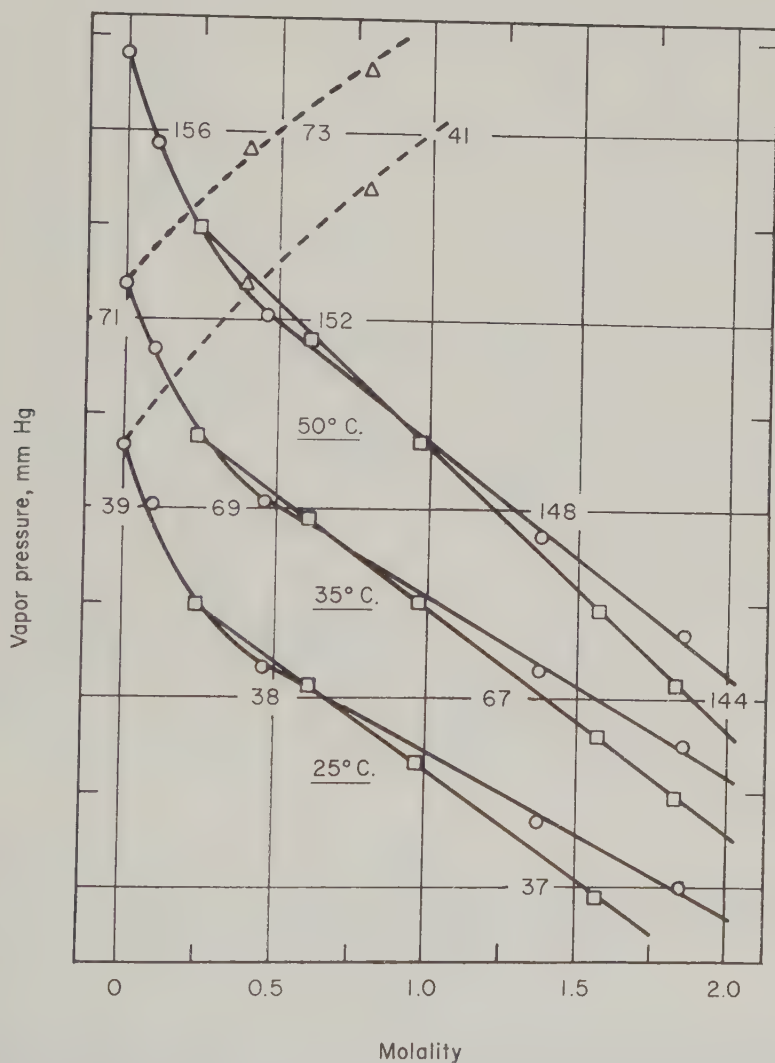


FIG. 3. Vapor pressure as a function of concentration for sodium dodecyl sulfate (○), sodium tetrapropylene benzene sulfonate (□), and sodium chloride (Δ) in 20.37% ethanol.

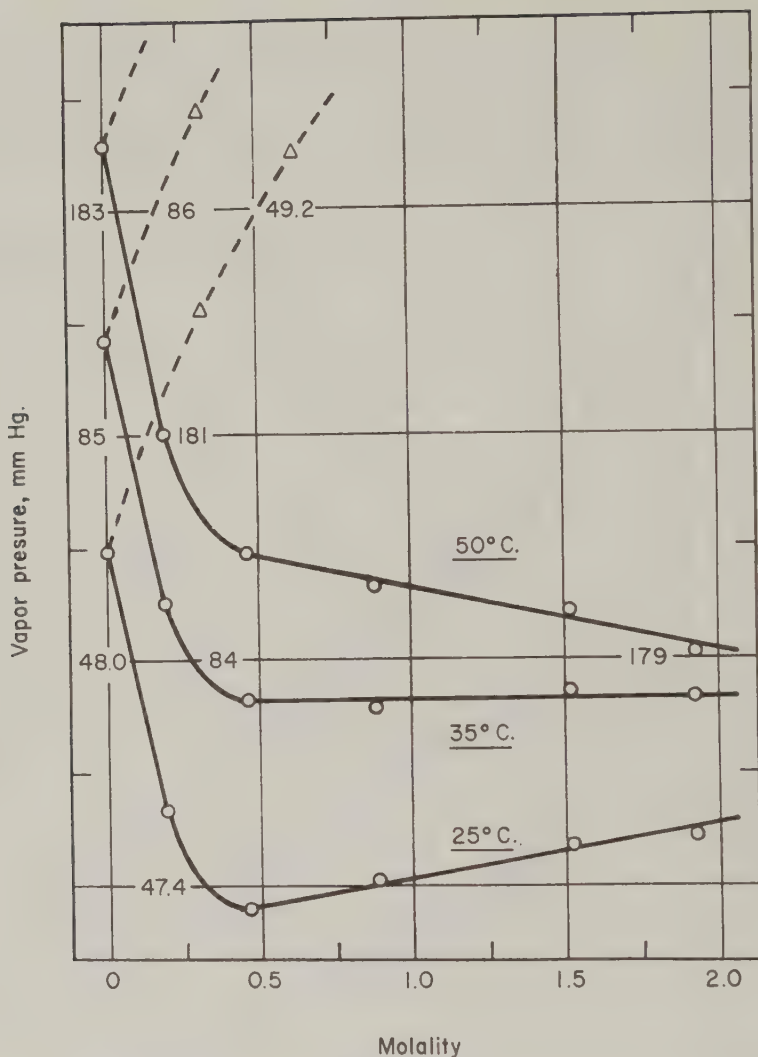


Fig. 4. Vapor pressure as a function of concentration for sodium dodecyl sulfate (O) and sodium chloride (Δ) in 44.81% ethanol.

DISCUSSION

Present results show that the addition of detergents to ethanol-water solutions lowers the vapor pressure at all detergent concentrations. Simple strong electrolytes have the opposite effect, as shown by the addition of sodium chloride. They raise the vapor pressure. The salting-out effect of an electrolyte has been ascribed to the congregation of molecules of the

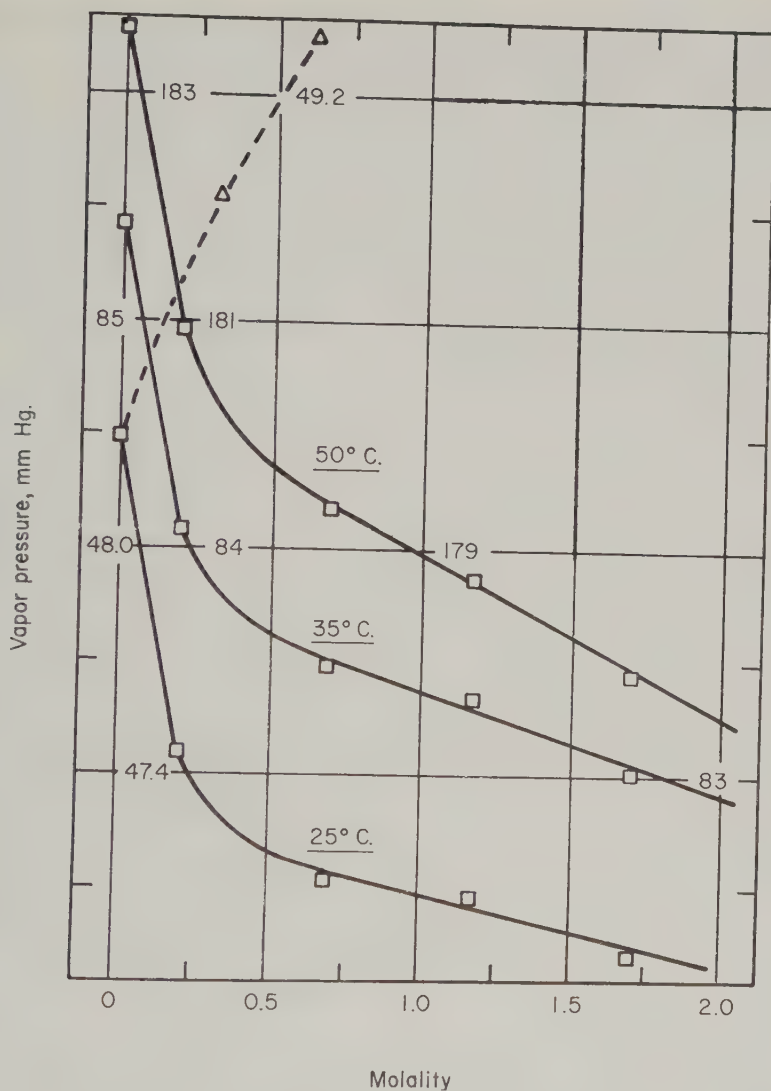


FIG. 5. Vapor pressure as a function of concentration for sodium tetrapropylene benzene sulfonate (\square) and sodium chloride (\triangle) in 44.81% ethanol.

polarizable solvent around the ions of the added electrolyte. In the present solutions of sodium chloride, water molecules are attracted by the ions more strongly than those of the alcohol. The latter are therefore displaced from the vicinity of the ions and their activity in the solution is consequently increased. Since the hydration of detergents will not be negligible,

it can be inferred from the observed lowering of vapor pressure that other effects operating in these solutions are of some importance.

In comparison with the results recorded in Figs. 2 and 3 the lowering of vapor pressure by a Raoult mechanism due to added detergent is likely to be small. Several workers (2, 6) have investigated the osmotic behavior of sodium dodecyl sulfate in aqueous solution. A plot of the square root of the molality vs. the osmotic coefficient shows an abrupt change of slope at a concentration roughly equal to the critical concentration for micelle formation (c.m.c.). Beyond this concentration the value of the osmotic coefficient falls rapidly. Treating the 20% ethanol solvent as a single solvent and using the osmotic coefficient valid in water, the correction to be applied to the vapor pressure of a 0.25 molal solution of sodium dodecyl sulfate amounts to 5% of the observed vapor pressure lowering. The validity of this conclusion may of course be questioned because of the assumption that the structure of the micelles is substantially the same in 20% ethanol as in water. From conductance measurements (7) Ward has shown that if the proportion of alcohol is doubled, the micelles seem to disappear completely. It would indeed be surprising if their state was still the same when they are thus halfway towards disappearance. However, even when the osmotic coefficient obtained for a 0.05 molal aqueous solution of sodium dodecyl sulfate is applied to the 0.25 molal solution of the detergent in 20% ethanol, the observed vapor pressure lowering is altered only by 10%.

The concentration of free paraffin-chain ions in equilibrium with the micelles cannot be accurately determined until the interionic effects are taken into account by appropriate activity coefficients. It is commonly accepted, however, that this concentration reaches a maximum value at just beyond the c.m.c. (8). For both detergents used in the present investigation the c.m.c. is under 0.01 molal in 5% ethanol at 20°C. In 30% ethanol the c.m.c. of sodium dodecyl sulfate equals this value. Therefore, it seems reasonable to neglect the possible salting-in effect of simple ions. Their relative importance will certainly diminish rapidly with increasing detergent concentration.

The data clearly indicate that there is strong interaction between the detergent micelles and alcohol molecules which is sufficient to overshadow the effects of detergent-water interaction. At the polar groups on the micelle surface water will undoubtedly be more strongly bound than the hydroxyl group. But the nonpolar part of the alcohol molecule will easily replace water along the hydrocarbon surface of the micelle. Support for the assumption of a hydrocarbon-water interface within each micelle can be found in the work of Stigter and Mysels (9) (*cf.* also reference 10). It seems likely that the more pronounced lowering of the vapor pressure by sodium tetrapropylene benzene sulfonate is associated with the anticipated larger hydrocarbon surface of the micelle.

By making the assumption that the concentration of ethanol in the solvent phase of detergent solutions, the concentrations of which are above the c.m.c., is approximately equal to that in an ethanol-water solution having the same vapor pressure, it is possible to calculate the apparent amount of ethanol associated with the detergent. (Although not strictly true, this assumption is satisfactory for present purposes. If the activity of the alcohol is reduced, the activity of the water will be increased and therefore the observed total vapor pressure lowering will be less than the decrease in the partial pressure of the alcohol.) Figure 6

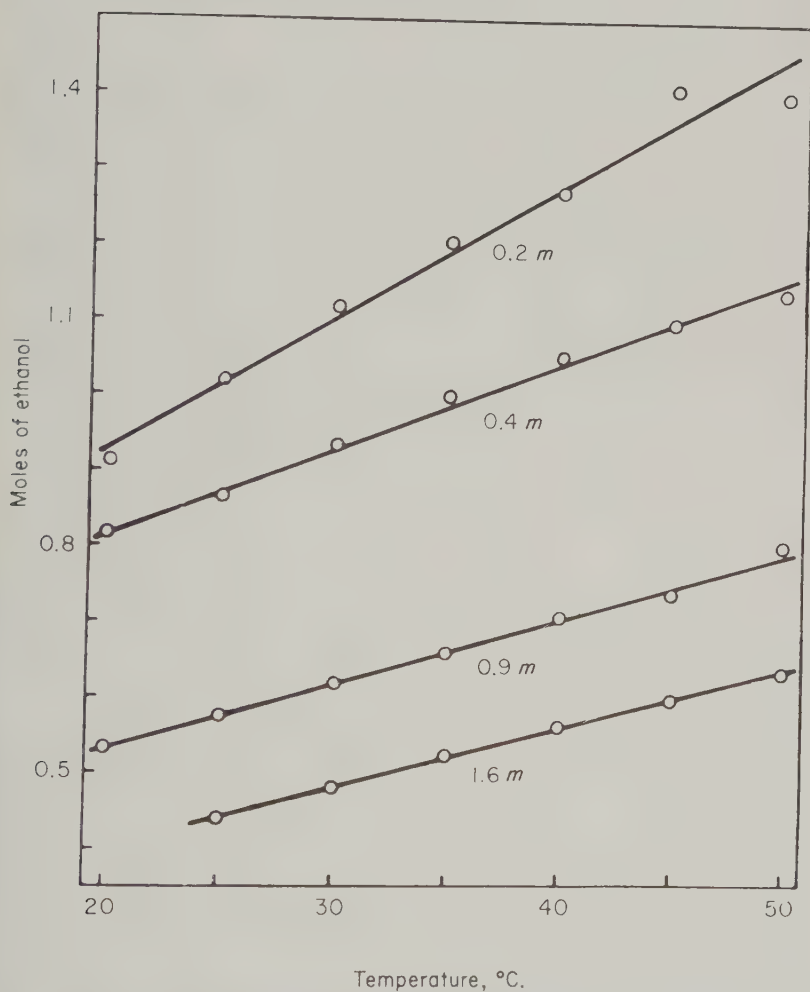


FIG. 6. Apparent amount of ethanol associated with 1 mole of sodium dodecyl sulfate vs. temperature for different detergent concentrations in 20.37% ethanol.

shows the result of these calculations for sodium dodecyl sulfate in 20% ethanol. With rise of temperature there is an increase in the amount of alcohol associated with the detergent. A similar result is obtained for sodium tetrapropylene benzene sulfonate in this solvent mixture and for both detergents in 5% and 45% ethanol. The explanation of this upward trend in the value with rising temperature is not immediately clear. A lower net binding of alcohol might have been expected. Thermal agitation of the detergent ions, however, constitutes a force tending towards disruption of the micelle. It is therefore tentatively suggested that with rise of temperature a somewhat greater area of hydrocarbon surface becomes available for alcohol uptake.

With increasing detergent concentration there is a marked decrease in the apparent amount of alcohol associated with the detergent (Fig. 6). These figures, however, are derived from the experimental data without taking the effects of detergent-water interaction into account. From the present point of view, the most important effect of this interaction is to increase the activity of the alcohol molecules in the solution. This is shown clearly by the results for sodium chloride in the mixed solvents (Figs. 3 and 4). Consequently the actual distribution of alcohol is more in favor of the detergent phase than the values given in Fig. 6 would suggest. Unfortunately it is not possible to make an exact correction for the effect of hydration in the present state of knowledge. Quantitative evaluation of solute-solvent interaction for even simple inorganic ions in water is a very recalcitrant problem. Nevertheless, with the limited information now available, it is possible to obtain approximate values for the distribution of ethanol between the aqueous and micellar phases in sodium dodecyl sulfate solutions.

The self-diffusion coefficient of micelles formed by sodium dodecyl sulfate in water and in aqueous sodium chloride solutions has been determined by Stigter, Williams, and Mysels (11) using the porous disc method. If the micelle is assumed to be spherical, comparison of the molecular weight obtained from these measurements with the value obtained from light-scattering measurements permits an estimate of hydration. Using Princen and Mysels's value for the micellar weight of sodium dodecyl sulfate determined from light-scattering data (12), it is found that a bimolecular layer of water of hydration accounts best for the results. This estimate has been tentatively accepted for the present calculation. It should be noted, however, that self-diffusion measurements obtained in fritted glass probably are vitiated by the hydrolysis catalyzed by the glass surface (12). The estimated charge on micelles of sodium dodecyl sulfate, at infinite dilution of micelles, corresponds to 25%–30% ionization (9). Although these free gegenions may be associated with 3 or 4 molecules of water (13), the total amount of water bound by them will obviously be

TABLE I

Approximate Distribution of Ethanol between Micelles of Sodium Dodecyl Sulfate and Water at 25°C.

Alcohol conc. (wt. %)	Detergent conc. (molarity)	Moles of alcohol bound per mole of detergent
5	0.05-0.40	0.56-0.54
20	0.05-0.40	1.84-1.70

small in comparison with that bound by the micelle. The hydration of sodium dodecyl sulfate in aqueous solution will therefore be taken as averaging around 10 molecules of water per detergent molecule.

No direct evidence is available on the degree of solvation of sodium dodecyl sulfate in alcohol-water mixtures. Ward (14) has observed a maximum in the conductance viscosity product for this compound at about 20% of ethanol. This is probably due to alteration in the solvation of the ions, though an alternative explanation has also been suggested; the effective viscosity for an ion solvated with water molecules and moving in the mixed solvent may be different from the viscosity of the mixed solvent in bulk (14). For the present calculations the assumption has been made that the hydration of sodium dodecyl sulfate in alcohol-water mixtures of low alcohol content is the same as in aqueous solution. If, as appears more likely, the hydration is smaller in the mixed solvents, then the actual distribution of alcohol will lie somewhere between the figures given in Table I and those presented in Fig. 6.

Knowing the amount of water immobilized by the polar groups of sodium dodecyl sulfate and thus not acting as solvent, it is possible to calculate the effective ethanol concentration of the solution when no detergent-alcohol interaction occurs. The amount of alcohol bound to the detergent is then the difference between the effective ethanol concentration of the solution before the uptake of alcohol by the micelles and the alcohol concentration of the solution after the uptake, this being calculated from the vapor pressure data by the method previously explained. Figures obtained in this way for the distribution of ethanol between the micelles of sodium dodecyl sulfate and water at 25°C. are shown in Table I.

Returning to the vapor pressure-concentration plots, two other findings are of some interest. For a 20% ethanol solvent the plot of vapor pressure vs. detergent concentration shows a slight change of slope from that observed with the more dilute solutions (Fig. 3). With 45% ethanol the change of slope is very pronounced; at low temperatures the curve for sodium dodecyl sulfate exhibits a well-defined minimum (Fig. 4).

Ward (7) observed a slight maximum in the equivalent conductance— $\sqrt{\text{concentration}}$ curve for sodium dodecyl sulfate in 20% ethanol, which

corresponds to the present result in this solvent mixture. But the conductance curves for 40% of alcohol onwards showed no unusual features. According to Ward the maximum can be explained in terms of regions of lowered dielectric constant around the micelles and increase in the viscosity of the solution; when there is 40% or more of alcohol, micelles are no longer formed.

Whereas it is impossible to say exactly what effects will be caused by charged micelles when their concentration is high, the fact that the vapor pressure decreases less rapidly with increasing detergent concentration is not perhaps unexpected. Very strong intermicellar influences must be operating in these solutions. Interaction could easily lead to a reduction in the amount of alcohol associated with the detergent through a change in micellar structure. Viscosity data on these solutions should be of considerable interest.

Whether or not micelles form in 45% ethanol, a lowering of vapor pressure would be expected on the addition of detergent. In fact, in the absence of colloidal aggregates the lowering is likely to be greater. Interaction between detergent and alcohol will still occur, the Raoult lowering of vapor pressure due to added detergent will now be important, and a reduction in the degree of hydration is highly probable. Present results are in accord with this expectation. But the alteration in vapor pressure as more detergent is added seems difficult to interpret without postulating some structural changes in the solution.

REFERENCES

1. McBAIN, M. E. L., AND HUTCHINSON, E., "Solubilization and Related Phenomena." Academic Press, New York, 1955.
2. HUFF, H., McBAIN, J. W., AND BRADY, A. P., *J. Phys. Chem.* **55**, 311 (1951).
3. FLOCKHART, B. D., *J. Colloid Sci.* **12**, 557 (1957).
4. HARROLD, S. P., *J. Invest. Dermatol.* **32**, 581 (1959).
5. WASHBURN, E. W., ed., International Critical Tables of Numerical Data, Vol. 3, p. 290 (1928).
6. HESS, K., AND SURÁNYI, L. A., *Z. physik. Chem.* **A184**, 321 (1939).
7. WARD, A. F. H., *Proc. Roy. Soc. (London)* **A176**, 412 (1940).
8. MURRAY, R. C., AND HARTLEY, G. S., *Trans. Faraday Soc.* **31**, 183, 206 (1935).
BRADY, A. P., AND SALLEY, D. J., *J. Am. Chem. Soc.* **70**, 914 (1948). ERIKSON, J. A., AND LINGAFELTER, E. C., *J. Colloid Sci.* **4**, 591 (1949). VOLD, M. J., *J. Colloid Sci.* **5**, 506 (1950).
9. STIGTER, D., AND MYSELS, K. J., *J. Phys. Chem.* **59**, 45 (1955).
10. PHILLIPS, J. N., *Trans. Faraday Soc.* **51**, 561 (1955).
11. STIGTER, D., WILLIAMS, R. J., AND MYSELS, K. J., *J. Phys. Chem.* **59**, 330 (1955).
12. MYSELS, K. J., AND PRINCEN, L. H., *J. Phys. Chem.* **63**, 1696 (1959).
13. BOCKRIS, J. O'M., *Quart. Revs. (London)* **3**, 173 (1949).
14. WARD, A. F. H., *J. Chem. Soc.* **1939**, 522.

SOME PROPERTIES OF THE CONCENTRATION PRODUCT IN COUNTERDIFFUSION¹

Frank R. Meeks and L. A. Veguilla²

Department of Chemistry, University of Cincinnati, Cincinnati 21, Ohio

Received March 14, 1961

ABSTRACT

By maximization of the concentration product of two species counterdiffusing through a medium, two approximations (one a function of time) are obtained for the position of the first Liesegang band. The expressions converge to the same value when the ratio of diffusion coefficients is unity. An expression of the Morse-Pierce form, relating band position to the square root of time after beginning of diffusion, is obtained as a straightforward result of the maximization. Physical significance of the derived quantities is discussed, and their range of validity is investigated.

INTRODUCTION

In theoretical work on the Liesegang phenomenon (periodic precipitation), two mathematical quantities are of frequent occurrence: the concentration product of the species involved in precipitation and the "Morse-Pierce" relation:

$$\frac{X_n}{t^{1/2}} = \text{constant}, \quad [1]$$

where X_n is a variable locating a Liesegang ring or band and t is time. Morse and Pierce (1) very early arrived at the conclusion that if the supersaturation product, H , was a constant, then Eq. [1] must follow, where

$$H \equiv C_A^a C_B^b \quad [2]$$

and H is identical to $K(X, t)$ of a previous paper (2) in this series. In Eq. [2] C_A^0 and C_B^0 are the initial concentrations of reactants A and B which form a precipitate of composition $A_a B_b$, and D_A and D_B are the diffusion coefficients of A and B, respectively. Since quantities in parentheses are lower limit, of integration in integrals of which the upper limits are infinity, Morse and Pierce reasoned that the only way in which H could

¹ Presented in part at the 135th National American Chemical Society Meeting, Boston, Massachusetts, Physical Chemistry Division.

² Present address: National Cash Register Co., Dayton, Ohio.

be constant would be for these limits to be constant. Here C_A and C_B are, of course, concentrations of A and B during supersaturation.

It is possible to be somewhat more general than Morse and Pierce by writing, similarly to Prager (3), a concentration product $K(x, t)$ which is not restricted to have a constant value. For counterdiffusion (as in, for example, the vapor-phase condensation work of Spotz and Hirschfelder (4), $K(x, t)$ takes on the form, not of that of Prager, but of the Morse-Pierce function. Prager's work was not concerned with counterdiffusion of the Spotz-Hirschfelder type. Wagner (5) has carried out a development similar to that of Prager.

In the present work, we are interested primarily in the maximal properties of $K(x, t)$. We are able to derive, incidentally, an expression of the form of Eq. [1] directly by maximization of $K(x, t)$ and to suggest a physical significance for it.

DERIVATIONS

Let

$$\alpha = \frac{X}{2\sqrt{D_A t}} \quad \text{and} \quad \beta = \frac{L - X}{2\sqrt{D_B t}},$$

the diffusion equation $D(\partial^2 c / \partial x^2) = \partial c / \partial t$ having been solved separately for A and B in a counterdiffusional process under the boundary conditions:

$$C_A = C_A^0 \quad \text{for} \quad X \leq 0; \quad C_B = C_B^0 \quad \text{for} \quad X \geq L;$$

$$C_A = C_B = 0 \quad \text{for} \quad 0 < x < L, t = 0.$$

Component A moves towards the right and B towards the left, accounting for the occurrence of $L - x$ in the numerator of β . Now $K(x, t)$ takes the form

$$K(x, t) = [C_A^0 \operatorname{erfc}(\alpha)]^a [C_B^0 \operatorname{erfc}(\beta)]^b. \quad [3]$$

Maximization of $K(x, t)$ with respect to x yields (6):

$$\exp(\alpha^2) \operatorname{erfc}(\alpha) = \mu \left(\frac{a}{b} \right) \exp(\beta^2) \operatorname{erfc}(\beta), \quad [3a]$$

where $\mu \equiv (D_B/D_A)^{1/2}$. For large values of α and β in Eq. [3a], it is possible to use an asymptotic approximation, as follows:

$$\exp(\alpha^2) \operatorname{erfc}(\alpha) = \pi^{-1/2} \left(\frac{1}{\alpha} - \frac{1}{2\alpha^3} + \frac{3}{4\alpha^5} - \dots \right),$$

which yields, neglecting all terms in α on the right except the first,

$$\beta \cong \mu \left(\frac{a}{b} \right) \alpha, \quad [4]$$

a similar approximation having been made for the expression involving β . From Eq. [4],

$$X_{\max.} \cong L \left(1 + \frac{a\mu^2}{b} \right)^{-1}, \quad [5]$$

locating the maximum in $K(x, t)$ with respect to x .

For large values of t (i.e., small values of α and β), the approximation of Eq. [5] is invalid, especially so if the diffusion constants are large. It is then possible, however, to use the procedure given (7) in the Appendix, resulting in the inequality, Eq. [8], of that section.

DISCUSSION

The analysis of Eq. [8] for the case $a = b$ will now be carried out. (The derivation of Eq. [8] for the general case $a = \gamma b$, where γ is a ratio of integers, is somewhat complicated by the stipulation $\gamma\mu < 1$. The present derivation is adequate when $\gamma\mu \sim 1$, but for values very much smaller than unity the Mean-Value Theorem must be applied differently from the way it is done in the Appendix. Also, for $\gamma\mu > 1$, it is sufficient simply to redevelop Eq. [8] by applying the Mean-Value Theorem to $F(\beta)$ instead of $F(\alpha)$, and the conclusions follow in the same manner as those presented below.

For $a = b$, Eq. [8] reduces to

$$X_{\max.} \leq \frac{L}{2\mu} + \frac{1 - \mu}{2\mu^3} (\pi D_B t)^{1/2}. \quad [9]$$

From the definition of μ , it follows that when $\mu = 1$ (both diffusing species having the same diffusion coefficient), the equality sign prevails and the maximum in $K(x, t)$ remains stationary in the center of the diffusion path. Salvinien (8) has very recently reached a similar conclusion for counter-diffusion when the reservoirs are exhaustible, using a different mathematical approach. For $\mu < 1$, the second term on the right-hand side of Eq. [9] is positive and it is possible for the maximum to move towards component B, the more slowly diffusing one.

It is, incidentally, possible to satisfy the conditions $\mu < 1$ but $\mu \cong 1$ in a number of ways involving different choices of a , b , and μ . Thus for $a/b = \gamma = 2$ and $\mu = 1/2$, $X_{\max.}$ remains stationary at $2/3L$. The precipitate in this case is A_2B and $D_A = 4D_B$; component A has a larger diffusion coefficient, which is one factor serving to establish the maximum in $K(x, t)$ nearer the reservoir of B, but this is slightly counteracted by the necessity of 2 moles of A per mole of B in the precipitate. A similar analysis can be made for $\gamma = 3$, $\mu = 1/3$, for which $X_{\max.} = 3/4L$, and other cases.

Equation [8] is of the form

$$X_{\max.} \leq mt^{1/2} + d, \quad [8']$$

since for a given reaction a , b , L , and μ are taken as constants. Of great interest is the $t^{1/2}$ dependence. Two cases may be considered: very large values of t and very small. In the latter instance, the term $mt^{1/2}$ can be neglected and $X_{\max.}$ is given as for $\mu = 1$. For very large t , the maximum migrates with time towards the more slowly diffusing reactant and the precipitate should eventually form between $L/2$ and the reservoir of B. It is possible to indicate a value of t above which it is not a good approximation to ignore the term $mt^{1/2}$. The condition

$$\frac{aL}{2a\mu + a - b} \gg \frac{(b - \mu a)(\pi D_B t)^{1/2}}{2a\mu^2 + (a - b)\mu}$$

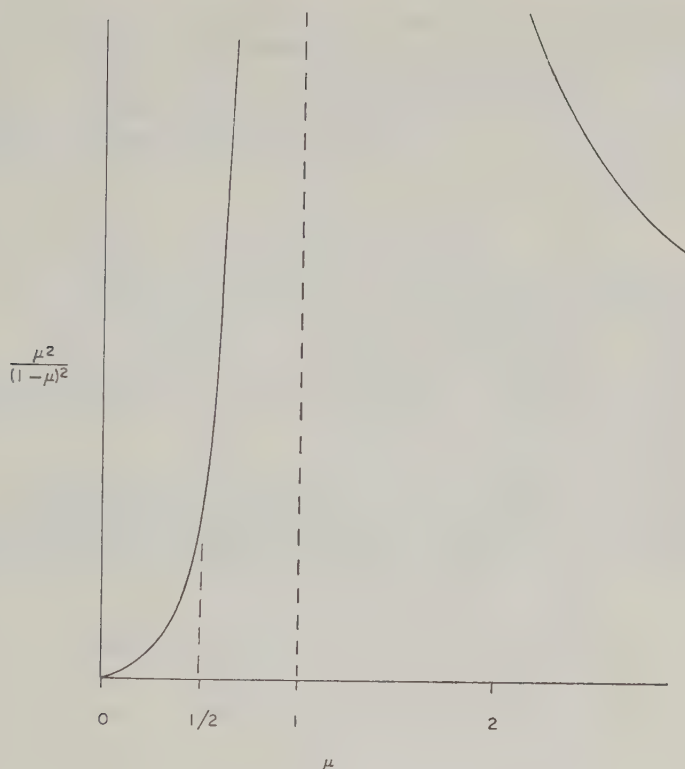
reduces to

$$t \ll \frac{L^2}{\pi D_B} \left(\frac{\mu}{1 - \mu} \right)^2$$

still for $a = b$. For $\mu = 1$, t must be less than infinity, which is to say that the term $mt^{1/2}$ can always be ignored. For $\mu \sim 0.5$, the term begins no longer to be negligible, as is seen from Fig. 1. (The branch of $\mu^2/(1 - \mu)^2$ for $\mu > 1$ is drawn into Fig. 1, but it is of no physical significance.) The more slowly B diffuses with respect to A (i.e., the smaller is μ), the larger the term $mt^{1/2}$ becomes. Physically, this means that a maximum in $K(x, t)$, once it has begun, moves rapidly in the direction of component B when μ is very small. A practical example of the application of Eq. [8] can be cited. Let the experiment of Spotz and Hirschfelder (4) be carried out in, say, a 10-cm. tube. For NH_3 and HCl in the vapor phase, the diffusion coefficients are approximately 0.3 and 0.2 $\text{cm}^2/\text{sec.}$, respectively, so that $\mu \cong 0.8$. Thus $L/2\mu \cong 6.25$ while $L/2\mu + (1 - \mu)(\pi D_{\text{NH}_3 t})^{1/2}/2\mu$ is approximately 8.25 for $t = 300$ sec., the approximate time at which the first Liesegang ring is observed. Since NH_4Cl becomes thermodynamically stable after approximately 15–20 sec. (as can easily be shown by evaluating $K(x, t)$), the maximum in $K(x, t)$ as represented by the ring has been migrating for $300 - 20 \cong 300$ sec. Without the term $mt^{1/2}$, an error of approximately 25% would be made in predicting $X_{\max.}$. Further experiments of the Spotz-Hirschfelder type, in which very long tubes of small diameter were used and in which accurate measurements have been made of the positions and times of formation of many successive rings, have been carried out in this laboratory and will be reported in the near future. Equation [8'] is obeyed in these latter experiments.

An evident property of $X_{\max.}$ as evaluated in this work is its independence of the reservoir concentrations. This suggests experiments in which C^0 is varied in some regular way for a series of experiments and positions of bands are observed; these are under way in this Laboratory (9).

The formal significance of Eq. [8] is that the position of the maximum


 FIG. 1. The function $\mu^2/(1 - \mu)^2$ versus μ .

in $K(x, t)$ is dependent upon $t^{1/2}$. When a band is deposited at X , when $t = t_1$, then $X \cong mt_1^{1/2} + d$, differing from Eq. [1] only in the presence of the constant d . If the effect of precipitation upon diffusion is slight, then for the second band at $t_2 (t_2 > t_1)$, $X_2 = mt_2^{1/2} + d$. The spacing between successive rings can be written $X_n - X_{n-1} = mt_n^{1/2}$, the Morse-Pierce relation exactly. This dependence has been observed experimentally in agar (10) under boundary conditions slightly different from those which obtain above, and in this laboratory on the aforementioned work on vapor-phase condensation of NH_4Cl from counterdiffusion of NH_3 and HCl (11).

SUMMARY

If the position of the first Liesegang band in a counterdiffusional system be taken to be that of the maximum in the concentration product, this position is a function of time as well as of the parameters of the diffusing systems. Maximization of the concentration product produces this dependence, an inequality of the form of the Morse-Pierce relationship. For

many laboratory situations, the inequality should be replaceable by an equality, resulting in a theoretical expression for the position of the first Liesegang band. In all the work of this paper, attention is confined to the results of an essentially new maximization of $K(x, t)$, and no discussion is offered at this time of the undoubtedly complicated interplay of diffusion and precipitation.

REFERENCES

1. MORSE, H. W., AND PIERCE, C. W., *Z. physik. Chem.* **45**, 589 (1903).
2. MEEKS, F. R., AND KOSENKRANIUS, H., *J. Colloid Sci.* (in press).
3. PRAGER, S., *J. Chem. Phys.* **25**, 279 (1956).
4. SPOTZ, E., AND HIRSCHFELDER, J. O., *J. Chem. Phys.* **19**, 1215 (1951).
5. WAGNER, C., *J. Colloid Sci.* **5**, 85 (1950).
6. "Tables of Probability Functions," F. W. A., W. P. A. of the City of New York (1941). Page XXV.
7. GANTSCHI, W., Private communication.
8. SALVINIEN, J., AND MOREAU, J. J., *J. chim. phys.* **57**, 518 (1960).
9. MEEKS, F. R., AND LINFERT, R. P., *J. Colloid Sci.* To be submitted.
10. CHATTERJI, A. C., AND BHAGWAN, H., *J. Colloid Sci.* **13**, 237 (1958).
11. MEEKS, F. R., AND GANOTE, C., To be submitted to *J. Colloid Sci.*

APPENDIX

Let

$$F(x) = e^{x^2} \int_x^\infty e^{-u^2} du \quad [6]$$

so that Eq. [2] becomes

$$F(\alpha) = \mu \left(\frac{a}{b} \right) F(\beta).$$

Since $F(x)$ is a decreasing function of x , then $\alpha > \beta$ when $\mu(a/b) < 1$, a condition which may be applied arbitrarily (7). Applying the Mean-Value Theorem to $F(\alpha)$, for $\alpha > \beta$,

$$F(\alpha) = F(\beta) + (\alpha - \beta)F'[\beta + \theta(\alpha - \beta)],$$

where $0 < \theta < 1$. Then

$$\alpha - \beta = \left[\mu \left(\frac{a}{b} \right) - 1 \right] F(\beta) \{ F'[\beta + \theta(\alpha - \beta)] \}^{-1}.$$

Now

$$-F''[\beta + \theta(\alpha - \beta)] = |F'[\beta + \theta(\alpha - \beta)]|$$

by inspection of Eq. [6]; further, since $\alpha > \beta$, it follows that

$$|F'(\alpha)| < |F'[\beta + \theta(\alpha - \beta)]|$$

and

$$\alpha - \beta < \left[1 - \mu \left(\frac{a}{b} \right) \right] F(\beta) [|F'(\alpha)|]^{-1}.$$

In view of the definition of $F(\alpha)$ and $F(\beta)$,

$$\alpha - \beta < \left[1 - \mu \left(\frac{a}{b} \right) \right] F(\alpha) \left[\mu \left(\frac{a}{b} \right) |F'(\alpha)| \right]^{-1}. \quad [7]$$

But $F'(\alpha) \equiv 2\alpha F(\alpha) - 1$ and $-F'(\alpha) = |F'(\alpha)|$, so that [6]:

$$\frac{|F'(\alpha)|}{F(\alpha)} = \frac{1}{F(\alpha)} - 2\alpha \geq \frac{1}{\alpha + \sqrt{\pi}/2},$$

which, when combined with Eq. [7], produces

$$\alpha - \beta \leq \left(\frac{b - \mu a}{\mu a} \right) \left(\alpha + \frac{\sqrt{\pi}}{2} \right).$$

Inserting the definitions of α and β , making partial use of the definition of μ , and rearranging, there results the following:

$$x_{\max.} \leq \frac{aL}{2a\mu + (a - b)} + \frac{(b - \mu a)(\pi D_B t)^{1/2}}{2a\mu^2 + (\alpha - \beta)\mu}. \quad [8]$$

CONDUCTIVITY OF MIXED SODIUM DECYL AND DODECYL SULFATES—THE COMPOSITION OF MIXED MICELLES¹

Karol J. Mysels and Raymond J. Otter

Chemistry Department, University of Southern California, Los Angeles 7, California

Received March 22, 1961

ABSTRACT

Precise measurements of conductivity of solutions of pure sodium decyl and dodecyl sulfates and their mixtures in the region of the critical micelle concentration (c.m.c.) are reported and the c.m.c. values of the mixed systems are evaluated. An empirical interpretation of these results is proposed which leads to a self-consistent assignment of composition to the mixed micelles. This interpretation is based on an extrapolation—on the conductivity vs. concentration plot—to obtain the concentration of monomers in a mixed solution in the same way in which the c.m.c. is obtained in a pure system. This extrapolated concentration is assumed to be the c.m.c. of the mixed monomers, again in analogy with the pure system. This concentration therefore determines the composition of the equilibrium monomers. The composition of the mixed micelles is then calculated by difference.

Whereas much is known about micellization in well-defined systems of a single micelle-forming component and in ill-defined mixtures of such components, there is relatively little work on well-defined mixtures of two or more micelle-forming components. A study of the interactions within mixed micelles holds, however, promise of shedding light upon their structure and the forces affecting it, in the same way the study of thermodynamic properties of ordinary solutions is contributing to our knowledge of these.

Previous work seems to have been confined to the determination of the critical micelle concentration (c.m.c.) (1-6) and to the development of theories accounting for its value in such systems (4-6). The general conclusion is that the mixed micelle can be considered as an ideal solution of its components and the observed c.m.c.'s thus accounted for. No attempt seems to have been made, however, to determine experimentally the composition of the mixed micelles, nor to evaluate the significance of the c.m.c. as a criterion of ideality. A closely related problem, the composition of the

¹ Presented in part at the symposium on the Structure of Micellar Solutions at the 139th National American Chemical Society Meeting, March, 1961.

mixed surface layer of such solutions, has been recently studied by Shinoda (7) but his experimental approach is not applicable to micelles.

The present paper presents some precise conductivity measurements for a number of mixed solutions of sodium decyl sulfate (NaDS) and sodium dodecyl (lauryl) sulfate (NaLS) in the c.m.c. region. These three-component solutions as well as their micellized and monomeric² parts may be characterized by their *concentration* in terms of total moles of surfactant per unit weight of solution and by the *composition* of this total surfactant in terms of mole fractions of each surfactant. The determination of precise c.m.c. values from these measurements is then discussed and a new empirical method of determining the composition of the mixed micelles presented. This leads to an evaluation of the changes in composition of the solution with concentration in these mixed systems. The following paper will present some thermodynamic observations and an interpretation of these empirical results.

EXPERIMENTAL

Materials

Sodium dodecyl and decyl sulfates were prepared as previously described from 99.8% pure alcohols obtained from Applied Research Laboratories, State College, Pennsylvania. The values of the equivalent conductivities of solutions of the NaDS agreed to within better than 0.15% over the concentration range 0 to 50×10^{-3} mole l.⁻¹ with measurements on three different independent samples prepared by Mrs. P. Kapauan (8) in this laboratory.

The equivalent conductivities of the NaLS were about 0.3 to 0.5 conductance unit lower than those obtained by Mukerjee, Mysels, and Dulin (9) on several different samples but were unchanged by further recrystallization from water or alcohol, followed by ether extraction. The slope of the two conductivity curves was otherwise identical, the curvature in the c.m.c. region being the same in both cases. Despite considerable effort we have been unable to trace the cause of this difference and have no reason to doubt the purity of either material.

The conductance measurements were carried out in an oil bath whose temperature was $25.00^\circ \pm 0.02^\circ\text{C}$. and constant to within 0.005°C . A Jones-Dyke (10) conductance bridge was used with a newly designed, magnetically stirred doughnut type dilution conductance cell described elsewhere (11). The cell constant was 2.9683 cm^{-1} . The solvent used was commercial distilled water which was carefully equilibrated against carbon dioxide in the air, and had a specific conductance of $3 \text{ to } 5 \times 10^{-6} \text{ ohm}^{-1}$

² The term "monomeric" is used throughout these two papers in opposition to "micellized" and is meant to include any dimers or ion pairs.

cm.⁻¹. In each series of measurements solutions of increasing concentration were prepared by adding known weights of a standard stock solution (1.0–0.1*M*) to a known weight of a more dilute solution, or of water, originally placed in the conductance cell. No buoyancy correction was applied to the weights of solution. The weight concentrations were converted to molal concentrations by using 288.4 and 260.3, respectively, for the formula weights.

RESULTS

Results of the conductivity measurements are shown in Table I and Figs. 1, 2, and 3. Table I gives selected numerical values obtained from smoothed large-scale graphs. Figure 1 shows the differential conductivity $\partial\kappa/\partial c$ (or more exactly, $(\kappa_2 - \kappa_1)/(c_2 - c_1)$ at $c = (c_1 + c_2)/2$), this is the best way of indicating the precision of the results and of showing the detailed behavior of the mixed systems. It also permits interpolation between values of Table I. A less detailed survey of the results is given by the plot of the equivalent conductivity, $\Lambda = \kappa/c$, in Fig. 2, which serves also to determine the usual value of the c.m.c. The plot of conductivity itself for the two pure components and a selected mixture in Fig. 3 shows much less detail but is the basis for our estimate of the composition of the micelles.

The strong interaction between the two components of our system is perhaps best indicated by Fig. 4, which shows the change in conductivity upon increasing the concentration of NaLS in a system in which the con-

TABLE I
Conductivities in the Sodium Decyl-Dodecyl Sulfate System at 25°C.

% NaDS	c.m.c. × 10 ³ (mole l. ⁻¹)	$K \times 10^6/\text{ohm}^{-1} \text{ mole}^{-1}\text{cm}^2$ at indicated $c \times 10^3/\text{mole l.}^{-1}$										
		c.m.c.										
		-1.0	-0.5	0	+0.5	+1.0	+2.0	+4.0	+6.0	+10	+15	+20
0	8.09	477	501	526	549	567	595	645	705	795	921	1045
10.78	8.55	509	533	561	581	597	645	685	740	841	971	1105
20.25)	8.78	525	552	575	596	617	653	717	777	887	1023	1160
20.06)												
34.78	10.16	616	642	664	689	710	746	812	874	896	1145	1289
49.12	11.46	697	724	742	776	799	840	912	961	1106	1275	1429
59.98	13.17	809	840	865	886	908	950	1029	1103	1245	1413	1573
71.00	15.40	956	984	1005	1030	1063	1096	1159	1257	1416	1584	1749
84.66	19.63	1221	1248	1273	1298	1322	1369	1459	1544	1705	1880	2045
94.95	27.24	1688	1713	1740	1760	1782	1827	1908	1987	2126	2282	2436
100.00	33.52	2061	2084	2105	2125	2143	2180	2243	2304	2417	2560	2704

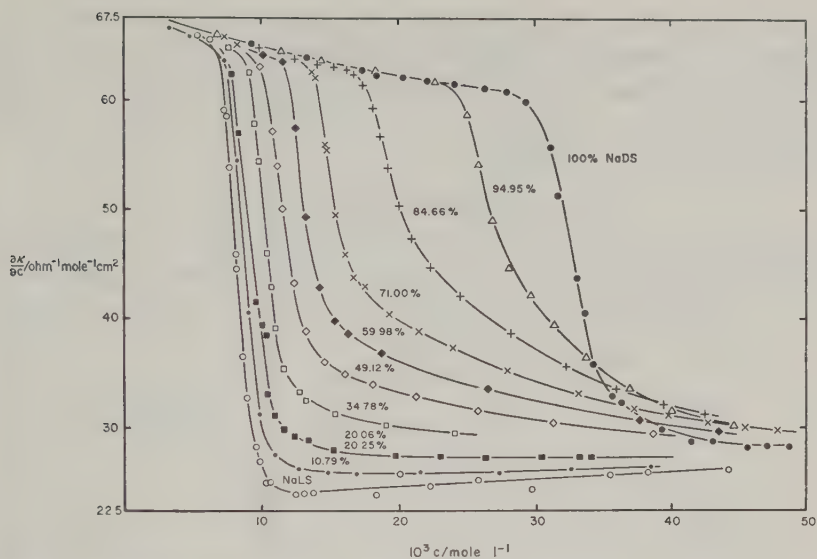


Fig. 1. Differential conductivity of NaLS-NaDS mixtures in the c.m.c. region.

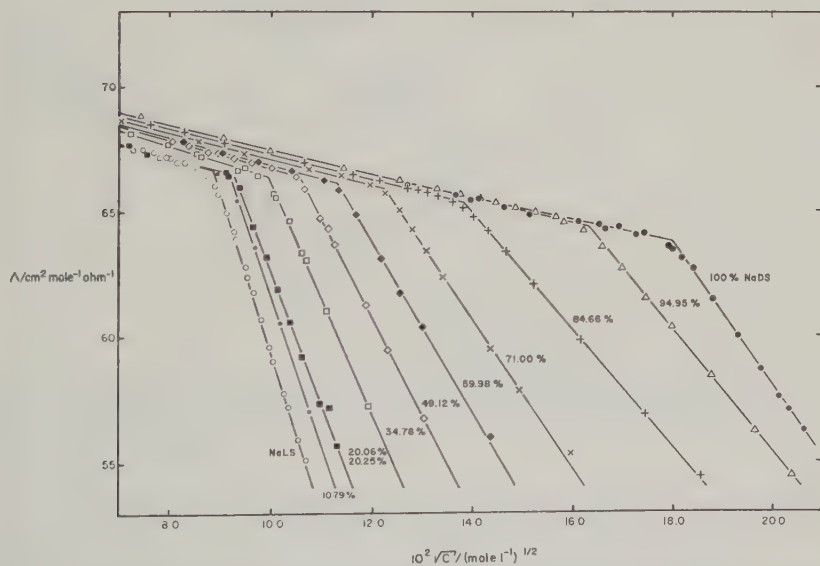


Fig. 2. Equivalent conductivities of NaLS-NaDS mixtures in the c.m.c. regions.

centration of NaDS is kept constant at several round values. The values for this graph are obtained from a large-scale graph similar to Fig. 3. It may be seen that addition of NaLS to water or low concentrations of NaDS increases the conductivity markedly at first and then somewhat less as

micelles begin to form. However, when the concentration of NaDS is high, the addition of NaLS can actually cause a decrease in conductivity as the formation of micelles is greatly facilitated. The dashed lines show what would be the effect of replacing NaLS by NaDS as the additive with correspondingly reduced interaction.

The Critical Micelle Concentrations

A useful definition of the c.m.c. is the concentration of surfactant at which the concentration of micelles would vanish if it were to decrease as

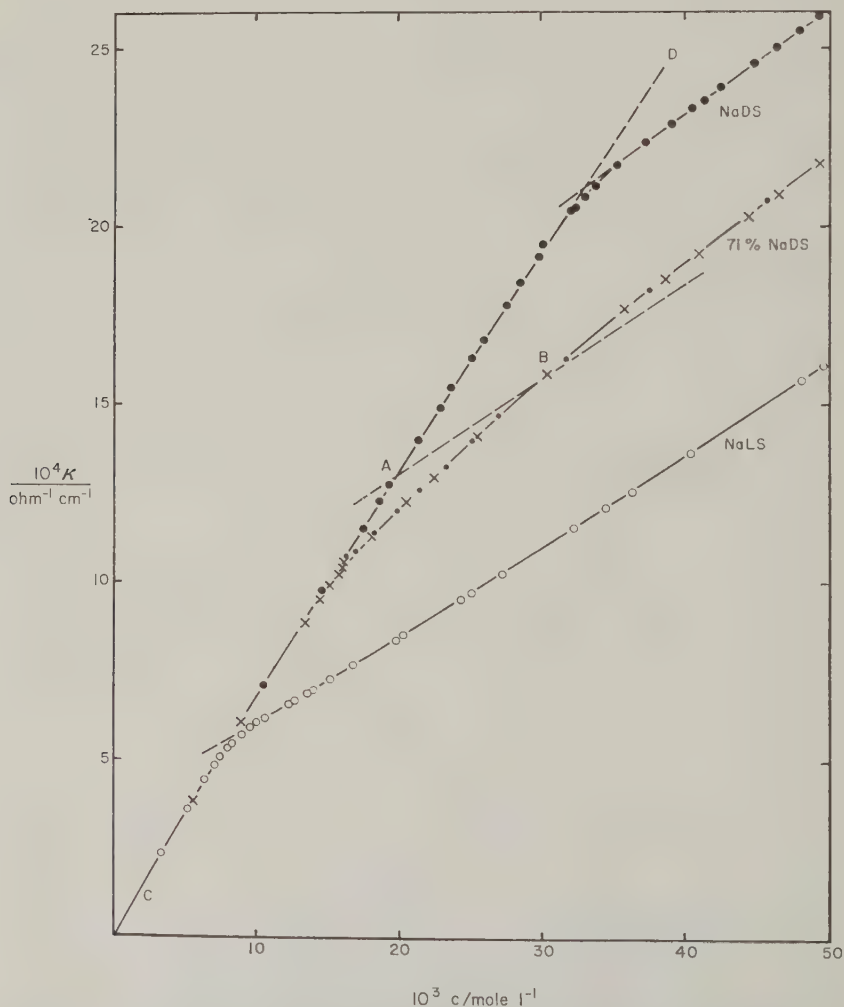


FIG. 3. The conductivities of pure NaLS, of pure NaDS, and of a mixture containing 71% NaDS. Line BA shows the extrapolation used for estimating the concentration of monomers (A) in equilibrium with micelles at point B. ●, X, O: experimental; •: calculated from diagonal line of Fig. 6.

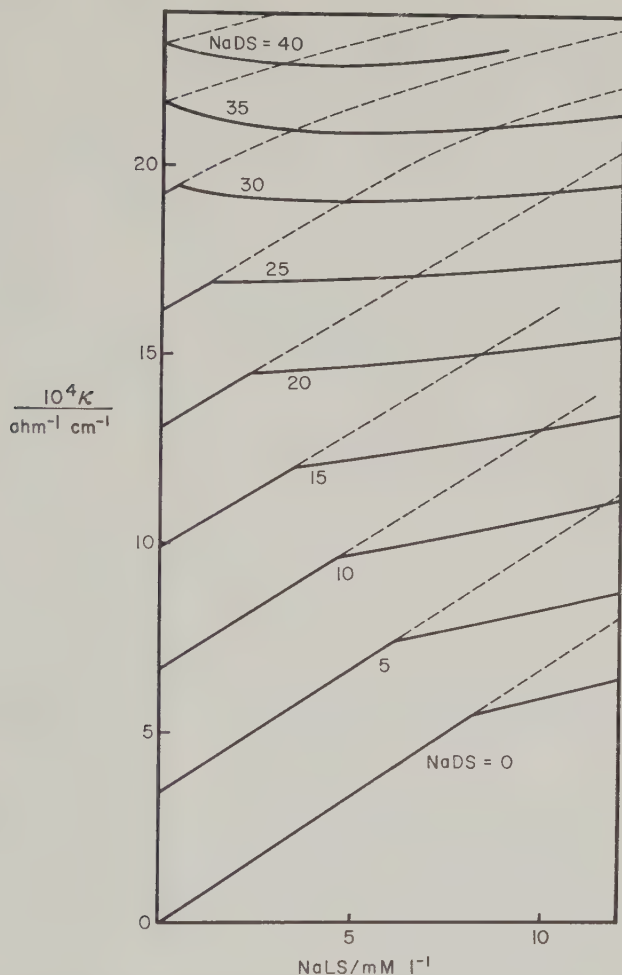


FIG. 4. The conductivity of the NaDS-NaLS system at several fixed concentrations of NaDS as a function of added NaLS. Dashed lines show the effect of replacing the added NaLS by NaDS.

it does at a slightly higher concentration. This is evaluated by extrapolating a selected property of the solution by straight lines from above and below the c.m.c. As shown by Fig. 2 such an extrapolation can be easily performed on a plot equivalent conductivity Λ vs. $c^{1/2}$ both for the pure components and for the mixtures. We call the values thus obtained c.m.c. I. Figure 3 shows that a similar extrapolation can be performed for the pure components on a κ vs. c plot but that the plot for the mixture is here too curved to make a linear extrapolation meaningful. Let us call the value obtained for the pure components by this second method c.m.c. II.

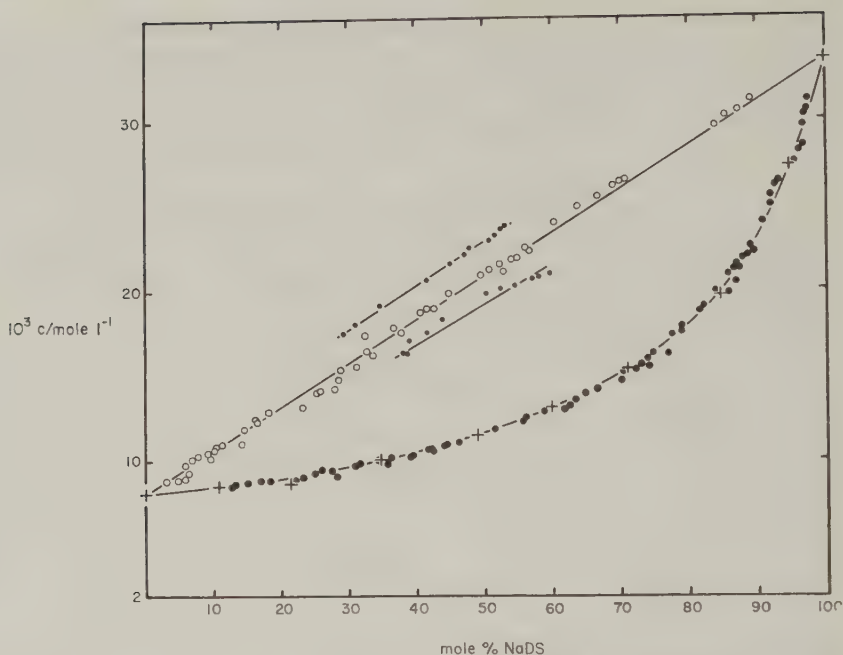


Fig. 5. C.m.c. values (lower curve) and mixed micelle compositions (upper line) in the NaLS-NaDS system. +: experimental c.m.c.; o: calculated mixed micelle compositions; •: same using the extreme slopes; •: c.m.c.'s calculated from the diagonal line.

As has been noted already by Ward (12) the two c.m.c. values thus obtained need not be the same. We find that c.m.c. I is lower than c.m.c. II by 2.8% for both pure components. This difference stems from the fact that an oblique straight line on one plot is not a straight line on the other so that different points are used in the extrapolation from above the c.m.c. and are extended differently.

In order to determine the composition of mixed micelles we will need the equivalent of c.m.c. II also for the mixed systems. We assign this value by applying the correction factor of 2.8%, valid for the pure systems, to the values of the c.m.c.'s I for the mixed ones. The c.m.c. II values thus obtained are listed in Table I and are shown by the crosses in Fig. 5. It should be noted that since the c.m.c. involves an extrapolation to zero concentration of micelles, the composition of mixed monomers and their concentration is that of the solution as a whole. The smooth curve of Fig. 5 thus gives us the composition of the monomeric ions at the c.m.c. for any mixed system.

The Composition of Mixed Micelles

The striking fact shown by Fig. 3 is that the conductivity of solutions of the pure components increases linearly above a narrow critical region

whereas that of the mixed system is curved over a wide concentration range. Qualitatively this difference must be due to the fact that in the pure system the composition of micelles and monomers is the same and must remain constant since only one component is present, whereas in the mixed system the compositions of micelles and monomers are different and change with overall concentration. The few micelles initially formed as the concentration increases are richer in one component (LS in our case) so that the composition of the monomeric solution is slightly enriched in the other (DS). This enrichment is increased as the concentration is increased and more micelles form. A change in micellar composition accompanies this enrichment and so on as the total concentration increases. Figure 6 shows a more quantitative picture of these changes. The important point is that above the c.m.c. micelles are in equilibrium with a monomeric solution whose composition differs from the overall composition of the system. Being enriched in the component having less tendency to micellize, this monomeric solution has a concentration higher than the original c.m.c. with a corresponding greater conductivity. This effect continues as the concentration increases, giving the observed curvature until, at very high concentrations, the composition of the micelles finally corresponds essentially to that of the overall system while the monomeric solution has a different equilibrium composition and undergoes no further change with increasing total concentration.

Another feature of Fig. 3 is that on this scale the conductivity of the monomeric solutions lies on a single, slightly curving line *CD* (Figs. 1 and 2 show that this is only an approximation) so that we can extrapolate readily the conductivity of a monomeric solution beyond its c.m.c. Vice versa, from the conductivity of the mixed monomeric solution we can obtain its concentration no matter what its composition.

Figure 3 shows also clearly that, for a *single* component system, the value of the c.m.c.—more precisely c.m.c. II—can be obtained from any point, provided it is slightly above the c.m.c., by linear extrapolation along a single slope (since all these points lie on a single straight line) back to the line *CD*. This slope is slightly different for NaLS and NaDS, but we can neglect this difference in the first approximation.

Let us now make the same back extrapolation to line *CD* along the same slope for the *mixed* system. This is shown by the line *AB* in Fig. 3. By analogy with the pure component case we would expect to reach the c.m.c. II value corresponding to the monomeric solution in equilibrium with the micelles at the starting point. Thus point *A* in Fig. 3 corresponds to the c.m.c. II of the monomeric solution in equilibrium with micelles of point *B*. From the lower line of Fig. 6 we know, however, the composition of monomers corresponding to this c.m.c. From the concentration and composition of the monomeric solution thus obtained for point *A* and from the overall composition at point *B* it is now easy to calculate the concentration

and composition of the micelles at that point. This is the desired quantity. It can be recorded graphically as shown in Fig. 5 by one of the open points having for coordinates the concentration (c.m.c.) of mixed monomers and the composition (mole %) of the mixed micelles.

The following numerical example may clarify this calculation: Point *B* in Fig. 3 corresponds to an overall concentration of 29.7 mM in a system containing 71% NaDS. Back extrapolation yields point *A* at 19.8 mM. According to Fig. 6, 19.8 mM corresponds to the c.m.c. of 84.8% NaDS. This gives the concentration of monomeric NaDS as $19.8 \times 0.848 = 16.79$ mM. The total DS concentration is $29.7 \times 0.71 = 21.09$ mM. Therefore the concentration of micellized NaDS is $21.09 - 16.79 = 4.30$ mM. Since the total concentration of micelles is the difference between the concentration of *A* and *B*, i.e., $29.7 - 19.8 = 9.9$ mM, we obtain the composition of the micelles as $(4.3/9.9) \times 10^2 = 43\%$ NaDS.

A similar calculation can be made for other points along the 71% curve of Fig. 3 and also for each of the similar curves obtained for the other compositions. In this way a series of partially overlapping groups of points shown in Fig. 5 is obtained. These can be all summarized within the experimental precision by the straight diagonal line shown. This line gives therefore the equilibrium monomeric concentration and micellar composition. The lower curve gives the corresponding monomer composition.

DISCUSSION

Sufficient assumptions to justify the above procedure would be that (1) the concentration and composition of monomers in equilibrium with micelles of a given composition are independent of the concentration of these micelles and (2) the equivalent conductivities of the two monomers and of micelles of any given composition are constant over the range of solutions involved in the extrapolation. These are clearly not correct assumptions, but neither are they necessary ones. The minimum necessary assumption would be that deviations from the above assumptions give a compensating effect such that the back extrapolation gives the c.m.c. of monomers having a composition in equilibrium with micelles of the desired composition. That the compensating factors can operate in this way—within the precision of Fig. 3—is shown by the straightness of the lines for the pure components. The unproven hypothesis is that the same compensation occurs in the mixed system.

A strong argument for the validity of this hypothesis is that the treatment is self-consistent, as shown by the fact that overlapping series of points all lying on the same line are obtained from experimental data for different compositions. In other words, the same equilibrium compositions of micelles and monomers can be obtained from two different overall compositions and concentrations. This is a rather sensitive test because small

changes in the chosen value for the c.m.c. can completely destroy the self-consistency and give series of points lying on disconnected segments.

In order to obtain consistent results it was necessary to use the next approximation in choosing the extrapolating slope, which, as already mentioned, is slightly different for NaLS and NaDS. We used a linear interpolation between the two extremes according to the conductivity at $40 \times 10^{-3} M$. The values used for each composition are listed in Table I. The short diagonal lines of Fig. 5 show the effect of using one or the other of the extreme slopes.

The straight line extrapolation requires omission of points very close to the c.m.c. We omitted those within $5 \times 10^{-3} M$. This is related to

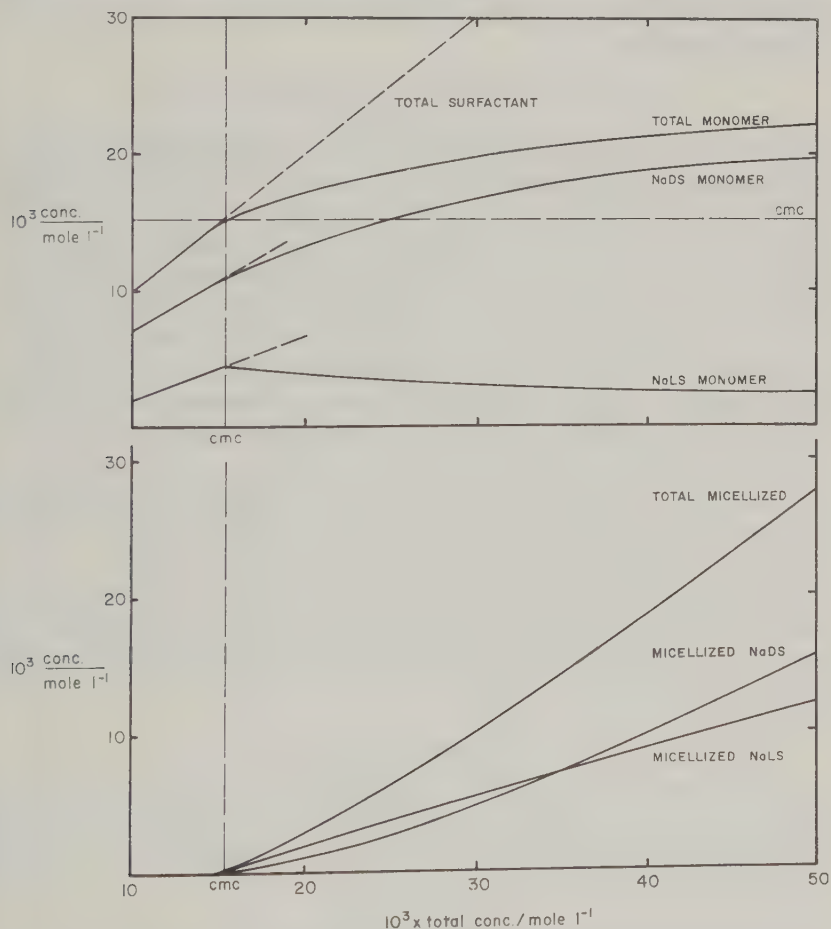


FIG. 6. Typical changes in concentration of monomeric (*above*) and micellized (*below*) components in a mixed system. Calculated for a 71% NaDS system on the basis of Fig. 5. Other compositions as well as ideal systems behave similarly.

the fact that even for the pure components the experimental points do not lie on the straight lines in this region. Conversely, if the equilibrium compositions of Fig. 5 are now used to calculate the position of the 71% line by reversing the procedure, the result—corresponding to the straight line for the pure component—shows only a minor deviation in the c.m.c. region from the experimental points. This deviation is not greater than that from the straight line for the pure components. This is shown in Fig. 3 by the small points and is an additional check on the self-consistency and accuracy of the procedure.

A similar procedure was used to calculate the c.m.c. II curve of Fig. 5 from the straight line of this figure combined with the experimental conductivities. The agreement shown by solid circles of Fig. 5 is obtained and is again satisfactory.

The Effect of Concentration in Mixed Systems

Figure 6 shows the application of the result of this empirical evaluation of the equilibrium compositions of monomers and micelles to a calculation of the changes in these two compositions as the overall concentration increases in a particular mixed system, the one containing 71% of NaDS. It may be noted that the composition of micelles continues to change even after the c.m.c. has been exceeded severalfold. The crossing of the two micellized concentrations means only that the micelles initially formed contained less than 50% of NaDS on a mole basis whereas at high concentration they tend, of course, to the 71% limit. The total concentration of monomers continues to increase markedly long after the c.m.c. is passed, although in a one-component system it would remain strictly constant at the c.m.c. level according to the assumptions made. This increase in concentration is, however, due only the DS^- , while the concentration of the monomeric LS^- actually decreases after reaching a maximum at the c.m.c.

Other compositions show very similar trends and ideal systems, discussed in the following paper, differ only quantitatively. The overall behavior is always quite analogous to that of a mixed vapor condensing upon being gradually and isothermally compressed.

ACKNOWLEDGMENTS

This work was supported in part by the Office of Naval Research and reproduction for purposes of the U. S. Government is permitted. We are indebted to Professor J. Th. G. Overbeek for helpful suggestions and to Mrs. P. Kapauan for her exploratory measurements on this system.

REFERENCES

1. CORRIN, M. L., AND HARKINS, W. D., *J. Colloid Sci.* **1**, 469 (1946).
2. KLEVENS, H. B., *J. Chem. Phys.* **14**, 742 (1946).

3. KLEVENS, H. B., *J. Phys. & Colloid Chem.* **52**, 130 (1948).
4. LANGE, H., *Kolloid-Z.* **131**, 96 (1953).
5. SHINODA, K., *J. Phys. Chem.* **58**, 541 (1954).
6. SHINODA, K., *J. Phys. Chem.* **58**, 1136 (1954).
7. SHINODA, K. AND MASHIO, K., *J. Phys. Chem.* **64**, 54 (1960).
8. MYSELS, K. J., AND KAPAUAN, P., *J. Colloid Sci.*, submitted.
9. MUKERJEE, P., MYSELS, K. J., AND DULIN, C. I., *J. Phys. Chem.* **62**, 1390 (1958).
10. DYKE, P. H., *Rev. Sci. Instr.* **2**, 379 (1931).
11. MYSELS, K. J., *J. Phys. Chem.* **65**, 1081 (1961).
12. WARD, A. F. H., *Proc. Roy. Soc. (London)* **176**, 412 (1940).

THERMODYNAMIC ASPECTS OF MIXED MICELLES— APPLICATION TO AN EMPIRICALLY ESTABLISHED EQUILIBRIUM¹

Karol J. Mysels and Raymond J. Otter

Chemistry Department, University of Southern California, Los Angeles 7, California

Received March 22, 1961

ABSTRACT

Relationships between the overall composition—in terms of mole fractions of two micelle-forming components—in a solution of these two components and the critical micelle concentration on the one hand and the composition of the mixed micelles on the other, are reviewed and activity coefficients introduced to account for the behavior of real systems. It is shown that the behavior of the critical micelle concentration is not a sufficient criterion for the ideality of the system, that the contribution to nonideality of the two components can be resolved, and that the ideality of the monomeric solution may be tested if the composition of mixed micelles is known. These considerations are applied to the results obtained in the preceding paper for the sodium decyl and dodecyl sulfates and indicate definite deviations from ideality for the whole system as well as for the monomeric solution. These deviations are, however, not very large and affect the mixed critical micelle concentration insignificantly.

List of Symbols

- a = one of the surfactants alone.
- A, B = constants.
- C = critical micelle concentration.
- f = activity coefficient in the micelle.
- g = concentration of counterions.
- $1, 2$ = the two components.
- i = any of the components.
- m = mixed system of mole fractions x_i .
- n = number of carbon atoms in surfactants.
- x = mole fraction in the total system.
- y = mole fraction in the micelles.
- β_i = $f_i \gamma_{iq} / \gamma_{ix}$.
- Δ = $n_1 - n_2$.
- γ = activity coefficient among the monomers.

¹ Presented in part at the symposium on the Structure of Micellar Solutions at the 139th National American Chemical Society Meeting, March, 1961.

θ = constant defined in Eq. [1].

ω = change of surface energy upon micellization.

In the preceding paper (1) we have reported conductivity measurement and proposed an interpretation in terms of equilibrium mole fractions in micelles and in the monomeric solution for the system sodium decyl sulfate (NaDS)-sodium dodecyl (lauryl) sulfate (NaLS). The present paper analyzes the general meaning of such an equilibrium in terms of deviations from ideality with particular application to this system.

The interpretation (2-4) of the formation of mixed micelles is based on what is known—or assumed—about the behavior of the pure system combined with the effect of the interaction of the two components in the micelle. For pure systems the c.m.c. and its changes as the concentration of counterions increases in the presence of an inert salt are known. A second micelle-forming component has two effects: (a) it introduces some counterions whose effect can thus be taken into account, and also (b) it changes the pure micelle into a mixed one which is a solution of the two components and thus is more easily formed. This second effect can be treated by assuming that the mixed micelle is an ideal solution, the activity of each component being proportional to its mole fraction in the micelle. Introduction of activity coefficients then permits transition to real systems.

IDEAL SYSTEMS

It is found experimentally (5-13) that the c.m.c. C of solutions of a single ionic surfactant, i , in the presence of salt can be described by the equation

$$\log C_{ig} = \log A_i - (\theta_i - 1) \log g, \quad [1]$$

where g is the total counterion concentration. Here A_i and θ_i are constants whose value depends on the nature of the surfactant. In general θ_i seems to be constant for a homologous series (9, 10) and differs but little for the two components of our system (11, 13). We will therefore omit the subscript and treat θ as a constant. It should be noted, however, that Lange (2) found large variations in θ for the higher alkyl sulfates and carried it as an independent variable in his development.

The constant A_i is given simply by the c.m.c. C_{ia} in the absence of added salt when the concentration of counterions is given by the ions accompanying the pure surfactant so that $g = C_{ia}$ and according to Eq. [1]

$$A_i = (C_{ia})^\theta. \quad [2]$$

We can define the c.m.c. C_m of a mixed system of overall mole fraction x_i of surfactant i in the usual way as the molar concentration of the solution when the concentration of micelles vanishes. This overall concentration C_m is therefore equal to the sum of the individual monomeric concentration C_{im} at this point and also to the counterion concentration g .

$$C_m = C_{1m} + C_{2m} = g. \quad [3]$$

By definition we also have at this point

$$C_{im} = x_i C_m. \quad [4]$$

We now assume ideal behavior and in particular, by analogy with ideal simple solutions where the ratio p/p_0 of the actual vapor pressure to that of the saturated vapor is equal to the mole fraction of the liquid, we make C_{im}/C_{ig} the ratio of the actual concentration of micelle-forming ions to the concentration at the c.m.c. (in the presence of the same counterion concentration) equal to the mole fraction y_i in the micelle:

$$C_{im} = y_i C_{ig}. \quad [5]$$

By combining the above equations one obtains for each component

$$\left(\frac{C_m}{C_{ia}}\right)^\theta = \frac{y_i}{x_i}. \quad [6]$$

Either y or x or C_m can be eliminated from these two equations, giving

$$C_m^\theta = \frac{(C_{2a} C_{1a})^\theta}{x_1 C_{2a}^\theta + x_2 C_{1a}^\theta}; \quad [7]$$

$$C_m^\theta = y_2 C_{2a}^\theta + y_1 C_{1a}^\theta; \quad [8]$$

and

$$\left(\frac{C_{2a}}{C_{1a}}\right)^\theta = \frac{y_1/y_2}{x_1/x_2}. \quad [9]$$

In view of Eq. [2] these can be more simply written also in terms of A_1 and A_2 .

Shinoda's (3) treatment differs from the above only in that he expresses the constant A_i in terms of n_i , the number of carbon atoms in the paraffin chain of the surfactant:

$$\log A_i = -n_i \omega / kT + B, \quad [10]$$

where ω and B are constants independent of the chain length in a homologous series and the former is interpreted as the change in surface energy upon micellization per methylene group. This leads to Eq. [8] above and to his Eq. [11], which can be written in our notation as

$$C_m^\theta = \frac{x_2 C_{2a}^\theta + x_1 C_{1a}^\theta e^{\Delta \omega / kT}}{x_2 + x_1 e^{\Delta \omega / kT}} \quad [11]$$

where $\Delta = n_1 - n_2$. Shinoda's approach, if pursued consistently, can actually eliminate one of the c.m.c.'s and permits replacement of Eqs.

[7]-[9] by the equivalent expressions in terms of ω :

$$C_m^\theta = C_{2a}^\theta / (x_2 + x_1 e^{\Delta\omega/kT}); \quad [12]$$

$$C_m^\theta = C_{2a}^\theta (y_2 + y_1 e^{\Delta\omega/kT}); \quad [13]$$

$$e^{\Delta\omega/kT} = \frac{y_1/y_2}{x_1/x_2}. \quad [14]$$

Thus the assumption of ideality leads not only to a definite mixed c.m.c. but also to a definite composition of micelles and to a relation between the composition of the mixed monomers and the mixed micelles.

COMPARISON WITH EXPERIMENT

Figure 1 shows the application of this ideal theory to the NaDS-NaLS system using $\theta = 1.68$. It is apparent that the observed values of the c.m.c. are rather close to the line predicted by the theory but that the composition of the micelles as obtained by our method (1) deviates markedly from

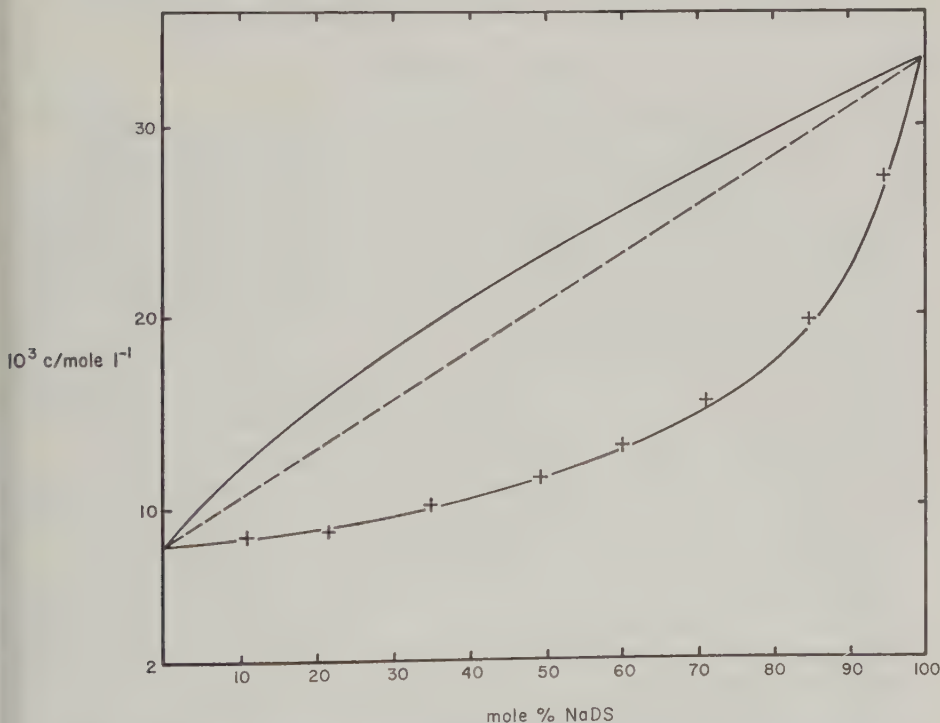


FIG. 1. The equilibrium compositions of micelles and monomers in the NaLS-NaDS system. Solid lines represent ideal behavior. +: experimental c.m.c. II; ---: composition of mixed micelles as obtained in preceding paper.

the theoretical line. The micelles are consistently richer in decyl sulfate than would be anticipated if the system were ideal. The deviation is much more than could be accounted for by minor errors in the measurement or in the extrapolation. It could be due either to a basic invalidity of our procedure or to a real deviation of the system from ideality. Pursuing this second possibility appears to be the more fruitful at present and in the following we shall assume the composition of the mixed micelles to be that given in the preceding paper.

The observed deviation from ideality could then be due to a preferential solubility of the decyl ion in the micelle or to a relatively greater reduction of activity of the dodecyl ion among the monomers or to a combination of these effects. Plausible structural arguments could be given for both effects. The following analysis indicates that nonideality of the monomers is at least a contributing cause.

NONIDEAL SYSTEMS

Deviation from ideality can be expressed in the customary manner by introducing activity coefficients. We replace therefore Eq. [5] by

$$C_{im}\gamma_{im} = y_i f_i C_{ig}\gamma_{ig}, \quad [15]$$

where the activity coefficient in the mixed micelle is f and in the solution it is γ . The first subscript indicates the component and the second its medium. Thus γ_{1m} and γ_{1g} indicate the activity of monomeric component 1 in the mixture and in a salt solution both having a concentration $g = C_m$ of counterions. Since it is possible that the activity of the monomer is affected not only by the ionic strength but also by specific interaction with other long-chain ions, the distinction may not be trivial.

It should be noted that no activity correction is needed in Eq. [1], which is empirically obtained without such corrections, nor in Eq. [3], for the conservation of mass, which assumes only that the monomeric surfactant is a strong salt. This is to be expected for the sodium salts (14).

The activity correction appears, therefore, in our final equations simply as a factor $f_i\gamma_{ig}/\gamma_{ix}$ multiplying the corresponding y_i whenever it appears.

Lange (2) has attempted to evaluate this factor by neglecting $f_i - 1$, assuming $\gamma_{ix} = \gamma_{ig}$ and calculating the latter from an extended Debye-Hückel theory taking the ionic radius as 8 Å. We feel that not enough is known at present to pursue the theoretical evaluation of this factor or of any of its components but that on the contrary the experiment can provide a useful evaluation of the whole factor and thus indicate the nonideality of the system. We therefore introduce $\beta_i = f_i\gamma_{ig}/\gamma_{im}$ and evaluate them from the known x_i , C_m , and C_{ia} , and from y_i determined empirically as ex-

plained in the preceding paper. Thus β_i is given by

$$\left(\frac{C_m}{C_{ia}}\right)^{\theta} = \beta_i y_i / x_i, \quad [16]$$

which corresponds to Eq. [6].

Figure 2 shows a plot of β_{NaDS} and β_{NaLS} for our systems obtained from a smoothed graph of observed C_m and y_i . It may be noted that β_{NaDS} is smaller and β_{NaLS} larger than unity throughout except perhaps for very low mole fractions of the decyl. The deviation from unity does not exceed 40%. The experimental error, estimated from the uncertainty in reading the graphs, becomes large as either mole fraction becomes small, but is reasonable for most compositions.

MEANING OF AN IDEAL MIXED C.M.C.

The opposite course of the two β 's is related to the fact that the experimental c.m.c.'s are close to those predicted by ideality. In fact, if one assumes that for a given value of x the ideal c.m.c. of Eq. [6] is exactly equal to the real c.m.c. of Eq. [16], one obtains

$$\beta_i y_{i,\text{real}} = y_{i,\text{ideal}}. \quad [17]$$

Since $y_1 = 1 - y_2$, this gives by eliminating the y_{ideal}

$$\beta_1 = \frac{1 - \beta_2 y_{2,\text{real}}}{1 - y_{2,\text{real}}}, \quad [18]$$

which shows that if the c.m.c. lies on the ideal line, the two β 's must either both equal unity or diverge therefrom in opposite directions. It also shows that the c.m.c. value may lie on the ideal line without ideal behavior of the system as a whole.

Hence determination of the mixed c.m.c. alone is not sufficient to prove the ideality of mixed micelles.

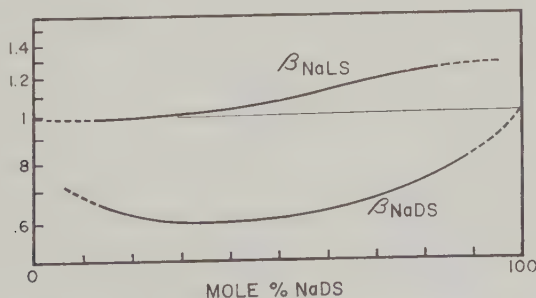


FIG. 2. The deviations from ideality of the two components of the NaLS-NaDS system as measured by the ratios β of activity coefficients according to Eq. [16].

INTERACTION OF MONOMERS

If one assumes that the monomers do not interact specifically so that their activity is primarily determined by the ionic strength, the distinction between the activity coefficients γ_{iz} and γ_{ig} (in the presence of equivalent concentrations of the second surfactant or of an inert salt) disappears and β_i becomes f_i , the activity coefficient in the mixed micelle. These two activity coefficients must, however, obey the Gibbs-Duhem relation. As has been shown recently by Redlich and Kister (15), a particularly easily tested consequence of this relation is that

$$\int_0^1 (\ln f_1 - \ln f_2) dx = 0, \quad [19]$$

which means that a plot of the two activity coefficients must cross and—on a semilogarithmic plot, such as Fig. 2—the areas enclosed on both side of the crossing must be equal. This is clearly not the case in our system. Hence, to the extent that our determination of the composition of mixed micelles is correct, there must be considerable interaction between the two monomers. In view of the marked dimerization indicated for the pure dodecyl salt (16) and its lack in the decyl one (13), this would not be surprising, but it clearly remains to be confirmed.

ACKNOWLEDGEMENTS

This work was supported in part by the Office of Naval Research and reproduction for purposes of the U. S. Government is permitted. We are grateful for the valuable comments of Prof. J. Th. G. Overbeek and Dr. D. Stigter.

REFERENCES

1. MYSELS, K. J., AND OTTER, R. J., *J. Colloid Sci.*, in the press.
2. LANGE, H., *Kolloid-Z.* **131**, 96 (1953).
3. SHINODA, K., *J. Phys. Chem.* **58**, 541 (1954).
4. SHINODA, K., *J. Phys. Chem.* **58**, 1136 (1954).
5. CORBIN, M. L., AND HARKINS, W. D., *J. Am. Chem. Soc.* **69**, 683 (1947).
6. MERRILL, R. C. AND GETTY, R., *J. Phys. & Colloid Chem.* **52**, 774 (1948).
7. KOLTHOFF, I. M., AND STRICKS, W., *J. Phys. & Colloid Chem.* **53**, 424 (1949).
8. LANGE, H., *Kolloid-Z.* **121**, 66 (1951).
9. HERZFELD, S. H., *J. Phys. Chem.* **56**, 959 (1952).
10. SHINODA, K., *J. Phys. Chem.* **59**, 432 (1955).
11. WILLIAMS, R., PHILLIPS, J. N. AND MYSELS, K. J., *Trans. Faraday Soc.* **51**, 728 (1955).
12. MATIJEVIC, E., AND PETHICA, B. A., *Trans. Faraday Soc.* **54**, 587 (1958).
13. MYSELS, K. J., AND KAPAUAN, P., *J. Colloid Sci.* **16**, 481 (1961).
14. MUKERJEE, P., AND MYSELS, K. J., *J. Phys. Chem.* **62**, 1400 (1958).
15. REDLICH, O., AND KISTER, A. T., *Ind. Eng. Chem.* **40**, 345 (1948).
16. MUKERJEE, P., MYSELS, K. J., AND DULIN, C. I., *J. Phys. Chem.* **62**, 1390 (1958); MUKERJEE, P., *ibid.* 1397 (1958). A negative result is reported, however, by F. VAN VOORST VADER, *Trans. Faraday Soc.* **57**, 110 (1961).

ELECTRIC CONDUCTIVITY OF SODIUM DECYL SULFATE SOLUTIONS

Karol J. Mysels and Paz Kapauan

Chemistry Department, University of Southern California, Los Angeles 7, California

Received March 22, 1961

ABSTRACT

A modified method of preparing the sodium decyl sulfate based on the insolubility of its alcoholate is described, and conductivity measurements in the highly dilute region and in the c.m.c. region in water and in the presence of salt are reported. The behavior of this compound seems quite normal throughout and it shows no indication of marked dimerization.

A previous paper from this laboratory (1) described and analyzed the electric conductivity of dilute solutions of sodium dodecyl sulfate. It indicated that at concentrations below the critical micelle concentration (c.m.c.) the amphipathic ion dimerizes to a more conducting entity. The marked deviation from the Onsager slope at concentrations below $10^{-3} M$ could thus be explained. It was therefore of interest to explore the corresponding behavior of the lower homolog, sodium decyl sulfate (NaDS), in the region of high dilution, and this is the subject of the present paper. At the same time conductivimetric determinations of the critical micelle concentration in water and in salt solutions were performed.

EXPERIMENTAL

Materials

NaDS was prepared by sulfonation of decyl alcohol with SO_3 vapor (Sulfan) and neutralization in aqueous solution with sodium hydroxide, care being taken to avoid extremes of acidity or alkalinity during the latter. The crude product thus obtained could not be purified by repeated recrystallization from water and extraction with ether because, once extracted with ether and thus freed of decyl alcohol, the sodium salt was too soluble to be recrystallized even at $0^\circ C$. On the other hand, the alcoholate (adduct) of two molecules of the salt with one of the alcohol¹ could be crystallized from water. Recrystallization gave products of increasing mushiness. Hence,

¹ This composition is assigned by analogy with the dodecyl compounds (2) and on the basis of the approximate yields obtained during preparative extraction with ether.

sulfonation was conducted with only two-thirds the theoretical amount of SO_3 , and, after neutralization, the crude product was recrystallized two or three times from water. After careful drying it was then extracted thoroughly with dry, freshly redistilled ether.

Decyl alcohol of 99.8% purity was obtained from Applied Science Laboratories, State College, Pennsylvania.

Conductivity measurements were made with the apparatus described previously (1) except that in the c.m.c. region we used newly designed dilution cells having a doughnut-shaped conductance path described elsewhere (3).

RESULTS AND DISCUSSION

Dilute Region

Equivalent conductivities in the dilute region are shown in Fig. 1. They summarize the results of seven separate determinations on three independent samples. Up to concentrations of $10^{-3} M$ they follow the Onsager slope very exactly and at high concentrations up to the c.m.c. they can be represented quite well by Robinson and Stokes' (4) equation

$$\Lambda = \Lambda^0 - \frac{B_1 \Lambda^0 + B_2}{1 + \kappa a} \sqrt{c} \quad [1]$$

in which the $1 + \kappa a$ term represents the deviation from the Onsager slope, κ is the Debye-Hückel parameter, and a is a measure of the closest approach. For the line shown in the Fig. $a = 7.5 \text{ \AA}$, which seems a reasonable value for the large ion considered. The limiting equivalent conductivity Λ^0 is

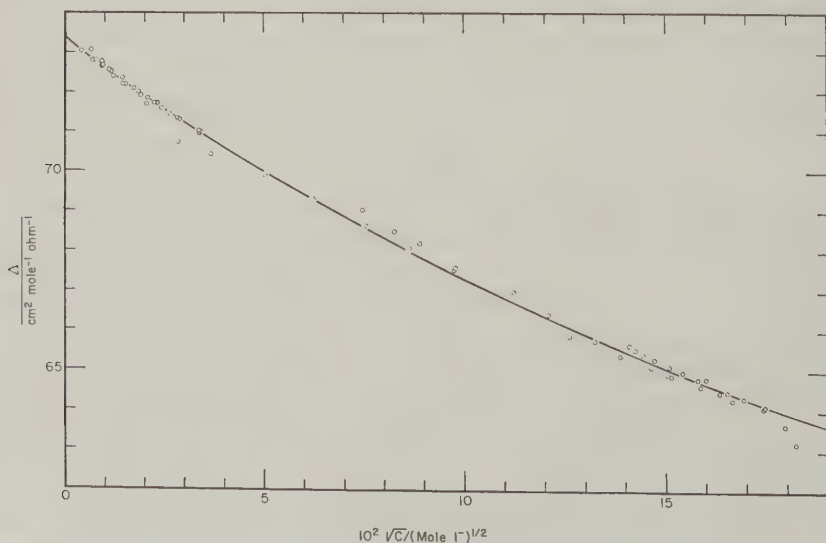


FIG. 1. The equivalent conductivity of sodium decyl sulfate at 25°C . Solid line drawn according to Eq. [1] with $a = 7.5 \text{ \AA}$.

73.4₀, which gives for the limiting conductivity of the DS⁻ ion 23.3. We thus find a difference of conductivities between the C₁₂ and C₁₀ sulfate ions of 1.7 which is very close to the difference, 1.74, found by McDowell and Kraus (5) between the C₁₀ and C₁₂ tetramethyl ammonium compounds. This seems to confirm the reasonableness of the infinite dilution value assigned previously (1) to the C₁₂ sulfate ion.

In contrast to the anomalies found (1) in the dilute region for the C₁₂ sulfate, the C₁₀ compound shows no indication of marked dimerization. In view of the numerous uncertainties involved and possible compensating factors, we cannot exclude, however, dimerization constants of the order of 10 or less, i.e., some 10 times smaller than for the C₁₂ compound.

The Critical Micelle Concentration

Extrapolation of data in the c.m.c. region on an equivalent conductivity vs. square root of concentration plot gives a value (c.m.c. I) of 0.0326 *M* and extrapolation on a conductivity vs. concentration plot gives a value (c.m.c. II) of 0.0335 *M*. This is close to the value 0.0322 reported by Prins (6) but seems significantly higher than the value of 0.031 reported by Tartar and Lelong (7).

The c.m.c. was also determined in 0.01, 0.1, and 0.3 *M* NaCl. The values lie closely on the straight line given by

$$\log [\text{c.m.c.}] = -2.426 - 0.645 \log (c + [\text{c.m.c.}]), \quad [2]$$

where *c* is the molarity of sodium chloride and the c.m.c. is in moles per liter. The slope of the line, 0.645, is only slightly lower than that, 0.679, found by the same method for the C₁₂ homolog (8).

ACKNOWLEDGMENT

This work was supported in part by the Office of Naval Research and reproduction for purposes of the U. S. Government is permitted.

REFERENCES

1. MUKERJEE, P., MYSELS, K. J., AND DULIN, C. I., *J. Phys. Chem.* **62**, 1390 (1958).
2. EPSTEIN, N. B., WILSON, A., JACOB, C. W., CONROY, L. E., AND ROSS, J., *J. Phys. Chem.* **58**, 860 (1954); EPSTEIN, M. B., WILSON, A., GERSHMAN, J., AND ROSS, JR., *ibid.* **60**, 1051 (1956).
3. MYSELS, K. J., *J. Phys. Chem.* **65**, 1081 (1961).
4. ROBINSON, R. A., AND STOKES, R. H., *J. Am. Chem. Soc.* **76**, 1991 (1954); "Electrolyte Solutions," p. 144. Academic Press, New York, 1959.
5. McDOWELL, M. J., AND KRAUS, C. A., *J. Am. Chem. Soc.* **73**, 2170 (1951).
6. PRINS, W., AND HERMANS, J. J., *Koninkl. Ned. Akad. Wetenschap. Proc.* **B59**, 298 (1956); PRINS, W., "Studies on Some Long-Chain Sodium Alkyl-1 Sulfates," Thesis, Leiden, 1955.
7. TARTAR, H. V., AND LELONG, A. L. M., *J. Phys. Chem.* **59**, 1185 (1955).
8. WILLIAMS, R. J., PHILLIPS, J. N., AND MYSELS, K. J., *Trans. Faraday Soc.* **51**, 728 (1955).

THE EFFECT OF TEMPERATURE ON THE CRITICAL MICELLE CONCENTRATION OF SOME PARAFFIN-CHAIN SALTS

B. D. Flockhart¹

Department of Chemistry, University College, Upper Merrion Street, Dublin

Received March 13, 1961

ABSTRACT

The variation in electrical conductance with change in concentration of aqueous solutions has been used in determining the critical micelle concentration of several isomeric sodium C₁₀ and C₁₄ alkyl sulfates at temperatures from 10° to 70°C. Values of the change in heat content ΔH_m associated with micelle formation have been estimated from these results and from similar observations in the literature using an equation of the Clausius-Clapeyron type. The significance of these ΔH_m values and their relation to current micelle theory are considered.

INTRODUCTION

Present evidence on aqueous solutions of paraffin-chain salts points to the formation with increasing concentration of colloidal aggregates, called micelles, over a narrow concentration range. Because of the smallness of the range it has become customary to talk of a critical micelle concentration (c.m.c.). Particular interest is attached to the value of the c.m.c., since it provides a measure of the ease of formation of micelles and how this is affected by changing conditions. Numerous reports have dealt with its dependence upon such factors as the size and shape of the paraffin chain, the nature of the polar group, and the addition of simple salts. Only a limited amount of work is at present available upon the effect of temperature. Knowledge of the temperature dependence of the c.m.c. is, however, of considerable importance, and it has already afforded valuable information on the aggregation process (1-3).

This study was undertaken to determine the effect of temperature on the c.m.c. of paraffin-chain salts which differ in (a) length of hydrocarbon chain, (b) position of polar group, (c) nature of polar group. Critical concentrations were determined from electrical conductance measurements. An equation of the Clausius-Clapeyron type has been used to calculate heats of micellization. The significance of these results and their relation to current theories of micelle formation are considered.

¹ Present Address: Department of Chemistry, The Queen's University, Belfast 9, Northern Ireland.

EXPERIMENTAL

The sodium *n*-alkyl sulfates (decyl, dodecyl, and tetradecyl) were kindly provided by Imperial Chemical Industries Limited, Manchester, and the other sodium alkyl sulfates (2-decyl, 2-tetradecyl, and 4-tetradecyl) by "Shell" Research Limited, Chester. Chemical analysis of the carbon, hydrogen, sulfur, and sodium content of the salts (except *n*-decyl and 4-tetradecyl) gave the theoretical values for their composition within the error of the determinations (C and H, $\pm 0.3\%$; S and Na, $\pm 0.5\%$). Homologs can therefore be present only in small amounts and distributed evenly on either side. The carbon content of sodium *n*-decyl sulfate was 0.4% above the theoretical figure, though the other elements were present in the required amounts. No minimum, however, was found in the surface tension-concentration curve. Sodium 4-tetradecyl sulfate was available only as a solution in water. Its preparation and purity have been described by Carrington and Evans (4). Water of conductance around 0.5×10^{-6} mho cm^{-1} at 25°C. was obtained by passing distilled water three times over an ion-exchange resin bed. As precautions had been taken to prevent the entry of traces of resin into the purified product, a further distillation was unnecessary.

The conductance bridge (5), cells, and procedure (6) have been described previously. Measurements were made at various temperatures over the range 0.2° to 75°C. The temperature was controlled to within $\pm 0.05^\circ$ or better.

RESULTS

Values for the c.m.c. have been obtained from both specific conductance-concentration plots and equivalent conductance- $\sqrt{\text{concentration}}$ plots, the concentration being expressed in moles per liter (these plots have been omitted from this communication, as they will be discussed in a forthcoming paper). Straight lines were drawn through the points lying below and above the region in which a rapid change of slope was observed, and the point of intersection was taken as the c.m.c. The methods were found to be about equally satisfactory for determining the value. Where measurements had been made over a fairly wide concentration range, it was necessary with the equivalent conductance data to fit a straight line to the points immediately above the c.m.c., since at higher concentrations this conductance falls off less rapidly with increasing concentration. In the specific conductance plot no departure from a linear relationship was clearly evident at these higher concentrations. Both plots show slight curvature near the c.m.c. For sodium 2-decyl sulfate, however, the curvature of the specific conductance plot is pronounced.

Values for the c.m.c. obtained from the specific conductance plot were

TABLE I
Comparison of Critical Micelle Concentrations of Sodium Alkyl Sulfates

Compound	Temp. (°C.)	Present work $M \times 10^3$	Published values $M \times 10^3$
n -C ₁₀	25	32.7	33.1 (3)
2-C ₁₀	25	45.6	
n -C ₁₂	25	8.16	8.08 (7); 8.1 (8) 8.3 (9); 8.35 (3)
n -C ₁₄	25	2.05	
	40	2.21	2.2 (10); 2.40 (11)
2-C ₁₄	25	3.27	
	60	4.04	3.74 (12)
4-C ₁₄	25	5.12	
	60	5.85	6.00 (12)
n -C ₁₀ , n -C ₁₄ (equimolar mixt.)	25	3.04	

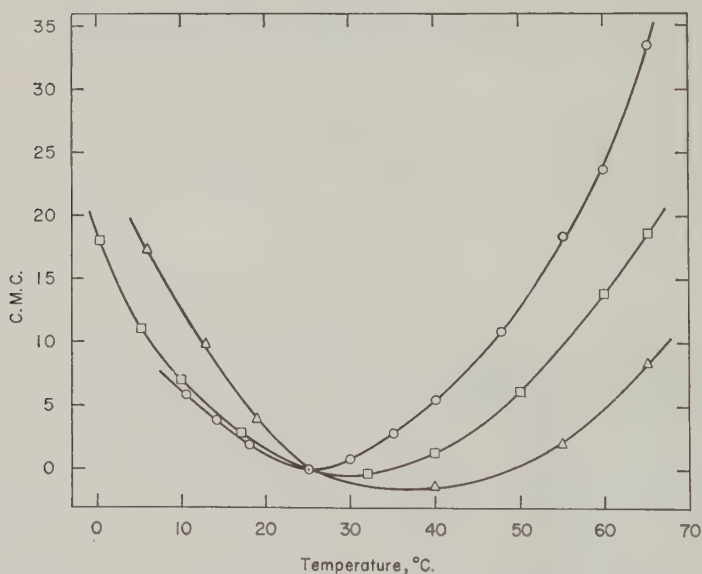


FIG. 1. Effect of temperature on the c.m.c. of sodium n -dodecyl sulfate (○), sodium n -decyl sulfate (□), and sodium 2-decyl sulfate (△). Percentage deviations from c.m.c. value at 25°C.

always higher than those obtained from the equivalent conductance curve. The actual difference varied somewhat from salt to salt, but was usually around 3%. The figures reported in this paper are mean values from the two procedures.

In Table I values for the c.m.c. of the salts are compared with some

published values obtained by either the conductivity or surface tension method.

Figures 1 and 2 show the present results in the form of deviation graphs to facilitate comparison of the effect of temperature on the different systems. The percentage deviation of the c.m.c. values, obtained at different temperatures, from the value of the c.m.c. at 25°C. is plotted as a function of temperature for the various salts and for a two-component salt mixture. Several further measurements on sodium dodecyl sulfate have been made since the last results were published (5). The limited solubility of the sodium tetradecyl sulfates in water prevented measurements being made at much lower temperatures.

The variation of the c.m.c. with temperature (i.e., a decrease and subsequent increase) is similar to that observed for a number of other paraffin-chain salt systems (3, 13-15). A peculiarity of the c.m.c. values is that the effect of shifting the sulfate group from the one to the two position is to increase the c.m.c. to a greater extent in the C_{14} system than in the C_{10} system. *A priori* one would expect the effect to be smaller in the C_{14} system, since a smaller fraction of the chain is involved.

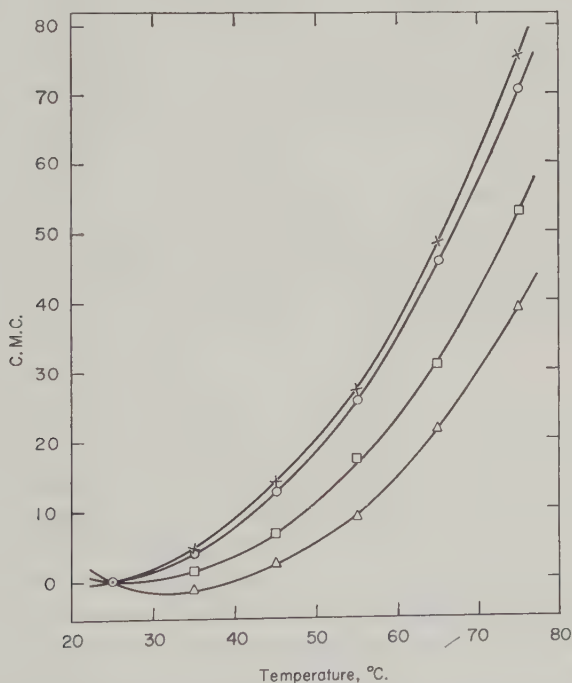


FIG. 2. Effect of temperature on the c.m.c. of sodium *n*-tetradecyl sulfate (O), sodium 2-tetradecyl sulfate (□), sodium 4-tetradecyl sulfate (Δ), and an equimolar mixture of sodium *n*-decyl sulfate and sodium *n*-tetradecyl sulfate (X). Percentage deviations from c.m.c. value at 25°C.

DISCUSSION

Most theories of micelle formation have emphasized energy considerations (16). Micellization is assumed to occur when the energy released by the aggregation of the hydrocarbon chains of the monomers is sufficient to overcome the electrical repulsion between the ionic groups and to balance the decrease in entropy accompanying the aggregation. Increasing the temperature would then be expected to increase the c.m.c. since the kinetic energy of the ions would be raised. Often a rise of temperature has this effect (reference 17 and Figs. 1 and 2, above 20° to 40°C.). But the effect is not large; this means that the energies involved in the aggregation process are small.

Calorimetric measurements have been made to determine directly the heat involved in micelle formation (2, 18). Although exact assessment of the heat was not possible, all the values obtained were small and some were positive. The existence of positive heat effects is at variance with earlier theories of micelle formation.

Goddard, Hoeve, and Benson (2) have provided a qualitative explanation of the small positive heats of micellization in terms of structural effects exhibited in water, as discussed by Frank and Evans (19). The hydrocarbon chain of the single ion is surrounded by a water (so-called iceberg) structure that results in a comparatively low-energy state, but the concomitant restriction to motion provides a driving force to aggregation. Hence at low temperatures micelle formation is an entropy and not an energy effect.

A number of papers have been published on heats of micellization, derived by indirect means. The temperature coefficient of the c.m.c. was first used for this purpose by Stainsby and Alexander (1). By treating the micelle as a separate phase with constant activity and ignoring small deviations from ideality, these workers derived the equation

$$\Delta H_m = -RT^2 d \ln (\text{c.m.c.})/dT, \quad [1]$$

where ΔH_m is the change in heat content when 1 mole of paraffin chain ions in the single ion form aggregate to the micellar form. More recently, Matijević and Pethica (20) obtained an equation very similar to this one, but containing an additional factor n on the right-hand side which is equal to 1 for complete ion exchange and 2 when no ion exchange occurs.

White and Benson (13) have used Eq. [1] to calculate heats of micellization for potassium octanoate. A comparison between these results and heats of micellization estimated from calorimetric measurements of heats of dilution shows that there are differences in the values obtained by the two methods. Although the derivation of ΔH_m from calorimetric data is very approximate, these workers are of the opinion that Eq. [1] leads to erroneous values of this quantity.

A likely source of error in the derivation of Eq. [1] is the assumption of approximate ideality below the c.m.c. Even though the deviations from ideality are only slight, they may be significant. The work of Mysels's school (21) has provided strong evidence for the reversible formation of dimers by the paraffin-chain ion in dilute solution. When dimerization takes place, the concentration of monomers becomes less than the stoichiometric concentration. At the critical micelle concentration the concentration of free monomers is therefore no longer equal to the stoichiometric c.m.c., as had been assumed by Stainsby and Alexander.

A more serious limitation upon the validity of the derivation is probably the neglect of surface effects. The two-phase treatment of micelles has received strong support from the solubilization and ultrafiltration studies of Hutchinson, Inaba, and Bailey (22). Yet, as these workers and more recently White and Benson (13) have pointed out, to entirely ignore surface effects when one of the phases is dispersed in almost molecular dimensions remains fundamentally incorrect.

Thus, as matters stand, the interpretation of the temperature coefficient of the c.m.c. by Eq. [1] to yield heats of micellization is somewhat uncertain. Until accurate direct measurements of ΔH_m are available, this uncertainty is likely to remain, unless of course further work permits a better evaluation of the assumptions on which the equation is based. The difficulties to be overcome in either case are formidable. For the present, however, it seems reasonable to use Eq. [1] to calculate heats of micellization, provided the limitations imposed on the meaning of ΔH_m so evaluated are borne in mind. In this connection it may be noted that according to Matijević and Pethica (20) the use of Eq. [1] is justified only when excess neutral electrolyte is present with one ion in common with the paraffin-chain salt. Since the present measurements were made without added electrolyte, the factor n (mentioned previously) should therefore be given some value between 1 and 2 and not arbitrarily put equal to unity, as in Eq. [1].

Values of ΔH_m calculated by the application of Eq. [1] to the present data and to similar observations in the literature (14, 15) are collected in Table II. Over the temperature range studied a plot of ΔH_m against temperature gives essentially a straight line. The values recorded in Table II are smoothed values summarizing the experimental results.

Examination of the data in Table II indicates the following facts:

1. At low temperatures ΔH_m is positive. The value decreases with increasing temperature and becomes negative above 20°–40°C. (potassium laurate, 47°C.).

2. For the primary alkyl sulfates the value of $-\Delta H_m$ increases with increase in the chain length.

3. Values of ΔH_m for an equimolar mixture of sodium n -decyl and

TABLE II
 ΔH_m (Kcal./Mole) Calculated from Equation [1]

Compound		Temperature (°C.)						
		10	20	30	40	50	60	70
Na <i>n</i> -C ₈ sulfate ^a	{29}	1.1	0.5	-0.1	-0.7	-1.2		
Na <i>n</i> -C ₁₀ sulfate	{29}	1.2	0.6	0	-0.6	-1.2	-1.8	
Na 2-C ₁₀ sulfate	{38}	1.6	1.0	0.4	-0.1	-0.7	-1.3	
Na <i>n</i> -C ₁₂ sulfate	{26}	1.2	0.4	-0.3	-1.1	-1.8	-2.6	
<i>n</i> -C ₁₂ sulfonic acid ^b	{26}		0.5		-1.1		-2.6	
K <i>n</i> -C ₁₂ carboxylate ^b	{47}		2.8		0.8		-1.3	
<i>n</i> -C ₁₂ ammonium chloride ^c	{31}		1.1			-2.0		
Na <i>n</i> -C ₁₄ sulfate	{21}			-0.7	-1.5	-2.3	-3.1	-3.9
Na 2-C ₁₄ sulfate	{27}			-0.2	-1.1	-1.9	-2.7	-3.5
Na 4-C ₁₄ sulfate	{32}			0.2	-0.7	-1.5	-2.3	-3.2
Na <i>n</i> -C ₁₀ sulfate	{20}			-0.8	-1.6	-2.4	-3.2	-4.0
Na <i>n</i> -C ₁₄ sulfate								

^a Smoothed values obtained from reference 3 by plotting recorded values of ΔH_m against temperature.

^b Calculated from data of reference 14.

^c Calculated from data of reference 15.

{ } Temperature at which change in sign of ΔH_m occurs.

n-tetradecyl sulfates are very similar to those obtained for the longer chain compound.

4. Shift of the polar group towards the middle of the chain leads to larger positive and smaller negative values for ΔH_m .

5. Replacement of the sulfate group by the sulfonate group alters the value of ΔH_m little. Replacement by the carboxyl group alters it appreciably.

The temperature variation of ΔH_m can be qualitatively understood in terms of the picture of iceberg formation mentioned earlier. As the temperature is raised there is a breakdown of the water structure and therefore an increase in the energy of the single ion state. Consequently the value of ΔH_m falls and eventually becomes negative.

With one exception (potassium laurate) the change in sign of ΔH_m occurs between 20° and 40°C. Evidence for the occurrence of the structural "melting" in liquid water between 25° and 40°C. has come from a number of studies. The strongest evidence is provided by the dependence of thermal conductance (23), heat capacity (24), and the pressure coefficient of viscosity (25) upon temperature. Surface and interfacial tension effects are consistent with the view (26). Other phenomena find a reasonable explanation on the basis of it (compare, for example, with reference 27). The fact that ΔH_m changes sign in approximately the temperature range within which something decisive happens in liquid water provides at least limited

support for Goddard, Hoeve, and Benson's explanation of the heat effects (2).

Positive heats of micellization for potassium laurate are higher than the corresponding values for sodium dodecyl sulfate and the change of sign occurs around 47°C. From calorimetric measurements, Hutchinson and Winslow (18) obtained a negative value for ΔH_m in potassium laurate solutions which was numerically less than that for sodium decyl sulfate. These workers attributed this result to the solubilization of lauric acid (formed by hydrolysis) in the micelle of potassium laurate, the heats of solubilization of a variety of solubilizates being slightly endothermic (28). This can hardly be the complete explanation. Present results are based on figures provided by Brady and Huff (14), who added alkali to suppress hydrolysis.

REFERENCES

1. STAINSBY, G., AND ALEXANDER, A. E., *Trans. Faraday Soc.* **46**, 587 (1950).
2. GODDARD, E. D., HOEVE, C. A. J., AND BENSON, G. C., *J. Phys. Chem.* **61**, 593 (1957).
3. GODDARD, E. D., AND BENSON, G. C., *Can. J. Chem.* **35**, 986 (1957).
4. CARRINGTON, R. A. G., AND EVANS, H. C., *J. Chem. Soc.* **1957**, 1701.
5. FLOCKHART, B. D., *J. Colloid Sci.* **12**, 557 (1957).
6. FLOCKHART, B. D., AND GRAHAM, H., *J. Colloid Sci.* **8**, 105 (1953).
7. WILLIAMS, R. J., PHILLIPS, J. N., AND MYSELS, K. J., *Trans. Faraday Soc.* **51**, 728 (1955).
8. HAFNER, F. D., PICCIONE, G. A., AND ROSENBLUM, C., *J. Phys. Chem.* **46**, 662 (1942).
9. SCHMID, G., AND LARSEN, E. C., *Z. Electrochem.* **44**, 651 (1938).
10. LOTTERMOSE, A., AND STOLL, F., *Kolloid-Z.* **63**, 49 (1933).
11. EVANS, H. C., *J. Chem. Soc.* **1956**, 579.
12. WIJGA, P. W. O. (Shell Laboratory, Amsterdam), Private communication.
13. WHITE, P., AND BENSON, G. C., *Trans. Faraday Soc.* **55**, 1025 (1959).
14. BRADY, A. P., AND HUFF, H., *J. Colloid Sci.* **3**, 511 (1948).
15. EGGENBERGER, D. N., AND HARWOOD, H. J., *J. Am. Chem. Soc.* **73**, 3353 (1951).
16. HARTLEY, G. S., "Aqueous Solutions of Paraffin-Chain Salts." Hermann and Cie, Paris, 1936. DEBYE, P., *Ann. N.Y. Acad. Sci.* **51**, 575 (1949). NAKAGAKI, M., *J. Chem. Soc. Japan* **72**, 113 (1951). OOSHIIKA, Y., *J. Colloid Sci.* **9**, 254 (1954). REICH, I., *J. Phys. Chem.* **60**, 257 (1956).
17. WRIGHT, K. A., ABBOTT, A. D., SIVERTZ, V., AND TARTAR, H. V., *J. Am. Chem. Soc.* **61**, 549 (1939). KLEVEN, H. B., *J. Phys. & Colloid Chem.* **52**, 130 (1948).
18. HUTCHINSON, E., MANCHESTER, K. E., AND WINSLOW, L., *J. Phys. Chem.* **58**, 1124 (1954). HUTCHINSON, E., AND WINSLOW, L., *J. Phys. Chem.* **60**, 122 (1956).
19. FRANK, H. S., AND EVANS, M. W., *J. Chem. Phys.* **13**, 507 (1945).
20. MATIJEVIĆ, E., AND PETHICA, B. A., *Trans. Faraday Soc.* **54**, 587 (1958).
21. MUKERJEE, P., MYSELS, K. J., AND DULIN, C. I., *J. Phys. Chem.* **62**, 1390 (1958). MUKERJEE, P., *J. Phys. Chem.* **62**, 1397 (1958). MUKERJEE, P., AND MYSELS, K. J., *J. Phys. Chem.* **62**, 1400 (1958). MUKERJEE, P., *J. Phys. Chem.* **62**, 1404 (1958).
22. HUTCHINSON, F., INABA, A., AND BAILEY, L. G., *Z. physik. Chem.* **5**, 344 (1955).

- HUTCHINSON, E., U. S. A. Navy Report, Project No. NR 054 244. HUTCHINSON, E., *Z. physik. Chem.* **21**, 38 (1959).
23. FRONTAS'EV, V. P., *Doklady Akad. Nauk S.S.S.R.* **111**, 1014 (1956).
24. GINNINGS, D. C., AND FURUKAWA, G. T., *J. Am. Chem. Soc.* **75**, 522 (1953).
25. BRIDGMAN, P. W., "The Physics of High Pressure," p. 346. Bell, London, 1949.
26. FRANKS, F., AND IVES, D. J. G., *J. Chem. Soc.* **1960**, 741.
27. FEATES, F. S., AND IVES, D. J. G., *J. Chem. Soc.* **1956**, 2798.
28. MCBAIN, M. E. L., AND HUTCHINSON, E., "Solubilization and Related Phenomena," p. 121. Academic Press, New York, 1955.

ULTRACENTRIFUGATION AND VISCOSITIES OF CRUDE OILS¹

P. B. Lorenz, R. J. Bolen, and H. N. Dunning

*Petroleum Research Center, Bureau of Mines, U. S. Department of the
Interior, Bartlesville, Oklahoma*

and I. A. Eldib

*Esso Research and Engineering Co., Process Research Division, Linden,
New Jersey*

Received December 13, 1960

ABSTRACT

Viscosities measured at three temperatures on ultracentrifuge fractions of several crude oils are compared with asphaltene content. The same comparison is made for solutions of asphaltenes in kerosene, gas oil, benzene, and decalin. The results indicate that asphaltene particles are solvated strongly in crude oil and only weakly in solvents. Dilution of crude oil desolvates asphaltenes.

The colloidal nature of petroleum was investigated recently by chemical studies of crude oils fractionated by ultracentrifugation (1). Viscosity is a particularly sensitive indicator of colloidal properties (2). Therefore the ultracentrifuge fractions described previously (1) have been studied viscometrically. The results re-emphasized the close relationship of the asphaltic colloidal components of crude oil. Therefore, the viscosity studies were expanded to include solutions of the pentane-insoluble portion of Tia Juana crude oil in various solvents.

Viscosities were measured at 38°, 54°, and 82°C., by ASTM method D445, with Cannon-Fenske viscometers for opaque liquids. The values were used as determined in centistokes (centipoise/density c.g.s.), because corrections for density changes amount to less than 2% of the viscosity changes observed.

The data for the West Texas oil are typical and are plotted in Fig. 1. The points approach the viscosity axis in a linear manner and are extrapolated in Fig. 1 to zero asphaltene concentration to give values representing a "solvent" for the asphaltenes. Limiting viscosity numbers are then calculated as follows:

$$[\eta] = \lim_{c \rightarrow 0} \frac{\nu - \nu_0}{\nu_0 c}$$

¹ Presented before the Division of Colloid Chemistry, American Chemical Society Meeting, Atlantic City, New Jersey (September 16, 1959).

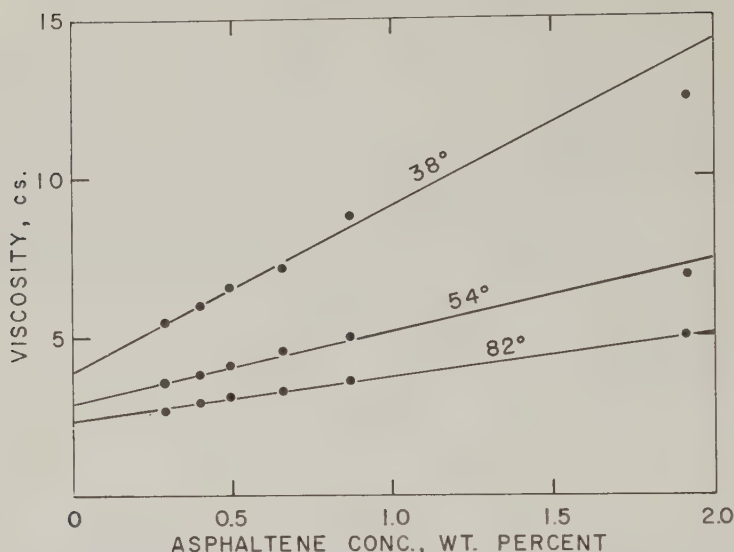


Fig. 1. Effect of asphaltene content and temperature on viscosities of ultracentrifuged fractions of West Texas crude oil.

TABLE I

Extrapolated Values of Viscosities and Voluminosity Factors for Asphaltenes in Ultracentrifuged Fractions

Temp. (°C.)	Kuwait	West Texas	Tia Juana	Lagunillas ^a
<i>v</i> ₀ (zero asphaltenes)				
38	4.45	3.99	6.3	7.29
54	3.80	2.99	5.0	5.59
82	2.43	2.34	4.0	3.24
<i>V</i> (voluminosity factors)				
38	30	62	38	16
54	26	37	24	10
82	20	30	11	8

^a Diluted to 62% crude oil with decalin.

where ν and ν_0 are the viscosities of the solutions and solvent, respectively, and c is the asphaltene concentration in weight-per cent.

Einstein's formula for viscosity can be modified for the present case to

$$[\nu] = 0.02V$$

where V is the rheological voluminosity.² Values of V for asphaltenes in the various oils are summarized in Table I.

² As $[\eta]$ is based on concentrations in wt.-%, the coefficient 0.02 contains the factors 0.88 for the density of crude oil and 1/1.10 for the specific volume of asphaltenes.

Asphaltene particles apparently are nearly spherical (3). Therefore, V is a measure of the maltene sheath thought to surround an asphaltene particle. The variations shown in Table I indicate that changes in this sheath may account for the discrepancies among asphaltene molecular weight determinations (4).

The effect of temperature was studied in terms of activation energies, E , derived from Arrhenius plots. Figure 2 is a typical Arrhenius plot for West Texas oil at 1 wt.-% asphaltenes. The data are not adequate for accurate values of E , but relative values at different asphaltene concentrations can be obtained by calculation from the parameters of Table I. The extrapolated viscosities for the solvent give values of E between 2 and 4 kcal./mole, which is typical of long-chain hydrocarbons. Asphaltenes increase E about

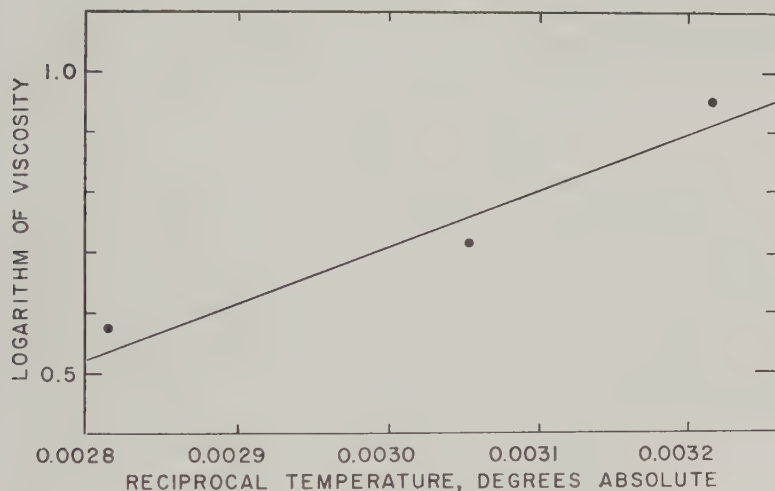


FIG. 2. Arrhenius plot of viscosity data for West Texas crude oil.

TABLE II

Voluminosity Factors of Asphaltene in Solvents and Changes in Activation Energies per Weight-Per Cent Asphaltene

Temp. (°C.)	Kerosene	Gas oil	Benzene	Decalin
Values of V				
25 ^a	—	—	3	—
38	5	3	3	2
54	5	2	2	2
82	2	2	—	2
$\Delta E/c$ (kcal./mole/wt.-%)				
	0.3	0.1	0.1	0.0

^a Data of Eckert and Weetman (4).

1 kcal./mole/wt.-% and thus make a major contribution to viscosity at moderate concentrations. A strong association, decreasing at higher temperatures, is indicated for asphaltenes in crude oil, suggesting marked solvation.

Viscosity values for the solutions of precipitated asphaltenes in solvents afford an illuminating comparison with crude oils. The data for the various solutions conform reasonably well with the Huggins equation (5):

$$\frac{\nu - \nu_0}{\nu_0 c} = [\nu] + k'[\nu]^2 c$$

where k' is a constant for a given system. Positive values of k' indicate poorer solvents (2) than in the case of crude oil, for which k' is essentially zero. Precipitated asphaltenes in solvents furthermore do not give the indications of marked solvation noticed with crude oil. Voluminosity and activation energy increases per wt.-% asphaltenes are small, as seen in Table II. Voluminosity factors give no information about the degree of aggregation of asphaltenes into micelles, but the low activation energy makes it improbable that the particles are significantly aggregated. These data indicate a small interaction between the asphaltene and most solvents and an almost negligible interaction with decalin.

In this connection, compare the data on Lagunillas crude oil with other oils (Table I). This oil is too viscous to centrifuge successfully and was diluted with decalin to 62% crude oil to give it the same viscosity as whole Tia Juana crude oil. The results of viscosity analysis on this mixture indicate that the asphaltenes have been desolvated somewhat by dilution. The colloidal properties of petroleum are therefore altered by addition of a diluent that is an indifferent solvent for asphaltenes.

REFERENCES

1. ELDIB, I. A., DUNNING, H. N., AND BOLEN, R. J., *J. Chem. and Eng. Data* (to be published).
2. MCGOURY, T. E., AND MARK, H., "Viscometry of dilute polymer solutions," Ch. 8, Supplement; in A. Weissberger, ed., "Technique of Organic Chemistry," Vol. 1, part 3, pp. 2399-2422. Interscience Publishers, New York, 1954.
3. RAY, B. R., WITHERSPOON, P. A., AND GRIM, R., *J. Phys. Chem.* **61**, 1296 (1957).
4. ECKERT, G. W., AND WEETMAN, B., *Ind. Eng. Chem.* **39**, 1512 (1947).
5. HUGGINS, M. L., *J. Am. Chem. Soc.* **64**, 2716 (1942).

THE MEASUREMENT OF DYNAMIC SURFACE TENSIONS OF SOLUTIONS OF SLOWLY DIFFUSING MOLECULES BY THE MAXIMUM BUBBLE PRESSURE METHOD

Roy J. Kuffner

The Lowell Technological Institute, Lowell, Massachusetts

Received December 27, 1960

ABSTRACT

A method is presented for the use of the maximum bubble pressure method of measuring surface tension, to measure dynamic surface tensions of solutions of slowly diffusing soluble molecules. Data obtained using this method on aqueous solutions of decanoic acid and decyl alcohol are also presented.

INTRODUCTION

The use of the maximum bubble pressure method to measure the surface tensions of solutions of slightly soluble solutes was described in a recent paper by Kuffner and co-workers (1). It was reported in this work that the maximum bubble pressure method could be used successfully in the study of aqueous solutions of slightly soluble solutes if (a) the single bubble variation of this method was employed and (b) if a "characteristic time" interval was allowed to elapse between bubbles. In an attempt to understand the contribution made by factor (b) it was found by the author that during the afore-mentioned time interval, the value for the surface tension of the solution was decreasing steadily with time and reached a minimum just before the "characteristic time" had elapsed. A method is presented here to measure this change in surface tension with time, together with some results of studies on decanoic acid and decyl alcohol.

EXPERIMENTAL

The maximum bubble pressure method for the determination of surface tension of liquids is based on the measurement of the maximum pressure necessary to blow a bubble in a liquid from the tip of a capillary. In practice the pressure is increased within the capillary until a bubble appears at the tip of a calibrated capillary orifice which has been placed in the experimental liquid at a predetermined depth. In applying this method to the study of solutions of slightly soluble solutes it is necessary for the gas/liquid interface at the opening of the capillary to be appropriately aged to obtain reproducible results. In the present extension of this method to the

measurement of dynamic surface tensions, the pressure in the capillary is maintained constant and the time lapse between the appearance of the bubbles is measured. Thus the time necessary for the gas/liquid interface at the capillary orifice to reach a surface tension sufficiently low for the pressure on the interface to cause the production of a bubble is determined. By varying this pressure and determining the above-mentioned time lapses the rate of change of surface tension with time can be determined for a solution.

The experimental details and description of the apparatus for this paper have been covered, except for a few additional instructions, in a recently published paper by Kuffner *et al.* (1). The additional instructions are as follows: As described in the above-mentioned paper, the capillary, with a gas pressure in excess of the probable pressure necessary to blow a bubble in pure water, is introduced immediately below the surface of the solution.

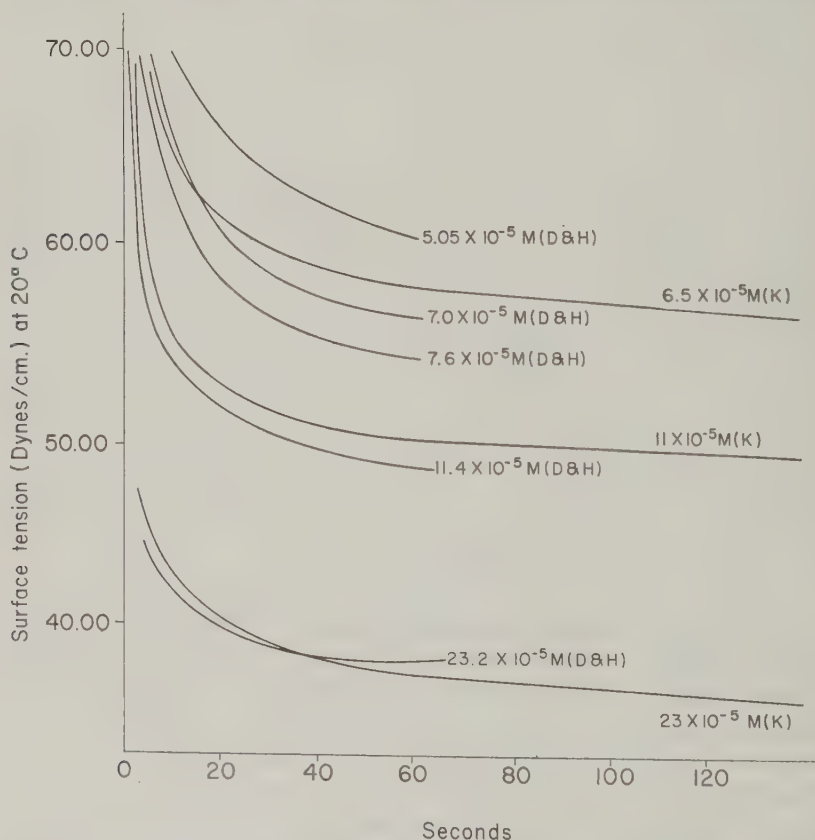


FIG. 1. Comparison between the results given by Defay and Hommelen (5) (D & H) and those obtained using the maximum bubble pressure method (K) on solutions of decanoic acid at 20°C.

Single bubbles begin to appear periodically at the orifice of the capillary opening. With the automatic lowering of the pressure in the capillary, due to the loss of gas in the capillary system as bubbles are blown, the bubbles will appear less and less frequently. It will be noticed that the pressure remains constant between bubbles and falls slightly when a bubble is blown. The system is in this sense "automatic," as the pressure need not be adjusted during a run. The time that elapses between any two successive bubbles is recorded with the pressure in the capillary, which is constant during this time. The above-mentioned pressure is the pressure that blows the second bubble of the pair. As the pressure in the capillary is reduced the time interval between bubbles will become greater to allow for more complete aging of the gas/liquid interface. It was found that a

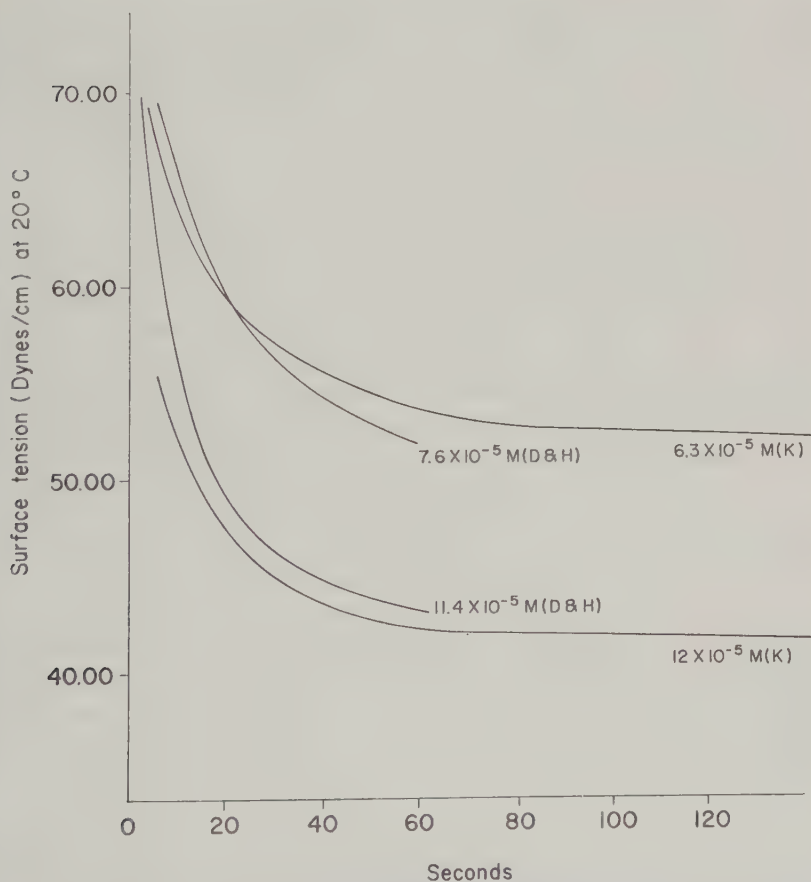


FIG. 2. Comparison between the results given by Defay and Hommelen (5) (D & H) and those obtained using the maximum bubble pressure method (K) on solutions of decyl alcohol at 20°C.

practical maximum time interval was eventually reached and a particular run was terminated. The temperature for this study was $20.0^{\circ} \pm .1^{\circ}\text{C}$.

The capillaries used in this study were between 0.008 and 0.010 cm. in radius, and the results were independent of the capillary sizes. The capillaries were drawn from Pyrex glass tubing.

The equation used to determine the surface tensions from the maximum bubble pressure is that used by Brown (2) and Belton (3) with corrections made for capillary depth below the surface of the solutions.

The curves presented are each individual runs. Averages were not used.

The individual points in a curve for any given solution were found to be reproducible in general to within a dyne.

The results of this research are presented in Figs. 1 and 2.

MATERIALS

The organic acid and alcohol were obtained from freshly opened "Eastman White Label" grade bottles and were used as received after obtaining the melting points (decanoic acid, 31.5°C . and decyl alcohol 5.8°C .). The water used was doubly distilled.

RESULTS AND DISCUSSION

In their recent papers Hommelen (4) and Defay (5) have discussed the significant experimental dynamic surface tension work that has been done to date on solutions of slowly diffusing molecules. They have pointed out probable sources of error that are inherent in the approaches of several investigators. They also presented a method of using the falling meniscus method for determining dynamic surface tensions for aqueous solutions of slowly diffusing solutes that was freed of these errors. Evaporation of solute during surface aging, pollution, and surface extension were the main errors that these authors were critical of. Evaporation of solute was found to give much higher values than were obtained when this source of error was removed. The results in this paper are in good agreement with those of Defay and Hommelen; as the maximum bubble pressure method is free of the above-mentioned difficulties with the exception of surface extension. The possibility of a slight surface extension error being introduced in the more rapidly formed bubbles is even further reduced because at higher pressures the meniscus at the capillary orifice is immediately curved so that surface extension during the forming of the bubble hemisphere is minimized.

REFERENCES

1. KUFFNER, R., BUSH, M. T., AND BIRCHER, L. J., *J. Am. Chem. Soc.* **79**, 1587 (1957).
2. BROWN, R., *Phil. Mag.* **13**, 578 (1932).
3. BELTON, J., *Trans. Faraday Soc.* **31**, 1413 (1935).
4. HOMMELEN, J. R., *J. Colloid Sci.* **14**, 385 (1959).
5. DEFAY, R., AND HOMMELEN, J. R., *J. Colloid Sci.* **14**, 401 (1959).

ON THE INTERPRETATION OF ELECTROKINETIC POTENTIALS

J. Lyklema and J. Th. G. Overbeek

van 't Hoff Laboratory, State University of Utrecht, The Netherlands

Received January 27, 1961

INTRODUCTION

Electrokinetic measurements are of considerable interest for the study of electrical double layers. It is customary to interpret electrokinetic data in terms of the so-called electrokinetic or ζ -potential. This is the potential of the slipping plane between the moving and the stationary phase, when the liquid far away from the interface is considered to be at zero potential.

The calculation of ζ from electrokinetic data is often uncertain because it involves the dielectric constant, ϵ , and the viscosity, η , and these may have abnormal values in part of the double layer. If one tries to correlate ζ with ψ_0 , the total potential drop across the double layer, more difficulties are encountered, such as uncertainties about the location of the slipping plane, the structure of the liquid inside the slipping plane, and discreteness of charges effects.

It is the purpose of this paper to contribute to the solution of these problems by considering the variability of the viscosity and dielectric constant in the double layer and proposing a model for the mechanics of the slipping process. We shall confine ourselves to aqueous solutions, taking electroosmosis and electrophoresis as the examples.

THE VARIABILITY OF THE DIELECTRIC CONSTANT IN THE ELECTRICAL DOUBLE LAYER

From double layer capacity evidence it is most likely that the dielectric constant in the inner region of the double layer is smaller than that of the bulk. This is due to saturation effects caused by the high field strengths in the double layer and to the structural influence of the adjacent phase. This decrease in ϵ can have a considerable influence on properties involving the inner region of the double layer (1-3).

It is therefore important in the establishment of the relation between ψ_0 and ζ . Whether it also influences the relation between ζ and the electrophoretic mobility, u , depends on the actual value of ϵ in the outer region of the double layer. The following reasoning will show that in this case saturation effects may usually be neglected.

A formula for the dielectric saturation of water is given by Booth (4)

based upon theories of Onsager and Kirkwood. This formula reads:

$$\epsilon = n^2 + \frac{28N\pi(n^2 + 2)\mu}{3\sqrt{73} E} L\left(\frac{\sqrt{73} E\mu(n^2 + 2)}{6kT}\right), \quad [1]$$

in which N represents the number of water molecules per cm^3 , n the refractive index, μ the dipole moment, E the acting electric field strength, and $L(z)$ the Langevin function. For low values of z , $L(z)$ may be replaced by the first term of its series expansion being $z/3$. From Eq. [1] one sees that ϵ is independent of E when this condition is fulfilled. Inserting the appropriate numerical values in Eq. [1] a quantitative relation between ϵ and E can be found. The dielectric saturation is 2% for $E = 5 \times 10^5$ v./cm. and 10% for $E = 1.5 \times 10^6$ v./cm. Such high field strengths can be produced only by a combination of high potential and high ionic strength, and are rarely found outside the slipping plane. This is illustrated in Table I giving the ζ -potentials required to reach the field strengths mentioned above.

From this table it may be concluded that it is mostly justified to use the bulk value of ϵ in the electrophoresis equation of Helmholtz-Smoluchowski:

$$u = \frac{\epsilon F}{4\pi\eta} \zeta, \quad [2]$$

where F is the applied field strength.

THE VARIABILITY OF THE VISCOSITY IN THE ELECTRICAL DOUBLE LAYER

A fully satisfactory theory for the dependence of the viscosity of liquids (especially water) on the strength of an applied electric field has not yet been given. Several workers investigated this dependency experimentally (5-14). In all cases η is found to increase with E . A quantitative formulation was given by Da.C. Andrade and Dodd (6):

$$\frac{\eta_E - \eta_{E=0}}{\eta_{E=0}} = \frac{d\eta}{\eta} = fE^2. \quad [3]$$

TABLE I

Values of the Diffuse Double Layer Potential (ζ) above Which the Dielectric Saturation Exceeds 2% and 10%, Respectively
(Gouy-Chapman picture; (1-1)-electrolytes)

Electrolyte concentration	Dielectric saturation of	
	2%	10%
1 molar	15 mv.	40 mv.
10^{-2} molar	94 mv.	148 mv.
10^{-4} molar	210 mv.	270 mv.

In this equation $\eta_{E=0}$ equals the viscosity with no field applied, and f represents the so-called viscoelectric constant. The following values were found (6):

$$\text{chloroform} \quad f = 1.89 \times 10^{-12} \text{ v.}^{-2} \text{ cm.}^2$$

$$\text{amylacetate} \quad f = 2.74 \times 10^{-12} \text{ v.}^{-2} \text{ cm.}^2$$

$$\text{chlorobenzene} \quad f = 2.12 \times 10^{-12} \text{ v.}^{-2} \text{ cm.}^2$$

Deviations of, for example, 10 % in the viscosity for these liquids can therefore be expected to occur at field strengths of

$$E > \sqrt{(10f)^{-1}} \sim 2 \times 10^5 \text{ v./cm.}$$

This is much lower than the field strength required for a 10 % change in ϵ ($E > 1.5 \times 10^6$ volts/cm.). Such field strengths may occur outside the slipping plane. The provisional conclusion must be that Eq. [2] requires a correction for the variation of the viscosity, whereas variations in ϵ may be neglected.

The argumentation given above is restricted to the three organic liquids mentioned. The viscoelectric constant of water (f_w) has not been measured. It can, however, be found from a theoretical reasoning.

To this purpose we start with Reynolds' equation for the viscosity of a liquid, written as

$$\eta = A \exp \left(\frac{\alpha}{kT} \right). \quad [4]$$

In this equation A is a constant and α can be interpreted as the activation energy of viscous flow. When the dipolar molecules of the liquid are oriented in an electric field this activation energy increases with a quantity α_{el} , leading to:

$$\eta + d\eta = A \exp \left(\frac{\alpha + \alpha_{el}}{kT} \right) = \eta \exp \left(\frac{\alpha_{el}}{kT} \right), \quad [5]$$

where

$$\alpha_{el} = B\mu^2 E_i^2. \quad [6]$$

E_i is the internal field strength and B is a structural specific constant of dimension [energy] $^{-1}$ and of the order $(kT)^{-1}$. It depends among other things on the coordination number and density of the liquid. For field intensities which are not too high the exponential in Eq. [5] may be expanded, retaining only two terms, which gives:

$$\frac{d\eta}{\eta} = \frac{B\mu^2}{kT} E_i^2 = \frac{B\mu^2 G^2}{kT} E^2, \quad [7]$$

when $E_i = GE$. Comparison of [7] with [3] yields:

$$f = \frac{B\mu^2 G^2}{kT}. \quad [8]$$

The factor G is given by (15)

$$G = \frac{3kT + \mu R^*}{3kT} \frac{1}{1 - g\alpha} \frac{3\epsilon}{2\epsilon + 1}, \quad [9]$$

where R^* is the reaction field;

$$R^* = \frac{g}{1 - g\alpha} \mu, \quad [10]$$

where g is a reaction field factor and equal to $\frac{1}{a^3} \frac{2n^2 - 2}{2n^2 + 1}$ (a representing the radius of the spherical molecule); α is the polarizability and can be calculated with the corrected Lorenz-Lorentz equation (15)

$$\frac{(n^2 - 1)(2n^2 + 1)}{12\pi n^2} = \frac{N\alpha}{1 - g\alpha}.$$

By inserting the appropriate values in [9] G can be calculated for water and the three organic liquids. With the aid of Eq. [8] the following values of B are found:

chloroform	$0.186 \times 10^{15} \text{ erg}^{-1}$
amylacetate	$0.154 \times 10^{15} \text{ erg}^{-1}$
chlorobenzene	$0.114 \times 10^{15} \text{ erg}^{-1}$
Mean value	$0.15 \times 10^{15} \text{ erg}^{-1}$

Though the structural properties of these liquids vary considerably their B -constants do not differ by more than a factor 5/3. Therefore the use of the mean B -value will probably lead to a reasonable estimate for the viscoelectric constant for water:

$$f_w = 10.2 \times 10^{-12} \text{ v.}^{-2} \text{ cm.}^2 \quad [11]$$

This value of f_w is used in the following section. As long, however, as f_w is not measured independently its value remains somewhat uncertain (see also reference 13).

The influence of the double layer field on the viscosity is illustrated by Table II. Comparison with Table I shows that the influence of the field on the viscosity is much more pronounced than that on the dielectric constant. It is seen that viscosity corrections are necessary in many cases.

CORRECTION OF THE HELMHOLTZ-SMOLUCHOWSKI EQUATION FOR THE VARIABILITY OF THE VISCOSITY

Consider a double layer at a flat interface, perpendicular to the x axis in an electric field of strength F parallel to this interface.

TABLE II
Values of the Diffuse Double Layer Potential (ζ) above Which a Viscosity Increase of 2% and 10%, Respectively Is Found
(Gouy-Chapman picture; (1-1)-electrolytes; $f_w = 10.2 \times 10^{-12} \text{ v.}^{-2} \text{ cm.}^2$)

Electrolyte concentration	Viscosity increase of	
	2%	10%
1 molar	1.4 mv.	3 mv.
10^{-2} molar	14 mv.	29 mv.
10^{-4} molar	88 mv.	128 mv.

Consider a volume element of thickness dx and area of 1 cm.^2 , also perpendicular to the x axis. The field exerts a force $F\rho dx$ on this volume element if ρ represents the space charge density. In the stationary state this force is just balanced by the force of viscous shear:

$$F\rho dx + \frac{d}{dx} \left(\eta \frac{dv}{dx} \right) dx = 0, \quad [12]$$

where v is the rate of streaming.

Substituting Poisson's equation in the form

$$\frac{d}{dx} \left(\epsilon \frac{d\psi}{dx} \right) = -4\pi\rho, \quad [13]$$

we find

$$-\frac{F}{4\pi} \frac{d}{dx} \left(\epsilon \frac{d\psi}{dx} \right) + \frac{d}{dx} \left(\eta \frac{dv}{dx} \right) = 0. \quad [14]$$

This equation can be integrated, utilizing the boundary conditions that far away from the surface ($x = \infty$) the velocity gradient and potential gradient are both zero. One obtains:

$$\frac{\epsilon F}{4\pi\eta} \left(\frac{d\psi}{dx} \right) = \left(\frac{dv}{dx} \right). \quad [15]$$

It is of interest to note that this equation is valid independent of the constancy of ϵ and η .

The second integration is now carried out with constant ϵ and leads to

$$u = \frac{\epsilon F}{4\pi} \int_0^\zeta \frac{d\psi}{\eta}, \quad [16]$$

where u represents the velocity at the point $x = d$, where $\zeta = \psi_d$, and where there is no shear for $x < d$. Then u is equal to the electrophoretic velocity.

The integration can be carried out if the relation between η and ψ is given. To this purpose we assume that η is correctly given by Eq. [3] written in the form

$$\eta_x = \eta_0 \left(1 + f \left(\frac{d\psi}{dx} \right)^2 \right), \quad [17]$$

where η_0 is the bulk viscosity and $(d\psi/dx)$, the double layer field strength, is given by the Gouy-Chapman theory as

$$\frac{d\psi}{dx} = \sqrt{\frac{32 \pi c R T}{1000 \epsilon}} \sinh \left(\frac{z F \psi}{2 R T} \right), \quad [18]$$

where c is the concentration of the $(z - z)$ -valent electrolyte in moles/liter and F is the Faraday.

From [16], [17], and [18] it follows that

$$u = \frac{\epsilon F}{4\pi\eta_0} \int_0^\zeta \frac{d\psi}{1 + \frac{32\pi c RT}{1000\epsilon} f \sinh^2 \left(\frac{zF\psi}{2RT} \right)}, \quad [19]$$

which for sake of simplicity can be written as

$$u = \frac{\epsilon F}{4\pi\eta_0} \int_0^\zeta \frac{d\psi}{1 + A \sinh^2 \left(\frac{\beta\psi}{2} \right)}. \quad [20]$$

The integration can be carried out analytically. It leads to three different equations, depending on the value of A .

The solution for $A < 1$ reads:

$$u = \frac{\epsilon F}{4\pi\eta_0} \frac{1}{\beta \sqrt{1 - A}} \cdot \ln \frac{\left(2 \exp \left(\frac{zF\zeta}{RT} \right) + \left(\frac{4}{A} - 2 \right) - \frac{4}{A} \sqrt{1 - A} \right) (1 + \sqrt{1 - A})}{\left(2 \exp \left(\frac{zF\zeta}{RT} \right) + \left(\frac{4}{A} - 2 \right) + \frac{4}{A} \sqrt{1 - A} \right) (1 - \sqrt{1 - A})}. \quad [21]$$

The solution for $A > 1$ reads:

$$u = \frac{\epsilon F}{4\pi\eta_0} \frac{2}{\beta \sqrt{A - 1}} \cdot \left\{ \operatorname{arctan} \frac{2 \exp \left(\frac{zF\zeta}{RT} \right) + \left(\frac{4}{A} - 2 \right)}{\frac{4}{A} \sqrt{A - 1}} - \operatorname{arctan} \frac{1}{\sqrt{A - 1}} \right\}. \quad [22]$$

For $A = 1$ both solutions approach to

$$u = \frac{\epsilon F}{4\pi\eta_0} \frac{2}{\beta} \operatorname{tgh} \left(\frac{zF\zeta}{2RT} \right). \quad [23]$$

For small values of ζ or the concentration ($A \propto c$) the following approximated solution of Eq. [20] may be useful:

$$u \approx \frac{\epsilon F}{4\pi\eta_0} \cdot \int_0^\zeta \left\{ 1 - A \sinh^2 \left(\frac{\beta\psi}{2} \right) \right\} d\psi = \frac{\epsilon F}{4\pi\eta_0} \left[\zeta - \frac{A}{2\beta} \{ \sinh(\beta\zeta) - \beta\zeta \} \right], \quad [24]$$

which can be further approximated for small ζ to

$$u \approx \frac{\epsilon \zeta F}{4\pi\eta_0} \left[1 - \frac{A\beta^2}{12} \zeta^2 \right]. \quad [25]$$

These equations show clearly the relation with the original equation of Helmholtz and Smoluchowski.

An illustration of these solutions is presented in Fig. 1. On the ordinate axis the difference is plotted between the potential of the slipping plane, $\zeta_{(\text{real})}$ and the "observed" potential, $\zeta_{\text{obs.}}$ (calculated simply from Eq. [2]).

The figure holds for monovalent electrolytes at 25° C. and $f_w = 10.2 \times 10^{-12} \text{ v.}^{-2} \text{ cm.}^2$. The approximation [24] is indistinguishable from the drawn curves within the 5% correction limit. The curve for $c = 0.035 \text{ mole/l.}$ corresponds with $A = 1$ (Eq. [23]); the 10^{-1} curve corresponds with $A > 1$ (Eq. [22]); and the other curves correspond with $A < 1$ (Eq. [21]). For low salt content the correction is expected to stay always below 5%. For somewhat higher salt contents ($> 10^{-2} \text{ mole/l.}$) the correction may reach 20% and even exceed this value in the case of the unfavorable combination of high ζ and high concentration. The correction limits the electrophoretic mobility regardless of the potential in the double layer. (See below, in particular, Fig. 4.)

SOME CONSIDERATIONS CONCERNING THE SLIPPING PROCESS

One of the most important aims of electrokinetic measurements is the correlation between ψ_0 and the electrophoretic velocity, u . If the electrical double layer consists of a molecular condenser with a potential drop $\psi_0 - \psi_\delta$ and a Gouy-Chapman diffuse double layer with a potential drop ψ_δ and if we assume that no slipping occurs within the molecular condenser, the problem resolves itself into the establishment of the relation between ψ_0 and ψ_δ and the relation between u and ψ_δ . The first relation is not relevant

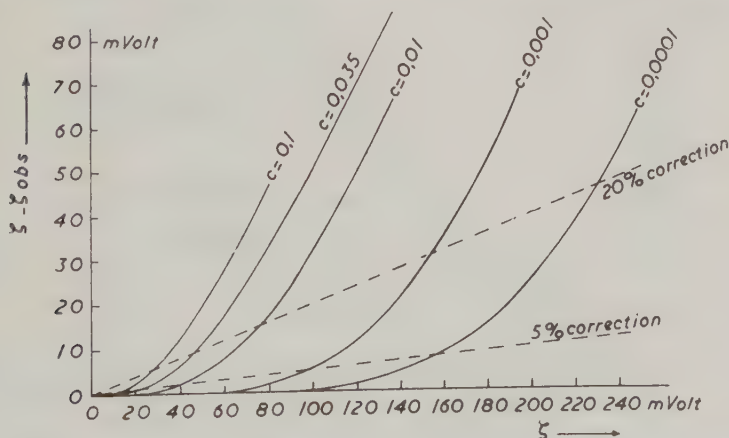


FIG. 1. Correction of the Helmholtz-Smoluchowski equation for the increase of the viscosity in the electrical double layer at different concentrations (c in moles/liter) of (1-1) electrolytes. $f_w = 10.2 \times 10^{-12} \text{ v.}^{-2} \text{ cm.}^2$; 25° C. The dotted lines indicate 5% and 20% correction.

for this paper; the calculation can, for example, be accomplished assuming that no specific adsorption occurs (16). We are here concerned with the second relation only.

From the preceding sections it is felt that the classical concept of a discrete slipping plane is too simple. There exists a slipping layer with a gradual transition from bulk fluidity to zero fluidity. This variation in viscosity may be due to the high electrostatic field strength, but this is not necessarily the only effect. A direct influence of the interface on the viscosity is also conceivable, in particular, an increase of the viscosity to very high values.

Discontinuities in the fluidity can be imagined in systems where solvated molecules are oriented in a peculiar way, behaving as an individual phase, for example, in so-called autophobic systems (17).

The actual relation between the observed electrokinetic potential, $\zeta_{\text{obs.}}$, and ψ_δ depends on the relative importance of the surface influence and double layer field influence on viscosity. As a matter of illustration we will discuss two extreme cases, one in which the viscosity is affected only by the viscoelectric effect and the other in which there is an immobilized layer of considerable thickness close to the surface.

a. No Direct Influence of the Surface on the Viscosity

For extremely low potentials the slipping plane is identical with the surface ($\zeta = \psi_\delta$). With increasing potential the viscoelectric effect causes the

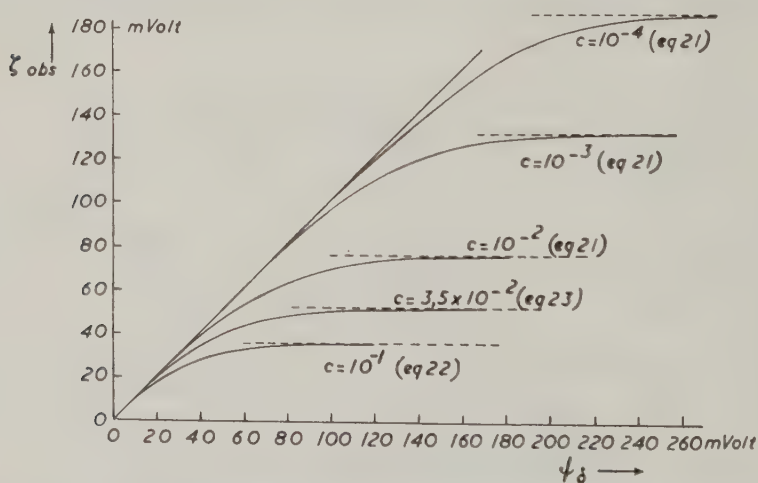


FIG. 2. Observed electrokinetic potential as a function of the surface potential in the absence of structural influence of the surface on the viscosity. Dotted lines: limiting values.

discrete slipping plane to be gradually replaced by a slipping layer of finite thickness. At last the viscosity can be so high that virtually no slip takes place at the interface. The slipping layer, the location of which is determined by the field strength, moves in outward direction with increasing potential, and this will eventually lead to a constant electrophoretic mobility (independent of ψ_δ , but dependent on the concentration). This dependency is illustrated in Fig. 2. The limiting values have been calculated from Eqs. [21]–[23] for ζ ($= \psi_\delta$) $\rightarrow \infty$. In Fig. 3 these limiting values are plotted as a function of the concentration. For low concentrations the relationship is linear with a slope of 58 mv. per tenfold increase in the concentration, but for higher concentrations the slope decreases.

1). At high ζ -potential the influence of the relaxation effect on electrophoresis should not be neglected. It also lowers the mobility.

2). In the given treatment f_w was considered to be independent of the concentration. This is probably an oversimplification (18). The influence of the concentration on f_w will change the curve of Fig. 3, and detailed analysis of the dependence of $\zeta_{\text{obs.}}$ from $\log c$ must be considered with a good deal of reservation.

Figure 2 can be exemplified by observed ζ -potentials on negative AgI which appear to be more or less independent of pI, i.e., of the surface potential ψ_0 over an appreciable range far from the zero point of charge. This followed from electrophoretic data (19–21), from streaming potentials (22), and also from sedimentation potentials at high ψ_0 as measured by Rutgers and Nagels (23), at least if correction was made for the relaxation effect. This constancy may be explained by the present theory. Recent data on

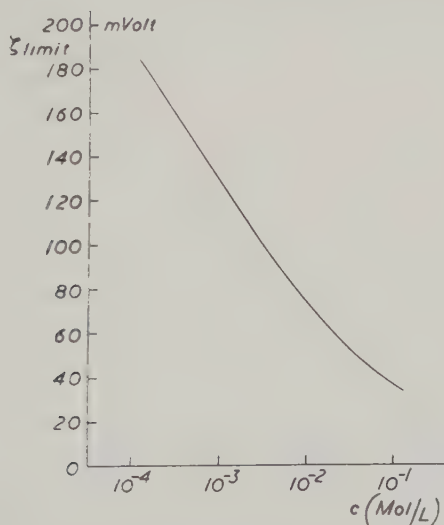


FIG. 3. Limiting values of $\zeta_{\text{obs.}}$

the ζ -potential at the oil-water interface as determined by Haydon (24) are also in qualitative agreement with the present picture especially with Fig. 2. For low potentials ζ and ψ_0 were identical. For higher ψ_0 $\zeta_{\text{obs.}}$ remained more or less constant. For high ψ_0 it decreased to some extent. This decrease must be explained by other factors, such as specific adsorption of ions and dependence of f_w on the composition of the solution. The constant zeta potentials are dependent not only on the concentration but also on the nature of the electrolyte and the nature of the soap (24); this—at least in part—may be due to the influence of concentration and nature of the solute on f_w .

b. Strong Influence of the Surface on the Viscosity

We assume now that several layers of molecules of the liquid are immobile with respect to the surface. The field strength outside this layer is already so low that the viscosity does not deviate very much from η_0 . This case can be treated as the classical, discrete slipping plane at a fixed distance (d) from the outer Helmholtz plane, with small viscosity correction $\zeta_{\text{obs.}} \sim \zeta_{\text{(real)}} = \psi_d$.

When specific adsorption of ions in the adhered layer may be neglected, $\zeta = \psi_d$ and ψ_δ are related through the equation

$$\exp\left(\frac{zF\zeta}{2RT}\right) = \frac{\exp(\kappa d) + \tanh\left(\frac{zF\psi_\delta}{4RT}\right)}{\exp(\kappa d) - \tanh\left(\frac{zF\psi_\delta}{4RT}\right)}, \quad [26]$$

where κ is the reciprocal Debye length.

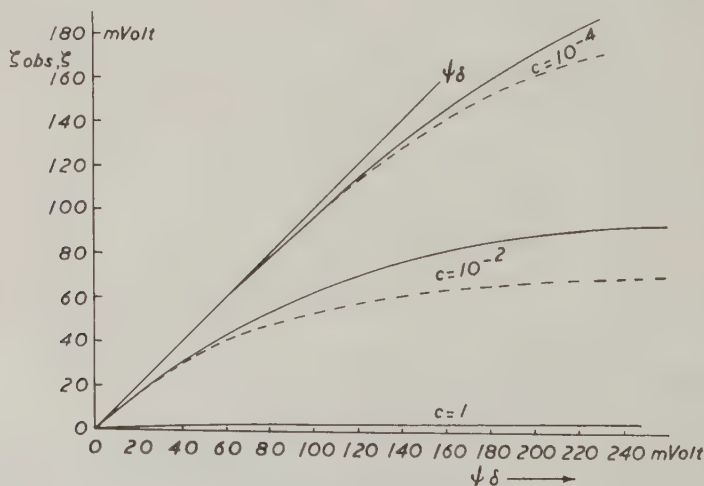


FIG. 4. Relation between the observed zeta potential, $\zeta_{\text{obs.}}$ (—), the potential of the slipping plane ζ (---), and the potential of the outer Helmholtz plane, ψ_δ .

The relation between ζ and ψ_δ is shown in Fig. 4 for three concentrations, $z = 1$ and $d = 10$ Å. The dotted curves represent the ζ_{obs} values, corrected for the viscoelectric effect with the help of Fig. 1.

For very high ψ_δ the potential of the slipping plane approaches a constant value (independent of ψ_δ) given by

$$\exp\left(\frac{zF\zeta}{2RT}\right) = \frac{1 + e^{-\kappa d}}{1 - e^{-\kappa d}}. \quad [27]$$

This constant value of ζ is seldom reached in practical cases. However, the electrophoretic mobility can become independent of ψ_δ at much lower potentials as a consequence of the viscoelectric correction. Comparison of Fig. 4 with Fig. 2 shows that in the case of Fig. 4 the constant electrophoretic mobilities are found at much higher surface potentials. Indeed the rate with which the electrophoretic velocity grows constant is a measure for the thickness of the solvated layer (influence of the surface) and for the magnitude of the viscoelectric constant (influence of the double layer viscosity). The limiting values of ζ_{obs} are, however, equal for both cases.

The relation between ζ_{obs} and c is governed by the influence of the concentration on the relations [21] [23] and [26]. This influence is given in Fig. 5 for three values of ψ_δ . It shows that the relation between ζ and $\log c$ is not linear. The slope varies with concentration and potential and is generally smaller than 58 mv. per tenfold change in concentration.

The observed zeta potential decreases more strongly with $\log c$ than the real one. At extremely high ψ_δ (limiting case) the slope is equal to that of Fig. 3. It should be noted that ψ_δ itself is usually a decreasing function of c ; this makes the slope of the curve relating ζ_{obs} and $\log c$ for constant ψ_0 steeper than that for constant ψ_δ .

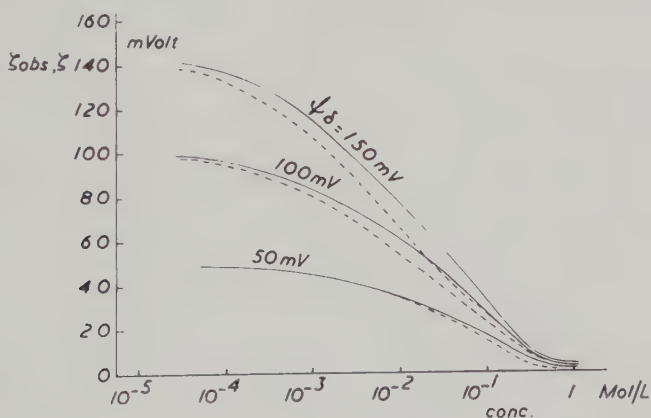


FIG. 5. Solid curves: relation between ζ and $\log c$ for constant slipping plane at 10 Å (1-1 electrolytes; diffuse double layer, for three values of ψ_δ). Dotted curves: corrected ζ -potential (ζ_{obs}).

An example of curves of this type are the ζ -log c curves for glass, as measured electroosmotically by Rutgers and De Smet (25).

The main point we wish to stress is that the effects calculated in this paper are sufficiently large and agreement with general experience is good enough to make a determination of the viscoelastic constant for water and aqueous solutions highly desirable.

SUMMARY

The variation of the dielectric constant and the viscosity in the electrical double layer are considered. The Helmholtz-Smoluchowski equation for the electrophoretic mobility requires only insignificant correction for variations in the dielectric constant; the variation in the viscosity can lead to considerable corrections, which increase with surface potential and concentration. Equations are given for the relation between electrophoretic mobility and surface potential and are illustrated by two examples. The concept of the slipping plane should be replaced by a slipping layer of finite thickness. At high surface potentials, the electrophoretic mobility is independent of the potential but depends on the electrolyte concentration.

REFERENCES

1. CONWAY, B. E., BOCKRIS, J. O'M., AND AMMAR, I. A., *Trans. Faraday Soc.* **47**, 756 (1951).
2. BRODOWSKY, H., AND STREHLOW, H., *Z. Elektrochem.* **63**, 262 (1959).
3. SPARNAAY, M. J., *Rec. trav. chim.* **77**, 872 (1958).
4. BOOTH, F., *J. Chem. Phys.* **19**, 391, 1327, 1615 (1951).
5. ANDRADE, E. N. DA. C., AND DODD, C., *Proc. Roy. Soc. (London)* **A187**, 296 (1946).
6. ANDRADE, E. N. DA. C., AND DODD, C., *Proc. Roy. Soc. (London)* **A204**, 449 (1951).
7. ALCOCK, E. D., *Physics* **7**, 126 (1936).
8. BJÖRNSTÅHL, Y., AND SNELLMAN, K. O., *Kolloid-Z.* **78**, 258 (1937).
9. CALKER, J. V., AND AUBKE, B., *Z. Physik* **131**, 443 (1952).
10. CHERNYUK, A. K., *Akad. Nauk S.S.S.R., Otdel. Tekh. Nauk Inst. Mashinovedeniya, Soveshchanie Vyazkosti Zhidkost. i Kolloid. Rastvorov* **2**, 62 (1944); *Chem. Abstr.* **40**, 3315¹⁻⁹ (1946).
11. CHMUTIN, M. S., *Uchenye Zapiski Stalingrad Gosudarst. Pedagog. Inst.* **1953** (No. 3) 92; *Chem. Abstr.* **50**, 4572ⁱ (1956).
12. HART, J., *Physica* **23**, 795 (1957).
13. HART, J., *J. Chem. Phys.* **29**, 960 (1958).
14. OSAMU KAMURA, I., *J. Chem. Soc. Japan* **64**, 895, 937 (1943).
15. BÖTTCHER, C. J. F., "Theory of Electric Polarisation," especially 11 sections. Elsevier, Amsterdam, Houston, London, New York, 1952.
16. GRAHAME, D. C., *Chem. Revs.* **41**, 441 (1947).
17. HARE, E. F., AND ZISMAN, W. A., *J. Phys. Chem.* **59**, 335 (1955).
18. HAYDON, D. A., Private communication.
19. TROELSTRA, S. A., AND KRUYT, H. R., *Kolloid-Z.* **101**, 182 (1942).
20. OTTEWILL, R. H., AND RASTOGI, M. C., Private communication.
21. BIJSTERBOSCH, B. H., Unpublished results.
22. PRAVDIĆ, V., AND MIRNIK, M., *Croat. Chem. Acta* **32**, 75 (1960).
23. RUTGERS, A. J., AND NAGELS, P., *J. Colloid Sci.* **13**, 140 (1958).
24. HAYDON, D. A., *Proc. Roy. Soc. (London)* **A258**, 319 (1960).
25. RUTGERS, A. J., AND SMET, M. DE, *Trans. Faraday Soc.* **41**, 758 (1945).

A SIMPLE APPARATUS FOR MEASUREMENT OF PROTEIN MONOFILM EXPANSION AT AIR-WATER INTERFACE IN RESPONSE TO SOLUBLE REACTANTS IN THE SUBSOLUTION¹

Charles Y. C. Pak² and John D. Arnold

Department of Medicine, University of Chicago, Chicago, Illinois

Received February 13, 1961

ABSTRACT

A new apparatus and technique for the study of the reaction of macromolecules at the air-water interface with soluble substances in the subsolution is described. A system of piston oils and plastic float with mercury seals is employed to monitor the monofilm area changes at constant pressure.

The reaction trays are milled from Teflon, which permits easy instrumentation and cleaning. The test monofilm is compressed to a predetermined pressure by a "piston oil" and is allowed to expand against the oil area on injection of a suitable reactant. The film expansion is isobaric owing to the unique characteristic of the piston oil. A plastic float with mercury seals divides the piston oil area from the test monofilm, and responds to small pressure changes in the latter by an appropriate displacement.

INTRODUCTION

It is the purpose of this paper to describe a technique and apparatus which will permit the study of the interaction of a protein monofilm with a soluble molecule of different chemical structure in the subsolution.

The technique requires that the monofilm be held at a constant pressure and the area be allowed to change. Isobaric surface area changes of this sort have been studied by several methods. Schulman and Stenhagen (1) studied isobaric film area changes by use of a modified Langmuir tray employing piston oils. Later, a constant pressure apparatus allowing a variable surface area was designed by Matalon and Schulman (2). This has been modified subsequently (3, 4) but is essentially a complex servo mechanism. In our laboratory, we have used an array of piston oils, a mercury seal with a plastic float, and a specially designed Teflon tray to show that the variable area response at constant pressure of the more elaborate machine can be obtained with an inexpensive apparatus.

¹ This research was supported by grants from USPHS 8-1593 C2 and USPHS C-3495(C2).

² Dr. Nathaniel I. and Marian Baskind Scholar, University of Chicago School of Medicine.

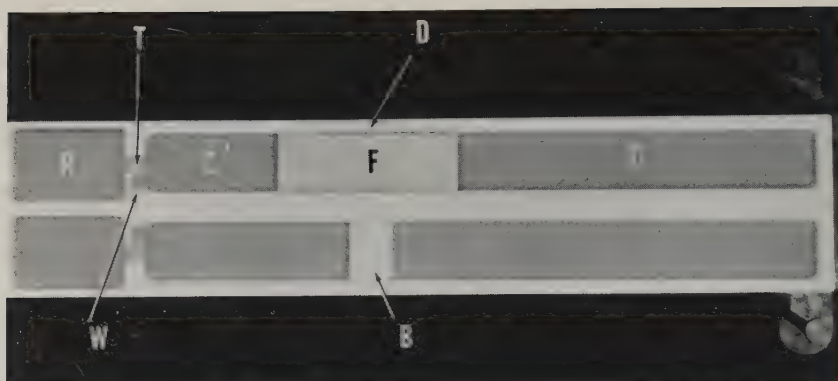


FIG. 1. A dual tray for measurement of surface film area changes. A pair of trays are milled from a Teflon block, $36.8 \times 7.6 \times 1.2$ cm. Compartment *R*, the reaction chamber, measures $5.0 \times 3.1 \times 0.3$ cm. and holds 4.65 ml. of solution when filled to the brim. Throat *T*, 0.9×0.9 cm. and 0.15 cm. deep, is designed to minimize subsurface diffusion from *R* to *C'*. The long compartment to the right of *T*, which includes *C* and *C'*, is $29.5 \times 2.5 \times 0.3$ cm. *C'*, together with *R*, is the area for developing the monofilm. *W* is the cup on which the surface film is made. *F*, 8 cm. long, is a freely movable float. *C* is a counter pressure area occupied by a piston oil. *B* is the solution separator dividing solution in compartment *C'* and *R* from solution in *C*. When the tray is filled with solution, *B* is just covered with liquid so that the float *F* will move freely. *D* is a small mercury drop between the float and tray.

The method of studying monofilm expansion is simple in principle: (1) A suitable monofilm of protein is formed which can be kept under a constant pressure, (2) with safeguards against incomplete mixing and erratic diffusion the subsolution is mixed with a soluble reactant, and (3) the change in surface area with time is then observed.

The apparatus has been especially designed to carry out these observations as easily and quickly as possible using small amounts of material. Since this is a new apparatus it will be described in some detail.

EXPERIMENTAL PROCEDURE

Description of Apparatus and Summary of Technique

Instead of the usual large Langmuir tray a pair of small trays are milled from a block of Teflon. A movable float is made from a thin sheet of cast Teflon and is used with mercury droplet seals. Two chambers may be made from each tray by a solution separator (*B*, Fig. 1). These are the mechanical components of the system.

In Fig. 1 a pair of trays are shown. The top tray has a movable float (*F*) in place. The bottom tray does not have the float in place to illustrate the positioning of the solution separator (*B*). Since the float must be freely movable a depth of solution of about 0.1 cm. is allowed over the solution separator.

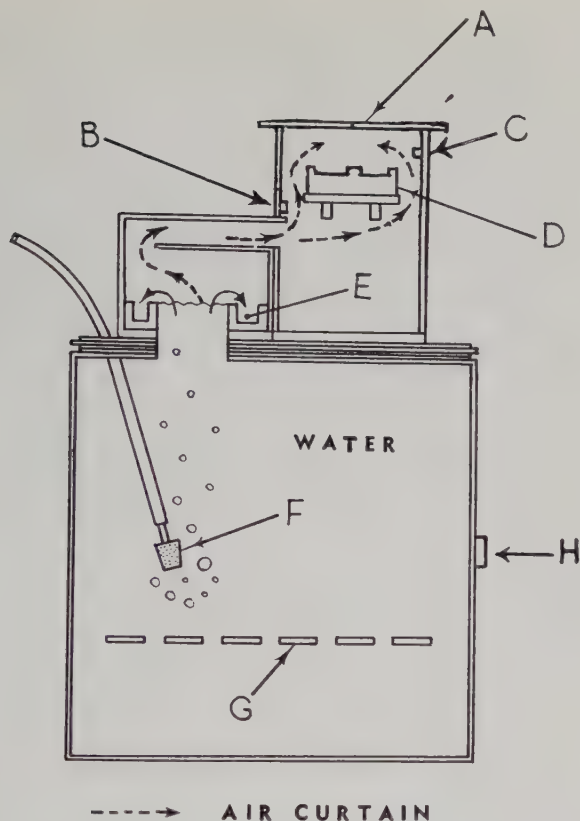


FIG. 2. Reaction incubator. The incubator is saturated with vapor formed by air bubbled into a water bath through a stone filter to remove air-borne contaminants (*F*). The water in this cleaning and humidifying bath is allowed to overflow constantly so that surface-seeking contaminants are removed as they form and do not get thrown up in the air curtain. This excess water is drained by *E*. Removable Lucite plates (*A*) allow easy access to the tray. The temperature of the incubator is controlled by the rheostat of water bath (*H*), and thermostat control (*B*), and is recorded on the telethermometer (*C*). By using a constant stream of clean humid air as an air curtain, the work on the trays can be carried out easily and with relatively little contamination of the air-water interface. It can be shown that evaporation from the tray surfaces is negligible.

The reaction compartment *R* provides a standard surface area of 15 cm.² and is connected to the cylinder compartment (*C'*) by a relatively narrow shallow throat. The depth of the throat is 0.15 cm., whereas in all other parts of the tray the solution is 0.3 cm. deep. This permits the transmission of surface pressure changes between *R* and *C'* but markedly reduces the diffusion of the soluble reactant from compartment *R* to compartment *C'*.

A small cup (*W*), 0.8 cm. in diameter and 0.3 cm. deep, is connected to

compartment C' by a wedge 0.1 cm. deep cut in the thin wall between C' and W . If these dimensions are followed the cup can be emptied by suction and the hydrophobic Teflon surfaces will prevent movement of solution back in the cup.

Since the experiments must be carried out under rigid temperature, humidity, and contamination control, a special incubator has been built in which an air curtain of clean moist air protects the surfaces of the tray and yet permits ready mechanical access to the solution surfaces (Fig. 2). Air and water temperatures can be maintained to within $\pm 0.25^\circ\text{C}$. It can be shown by a simple experiment that the evaporation from solution surfaces is minimal. Two thermometers, one with a plain bulb, and the other wrapped in wet cloth, recorded the same temperature after 30 minutes in the incubator.

In the test procedure, the monofilm is spread on compartments C' and R (Fig. 1). When spreading is complete, a piston oil is placed on compartment C . The float moves in response to the change in surface tension, until the surface pressure of the test film becomes equal to that of the piston oil.

The monofilm is then reacted with the test material which is injected under the surface film in compartment R . The reaction capacity of the monofilm is then measured by the movement of the float to the right into the region of the piston oil.

Piston Oils

As first studied by Carey and Rideal (5-7) and later by Langmuir (8), a variety of oils and mixtures of oils have the ability to maintain a constant pressure despite a marked change in area.

A list of piston oils and mixtures of piston oils with the pressure established by each, as measured by us, is given in Table I. Most of these are unstable on alkaline solution. If the reaction is studied over a neutral or alkaline solution, a two-compartment tray may be used. The solution separator (B , Fig. 1) is then used to separate the buffer solution in compartments R and C' from an acid solution in compartment C . On the right compartment C , on which piston oil is placed, is customarily filled with 0.01 N HCl to prevent saponification of the piston oil.

Unfortunately, the behavior of piston oils has been only incompletely studied. Some piston oils and mixtures are much more responsive in the contraction phase than they are in the expansive phase. Others become inert after a lapse of time. Even when they are studied at 0.01 N HCl solution, they often fail to maintain the constant pressure if their area is compressed more than 60%-75% of the original area. The range through which the surface area of the test film in compartment R may change, is thus limited by the maximal compressibility of a given oil.

TABLE I
Survey of Piston Oils

Piston oil	Pressure (<i>dynes-cm.</i>)
Oleic acid (USP, Merek)	32.0
Linoleic acid (Tech, Matheson & Coleman)	30.2
Ethyl laurate (Highest Purity, Eastman Organic)	19.7
Ethyl myristate (Highest Purity, Eastman Organic)	18.7
66.7% Ethyl laurate in mineral oil (Heavy, Sargent)	17.7
60% Ethyl laurate mineral oil (Heavy)	16.8
50% Ethyl laurate in mineral oil (Heavy)	15.5
40% Ethyl laurate in mineral oil (Heavy)	13.6
30% Ethyl laurate in mineral oil (Heavy)	11.4
Tri- <i>m</i> -tolyl phosphate (tri-cresyl phosphate or TCP Practical, Eastman Organic)	9.7
20% Ethyl laurate in mineral oil (Heavy)	9.1
15% Ethyl laurate in mineral oil (Heavy)	6.9
10% Ethyl laurate in mineral oil (Heavy)	4.5
Mineral oil (Heavy, Sargent)	0

The surface pressure of the piston oil was measured using a vertical pull balance (Wilhelmy type) on 0.01 *N* HCl solution at 22° C. every 5 minutes. The above oils can withstand 60%–75% compression of area without detectable change in pressure for 30 minutes. The glass slide of the balance was dipped gently into the solution a few times before each measurement to remove deposited oil film in an attempt to eliminate contact angle changes.

Movable Float and Mercury Seals

There are a number of problems associated with the use of a movable float in a system with surface-active agents. The most important of these is that of leakage of material around the float and the frictional resistance of the float against the sides of the tray.

Since the float could be made of thin plastic sheets of Teflon³ a predictable degree of fit between float and tray may be established by trial and error. It has been found that a 0.005- to 0.006-inch space (or 5 to 6 mils) on each side is necessary in order to minimize frictional resistance to movement of the float. This space, however, will allow a considerable escape of high-pressure film to the low-pressure side. To prevent leakage without increasing the frictional resistance of the tray, a small droplet of mercury is placed in a tiny cup milled from the tray so that the circumference of the droplet reaches the edge of the float (*D* Fig. 1; close-up, Fig. 3).

It is obvious that the fit between the tray, mercury, and the float will

³ Although Kel-F, Teflon, mylar, and aluminum foil work adequately as floats, the cast Teflon film, Type C (Dilectrix Co., 60 Ocean Avenue, Lynbrook, New York), at 0.002 inch thickness, has been easiest to clean, form, and use. It also appears to be most chemically resistant.

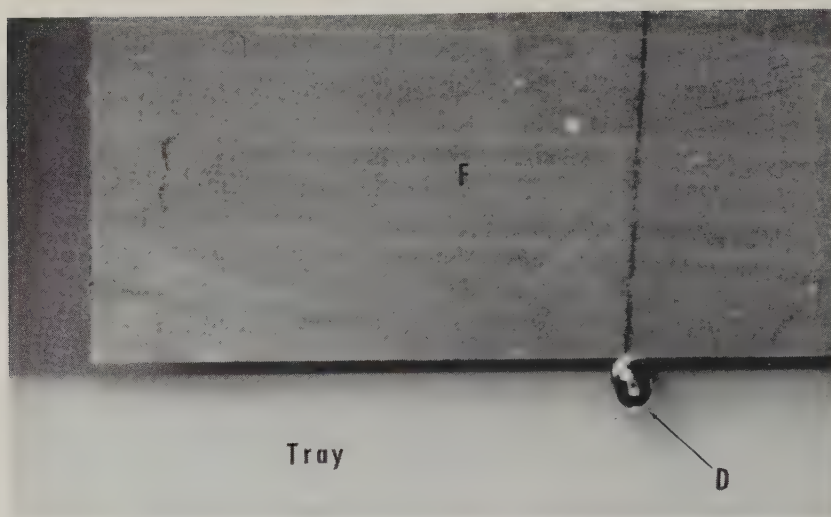


FIG. 3. A magnified view of the mercury seals (D) and float (F). A mercury droplet 0.00104 cm.^3 (1.04 lambda) in volume is placed in a cup (D) in the tray.

TABLE II
Effect of Mercury Droplet Size and Clearance

Clearance (mil)	Hg droplet (lambda)	$\frac{100 \Delta A}{A}$
4.5	0.52	69.5 ± 1.2
5.5	0.52	74.5 ± 0.5
5.5	0.60	71.5 ± 0.9
5.5	1.04	45.0 ± 1.2

The expansion of the monofilm is impeded by the resistance to movement of the float, which is a function of mercury size and the distance (clearance) between float and tray. The size of the mercury droplet was chosen such that the droplet (1) would remain in the hole in the tray without falling (Fig. 3) and (2) would prevent the escape of surface films (Fig. 4). Under the same clearance, the exact size of the droplet is not critical: 15% increase in droplet size from 0.52 to 0.60 lambda does not alter the monofilm expansion appreciably. A volume of 0.5 ml. of 4.8 mg. % porcine alpha globulin (Pentex, Inc.) was injected below pork insulin monofilm (Iletin U-40).

depend on the size of the mercury drop and the cup in the tray in which it sits. A hole in the tray 0.0312 inch in diameter and 0.02 inch deep was found to be most desirable. It can accommodate 0.00052-cm.^3 to 0.00104-cm.^3 (or 0.52- to 1.04-lambda) mercury drops. The mercury drops can be produced with relative ease to within $\pm 0.00003 \text{ cm.}^3$ by a calibrated 4-lambda micropipette which is attached to a 1-ml. syringe by a short rubber tubing. Table II shows the effect of the clearance between the float and

tray and the size of the mercury drop on the reaction. If the same clearance and same size mercury droplets are utilized, different trays of varying widths will give nearly identical reactions.

The efficiency of the mercury seal in preventing leakage is indicated by Fig. 4. A single tray and float were studied with and without a mercury droplet seal. On one side of the float tri-*m*-tolyl phosphate (tricresyl phosphate or TCP) was spread. On the other side of the float, the vertical pull balance on the initially clean surface measured the surface pressure developed by the leaking oil. With a mercury seal, a clean surface was maintained for a period of more than 30 minutes, but the float without the

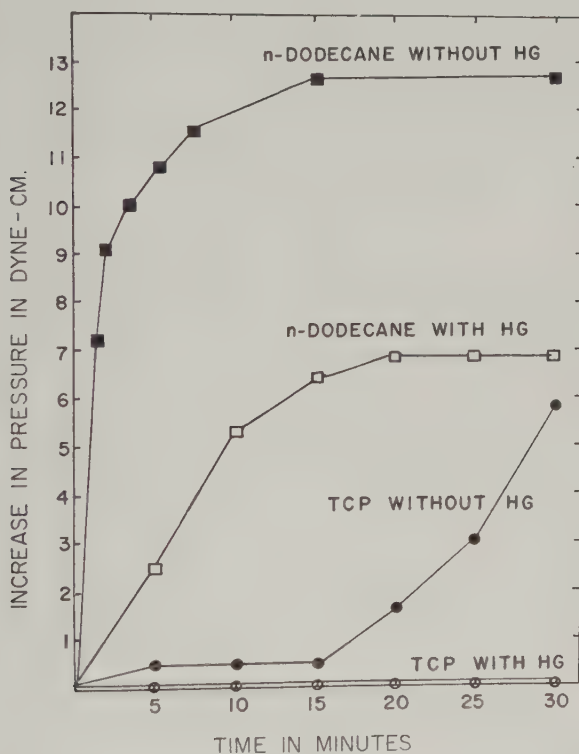


FIG. 4. Efficiency of mercury seals. A tray and float as in Fig. 1 top was studied with and without mercury seals as a test of the efficiency of the seals in preventing escape of film from one side of the float to the other. TCP and *n*-dodecane, at 9.7 and 12.7 dynes-cm. pressure, respectively, were placed in *R* and *C'* of the tray. A vertical pull balance was placed in *C*. It is apparent that the mercury seals are effective for pressure differences as high as 9.7 dynes-cm. but are not effective for higher pressures. Experiments were performed using 1.04- λ mercury droplets at 6-mil clearance between float and tray. Similar results were obtained with 0.52- λ droplets at 5.5-mil clearance.

mercury seal allowed 6.8 dynes-cm. pressure of contaminating material to pass in the same period of time.

The effect of the mercury droplet on frictional resistance of the float can be estimated by the following experiment. The initial resistance of starting from a static position was tested by placing two piston oils of small pressure differences on either side of the float with the float at rest. It requires a pressure difference of 0.125 dyne-cm. to consistently put the float in motion. Once in motion, however, a pressure difference of 0.06 dyne-cm. was the minimal force able to continue motion of the float. In this instance the width of the tray was about 2.5 cm.

It is highly desirable to maintain the mercury seal throughout the test procedure. Before compression by oil, the mercury droplets are placed on the far left edge of the float; after compression, the mercury droplets are still retained, preferably on the far right side of the float to allow for the subsequent expansion of the monofilm on injection of reactant. If the best conditions are to be met, the total excursion of float on compression by piston oil should not be greater than the area of the float, or 20 cm.².

Spreading of Monofilm

It has been customary to spread the monofilm at a fixed area of 40 cm.² or $\frac{8}{3}$ of the reaction area (*R*, Fig. 1). The amount of substance to be spread and the time allowed for spreading are determined by trial and error so as to give an initial monofilm area not greater than 35 cm.², and not less than 20 cm.², on compression by piston oil. If time of spreading is adequate and spreading complete, the behavior of the test film, whether spread on a 60-cm.² or 40-cm.² area, appears to be the same, as demonstrated by Table III.

Before spreading, the surfaces must be cleaned by the usual technique using flat Teflon bars. The shallow depth of the tray (0.3 cm.) facilitates the diffusion of surface-active impurities to the interface, which is complete in about 5 minutes (Table IV). To insure effective removal of these im-

TABLE III
Effect of Initial Surface Area of Spreading

Area of spreading (cm. ²)	Compressed area (cm. ²)	$\frac{100 \Delta A}{A}$
40	32.5	40.0
60	32.75	38.4

A volume of 0.05 ml. of 20 mg. % bovine albumin (Pentex, Inc.) was spread for 15 minutes at 40-cm.² and 60-cm.² areas. Formation of nearly the same film areas on compression by TCP suggests that spreading was complete. The two monofilms gave similar expansions on injection of 0.5 ml. of 12.5 mg. % alpha globulin even though they were spread on different areas.

purities, the solutions were allowed to stand in the tray for this period before their surfaces were cleaned. Subsequent contamination is very slow to develop.

The monofilm was formed from solutions of concentrations of not more than 24 mg. % by means of a constant flow injector. A motor of predetermined speed was used to turn the head of a micrometer syringe, to deliver a constant amount onto the surface, usually at a rate of 0.01 ml. per minute. In our hands more reproducible spreading occurs with this apparatus than by any manual technique.

A modified method of Bull (9) was used for placing the film on the interface. The 27-gage needle, attached to the micrometer syringe of constant flow injector, was lowered into the surface and gradually withdrawn, so that a cone of liquid formed around the tip of the needle. It was then raised as far as possible without breaking the cone. Larger gage needles or pipettes with blunt ends gave poorer spreading. Figure 5 shows how reproducible the formation of insulin monolayers may be by this method.

The film is formed initially on the surface of the small cup (*W*, Fig. 1).

This procedure was suggested by the experiments of Trurnit (10). After the monofilm covers all the available area in compartments *C'* and *R*, the excess which does not enter the interface will remain in solution in the side cup *W*. Material which is in solution may interfere with the reaction by spontaneous diffusion into the film (10, 11). This can be prevented by emptying the side cup *W* after spread is nearly complete.

Injection of Reactant

The test material (reactant) is injected under the monofilm in *R* through a small aperture in the side of the tray (Fig. 6). The injection is made from

TABLE IV
Removal of Impure Film by Sweeping

Number of minutes buffer was allowed to stand in tray before cleaning the surface by sweeping	Area of nucleohistone film ($cm.^2$)
0	26.7 ± 1.8
1	30.2
2	30.8
3	31.8
5	31.9 ± 0.1

When the surface of buffer solution is not swept, impure film may form from surface-active impurities in the solution, which will interfere with the spreading of the test monofilm. Such films, however, can be removed by sweeping the surface of the buffer 5 minutes after the solution has been placed in the tray by means of Teflon bars.

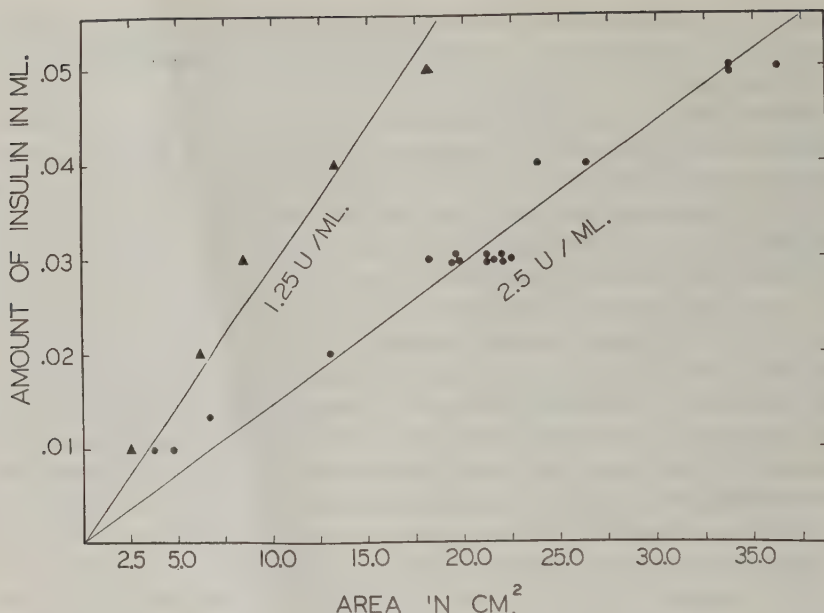


FIG. 5. Reproducibility of insulin monofilm formation. Two dilutions of crystalline zinc insulin (Iletin U-40, Lilly, 1.25 units/ml. and 2.5 units/ml.) were introduced on a fixed area of 40 cm.² over Mellvaine's phosphate-citric acid buffer at 31°C. for varying periods. After spreading, the films were compressed by TCP. The areas obtained were proportional to the amount of insulin introduced for both dilutions of insulin. This figure gives some indication of the reproducibility of the film area by this technique.

a 500-lambda micropipette (Sargent), at the end of which is added a small plastic tube which inserts directly under the monofilm.

Since the rate of monofilm reaction will depend on diffusion to the surface, the mixing of the reactant in the subsolution should be rapid and complete. The reaction tray, with the relatively shallow depth of 0.3 cm. and relatively small volume of 4.65 ml., is particularly adapted for rapid easy mixing. The efficiency of mixing is a function of the temperature, diffusion characteristic of the reactant, the volume of the reactant injected, and number of injections. For rapidly diffusible molecules at 31°C., as shown by dye in Fig. 6, mixing is essentially complete on primary injection of 500 lambda in 40 seconds. When the reactant molecules are more viscous or of low diffusion rate, it may be necessary to draw up the subsolution into the micropipette and reinject.

For very viscous solutions of the character of DNA it has not been possible to obtain complete mixing without disturbing the film or the time sequence of the reaction.

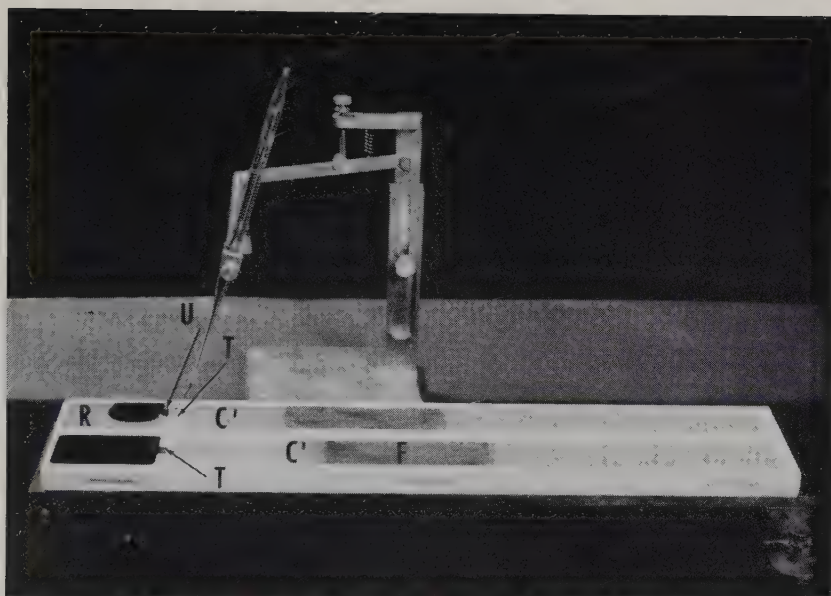


FIG. 6. Injection of reactant. In the upper tray, the test material (in this case a dye) is being injected under the test film and allowed to mix with subsolution. The mixing is fast and relatively complete without appreciable escape through the throat (T) as seen in the bottom tray when the injection is sufficiently vigorous. As diffusion and turbulence from the injection completes mixing and carries the test molecules to the surface, the reaction is measured by displacement of the float (F) to the right, as is shown in the lower tray.

Function of Throat (T)

The function of the shallow throat between R and C' is to limit the diffusion of test materials in the solution to the region of the reaction surface R as seen in Fig. 6. Table V shows that surface diffusion across the throat is negligible. If diffusion of test material occurs from compartment R to C' , the diffused molecules will react with the monofilm in C' and add to the reaction. It can be seen that insulin monofilms confined to R give the same response to gamma globulin injection as do the films which extend into compartment C' .

On Cleaning

The Teflon trays and bars are cleaned in Lakeseal,⁴ and kept in 0.05 N HCl solution for at least 10 minutes before use. The underwater glass Teflon⁵ barriers (B) are similarly washed and kept in 0.05 N HCl solution

⁴ Lakeseal is a laboratory cleanser manufactured by Finger Lakes Chemical Company, Inc., Etna, New York.

⁵ Glass-filled Teflon is used because it is more wettable than Teflon and permits a shallower layer of water to cover it. It is easy to form and clean.

TABLE V
Function of the Throat (T)

Total insulin monofilm area on compression (cm^2)	Area in C' occupied by insulin monofilm (cm^2)	$\frac{100 \Delta A}{A}$
15.5	0.1	48.3
18.7	3.3	50.0
35.3	19.9	53.3
36.7	21.3	50.0

Predetermined amounts of insulin were spread so as to give different film areas on compression by TCP. All these films filled the reaction compartment and extended into the compartment C' beyond the throat (T) to varying extent. When such films were reacted against 0.5 ml. of 24 mg. % porcine gamma globulin (Pentex, Inc.), nearly identical expansions were noted, suggesting that the diffusion of substrate molecules across the throat from R to C' is insignificant.

for at least 30 minutes. The floats are washed in Lakeseal, immersed in 10 % ethyl alcohol for 30 minutes, rinsed in glass-distilled water, and kept dry in a desiccator. They must be completely dry before use; wet floats will give erroneous results. Between use, they are kept between two glass plates to maintain their shape. They can be repeatedly used, unless they lose their shape or their hydrophobic surface character. Both the micro-pipette for delivery of mercury seals and mercury must be acid-washed.

Description of Test Procedure

The test is performed at a temperature regulated to within $\pm 0.25^\circ\text{C}$. The following procedure has been employed:

1). The tray is removed from 0.05 N HCl solution, rinsed with distilled water and placed in incubator (Fig. 2).

2). The compartments in the tray are filled to the edge with a predetermined amount of buffer. The solution separator (B) by virtue of its hydrophobic surface keeps the buffer in compartment C' and R until 0.01 N HCl is added to compartment C (Fig. 1).

3). The float (F) is placed over the solution separator (B) without connecting the two solutions. The hydrophobic surface character of the float and the solution separator keeps the two solutions separated.

4). The solutions are allowed to stand for 5 minutes to allow the surface-active impurities to diffuse to the surface. The surfaces are then swept with flat Teflon bars. The buffer solution in compartments C' and R is then connected to dilute acid solution in compartment C by to and fro horizontal movement of the float by bars placed on the free edges of the float. The area of admixture of buffer and acid is thus confined to a shallow region under the float.

5). The float is held by a bar in a predetermined position so as to give 40 cm.² of surface in compartments C' and R' . Into this surface area, the substance to be spread is introduced by means of a constant flow injector on the surface of W .

6). The time allowed for spreading is determined for each monofilm. In general, 15 minutes was found to be sufficient. Two minutes before completion of spreading, mercury drops are placed on the far left end of the float.

7). On completion of spreading, the Teflon bar holding the float is removed, and the monofilm is compressed by two drops of selected piston oil deposited on compartment C . The area of the test film should be large enough so that the float comes to equilibrium at a point where the mercury seals protect it.

8). The oil is allowed to equilibrate with the test film. This period of equilibrium must be determined for each film and each piston oil. In the meantime, the test solution to be injected into the substrate below the monofilm is mixed with an appropriate solvent and brought to temperature. The test solution is made just before use unless otherwise stated.

9). After equilibration, 0.5 ml. of the mixture is injected under the monofilm.

10). The position on the left edge of the float is recorded at the start of the injection, and every 1 to 5 minutes thereafter for 15 minutes to 1 hour. The reaction is expressed in terms of monofilm expansion, or the per cent change in area of the monofilm covering the area of compartment R , which is 15 cm.²; i.e., $100 \cdot \Delta A/A$ since this is the area exposed to the reacting molecules.

All the experiments reported in this paper were performed under the following conditions unless otherwise stated: McIlvaine's pH 7.4 buffer, 31°C. temperature, 15 minutes of spreading, TCP piston oil at 5 minutes of equilibration, 5.5-mil clearance between float and tray, 0.52-lambda mercury droplets, and 15 minutes of reaction period.

RESULTS

Factors Affecting Total Expansion of Monofilm

When the soluble reactant is injected below the test monofilm of another molecular species, the monofilm will usually expand against the constant pressure of the piston oil. The film expansion is modified by the following variables:

1. *Concentration of the substrate (reactant)*. The concentration of reactant is expressed as milligrams or micrograms per milliliter of solution in compartment R /cm.² surface film of compartment R . The rate of monofilm expansion depends on the efficiency of mixing of the reactant in the sub-solution. For plasma protein reactants, mixing is apparently complete on

primary injection, since repeated injections by withdrawal and reinjection of subsolution will not alter the film expansion rate.

Provided the mixing of the reactant in the subsolution is rapid and complete, the total expansion of the test monolayer is proportional to the concentration of the reactant within rather wide limits. For protamine sulfate-insulin monofilm interaction, this proportionality is maintained up to the protamine sulfate concentration of 5.5 micrograms/milliliter/cm.² or at about 110 % expansion of insulin monofilm (Fig. 7). Beyond this film expansion, the reaction is no longer proportional to the reactant concentration.

This loss of proportionality is sometimes due to the change in compression pressure of the piston oil. The 110 % increase in the monofilm causes a 50 % to 60 % contraction of the piston oil area. At that point, an increase in pressure of some oils begins to occur.

Figure 7 also demonstrates that the film expansion is not linear with reactant concentration below 40 %. Poor reproducibility is also shown at

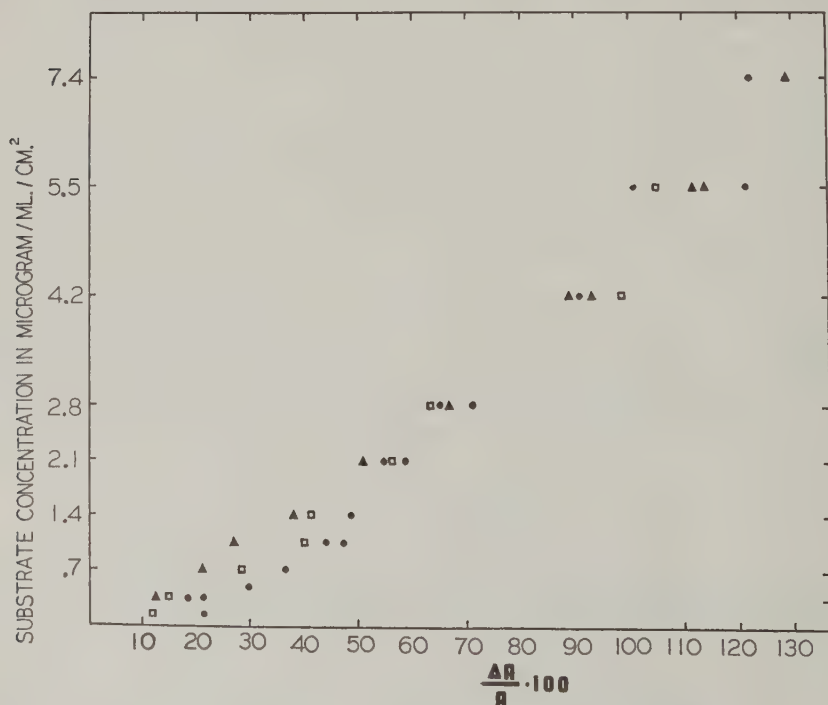


FIG. 7. Effect of concentration of soluble molecules in subsolution on film expansion. Pork insulin monofilms were reacted with protamine sulfate (Lilly, NF) to demonstrate reproducibility and linearity of reaction. Different symbols represent three different months in which the experiments were performed (0.8-lambda mercury droplets; 30 minutes of reaction).

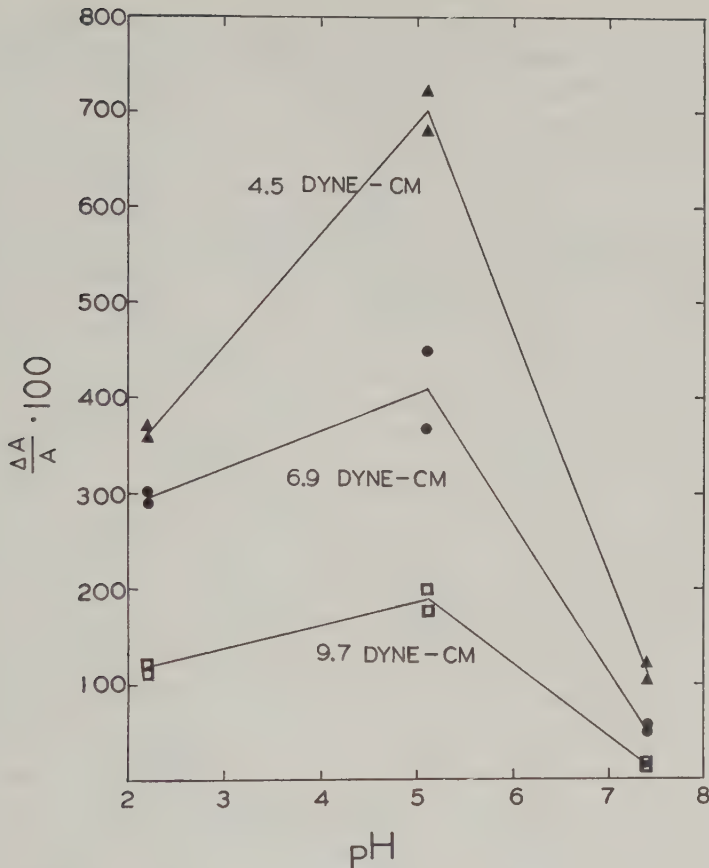


FIG. 8. Effect of pH and compression pressure. Pork insulin (isoelectric point of 5.3) monofilm was reacted with 0.35 microgram/milliliter/cm.² porcine albumin (Pentex, Inc., isoelectric point 4.9) to show that their total reaction is greatest between their isoelectric points. The reaction is reduced by increasing compression pressures.

this range. However, when smaller mercury drops are used (0.52 lambda instead of 0.8), proportionality between film expansion and reactant concentration is maintained down to 16% during 30 minutes of reaction.

2. *Effect of pH.* The effect of pH on the total film expansion will depend on the specific biologic system studied. For pork insulin monofilm-porcine albumin reactant system, the expansion appears to be greatest between their isoelectric points and lowest on the basic side (Fig. 8).

For insulin monofilm-protamine sulfate reactant system, the expansion is greatest between the two isoelectric points, and lowest on the acid side of the isoelectric point of insulin.

3. *Effect of compression pressure.* Figure 8 also demonstrates an inverse

relationship between the total film expansion and compression pressure. The expansion is reduced as piston oil pressure is increased. As will be shown in a later paper, the pressure may be a critical factor in demonstrating specific reactions.

4. *Effect of buffer.* The ionic strength of McIlvaine's buffer from one-half to threefold concentration had no effect on the insulin monofilm-protamine reactant system. McIlvaine's buffer was used for all this study since it permits greater and more reproducible film expansion than acetate, boric acid, or veronal buffers. The expansion curves produced with some buffers are harder to interpret (Fig. 9).

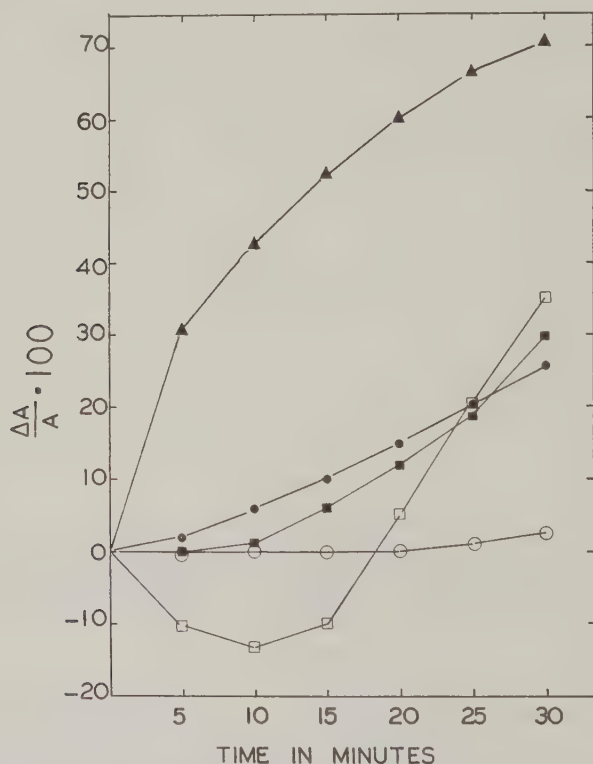


FIG. 9. Effect of buffer solutions. 2.9 microgram/milliliter/cm.² protamine sulfate was reacted with pork insulin monofilm in different buffers at pH 7.4. In McIlvaine's phosphate-citric acid buffer, the total expansion is initially very rapid, and gradually decreases, reaching 71% in 30 minutes (solid triangles). The same reaction is much reduced in 0.01 N sodium acetate + 0.14 N sodium chloride (solid circles), veronal (open squares), Clark's boric acid-potassium chloride (open circles), and McIlvaine's buffer + 10 mg.% tannic acid (closed squares). The reaction in sodium acetate + sodium chloride buffer is almost linear with time. In veronal buffer, the initial contraction of film is followed by a rapid linear expansion.

5. *Effect of temperature.* The Q_{10} value between 28°C. to 38°C. for insulin monofilm-pork alpha globulin system is found to be 1.73. It is thus very important to control temperature. Since the critical temperature is that of the water surface it is equally important to regulate the rate of evaporation. The reaction incubator with moist air curtain makes this possible.

DISCUSSION

The development of certain fluoroplastics, such as Teflon, with surface characteristics similar to those of paraffin but with greater mechanical strength, has permitted a new approach and much simpler instrumentation than has been possible in the past with the classical Langmuir tray.

The reaction tray, milled from a Teflon block, is designed particularly for the measurement of monofilm expansion at constant pressure. The tray is considerably smaller than the ordinary Langmuir trough, holding only about 35 ml. of solution, and is easy to clean and handle. The function of the throat (T , Fig. 1) in restricting the reacting film area to compartment R , and the method of injection of soluble reactant have been discussed. The mixing of soluble reactant in the subsolution in compartment R is rapid and complete owing chiefly to the shallowness of the tray and the small volume of the compartment (4.65 ml.). The small depth of the tray (0.3 cm.) also facilitates the diffusion of surface-active impurities from the test solution to the interface, allowing for their removal by sweeping before spreading of the test monofilm (Table IV).

A system of piston oils and movable plastic float with mercury seals permits an easier and perhaps better measurement of isobaric monofilm expansion than has been previously possible. The float is held in equilibrium between the test monofilm and the piston oil. When a suitable soluble reactant is injected below the test film, and penetration takes place, the float is displaced along the surface as a new equilibrium is reached. The unique property of the piston oil allows this process to take place at constant pressure even though the area of the oil film changes. The float is very sensitive to surface pressure changes in the monofilm. A pressure as low as 0.06 to 0.125 dyne-cm. will start it in motion. Its movement is furthermore automatic; i.e., manual adjustments are not necessary to bring it to equilibrium.

For the film expansion to be meaningful and reproducible, several conditions must be satisfied. First, the fit of the mercury droplet between the tray and float is made so that the resistance to movement of the float would be minimal and the leakage of surface film prevented. Secondly, the piston oil must exert the same pressure throughout the test procedure. Many piston oils change their surface pressure on exposure to a basic solution or on compression of their area to less than 40% to 25% of the original area. Finally, the various experimental conditions, such as tem-

perature, pH, and buffer medium, must be rigidly controlled. The dependence of total monofilm expansion on these variables has been demonstrated.

With these safeguards, the apparatus permits a rapid and easy approach to the measurement of monofilm expansion at a constant pressure.

ACKNOWLEDGMENT

The authors would like to thank Dr. Herman E. Ries, Jr., Research and Development, Standard Oil Company (Indiana), for his critical reading of the manuscript.

REFERENCES

1. SCHULMAN, J. H., AND STENHAGEN, E., *Proc. Roy. Soc. (London)* **126B**, 356 (1938).
2. MATALON, R., AND SCHULMAN, J. H., *J. Colloid Sci.* **4**, 89 (1949).
3. MATALON, R., *J. Colloid Sci.* **8**, 53 (1953).
4. GODDARD, E. D., AND SCHULMAN, J. H., *J. Colloid Sci.* **8**, 309 (1953).
5. CARY, A., AND RIDEAL, E. K., *Proc. Roy. Soc. (London)* **109A**, 301 (1925).
6. CARY, A., AND RIDEAL, E. K., *Proc. Roy. Soc. (London)* **109A**, 318 (1925).
7. CARY, A., AND RIDEAL, E. K., *Proc. Roy. Soc. (London)* **109A**, 331 (1925).
8. LANGMUIR, I., *J. Chem. Phys.* **1**, 756 (1933).
9. BULL, H., *J. Biol. Chem.* **125**, 585 (1938).
10. TRURNIT, H. J., *J. Colloid Sci.* **15**, 1 (1960).
11. KAPLAN, J. G., AND FRASER, M. J., *J. Biol. Chem.* **210**, 57 (1954).

MOLECULAR TILT IN FATTY ACID MULTILAYERS

J. B. Bateman and E. J. Covington¹

U. S. Army Chemical Corps, Fort Detrick, Frederick, Maryland

Received February 15, 1960, revised March 22, 1961

ABSTRACT

The optical properties of films of Ba-Cu-H stearate formed by successive monolayer transfer from the air-water interface to a solid carrier have been studied by two methods: (a) the Hartman method, which gives thickness and refractive index of stepped multilayers for an incident s-ray, and (b) the Mattuck method, which gives thickness and refractive index of thin film increments upon a suitable multilayer carrier. It has been found (a) that the Hartman multilayers show directional properties with respect to the direction of "dipping" during monolayer transfer, and (b) that the apparent refractive indices found by the Mattuck method vary considerably with film pressure of transfer. These findings are interpreted quantitatively in terms of molecular tilt imposed by the process of monolayer transfer from the original *a/w* interface. Preliminary data on films of Ba-Cu-H nonadecanoate show these to be unstable and nonhomogeneous, with much looser molecular packing than in the case of the corresponding stearates. On the average the hydrocarbon chains are very nearly normal to the slide.

The orientation of the molecular axes of long-chain fatty acids in various conditions—in crystals, in monolayers on water, and in built-up multilayers on solid surfaces—is a matter of some interest in view of the well-known polymorphism (1) of these substances, which arises partly from the existence of several different modes of lateral association of the chains. It might be supposed that these would be encountered in monolayers and multilayers and would influence their optical properties in a manner which would also be of some practical interest in connection with recent optical methods of determining the thickness and refractive index of thin films (2-4) which require the use of well-characterized, homogeneous, and preferably isotropic, multilayer plates; these have usually consisted of fatty acid multilayers.

The present paper reports observations on stearate and nonadecanoate films which are interpreted in terms of variations in molecular tilt with the conditions of transfer from air-liquid monolayer to solid carrier.

¹ Present address—General Electric Research Laboratory, Schenectady, New York.

MATERIALS AND METHODS

Optical Methods

The optical methods used were essentially those of Hartman *et al.* (2) and Mattuck *et al.* (3, 4) with modifications to be mentioned shortly. The former method permits measurements of the thickness and refractive index of thick multilayers when these can be built up on chromium-plated slides in a series of suitable steps. The Mattuck method permits measurement of the thickness and refractive index of very thin ($10 \leq d \leq 250$ Å.) homogeneous films deposited in any way upon a suitable optical multilayer gauge.

Hartman Method

When a flat chromium-plated slide coated with a transparent homogeneous film (thickness Nd and refractive index n) is illuminated with white light plane-polarized with the electric vector perpendicular to the plane of incidence (*s*-ray), the reflected intensity will pass through a minimum when

$$\delta = \delta_0 + 2\pi m = (n^2 - \sin^2 \phi)^{1/2} \frac{4\pi dN}{\lambda}, \quad [1]$$

where δ is the optical path difference, ϕ is the angle of incidence, λ is the wavelength, d is the thickness per double layer, N is the number of superimposed double layers, and m is the fringe order, 0, 1, 2 \dots . It follows that

$$m = [2d(n^2 - \sin^2 \phi)^{1/2}] \left(\frac{N}{\lambda} \right) + c = b \left(\frac{N}{\lambda} \right) + c, \quad [2]$$

where c is a constant, so that the expression in brackets can be evaluated by locating the fringe wavelength for several orders, keeping ϕ constant. Further, by repeating these measurements at several different angles of incidence, n and d can be determined easily by solving the equation

$$b^2 = 4(n^2 d^2 - d^2 \sin^2 \phi) \quad [3]$$

by the method of least squares.

In the experiments on directional effects in nonadecanoate multilayers, it was assumed that the metrical thickness of the films is independent of the direction from which they are viewed. Using one prime and two primes, respectively, to denote values applicable when, at constant angle of incidence ϕ_1 , the incident *s*-rays are in two mutually perpendicular directions (see nomenclature, p. 542), one obtains from Eq. [3]

$$(b')^2 + (b'')^2 = 4d^2[(n')^2 + (n'')^2] - 8d^2 \sin^2 \phi_1; \quad [4]$$

$$(b')^2 - (b'')^2 = 4d^2[(n')^2 - (n'')^2]; \quad [5]$$

which can readily be solved for d , n' , and n'' .

Mattuck Method

This method in its original form requires the use of a stepped optical base consisting of a chromium-plated slide coated with about 20 stearate double layers in one portion and about 40 in another. These two thicknesses are chosen in order to satisfy the zeroth order conditions for zero reflection coefficients at about the same visible wavelength when the thinner step reflects the *s*-ray and the thicker step reflects the *p*-ray. When the two steps are covered with a thin film of unknown thickness *d* and refractive index *n*, the fringes are displaced by $\Delta\lambda^s$ and $\Delta\lambda^p$, respectively. Because of the different forms of the Fresnel reflection coefficients for the *s* and *p* rays, these displacements are different functions of *n* and *d* and simultaneous solutions are possible with several degrees of approximation according to the accuracy desired.² In their simplest form the equations can be written

$$n \approx a \left(\frac{\alpha^s \Delta\lambda^s}{\alpha^p \Delta\lambda^p} \right)^{1/2}; \quad [6]$$

$$d \approx \frac{b \alpha^s \alpha^p \Delta\lambda^s \Delta\lambda^p}{(2.25 \alpha^s \Delta\lambda^s - \alpha^p \Delta\lambda^p)}; \quad [7]$$

where *a* and *b* are constants, α^s and α^p are calibration constants, and $\Delta\lambda^s$, $\Delta\lambda^p$ are the measured fringe shifts. In the present work the calculations have been made to a somewhat better degree of approximation by using Mattuck's (3) equations 8-12.

The method has been modified in the following respects: (1) The optical base is built up to give the first, instead of the zero, order interference fringes, with about 61 and 80 double layers for the *s* and *p* rays, respectively. The displacements $\Delta\lambda$ caused by an unknown film are smaller than with the zeroth-order slides, but there is an over-all gain in precision and convenience of measurement because the first-order fringes are much sharper (Fig. 1). (2) Measurements with *s*- and *p*-rays were made at a single angle of incidence, 81°, instead of $\phi^s = 79^\circ 10'$ and $\phi^p = 82^\circ 30'$ for strictly zero reflection coefficients. The compromise resulted in negligible loss of accuracy and considerable gain in convenience. (3) The built-up multilayers

² Faucher, McManus, and Trurnit (5) have suggested recently that film refractive index and thickness might be determined simultaneously by using only the *s*-ray and measuring at two wavelengths the numbers of double layers corresponding to the minimum reflected intensity. The pertinent equation for minimum reflected intensity can be written: $\tan 2zNd = -az/(b - z^2)$, where *z* is a function of film refractive index and angle of incidence, *N* is number of monolayers, *d* is thickness per monolayer, and *a* and *b* are functions of the complex index of refraction of the metal base. Thus, if one ignores dispersion in the film material itself, the possibility of solving simultaneously for *n* and *d* at two wavelengths rests solely upon the dispersion of the refractive index of the metal base. The principle is thus quite different from that of the Mattuck method discussed here, and the feasibility of the procedure remains to be demonstrated in quantitative terms.

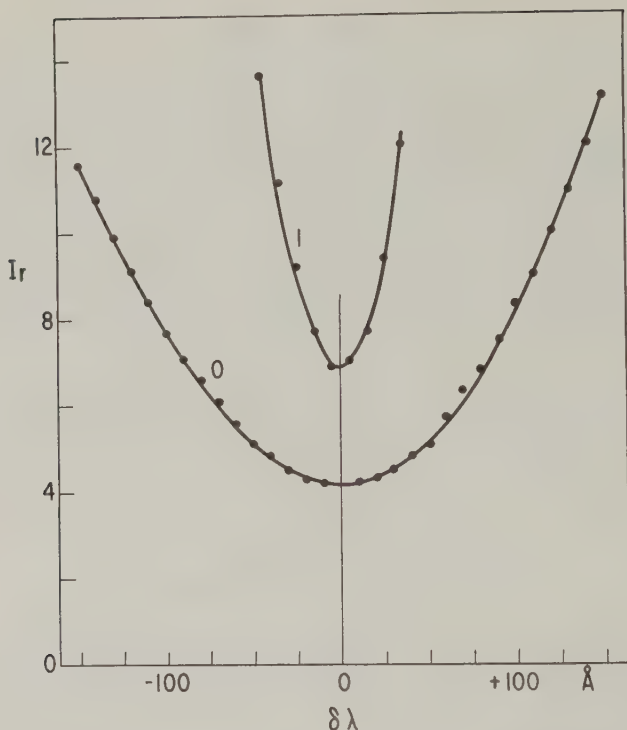


FIG. 1. Reflected intensity as a function of wavelength for zeroth and first-order Ba-Cu-H stearate multilayers on chromium. The number of double layers is 19 and 61 for the zeroth and first order, respectively, the angle of incidence is 81° , and the data refer to the s-ray.

were composed of Ba-Cu-H stearate rather than Ba-H stearate used formerly (q.v.). (4) Each slide used was individually calibrated by the addition of a few further stearate layers prior to deposition of the unknown; previously, average values of the calibration constants had been used. As in earlier work, the fringes were always measured at a number of points on the slide; because of the great uniformity of the new multilayers, this served principally to demonstrate occasional surface imperfections in the chromium slides.

Technique of Monolayer Spreading and Transfer

The process of preparing built-up multilayers has not been adequately described in the literature, although several of the individual steps have received detailed attention. Our unsuccessful first attempts to obtain uniform films led us to examine the matter in detail and to develop a standardized procedure.

Film Tray

The Plexiglas film tray is sketched in Fig. 2. Tray and all parts are coated with paraffin wax. The depth is 0.9 cm. except at positions 1 and 4, where there are troughs deep enough to accommodate the slides which are being dipped. At 3 there is a ground glass ring of the kind described by Langmuir and Schaefer (6), of such a depth that the aqueous solution filling the trough just covers the ring when the level is precisely adjusted to the tip of a hydrophobic glass pointer. The floating piston 2 is cut from polyethylene sheet. The sweeping barrier 5 is of Plexiglas.

Aqueous Subphase

The Blodgett "a" solution (7) containing BaCl_2 and KHCO_3 at pH 7.0 has been widely used in preparing films for transfer; the resulting film is composed of stearic acid mixed with the barium soap, which may be designated Ba-H-St. Such films are not of sufficient uniformity for the present purposes; moreover, as Blodgett (8) has shown, some film substance is lost upon immersion in water. We find that extremely uniform and stable built-up multilayers are obtained from Ba-Cu-H-St monolayers formed on the following subphase: $10^{-4} M \text{BaCl}_2$, $2 \times 10^{-4} M \text{KHCO}_3$, $10^{-7} M \text{CuCl}_2$ in laboratory distilled water; the pH is 6.8 and the temperature should not exceed 20°C . This specification is not complete, since our laboratory distilled water, of specific resistance 74,000 ohms-cm., was shown by spectrographic analysis to contain traces of B, Si, Al, Fe, Mg, Ca, and Cu. Blodgett and Langmuir (7) also used water known to be contaminated with trace elements, although they considered that the specific resistance should not be less than 300,000 ohms-cm.

Stearic Acid Solution

The stearic acid (Eastman, m.p. $69.5^\circ\text{--}70^\circ\text{C}$.) was dissolved in benzene (Baker's AR.) at a concentration $3 \times 10^{-2} M$. Unsatisfactory results were obtained when the solution was too dilute, in conformity with the results of LaMer and Robbins (9), who noted an increase in area of stearic acid

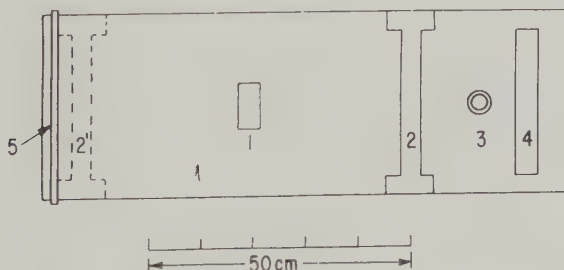


FIG. 2. Plexiglas trough for fatty acid monolayers. See text.

monolayers formed from dilute solutions. Archer and LaMer (10, 11) give reasons for considering other solvents preferable to benzene, and they recommend use of 0.014 *M* stearic acid in petroleum ether.

Nonadecanoic Acid

The purified nonadecanoic acid, m.p. 68°–69°C., was prepared by Professor H. A. Smith of the University of Tennessee.

Spreading Technique

With the polyethylene float in position 2 (Fig. 2) the stearic acid solution is dropped from a micropipette upon the surface of the subphase at the center of the ring 3; the ring retains the solution while permitting outward spreading of the monolayer formed as the benzene evaporates. Its function is thus to protect the paraffined edges of trough and barriers from the solvent action of benzene and possibly to prevent occlusion of residual benzene by the monolayer. The solution is delivered from the micropipette so rapidly that it always remains visible on the surface. Rapid spreading against a resistance is considered important because impurities in the subphase are less likely to enter an interface already occupied by a monolayer. Spreading is continued until the float has been propelled to position 2'. The last drop of solution remains on the subphase surface as a lens and is removed with an aspirator. After a few minutes the piston oil is applied to the clean surface to the left of 2' with a clean platinum wire.

Piston Oils

In the routine transfer of stearate monolayers to solid surfaces, the films were compressed to 29 dynes/cm. using oleic acid as piston oil. Commercial oleic acid is freed of oxidation products, which lower its surface pressure, by contact with diatomaceous earth, and the product is stored in the dark. Other piston oils used were castor oil (~ 16 dynes/cm.) and tri-*m*-cresyl phosphate (~ 9 dynes/cm.).

Film Transfer Technique

The clean chromium-plated glass slides, made hydrophobic by rubbing with cotton wool, were mounted on an automatic dipping device of adjustable speed. In preparing stepped multilayers several slides were dipped at once in the trough 4 (Fig. 2) at about 5 cm./min. In transferring monolayers for calibration or as unknowns, individual slides were dipped in trough 1, where the film is thought to be more uniform.

Optical Uniformity of Multilayer Slides

A prerequisite for any valid experimental use of the Hartman and Mattuck methods is that the stepped multilayers shall be homogeneous;

in the case of the Mattuck method this requirement takes a more stringent form, since optical homogeneity must be supplemented by strict chemical and physical identity of the *s* and *p* interfaces which are to receive the unknown film. Bateman (unpublished experiments), in attempting to characterize a number of polycyclic organic substances by the Mattuck method, observed in several instances that the reactivities of the zeroth-order *s* and *p* Ba-H stearate interfaces toward these substances were so strikingly different as to make optical measurements fruitless. Schaefer (12) had previously noticed that the surface properties of Ba-H stearate multilayers were periodic functions of the number of double layers, and had attempted to account for this in terms of a cumulative migration of portions of each successive monolayer into vacancies in the underlying layers; Sobotka (13) also discussed this question in somewhat similar terms. In line with this hypothesis, Mattuck noted that the position of the *s* fringe would often shift by as much as ± 4 Å. within a few days. The question needs closer examination, but it is significant that the Ba-Cu-H stearate slides now in use are stable for several months. We have also noted, by means of measurements with a cathetometer, that whereas in our earlier experiments the height of the meniscus during film transfer varied periodically with the number of layers on the slide, it now remains unchanged after the seventh double layer.

RESULTS

Optical Properties of Ba-Cu-H Stearate Multilayers

Stepped slides with six orders were built up by transfer of Ba-Cu-H stearate monolayers under 29 dynes/cm. pressure, and first examined with the *s*-ray incident at right angles to the dipping direction and with the electric vector therefore coinciding with the dipping direction. The slides were then turned through 90° and the measurements repeated.

Figure 3 illustrates the validity of Eqs. [2] and [3] for one of the slides so examined. It was found (Table I) by use of Eqs. [4] and [5] that changing the orientation of the incident light with respect to the direction of deposition of the monolayers appeared to have a slight effect upon the apparent index of refraction, the index for light incident at right angles to the dipping direction, $(n^s)'$, being about 0.002 higher than $(n^s)''$. Unfortunately a quantitative statement of the reliability of this difference, based as it is on only two experiments, cannot be made, but the result is believed to be qualitatively valid.

Optical Properties of Ba-Cu-H Stearate Double Layers on Stepped Multilayers

Ba-Cu-H stearate films were transferred to calibrated stepped Ba-Cu-H stearate reflectors at three different surface pressures and the optical con-

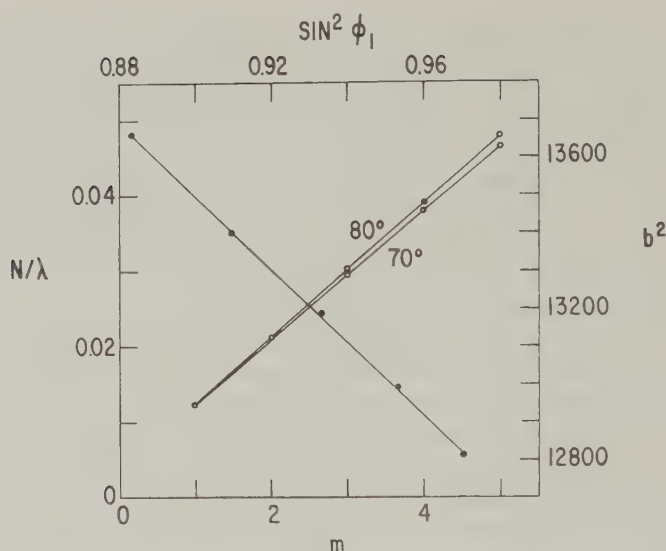


FIG. 3. Experimental data illustrating Hartman method of determining film thickness per monolayer and refractive index. Ba-Cu-H stearate multilayers on chromium. Open circles: N/λ as a function of m (text Eq. [2]) for angles of incidence 70° and 80° . Closed circles: b^2 ($\sin^2 \phi_1$), text Eq. [3], for angles of incidence 70.0° , 72.5° , 75.0° , 77.5° , and 80.0° .

TABLE I
Optical Properties of Ba-Cu-H Stearate Multilayers
(Hartman Method)
 $d = 49.50 \text{ \AA}$.

Incident beam at right angles to dipping direction $(n^s)'$	Incident beam in plane of dipping direction and surface normal $(n^s)''$
1.510	1.508

stants determined by Mattuck's method, using Mattuck's (3) equations 8-12. The results (Table II) show that the metrical thickness per double layer decreases with decreasing surface pressure, while the apparent refractive index increases. The slides were mounted for optical examination in the customary way with the dipping direction vertical and the plane of incidence horizontal. The limits of error given for these slides were calculated using Mattuck's (3) equation 35, where the standard deviations of the computed n and d values are stated in terms of the deviations of the fringes. The standard deviations of the s and p fringes were averaged over all the slides for this work and the values used in the computations were $\sigma_s = \sigma_p = \pm 1.3 \text{ \AA}$.

TABLE II
Optical Constants of Ba-Cu-H Stearate Films
 Dipping axis vertical, plane of incidence horizontal
 (Mattuck Method)

Slide no.	Transfer Pressure (dynes/cm.)	No. of double layers	d (Å.)	n
1	29	2	49.40 ± 2.5	1.512 ± 0.017
		6	49.18 ± 1.4	1.511 ± 0.010
2	16	4	47.89 ± 1.7	1.518 ± 0.014
3	9	4	45.16 ± 1.6	1.528 ± 0.014

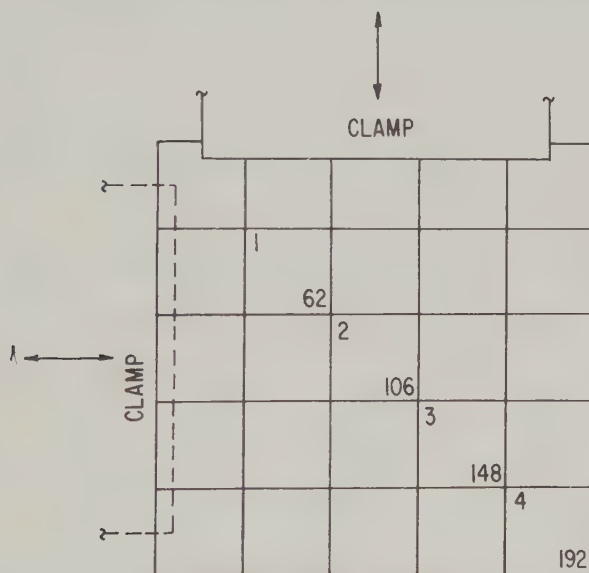


FIG. 4. "Checkerboard" multilayers, for study of s-ray fringes by Hartman method, formed by dipping in two directions at right angles. Left and right numbers in diagonal squares refer to fringe order and number of Ba-Cu-H stearate double layers, respectively.

Optical Properties of Ba-Cu-H Stearate Multilayers Transferred Symmetrically in Two Directions at Right Angles

The occurrence of directional effects with respect to the dipping axis suggested that in attempting to prepare homogeneous stepped reflectors for the Mattuck method it might be expedient to transfer the double layers alternately in two directions at right angles. A preliminary test was made by building the "checkerboard" slide illustrated in Fig. 4 in such a

way that the four s-ray orders in the diagonal squares were each composed of equal numbers of double layers dipped at right angles. With only four orders it proved impossible to measure n and d with an accuracy comparable to that of the values in Table I, but a comparison was made of the average apparent change of fringe wavelength when the checkerboard slide and the ordinary Hartman slide were rotated through 90° . The average shift for the regular Hartman slide was 9.8 Å., and for the checkerboard slide 2.7 Å.

Ba-Cu-H-Nonadecanoate Films

Preliminary measurements were made on transferred monolayers of this acid as a representative of the odd carbon series. The precision attainable was disappointing, as will be seen from the variation among the results given in Table III. Furthermore, considerable molecular rearrangement took place during two months following preparation of one of the multi-layer slides, the change being in the direction of denser packing approaching that which, for unknown reasons, was attained immediately after preparation of the multilayers on another occasion. In none of the results, however, is there any reliable indication of a directional variation of n^s ;

TABLE III
Apparent Optical Constants of Ba-Cu-H Nonadecanoate Films
Transfer pressure 29 dynes/cm.

Slide	Method	d (Å.)	n	$(n^s)'$	$(n^s)''$
—	Mattuck	56.1	1.487	—	—
I	Hartman	51.21	—	1.514	1.515
II	Hartman	53.91	—	1.470	1.470
II ^a	Hartman	52.53	—	1.491	1.491

^a remeasured two months later.

n = refractive index measured by Mattuck method.

$(n^s)'$ = refractive index for s-ray incident at 81° at right angles to monolayer transfer direction.

$(n^s)''$ = value for incidence parallel to dipping direction.

TABLE IV
Deposition Ratios

Film	Piston oil	Transfer Pressure (dynes/cm.)	Deposition ratio	Reference
BaH stearate	Oleic acid	29	0.99	Langmuir <i>et al.</i> (14)
BaCuH stearate	Oleic acid	29	0.99–1.00	This paper
BaH stearate	Castor oil	16	0.95–0.96	Schaefer (12)
BaCuH stearate	Tri- <i>m</i> -cresyl phosphate	9	0.96–0.97	This paper

such variation, if it exists, is probably substantially less than that found in the case of the corresponding stearate.

Deposition Ratios

The area of a Ba-Cu-H stearate monolayer consumed was compared with the slide area covered by dipping a number of chromium-plated slides simultaneously. The results obtained with two different film pressures are shown, with comparable values from the literature, in Table IV.

DISCUSSION

Blodgett and Langmuir (7) reported that built-up films of Ba-H stearate behave like positive uniaxial crystals with the optic axis perpendicular to the film. The directional properties of the *s*-ray reflection coefficients of our

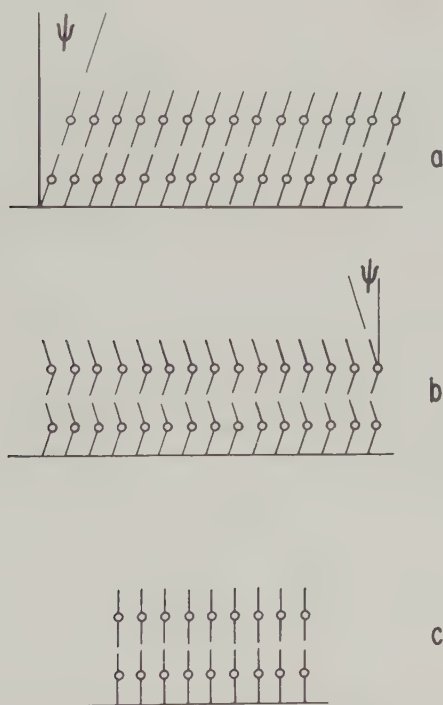


FIG. 5. Two hypothetical configurations of stearate molecules in monolayers transferred to a solid carrier. Straight lines represent hydrocarbon chains and circles represent interacting pairs of carboxyl groups and associated cations (H^+ , Cu^{++} , or Ba^{++}). In 5a the fully extended hydrocarbon chains in the double molecules are coaxial and tilted in the dipping direction at an angle ψ to the slide normal ("extended configuration"). In 5b the axial tilt is assumed to be constant with respect to the direction of motion of the slide during monolayer transfer ("herring-bone configuration"). Figure 5c illustrates the fact that in both configurations the long molecular axes are perpendicular to the slide in the transverse direction.

Ba-Cu-H stearate multilayers in relation to the direction of dipping (or the highly correlated direction of monolayer compression) (Table I) suggest that the angle between the optic axis and the slide normal, in the plane defined by the slide normal and the long axis of the slide, is different from 0° . This result would be obtained if the multilayers consisted of the traditional superimposed bimolecular sheets in which the common long axes of the double molecules had become tilted by the dipping process, as illustrated in Fig. 5a. Such a model for stearic acid has been proposed by Germer and Storks (15, 16), on the basis of electron diffraction data, and by Clark and Leppla (17). Since the molecular axes in such a multilayer would remain at right angles to the width of the slide, the refractive index for an incident *s*-ray parallel to the dipping direction would equal the ordinary uniaxial refractive index n_0 ; for an incident ray at right angles to the dipping direction it would be greater than n_0 . This corresponds to the result reported in Table I. However, such a film structure would be inconsistent with Blodgett and Langmuir's result, since the optic axis would be tilted at an angle ψ to the slide normal in the dipping direction. An alternative model will reduce the discrepancy; if alternate molecular layers were tilted equally in opposing directions, as the putative mechanism of the dipping process might suggest, there would result a crystal having its optic axis perpendicular to the slide but still showing directional variation of n^s . This, the "herring-bone" model, is illustrated in Fig. 5b.

It will be shown that both these structures—the "extended" and the "herring-bone"—provide satisfactory interpretation of the remaining results of this study (Table II).

The variation of refractive indices n^s and n^p with angle of tilt ψ can easily be calculated for two cases. (1) For rays incident in the plane of the slide normal and the short dimension of the slide; this will be referred to as "transverse incidence" and will always be designated by a prime, e.g., $(n^p)'$. (2) For rays incident in the plane of the slide normal and the long dimension, or the dipping direction; this will be called "longitudinal incidence," with two primes, e.g., $(n^p)''$. The nomenclature is illustrated in the conventional "indicatrix" diagram of Fig. 6.

Considering first the *s*-ray index $(n^s)'$ for transverse incidence, this is given by

$$[(n^s)']^2 = \frac{n_e^2 n_0^2 (1 + \tan^2 \psi)}{n_0^2 \tan^2 \psi + n_e^2} \quad [8]$$

and is independent of angle of incidence. Choice of values for n_0 and n_e is not easy; we shall use $n_0 = 1.51$ and $n_e = 1.56$, representing a compromise based upon several given by Blodgett and Langmuir (7). The difference $(n^s)' - (n^s)''$, equal to 0.002 (Table I), then corresponds to a molecular tilt of about 11° . The entire curve $[(n^s)'](\psi)$ is shown graphically in Fig. 7.

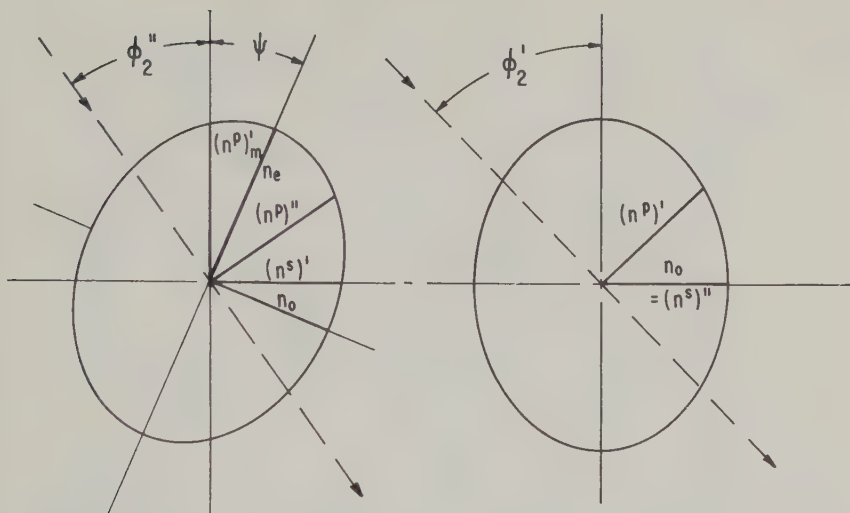


FIG. 6. Refractive index diagrams corresponding to the molecular configurations shown in Fig. 5a. The extraordinary index of refraction n_e is assumed to coincide with the direction of the long molecular axis. The symmetry is monoclinic but the simplifying assumption is made that there is a single ordinary index n_o . The indices of refraction for s- and p-rays passing through the film at angles of refraction ϕ_2 are indicated, a single prime referring to "transverse" rays (see text) and a double prime to "longitudinal" rays.

The behavior of $n^p(\psi)$ for transverse and longitudinal incidence is also illustrated in Fig. 7 for the single angle of incidence most frequently used in the present work; $\phi_1 = 81^\circ$. The pertinent equations, easily derived, are:

$$\frac{1}{[(n^p)'']^2} = \frac{\cos^2(\phi_2 + \psi)}{n_o^2} + \frac{\sin^2(\phi_2 + \psi)}{n_e^2}; \quad [9]$$

$$\frac{1}{[(n^p)']^2} = \frac{\cos(\phi_2 - 90^\circ)}{[(n^p)'_m]^2} + \frac{\sin^2(\phi_2 - 90^\circ)}{n_o^2}, \quad [10]$$

where the maximum refractive index for the p' ray, $(n^p)'_m$, is given by

$$\frac{1'}{[(n^p)'_m]^2} = \frac{\cos^2 \psi}{n_e^2} + \frac{\sin^2 \psi}{n_o^2}. \quad [11]$$

It will be noted that the curves for $(n^s)'$ and $(n^p)'$ are symmetrical about $\psi = 0$ so that they apply to the results of experiments involving incident and reflected rays, and also to both extended and herring-bone structures. The curve for $(n^p)''$, on the other hand, is antisymmetrical, and is applicable only to transmitted rays; for experiments involving reflection, the values must be averaged over $\pm\psi$. Thus observations in the two opposing longitudinal directions are not of much value in the study of molecular orientations.

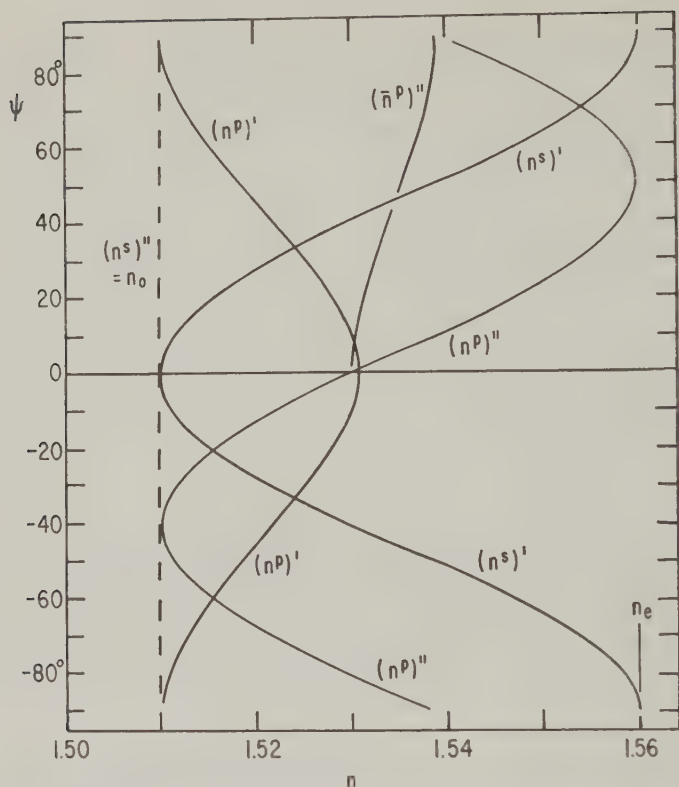


FIG. 7. Variation of multilayer refractive index with angle of tilt, ψ , of long molecular axis with respect to slide normal in dipping direction. See text equations [8] to [11]. The n^s indices apply to any angle of incidence. The n^p indices are calculated for an angle of incidence 81° . Single prime refers to "transverse" incidence and double prime to "longitudinal" incidence. Note that the curve for $(n^p)''$ applies only to a transmitted ray; for reflected rays the averaged values $(\bar{n}^p)''$ about $\pm\psi$ must be used.

Next, in order to determine whether the variation of apparent refractive index, n , of Ba-Cu-H stearate layers (determined by the Mattuck method—Table II) with monolayer transfer pressure can be explained in terms of variation of molecular tilt ψ , it is necessary to estimate values of $(n^p)'$ corresponding to the measured values n which were calculated on the assumption that the films are isotropic. Obviously, in absence of further information a given value of n is compatible with many pairs of values $(n^p)'$, $(n^s)'$, and the locus of these has been calculated by adapting Mattuck's (3) equation 43 in the form

$$\frac{1}{[(n^p)']^2}(\psi) = 1 - \frac{1.022}{n^2} \{[(n^s)']^2(\psi) - 1\}, \quad [12]$$

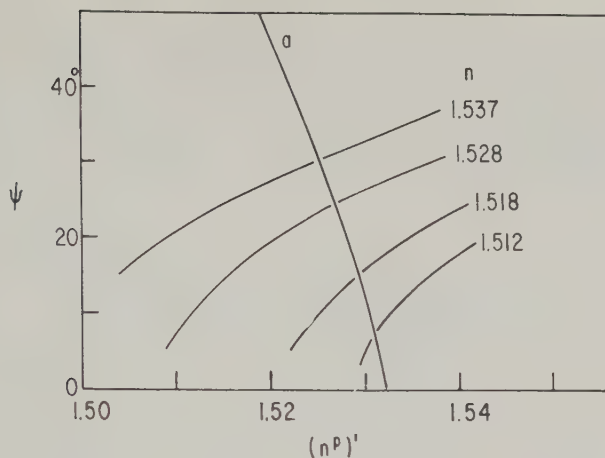


FIG. 8. Determination of angle of molecular tilt for Ba-Cu-H stearate layers from measurements of apparent index of refraction by the Mattuck method. Curve (a) shows $(n^p)'(\psi)$, taken from Fig. 7. Other curves show values of $(n^p)'(\psi)$ compatible with the values n measured by the Mattuck method, according to text equation [12].

where $[(n^p)'](\psi)$ is given by Eq. [8]. The simultaneous solution of [10] and [12] for the three values of n in Table II is shown in Fig. 8. The values of ψ are given in Table V and the relative thicknesses are compared with $d_0 \cos \psi$.

The calculated angles of tilt are clearly compatible with the measured thickness per double layer, d , because d and $d_0 \cos \psi$ are in close agreement. The functional dependence of molecular tilt upon transfer pressure F is very well represented by the equation $\psi F = 227 \text{ degree dyne cm.}^{-1}$. Furthermore, the small orientation effect, 0.002, observed when the s-ray refractive index of multilayers is measured by the Hartman method (Table I), is very close to that predicted with the aid of Fig. 7 from the molecular tilt, 7.3° , calculated by the Mattuck method for films transferred at the same surface pressure, 29 dynes/cm. (Table V).

It is of some interest to review earlier results from the present standpoint. We may adopt the value 48.84 Å. given by Müller (18) as the extended length of the stearic acid bimolecule. For the pure Ba soap, 51.0 Å. would seem a reasonable but rather uncertain value so that in built-up films consisting partly of the free acid the effective length might vary by some 2.2 Å. If there is about 57% soap under our experimental conditions, as the measurements of Langmuir and Schaefer (19) would suggest, the length would be 50.07 Å., in fair agreement with 49.8 Å. for d_0 given in Table V. However, the actual percentage of soap in the transferred layers is a matter of some uncertainty (20).

Hartman and co-workers (2) found for BaH stearate $(n^s)' = 1.508$, in

TABLE V

*Molecular Tilt in Monolayers Transferred at Different Surface Pressures*Assuming $n_0 = 1.510$, $n_e = 1.560$, $\phi_1 = 81^\circ$

Film	Transfer pressure, F (dynes/cm.)	$(n^p)'$	$(n^e)'$	ψ (deg.)	$F\psi$	d meas. (Å.)	$d_0 \cos \psi$	Ref.
BaCuH stearate	∞	—	—	0		—	49.8	This paper
	29	1.5308	1.5108	7.3	211.7	49.40	49.40	
	16	1.5292	1.5130	15.5	248.0	47.89	47.91	
	9	1.5266	1.5184	24.7	222.3	45.16	45.27	
Stearic acid	∞	—	—	0		—	48.84	Müller (18)
	29	1.5250	1.5226	30.3	878.7	41.9	42.17	Mattuck <i>et al.</i> (4)

fair agreement with our assumed value 1.510 for n_0 , and $d = 45.7$, which is too low, and perhaps attributable to the Schaefer "filling-in" phenomenon (12), which would make the effective number of complete double layers less than the number of dips. Mattuck, Petti, and Bateman (4) found $(n^p)' = 1.508$ by the Abelès method, corresponding to $\phi_1 = 56.45^\circ$, so that in this case $(n^p)'$ should be a little larger than n_0 . It is possible that our assumed value for n_0 , 1.51, is a little too high; Blodgett and Langmuir (7) found $n_0 = 1.491$. Using the Mattuck method, the same workers found $n = 1.486$ and $d = 49.3$; this result is difficult to interpret in the present terms and may have been due to unsymmetrical film transfer of the type already mentioned.

Stearic acid showed a very high apparent index, 1.537, with $d = 41.9$ Å. These values are both consistent with a molecular tilt of 30.3° (Table V), and it is of interest that the resulting thickness $d_0 \cos \psi$ is quite close to values of $c \sin \beta$ given by Schoon (21, 22) for two crystalline forms of stearic acid, viz., 43.85 and 39.85 Å. Other values have been given elsewhere (23–26). The value given by Mattuck and co-workers of $(n^p)'$ for stearic acid, 1.549, finds no ready explanation, because a value not very much greater than n_0 would be anticipated.

The tilting of molecules in films transferred at low pressures is perhaps most plausibly related to the transfer process itself, rather than to orientation on the liquid surface during compression, since the necessary slip between adjacent hydrocarbon chains would occur more readily under these circumstances. By the same token, the lower deposition ratios (Table IV) are comprehensible as associated with intermolecular slip, whereas stretching and slipping of a close-packed film with all residual interactions fully engaged would be much more difficult.

The present data demonstrate anew the high degree of molecular organization in stearate multilayers along the direction of the long molecular

axis. For convenience in presenting the results, the conventional idea of an equally well-developed lamellar organization, corresponding to preservation of the individuality of the parent monolayers, has also been adopted. In reality the data provide no direct evidence concerning lamellar structure and are equally compatible with the idea (27, 28) that considerable molecular rearrangement subsequent to monolayer transfer has resulted in formation of soap crystallites (which determine the dominant X-ray spacing) embedded in a matrix of stearic acid.

The data on Ba-Cu-H nonadecanoate films are consistent with the assumption that the molecular packing of the odd carbon acids tends to be looser than that in the even acids—an assumption which finds support in the well-known alternation of physical properties in the odd and even series (25) and in stereochemical considerations which suggest differences in carboxyl orientation relative to chain direction (26). Whether because of impurities or for intrinsic stereochemical reasons, the molecular packing is apparently initially rather loose, especially (as shown by the apparent thickness of 56.1 Å. and the low refractive index) in the first few transferred monolayers. In one instance considerable rearrangement has been observed, although the lack of directional variation shows that usually an average axial orientation very nearly normal to the slide is preserved. The values of d are compatible with this conclusion, except in the case of the Hartman slide *I*, where the apparent thickness 51.21 Å. is actually slightly less than might be calculated for pure nonadecanoic acid by adding 2.54 Å. to the length, 48.84 Å., of stearic acid, viz., 51.38 Å. In this instance the refractive index values suggest a molecular tilt of about 5° , increasing the length of the molecule to 52.30 Å. It is not obvious why in this instance the films should apparently be free of the Ba and Cu soaps, and the discrepancy may be due to film inhomogeneity, rendering the Hartman method inapplicable.

ACKNOWLEDGMENTS

We are happy to acknowledge the gift of a sample of nonadecanoic acid from Professor Hilton A. Smith of the University of Tennessee. Arthur L. Rosen has co-operated ably in some of the experimental work.

REFERENCES

1. FRANCIS, F., PIPER, H., AND MALKIN, T., *Proc. Roy. Soc. (London)* **128A**, 214-252, 1930.
2. HARTMAN, R. E., HARTMAN, R. S., LARSON, K., AND BATEMAN, J. B., *J. Opt. Soc. Amer.* **44**, 197-198, 1954.
3. MATTUCK, R. D., *J. Opt. Soc. Amer.* **46**, 621-628, 1956.
4. MATTUCK, R. D., PETTI, R. D., AND BATEMAN, J. B., *J. Opt. Soc. Amer.* **46**, 782-789, 1956.
5. FAUCHER, J. A., McMANUS, G. M., AND TRURNIT, H. J., *J. Opt. Soc. Amer.* **48**, 51-54, 1958.

6. LANGMUIR, I., AND SCHAEFER, V. J., *J. Franklin Inst.* **235**, 119-162, 1943.
7. BLODGETT, K. B., AND LANGMUIR, I., *Phys. Rev.* **51**, 964-982, 1937.
8. BLODGETT, K. B., *J. Phys. Chem.* **41**, 975-984, 1937.
9. LAMER, V. K., AND ROBBINS, M. L., *J. Phys. Chem.* **62**, 1291-1295, 1958.
10. ARCHER, R. J., AND LAMER, V. K., *Ann. N. Y. Acad. Sci.* **58**, 807-829, 1954.
11. ARCHER, R. J., AND LAMER, V. K., *J. Phys. Chem.* **59**, 200-208, 1955.
12. SCHAEFER, V. J., *J. Phys. Chem.* **45**, 681-701, 1942.
13. SOBOTKA, H., *J. Colloid. Sci.* **11**, 435-444, 1956.
14. LANGMUIR, I., SCHAEFER, V. J., AND SOBOTKA, H., *J. Am. Chem. Soc.* **59**, 1751-1759, 1937.
15. GERMER, L. H., AND STORKS, K. H., *J. Chem. Phys.* **6**, 280-293, 1938.
16. GERMER, L. H., AND STORKS, K. H., *Proc. Natl. Acad. Sci.* **23**, 390-397, 1937.
17. CLARK, G. L., AND LEPLA, P. W., *J. Chem. Soc.* **58**, 2199-2201, 1936.
18. MÜLLER, A., *Proc. Roy. Soc. (London)* **114A**, 542-561, 1927.
19. LANGMUIR, I., AND SCHAEFER, V. J., *J. Am. Chem. Soc.* **58**, 284-287, 1936.
20. SOBOTKA, H., DEMENY, M., AND CHANLEY, J. D., *J. Colloid. Sci.* **13**, 565-568, 1958.
21. SCHOON, T., *Z. physik. Chem.* **39B**, 385-410, 1938.
22. SCHOON, T., *Strukturber.* **6**, 238-240, 1938.
23. ABRAHAMSSON, S., AND VON SYDOW, E., *Acta Cryst.* **7**, 591-592, 1954.
24. VON SYDOW, E., *Acta Cryst.* **8**, 557-560, 1955.
25. DEUEL, H. J., JR., "The Lipids," Vol. 1. Interscience, New York, 1951.
26. VON SYDOW, E., *Arkiv Kemi* **9**, 231-254, 1956.
27. HOLLEY, C., *Phys. Rev.* **53**, 534-537, 1938.
28. BERNSTEIN, S., *J. Am. Chem. Soc.* **62**, 374-378, 1940.

INTERFACIAL PHENOMENA

By J. T. DAVIES, *Professor of Chemical Engineering and Director of the Department, University of Birmingham*

and SIR ERIC RIDEAL, *Former Professor of Colloid Science, University of Cambridge*

July 1961, 474 pp., \$14.00

This book satisfies the need for a unified, comprehensive account of the properties of surfaces and interfaces, including adsorption. It gives an up-to-date presentation of the fundamentals of the subject and a systematic account of recent research, including more than one thousand references. Many of the results and treatments presented have not been published before.

Chemists and physicists working on surface or colloidal phenomena, chemical engineers, and also biologists interested in the properties of the surfaces of living cells, will find this book of interest. The systematic manner of presentation makes the work suitable as a text in advanced courses, and the extensive coverage of recent research makes it highly useful for all engaged in research in this field.

The Physics of Surfaces
Electrostatic Phenomena
Electrokinetic Phenomena
Adsorption at Liquid Interfaces
Properties of Monolayers

Reactions at Liquid Surfaces
Diffusion through Interfaces
Disperse Systems and Adhesion
PRINCIPAL SYMBOLS
AUTHOR INDEX — SUBJECT INDEX.

Advances in CATALYSIS and Related Subjects

*Edited by D. D. ELEY, Nottingham, P. W. SELWOOD, Evanston, Illinois
and PAUL B. WEISZ, Paulsboro, New Jersey*

*Advisory Board: PETER J. DEBYE, Ithaca, New York, P. H. EMMETT, Baltimore,
W. JOST, Göttingen, E. K. RIDEAL, London
and H. S. TAYLOR, Princeton, New Jersey*

Volume 12

1960, 324 pp., \$11.00

The Wave Mechanics of the Surface Bond
in Chemisorption

By T. B. GRIMLEY, *University of
Liverpool*

Magnetic Resonance Techniques in
Catalytic Research

By D. E. O'REILLY, *Gulf Research &
Development Company, Pittsburgh,
Pennsylvania*

Base-Catalyzed Reactions of Hydrocarbons

By HERMAN PINES, *Northwestern
University, and LUKE A. SCHAAP,
Standard Oil Company,
Whiting, Indiana*

The Use of X-Ray K-Absorption Edges in the
Study of Catalytically Active Solids

By ROBERT A. VAN NORDSTRAND,
*Sinclair Research Laboratories, Inc.,
Harvey, Illinois*

The Electron Theory of Catalysis on
Semiconductors

By TH. WOLKENSTEIN, *University of
Moscow*

Molecular Specificity in Physical
Adsorption

By D. J. C. YATES, *University of
Cambridge*

AUTHOR INDEX — SUBJECT INDEX.



ACADEMIC PRESS, *New York and London*

111 Fifth Avenue, New York 3

17 Old Queen Street, London, S.W. 1

*Academic Press, Publishers
are pleased to announce*

Journal of Catalysis

Volume 1, Number 1, February, 1962

Editors:

J. H. DE BOER
Technological University of Delft

P. W. SELWOOD
Northwestern University

To be assisted by an editorial board of distinguished scientists,
to be announced shortly.

ARTICLES dealing with original studies in heterogeneous catalysis as well as homogeneous catalysts will be welcomed in this new periodical. Studies relating catalytic properties with chemical processes at surfaces, including the study of surfaces by various physical means will be included in the scope of this journal, as will molecular rate processes, studies of the chemistry of surfaces, and most emphatically also engineering studies related catalysis.

Volume 1 will consist of six issues to be released at bi-monthly intervals during 1962.

Manuscript should be sent to either of the editors:

PROFESSOR J. H. DE BOER
Laboratory of Chemical Engineering
Technological University of Delft
Julianalaan 136
Delft, The Netherlands

PROFESSOR P. W. SELWOOD
Department of Chemistry
Northwestern University
Evanston, Illinois
U. S. A.



ACADEMIC PRESS, *New York and London*

111 FIFTH AVENUE, NEW YORK 3, NEW YORK

17 OLD QUEEN STREET, LONDON, S.W.1

Protein Structure

By HAROLD A. SCHERAGA, *Cornell University, Ithaca, New York*

August 1961, 306 pp., \$8.00

The primary aim of this book is to present some of the quantitative aspects of the physicochemical approach to the protein structure problem, including gross and internal structure. In discussing gross structure, polymer principles have been applied. In considering the more detailed aspects of internal structure, attention has been directed to interactions between polar groups and nonpolar ones. The material is developed from first principles, assuming a background of elementary physical chemistry.

The book has evolved from a series of lectures given for C.S.I.R.O. in Melbourne, based on research carried out in the author's laboratory during the past decade. It will be of interest to all students and research workers engaged in the study of the structure of biological activity of proteins. It will also be of value to workers in other biological sciences in which the principles of protein structure and activity are of interest.

CONTENTS:

Hydrodynamic Properties of Protein Solutions
Internal Structure; Effect of Hydrogen Bonding
on Side-Chain Reactivity
Limited Proteolysis
Denaturation

Limited Proteolysis and Aggregation in the
Fibrinogen-Fibrin Conversion
Some Experimental Methods
Configurational Studies of Insulin, Lysozyme,
and Ribonuclease
REFERENCES—SUBJECT INDEX.

Protein Biosynthesis

*Proceedings of the Symposium held under the auspices of
U.N.E.S.C.O., at Wassenaar, August 29—September 2, 1960
Edited by R. J. C. HARRIS, Imperial Cancer Research Fund, London*

June 1961, 409 pp., \$14.00

Contents available upon request.

This international symposium was sponsored jointly by U.N.E.S.C.O., C.I.O.M.S., and the Netherlands Cancer Institute. This book includes not only the papers but also the major contributions to the discussion. It provides the first authoritative and complete account of progress in this rapidly expanding field.

The treatment is primarily biochemical. All major research groups in this field were represented. This volume will be useful not only to biochemists but also to those cytologists, biophysicists, and chemists who are interested in such topics as the function of nucleic acids, the structure of cytoplasm, the properties of ribosomes, the biosynthesis of viruses, and the synthesis of antibodies.

Amino Acids, Proteins and Cancer Biochemistry

*Papers presented at the JESSE P. GREENSTEIN MEMORIAL SYMPOSIUM, Division
of Biological Chemistry, American Chemical Society, September 16, 1959*

*Edited by JOHN T. EDSALL, Harvard University
Preface by SIDNEY W. FOX and JULIUS SCHULTZ*

1960, 244 pp., \$7.00

We believe that this book, which includes all of the papers given at the Symposium, will make an important contribution in portraying some of the

major current developments in amino acid and protein chemistry and in the biochemistry of cancer—the two great fields in which Greenstein's work was preeminent.”

—From the Preface

ACADEMIC PRESS, NEW YORK AND LONDON

111 FIFTH AVENUE, NEW YORK 3, N. Y.
17 OLD QUEEN STREET, LONDON S.W. 1



Radical Polymerization

By J. C. BEVINGTON

University of Birmingham, England

August 1961, 188 pp., 37s.6d./\$6.00

THIS BOOK IS DIRECTED not only to specialists but also to all who are interested in the reactions of free radicals. Others who will find it of value are those concerned with nonradical polymerizations, those whose chief interest lies in the structure of high polymers, and students already familiar with the general concepts of chain reactions and the fundamentals of radical chemistry, for whom it will serve as a bridge between standard textbooks and original papers.

Elaborate kinetic analysis is avoided; emphasis is placed rather on the relationships between the detailed mechanism of polymerization and the composition and structure of the resulting macromolecules. References to original papers are numerous; and include some as recent as mid-1960.

CONTENTS

General Introduction

Production of Radicals

Initiation of Polymerization

Growth Reactions

Transfer Reactions

Interaction of Radicals

Retardation and Inhibition

References

AUTHOR INDEX—SUBJECT INDEX.



ACADEMIC PRESS, LONDON AND NEW YORK

17 Old Queen Street
London, S.W.1, England

111 Fifth Avenue
New York 3, New York

DIFFUSION AND THE KINETICS OF ADSORPTION OF ALIPHATIC ACIDS AND ALCOHOLS AT THE WATER-AIR INTERFACE¹

Robert S. Hansen

*Institute for Atomic Research and Department of Chemistry, Iowa State University,
Ames, Iowa*

Received December 29, 1960, revised received March 27, 1961

ABSTRACT

Hansen and Wallace (1) and Defay and Hommelen (2) have recently published independent studies of the time-dependent surface tensions of aqueous solutions of aliphatic acids and alcohols. Whereas experimental results in systems studied by both sets of workers appear to be in reasonably close agreement, Hansen and Wallace interpreted their results in terms of a barrier-limited adsorption process, Defay and Hommelen in terms of a diffusion-limited process.

A treatment of adsorption kinetics is presented which takes explicit account of the diffusion process without presupposing the absence of an adsorption barrier, a new equation suitable for the treatment of experimental data is derived, and its utility is discussed. It is shown that available data point to a substantial depletion of the subsurface concentration at intermediate times and that the treatment of Hansen and Wallace, presupposing exclusive barrier limitation, cannot be correct. On the other hand, the initial proportionality of spreading pressure to time cannot be explained by an adsorption process limited exclusively by diffusion if it is supposed that the spreading pressure depends on the number of solute molecules in the surface layer in the same manner in the dynamic process and at equilibrium. Two hypotheses are advanced to account for the apparent barrier limitation at low times and diffusional limitation at intermediate times. First, the mechanism of transfer from subsurface to surface may be fast but not infinitely so (small barrier hypothesis). For the linear isotherm it is shown that this hypothesis leads to an adsorption proportional to time at low times, and to that given by diffusion theory with a time lag at long times. Reasons for expecting this behavior to be fairly general are given. Second, adsorption may be exclusively diffusion-controlled, but the concentration depletion near the surface contributes in the initial period of adsorption an effective spreading pressure $-nRT$, where n is the number of moles of solute per square centimeter in the surface layer. A model giving rise to this correction term is suggested and its plausibility discussed.

INTRODUCTION

Hansen and Wallace (1) and Defay and Hommelen (2, 3) have recently published extensive independent studies of the dependence of surface tension

¹ Contribution No. 979. Work was performed in the Ames Laboratory of the U. S. Atomic Energy Commission.

of aqueous solutions of aliphatic acids and alcohols (from 5 to 10 carbons) on concentration and time. In both cases measurements were made by the vibrating jet method. Heptanol-1 was the only solute studied by both sets of workers, and results of the two sets of workers at comparable concentrations appear to agree within experimental error. The qualitative variations of spreading pressure with time, concentration, and type of solute observed in the Brussels laboratory and in our own appear to be closely similar (remarkably so, considering that our treatment of vibrating jet data is quite different from theirs and in our opinion has a sounder basis (4)). Despite the basic agreement on experimental facts, Hansen and Wallace proposed a barrier-limited adsorption mechanism to explain their results, Defay and Hommelen a diffusion-limited adsorption mechanism. The present work compares these two points of view, examining the extent to which the available experimental evidence is capable of resolving between them. Incident to this comparison the kinetics of adsorption involving simultaneous diffusion and barrier limitations to adsorption rate are briefly treated, and a new equation particularly suited to analysis of such systems is presented. The assumptions basic to the inference of adsorption kinetics from observed dependence of spreading pressure on time are discussed as possible sources of a discrepancy between experiment and theory. Finally, two hypotheses are presented which appear to be capable of rationalizing the apparent barrier limitation to adsorption at short times, followed by diffusion limitation at long times.

THEORETICAL

Both Hansen and Wallace (1) and Defay and Hommelen (2)² assumed that for a given solute the spreading pressure depended only on the number of solute molecules in the surface layer, i.e., $\pi(t) = f\{n(t)\}$, where $\pi(t)$ is the spreading pressure at time t and $n(t)$ the number of solute moles/cm.² adsorbed. The form of f was determined by application of the Gibbs adsorption theorem to the dependence of spreading pressure on concentration at equilibrium to obtain $\pi(t \rightarrow \infty) = f\{n(t \rightarrow \infty)\}$. The number of solute moles adsorbed at any time could therefore be inferred from the observed spreading pressure at that time. If adsorption kinetics are diffusion controlled, subsurface and surface are presumed to be in equilibrium and the subsurface concentration $C(0, t)$ can also be inferred from the observed $\pi(t)$. In considering the possibility of a diffusion-limited adsorption mecha-

² However, Defay and Hommelen considered this assumption justified only if subsurface and surface were in equilibrium, i.e., if adsorption were diffusion limited. Defay has maintained that in general the boundary tension reflects both surface and subsurface composition; his views on this point have been set forth in *J. chim. phys.* **51**, 299 (1954).

nism both groups used the equation of Ward and Tordai (5)

$$n(t) = 2 \sqrt{\frac{D}{\pi}} \left\{ C_0 t^{1/2} - \int_0^t C(0, t - \tau) d\tau^{1/2} \right\}. \quad [1]$$

Hansen and Wallace evaluated the functions $n(t)$ and $C(0, t)$ from observed $\pi(t)$ as previously explained, calculated an apparent diffusion coefficient from Eq. [1], and compared it with the known diffusion coefficient of the solute. They found that the apparent diffusion coefficient increased with time and increased with concentration, but at all times and concentrations was less than the known diffusion coefficient of the solute. At low concentrations and low times calculated diffusion coefficients were less than correct diffusion coefficients by factors of ten or more; at high concentrations and long times calculated diffusion coefficients approached correct diffusion coefficients rather closely in some cases. Defay and Hommelen also chose this as one method for treatment of their data, but apparently much less extensively. Diffusion coefficients were calculated for a single (intermediate) time for a given rate curve, and for at most two rate curves per system. Defay and Hommelen, in a second method, plotted the surface tension against $t^{1/2}$ and observed that the slope of this plot was nearly zero at low times, curved rather sharply to a strongly negative value, then curved gently toward less negative values. They extrapolated that portion of the plot having a strongly negative slope to 72 dynes/cm. (this extrapolation of a curve was doubtless equivalent to and for precision should be described as the 72 dyne/cm. intercept of the tangent to the curve at its point of inflection), and proposed that the time corresponding to the intercept at 72 dynes/cm. should be given by Eq. [1] with $n(t) = 2 \times 10^{-10}$ moles/cm.², $D = 5 \times 10^{-6}$ cm.²/sec., and omitting the second term in the parentheses in Eq. [1] as corresponding to back diffusion from the surface not yet extensively developed at low surface coverages. The diffusion coefficient was selected as a suitable mean value for the substances considered (ranging from hexanol-1 to lauric acid) and the value of n was about $\frac{1}{3}$ that required for a saturated monolayer. Observed intercept times were greater than intercept times calculated in this manner by a nearly constant factor estimated from their Fig. 2 to be slightly greater than 3. Defay and Hommelen suggested that this discrepancy might well be accounted for by neglect of the back diffusion term in Eq. [1].

The treatment of Hansen and Wallace and the first treatment of Defay and Hommelen are in principle exact tests of the theory of diffusion-limited adsorption kinetics (subject to the previously mentioned assumptions involved in the inference of $n(t)$ and $C(0, t)$ from observed $\pi(t)$); the second treatment of Defay and Hommelen is an order of magnitude test (subject to the same assumptions) and estimation of its reliability does not appear

to be a very tractable theoretical problem. It cannot be said with confidence, for example, whether or not the threefold difference between observed and calculated intercept times should be considered significant evidence that factors other than diffusion influence the adsorption kinetics.

The basic differences in interpretations of very similar sets of data can be stated briefly as follows: Defay and Hommelen considered neither the initial zero slope of their plot of spreading pressure against $t^{1/2}$ nor the fact that their observed intercept time exceeded the calculated value threefold significant evidence of nondiffusional factors, whereas precisely similar considerations (spreading pressure initially proportional to t rather than to $t^{1/2}$, apparent diffusion coefficients considerably less than known solute diffusion coefficients) led Hansen and Wallace to abandon the diffusion-controlled mechanism.

The author has recently given a theoretical analysis of the functions $C(0, t)$, $n(t)$, and $\pi(t)$ for diffusion-controlled adsorption of solutes obeying the Langmuir adsorption isotherm (6). The function $\pi(t)$ should be linear in $t^{1/2}$ at low t , or should show an infinite slope initially if plotted against t , and it was pointed out that this behavior must be expected of all solute such that adsorption is proportional to concentration at sufficiently low concentration. This behavior does not seem to be found for any spreading pressure-time data obtained anywhere at sufficiently low times to permit reliable extrapolation to the origin. On the other hand, spreading pressure-time data are now available for solutes in which the time scales vary over 5 orders of magnitude; the rather close order of magnitude agreement between the observed and calculated intercept times of Defay and Hommelen makes the outright abandoning of the diffusion factor by Hansen and Wallace suspect. Further evidence in this direction is furnished by the good order of magnitude agreement between observed spreading pressures and those calculated from the asymptotic expression, valid at long times, derived by the author (6) for diffusion-controlled adsorption kinetics. The available evidence indicates that either the method of inferring $n(t)$ and $C(0, t)$ from observed $\pi(t)$ is incorrect at low times or else diffusion is initially not rate limiting. We shall return later to this method of inference, but for the time being we ask whether it is possible to prove from existing data whether diffusion plays a significant limiting role in the adsorption kinetics as adsorption proceeds even if it is not rate limiting. Equation [1] is not well suited for this purpose, and we shall therefore derive a more suitable test equation.

Consider a semi-infinite slab of solution with surface at $x = 0$, solution occupying the half space $x > 0$. Let $C(x, t)$ be the concentration of solution at position x and time t , C_0 the initial (uniform) concentration, D the solute diffusion coefficient, and $n(t)$ the moles solute adsorbed per unit area of surface. We suppose diffusion to obey Fick's law but do not suppose diffu-

sion to be necessarily rate limiting. In other words, we suppose that a barrier to surface entry may exist, and that $n(t)$ may not necessarily be in equilibrium with $C(0, t)$. Then where $C_{xx} = \partial^2 C / \partial x^2$, $C_t = \partial C / \partial t$, etc., the following boundary value problem is generated:

$$DC_{xx}(x, t) = C_t(x, t) \quad (x > 0, t > 0) \quad [2a]$$

$$C(x, 0) = C_0 \quad [2b]$$

$$\lim_{x \rightarrow \infty} C(x, t) = C_0 \quad [2c]$$

$$DC_x(0, t) = n_t(t), \quad [2d]$$

which becomes on application of the Laplace transformation (7) where $c(x, s)$ and $\nu(s)$ are the transforms of $C(x, t)$ and $n(t)$

$$Dc_{xx} = sc - C_0 \quad [3a]$$

$$\lim_{x \rightarrow \infty} c(x, s) = \frac{C_0}{s} \quad [3b]$$

$$Dc_x(0, s) = s\nu(s); \quad [3c]$$

therefore

$$c(x, s) = \frac{C_0}{s} - \left(\frac{s}{D}\right)^{1/2} \nu(s) e^{-(s/D)^{1/2} x}. \quad [3d]$$

There is not a standard inversion for $c(x, s)$, but for $x = 0$ we may write either

$$c(0, s) = \frac{C_0}{s} - \frac{s\nu}{\sqrt{sD}} \quad [4a]$$

or

$$\nu(s) = D^{1/2} \left\{ \frac{C_0}{s^{3/2}} - \frac{c(0, s)}{s^{1/2}} \right\}. \quad [4b]$$

Equation [4b] inverts directly to Eq. [1], but Eq. [4a] inverts to

$$C_0 - C(0, t) = \frac{2}{\sqrt{\pi D}} \int_0^t n_t(t - \tau) d\tau^{1/2}, \quad [5]$$

which is new and particularly useful for the present problem. Both Eq. [1] and Eq. [5] are valid whether or not an entry barrier exists; absence of such a barrier is assumed only when n in Eq. [1] or n_t in Eq. [5] is assumed to be in equilibrium with $C(0, t)$. From the standpoint of mechanism inference Eq. [5] permits calculation of $C(0, t)$ from observed $\pi(t)$, providing $\pi(t)$ can be related unambiguously to $n(t)$. Consistent with previously made assumptions, $\pi(t)$ would depend on $n(t)$ in the same manner as at equilib-

rium, so that $\pi(t)$ implies $n(t)$, $n_t(t)$ can be obtained by graphical differentiation, and the integral on the right side of Eq. [5] evaluated graphically. If $C(0, t)$ is less than C_0 at any time diffusion cannot be neglected entirely in analysis of the adsorption mechanism; a possible barrier mechanism would involve establishing a relation of the sort $n_t = F\{C(0, t), n(t)\}$ and rationalizing it mechanistically. Hansen and Wallace presented such an analysis ignoring the diffusion factor on bases previously discussed; their analysis can be correct only if $C(0, t) = C_0$ at all t .

Defay and Hommelen (8) consider the initial slope of the plot of π against $t^{1/2}$ to be low but probably not zero, and attribute the low initial slope to the fact that the longer chain aliphatic compounds most extensively studied have a very appreciable lateral interaction. Spreading pressure-concentration and surface excess-spreading pressure curves both have very appreciable positive curvatures initially and rather sigmoid shapes poorly represented by corresponding curves derived for Langmuir isotherms. It was therefore considered important to analyze spreading pressure-time data such that (1) accurate surface equation of state data were available for the water-solute system and (2) $n(t)$ could be extrapolated objectively to zero time. Frumkin (9) has presented such data for octanoic and decanoic acids, found his data to be well represented by

$$\pi = -A \log_{10} (1 - \theta) - a''\theta^2$$

$$BC = \frac{\theta}{1 - \theta} \times 10^{-2a''\theta}$$

with $n_m = A/2.303RT$, $\theta = n/n_m$, and has tabulated A and a'' for octanoic, decanoic, and dodecanoic acids. Spreading pressure-time data for octanoic acid at concentrations $0.74 \times 10^{-3} M$, $1.1 \times 10^{-3} M$, and $1.5 \times 10^{-3} M$ given by Hansen and Wallace, and for decanoic acid at concentration $0.47 \times 10^{-4} M$ given by Addison (10) satisfied the second criterion (a number of curves which had been previously thought to justify extrapolation of $\pi(t)$ curves to the origin did not permit unambiguous extrapolation of $n(t)$ curves to the origin for such just reasons as those suggested by Defay and Hommelen).

Raw spreading pressure-time data for the indicated solutes and concentrations were transformed point by point (i.e., without prior smoothing of data) to amount adsorbed-time data by means of Frumkin's equation of state. Smooth curves were drawn through the $n(t)$ data to obtain the functions $n(t)$, the functions $n(t)$ were differentiated graphically to obtain the functions $n_t(t)$, and the integral on the right side of Eq. [5] was evaluated graphically. Diffusion coefficients were calculated from Longworth's (11) empirical formula corrected to 20°C. to be $5.12 \times 10^{-6} \text{ cm.}^2/\text{sec.}$ for octanoic acid, $4.72 \times 10^{-6} \text{ cm.}^2/\text{sec.}$ for decanoic acid. Functions $C(0, t)$ were then

calculated by means of Eq. [5]. Uncertainties in rounding of the functions $n(t)$ and corresponding uncertainties in the graphical differentiation to obtain the functions $n_i(t)$ led to uncertainties in the value of the integral in Eq. [5] of about 30%.

In all cases $C(0, t)$ was found to be significantly less than C_0 in the intermediate time range. Calculated minimum values (uncertainty about 0.30) for $C(0, t)/C_0$ were 0.5, 0.0, 0.0, and 0.7 for the octanoic acid solutions of concentrations $0.74 \times 10^{-3} M$, $1.1 \times 10^{-3} M$, and $1.5 \times 10^{-3} M$ and for the decanoic acid solution of concentration $0.47 \times 10^{-4} M$. Diffusion therefore plays a significant role in limiting the rate of adsorption in these cases. Other systems and solutions of the above solutes at other concentrations studied in our laboratory and at Brussels appear to behave in a qualitatively similar manner, although the data were not susceptible to the above analysis because of the impossibility of extrapolating spreading pressure-time data to the origin objectively. It can be safely presumed from their similarity in qualitative behavior to the systems analyzed that diffusion plays a significant role in limiting adsorption in these systems also. The analysis of Hansen and Wallace ignores this factor, assuming $C(0, t) = C_0$ at all times. Therefore, it cannot be correct. It would be possible in principle to modify their analysis by re-expressing their kinetic mechanism $n_i = g\{C(0, t), n\}$, the forms of F and g differing only through the transition state activity coefficient which would then vary much less with spreading pressure than in the original analysis. Precision of the functions $C(0, t)$ obtained from Eq. [5] does not justify this modification with present data.

On the other hand $\lim_{t \rightarrow 0} C(0, t)/C_0 = 1$ for all four of the above sets of data, whereas a theory based solely on diffusion would require this limit to be zero. This discrepancy is a consequence of the linear variation of π with t rather than with $t^{1/2}$ at low times, a behavior which seems to be characteristic rather than exceptional.

These facts can be summarized as follows: if it is assumed that spreading pressures depend on amounts of solute adsorbed and on subsurface concentration in the same manner in dynamic and equilibrium systems, and if amounts of solute adsorbed and subsurface concentrations are inferred from observed spreading pressure-time data on this basis, then adsorption limited solely by diffusion fails to explain the initial linear variation of spreading pressure with time, but except for this initial behavior diffusion must play an important role in limiting the adsorption rate. The adsorption appears to be diffusion controlled except for an initial time lag; times required to reach any particular spreading pressure are always longer than would be expected if diffusion were the only limiting factor.

There appear to be two principal theoretical approaches to the rationalization of these facts. First, there may be a small barrier to surface entry, either in the form of a process for transfer of solute from subsurface to sur-

face whose rate is proportional to some power of $C(0, t)$ and whose rate constant is rather large, or in the form of a surface structure for the solvent which furnishes an initial barrier to entry but which becomes disorganized ("melted") after a small amount of solute has entered the surface. In either of these cases, diffusion will eventually become rate limiting, but will not be rate limiting initially. Second, adsorption may be diffusion-controlled at all times, but the dynamic spreading pressure may not depend on the number of solute molecules in the surface in the same manner as at equilibrium. There are two possible sources of a difference in dependence of spreading pressure on surface composition between equilibrium and dynamic systems: (1) the adsorbed molecules may be differently oriented; for instance they might be optimally oriented in the equilibrium system, randomly oriented in the dynamic system; (2) the diffusional concentration gradient in the dynamic system (not found in the equilibrium system) contributes to the observed spreading pressure. We shall examine briefly these theoretical approaches.

To discuss the first (small barrier) case we consider two modifications of Eq. [2d]:

$$DC_x(0, t) = n_t(t) = \left(\frac{dg}{dC} \right)_{C(0, t)} C_t(0, t) \quad [6a]$$

if diffusion controlled, and

$$DC_x(0, t) = h\{C(0, t), n\} \{g[C(0, t)] - n\} \quad [6b]$$

if barrier controlled, where $n = g(C)$ is the equilibrium adsorption isotherm. Equation [6b] would include the surface structure barrier case, with h for that case depending on n in such a way as to increase fairly rapidly with n . We ask to what extent the function $n(t)$ depends on which of the boundary conditions [6a] and [6b] is to be satisfied. We consider first the special case $g = MC$, $h = k/M$, which has been solved exactly for both cases by Sutherland (12) with the results

$$\frac{n(t)}{MC_0} = 1 - e^{Dt/M^2} \operatorname{erfc} \frac{\sqrt{Dt}}{M} \quad [7a]$$

if diffusion controlled,

$$\frac{n(t)}{MC_0} = 1 - \frac{\beta}{\beta - \alpha} e^{Dt\alpha^2} \operatorname{erfc} \alpha\sqrt{Dt} + \frac{\alpha}{\beta - \alpha} e^{Dt\beta^2} \operatorname{erfc} \beta\sqrt{Dt} \quad [7b]$$

if barrier limited, where

$$\alpha = \frac{k}{2D} - \left(\frac{k^2}{4D^2} - \frac{k}{MD} \right)^{1/2}; \quad \beta = \frac{k}{2D} + \left(\frac{k^2}{4D^2} - \frac{k}{MD} \right)^{1/2}$$

(Sutherland's formulas are equivalent to replacing k/MD in α and β by

k/MD^2 , and are incorrect in this respect). To compare the implications of Eqs. [7a] and [7b] consider the following limiting behaviors of $e^{x^2} \operatorname{erfc} x$:

$$e^{x^2} \operatorname{erfc} x = 1 - \frac{2}{\pi^{1/2}} x + x^2 - \frac{4}{3\pi^{1/2}} x^3 + \cdots \quad (x \text{ small}) \quad [8a]$$

$$= \frac{1}{\pi^{1/2} x} \left\{ 1 - \frac{1}{2x^2} + \frac{3}{4x^4} - \cdots \right\} \quad (x \text{ large}). \quad [8b]$$

Applying these formulas to Eqs. [7a] and [7b] we find: For small t

$$\frac{n(t)}{MC_0} = \frac{2}{M} \left(\frac{Dt}{\pi} \right)^{1/2} \left\{ 1 - \frac{(\pi Dt)^{1/2}}{2M} + \cdots \right\} \quad [9a]$$

if diffusion limited, and

$$\frac{n(t)}{MC_0} = \frac{kt}{M} \left\{ 1 - \frac{4kt^{1/2}}{3(\pi D)^{1/2}} + \cdots \right\} \quad [9b]$$

if barrier limited. For large t

$$\frac{n(t)}{MC_0} = 1 - \frac{M}{(\pi Dt)^{1/2}} \left(1 - \frac{M^2}{2Dt} + \cdots \right) \quad [10a]$$

if diffusion limited, and

$$\frac{n(t)}{MC_0} = 1 - \frac{M}{(\pi Dt)^{1/2}} \left(1 - \frac{M^2}{2Dt} + \frac{M}{kt} + \cdots \right) \quad [10b]$$

if barrier limited.

We note that diffusion-limited and barrier-limited mechanisms lead to a pronounced difference in the dependence of n on t at low t ; that $n(t)$ is proportional to $t^{1/2}$ at low t in the former case and to t^1 in the latter should be especially noted. The correspondence between Eqs. [10a] and [10b] at long times is on the other hand remarkable; coefficients of the $t^{-1/2}$ terms are identical (regardless of the magnitude of k), and the coefficients of the $t^{-3/2}$ terms will be substantially equal if $k \gg 2D/M$. The author's asymptotic expression for large t (6)

$$\frac{C(0, t)}{C_0} = 1 - \frac{\bar{n}}{C_0 \sqrt{\pi Dt}}, \quad t \text{ large} \quad [11]$$

(\bar{n} = equilibrium value of n) does not depend on any assumptions as to surface entry barrier or mechanism by which it is surmounted, and from the preceding example it may be inferred that parameters describing barrier and mechanism first appear in the coefficient of $t^{-3/2}$ in general. It is also possible to write Eq. [10b] in the form

$$\frac{n(t)}{MC_0} = 1 - \frac{M}{\sqrt{D(t - \tau)}} \left(1 - \frac{M^2}{2D(t - \tau)} + \cdots \right), \quad [12]$$

with $\tau = 2M/k$, which is identical in form with Eq. [10a], and corresponds to a diffusional behavior at long times with a time lag τ . This qualitative behavior accords well with experimental observation.

We consider next the possibility that the spreading pressure depends on surface composition in different manners in equilibrium and dynamic systems. If the rate of orientation of adsorbed molecules were markedly slower than the rate of entry, and if the boundary tension depended strongly on orientation, such a difference might be expected. Relevant experimental information is limited; the surface potential studies of Posner and Alexander (13) indicate that the rate of orientation is indeed considerably less than the rate of entry, but also indicate that the boundary tension does not change much during the orientation process. Further, at sufficiently low surface concentrations the spreading pressure should be approximately nRT regardless of orientation, and it is in the low coverage region where the discrepancy between experiment and theory is most pronounced. A slow orientation process therefore does not seem to provide a plausible explanation for the discrepancy.

A second source of a difference in dependence of spreading pressure on surface composition in equilibrium and dynamic systems is the diffusional concentration gradient existing in the latter system. A striking consequence of the existence of this gradient is apparent in the boundary value problem formulated by Eqs. [2]: the Gibbsian surface excess is zero for all finite time, in the sense that

$$\Gamma = \int_0^\infty \{C(x, t) - C_0\} dx + n(t) = 0 \quad [13]$$

by material balance. Hansen and Wallace referred to $n(t)$ as a surface excess (incorrect in terms of common usage), Defay and Hommelen referred to $n(t)$ as a surface concentration (correct), and both denoted it by Γ , an unfortunate notation.

Fordham (14) appears to be the first to suggest that the diffusional concentration gradient might be the source of a spreading pressure increment. Fordham presented a theory of this increment based on thermodynamic arguments. From a theoretical point of view Fordham's theory seems incorrect in neglecting the solvent completely in contemplated transfer processes; from a practical point of view his theory implies that the spreading pressure for a given n should be greater in a dynamic system than at equilibrium, and this is in the wrong direction to explain existing discrepancy between theory and experiment.

A conceptual picture of the spreading pressure measurement capable of rationalizing the discrepancy between observed and diffusion-theoretical dependence of surface tension on time is the following: the spreading pressure measurement sums the difference in spreading pressure due to a slab

of liquid of thickness dx and concentration $C(x, t)$ and a corresponding slab of liquid of bulk concentration C_0 over all x . For the cases of interest $C(x, t)$ and C_0 are always small; the spreading pressures due to these slabs should therefore be those for ideal films, $C(x, t) RT dx$ and $C_0 RT dx$. The total spreading pressure should therefore be

$$\pi_{\text{dyn}} = \pi(n) + RT \int_0^\infty [C(x, t) - C_0] dx \quad [14]$$

$$= \pi(n) - nRT, \quad [14a]$$

where $\pi(n)$ is the spreading pressure due to a surface concentration n at equilibrium as given by the surface equation of state. Now $\pi(n)$ must be capable of expression in virial form

$$\pi(n) = nRT + \alpha_2 n^2 + \alpha_3 n^3 + \dots \quad [15]$$

and therefore

$$\pi_{\text{dyn}} = \alpha_2 n^2 + \alpha_3 n^3 + \dots \quad [16]$$

and the effect of the concentration gradient has been to cancel the leading term in $\pi(n)$. If n varies as $C_0 t^{1/2}$ for low t , as required by diffusion theory, π_{dyn} will vary as $C_0^2 t$ at low t , as observed by Hansen and Wallace. Further, the coefficient of proportionality can be calculated from the equation of state, and agrees fairly well (within 30%) with the observed value for octanoic acid at low concentrations. Two reservations to this treatment are important, however. First, it is not at all clear that the conceptual picture on which it is based corresponds to spreading pressure measurement. Second, Eq. [14a] purports to apply for all finite time, whereas in the experiments under discussion the difference between π_{dyn} and $\pi(n)$ becomes small compared to nRT at easily observable times in many cases. This second difficulty arises from the semi-infinite slab model used in Eqs. [2]; use of a finite slab model will modify the nRT term in [14a] in such a way as to cause it to have the value nRT at times satisfying $\sqrt{Dt} \ll 1$, and the value 0 if $\sqrt{Dt} \gg 1$, where 1 is the thickness of the slab. The "persistence time" of the correction term is hence of the order $1^2/D$; in a representative vibrating jet experiment $1 = 5 \times 10^{-2}$ cm., $D = 5 \times 10^{-6}$ cm.²/sec., and the calculated "persistence time" of 500 sec. is long by a factor of about 10^4 .

ACKNOWLEDGMENTS

I am indebted to Prof. Raymond Defay for stimulating written discussion, and to Prof. Defay, Prof. F. P. Buff, Prof. K. Ruedenberg, Dr. J. R. Hommelen, Dr. E. L. Mackor, and Dr. A. J. B. Spaul for stimulating oral discussion. I am also indebted to the National Science Foundation for a Senior Postdoctoral Fellowship September, 1959 to September, 1960, in the course of which the preceding discussion occurred and a number of the ideas in this paper germinated.

REFERENCES

1. HANSEN, R. S., AND WALLACE, T. C., *J. Phys. Chem.* **63**, 1085 (1959).
2. DEFAY, R., AND HOMMELEN, J. R., *J. Colloid Sci.* **14**, 411 (1959).
3. DEFAY, R., AND HOMMELEN, J. R., *J. Colloid Sci.* **13**, 553 (1958).
4. HANSEN, R. S., PURCHASE, M. E., WALLACE, T. C., AND WOODY, R. W., *J. Phys. Chem.* **62**, 210 (1958).
5. WARD, A. F. H., AND TORDAI, L., *J. Chem. Phys.* **14**, 453 (1946).
6. HANSEN, R. S., *J. Phys. Chem.* **64**, 637 (1960).
7. CHURCHILL, R. V., "Modern Operational Mathematics in Engineering", Chapters 1, 2. McGraw-Hill, New York, (1944).
8. DEFAY, R., AND HOMMELEN, J. R., Private communication.
9. FRUMKIN, A., *Z. physik. Chem.* **116**, 466 (1925).
10. ADDISON, C. C., *J. Chem. Soc.* **1946**, 579.
11. LONGSWORTH, L. G., *J. Am. Chem. Soc.* **75**, 5705 (1953).
12. SUTHERLAND, K., *Australian J. Sci. Research A* **5**, 683 (1952).
13. POSNER, A. M., AND ALEXANDER, A. E., *Trans. Faraday Soc.* **45**, 651 (1949).
14. FORDHAM, S., *Trans. Faraday Soc.* **50**, 593 (1954).

DETERMINATION OF PARTICLE SIZE OF POLYSTYRENE LATEXES BY LIGHT SCATTERING¹

Gjuro Deželić and Josip P. Kratochvil²

Laboratory of Physical Chemistry, Faculty of Science, and Department of Applied Biochemistry, "Andrija Štampar" School of Public Health, Faculty of Medicine, University of Zagreb, Zagreb, Croatia, Yugoslavia

Received January 23, 1961; revised March 27, 1961

ABSTRACT

An extensive and more complete study of light scattering of three BASF and eight Dow polystyrene latexes was undertaken. The measurements were performed at four wavelengths of the mercury arc, and theoretical functions, published in a foregoing paper, were applied. Five different methods of determination of particle size by light scattering were used: transmission, scattering at 90°, dissymmetry, polarization ratio, and positions of maxima and minima in angular distribution. The results are in good agreement with earlier data obtained on some of the latexes investigated in this work. It was found that the particle sizes are generally smaller than those obtained by electron microscopy. Any definitive explanation of this behavior could not be found.

INTRODUCTION

Monodisperse polystyrene latexes (1) are very convenient systems for investigation by light scattering. Because of their spherical shape the Mie theory of scattering by spheres (2) can be applied very successfully.

During the last decade a number of papers have appeared in that field. The size of a latex was determined from the angular position of the first minimum of intensity of scattered light by Dandliker (3). Alfrey *et al.* (4) measured the dissymmetries of three polyvinyltoluene latexes of medium size and tried to determine their diameters in terms of the Rayleigh-Gans theory. The same theory was also applied to the determination of latex diameters from dissymmetry by Burnett *et al.* (5) for a polydisperse polystyrene latex, and by Rosik and Vilim (6) for a number of monodisperse polystyrene latexes prepared by the authors themselves. A monodisperse latex from lower size range was investigated by Goring *et al.* (7) and Sokol (8) mainly for the purpose of calibrating light-scattering instruments. La Mer and Plesner (9) investigated the higher order Tyndall spectra, and

¹ Contribution No. 92 from the Laboratory of Physical Chemistry (P.O. Box 131, Zagreb, Yugoslavia).

² Present address: Clarkson College of Technology, Potsdam, New York.

Kerker (10) evaluated their results in terms of the Mie theory. The most extensive theoretical and experimental work was done by Heller and co-workers (11–17). Their results include calculations of Mie functions and experimental studies of latex density, refractive index, specific turbidity, and scattering at 90° . Bateman *et al.* (18) used transmission data to evaluate particle size and concentration. Recently Kerker and Matijević (19) compared polarization ratios and dissymmetries of four monodisperse polystyrene latexes with the Mie theory.

In our work we have tried to expand these earlier investigations to cover a wider range of particle sizes and several refractive indices for various wavelengths in order to obtain a clearer idea of the light scattering of latexes and of the general applicability of the Mie theory to spherical particles. Our investigations include measurements of transmission, scattering at 90° , dissymmetry, polarization ratio, and angular positions of maxima and minima of intensity of scattered light, all at several wavelengths.

EXPERIMENTAL

Materials

The measurements were performed on polystyrene latexes obtained from the Dow Chemical Company, Midland, Michigan, and the Badische Anilin- & Soda-Fabrik AG., Ludwigshafen a. Rhein, Germany. Table I lists data supplied by the producers for these samples. For definitions of tabulated quantities see a preceding publication (20). The samples contained about 1 % of solid for BASF and 10 % for Dow latexes. A relatively low concentration and limited quantity of BASF latexes prevented more detailed study. BASF latexes were old and rather aggregated (this could arise from the decreased latex stability generally occurring with dilution). This source of trouble was at least partially avoided by centrifugation and filtration through Millipore HA filters. The amount of aggregates in concentrated Dow latexes is negligible (3) and to avoid aggregation during the experimentation all measurements were carried out within a short time after dilution. The usual technique was as follows: the samples were diluted to a 0.5 % solution, and centrifugation at 400 *g*, sufficient to remove possible aggregates (12), was undertaken. The concentration of these centrifuged samples was determined gravimetrically by evaporation and drying in vacuum over P_2O_5 at $100^\circ C$. Dilutions were made volumetrically using a recalibrated burette and volumetric flasks. All glassware was rinsed with water redistilled from a special apparatus constructed to obtain water as dust-free as possible. A similar apparatus is described in the literature (21).

Transmission Measurements

Turbidity was measured by means of a Beckman Model DU spectrophotometer with a specially built attachment. This device is described

TABLE I
Standard Polystyrene Latexes

Sample	BASF-latexes		m_w/m_n
	$D_n(m\mu)$	$D_w(m\mu)$	
1	35	37	1.21
2	42	47	1.33
3	68	72	1.17

Sample	Dow-latexes		$s (m\mu)$
	$\bar{D} (m\mu)$	$s (m\mu)$	
LS-040-A	88	8	
15N-23	138	6	
LS-055-A	188	8	
LS-057-A	264	6	
LS-061-A	365	8	
LS-063-A	557	11	
LS-066-A	814	10	
LS-067-A	1171	13	

\bar{D} —arithmetic mean average diameter.

D_n —number-average diameter.

D_w —weight-average diameter.

s —standard deviation of a measurement.

m_w/m_n —polydispersity ratio.

in detail elsewhere (22) and closely resembles the construction of Bateman *et al.* (18). In this way the errors due to multiple scattering, corona effects, and stray reflections (13) are eliminated. Values of τ/c were practically independent of the concentration—a finding in agreement with the results of other authors (12, 18). Here τ denotes turbidity, and c concentration in grams per gram of solution. Cells with 10 cm. path length were used and the cell walls were blackened. The cells were matched before each series of measurements.

Angular Scattering

For angular light-scattering measurements an Oster-Aminco light-scattering photometer (23) was used. The measurements were performed as described previously (24), but some improvements in the electric circuit were undertaken (25). The microammeter originally attached to the apparatus was replaced with a spot galvanometer (manufactured by Norma, Vienna, Austria) of greater sensitivity. This instrument also allows a stepwise variation of sensitivity by means of a built-in Ayrton shunt. To obtain fine zero adjustment a combination of a variable 20 $k\Omega$ resistor in series with a 10 $k\Omega$ resistor was inserted in parallel to the 100 Ω Helipot.

Calibration of the electrometer tube was carried out by putting known

voltages on the grid of the tube by means of a precise potentiometer. The linearity was good in the first third of the scale, but at the full deflection of the galvanometer deviations over 5% were observed. The meter multiplier resistors were calibrated by comparing the galvanometer deflections for two successive resistors at constant sensitivity of apparatus.

The differences in sensitivity of the 1P21 photomultiplier tubes to horizontally and vertically polarized light were determined. The polaroids were carefully adjusted. The I_H'/I_V' ratios depended on wavelength and varied from tube to tube. Here is an example:

$\lambda_0(\text{m}\mu)$	578	546	436	405
I_H'/I_V'	1.101	1.080	1.045	0.933

where I_H' and I_V' are galvanometer readings for horizontally and vertically polarized light, respectively. These ratios are correction factors by which the measured polarization ratios should be divided.

For measuring intensity at 90° , dissymmetry and polarization ratio semioctagonal cells by Hellma GMBH, Müllheim/Baden, Germany, were used. Cylindrical cells by Aminco, Silver Spring, Maryland, were used for obtaining angular scattering diagrams.

The cells were cleaned in an apparatus according to Thurmond (26).

RESULTS

The density and refractive index of polystyrene latex particles are known. Heller and Pugh (14, 15) made extensive studies and found for the density of particles a value $\rho_2 = 1.057 \pm 0.002 \text{ g.cm.}^{-3}$. For the refractive index they obtained $n = 1.602 \pm 0.008$ at $\lambda_0 = 546.1 \text{ m}\mu$ and 25°C . For water suspensions at 25°C , this makes $\rho_2/\rho_1 = 1.060$ and $m = 1.200$ at $\lambda_0 = 546.1 \text{ m}\mu$, with last figures uncertain to ± 1 . Here ρ_1 and ρ_2 are the densities of the solution and of the particles, respectively, and m is the relative refractive index ($m = n/n_0$, where n is the refractive index of the particle and n_0 the refractive index of the surrounding medium).

To calculate the refractive indices at other wavelengths we used the formula of Bateman *et al.* (18)

$$n = 1.5683 + \frac{1.0087 \times 10^{-10}}{\lambda_0^2}, \quad [1]$$

where λ_0 is the wavelength of light in vacuum in centimeters. We obtained the following values of m for the four wavelengths of the mercury arc (uncertainty in last figure ± 1):

$\lambda_0(\text{m}\mu)$	578.0	546.1	435.8	404.7
m	1.199	1.200	1.210	1.214

These values are used for computing theoretical functions, necessary for evaluating the experimental data. The theoretical functions computed are published separately (27).

Transmission Measurements

The results of transmission measurements agree very well with those of previous authors (12, 18). Generally, the dependence of τ/c on concentration could be neglected. Only for the lowest sizes of latex particles a remarkable increase of specific turbidity with concentration could be noted. In all cases, however, the second virial coefficient A_2 was positive and of a finite value, although it was determined with a rather great experimental error (because of the very small value of the slopes of c/τ vs. c plots). The standard coefficients of variation of $(\tau/c)_0$ values (and also $(c/\tau)_0$ values) were not higher than $\pm 2\%$. In comparing $(c/\tau)_0$ values taken as mean values of c/τ with $(c/\tau)_0$ values obtained by the method of least squares, we obtained relative differences Δ of about 1%, i.e., the error in neglecting the concentration dependence of specific turbidities was smaller than the experimental error. Only for the smallest latex LS-040-A Δ was greater than the experimental error. The relative differences for particle diameters Δ' , obtained in the same way as Δ , are still smaller, except for the latexes LS-066-A and LS-067-A, whose specific turbidities lie on the flat part of the $(\tau/c)_0$ vs. α curve (Fig. 1). The values of A_2 , Δ , and Δ' for Dow latexes are presented in Table II.

The evaluation of particle sizes was done using arithmetic means of τ/c , obtained at various concentrations. For comparison with the theoretical values of $(\tau/c)_0$ the experimental values must be standardized (11, 24, 27). Here index s denotes the standard value.³

$$(\tau/c)_{0,s} = (\tau/c)_0 \cdot (\rho_2/\rho_1) \cdot (\lambda/\lambda_s). \quad [2]$$

From these standard values and a theoretical $(\tau/c)_0$ vs. α curve of proper m it is possible to obtain values of α . Here α is the relative particle diameter ($\alpha = \pi D/\lambda$). Figure 1 shows our results for $\lambda_0 = 546.1 \mu$. The full curve is theoretical; the circles are experimental $(\tau/c)_{0,s}$ values using the diameters from electron microscopy. The results at other wavelengths showed the same pattern. In Fig. 2 the region of smaller particle sizes is augmented. Table III lists the results of transmission measurements.

The electron microscopic data represent weight-average diameters for BASF latexes and arithmetic mean average diameters for Dow latexes. The difference between the weight-average and arithmetic mean average diameters, calculated for several samples from histograms obtained by

³ It should be noted that the expression given in reference 11, p. 503, and used in our previous paper (24) (Eqs. [17] and [21]) must be replaced by the above correct expression, since in the definition of specific quantities λ instead of λ_0 is used.

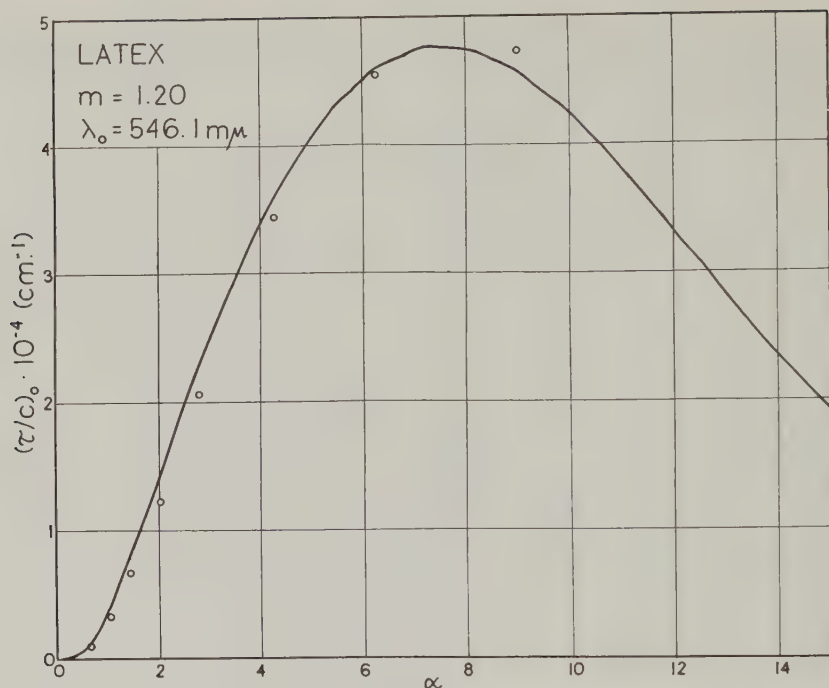


FIG. 1. Specific turbidity versus relative diameter. Curve is obtained from Mie theory for $\rho_1 = \rho_2$, $\lambda_0 = 546.1 \text{ m}\mu$, and $m = 1.20$; circles are experimental standardized values measured at the same wavelength.

TABLE II

Second Virial Coefficients A_2 and Relative Differences for $(c/\tau)_0$ and D Values

Dow latexes

The relative differences are between values obtained from arithmetic means and those obtained by the method of least squares. The differences are Δ for $(c/\tau)_0$ and Δ' for D . Transmission measurements at $\lambda_0 = 546.1 \text{ m}\mu$.

Sample	$A_2 \times 10^7$	$\Delta\%$	$\Delta'\%$
LS-040-A	12.5	3.1	0.88
15N-23	10.7	1.22	0.65
LS-055-A	1.72	0.62	0.25
LS-057-A	3.12	0.81	0.56
LS-061-A	4.65	1.17	1.00
LS-063-A	3.89	1.62	1.32
LS-066-A	5.42	0.41	0.59
LS-067-A	2.28	1.34	-1.63

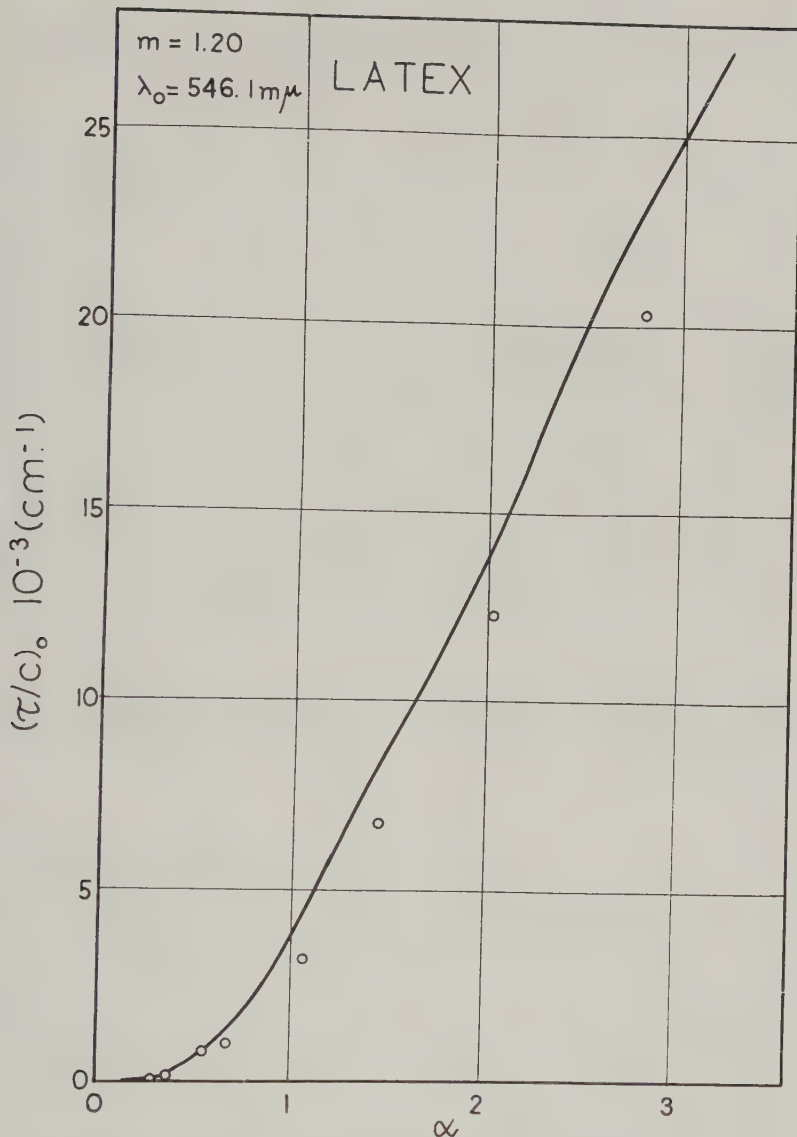


FIG. 2. Specific turbidity versus relative diameter. The conditions are the same as in the case of Fig. 1; the region of smaller particle sizes is augmented.

electron microscopy and estimated for other samples assuming the same type of distribution, has a value of 0.8 % for LS-040-A sample and decreases continuously amounting to 0.1 % in the case of LS-066-A and LS-067-A samples. This shows a good monodispersity of Dow latexes and allows comparison of light scattering and electron microscopic diameters.

TABLE III
Specific Turbidities $(\tau/c)_0$ and Particle Diameters D ($m\mu$) Obtained from Transmission Measurements

Sample	$\lambda_0(m\mu)$							
	578		546		436		405	
	$(\tau/c)_0 \times 10^{-3}$ ($cm.^{-1}$)	D ($m\mu$)	$(\tau/c)_0 \times 10^{-3}$ ($cm.^{-1}$)	D ($m\mu$)	$(\tau/c)_0 \times 10^{-3}$ ($cm.^{-1}$)	D ($m\mu$)	$(\tau/c)_0 \times 10^{-3}$ ($cm.^{-1}$)	D ($m\mu$)
BASF 1	0.0446	30.4	0.0556	30.6	0.1441	29.8	0.203	30.1
BASF 2	0.1235	42.8	0.1532	43.0	0.425	41.8	0.601	41.4
BASF 3	0.662	73.2	0.787	71.6	1.590	66.2	2.04	65.0
Dow LS-040-A	0.692	77.0	0.877	76.5	2.24	75.4	3.08	75.0
Dow 15N-23	2.42	120	3.01	120	7.10	119	9.40	119
Dow LS-055-A	5.25	166	6.35	168	13.00	167	16.43	167
Dow LS-057-A	9.90	240	11.59	241	23.6	241	29.6	239
Dow LS-061-A	16.66	330	19.16	328	34.8	330	42.7	329
Dow LS-063-A	28.8	528	32.5	526	52.6	520	61.0	514
Dow-LS-066-A	38.9	783	42.9	799	59.3	785	64.1	768
Dow LS-067-A	40.3	1260	42.5	1200	44.0	1143	41.1	1137

It must be noted that the weight average is valid only for specific turbidities and specific intensities in the Rayleigh region. For greater particle sizes and other light-scattering functions there are different types of averages (28).

Angular Scattering

The specific intensities $(I_{90}/I_{0c})_0$ can be determined experimentally by means of the expression $(I_{90}/I_{0c})_0 = C (I'_{90}/c)_0$, where C is the instrument constant (24) and I'_{90} is the galvanometer reading of light scattered at 90° . The instrument was calibrated with Ludox (24) using the method of Maron and Lou (29).

The measurements were performed at two solid angles, which could be changed by inserting two different receiver nosepieces with appropriate rectangular stops. The stops were 1.5×2.8 mm. and 0.5×2.8 mm., and the planar angles ω (defined as in reference 16, Fig. 1; they are a simpler measure of solid angles) 1.23° and 0.42° , respectively.

The feature of the (I_{90}/I_{0c}) vs. c plots for both ω was the same as found by Tabibian and Heller (16), although better agreement was obtained for $\omega = 0.42^\circ$. The error of the extrapolated $(I_{90}/I_{0c})_0$ values depended on the particle size and on the curvature of the plots. The average error amounted to about 4% and did not exceed 7%.

As in the case of specific turbidities, the experimental specific intensities

$(I_{90}/I_{0c})_0$ must be standardized for comparison with the theoretical values, using the expression

$$(I_{90}/I_{0c})_{0,s} = (I_{90}/I_{0c})_0 \cdot (\rho_2/\rho_1) \cdot (\lambda/\lambda_s). \quad [3]$$

Figure 3 is a graphical representation of our results for $\omega = 1.23^\circ$ at $\lambda_0 = 546.1 \text{ m}\mu$. The solid curve is theoretical; the circles are experimental results. Tables IV and V summarize all data obtained by the method of scattering at 90° .

Dissymmetry Measurements

Dissymmetries $z = I'_{45}/I'_{135} = i_{135}/i_{45}$ with unpolarized incident light were measured. Here the subscripts of the experimental relative intensities I' and theoretical intensities i mean the scattering angle θ and γ , respectively. Here γ is defined as the angle between the direction of observation and the reverse direction of the primary beam. Between γ and θ exists the relation $\theta = 180^\circ - \gamma$. The intensity $i_\gamma = (i_1 + i_2)_\gamma/2$ follows from the Mie theory and is defined as usually (19, 30).

To eliminate the influence of the multiple scattering, the values extrapolated to zero concentration were used and compared with the theory. As a first approximation linear extrapolations were made.

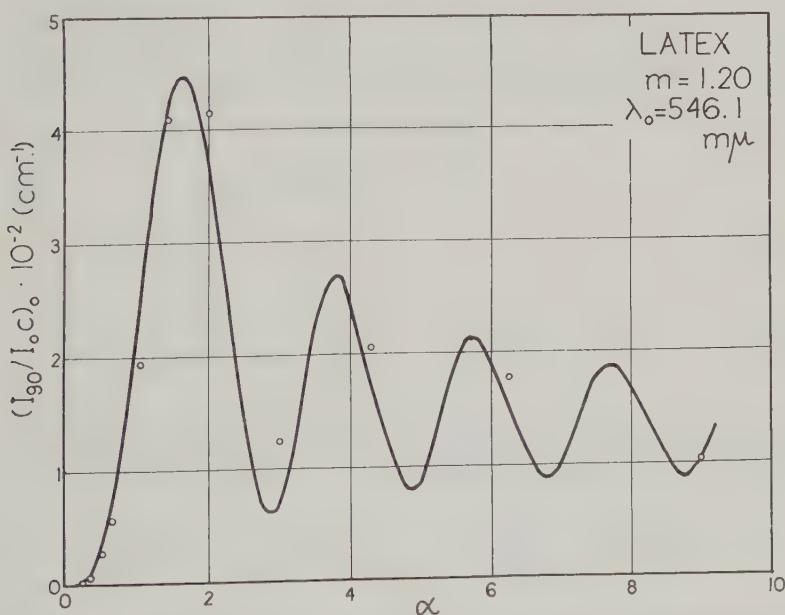


FIG. 3. Specific intensity at 90° versus relative diameter. Curve is obtained from Mie theory for $\rho_1 = \rho_2$, $\lambda_0 = 546.1 \text{ m}\mu$, and $m = 1.20$; circles are experimental standardized values measured at the same wavelength ($\omega = 1.23^\circ$).

TABLE IV
Specific Intensities $(I_{90}/I_0)_0$ and Particle Diameters D ($m\mu$) from
Scattering at 90° ; $\omega = 1.23^\circ$

Sample	$\lambda_0(m\mu)$							
	578		546		436		405	
	$(I_{90}/I_0)_0 \times 10^{-2}$ (cm^{-1})	D ($m\mu$)	$(I_{90}/I_0)_0 \times 10^{-2}$ (cm^{-1})	D ($m\mu$)	$(I_{90}/I_0)_0 \times 10^{-2}$ (cm^{-1})	D ($m\mu$)	$(I_{90}/I_0)_0 \times 10^{-2}$ (cm^{-1})	D ($m\mu$)
BASF 1	0.0200	26.9	0.0268	28.0	0.0796	29.2	0.1298	30.0
BASF 2	0.0718	42.9	0.0915	42.4	0.250	42.0	0.379	42.4
BASF 3	0.202	59.0	0.254	58.5	0.624	56.4	0.865	57.3
Dow LS-040-A	0.407	69.6	0.535	76.1	1.32	72.5	1.86	74.9
Dow 15N-23	1.43	121	1.82	122	4.06	120	4.43	110
Dow LS-055-A	3.18	182	3.87	174	6.16	171	4.90	199
Dow LS-057-A	3.64	256	3.92	240	2.66	244	1.16	257
Dow LS-061-A	1.44	330	1.17	338	2.23	342	2.95	322
Dow LS-063-A	2.07	541	1.96	554	1.76	535	2.02	498
Dow LS-066-A	1.78	816	1.67	792	2.26	820	1.72	802
Dow LS-067-A	1.14	1140	0.980	1171	1.92	—	1.82	—

Dissymmetries, especially the higher values, are strongly affected by the reflections on the glass walls of the cell. A reflection correction as given by Oth *et al.* (31) and modified by Sedláček (32) was applied to measured dissymmetries:

$$z_{\text{corr.}} = \frac{z - 1 + C_0}{1 - (1 - C_0)z}, \quad [4]$$

with

$$C_0 = 1$$

$$- \left(\frac{n_{21} - 1}{n_{21} + 1} \right)^2 + \left(\frac{n_{32} - 1}{n_{32} + 1} \right)^2 \left[1 - \left(\frac{n_{21} - 1}{n_{21} + 1} \right)^2 \right] \left[1 - \left(\frac{n_{12} - 1}{n_{12} + 1} \right)^2 \right]. \quad [5]$$

Here n is the refractive index and the subscripts 1, 2, and 3 refer to the solution, glass, and air, respectively. In our case for the semioctagonal cells and water solutions we had the following C_0 values:

$\lambda_0(m\mu)$	578	546	436	405
C_0	0.9612	0.9608	0.9601	0.9598

The application of this correction, based on Fresnel's reflection formulas, is of the utmost importance in the case of higher dissymmetries. For example, if the measured apparent dissymmetry at $\lambda_0 = 546 m\mu$ is $z = 15.0$, the corrected value would be $z_{\text{corr.}} = 36.3$, i.e., the real dissymmetry is

TABLE V

Specific Intensities $(I_{90}/I_{0c})_0$ and Particle Diameters D ($m\mu$) from Scattering at 90° ;
 $\omega = 0.42^\circ$

Sample	λ_0 ($m\mu$)			
	546		436	
	$(I_{90}/I_{0c})_0$ $\times 10^{-2}$ (cm^{-1})	D ($m\mu$)	$(I_{90}/I_{0c})_0$ $\times 10^{-2}$ (cm^{-1})	D ($m\mu$)
Dow LS-040 A	0.479	73.6	1.39	74.5
Dow 15N-23	1.74	120	3.98	119
Dow LS-055-A	3.40	167	5.74	185
Dow LS-057-A	3.87	242	3.00	239
Dow LS-061-A	1.02	336	2.20	340
Dow LS-063-A	2.12	530	1.98	544
Dow LS-066-A	1.70	791	2.23	823
Dow LS-067-A	1.10	1180	1.54	—

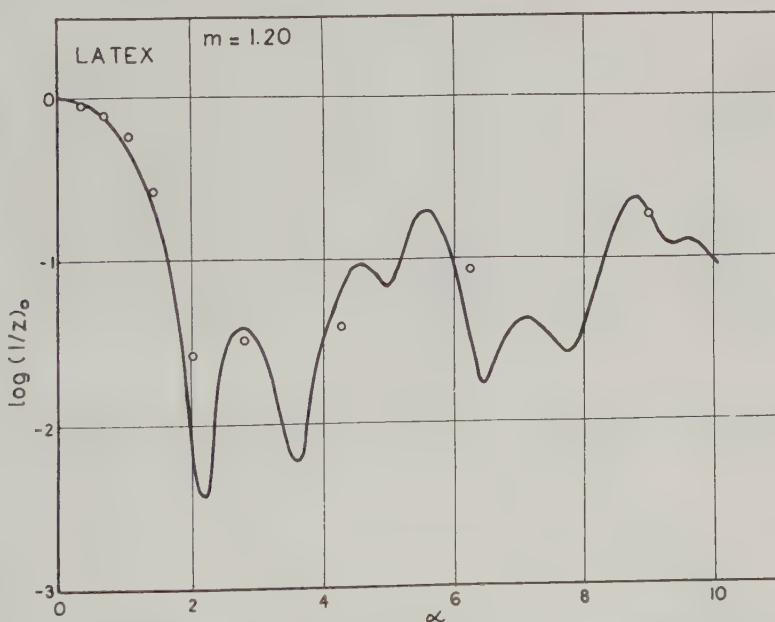


FIG. 4. Logarithm of the function of dissymmetry versus relative diameter. Curve is obtained from Mie theory for $m = 1.20$; circles are experimental values measured at $\lambda_0 = 546.1 m\mu$ ($\omega = 1.23^\circ$).

more than twice that of the measured one. For extremely great values of z this correction falls out since the function at $z = 1/(1 - C_0)$ becomes infinite (in the above case at $z = 25.5$). Our results showed a good agreement with other light-scattering data, although because of the linear

extrapolation of dissymmetries to zero concentration a greater experimental error (in some cases as much as 10%) was involved.

In Fig. 4 the results of dissymmetry measurements at $\lambda_0 = 546.1 \text{ m}\mu$ are represented. In Tables VI and VII all dissymmetry data are summarized. The diameters were obtained by setting $\log(1/z_{0,\text{corr.}})$ values in a theoretical plot of proper relative refractive index. The dissymmetries of BASF latexes were too high owing to the remarkable aggregation formerly mentioned. The measurements were performed with both nosepieces. No significant discrepancies between the data could be observed.

TABLE VI

Dissymmetries z_0 and $z_{0,\text{corr.}}$, and Resulting Particle Diameters D ($\text{m}\mu$); $w = 1.23^\circ$

Sample	$\lambda_0 (\text{m}\mu)$											
	578			546			436			405		
	z_0	$z_{0,\text{corr.}}$	$D (\text{m}\mu)$	z_0	$z_{0,\text{corr.}}$	$D (\text{m}\mu)$	z_0	$z_{0,\text{corr.}}$	$D (\text{m}\mu)$	z_0	$z_{0,\text{corr.}}$	$D (\text{m}\mu)$
BASF 2	1.095	1.10	52	1.10	1.10	54	1.12	1.12	42	1.19	1.20	51
Dow LS-040-A	1.19	1.20	73	1.23	1.25	78	1.38	1.40	76	1.50	1.60	82
Dow 15N-23	1.52	1.62	123	1.65	1.72	120	2.30	2.50	120	3.38	3.88	133
Dow LS-055-A	2.65	2.91	171	3.33	3.81	181	7.15	10.02	171	17.0	53.6	178
Dow LS-057-A	10.5	17.8	241	14.2	32.0	240	17.9	62.3	245	14.8	36.6	238
Dow LS-061-A	15.5	38.9	344	14.0	30.9	333	18.0	63.5	334	14.3	33.7	374
Dow LS-063-A	14.0	30.5	551	11.0	19.2	536	6.80	9.40	536	11.0	19.5	584
Dow LS-066-A	5.3	6.6	800	8.0	11.6	776	10.3	17.8	836	6.2	8.2	795
Dow LS-067-A	7.5	10.6	1153	4.50	5.41	1175	10.3	17.8	—	5.65	5.20	—

TABLE VII

Dissymmetries z_0 and $z_{0,\text{corr.}}$, and Resulting Particle Diameters D ($\text{m}\mu$); $\omega = 0.42^\circ$

Sample	$\lambda_0 (\text{m}\mu)$					
	546			436		
	z_0	$z_{0,\text{corr.}}$	$D (\text{m}\mu)$	z_0	$z_{0,\text{corr.}}$	$D (\text{m}\mu)$
Dow LS-040-A	1.26	1.28	83	1.38	1.40	76
Dow 15N-23	1.70	1.79	122	2.13	2.31	118
Dow LS-057-A	14.8	35.1	241	18.9	77.0	243
Dow LS-061-A	15.0	36.6	326	20.0	98.8	342
Dow LS-066-A	8.7	13.2	784	12.0	22.9	826
Dow LS-067-A	5.30	6.60	1190	12.0	22.9	—

Polarization Ratio

Measurements of the polarization ratio $\rho_{90} = I'_{90,H}/I'_{90,V} = (i_2/i_1)_{90}$ were carried out with unpolarized incident beam and the polaroids placed before the photomultiplier tube. Because of the weak intensities of horizontally

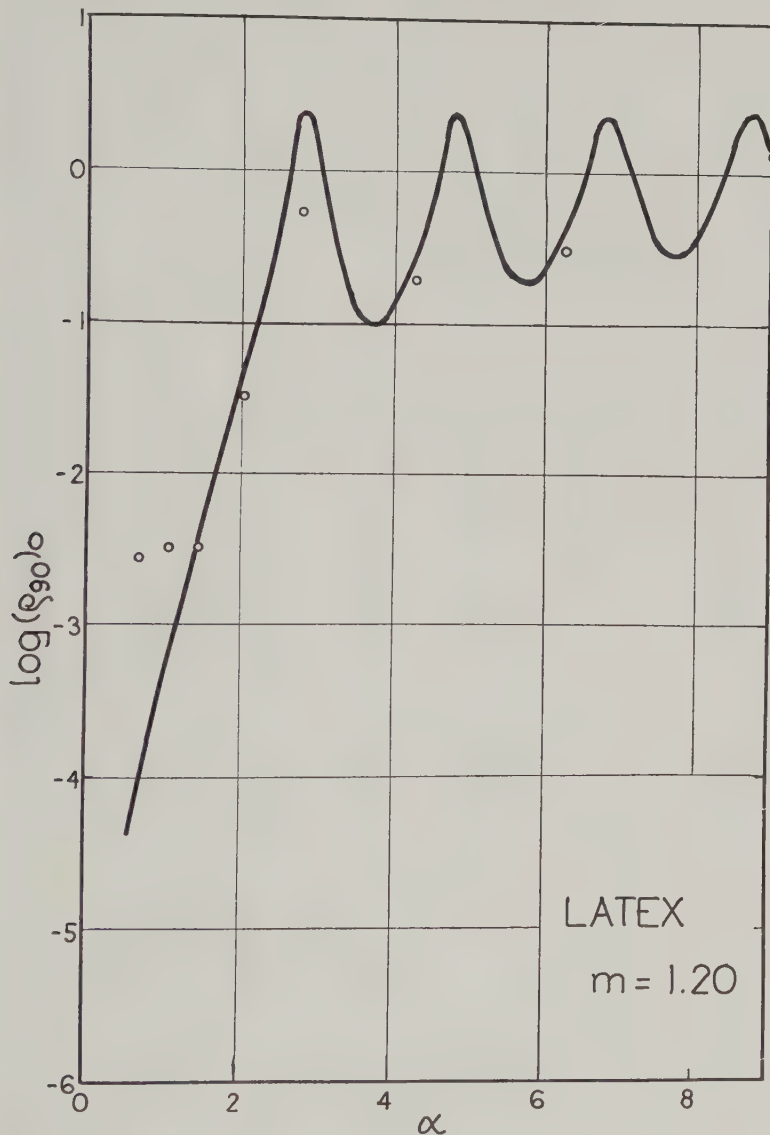


FIG. 5. Logarithm of polarization ratio versus relative diameter. Curve is obtained from Mie theory for $m = 1.20$; circles are experimental values measured at $\lambda_0 = 546.1 \text{ m}\mu$ ($\omega = 1.23^\circ$).

TABLE VIII
Polarization Ratios $(\rho_{90})_0$ and Resulting Particle Diameters D ($m\mu$)

Sample	λ_0 ($m\mu$)							
	578		546		436		405	
	$(\rho_{90})_0$ $\times 10$	D ($m\mu$)	$(\rho_{90})_0$ $\times 10$	D ($m\mu$)	$(\rho_{90})_0$ $\times 10$	D ($m\mu$)	$(\rho_{90})_0$ $\times 10$	D ($m\mu$)
Dow LS-057-A	0.252	264	0.322	252	3.05	250	10.48	251
Dow LS-061-A	3.44	338	5.45	332	2.58	336	1.94	318
Dow LS-063-A	1.33	553	1.94	541	5.85	536	4.15	506
Dow LS-066-A	2.36	823	3.06	797	2.68	793	6.96	800
Dow LS-067-A	5.54	1123	13.5	1169	9.85	—	7.15	—

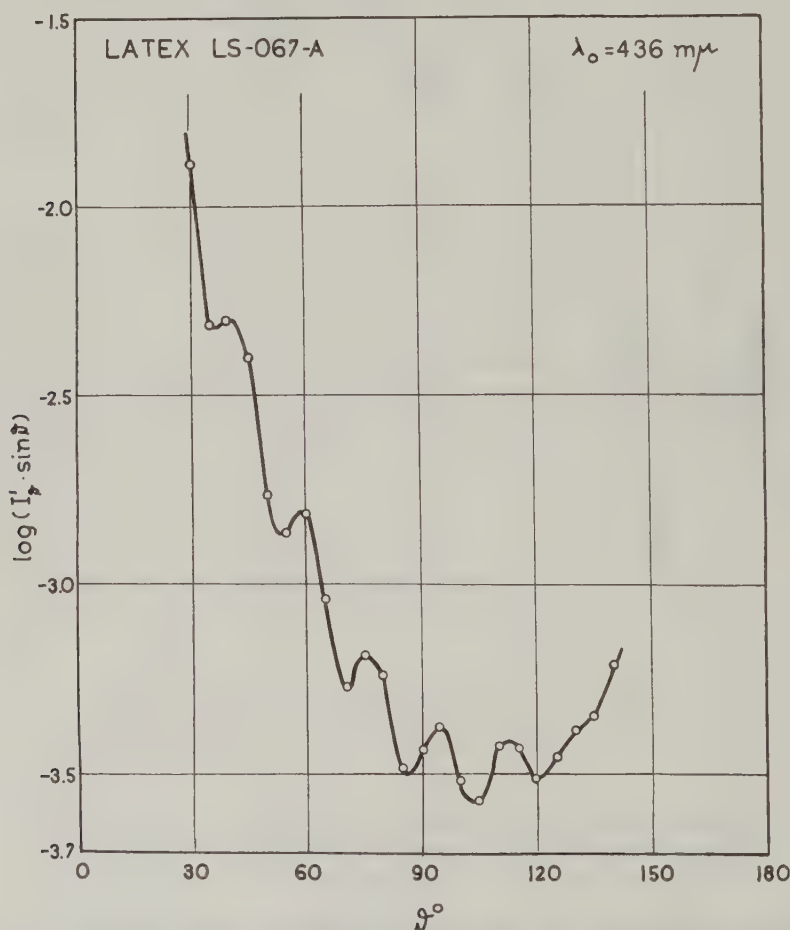


FIG. 6. Angular scattering diagram of the latex Dow LS-067-A measured with unpolarized incident light at $\lambda_0 = 435.8 m\mu$.

TABLE IXa

Positions of Maxima $\vartheta^\circ_{\max.}$ of the Order n and Resulting Particle Diameters D ($m\mu$)
Measured at $\lambda_0 = 436\ m\mu$ (Dow Latexes)

Sample	n	1	2	3	4	5	6	7	\bar{D} ($m\mu$)
LS-061-A	$\vartheta^\circ_{\max.}$	101							
	$D' (m\mu)$	376							376
	$D (m\mu)$	365							365
LS-063-A	$\vartheta^\circ_{\max.}$	58	99	—					
	$D' (m\mu)$	585	550						568
	$D (m\mu)$	535	538						536
LS-066-A	$\vartheta^\circ_{\max.}$	—	60	91	123	—			
	$D' (m\mu)$		854	786	787				809
	$D (m\mu)$		834	786	770				797
LS-067-A	$\vartheta^\circ_{\max.}$	—	40	60	76	94	113	—	
	$D' (m\mu)$		—	1126	1168	1158	1181		1158
	$D (m\mu)$		—	1150	1168	1158	1181		1164

TABLE IXb

Positions of Minima $\vartheta^\circ_{\min.}$ of the Order n and Resulting Particle Diameters D ($m\mu$)
Measured at $\lambda_0 = 436\ m\mu$ (Dow Latexes)

Sample		$n = 0$							
		$\vartheta^\circ_{\min.}$				$D (m\mu)$			
LS-040-A		96				76			
15N-23		110				118			
LS-055-A		—				—			

Sample	n	$n = 1-8$								\bar{D} ($m\mu$)
		1	2	3	4	5	6	7	8	
LS-057-A	$\vartheta^\circ_{\min.}$	108								
	$D' (m\mu)$	240								240
	$D (m\mu)$	248								248
LS-061-A	$\vartheta^\circ_{\min.}$	80	122							
	$D' (m\mu)$	310	380							345
	$D (m\mu)$	324	386							355
LS-063-A	$\vartheta^\circ_{\min.}$	52	86	123						
	$D' (m\mu)$	462	504	540						502
	$D (m\mu)$	495	534	549						526
LS-066-A	$\vartheta^\circ_{\min.}$	—	55	81	107	131	—			
	$D' (m\mu)$		770	759	778	820				782
	$D (m\mu)$		797	790	778	829				798
LS-067-A	$\vartheta^\circ_{\min.}$	—	36	54	70	87	104	121	—	
	$D' (m\mu)$		1064	1110	1130	1148	1153	1148		1126
	$D (m\mu)$		1148	1172	1150	1168	1163	1148		1156

polarized light only the nosepiece with $\omega = 1.23^\circ$ was used. The polarization ratios depended on the concentration. Excellent straight lines were obtained which could easily be extrapolated to zero concentration. All extrapolated values $(\rho_{90})_0$ were corrected for the different sensitivity of the photomultiplier tube to horizontally and vertically polarized light. The particle diameters were obtained from experimental $\log(\rho_{90})_0$ values and theoretical plots.

In Fig. 5 the results obtained at $\lambda_0 = 546.1 \text{ m}\mu$ are compared with the theoretical curve. Only the results for smaller sizes disagree with theoretical values. It will be shown later that these data are erroneous. In Table VIII all results are presented except those for latexes of the smallest particle sizes.

Angular Positions of Maxima and Minima

Measurements of the angular dependence of the intensity of scattered light were carried out by using cylindrical cells and $\omega = 0.42^\circ$. Under these conditions the radiation envelope of a fluorescein solution was fully symmetric showing the absence of cell irregularities. To correct for the scattering volume seen by the photomultiplier all galvanometer deflections, corrected for the nonlinearity of the electrometer tube and for the deviations in meter multiplier ratios, were multiplied by $\sin \theta$. Thus the quantity $I_\theta' \sin \theta$ is proportional to i_γ . Logarithmic plots of $I_\theta' \sin \theta$ vs. θ were used to evaluate the positions of the extrema graphically. Because no precise theo-

TABLE X

Positions of Maxima $\vartheta^\circ_{\text{max.}}$ and Minima $\vartheta^\circ_{\text{min.}}$ of the Order n and Resulting Particle Diameters D ($\text{m}\mu$) Measured at $\lambda_0 = 546 \text{ m}\mu$
(Dow latexes)

Sample	n	1	2	3	4	5	6	\bar{D} ($\text{m}\mu$)
<i>Maxima</i>								
LS-066-A	$\vartheta^\circ_{\text{max.}}$	47	80					
	D' ($\text{m}\mu$)	890	830					860
	D ($\text{m}\mu$)	833	820					826
LS-067-A	$\vartheta^\circ_{\text{max.}}$	—	55	76	101			
	D' ($\text{m}\mu$)		1165	1168	1160			1164
	D ($\text{m}\mu$)		1151	1168	1160			1160
<i>Minima</i>								
LS-066-A	$\vartheta^\circ_{\text{min.}}$	42	72	104				
	D' ($\text{m}\mu$)	710	749	768				742
	D ($\text{m}\mu$)	806	790	793				796
LS-067-A	$\vartheta^\circ_{\text{min.}}$	—	50	70	91	116		
	D' ($\text{m}\mu$)		1049	1088	1112	1130		1095
	D ($\text{m}\mu$)		1113	1151	1185	1160		1152

retical data exist and to simplify the whole procedure only one very diluted solution of each latex was evaluated. By comparing the angular diagrams at several concentrations it was not possible to observe any remarkable shift of extrema at higher concentrations. Only a blurring of the extrema appears.

In Figure 6 the angular diagram of Dow latex LS-067-A measured at $\lambda_0 = 435.8 \text{ m}\mu$ is represented.

Since the theoretical functions were computed for the case of $m = 1.200$ and the measurements were for the most part carried out at $m = 1.210$ ($\lambda_0 = 435.8 \text{ m}\mu$), an additional correction must be introduced. From the consideration of Nakagaki and Heller (17) it can be concluded that all results obtained at $m = 1.210$ and evaluated with functions for $m = 1.200$ are about 0.7% too high. This is an average estimate, but because of its small value the approximation is probably a good one.

In Tables IX and X the positions of extrema θ_e° are listed. Here D' represents the diameters evaluated from the data of Nakagaki and Heller (17) and D the values from our estimated data (27).

DISCUSSION

Several latexes used in this study had already been investigated by the methods of light scattering (12, 18, 19). Table XI summarizes results from the literature. Only data obtained by methods used in this paper are listed. Δ is the relative difference from electron microscopic data (D_{EM}).

A summarizing review of our results is given in Table XII. From our results it can be concluded, in agreement with previous authors, that the

TABLE XI

Earlier Results Obtained on Polystyrene Latexes Investigated in This Paper

Sample	Heller <i>et al.</i>		Bateman <i>et al.</i>		Kerker and Matijevic	
	$D(\text{m}\mu)$	$\Delta(\%)$	$D(\text{m}\mu)$	$\Delta(\%)$	$D(\text{m}\mu)$	$\Delta(\%)$
Dow 15N-23					129 ^d	-6.5
Dow LS-057-A			240 ^b	-9.1	260 ^d	-1.5
			245 \pm 5 ^c	-7.2		
Dow LS-063-A	538 ^a	-3.4			546 ^d	-2.0
Dow LS-066-A	765 ^a	-6.0	820 ^b	+0.74		
			802 \pm 33 ^c	-1.5		
Dow LS-067-A			1160 ^b	-0.94		
			1168 \pm 37 ^c	-0.26		

^a From transmission at 546 $\text{m}\mu$.

^b From transmission at 560 $\text{m}\mu$.

^c From transmission at eight wavelengths (370-950 $\text{m}\mu$), averaged value.

^d From polarization ratio ρ_{90} at 546 $\text{m}\mu$.

TABLE XII
Review of All Latex Diameters Obtained by Light Scattering

Sample	$D_{EM} (m\mu)$	$D(m\mu)$					$\bar{D} (m\mu)$
		(1)	(2)	(3)	(4)	(5)	
BASF 1	37	30.2 ± 0.3	28.5 ± 1.2^a	—	—	—	29.4
BASF 2	47	42.2 ± 0.8	42.4 ± 0.4^a	50 ^a	—	—	44.9
BASF 3	72	69 ± 4	57.8 ± 1.2^a	—	—	—	64.0
Dow	88	76.0 ± 0.9	73.3 ± 2.9^a	78 ± 4^a	—	76 ^c	76.2
LS-040-A			74.0 ^b	79.8 ^b			
Dow	138	120 ± 1	118 ± 5^a	124 ± 6^a	—	118 ^c	120
15N-23			120 ^b	120 ^b			
Dow	188	167 ± 1	182 ± 13^a	175 ± 5^a	—	—	175
LS-055-A			176 ^b	—			
Dow	264	240 ± 1	249 ± 15^a	241 ± 3^a	254 ± 7	248 ^c	245
LS-057-A			240 ^b	242 ^b			
Dow	365	329 ± 1	333 ± 9^a	346 ± 19^a	331 ± 9	360 ± 32^c	339
LS-061-A			338 ^b	334 ^b			
Dow	557	522 ± 6	526 ± 25^a	552 ± 23^a	534 ± 2	531 ± 21^c	534
LS-063-A			537 ^b	—			
Dow	814	784 ± 4	808 ± 4^a	802 ± 25^a	803 ± 14	805 ± 21^c	803
LS-066-A			807 ^b	805 ^b		808 ± 18^d	
Dow	1171	1185 ± 58	1156 ^a	1164 ^a	1146	1158 ± 16^c	1167
LS-067-A			1180 ^b	1190 ^b		1155 ± 22^d	

(1)—Transmission

(2)—Scattering at 90°

(3)—Dissymmetry

(4)—Polarization ratio

(5)—Location of extrema

 D_{EM} —Diameter from electron microscopy \bar{D} —arithmetic mean of diameters obtained by light scattering.^a $\omega = 1.23^\circ$ ^b $\omega = 0.42^\circ$ ^c $\lambda_0 = 436 m\mu$ ^d $\lambda_0 = 546 m\mu$.

Mie theory can be very satisfactorily applied to the light scattering of polystyrene latexes. The diameters from light-scattering measurements are lower than those from electron microscopy, and only a few exceptions to this behavior could be noted. This can be seen very clearly from the tables and figures represented in this paper. Most striking is the fact that both the methods which depend on concentration (transmission, scattering at 90°) and those independent of calibration and concentration (dissymmetry, polarization ratio, angular positions of extrema) are in agreement with one another. Even if a systematic error in concentration could be involved in the first group of methods such an error could not occur in the other methods.

The one remarkable exception found can easily be explained as resulting from the presence of aggregation in the BASF sample that could not be eliminated by centrifugation and filtration. It is clear that both the specific turbidity and specific intensity at 90° could be influenced by the presence of aggregates, but not in such a proportion as dissymmetry.

The erroneous results of polarization ratio for small particle sizes are a consequence of the impossibility of measuring extremely low polarization ratios with polaroid discs. This is a possible source of error discussed by Geiduschek (33). It should be noted that Kerker and Matijević (19) measured successfully ρ_{90} for the Dow 15N-23 sample using Glan-Thompson prisms, a much more sensitive device.

The results obtained from locations of maxima and minima are less accurate compared with other data, but they still agree well.

The existence of small but finite second virial coefficients is a fact not observed by previous authors (12, 18). The virial coefficients show a tendency to decrease with increasing particle size (having in mind the great experimental error made in measuring them) similarly to the general behavior of the second virial coefficients of macromolecules.

It is obvious that for practical purposes the multivaluedness of the light-scattering functions at large relative diameters makes it difficult to determine particle size. The specific turbidities in the particle size range investigated covers only the first turbidity maximum, but because of the slow change in the region of maximum the precision of the size determination is diminished. By the use of several methods at the same time, as in this work, it is possible to make a reliable estimate of the particle size. The procedures described are, of course, restricted to monodispersed samples of stable particles.

If the particle size of the system changes during the time, e.g., in the case of particle growth during a precipitation or coagulation process, only the methods independent of concentration can be used. Dissymmetry and polarization ratio methods can be applied if the solution is sufficiently diluted. It seems that the method of location of extrema is least influenced by the multiple scattering. The only disadvantage of this method is uselessness in the region of $\alpha < 2$. The location of minima of zero order is also of limited value since these minima disappear at $\alpha > 1.40$ and the overall precision of determination is not sufficiently high.

The lower light-scattering results of latex diameters may indicate a systematic error in electron microscopic data, but it is possible that these discrepancies arise from the colloid electrolyte character of latexes. Latexes consist of polystyrene and detergent molecules (34), and therefore the spherical particles should be electrically charged (using an ultramicroscopic electrophoresis apparatus we found that the charge of particles is negative). It can be expected that they behave like Ludox solutions (24, 35) and other charged colloids in the presence of electrolytes, i.e., in the case

of no electrolyte content the light-scattering data are apparently lower. We hope to obtain a final answer to this problem by further investigations.

ACKNOWLEDGMENTS

We are grateful to Dr. J. W. Vanderhoff of the Dow Chemical Company and to Dr. G. Hummel of the Badische Anilin- & Soda-Fabrik for a supply of polystyrene latexes, and to Professors B. Težak and V. B. Vouk for their interest in this work.

REFERENCES

1. BRADFORD, E. B., AND VANDERHOFF, J. W., *J. Appl. Phys.* **26**, 864 (1955).
2. MIE, G., *Ann. Physik* **25**, 377 (1908).
3. DANDLIKER, W. B., *J. Am. Chem. Soc.* **72**, 5110 (1950).
4. ALFREY, T., JR., BRADFORD, E. B., VANDERHOFF, J. W., AND OSTER, G., *J. Opt. Soc. Amer.* **44**, 603 (1954).
5. BURNETT, G. M., LEHRLE, R. S., OVENALL, D. W., AND PEAKER, F. W., *J. Polymer Sci.* **29**, 417 (1958).
6. ROSIK, L., AND VILIM, O., *Chem. Listy* **53**, 757 (1959).
7. GORING, D. A. I., SENEZ, M., MELANSON, B., AND HUQUE, M. M., *J. Colloid Sci.* **12**, 412 (1957).
8. SOKOL, F., *Chem. Zvesti* **12**, 69 (1958).
9. LA MER, V. K., AND PLESNER, J. W., *J. Polymer Sci.* **24**, 147 (1957).
10. KERKER, M., *J. Polymer Sci.* **28**, 429 (1958).
11. HELLER, W., AND PANGONIS, W. J., *J. Chem. Phys.* **26**, 498 (1957).
12. TABIBIAN, R. M., HELLER, W., AND EPEL, J. N., *J. Colloid Sci.* **11**, 195 (1956).
13. HELLER, W., AND TABIBIAN, R. M., *J. Colloid Sci.* **12**, 25 (1957).
14. PUGH, T. L., AND HELLER, W., *J. Colloid Sci.* **12**, 173 (1957).
15. HELLER, W., AND PUGH, T. L., *J. Colloid Sci.* **12**, 294 (1957).
16. TABIBIAN, R. M., AND HELLER, W., *J. Colloid Sci.* **13**, 6 (1958).
17. NAKAGAKI, M., AND HELLER, W., *J. Chem. Phys.* **32**, 835 (1960).
18. BATEMAN, J. B., WENECK, E. J., AND ESHLER, D. C., *J. Colloid Sci.* **14**, 308 (1959).
19. KERKER, M., AND MATIJEVIĆ, E., *J. Opt. Soc. Amer.* **50**, 722 (1960).
20. DEŽELIĆ, GJ., WRISCHER, M., DEVIDÉ, Z., AND KRATOHVIL, J. P., *Kolloid-Z.* **171**, 42 (1960).
21. PRICE, F. P., BELLAMY, W. D., AND LAWTON, E. J., *J. Phys. Chem.* **58**, 821 (1954).
22. DEŽELIĆ, GJ., *Croat. Chem. Acta*, in press.
23. OSTER, G., *Anal. Chem.* **25**, 1165 (1953).
24. DEŽELIĆ, GJ., AND KRATOHVIL, J. P., *Kolloid-Z.* **173**, 38 (1960).
25. SCATCHARD, G., AND BREGMAN, J., *J. Am. Chem. Soc.* **81**, 6095 (1959).
26. THURMOND, C. D., *J. Polymer Sci.* **8**, 607 (1952).
27. DEŽELIĆ, GJ., *Croat. Chem. Acta*, in press.
28. MEEHAN, E. J., AND BEATTIE, W. H., *J. Phys. Chem.* **64**, 1006 (1960).
29. MARON, S. H., AND LOU, R. L. H., *J. Polymer Sci.* **14**, 29 (1954).
30. GUMPRECHT, R. O., AND SLIEPCEVICH, C. M., "Tables of Light-Scattering Functions for Spherical Particles." University of Michigan Press, Ann Arbor, 1951.
31. OTH, A., OTH, J., AND DESREUX, V., *J. Polymer Sci.* **10**, 551 (1953).
32. SEDLAČEK, B., *Chem. Listy* **47**, 1113 (1953).
33. GEIDUSCHEK, E. P., *J. Polymer Sci.* **13**, 408 (1954).
34. SMITH, W. V., *J. Am. Chem. Soc.* **70**, 3695 (1948).
35. DEŽELIĆ, GJ., AND KRATOHVIL, J. P., in preparation.

THE PREPARATION OF MONODISPERSE SILVER BROMIDE AND SILVER IODIDE SOLS

R. H. Ottewill and R. F. Woodbridge

Department of Colloid Science, University of Cambridge, Cambridge, England

Received February 2, 1961

ABSTRACT

The preparation of sols of silver bromide and silver iodide with a high degree of monodispersity is described. The methods employed utilized the dilution of silver halide complex solutions with distilled water, in both the excess halide and excess silver regions, and the cooling of hot silver bromide solutions in the region of ionic solubility. All the sols prepared exhibited Higher Order Tyndall Spectra (HOTS). Electron microscope observations were used to examine the degree of monodispersity of the sols and the shape of the particles.

INTRODUCTION

A monodisperse sol may be defined as one in which all the particles have exactly the same size and shape. A theory of monodisperse sol production has been proposed by La Mer and his co-workers (1, 2), and the preparation and properties of monodisperse sulfur sols have been thoroughly investigated by this school (3-8). The methods proposed should in theory allow almost any insoluble material to be prepared in a monodisperse form provided that suitable reactions can be found. It seems surprising therefore that relatively few monodisperse sols have been prepared, since the advantages of working with monodisperse systems in colloid experiments are immediately obvious. The systems prepared in monodisperse form, so far, apart from sulfur include selenium (9), silver chloride in 95% ethanol (10), barium sulfate (11), gold (12), lead iodate (13, 14), lanthanum iodate (14), and polystyrene latexes (15). However, the preparation of monodisperse colloidal silver bromide and iodide does not appear to have been reported in the literature. Silver iodide has long played a major role in the development of the theory of lyophobic colloid chemistry, and has been extensively investigated in the schools of Kruyt and Overbeek (16) and Težák (17). Silver bromide, moreover, is of great importance in the photographic industry. It would therefore appear of particular importance that methods should be available for the preparation of these materials in monodisperse form. This subject has recently been investigated in detail in these laboratories, and successful methods have been developed for the

preparation of monodisperse silver iodide and bromide sols. A preliminary account of these experiments is given in the present paper.

THEORETICAL

The basis of monodisperse sol production may be summarized, following La Mer and his co-workers, by reference to Fig. 1. Thus if a reaction occurs which continuously generates molecules of a disperse phase, the concentration of these molecules increases steadily, passes the point of saturation *A*, and reaches a point *B* at which the rate of self-nucleation becomes appreciable; as *D* is approached the rate of nucleation rises rapidly. However, if the rate of production of molecules is slow the sudden appearance of nuclei relieves the supersaturation so rapidly and effectively that the region of nucleation (II) is restricted in time and no new nuclei are formed after the initial outburst. The nuclei produced grow uniformly by a diffusion process (region III) and a sol of monodisperse particles is obtained (1, 2).

As pointed out by La Mer and Dinegar (1), nothing in the theory limits the mechanism by which the value of the critical limiting supersaturation is reached: "Supersaturation can be achieved not only by building up the concentration of dissolved material in a medium of constant solubility—but also starting with a certain concentration of material and then decreasing

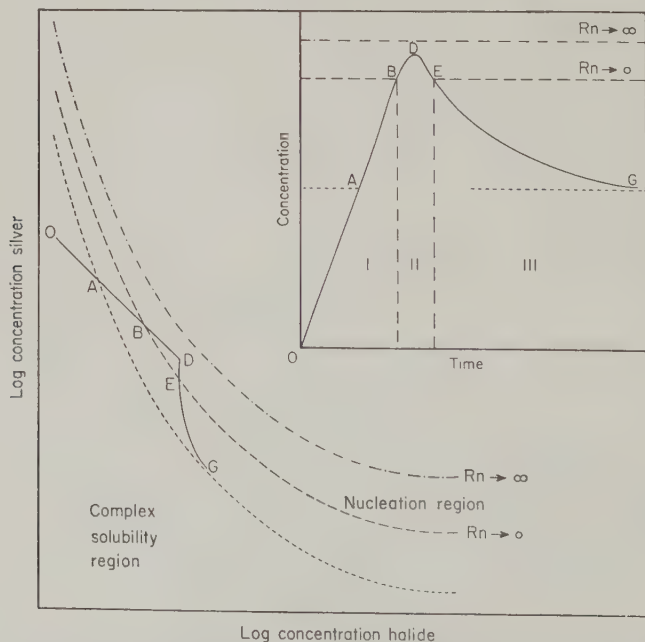


FIG. 1. Schematic representation, following La Mer, of conditions for the preparation of monodisperse silver halide sols: - - - - critical limiting supersaturation curve, - · - · - critical supersaturation curve, · · · · solubility curve. R_n = rate of nucleation. *Insert*: Concentration of disperse phase in molecular solution against time.

the solubility either by lowering the temperature or by adding a miscible non-solvent."

In the case of silver halides it is well known that soluble complexes are formed in the regions of both halide and silver excess, and the regions of complex solubility have been investigated in detail by Težak and his collaborators (18, 19) and by Leden *et al.* (20-23). Thus theoretically it is possible to cross the complex solubility line by dilution with water and achieve a supersaturation value which produces just one brief burst of nuclei. This situation can be made clear by reference to Fig. 1. Thus starting with a solution in the complex solubility region *O*, on dilution with water to the point *D* nucleation occurs; a drop in concentration of the molecular disperse phase then occurs, and the particles grow by diffusion in the region *EG*. The letters *O A B D E G* refer to the same regions as described in Fig. 1A. One disadvantage of this method of preparation is that the sol produced usually contains a large excess of the silver halide solvent; since this is usually an electrolyte, rapid removal or dilution is necessary to prevent coagulation.

In the case of silver bromide, the solubility of which at 100°C. is forty times that at 20°C., the preparation can be carried out in the region of

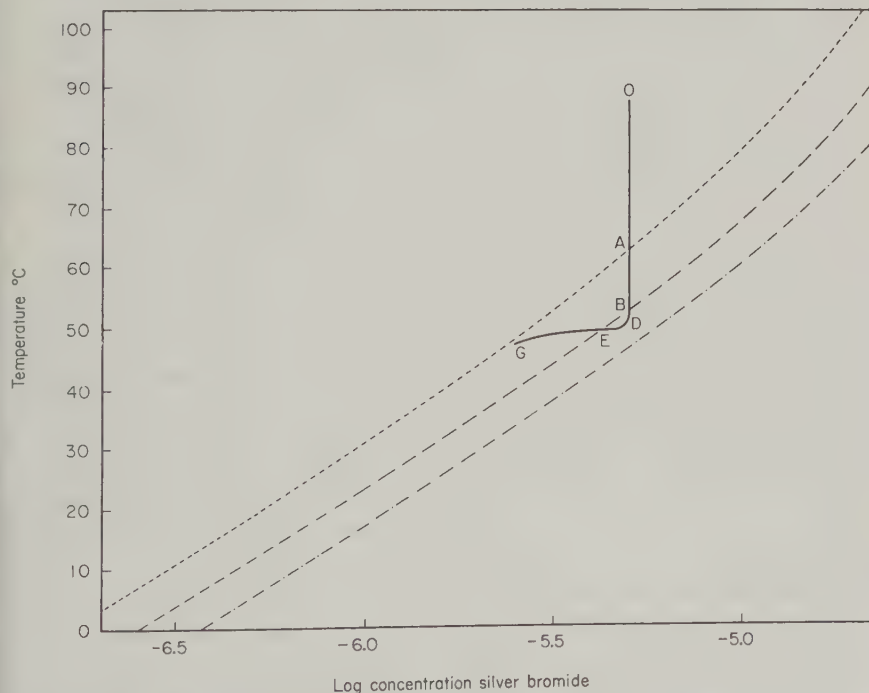


FIG. 2. Preparation of monodisperse silver bromide sols by cooling: - - - - critical limiting supersaturation curve, - · - · - critical supersaturation curve, · · · · solubility curve (data of Gledhill and Malan (24)).

ionic solubility (see Fig. 6). This method of preparation can be understood by reference to Fig. 2, in which the solubility of silver bromide against temperature is plotted according to the data of Gledhill and Malan (24). Thus if a solution of silver bromide is made (*O*), on controlled cooling, the solubility curve is crossed at *A* and nucleation occurs at *D* followed by growth in the region *EG*. By this method a sol can be prepared which is virtually free of extraneous electrolyte.

EXPERIMENTAL

Materials

Distilled water was passed through a Bio-deminrolit mixed bed ion-exchange resin and then redistilled from an all-Pyrex apparatus. All chemicals used were of A.R. grade. Solutions used were filtered through a no. 5 Pyrex sintered glass filter; this filtration, however, did not appear to be essential in order to obtain monodisperse sols. Unless otherwise stated all preparations were carried out at room temperature (ca. 20°C.).

Preparation of Monodisperse Sols by Dilution of Complex Solutions

General Procedure. The monodispersity of the sols produced was found to be very dependent on the method of mixing, and it was found necessary to control this carefully in order to obtain reproducible results. Provided the same method of mixing was employed and the concentrations of reactants were kept within certain ranges (see later) the particles were of the same shape and there was little variation in the particle-size distribution curves for different preparations. The following procedures were adopted.

A known volume of complex solution the composition of which corresponded to a point in the complex solubility region (e.g., *O* in Fig. 1) was placed in a beaker. The solution was then diluted by rapidly pouring into it about two to three times its own volume of water with fairly rapid stirring. After addition of water the stirrer was switched off and the sol left to stand for particle growth to occur. The degree of monodispersity of the sol and the particle size depended upon the volumes and concentrations of the solutions used and upon the rates of addition and stirring employed. When all these factors were kept constant reproducible preparations were obtained. All the preparations described in this paper using dilution of the complex solutions were carried out by this procedure.

Similar preparations were obtained by placing about 3 ml. of a more concentrated complex solution (to give the same final sol concentration as the earlier method) in a flask so as to completely cover the bottom of the vessel. Approximately 80 ml. of water were then injected into this solution either from a large syringe or a polythene wash bottle. Results by this

method, however, were not as reproducible as those obtained by the first method.

The method employed by Herak *et al.* (14) in which the water was slowly poured down the side of a beaker into the complex solution also produced a monodisperse sol. However, the sols produced had a much larger particle size and the results were less reproducible than those obtained by the other methods described above.

In all cases sols were formed within 1 minute of mixing and exhibited at this stage well-defined higher order Tyndall spectra (HOTS). After preparation the sols were usually further diluted with water to a known volume in order to lower the electrolyte concentration and thus prevent the occurrence of coagulation. Alternatively, the electrolyte was removed from the sols either by electrodialysis or by passage through a column of mixed bed ion-exchange resin. In both cases, however, there was a decrease in sol concentration owing to adherence of particles either to the resin or to the dialysis membrane.

Concentration of the sols was achieved by allowing them to sediment (under gravity or a weak centrifugal field), removing the bulk of the supernatant, and then washing, resedimenting, and dispersing the sediment in a small volume of water. When centrifugation was employed careful control was essential, otherwise the particles adhered tenaciously to the centrifuge tube and were not redispersible. Coagulation occurred to a small extent during concentration but the sols produced were excellent for microelectrophoresis since the single particles were easily distinguishable from the coagula in the ultramicroscope beam.

Particle counts on sols using the counter described by Ottewill and Wilkins (25) showed that the number concentration of the freshly prepared sols was of the order of 10^7 particles per milliliter.

Electron Microscopy. Samples for electron microscopy were obtained by centrifuging the particles onto the surface of a freshly cleaved mica disc. The disc after washing with water and drying was coated with evaporated carbon (26) and then shadowed with chromium vapor at a 60° angle. The shadowed carbon film was then floated off the mica by slow immersion of the disc in concentrated potassium cyanide solution. After the silver halide particles had dissolved, the carbon-chromium film was washed with water and transferred to a copper grid. The electron microscope used for all observations was a Siemens Elmiskop I.

RESULTS

Preparation by Dilution of Complex Solutions

A large number of experiments have been carried out over ranges of the complex solubility curves both in the halide ion excess region and in

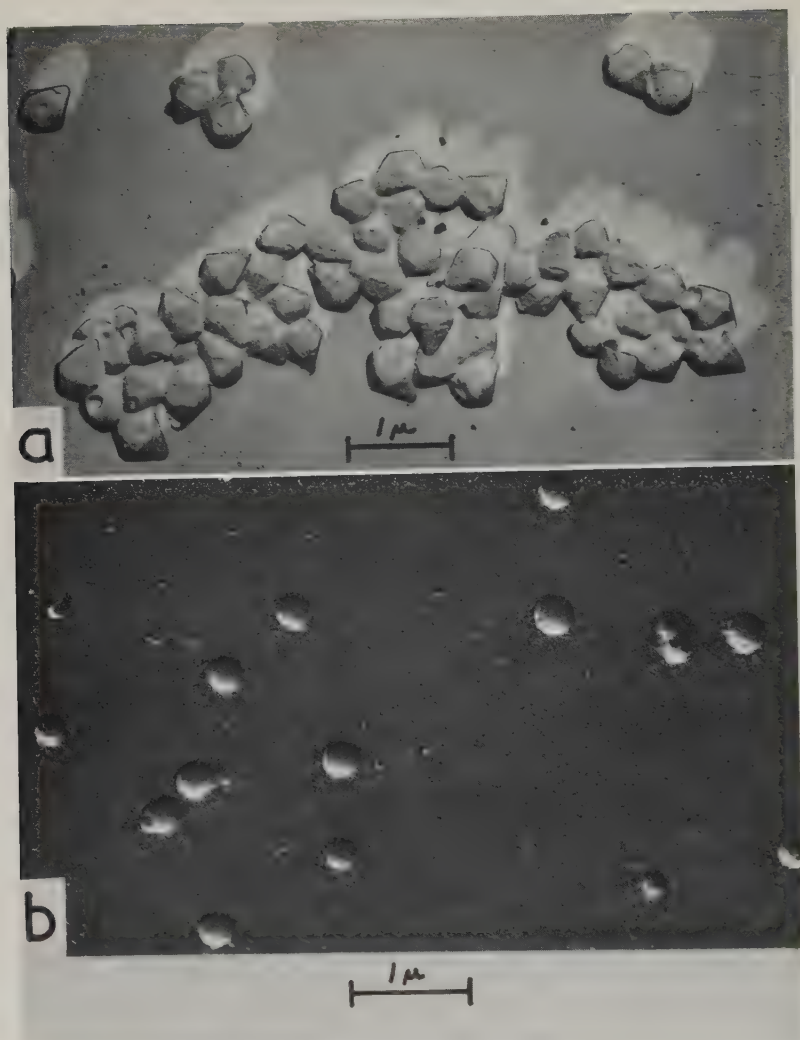


FIG. 3. Silver iodide sols. Electron micrographs of carbon replicas shadowed with chromium. (A) preparation in iodide excess region shadowed at a 60-degree angle; (B) preparation in silver excess region, shadowed at a 40-degree angle.

the silver ion excess region. Since these experiments are too extensive to elaborate in detail only those giving the best results are described. Stock solutions of the complex solutions were made up either by dissolving washed precipitated silver halide in the appropriate halide solvent or, more conveniently, by carefully mixing solutions of silver nitrate and the appropriate halide.

Silver Iodide Sols

Iodide Excess Region. One hundred and fifty milliliters of a solution which was $3 \times 10^{-5} M$ with respect to silver iodide and $0.1 M$ with respect to potassium iodide was diluted to 500 ml. with distilled water. The resulting sol, after about 1 minute, showed two red bands at angles of approximately 45° and 90° to the direction of the incident radiation. Provided that the electrolyte concentration was lowered by dilution or electrolyte was removed by dialysis or treatment with ion-exchange resins, the HOTS lasted until the sol particles sedimented. If excess electrolyte was not removed the HOTS disappeared after several hours. A typical electron micrograph of carbon replicas of the sol particles is given in Fig. 3(A); the particles were hexagonal bipyramids. A particle-size distribution curve for this sol is given in Fig. 5(A). The mean radius of a sphere equal in volume to the particle was 0.389μ with a standard deviation of 0.042 and a coefficient of variation of 10.8%.

Silver Excess Region. Fifty milliliters of a solution which was $6 \times 10^{-5} M$ with respect to silver iodide and $0.2 M$ with respect to silver nitrate was diluted to 200 ml. with distilled water. The HOTS of the resultant sol, which were always obtained within about 1 minute of mixing and lasted for several hours (even without removal of electrolyte), were variable, red bands sometimes appearing in the forward direction and sometimes in the backward. The degree of monodispersity, however, as judged by electron microscopy (see Fig. 3(B)) was not as good as that attained with the other sols in this paper, and the method of mixing was also found to be much more critical.

Silver Bromide Sols

Bromide Excess Region. Forty milliliters of solution which was $1.5 \times 10^{-4} M$ with respect to silver bromide and $0.78 M$ with respect to ammonium bromide was diluted to 300 ml. with distilled water. The resulting sol showed after ca. 1 minute HOTS with 3 red bands at approximately 35° , 70° , and 100° to the incident beam. Whilst electrolyte remained the HOTS lasted for several hours; the actual time depended on the degree of dilution. These sols were very reproducible and the particles were regular octahedra. A typical electron micrograph of particles, of side 0.40μ , is given in Fig. 4(A).

Silver Excess Region. One hundred milliliters of a solution which was $1.6 \times 10^{-5} M$ with respect to silver bromide and $0.4 M$ with respect to silver nitrate was diluted to 400 ml. with distilled water. The resulting sol showed HOTS with two red bands at angles of approximately 70° and 140° to the forward direction. On removal of excess electrolyte the HOTS remained visible until the sol sedimented. An electron micrograph of carbon

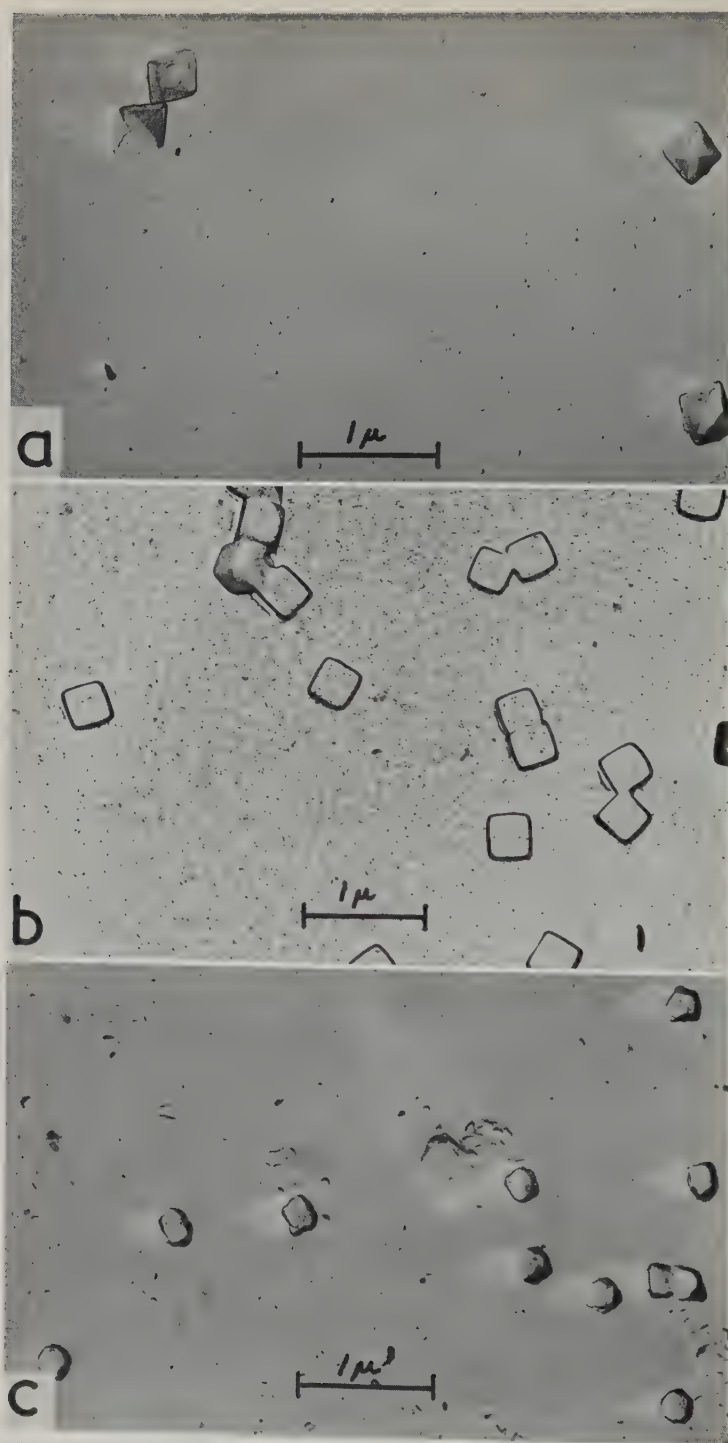


FIG. 4. Silver bromide sols. Electron micrographs of carbon replicas shadowed with chromium at a 60-degree angle. (A) preparation in bromide excess region; (B) preparation in ionic solubility region; (C) preparation in silver excess region.

replicas of typical particles from this type of sol is shown in Fig. 4(C), and a particle-size distribution curve is given in Fig. 5(B). The particles were of somewhat irregular shape with a tendency to octahedral form. For the purpose of particle-size analysis the dimension used was the average of two measurements taken at right angles across the particle; the mean was 0.425μ with a standard deviation of 0.047 and a coefficient of variation of 11.0%.

Ionic Solubility Region. Two hundred and fifty milliliters of boiling $4 \times 10^{-5} M$ silver nitrate solution was quickly poured into 250 ml. of rapidly stirred boiling $4 \times 10^{-5} M$ potassium bromide solution contained in a thin-walled 1-liter beaker. The solution was then left to cool to 20°C . in the dark with slow stirring. The resulting sol showed HOTS with two red bands at approximately 20° and 50° to the incident beam (also a faint one at 80°). Examination of carbon replicas in the electron microscope showed the particles to be perfect cubes (Fig. 4(B)). Particle-size analysis (Fig. 5(C)) gave for the mean length of the side 0.353μ , with a standard deviation of 0.036 and a coefficient of variation of 10.1%. The monodispersity of this sol depended on the rate of cooling and on the solution's being kept homogeneous during this process. Provided these variables were controlled the monodispersity of the sol was very reproducible; best results were achieved with fairly rapid cooling in air. Because of the low

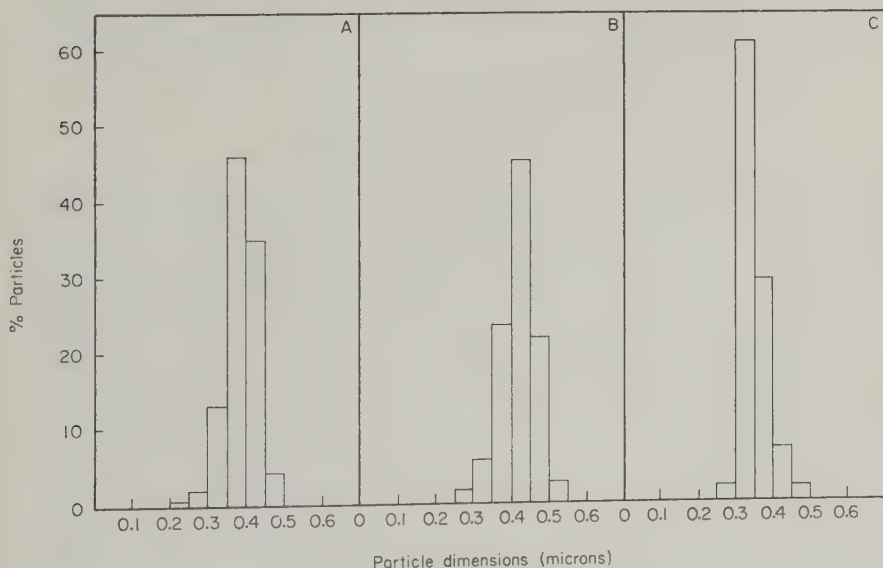


FIG. 5. Particle-size distribution curves for silver iodide and silver bromide sols. (A) silver iodide preparation from iodide excess region; (B) silver bromide preparation from silver excess region; (C) silver bromide from ionic solubility region.

concentration of the resultant sol this method was not used for silver iodide; apart from this point there does not appear any reason why it should not be utilized.

DISCUSSION

The conditions for the preparation of silver bromide sols can best be discussed by reference to the solubility curve for silver bromide in the ionic solubility and complex solubility regions. This curve has been investigated in detail at 25°C. by Kratochvil, Težak, and Vouk (19) and by Berne and Leden (20). The curve shown in Fig. 6 has been constructed from their data. Only the silver bromide case will be discussed since the preparation of silver iodide sols is essentially similar.

Experimentally, the silver bromide sols in the bromide excess region showing the highest degree of monodispersity by electron microscopy and the best HOTS were obtained by dilution such that the solubility curve was crossed in the range pAg 3.0 to 4.2, that is, by starting with solutions

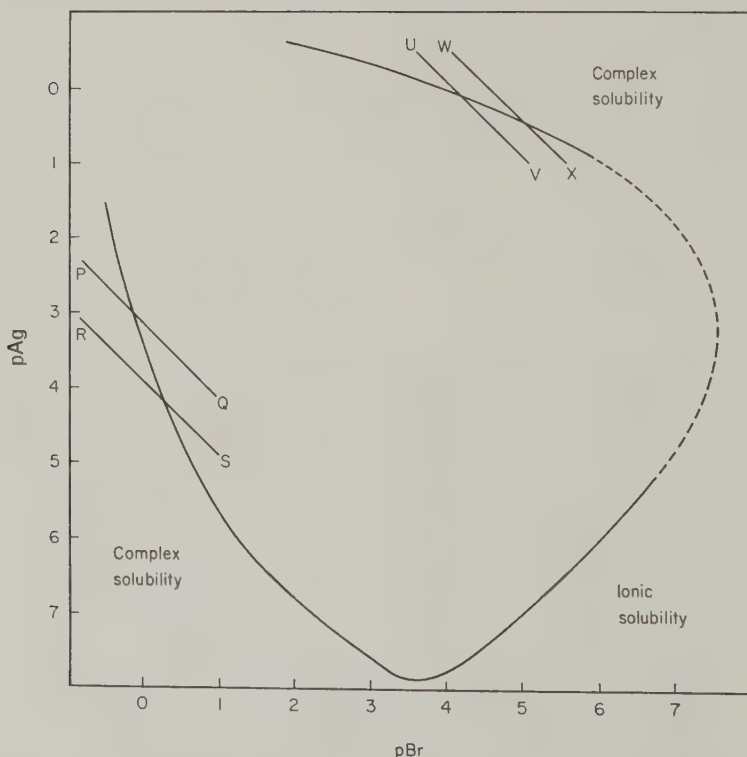
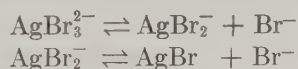


FIG. 6. Solubility curve for silver bromide in complex and ionic solubility regions. $PQRS$, region of best monodispersity in excess bromide; $UVWX$, region of best monodispersity in excess silver.

having a composition in the region PR and diluting into the region QS . It was impossible to define these limits sharply and the limits given define only the region in which monodisperse sols of reasonable stability and concentration were obtained. Above the line PQ it was found that the final electrolyte concentration was too high for convenient preparation, i.e., coagulation was rather rapid; in this region, moreover, the preparation appeared to be unduly sensitive to the method of mixing. Below the line RS the sols obtained were rather too dilute with respect to particle number per milliliter to enable concentration to be effected and the degree of monodispersity was not satisfactory. This is possibly caused by the fact that in this region the slope of the solubility curve approaches unity. Thus the boundary is crossed at a very shallow angle, and nucleation occurs over an extended period of time. In the case of silver bromide sols prepared in the presence of excess silver the pBr region 4.2 to 5.0 was found to be the most effective. Again, in this region, the slope of the solubility-curve approached unity and mixing was found to be a critical factor.

In the case of silver iodide sols the most effective regions were found to be pAg 4.5 to 5.2 in the iodide excess region and pI 4.1 to 5.0 in the silver excess region. The solubility curve was constructed from the data of Kratochvil, Težak, and Vouk (19).

It would appear from the experimental work that nucleation occurs quite rapidly after the complex solubility curve is crossed. Kratochvil, Težak, and Vouk (19) give the formula of the complex in the bromide excess region as AgBr_3^{2-} and thus on dilution molecular silver bromide is probably formed by dissociation of the complex in the following manner,



The fact that monodisperse sols were formed suggested that these reactions were reasonably slow (i.e., with half-lives of the order of seconds). In order to test this hypothesis experiments were carried out in a spectrophotometer adapted for rapid mixing and automatic recording (27). A solution of the silver bromide complex was added to water in the spectrophotometer cell to give conditions such that the sol formed was the same as that described earlier (see above). The resultant curve of optical density against time is shown in Fig. 7. The induction period was not completely reproducible but was always in the region of 3 to 7 seconds, suggesting that nucleation was delayed until the concentration of "molecular" silver bromide had reached the critical value, in agreement with La Mer's hypothesis (1, 2). The experiment was then repeated with the water replaced by a dilute silver nitrate solution. Concentrations in the region 10^{-6} to 10^{-11} M were investigated, and it was found that at pAg values less than 10 the induction period disappeared completely. This

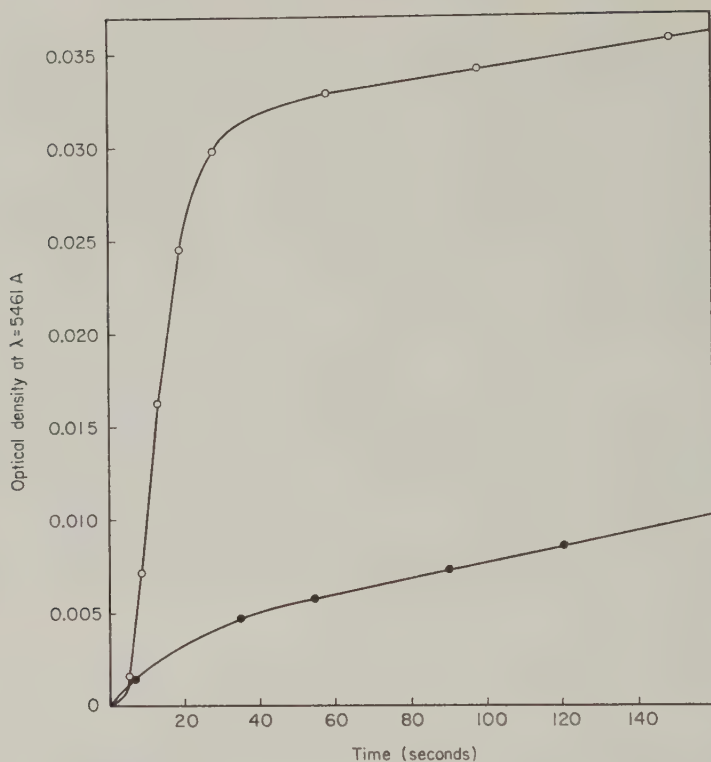


FIG. 7. Decomposition of silver bromide complex, - ○ - by addition of distilled water; - ● - by addition of 10^{-9} M silver nitrate.

suggested that immediate nucleation had occurred owing to reaction of the silver ions already present in the water with bromide ions. The resultant sol was one of many small particles.

It would appear plausible that nucleation occurs during mixing in the concentration gradient of the formed boundary regions. The nuclei then become distributed throughout the solution and growth continues by diffusion of the molecular silver bromide formed by the "relatively" slow decomposition of the complex (region III, Fig. 1, inset). It is of interest in this connection that slow mixing, as used by Herak *et al.* (14), produced a small number of nuclei and thus large particles. Rapid mixing using a Hartridge-Roughton mixing chamber (28) produced a large number of nuclei and a sol of small particles. The method of mixing primarily employed in the present work was intermediate between these two extremes and gave particles of the order of 0.3 to 0.6μ in diameter in a fairly reproducible way.

The silver bromide particles formed in the bromide excess region were

regular octahedra, whereas those produced in the region of ionic solubility by cooling, a region where silver and bromide ions were present in virtually equal concentrations, were cubes. The shape of the particles produced in the excess silver region was not easy to determine although a tendency to octahedral growth was apparent.

In the case of silver iodide the shape of the particles formed in the excess iodide region suggested that these were in the form of β -hexagonal silver iodide. This is in agreement with observations that silver iodide formed in the presence of an excess of iodide ions is hexagonal (29, 30). In the presence of excess silver the particle shape was not so well defined. From electron micrographs of shadowed carbon replicas the particles appeared to be rounded hexagonal plates. "Rounding off" appeared to be a common feature of the crystals in many fresh sol preparations, with perfection occurring on aging.

The methods developed and described in this communication have led to the preparation of sols of silver bromide and silver iodide of a high degree of monodispersity. All the sols prepared exhibited HOTS. The latter phenomenon does not necessarily mean that the sols are completely monodisperse, but it is usually a criterion that they are nearly so (7). This is confirmed by the present work. Detailed optical and electrokinetic experiments on the sols described in this paper are in progress and will appear in a later publication.

We wish to thank Messrs Ilford Ltd. for a grant which has defrayed the cost of this investigation. It is also a pleasure to thank Mr. H. O. Dickinson and Mr. C. Waller for stimulating discussions on this subject and Mr. R. W. Horne for taking the electron micrographs.

REFERENCES

1. LA MER, V. K., AND DINEGAR, R. H., *J. Am. Chem. Soc.* **72**, 4847 (1950).
2. LA MER, V. K., *Ind. Eng. Chem.* **44**, 1270 (1952).
3. LA MER, V. K., AND BARNES, M. D., *J. Colloid Sci.* **1**, 71 (1946).
4. BARNES, M. D., AND LA MER, V. K., *J. Colloid Sci.* **1**, 79 (1946).
5. JOHNSON, I., AND LA MER, V. K., *J. Am. Chem. Soc.* **69**, 1184 (1947).
6. BARNES, M. D., KENYON, A. S., ZAISER, E. M., AND LA MER, V. K., *J. Colloid Sci.* **2**, 349 (1947).
7. LA MER, V. K., *J. Phys. & Colloid Chem.* **52**, 65 (1948).
8. ZAISER, E. M., AND LA MER, V. K., *J. Colloid Sci.* **3**, 571 (1948).
9. WATILLON, A., VAN GRUNDERBEECK, F., AND HAUTECLER, M., *Bull. soc. chim. Belges* **67**, 5 (1958).
10. GINELL, R., GINELL, M. A., AND SPOERRI, E. P., *J. Colloid Sci.* **2**, 521 (1947).
11. TAKIYAMA, K., *Bull. Chem. Soc. Japan* **31**, 950 (1958).
12. TAKIYAMA, K., *Bull. Chem. Soc. Japan* **31**, 944 (1958).
13. HERAK, M. J., HERAK, M. M., TEŽAK, B., AND KRATOCHVIL, J., *Archiv. Kem.* **27**, 117 (1955).
14. HERAK, M. J., KRATOCHVIL, J., HERAK, M. M., AND WRISCHER, M., *Croat. Chem. Acta* **30**, 221 (1958).

15. BRADFORD, E. B., AND VANDERHOFF, J. W., *J. Appl. Phys.* **26**, 864 (1955);
BRADFORD, E. B., VANDERHOFF, J. W., AND ALFREY, T., *J. Colloid Sci.* **11**, 135 (1956).
16. OVERBEEK, J. TH. G., in KRUYT, H. R., ed., "Colloid Science," Vol. 1. Elsevier, Amsterdam, 1952.
17. TEŽAK, B., MATIJEVIĆ, E., SCHULZ, K. F., KRATOCHVIL, J., MIRNIK, M., AND VOUK, V. B., *Discussions Faraday Soc.* **18**, 63 (1954).
18. VOUK, V. B., KRATOCHVIL, J., AND TEŽAK, B., *Archiv. Kem.* **25**, 219 (1953).
19. KRATOCHVIL, J., TEŽAK, B., AND VOUK, V. B., *Archiv. Kem.* **26**, 191 (1954).
20. BERNE, E., AND LEDEN, I., *Z. Naturforsch.* **8a**, 719 (1953).
21. LEDEN, I., AND PARCK, C., *Acta Chem. Scand.* **10**, 535 (1956).
22. LEDEN, I., *Acta Chem. Scand.* **10**, 540 (1956).
23. LEDEN, I., *Acta Chem. Scand.* **10**, 812 (1956).
24. GLEDHILL, A., AND MALAN, G. MCP., *Trans. Faraday Soc.* **50**, 126 (1954).
25. OTTEWILL, R. H., AND WILKINS, D. J., *J. Colloid Sci.* **15**, 512 (1960).
26. BRADLEY, D. E., *Brit. J. Appl. Phys.* **10**, 198 (1959).
27. OTTEWILL, R. H., AND SIRS, J. A., *Bull. Photoelectric Spectrometry Group* **10**, 262 (1957).
28. HARTRIDGE, H., AND ROUGHTON, F. J. W., *Proc. Roy. Soc. (London)* **A104**, 376 (1923).
29. TRILLAT, J. J., AND LALOEUF, A., *J. chim. phys.* **46**, 168 (1949).
30. HORNE, R. W., AND OTTEWILL, R. H., *J. Phot. Sci.* **6**, 39 (1958).

ELECTROCHEMISTRY OF SILVER IODIDE¹ THE CAPACITY OF THE DOUBLE LAYER AT THE SILVER IODIDE-WATER INTERFACE

J. Lyklema and J. Th. G. Overbeek²

van't Hoff Laboratory, Sterrenbos 19, Utrecht, The Netherlands

Received February 30, 1961

I. INTRODUCTION

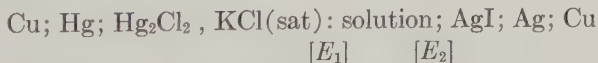
Extensive and accurate data on the properties of the electrical double layer on mercury have been collected by several investigators (e.g., by Grahame (1) and by Frumkin (2)). Data on other double layers are much more scanty. It is the purpose of the present paper to extend the existing data on silver iodide (Verwey (3), Verwey and Kruyt (4), De Bruijn (5), van Laar (6), Mackor (7)) particularly by using a greater variety of counter ions and co-ions.

Silver iodide has an important advantage over mercury as a subject for study of electrochemical properties of interfaces, in that the properties of colloidal AgI (e.g., stability, electrophoresis) are well known and are available for comparison with electrochemical data. It has the disadvantage (compared to mercury) that the range over which the interfacial potential difference can be varied is much less (ca. 450 mv. as compared to 2400 mv.).

II. EXPERIMENTAL PART

a). Outline of Method

The first aim of the experiments was the determination of the surface charge (σ) as a function of the potential difference across the interface. The galvanic cell:



¹ Based on the doctor's thesis of J. Lyklema, "Adsorptie van Tegenionen" (Adsorption of Gegenions), Utrecht, 1957.

² The second author expresses his gratitude to the Petroleum Research Fund for supporting his stay at the University of Southern California, Los Angeles 7, California, in 1959-1960 during which this paper was written.

was used for this purpose. The e.m.f. of this cell, E_{cell} , reflects any changes in the properties of the solution through E_1 and E_2 . When the concentrations in the solution are not too high E_1 can be kept virtually constant (see below), in which case

$$dE_{\text{cell}} = dE_2. \quad [1]$$

The changes in the solution involved variations in the concentrations of the potential-determining (Ag^+ , I^-) ions and in the concentrations and natures of indifferent ions. The ionic strength of the solution was kept constant during the process first mentioned.

The surface charge is defined through

$$\sigma = F(\Gamma_{\text{Ag}^+} - \Gamma_{\text{I}^-}), \quad [2]$$

in which Γ_{Ag^+} and Γ_{I^-} represent the number of equivalents of silver and iodide ions, respectively, adsorbed per square centimeter. These quantities can be found from a simple material balance when the concentrations of Ag^+ or I^- ions are known; these in turn can be evaluated directly from E_{cell} .

The surface charge, defined by [2], is the thermodynamic analog of the electrical charge on the mercury interface in surface electrochemical investigations. It is identical with the true surface charge provided Ag^+ and I^- are the only specifically adsorbed ions.

It should be kept in mind that calibrations have to be carried out for each type and concentration of electrolyte in order to allow for variations in the liquid junction potential, E_1 , and in the activity coefficients of the potential-determining ions.

In order to increase the available adsorbing surface the solution contained a suspension of finely divided silver iodide, which must be in equilibrium with the silver iodide of the electrode.

It is customary and advantageous to choose the zero point of charge (z.p.c.) as the reference point for E_2 and σ ; $E_2 - E_2(\text{z.p.c.})$ will be called ψ , the double layer potential. The z.p.c. can be determined by several independent methods. For silver iodide in dilute solutions of monovalent electrolytes at 25°C., van Laar (6) found it to be located at

$$-\log C_{\text{I}^-} = P_{\text{I}^-} = 10.56. \quad [3]$$

From $d\sigma$ and dE_2 the differential capacity of the double layer C is found through

$$C = \frac{d\sigma}{dE_2}. \quad [4]$$

b). Essential Parts of the Experimental Setup

The actual measurements consist in determinations of E_{cell} after addition of successive small amounts of a silver or an iodide salt solution. As

it takes a long time before the adsorption equilibrium is established, particularly near the equivalence point, the establishment of one single adsorption isotherm may require several days, during which the liquid junction potential E_1 must be constant and reproducible. Errors resulting from the contamination of the solution by KCl from the salt bridge (and consequent precipitation of AgCl) must therefore be minimized. This was achieved by using a salt bridge as described previously by van Laar (8). In this salt bridge, in which the mixture of KNO_3 and NaNO_3 (8) is substituted by a saturated KCl solution, the KCl is discharged under a known excess pressure through a very narrow hole into the solution. In our case only 1.3×10^{-8} g.-equivalents of KCl per hour were introduced into about L/4 of the solution. In lengthy experiments a small correction for precipitated AgCl was inevitable. The adsorption capacity of the AgCl, however, was negligible.

The silver iodide electrodes were prepared electrolytically essentially after De Bruijn (5a). Their standard potentials remained constant within 0.1 mv. during a couple of titrations, and within 1 or 2 mv. for a year or longer.

The purest chemicals commercially available were used. In most cases they were of AnalaR quality. Whenever necessary they were recrystallized until the chloride impurity was small compared with the amount of chloride introduced by the salt bridge.

The e.m.f.'s were measured with a Philips pH-meter (type GM 4491) at 20°C. under standard conditions of stirring and an excess pressure of 1 atm. on the KCl. Readings were generally reproducible within 0.3 mv.

Recent unpublished experiments in our laboratory by R. S. Hansen and B. H. Bijsterbosch resulted in incompletely reversible adsorption isotherms of deviating shapes. Though the origin of these irregularities is not yet fully understood they have probably to do with impurities of the reagents. In order to confirm the reliability of the results described in this paper, E. J. van Tellingen and D. van Wijngaarden conducted some experiments on AgI which was filtered off once after charging it negatively and once after charging it positively in the hope of discarding all charged impurities (surfactants, chloride, etc.). Though their isotherms still deviated slightly from the ones published here at the silver side of the z.p.c. in 10^{-3} KNO_3 solution, the 10^{-1} isotherms of this paper and especially the influence of the nature of the counter ion (Li, K, Rb) were confirmed within experimental error.

c). Surface Area and Aging

In order to transform the adsorption into a specific surface charge the specific surface area of the suspension must be known. None of the methods used, however, is felt to be entirely satisfactory. In the methods where the AgI precipitate has to be dried, as in the B.E.T. gas adsorption methods, the surface area might be changed irreversibly. In the "wet" methods, such as the methylene blue adsorption, the area per adsorbed molecule is

rather uncertain. The situation is further complicated by the decrease of the adsorption capacity on aging.

In the subsequent section a surface area of $5.76 \text{ m}^2/\text{gram}$ is used. This value was found by an indirect method, namely, by measuring the differential capacity of AgI per gram at the z.p.c. in 10^{-3} M KF or NaF solution and by assuming that the differential capacity per square centimeter of AgI under these conditions is the same as that for Hg. The latter value is known from the work of Grahame (1). This assumption is based on the consideration that in dilute electrolyte solutions at the z.p.c. the total capacity per square centimeter should be governed chiefly by its diffuse part and this should be independent of the nature of the interface. The great similarity of capacities on AgI and mercury under these conditions near the z.p.c. provides some experimental justification for this assumption.

We have tried to check this surface area by means of some direct adsorption methods (Table I) but none of these methods is accurate enough to allow more than a confirmation of the order of magnitude.

In methods 2, 3, and 4 use was made of the molecular area of the adsorbed molecules on coal. The first value of method 5 was calculated with a molecular area of the methylene blue molecule of 197 \AA^2 (Graham, on coal (9)), the second one with 386 \AA^2 (v. d. Heuvel, on BaSO_4 (10)).

From a theoretical point of view the sixth method is outstandingly attractive. This method was previously used by Schofield (11) on clay suspensions. It is based on the expulsion of co-ions (e.g., SO_4^{--} -ions from a negatively charged surface). The relative concentration increment of repelled ions written as $\Delta c/\sqrt{c}$ is proportional to the surface area. The advantages of this method are: (a) it measures a surface area in the conditions of experimental interest (wet); (b) it measures what may be regarded as the "electrochemical" surface; (c) the co-ion distribution can

TABLE I
Surface Area Determination of AgI Suspensions

No.	Method	Temp.	AgI sample		Surface area ($\text{m}^2/\text{g.}$)
			Condition	Age	
1	Double layer capacity	Room	Wet	100 days	5.76
2	BET with N_2 -vapor	-196°C.	Dried	Freshly prepared	12
3	BET with CCl_4 -vapor	Room	Dried	Very old	0.85
4	BET with benzene vapor	Room	Dried	100 days	4-6
5	Ads. of methylene blue	Room	Wet	100 days	3.8; 7.4
6	Negative adsorption of sulfate ions	Room; 5°C.	Wet	100 days	5-6

be exactly calculated by the Gouy-Chapman theory. However, the experimental precision so far obtained has been low owing principally to the small values of $\Delta c/\sqrt{c}$ so that the agreement between areas obtained in this way with those obtained from double layer capacitance must be fortuitously good.

III. RESULTS AND DISCUSSION

a). Double Layer Capacities in Solutions of Monovalent Symmetrical Electrolytes

The adsorption of potential-determining ions on AgI expressed as σ as a function of ψ is given in Fig. 1 for three concentrations of KF. (It is known from the work on mercury (1) that the fluoride ion shows no tendency to specific adsorption; the same is expected to be true for AgI.)

The isotherms of Fig. 1 are independent of the direction in which σ and ψ are changed. In the study of a given electrolyte, the curves were established as follows. The suspension was made positive by addition of some AgNO_3 , the salt concentration adjusted, and then titrated, with a KI solution to the extremity of the measurable range at the negative side. The electrolyte concentration was then increased to $10^{-1} M$ and titrated backward as far as possible. The point of intersection with the abscissa of the 10^{-1} curves, found in this way appeared to be displaced slightly (generally less than 10 mv.) from that of the 10^{-3} curves. This can be attributed either to a shift of the z.p.c. with the electrolyte concentration or to (an accumulation of) experimental errors. To make isotherms comparable the 10^{-1} curve was shifted parallel to the abscissa; this means that the z.p.c. in 10^{-1} solutions was taken equal to that of 10^{-3} solutions. The ones last mentioned were, in turn, taken to correspond to the value of Van Laar (see Section II, a).

The manipulation has only a minor influence on the capacity (slope of the curve).

On the silver side of the z.p.c. a correction had to be made for silver ion consumed by precipitation of AgCl , the chloride being delivered by the salt bridge. For justification of this correction see Section III, c.

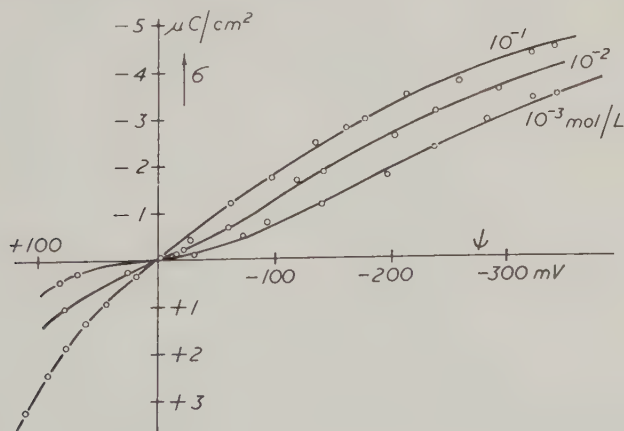


FIG. 1. Adsorption of I^- and Ag^+ ions on AgI in solutions of KF.

The adsorption isotherms show a close resemblance to similar isotherms obtained previously in NaClO_4 (Mackor (7c)) and $\text{KNO}_3 + \text{NaNO}_3$ mixtures (Van Laar (6)). There is also some analogy with isotherms on mercury (Grahame (1)) or on silver sulfide (Iwasaki and de Bruyn (12)).

By graphical differentiation of the isotherms of Fig. 1 the corresponding differential capacities are obtained. They are presented in Fig. 2. By way of comparison the theoretical diffuse double layer capacity Cd as calculated from the Gouy-Chapman theory is given in Fig. 2 (dotted line) for 10^{-3} and $10^{-2} M$ solutions of a monovalent binary electrolyte.

The observed capacity C closely resembles the theoretical Cd in solutions of low concentration near the z.p.c.

This is exactly what must be expected from the Gouy-Stern theory. According to this theory the double layer consists of a diffuse and a non-diffuse part. Their capacities Cd and Cm , respectively, are in series, and provided there is no specific adsorption:

$$\frac{1}{C} = \frac{1}{Cd} + \frac{1}{Cm}. \quad [5]$$

The value of Cd can be calculated to be

$$Cd = \sqrt{\frac{\epsilon n e^2}{2\pi k T}} \cosh\left(\frac{y}{2}\right), \quad [6]$$

in which ϵ is the dielectric constant, n the number of ions of either sign per milliliter in the bulk, e the elementary charge, k the Boltzmann con-

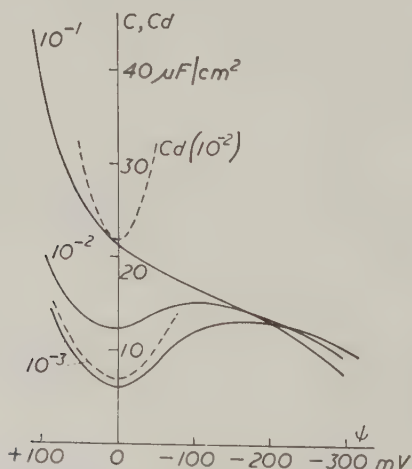


FIG. 2. Differential capacity C of the double layer on AgI in 10^{-3} , 10^{-2} , and $10^{-1} M$ KF-solutions as a function of the potential. Dotted lines: capacity Cd according to the diffuse double layer theory.

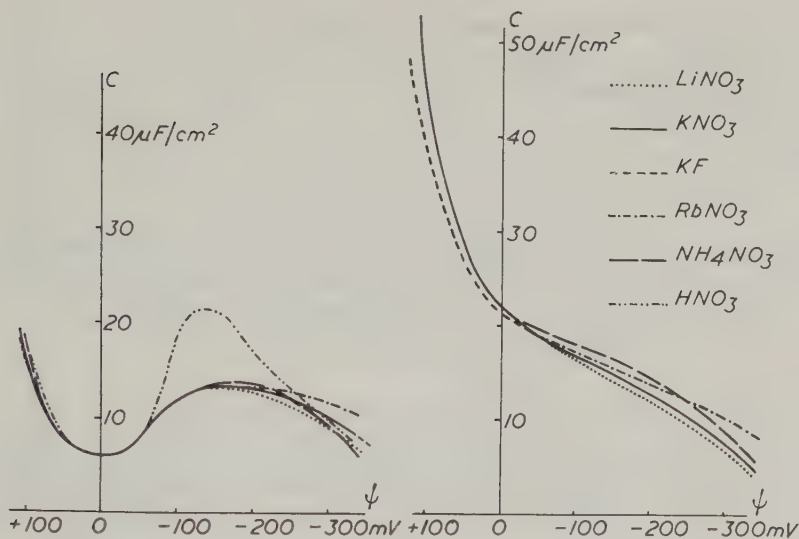


FIG. 3. Differential capacity of the double layer on AgI in solutions of some monovalent nitrates and KF. *a.* 10^{-3} mole/l. *b.* 10^{-1} mole/l.

stant, T the absolute temperature, and $y = e\psi_s/kT$. The potential ψ_s on the boundary between the diffuse double layer and the molecular condenser can be calculated from

$$\sigma = \sqrt{\frac{2\epsilon n k T}{\pi}} \sinh \frac{y}{2}. \quad [7]$$

As follows from Fig. 2 the total capacity is smaller than the diffuse one. This is in agreement with Eq. [5]. Especially at very high potentials $Cd^{-1} \sim 0$ (see Eq. [6]), and the capacity is governed predominantly by its nondiffuse part, which appears to be independent of the electrolyte concentration, as was also found to be the case for mercury (1).

The capacity rises sharply as the AgI is made increasingly positive. For mercury such a behavior is due to specific adsorption of anions. The behavior of AgI may have the same explanation. At any rate we shall limit our considerations mainly to negative surfaces.

All capacity curves show some tendency to decrease at very high negative potentials. This can possibly be attributed to the fact that the adsorption of I^- ions on AgI proceeds only on active centers which will be saturated long before the total surface area is occupied. A further discussion of this possibility is published elsewhere by one of us (13).

The influence of the nature of the counter- and co-ion is illustrated in Fig. 3, from which the following may be read:

a). As expected all capacities merge in the region where the diffuse part of the double layer prevails.

b). The influence of the co-ion is negligible within the experimental error: compare, for example, KF and KNO_3 on negative AgI or KNO_3 and RbNO_3 on positive AgI.

c). The influence of the cations at the negative side follows the lyotropic order:



This sequence was also found for mercury by Grahame (14) and is reflected in the flocculation values of the negatively charged AgI-sol (15).

d). The capacity on the positive side decreases in the order



In Fig. 3 the NaClO_4 -curve is not given for the sake of clarity.

e). The shapes of the HNO_3 and NH_4NO_3 -curves are somewhat deviating. The proton, owing to the small dimensions of the H_3O^+ ion, seems to be able to follow the diffuse pattern up to a higher surface potential. The character of the NH_4NO_3 -curve might be connected with a possible specific relation between the AgI and the NH_4^+ -ion (complex formation).

The phenomena described in this section can be illustrated by Fig. 4, giving Stern capacities for some monovalent electrolytes, calculated from

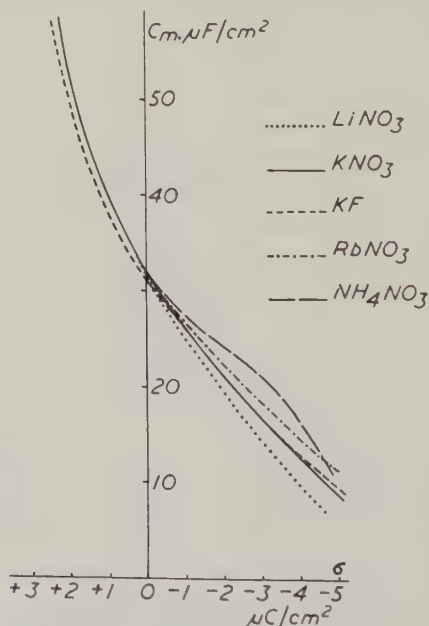


FIG. 4. Differential capacity of the molecular condenser of the double layer on AgI in solutions of some monovalent electrolytes.

the experimental 10^{-1} capacity curves with the aid of Eqs. [5], [6], and [7].

The curves are qualitatively similar to those for mercury, the capacities are of the same order of magnitude, and the specific influence of ions is in the same order (1, 14). There are, however, a few striking quantitative differences. The Stern capacity changes more strongly with surface charge for AgI than for mercury and the lyotropic effects are also more pronounced for AgI. Both these effects might be connected with the somewhat more discrete character of the double layer for AgI (13).

b). Double Layer Capacities in Solutions of Asymmetrical Electrolytes

Sets of representative capacity curves are given in Figs. 5, 6, 7, 8, and 9. In these curves the solid lines represent the experimental capacities, whereas the dotted lines represent the diffuse capacities now to be calculated from

$$Cd = \sqrt{\frac{\epsilon n e^2}{8\pi k T}} \cdot z_- z_+ \frac{|e^{-z_- y} - e^{-z_+ y}|}{\sqrt{-z_- e^{-z_+ y} + z_+ e^{-z_- y} + z_- - z_+}}. \quad [8]$$

In [8] z_- and z_+ are the valencies of the negative and the positive ion (sign included), and n is the electrolyte concentration in neutral molecules/cm.³; for $z_+ = 1$ and $z_- = -1$ [8] changes into [6].

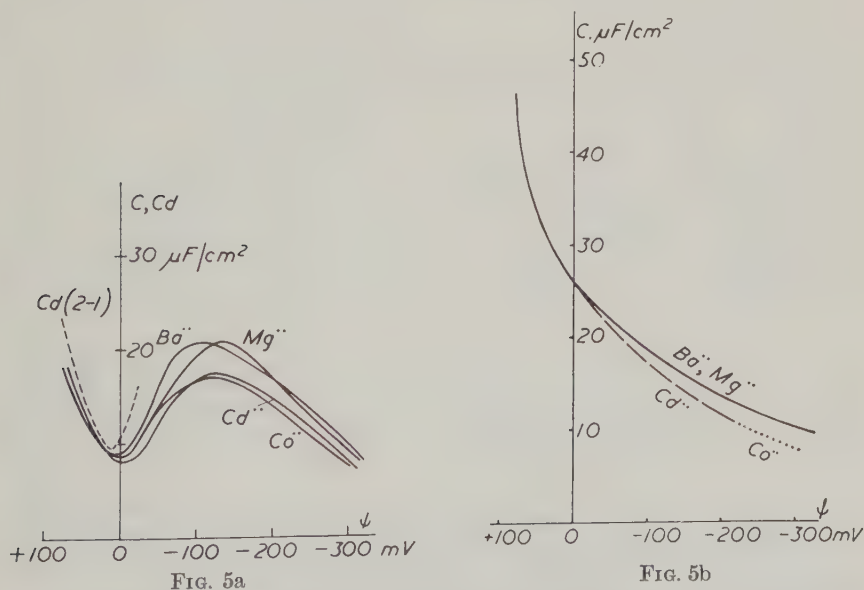


FIG. 5. Differential capacity of the double layer on silver iodide in solutions of some bivalent nitrates. *a.* 10^{-3} mole/l. Dotted line: Cd . *b.* 10^{-1} mole/l.

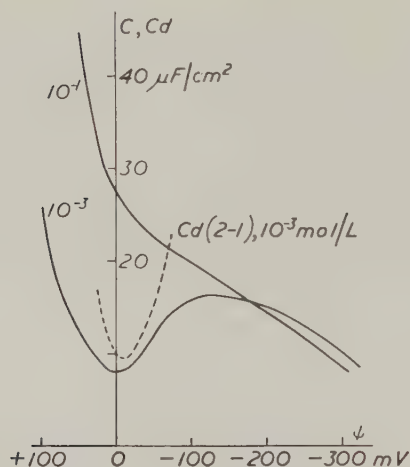


FIG. 6. Differential capacity of the double layer on AgI in 10^{-3} and 10^{-1} M K_2SO_4 . Dotted: Cd in 10^{-3} M solution.

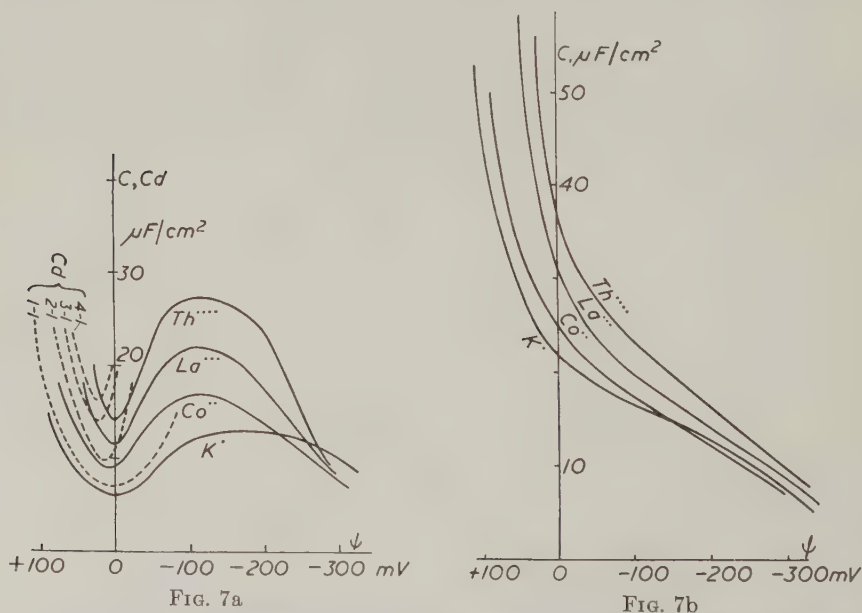


FIG. 7. Differential capacity of the double layer on AgI. Influence of the charge of the cation. a. 10^{-3} mole/l. Dotted lines: Cd. b. 10^{-1} mole/l.

From these figures the following can be read:

- It is seen that the qualitative appearances of these curves are of the same character as those of the (1-1) curves (Figs. 3 and 4).
- The lyotropic order for bivalent cations on negative AgI is



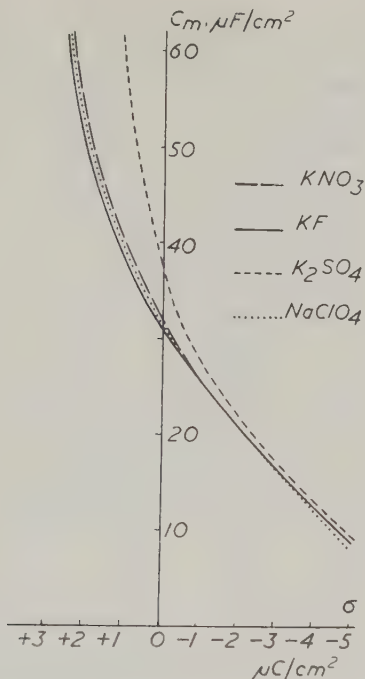


Fig. 8. Differential capacity of the molecular condenser of the double layer on AgI. Influence of the anion.

The mutual differences are somewhat less pronounced than those between the monovalent cations. This is also the case with their flocculation values (15).

c). The capacity maximum at the negative side of the z.p.c. in 10^{-3} *M* solutions is reached at a lower (less negative) potential than in 10^{-3} (1-1) solutions. Furthermore the capacities at the maximum are higher. This can be seen as a consequence of the stronger compression of the diffuse part of the double layer by the multivalent counter ion. As a further consequence of the great increase in *Cd*, *Cm* (which is less dependent on ψ) can prevail at lower surface potentials.

d). On increasing cationic charge the capacity of the diffuse part shows an increasing minimum value and a stronger curvature. This is reflected in the experimental 10^{-3} *M* curves in the region near the zero point of charge.

e). Theoretically a shift in the minima of *Cd* to the side of positive surface charge is expected. This is not clearly reflected in the experimental curves (Fig. 7a). However, the experimental determination of the minimum of *C* involves the establishment of the point of inflection in curves of the type of Fig. 1 (10^{-3} curve) in a region of low slope. This process cannot be performed without some arbitrariness. The uncertainty in the establish-

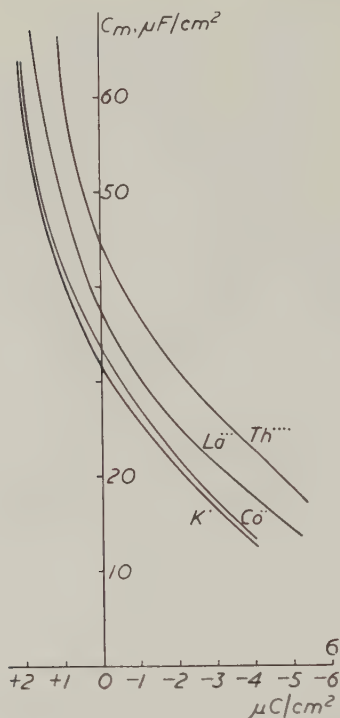


FIG. 9. Differential capacity of the molecular condenser of the double layer on AgI. Influence of the charge of the cation.

ment of the experimental minimum is accompanied by some uncertainty as to the exact location of the z.p.c. in millimolar solutions of asymmetrical electrolytes. It deviated from its value in 10^{-3} KNO_3 by a small amount, as was found by van Laar (6) and by us. The deviations, however, were poorly reproducible and not very systematic. For that reason we preferred to make use of the well-established z.p.c. in 10^{-3} KNO_3 . Consequently this problem must be considered to be not yet solved.

In this connection it should be noted that no real significance has to be attributed to the fact that at positive $\text{AgI } C > Cd$ for La^{3+} and Th^{4+} , which would mean that C_m should be negative.

c). Cases of Pseudocapacity

The electrolytes treated above showed no specific relation to Ag^+ or I^- ions. When this condition is not fulfilled, the adsorption process can be accompanied by a supplementary Ag^+ or I^- ions consuming process, leading to a nonreal capacity ("pseudocapacity").

Chloride ions interfered by precipitation of AgCl . Experiments in which a known amount of chloride ions was added showed that precipitation of

AgCl (consumption of Ag^+ without change in e.m.f.) occurred at the value calculated from the solubility product of AgCl. The conclusion that this precipitation is not influenced by the presence of suspended AgI could be employed in the correction for KCl, delivered by the salt bridge, as described in Section II, *b*.

Lead can interfere by precipitation of PbI_2 but the solubility product is so high that it is not reached. Capacity curves were of the same type as those presented in Fig. 5. (Curves are not given for sake of clarity.)

Thallium forms a sparingly soluble iodide with a solubility product of 3.6×10^{-8} . This is reached easily in not too dilute solutions of TlNO_3 . Before the solubility product was reached the capacity was markedly higher than those of the other monovalent electrolytes. The solubility product could be established experimentally from the (known) Tl^+ -concentration and the p_{I^-} at which the consumption of iodide ions increases sharply under formation of a precipitate of TlI (the bright yellow color of which could be distinguished easily from the pale yellow of the AgI). We found 1.9×10^{-9} , independent of the amount of AgI and Tl^+ -concentration. It is possible that an epitaxis of TlI on AgI is responsible for this deviation from the literature value. A similar effect was found by Bergna and de Bruyn (16), who found Ag_2O to precipitate on positive AgI before its solubility product was reached. In connection with the anomalous behavior of Tl^+ its low flocculation value can be mentioned ($\frac{1}{5}$ of that of other monovalent electrolytes).

Cadmium. In the greater part of the potential range Cd^{2+} behaved about as Co^{2+} (Fig. 5). At high iodide concentration in $10^{-1} M \text{Cd}(\text{NO}_3)_2$ -solution a too high consumption of I^- -ions was observed before the solubility product was reached. We presume that the complex formation



is responsible. From the estimated deviation of the "normal" behavior, the concentration of CdI^+ can be found. As further the equilibrium concentrations of Cd^{2+} and I^- are known, the equilibrium constant can be evaluated. We found

$$p_K = -\log \frac{[\text{CdI}^+]}{[\text{Cd}^{2+}][\text{I}^-]} = 1.89$$

in reasonable agreement with $p_K = 1.76$ as found by Quintin and Pelletier (17).

In the region of complex formation the capacity curve is omitted in Fig. 5*b*.

SUMMARY

A method is described for obtaining differential double layer capacities on silver iodide. Especially the influence of the nature and concentration

of indifferent electrolytes was investigated, viz., the nitrates of Li⁺, K⁺, Rb⁺, NH₄⁺, H⁺, Tl⁺, Mg²⁺, Ba²⁺, Co²⁺, Cd²⁺, Pb²⁺, La³⁺, Th⁴⁺, the fluoride, chloride, and sulfate of K⁺, NaClO₄ in 10⁻³ and 10⁻¹ M solutions. Capacities showed definite analogy with those on mercury. The influence of the counter ion was in the lyotropic order. The capacity of the molecular condenser, calculated with the assumption of absence of specific adsorption, was independent of the electrolyte content.

REFERENCES

1. GRAHAME, D. C., *Chem. Revs.* **41**, 441 (1947).
2. FRUMKIN, A. N., *Ergeb. exakt. Naturw.* **7**, 235 (1928).
3. VERWEY, E. J. W., *Proc. Koninkl. Akad. Wetenschap. Amsterdam* **36**, 225 (1933); *Chem. Revs.* **16**, 363 (1935).
4. VERWEY, E. J. W., AND KRUYT, H. R., *Z. physik. Chem.* **A167**, 137, 149, 312 (1933).
5. BRUIJN, H. DE, *Rec. trav. chim.* **61**, 5, 12, 21, 189, 193 (1942).
6. LAAR, J. A. W. VAN, Thesis, State University of Utrecht, 1952.
7. MACKOR, E. L., *Rec. trav. chim.* **70**, 663, 747, 763, 841 (1951).
8. LAAR, J. A. W. VAN (to N. V. Philips Gloeilampenfabrieken, Eindhoven, Netherlands), Dutch Patent 79,472, Nov. 15, 1955.
9. GRAHAM, D., *J. Phys. Chem.* **59**, 896 (1955).
10. HEUVEL, W. V.D., *Koninkl. Vlaam. Acad. Wetenschap. Belg. Kl. Wetenschap.* **17**, No. 8 (1955).
11. SCHOFIELD, R. K., *Trans. Faraday Soc.* **42b**, 219 (1946); *Nature* **160**, 408 (1949).
SCHOFIELD, R. K., AND TALIBUDDIN, O., *Discussions Faraday Soc.* **No. 3**, 51 (1948).
12. IWASAKI, I., AND BRUYN, P. L. DE, *J. Phys. Chem.* **62**, 594 (1958).
13. LYKLEMA, J., to be published.
14. GRAHAME, D. C., *J. Electrochem. Soc.* **98**, 343 (1951).
15. KRUYT, H. R., AND KLOMPÉ, M. A. M., *Kolloid-Beih.* **54**, 484 (1942).
16. BERGNA, H., AND BRUYN, P. L. DE, *Mass. Inst. Technol. Progr. Rept.* **No. 31** (April 30, 1956); *ibid* **No. 32** (July 31, 1956).
17. QUINTIN, M., AND PELLETIER, S., *J. chim. phys.* **54**, 226 (1956).

FLOCCULATION-DISPERSION BEHAVIOR OF QUARTZ IN THE PRESENCE OF A POLYACRYLAMIDE FLOCCULANT

T. W. Healy

Mining Department, University of Melbourne, Australia¹

Received March 14, 1961

ABSTRACT

Electrokinetic, adsorption, and subsidence studies on quartz dispersions in the presence of a commercial, synthetic, polyacrylamide type flocculant are reported.

Additional evidence is given for the bridging mechanism of polymer flocculation. This model is extended to include the effect of agitation on the adsorption of polymer and on subsequent flocculation.

INTRODUCTION

Considerable interest is being directed towards understanding the mechanism of adsorption of macromolecules on dispersed inorganic solids and the flocculation-dispersion phenomena associated with this adsorption.

Several factors hinder quantitative analysis of the problem, among these being the difficulty of obtaining monodisperse polymer samples and the general lack of information on the forces responsible for the adsorption of polymers at the solid-liquid interface. Furthermore, the stability of aqueous suspensions of insoluble inorganic compounds, in the presence of polymer flocculants, is influenced by many variables (1, 2).

An attempt has been made in this study to understand the effect of three of the more important variables on the adsorption-flocculation process for the system quartz-Separan 2610. Separan 2610 is a partially hydrolyzed polyacrylamide flocculant supplied by the Dow Chemical Corporation. Variables studied were surface charge of the solid-liquid interface and the intensity and time of agitation.

It has been suggested, but not proved, that the variation of zeta potential of the solid-liquid interface will have little effect on the mechanism of polymer flocculation (2). Likewise the bridging theory of polymer flocculation, accepted by most workers in this field (1-3, 4) merits further substantiation.

Certain aspects of the effect of agitation have been reviewed by Linke and Booth (5) and other workers (2). In these particular studies, no dis-

¹ Present address: Chemistry Department, Columbia University, New York 27, New York.

tion was made between time and intensity of agitation; see, however, reference 1. The effect of both these variables is important to the understanding of the mechanism of polymer flocculation.

EXPERIMENTAL

Samples of clean reef quartz from Diamond Creek and Buninyong areas in Victoria were used in the preparation of sized fractions of quartz for zeta potential, adsorption, and subsidence measurements. The quartz was stage ground under conductivity water in an Abbe type pebble mill. Samples of $-14 + 20$ mesh (Tyler) and $-48 + 65$ mesh (Tyler) material were removed, and stored under conductivity water for zeta potential measurements. The quartz used in the adsorption and subsidence work was 95% -400 mesh (Tyler). One stock solution of this pulp was used for all adsorption and subsidence work.

Conductivity water was prepared by passing once-distilled water through a mixed cation, anion exchange resin column.

Freshly prepared solutions of the synthetic flocculant Separan 2610, described by Dow as a partially hydrolyzed polymer of acrylamide and other monomers, were used throughout the project. They had an average molecular weight of one million. This was estimated by ionic group titration together with information from the Dow Chemical Corporation.

1. Measurement of Electrokinetic Potentials

The electrokinetic potential (ζ) of quartz was determined by a streaming potential technique which was a modification of that used by Buchanan and Heymann (6). The electrokinetic potential is defined as the electrical potential at the plane of shear with respect to a point in the bulk liquid which is considered to be at zero potential. With the convention that a negative zeta potential corresponds to a negative surface charge, the zeta potential was calculated from the measured streaming potential by means of the Helmholtz-Smoluchowski equation

$$\zeta = -\frac{4\pi\eta}{D} \cdot \frac{EC}{RP}, \quad [1]$$

where η is the viscosity, D is the dielectric constant of the liquid, E is the measured streaming potential when liquid is forced through a plug by a pressure P . Here C/R is the specific conductance of liquid which permeates the plug, C being the plug constant and R the electrical resistance between the electrodes during streaming.

No deviation from linearity was observed for the E/P vs. P plot for the pressure range 18–28 cm. Hg. Streaming potentials were measured with a Cambridge valve potentiometer, and plug resistances and solution conductances were determined by means of an a.c. bridge, Philscope type G.M. 4144.

Zeta potentials were reproducible to ± 1.0 mv. at low values, and to ± 2.0 mv. at high values.

2. Adsorption Measurements

A conductivity method, similar to that of Black (7), was used to determine adsorption of Separan on quartz. The apparatus consisted of a Pyrex glass conductivity cell into which was fixed a rotor blade stirrer. Agitation conditions in the cell were varied by means of a rheostat on the stirrer motor. If 10 units represents one full scale of the rheostat, then conditions of gentle, mild, and violent agitation correspond to scale readings of 1, 3, and 5 units, respectively. For settings above 6, turbulence and whirlpool action in the cell caused air entrapment within the pulp.

Residual polymer concentration after adsorption was read off a calibration curve of electrical resistance vs. polymer concentration, due allowance being made for the contribution of soluble silica.

3. Subsidence Measurements

Subsidence rates were determined from the slope of the initial constant rate period of the height of subsiding column vs. time plots. (No initiation period was observed, and curves were all of Type II, of Smellie and La Mer (8).) The flocculated pulps were allowed to stand undisturbed in Pyrex glass cylinders, 6 cm. in diameter.

A standard procedure for mixing flocculant solution with the pulp was obtained empirically, *viz.*, ten end-over-end rotations of the cylinder at constant speed, during which 100 ml. of the desired flocculant solution was added in three increments, after the second, fifth, and eighth cycles, respectively. By this procedure it was possible to obtain subsidence rates, for a given flocculated sample, which did not vary by more than ± 1.0 cm./min.

RESULTS

1. Electrokinetic Potentials

In the subsequent discussion, the change in zeta potential, calculated from the measured streaming potential by means of Eq. [1], is used as a measure of the variation of adsorption behavior of macromolecules at surfaces and not as a quantitative measure of the charge density in the electrical double layer of quartz.

Furthermore, it must be stressed that inherent limitations in electrokinetic techniques and in calculation of zeta potentials from streaming potentials by Eq. [1] do not allow quantitative correlation of zeta potentials with aggregation phenomena (9).

The variation of the zeta potential of quartz with Separan 2610 concentration is shown in Fig. 1. After determination of the zeta potential at each concentration, approximately 6 liters of conductivity water was streamed through the plug of quartz, and the zeta potential was redeter-

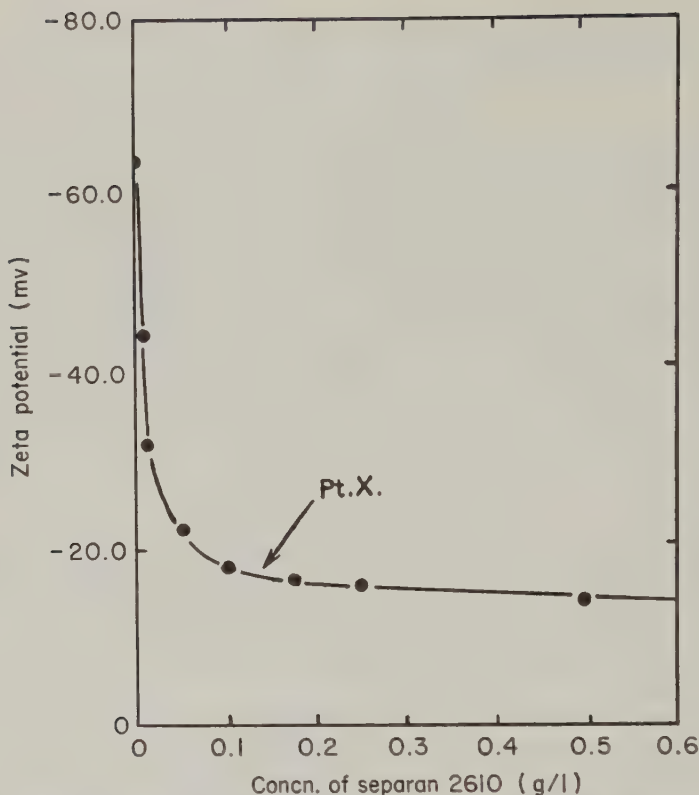


FIG. 1. Zeta potential of quartz in aqueous solutions of Separan 2610 at pH 5.9.

mined during streaming of the sixth liter of water. The results of these tests are summarized in Table I.

For the system noted in these results, -16.5 mv. is referred to as the "wash-back" potential (Point X in Fig. I). For concentrations up to and including 0.1 g./liter there is no significant alteration in zeta potential after the wash procedure. However, for concentrations greater than 0.1 g./liter the potential after washing attained a constant value of -16.5 mv. As washing did not alter the zeta potential of quartz in Separan 2610 solutions up to 0.1 g./liter, the adsorption of polymer to this stage is therefore considered to be irreversible to washing. Although the potential decreases at concentrations greater than 0.1 g./liter the adsorption is reversed by washing.

2. Adsorption Measurements

Adsorption results are reported in Fig. 2 and are summarized in Table II. The time to attain steady-state adsorption, for the above system, was

TABLE I
Summary of Zeta Potential Data

Concentration of Separan 2610 (g./liter)	Zeta potential of quartz in test solution (mv.)	Zeta potential ¹ of quartz after plug washing (mv.)
0	-63.0	-63.0
0.001	-43.5	-44.0
0.010	-31.5	-31.5
0.050	-21.5	-22.0
0.100	-17.5	-18.0
0.175	-16.0	-16.5
0.250	-15.5	-16.5
0.500	-13.5	-16.5
0.750	-12.5	-16.5

¹ Determined in conductivity water.

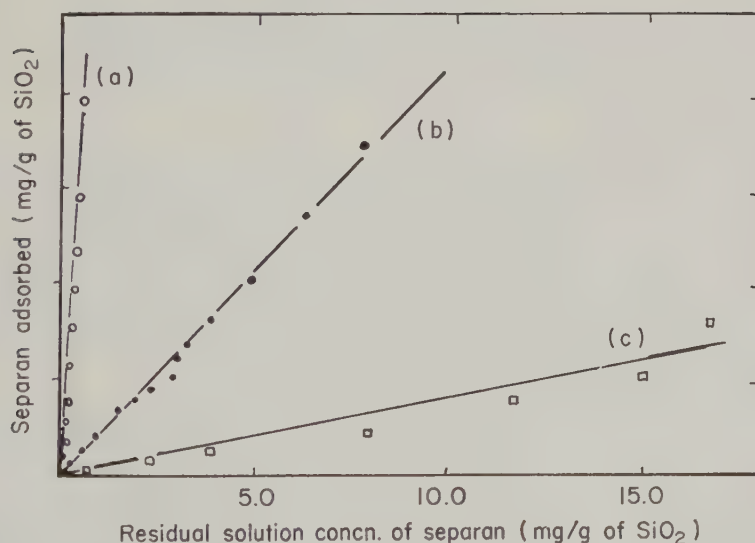


FIG. 2. Adsorption behavior of quartz-Separan 2610 under conditions of (a) mild, (b) medium, and (c) strong intensity of agitation.

too rapid to measure, i.e., less than 2 secs. after addition of polymer solution to the cell. Prolonged time of agitation, at any one fixed intensity, did not alter the residual polymer concentration in solution. Furthermore, as the intensity of agitation was increased the average floc size of the pulp decreased.

Analysis of the shape of the adsorption curves is not possible since assumptions in using the conductimetric method cannot be substantiated

TABLE II

Adsorption of Separan 2610 on Quartz as a Function of Intensity of Agitation

Polymer added (mg./g. of quartz)	Conditions of agitation		
	Gentle	Mild Polymer adsorbed (mg./g. quartz)	Violent
0.33	0.33	0.27	0.10
0.67	0.67	0.50	0.16
1.67	1.58	1.15	0.40
3.33	3.00	2.30	0.70
6.67	6.48	4.75	1.65

in the scope of the present study. However, the wide separation of amount adsorbed with change in intensity of agitation is of particular interest.

3. Subsidence Results

The effect of polymer addition on the subsidence rate is shown in Fig. 3. Similar optimum behavior was shown at other pulp densities between 3 % and 15 % solids (by weight) and has been observed for other polyacrylamide type flocculants (5).

The effect on the subsidence rate of time of agitation at a fixed intensity is shown in Fig. 4, in which curves 1, 2, and 3 represent Separan 2610 additions of 7.5×10^{-5} , 20.0×10^{-5} , and 42.5×10^{-5} g./g. of solids, respectively. The greater the initial polymer concentration, the more resistant are the flocs to redispersion. For the highest concentration (No. 3) redispersion was not observed until pre-agitation was eight times the standard value, whereas at low concentrations (No. 1) significant redispersion occurred at twice standard pre-agitation.

The pertinent experimental results may be summarized as follows:

1. There is a rapid decrease in zeta potential of quartz with increasing Separan concentration. The potential is not reduced to zero.
2. With increasing intensity of agitation: *a.* the amount of polymer adsorbed decreases, and *b.* the average floc size of the pulp decreases.
3. With increasing time of agitation at a fixed intensity: *a.* the amount of polymer adsorbed does not change, but *b.* the degree of flocculation (or average floc size) decreases.
4. The resistance of the flocs to redispersion increases as polymer concentration increases.

DISCUSSION

From Fig. 1 it can be seen that a substantial reduction in the magnitude of the zeta potential occurs at low solution concentrations, although with increasing concentration of polymer the zeta potential is not reduced to

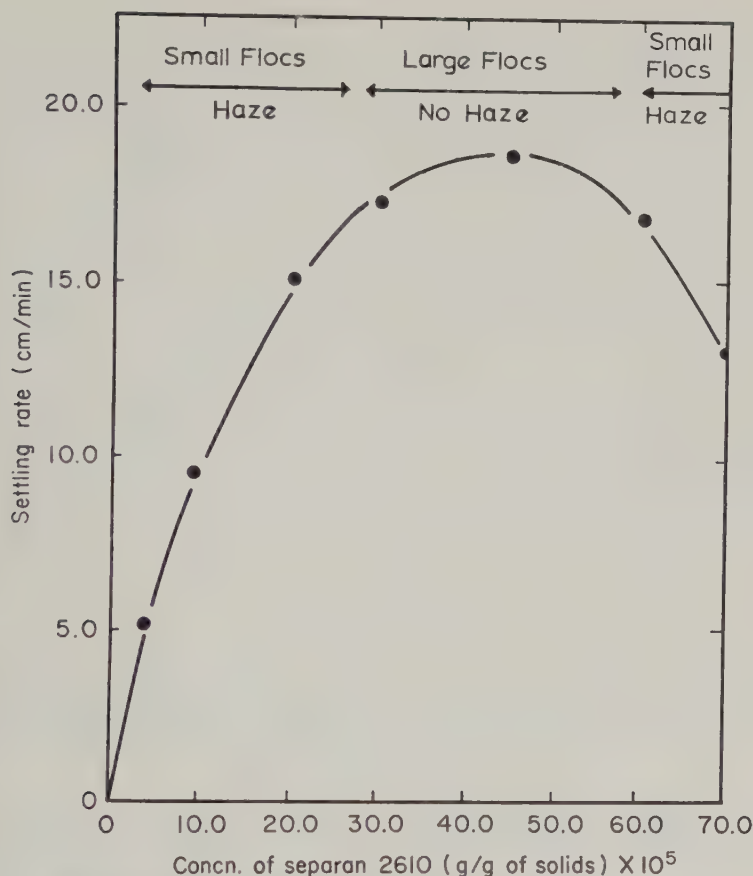


FIG. 3. Effect of flocculant addition on the settling rate of a quartz pulp of 5% solids (pH 5.9).

zero. Point X (Fig. 1) corresponds to a potential energy barrier of approximately $0.5 kT$. This barrier is low enough to allow rapid coagulation to proceed. However, the flocculation shown in Fig. 3 is much more extensive than that shown by, for example, inorganic ion adsorption. Some additional mechanism must be introduced to explain flocculation by polymeric compounds. It would appear that the zeta potential reduction accompanying polymer adsorption is a subsidiary mechanism to that of bridge formation by the polymer molecules between adjacent solid particles in the pulp.

The significance of the wash-back effect shown in Table I is not completely understood. It would seem that the adsorption reaction must be agitation controlled. The first polymer chains can attach at many points on the surface. As the polymer concentration increases the surface becomes more and more covered and each additional molecule adsorbed is held at

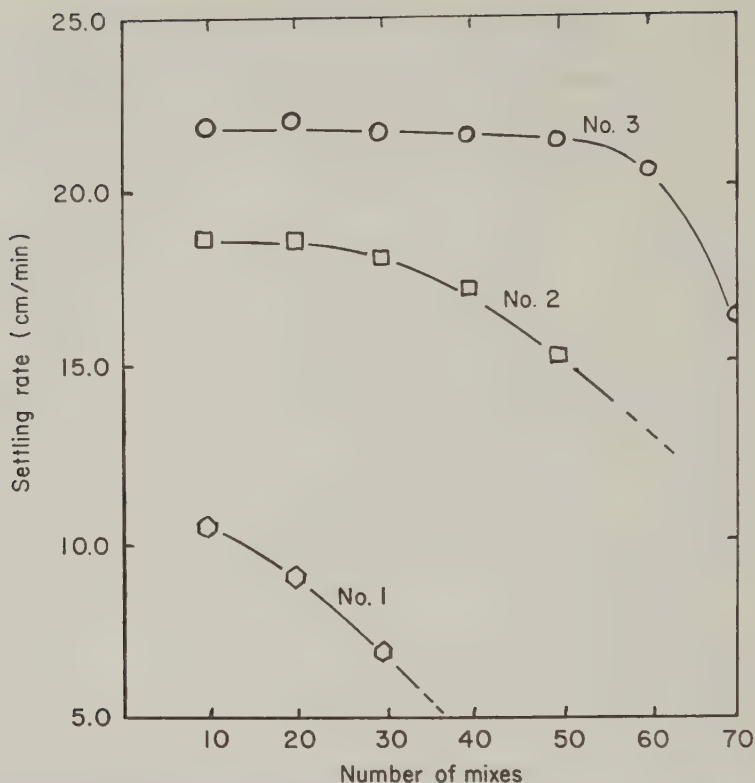


FIG. 4. Effect of extent of agitation on settling rate of quartz pulps at three flocculant additions. (For Key see text.)

fewer and fewer sites. At any condition of shear there is a critical number of sites at which the polymer chain must be attached for it to remain adsorbed. This model also seems to fit the subsidence data.

The optimum effect shown in Fig. 3 will not be discussed in detail. It has been observed by other workers (1, 3, 5) and may be summarized as follows: The degree of flocculation, at any particular concentration of polymer depends on (a) the length and number of extended segments, and (b) the available surface onto which extended segments can bridge.

This bridging model of the flocculation process can be extended to explain the observations given above. First, since individual chains adsorb at only a fraction of the active sites per molecule (10), the more intense the agitation the more difficult it is for polymer to adsorb a critical number of groups and stay attached; i.e., as intensity of agitation increases, the amount of polymer adsorbed decreases (Fig. 2).

Second, increasing time of agitation at a fixed intensity does not change the amount of polymer adsorbed, but the degree of flocculation decreases

(i.e., redispersion). Also the rate of redispersion at low concentrations of polymer is greater than at high concentrations. Consider the floc of solid particles bridged together by polymer chains. There will be random movement, partly restricted, of the units of the floc. During this motion the bridging segments of the polymer are reduced in length and number by adsorption on adjacent or individual particles, and the flocs themselves become less resistant to shear. At low surface coverage (low polymer addition), adsorption of extended segments is more rapidly accomplished than at high surface coverage. Furthermore a longer time, at any fixed intensity of agitation, is required at the higher concentrations of polymer, since the probability of an extended segment finding free surface onto which it can adsorb is less than at low surface coverage.

Finally it must be stressed that the above discussion is based on observations of the system quartz-polyacrylamide. Other mineral-polymer systems may show divergence from the present system. The bridging model of polymer flocculation would seem adequate at present. Further information on the adsorption forces responsible for initial adsorption of polymer is needed to test the model in more detail.

ACKNOWLEDGMENTS

The author gratefully acknowledges the award of a Consolidated Zinc Metallurgical Research Scholarship.

He also wishes to thank those personnel of the Mining Department, University of Melbourne, who assisted him in many ways in this project.

REFERENCES

1. LA MER, V. K., SMELLIE, R. H., JR., AND LEE, PUI-KUM, *J. Colloid Sci.* **12**, 230 (1957).
2. McCARTY, M. F., AND OLSON, R. S., *Mining Eng.* **11**, 61 (1959).
3. LA MER, V. K., AND SMELLIE, R. H., JR., *J. Colloid Sci.* **11**, 709, 711 (1956).
4. RUEHRWEIN, R. A., AND WARD, D. W., *Soil Sci.* **73**, 485 (1952).
5. LINKE, W. F., AND BOOTH, R. B., Preprint, American Institute of Mining and Metallurgical Engineers, Annual Meeting, 1959.
6. BUCHANAN, A. S., AND HEYMANN, E., *Proc. Roy. Soc. (London)* **195**, 150 (1948).
7. BLACK, A., M. Eng. Sci. Thesis, Melbourne, Australia, 1952.
8. SMELLIE, R. H., JR., AND LA MER, V. K., *J. Colloid Sci.* **11**, 720 (1956).
9. BIKERMAN, J. J., "Surface-Chemistry—Theory and Applications." Academic Press, New York, 1958.
10. ULMAN, R., KORAL, J., AND EIRICH, F. R., *Proc. 2nd. Intern. Congr. Surface Activity* **3**, 485 (1957).

THERMODYNAMICS OF POLY(METHYL ACRYLATE)
MONOLAYERS

J. Llopis and J. A. Subirana

*Instituto de Química Física "Rocasolano", Madrid, Spain**Received March 20, 1961*

ABSTRACT

Monolayers of poly(methyl acrylate) spread at the a/w interface have been studied at different temperatures. Samples of carefully fractionated polymer have been used in order to study the influence of molecular weight. In each case the compression isotherms have been obtained and the surface pressures π have been plotted as a function of temperature T , for given values of area A . The representations of πA vs. $1/A$ allow conclusions to be drawn on the variation of the second virial coefficient B as a function of temperature. If the values of B thus obtained are plotted versus $1/T$ straight lines may be fitted to the experimental points. The behavior of the monolayers is different below or above the "ideal temperature" θ at which the coefficient B is zero. On the other hand, the spreading entropies s_s and enthalpies h_s can be determined from the slopes of the curves π vs. T . It is shown that for high values of the area both s_s and h_s are nearly linear with $1/A^2$, tending to zero when $A \rightarrow \infty$. The equation of state of these polymer monolayers has been discussed, and it may be seen that surface pressure is mainly produced at the segment-segment contacts.

The regular chemical constitution of synthetic linear polymers allows us⁸ to think that their behavior as monolayers might be simpler than that of other macromolecular substances. Even so it is convenient to choose a polymer in which the inter- and intramolecular forces are not very great and the hysteresis effects in the successive compressions and expansions of the monolayer are negligible. The chosen substance for this study has been poly(methyl acrylate). This is a linear polymer of head-to-tail structure, with a paraffinic main chain having ester groups ($-\text{COOCH}_3$) regularly attached. In this paper we have studied the influence of temperature and molecular weight on monolayers of this polymer. The samples used have been carefully fractionated.

The influence of temperature on the compression isotherms of these monolayers allows us to separate the enthalpic and entropic contributions to the surface pressure π . The compression isotherms, π vs. A (area), may be expressed as

$$\pi A = RT \left[\left(\frac{1}{M_n} \right) + B \left(\frac{1}{A} \right) + C \left(\frac{1}{A^2} \right) + \cdots \right], \quad [1]$$

M_n being the number-average molecular weight and $B, C \dots$ the virial coefficients.

These coefficients usually depend on temperature, and the form of this dependence, mainly for the second coefficient B , may supply valuable data for a better understanding of the interactions in the monolayer. In this paper it is shown that there is a temperature θ at which the coefficient B is zero, and the behavior of the monolayer is different below and above this temperature.

It is known (1) that the influence of molecular weight, on the monolayers of synthetic polymers is negligible under the usual experimental conditions (surface pressure above 0.2 dynes cm^{-1}), provided that the molecular weight is high enough (>2000). However, the surface technique has been used to evaluate molecular weights, and therefore it would be convenient to clarify under what conditions this method will be suitable for such determinations. Accordingly the behavior of five fractionated samples of molecular weights ranging between 4,000 and 750,000 has been studied at low surface pressures. We have also established the convenience of working above the "ideal" temperature, θ .

PREPARATION OF THE SAMPLES OF POLY(METHYL ACRYLATE)

Different transfer agents were used in the polymerizations to obtain a range of molecular weights. The concentration of initiator (benzoyl peroxide) was always relatively high and did not have much influence on the molecular weight obtained.

The polymers were fractionated using acetone as solvent and a methanol-water (7:3) mixture as precipitant. In one case (sample A) the precipitant was water only. In each case one fraction was chosen and carefully re-fractionated to obtain a more homogeneous sample.

The molecular weights were established by the viscosity of solutions in benzene or ethyl acetate, using the relations described in the literature (Table I). In two cases (samples B and C) the equation used was extrapolated, introducing a possible source of error.

Table I summarizes the most important data concerning the polymerizations. Sample C was obtained by refractionation of the first fraction of sample B. Sample E was first precipitated with petrol ether from its solution in benzene, in order to eliminate the substances of low molecular weight, before the actual fractionation.

EXPERIMENTAL TECHNIQUE

The surface balance used was described elsewhere (6). Its sensitivity per degree of torsion of the wire was about 0.060 dyne cm^{-1} . The balance was enclosed in a wooden box to allow thermostatic control. The substrate was kept at constant temperature (within 0.1°C.) with a glass coil immersed

TABLE I
Description of Samples

Sample	Transfer agent	Number of fractions	Molecular weight of fraction used	References
A	Br ₄ C	9	4,100	2
B	Isopropyl benzene	7	17,000	3, 4
C	Isopropyl benzene	5	34,000	3, 5
D	Ethyl acetate	3	140,000	5
E	Benzene	8	750,000	5

in the trough and supplied with water from a bath at the working temperature.

All experiments were carried out at the air/water (10^{-3} N HCl) interface. The polymer was dissolved in benzene (0.2–1.0 mg./ml.) and the monolayers were spread with an "Aglä" microsyringe. It was confirmed that neither the acidity of the substrate nor the concentration of the polymer in the spreading solution has any influence on the force-area curves. The compression was initiated 4 minutes after spreading the monolayer and was performed slowly and continuously with a motor. The absence of hysteresis was confirmed by the fact that successive compression and expansion isotherms coincided. The behavior of these monolayers was studied between 5°C. and 50°C.

EXPERIMENTAL RESULTS

The Compression Isotherms

The compression isotherms of the monolayers were usually determined between 20°C. and 50°C. Some curves were also obtained between 5°C. and 20°C. for samples A and D. The results obtained with sample D have been described in a recent paper (6).

It is well known (1) that polymers having a great internal cohesion, e.g., nitrocellulose, nylon, and poly(acrylonitrile), do not spread well at the air/water interface. Therefore, it is important to know first of all if the polymer to be studied spreads perfectly. This may be verified by spreading different amounts of polymer from several solvents and different concentrations. Spreading is good if pressure is reproducible for a given area *A*. The behavior of sample D was studied in detail, monolayers being spread from solutions ranging between 0.2 mg./ml. and 1.1 mg./ml. and with compression started at different initial areas. The results obtained were reproducible within experimental error.

The effect of the solvent retained in the monolayer is also to be considered, since it may have a great influence, as Robbins and La Mer have shown recently (7). In our case this effect has no observable influence,

probably because the side chains of poly(methyl acrylate) are very short and the retention of solvent among them is difficult. The great effect of the spreading solvent observed by Robbins and La Mer on monolayers of stearic acid and stearyl alcohol is due to the interaction of benzene with the long paraffinic chains of these compounds.

The representation π vs. $1/A$ is more suitable for study of the compression isotherms, since it gives curves passing through the origin, and hence the graphical fitting of a curve to the experimental points may be done more easily. Moreover, the slope at the origin is negligible for high enough molecular weights and it facilitates the drawing of the interpolated curves.

The results of eight experiments performed with sample D at 35°C. are represented in Fig. 1. Four spreading solutions of 0.27₈, 0.44₀, 0.67₃, and 1.1 mg./ml., were used, while the initial area ranged between 8 and 15 m.²/mg. The isotherms corresponding to 20°C. and 50°C. are also represented.

From isotherms like those in Fig. 1, curves of π vs. T may be drawn, for given values of A . The curves corresponding to sample D appear in a preceding paper (6). It is observed that the surface pressure varies very little between 10°C. and 25°C. and it is difficult to decide whether or not there exists a minimum between these temperatures. On the other hand,

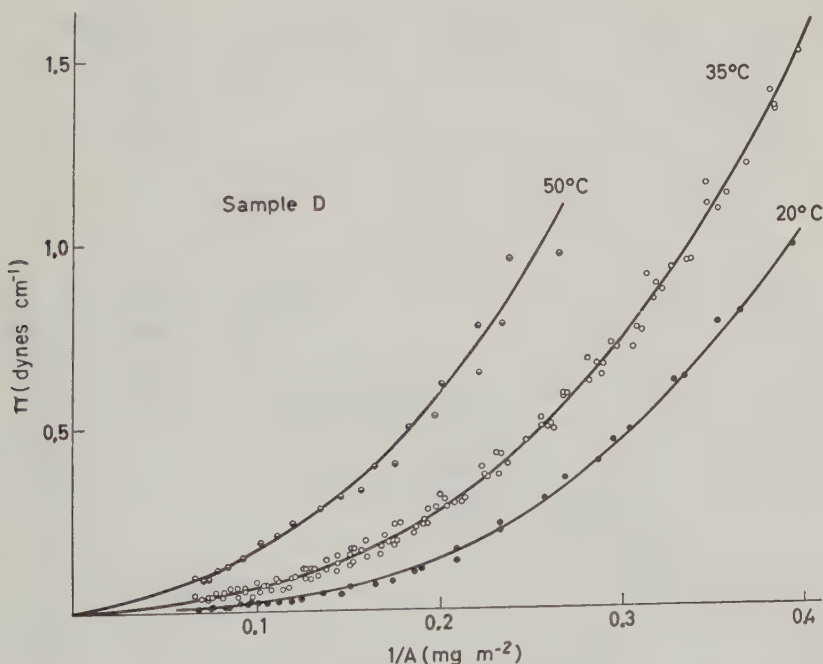


Fig. 1. Compression isotherms, π vs. $1/A$, at different temperatures. Sample D.

the surface pressure increases rapidly for temperatures above 25°C. All the samples show similar behavior, but at high areas the surface pressure increases with decreasing molecular weight.

Figure 2 shows the values of πA vs. $1/A$, for sample B at six temperatures. The points plotted in the figure have been obtained from the interpolated π vs. T curves, for a set of values of A , so that the scatter of the experimental results is minimized.

The intercept $(\pi A)_0$ of these curves depends on the molecular weight, and they may be represented by an empirical equation such as [1]. For low values of $1/A$ the high-order terms may be omitted and the plot is linear. This linear part is longer and its slope greater at higher temperature, and it is also longer with increasing molecular weight. Figure 3 shows the plot of πA vs. $1/A$ at 35°C. with two samples, A and E, of very different molecular weight. For sample A the linear part is much reduced.

The second virial coefficient B may be determined from the initial slope of the plot πA vs. $1/A$ (Fig. 2). The values of B thus obtained are plotted in Fig. 4 against $1/T$, for all the samples of polymer here studied. Straight lines with negative slopes may be fitted to the experimental points. These lines have a common point of the $1/T$ axis and therefore B may be written

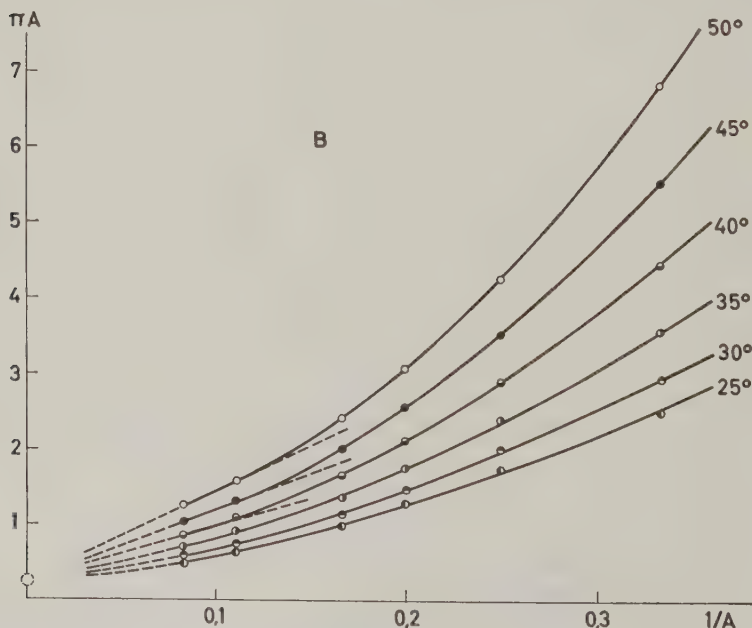


FIG. 2. Plots of πA vs. $1/A$ for different values of temperature. Sample B, molecular weight $M_n = 17,000$.

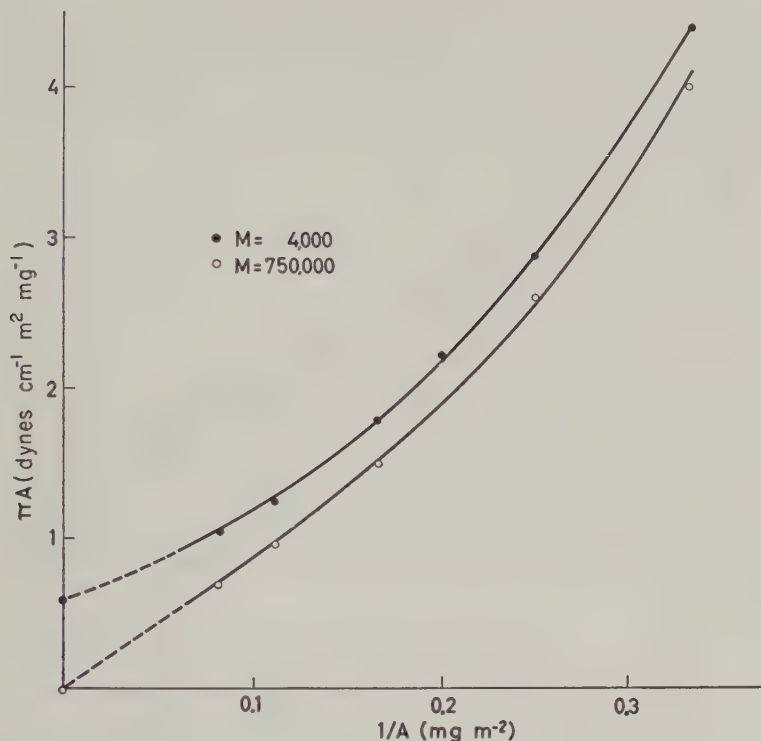


FIG. 3. Plots of πA vs. $1/A$. Samples A and E. Temperature 35°C.

as:

$$B = \varphi \left(1 - \frac{\theta}{T} \right), \quad [2]$$

where $\theta = 292.7^\circ\text{K}$. (19.5°C .). The values of φ are given in Table II. It may be seen that φ shows a slight tendency to increase with molecular weight.

Curves rather than straight lines would better fit the experimental points represented in Fig. 4, and it would be necessary to add higher terms in expression [2]. Nevertheless, the parameters φ and θ calculated from the straight lines are useful in the interpretation of the results.

Thermodynamic Spreading Functions

The spreading functions may be obtained from the plots of π against T , for given values of the area A . The equations to be used are

$$s_s = \left(\frac{\partial \pi}{\partial T} \right)_A; \quad h_s = T \left(\frac{\partial \pi}{\partial T} \right)_A - \pi. \quad [3]$$

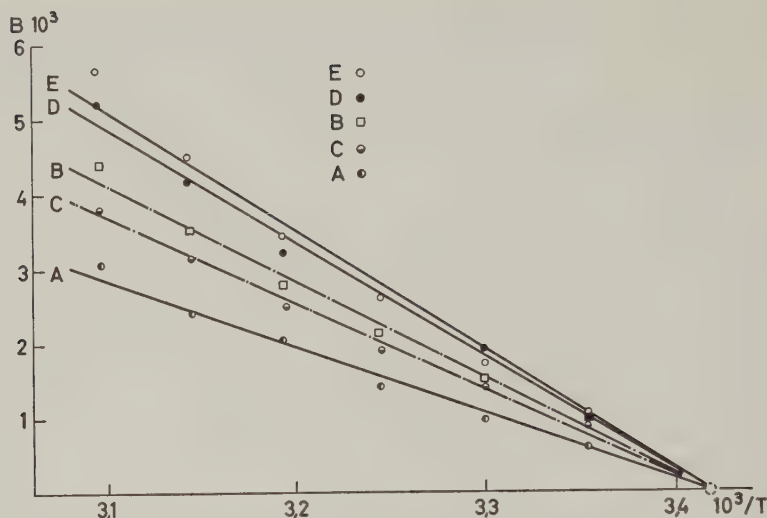


FIG. 4. Values of the second virial coefficient B vs. $1/T$. Samples of different molecular weight.

TABLE II
Values of φ for the Samples

	Sample				
	A	B	C	D	E
M_n	4,000	17,000	34,000	140,000	750,000
$\text{Log } M_n$	3.61	4.0	4.21	5.14	5.87
$\varphi \cdot 10^2 \text{ m.}^2\text{mg.}$	3.3 ₅	4.4 ₅	4.0 ₀	5.3 ₅	5.4 ₅

The formal analogy of these functions with the corresponding dilution terms for bulk solutions has been established elsewhere (8).

The values of h_s and s_s have been calculated for all samples at 25°C. and 50°C. The plots of both functions against $1/A^2$ for sample D have been discussed in reference 6, and it can be seen that the fitted curves are linear up to areas of 4 or 5 m.²/mg. The values obtained with the other samples are nearly the same and plots versus $1/A^2$ are similar, but the initial slope has a tendency to increase with molecular weight.

The values obtained at 25°C. for both h_s and s_s are not very reliable, since at this temperature the ways of fitting the curves π vs. T to the experimental points has a remarkable influence on the values of the slope $(\partial\pi/\partial T)_A$.

The observed parallelism between h_s and s_s seems to be general for all macromolecular substances for which these functions have been calcu-

lated (8). From [3] it may be seen that the formal cause of this behavior is the fact that $\pi \ll Ts_s$ and, furthermore, the variations of π and s_s with $1/A^2$ are very similar.

If the second virial coefficient may satisfactorily be approximated by [2], then Eq. [1] may be written without the higher terms as:

$$\pi = RT \left[\frac{1}{M_n A} + \varphi \left(1 - \frac{\theta}{T} \right) \frac{1}{A^2} \right]; \quad [4]$$

and then [3] becomes

$$s_s = \frac{R}{M_n A} + R\varphi \frac{1}{A^2}; \quad h_s = R\varphi\theta \frac{1}{A^2}. \quad [5]$$

The term R/M_n is very small for high polymers and, therefore, the plots of h_s and s_s versus $1/A^2$ must be linear as long as higher terms are negligible, in agreement with the experimental results. The parameters φ and θ may be also calculated from the slopes of these straight lines and the values thus obtained at 40°C. agree fairly well with those of Table I. This fact may be a help in the extrapolation of the curves πA vs. $1/A$, used to determine molecular weights.

According to [5] h_s and s_s should be independent of temperature. However, for temperatures higher than 30°C. the values of the slopes $(\partial\pi/\partial T)_A$ seem to increase slightly with temperature, and therefore s_s will also increase. This variation could be taken into account by considering higher terms in [2] and therefore in [5], but the scatter of the experimental results does not allow an accurate estimate of the dependence of s_s on T .

DISCUSSION

The equation of state of the monolayer should take account of all molecular interactions. The easiest way is to estimate these interactions through a term proportional to $1/A^2$, as Saraga and Prigogine have done (9). In some cases the equation thus obtained is sufficient to account for the experimental results, especially those involving the second virial coefficient.

However, because of their great importance in the equation of state, it is necessary to have a better knowledge of such interactions. On the basis of the quasi-lattice theory it may be assumed that the interactions take place only between nearest neighbors. When the number of contacts and its influence on the number of available configurations are computed, an expression for the thermodynamic functions can be derived.

The same parameters will be used here as in Münster's (10) work, where the subscripts 1 and 2 designate the substrate (solvent) and the polymer (solute), respectively. The energy of configuration is given by

$$E^* = z(X_{11}u_{11} + X_{12}u_{12} + X_{22}u_{22}), \quad [6]$$

where u_{11} , u_{12} , and u_{22} are the interaction energies of each kind of contact and zX_{11} , zX_{12} , zX_{22} are the total numbers of contacts between nearest neighbors, z being the coordination number of the two-dimensional lattice.

The number of contacts satisfies the following equations:

$$\begin{aligned} N_1 &= 2X_{11} + X_{12}; \\ qN_2 &= 2X_{22} + X_{12}; \end{aligned} \quad [7]$$

where N_1 and N_2 are the total number of molecules and q is the number of nearest neighbors of a polymer molecule.

Equation [6] may be written

$$E^* = E_0 + zu_m X_{22}, \quad [8]$$

where

$$E_0 = \frac{z}{2} (N_1 - qN_2)u_{11} + zqN_2 u_{12}; \quad [9]$$

$$u_m = u_{11} + u_{22} + 2u_{12}. \quad [10]$$

Now, the partition function of the surface solution may be written and the summation replaced by its maximum term

$$\frac{Q(T)}{N_1! N_2!} = e^{-E_0/kT} g(N_1, N_2, \bar{X}_{22}) e^{-z\bar{X}_{22}u_m/kT}, \quad [11]$$

where $g(N_1, N_2, X_{22})$ is the number of possible configurations with zX_{22} segment-segment contacts and \bar{X}_{22} is the number of these contacts corresponding to the maximum term of the sum.

If G_μ be the surface free energy of mixing, then an expression for the surface pressure π may easily be obtained from Eq. [11].

$$\pi = -\frac{\partial G_\mu}{\partial A} = -kT \frac{\partial \ln g}{\partial A} + u_m \frac{\partial (z\bar{X}_{22})}{\partial A}. \quad [12]$$

At this stage some simplifications must be introduced to calculate this expression. In the zeroth approximation (11), \bar{X}_{22} is evaluated by assuming a random mixing. The error introduced by this approximation will probably be negligible, as it is for the theory of solutions (12). Therefore,

$$\bar{X}_{22} = \frac{1}{2} \frac{(qN_2)^2}{N_1 + qN_2}. \quad [13]$$

The monolayer may be visualized as a surface solution consisting of molecules of the substrate and polymer molecules lying on it with the hydrophilic groups penetrating into the substrate. The number of external contacts of a polymer molecule (r -mer) within the surface layer may be

expressed by

$$zq = r(z - 2) + 2, \quad [14]$$

where the second term is negligible for large r . From Eqs. [13] and [14] the number of contacts $z\bar{X}_{22}$ may be expressed in the following way

$$z\bar{X}_{22} = \frac{(z - 2)^2 A_0}{2M_0} \frac{1}{(zA - 2A_0)}, \quad [15]$$

where rM_0 is the molecular weight of the polymer and A_0 the area in the close-packed state. According to the results of Benson and McIntosh (13), $A_0 = 1.5 \text{ m}^2 \text{ mg}^{-1}$ for poly(methyl acrylate).

By differentiating Eq. [15] it is now possible to calculate the second term of Eq. [12]

$$\frac{\partial(z\bar{X}_{22})}{\partial A} = -\frac{(z - 2)^2 A_0}{2zM_0} \frac{1}{\left[A - \left(\frac{2\bar{X}z}{z}\right) A_0\right]^2}. \quad [16]$$

In the first term on the right-hand side of Eq. [12], let g be regarded as the product of two factors: g_c (the chain configuration factor) and g_m (the contact configuration factor). The first one changes with that part of the expansion which does not alter the numbers of contacts of different kinds; the second one is associated with the change in these numbers accompanying expansion. The elementary processes by which these numbers change involve a change of internal energy u_m and a change in configurational entropy s_m . It is this change of entropy which alters g_m and it can be included in the second term on the right-hand side of Eq. [12] if u_m is replaced by the change in free energy $u_m - Ts_m$. At constant pressure and volume this is also the change in free enthalpy, and the parameter, w , can be introduced where:

$$w = h_m - Ts_m. \quad [17]$$

Equation [12] then reads

$$\pi = -kT \frac{\partial \ln g_c}{\partial A} + w \frac{\partial(\bar{X}_{22}z)}{\partial A}. \quad [12']$$

The exact calculation of g_c has not yet been possible, and it is necessary to proceed in an approximate way, especially for monolayers, where the orientation of hydrophilic and hydrophobic groups introduces an additional complication. A semi-empirical parameter, p , may be introduced in the equation of Flory-Huggins, as Kawai has done (14). Let i be the number of polymer molecules already present in the quasi-lattice and r the number of segments in a macromolecule. The expected number of available sites

for the j segment of molecule $i + 1$ will be:

$$\nu_{ij} = z' \left(1 - \frac{r_i}{N_1 + rN_2} p \right), \quad [18]$$

where z' is slightly different from z .

The parameter p represents the effectiveness of the molecules already present in the monolayer in restraining the randomness of segment j . This parameter has a complicated nature, but it will be greater for molecules having a higher flexibility. Generally speaking, macromolecules will show a restricted flexibility at the interfaces, since their segments are oriented according to their affinity toward the limiting phases. A change in the chain configuration will require that some groups leave temporarily the interface, having to overcome a large potential barrier. Hence, p will probably be very small, even in monolayers of the expanded type such as those of poly(methyl acrylate).

The method of Singer (15) has been applied by Kawai and from Eq. [18] is derived the following expression for the configurational surface pressure:

$$\pi_c = -kT \frac{\partial \ln g_c}{\partial A} = \frac{kT}{A_0} \left[\left(\frac{1}{r} - 1 \right) \frac{A_0}{A} - \frac{1}{p} \ln \left(1 - \frac{pA_0}{A} \right) \right]. \quad [19]$$

However, the meaning ascribed by Kawai to the parameter p is somewhat different from ours. As it has already been shown, p is here very small, and therefore π_c nearly coincides with the ideal surface pressure.

From the foregoing arguments it may be seen that surface pressure is mainly produced by the repulsion at the segment-segment contacts. When any of these contacts is broken, the entropy of the monolayer increases by the increment of disorder produced by the polymer chains. This entropy increment is in part compensated by the enthalpy increment due to the rupture of the contact. The surface pressure is then produced by the non-compensated entropy.

In what follows only the results obtained for $T > 25^\circ\text{C}$. will be discussed, since at lower temperatures the interpretation of the experimental facts requires another approach.

From Eqs. [12], [16], [17], and [19] the following equation of state is obtained:

$$\pi = -\frac{kT}{rA} - \frac{b(h_m - Ts_m)}{(A - a)^2}. \quad [20]$$

From this equation for large values of r , the following expression for the spreading entropy is deduced:

$$s_s = \frac{bs_m}{(A - a)^2} \quad [21]$$

and a similar expression for the spreading enthalpy h_s . The range of validity of these relationships will increase as the molecular weight increases.

In Fig. 5 the values of s_s^{40} are plotted against $1/(A - a)^2$, where $a = 0.4$ m.²/mg. The points shown correspond to samples D and E of higher molecular weight. In these cases it may be seen that molecular weight has not yet had influence. In Fig. 6 the surface pressure π is plotted against $1/(A - a)^2$ for the same samples and two values of temperature. It can be seen that the plots are linear; therefore Eq. [20] describes satisfactorily the experimental facts, in spite of the approximations introduced in its derivation.

To discuss the results concerning the second virial coefficient a new parameter will be introduced

$$\theta = \frac{h_m}{s_m}, \quad [22]$$

and it will be called "ideal temperature," after Flory (16). The equation of state for very large r may now be written

$$\pi = bTs_m \left(1 - \frac{\theta}{T}\right) \frac{1}{(A - a)^2}. \quad [23]$$

For samples D and E of high molecular weights, this equation accounts fairly well for the observed variations of the second virial coefficient with temperature. Comparing now Eqs. [4] and [23], one obtains

$$\varphi = \frac{bs_m}{R}. \quad [24]$$

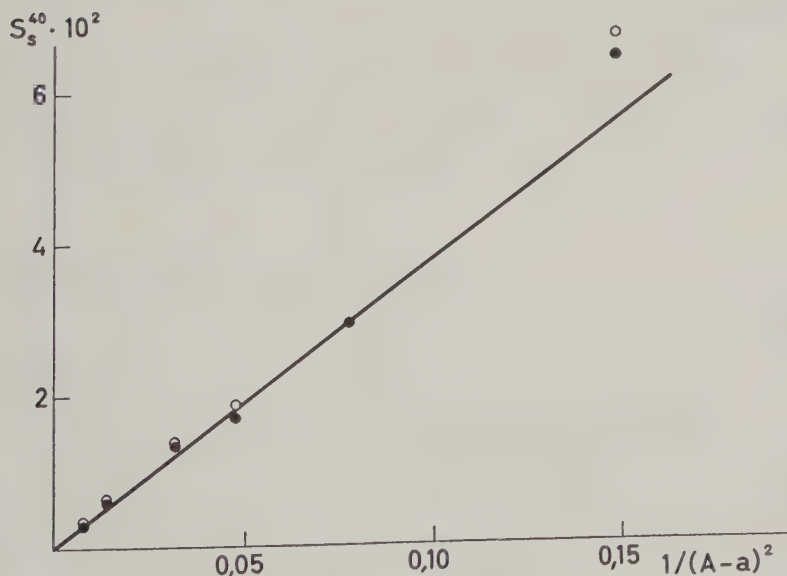


FIG. 5. Spreading entropies s_s^{40} plotted against $1/(A - a)^2$. Samples D and E.

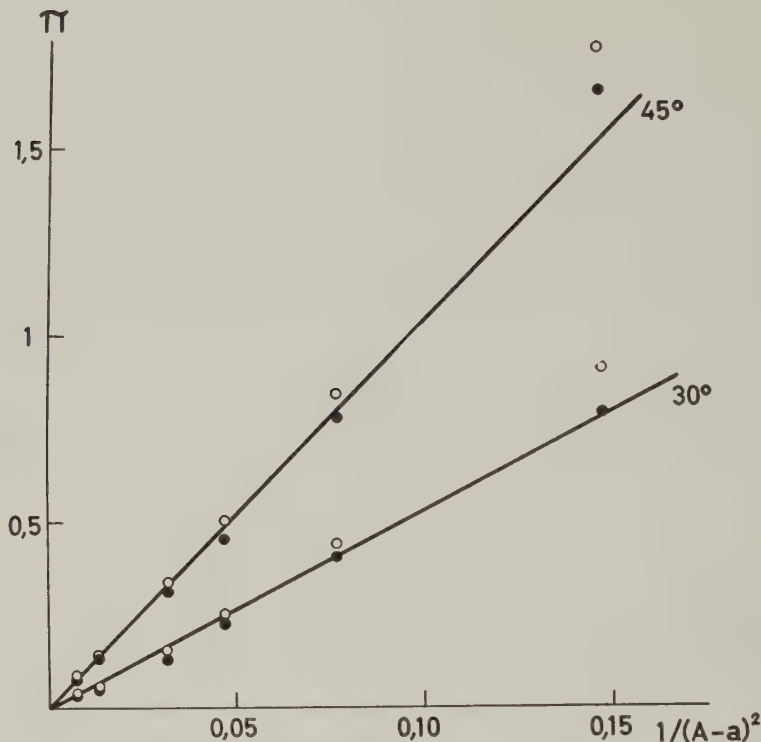


FIG. 6. Plots of surface pressure π vs. $1/A - a)^2$. Samples D and E. Two values of temperature.

For the experimental values of $\varphi = 5.4 \times 10^{-2} \text{ m.}^2/\text{mg.}$ and $\theta = 292.7^\circ\text{K.}$ (Table II), the following values are obtained

$$\begin{aligned} s_m &= 1.3 \times 10^8 \text{ erg } ^\circ\text{K.}^{-1} \text{ mole}^{-1}; \\ h_m &= 3.8 \times 10^{10} \text{ erg mole}^{-1}. \end{aligned} \quad [25]$$

It is remarkable that the value of h_m is of the same order of magnitude as the value $5.0 \times 10^{10} \text{ erg mole}^{-1}$ obtained by Saraga and Prigogine for the interaction $\text{CH}_2\text{—H}_2\text{O}$ in solutions of long-chain esters.

The parameter θ has an interesting physical meaning. From Eq. [23] it may be seen that π would be negative for $T < \theta$. In fact, at these temperatures a demixing will take place and Eq. [23] no longer holds, since a condensed surface phase will be separated. As explained by Flory (16), at temperature θ the interface ceases to be a poor solvent and becomes a good one. Therefore, it is necessary to work in the neighborhood of the corresponding θ temperature to obtain monolayers of a given polymer. For $T \gg \theta$ the interface is a good solvent and the monolayer tends to be dissolved in the substrate.

The experimental values of parameters h_m , s_m , and θ will depend on the polymer under study. For polymers having the same hydrophilic groups, s_m will not be very different while h_m will be greater for polymers having longer hydrocarbon side chains and hence θ will also increase.

On the other hand, the behavior of monolayers below temperature θ is complicated and is not quite clearly understood. In the vicinity of θ a minimum in the curves π vs. T is often observed (6, 17). This fact is difficult to explain from a thermodynamical point of view. Probably it is due to hysteresis effects, and a "surface gel" is formed with a long time required to attain the equilibrium state for each value of the area.

REFERENCES

1. CRISP, D. J. in Danielli, Pankhurst, and Riddiford, eds., "Surface Phenomena in Chemistry and Biology," p. 23 Pergamon Press, London, 1958.
2. SAKURADA, I., NAKAJIMA, A., AND AOKI, A., *J. Polymer Sci.* **35**, 507 (1959).
3. GADKARY, S. D., AND KAPUR, S. L., *Makromol. Chem.* **17**, 29 (1955).
4. SEN, J. N., CHATERJEE, S. R., AND PALIT, S. R., *J. Sci. Ind. Research (India)* **11B**, 90 (1952).
5. GUZMÁN, G. M., *Anales real soc. españ. fis. y quim. (Madrid)* **50B**, 631 (1954).
6. LLOPIS, J., AND SUBIRANA, J. A., *3rd Intern. Congr. Surface Activity Köln* (1960) II, 149, Verlag der Universitätsdruckerei, Mainz.
7. ROBBINS, M. L., AND LA MER, V. K., *J. Colloid Sci.* **15**, 123 (1960).
8. LLOPIS, J., *Anales real soc. españ. fis. y quim. (Madrid)* **56B**, 669 (1960).
9. SARAGA, L. T. M., AND PRIGOGINE, I., *Mém. service chim. etat* **38**, 109 (1953).
10. MÜNSTER, A., in H. Stuart, ed., "Die Physik der Hochpolymeren," vol. 2, pp. 99, 154. Springer, Berlin, 1953.
11. GUGGENHEIM, E. A., "Mixtures," p. 216. Clarendon, Oxford, 1952.
12. PRIGOGINE, I., "The Molecular Theory of Solutions." North Holland Publishing Co., 1957.
13. BENSON, G. C., AND MCINTOSH, R. L., *J. Colloid Sci.* **3**, 323 (1948).
14. KAWAI, T., *J. Polymer Sci.* **35**, 401 (1959).
15. SINGER, S. J., *J. Chem. Phys.* **16**, 872 (1948).
16. FLORY, P. J., "Principles of Polymer Chemistry." Cornell University Press, Ithaca, New York, 1953.
17. LLOPIS, J., AND REBOLLO, D. V., *Arch. Biochem. Biophys.* **88**, 142 (1960).

LETTERS TO THE EDITOR

APPROACH OF A SOLID SPHERE TO A RIGID PLANE
INTERFACE

As part of a study of the coalescence of drops in gravity fields, Charles and Mason (1) derived the following relationship for the close approach of a solid sphere immersed in a viscous fluid to an unbounded horizontal plane:

$$u = \frac{dh}{dt} = -\frac{Fh}{6\pi\eta_2 b^2}, \quad [1]$$

where u is the velocity of approach, b is the radius of the sphere, h ($> b$) is the minimum separation between sphere and plane, η_2 is the viscosity of the suspending fluid, and F the force on the sphere normal to the plane.

The calculation is readily extended to two spheres of radius b_1 and b_2 being pushed together by the force F at a rate

$$\frac{dh}{dt} = -\frac{Fh}{6\pi\eta_2} \left[\frac{1}{b_1} + \frac{1}{b_2} \right]^2. \quad [2]$$

This case is of interest in studying the approach and coalescence of spheres in electric and shear fields (2).

This note deals with an experimental verification of Eq. [1] by measuring the sedimentation of a sphere through a Newtonian liquid towards a horizontal surface. A simplification is made by first determining the Stokes velocity

$$V_s = \frac{F}{6\pi\eta_2 b},$$

which enables F/η_2 to be eliminated from Eq. [1] to yield

$$-\frac{dh}{dt} = \frac{V_s h}{b}. \quad [3]$$

Integration of [3] gives

$$-\log_e h = \frac{V_s t}{b} + k. \quad [4]$$

Thus to check the theory (Eq. [3]), the physical properties of the liquid used need not be known.

The rate of approach of nylon spheres to a horizontal plane glass surface through UCON oil 50 HB 5100 (Union Carbide Chemicals Company,

$\rho = 1.065$ g./c.c., $\eta = 30$ poises) was measured. The vessel was a rectangular aquarium ($15 \times 15 \times 24$ cm.) mounted on rubber inside a constant-temperature bath at $20.0^\circ\text{C.} \pm 0.01$. The plane surface was a 10 cm. square glass plate floating on mercury. The aquarium was filled with the oil to a depth of about 18 cm. above the plate.

The approach of single spheres to the glass plate was filmed with a 16 mm. Bolex-Paillard cine camera fitted with a 25-mm. lens. The camera

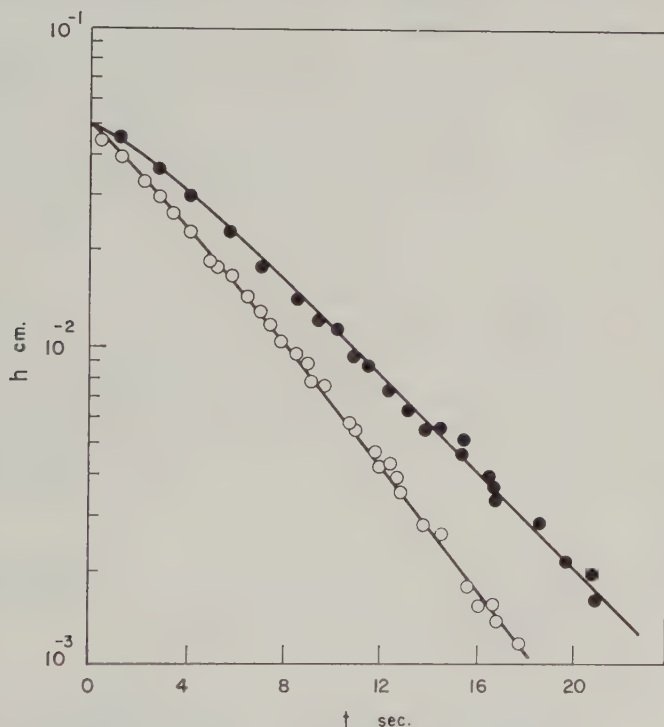


FIG. 1. Semilogarithmic plot: h versus time for $b = 0.2775$ cm. (open circles) and 0.1988 (solid circles).

was aligned axially with one ocular ($10\times$) of a stereo microscope, the objective ($10\times$) of which was focused on the sphere and interface. Timing was provided by having the source of illumination, a 6-volt microscope lamp, operated by a Robot Impulse Timer.

The film was subsequently projected at a magnification of approximately $60\times$ and the distance between the sphere and its image on the upper surface of the glass was measured to $\pm 5 \mu$. The separation between sphere and plane was one-half the measured distance. The film magnification was determined from the known diameter of the spheres.

Duplicate runs were conducted with nylon spheres ($\rho = 1.18$ g./cm.³) of

LETTERS TO THE EDITOR

APPROACH OF A SOLID SPHERE TO A RIGID PLANE
INTERFACE

As part of a study of the coalescence of drops in gravity fields, Charles and Mason (1) derived the following relationship for the close approach of a solid sphere immersed in a viscous fluid to an unbounded horizontal plane:

$$u = \frac{dh}{dt} = -\frac{Fh}{6\pi\eta_2 b^2}, \quad [1]$$

where u is the velocity of approach, b is the radius of the sphere, h ($> b$) is the minimum separation between sphere and plane, η_2 is the viscosity of the suspending fluid, and F the force on the sphere normal to the plane.

The calculation is readily extended to two spheres of radius b_1 and b_2 being pushed together by the force F at a rate

$$\frac{dh}{dt} = -\frac{Fh}{6\pi\eta_2} \left[\frac{1}{b_1} + \frac{1}{b_2} \right]^2. \quad [2]$$

This case is of interest in studying the approach and coalescence of spheres in electric and shear fields (2).

This note deals with an experimental verification of Eq. [1] by measuring the sedimentation of a sphere through a Newtonian liquid towards a horizontal surface. A simplification is made by first determining the Stokes velocity

$$V_s = \frac{F}{6\pi\eta_2 b},$$

which enables F/η_2 to be eliminated from Eq. [1] to yield

$$-\frac{dh}{dt} = \frac{V_s h}{b}. \quad [3]$$

Integration of [3] gives

$$-\log_e h = \frac{V_s t}{b} + k. \quad [4]$$

Thus to check the theory (Eq. [3]), the physical properties of the liquid used need not be known.

The rate of approach of nylon spheres to a horizontal plane glass surface through UCON oil 50 HB 5100 (Union Carbide Chemicals Company,

$\rho = 1.065$ g./c.c., $\eta = 30$ poises) was measured. The vessel was a rectangular aquarium ($15 \times 15 \times 24$ cm.) mounted on rubber inside a constant-temperature bath at $20.0^\circ\text{C.} \pm 0.01$. The plane surface was a 10 cm. square glass plate floating on mercury. The aquarium was filled with the oil to a depth of about 18 cm. above the plate.

The approach of single spheres to the glass plate was filmed with a 16 mm. Bolex-Paillard cine camera fitted with a 25-mm. lens. The camera

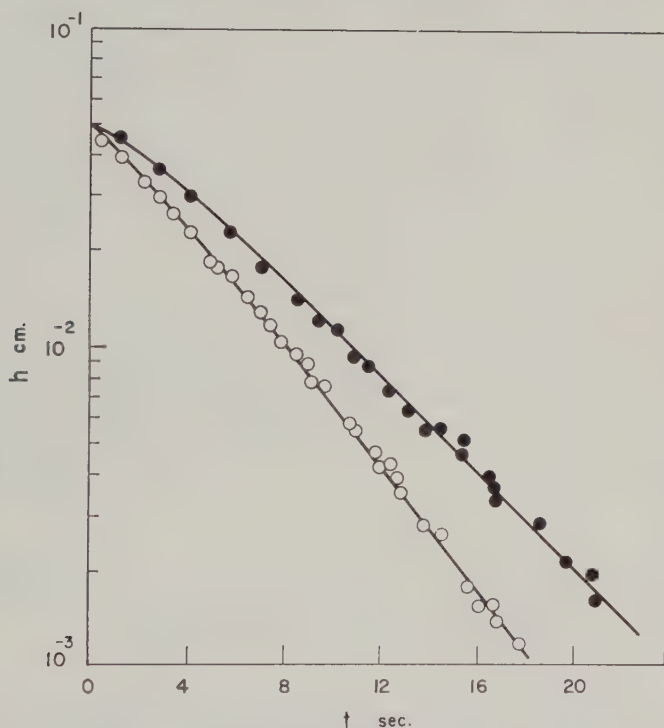


FIG. 1. Semilogarithmic plot: h versus time for $b = 0.2775$ cm. (open circles) and 0.1988 (solid circles).

was aligned axially with one ocular ($10\times$) of a stereo microscope, the objective ($10\times$) of which was focused on the sphere and interface. Timing was provided by having the source of illumination, a 6-volt microscope lamp, operated by a Robot Impulse Timer.

The film was subsequently projected at a magnification of approximately $60\times$ and the distance between the sphere and its image on the upper surface of the glass was measured to $\pm 5 \mu$. The separation between sphere and plane was one-half the measured distance. The film magnification was determined from the known diameter of the spheres.

Duplicate runs were conducted with nylon spheres ($\rho = 1.18$ g./cm.³) of

radii 0.1587, 0.1988, and 0.2775 cm. The terminal velocity V_t was determined from cathetometer readings as the sphere descended well above the surface.

TABLE I
Summary of Data

Sphere radius (cm.)	$10^3 V_t$ (cm./sec.)	Ladenburg correction factor	$10^3 V_s$ (cm./sec.)	$-10^3 (d \log_{10} h/dt)$	
				Expt.	Eq. [4]
0.1587	1.09	1.08	2.03	5.93	5.61
0.1988	3.09	1.11	3.37	7.42	7.47
0.2775	5.30	1.15	5.94	9.77	9.55
				experimental	
				Mean slope $\frac{\text{experimental}}{\text{calculated}} = 1.02$	

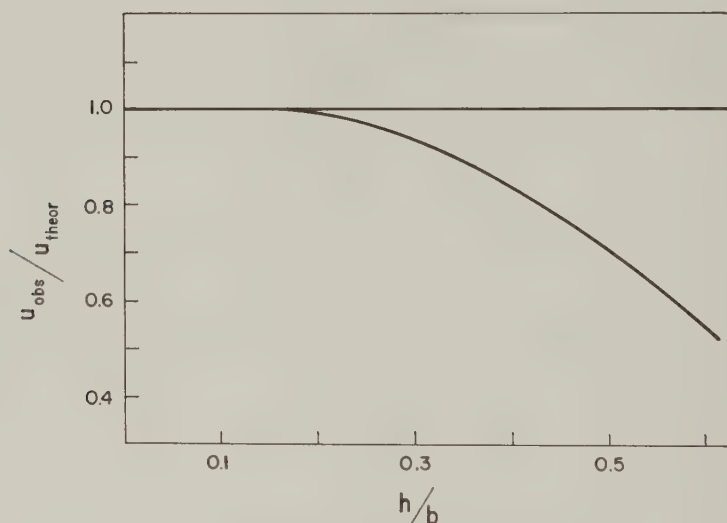


FIG. 2. Summary plot of $u_{\text{obs.}}/u_{\text{theor.}}$ as a function of (h/b) .

The Stokes velocity was obtained by correcting the observed terminal velocity for end and wall effects, using the Ladenburg (3) expression for a cylindrical tube

$$V_s = V_t \left(1 + 2.4 \frac{b}{R} \right) \left(1 + 3.3 \frac{b}{H} \right), \quad [5]$$

where R is the radius of the cylinder and H the height of fluid in the vessel; R was taken to be the radius of the inscribed circle in the vessel.

Figure 1 is a plot of $\log h$ versus time for the two larger spheres, with the time scales superimposed to coincide at $h = 0.05$ cm. Initially curved, the plots become linear at $h \leq 0.01$ cm. approximately. Values of the slope of the linear portion constructed by the method of least squares are listed in Table I. The agreement with Eq. [4] is good.

Figure 2 shows the variation of $(u_{\text{obs.}}/u_{\text{theor.}})$ with h/b for the three spheres; $u_{\text{obs.}}$ was obtained by fitting a polynomial to the $\log_e h$ vs. t data, and $u_{\text{theor.}}$ from Eq. [3].

Equation [3] holds within 1% when $(h/b) \leq 0.2$. Because of symmetry it is reasonable to suppose that Eq. [2] will hold to the same accuracy when $(h/b) \leq 0.4$. Equation [2] is similar to but not identical with an equation derived by Mooney (4).

This work was conducted with financial assistance from the Defence Research Board of Canada (DRB Grant 9510-05).

REFERENCES

1. CHARLES, G. E., AND MASON, S. G., *J. Colloid Sci.* **15**, 105 (1960).
2. ALLAN, R. S., AND MASON, S. G., Forthcoming publication.
3. LADENBURG, R., *Ann. Physik.* **22**, 287 (1907); *ibid.* **23**, 9444 (1907).
4. MOONEY, M., *J. Colloid Sci.* **12**, 575 (1957).

*Pulp and Paper Research Institute
of Canada and the Department of Chemistry,
McGill University,
Montreal, Canada.
June 13, 1961.*

G. D. M. MacKAY
S. G. MASON

CONCENTRATION DEPENDENCE OF THE DILUTE SOLUTION VISCOSITY OF POLYSTYRENE

It has become common practice to relate the dilute solution viscosities of polymer solutions to the solution concentration using the equation of Huggins (1):

$$\frac{\eta_{sp}}{c} = [\eta] + k'[\eta]^2 c.$$

The parameter k' of this equation has in general been found to be characteristic of a given solute-solvent system, being essentially constant for solutions, in a given solvent, of different members of a polymer homologous series. This parameter is, however, significantly changed for the same polymer fraction in different solvents.

In the careful measurement of the intrinsic viscosity of polystyrene in toluene it is observed that the parameter k' in the above equation increases with a decrease in molecular weight. Table I lists the intrinsic viscosities and Huggins' k' values obtained on several narrow molecular weight dis-

tribution anionically polymerized and broad distribution thermally polymerized polystyrenes covering a range in molecular weight from 10,500 to 1,200,000. Viscosities were determined in toluene at 25°C. with the use of a Ubbelohde-type viscometer having a solvent flow time of 225 sec. Molecular weight distributions were characterized by sedimentation velocity analysis as previously reported (2). It can be seen from this data

TABLE I
Intrinsic Viscosities in Toluene at 25°C.

Polymer	\overline{M}_w	$\overline{M}_w/\overline{M}_n$	$[\eta]$	k'
<i>Anionic Polystyrene</i>				
S0	10,500	1.64	0.0766	0.51
S1	13,800	1.50	0.102	0.50
S2	20,500	1.95	0.137	0.44
S3	54,000	1.35	0.276	0.39
S4	78,100	1.18	0.358	0.36
S5	110,000	1.16	0.439	0.35
S6	125,000	1.08	0.515	0.36
S7	141,000	1.08	0.578	0.33
S8	171,000	1.07	0.640	0.34
S9	210,000	1.11	0.727	0.32
S10	249,000	1.04	0.840	0.37
S11	819,000	1.18	1.951	0.34
S12	1,200,000	1.19	2.723	0.36
<i>Thermal Polystyrene</i>				
B1	118,000	2.41	0.411	0.35
B2	187,000	1.90	0.668	0.35
B3	214,000	1.94	0.712	0.33
B4	255,000	1.96	0.787	0.33
A1	262,000	2.38	0.811	0.35
B5	285,000	1.77	0.892	0.35
A2	351,000	2.23	1.008	0.32
A3	416,000	2.47	1.122	0.36
B6	447,000	2.85	1.233	0.33

that the value of k' , which has a relatively constant value of 0.34 for high molecular weight polymers, exhibits a significant continuous increase with decreasing molecular weight for polymers of molecular weight below 60,000, reaching a value of 0.51 for a molecular weight of 10,500. Although the lower molecular weight anionic polymers have greater heterogeneity than the higher molecular weight anionic polymers, this increased heterogeneity can not account for the increase in k' since no increase in k' is observed for the even more heterogeneous thermal polystyrene. It is also unlikely that end group polymer association can account for this increased k' since all

the anionic polymers were terminated with water leaving the polymer ends free of polar groups. Although a complete physical understanding of this increase in the Huggins' k' at low molecular weight is open to speculation, the present data rather conclusively exhibit this interesting phenomenon.

REFERENCES

1. HUGGINS, M. L., *J. Am. Chem. Soc.* **64**, 2716 (1942).
2. McCORMICK, H. W., *J. Polymer Sci.* **36**, 341 (1959).

H. W. McCORMICK

*Physical Research Laboratory,
The Dow Chemical Company,
Midland, Michigan*

Received September 28, 1961

BOOK REVIEW

Scientific Russian Reader. By NINA A. SYNIAWSKA, Ph.D. Columbia University Press, New York, 1961. 177 pp. Price \$5.00.

This book will be welcomed by students of Russian who have achieved a reasonably good knowledge of the language and who wish to extend their competence in reading and translating articles from the current Soviet scientific and technical literature. The material which Dr. Syniawska has compiled is reproduced in its original typographic form and includes papers from contemporary work in physics, chemistry, and biology, as well as a number of popular science articles.

The contents of this useful book are arranged in order of increasing difficulty. A few sample English translations are included, along with a substantial glossary of scientific and technical words pertinent to the text. It is this reviewer's opinion that a serious study of this book by those with a sufficiently strong background in Russian, such as is now readily available in this country, will be well worth the effort.

Theodore Shedlovsky, New York, New York

ERRATUM

Volume 16, Number 2, April 1961. In the Letter to the Editor entitled "Streaming Potential and Turbulence" by P. R. Stewart and N. Street, pp. 192-194, the voltages shown in the ordinates of Figs. 1 and 2 should be multiplied by 10^{-1} for Capillary II and by 10^{-2} for Polystyrene and Teflon.

AUTHOR INDEX

A		HERZ, A. H.,	199
ALEXANDER, A. E.,	57	HORINO, TUNEO,	411
ALLAN, R. S.,	150	HUNTER, R. J.,	190
ARANOW, RUTH H.,	127	K	
ARNOLD, JOHN D.,	513	KAPUAN, PAZ,	481
B		KAWAI, HIROMICHI,	262, 411
BATEMAN, J. B.,	531	KAWASAKI, KOJI,	405
BECHER, PAUL,	49	KAY, WALTER S.,	182
BOLEN, R. J.,	493	KOCH, M. JOAN,	327, 345
BRESCIA, FRANK,	438	KOSZMAN, IHOR,	375
BROOKS, J. H.,	442	KRATOHVIL, JOSIP P.,	561
C		KRISHNAN, R. S.,	41
CHAPPELEAR, D. C.,	186	KUFFNER, ROY J.,	497
CHARLES G. E.,	150	L	
COVINGTON, E. J.,	531	LESTER, G. R.,	315
D		LITT, MORTON,	297
DANNHAUSER, WALTER,	101	LLOPIS, J.,	618
DEŽELIĆ, GJURO,	561	LORENZ, P. B.,	493
DUNNING, H. N.,	493	LYKLEMA, J.,	501, 595
E		M	
EGAN, JAMES J.,	68	MACKAY, G. D. M.,	632
ELDIB, I. A.,	493	MACRITCHIE, F.,	57, 442
F		MARCHESSAULT, R. H.,	327, 345
FERRY, JOHN D.,	101, 166	MASON, S. G.,	150, 210, 238, 632
FISHMAN, MYER M.,	392	MCCORMICK, H. W.,	635
FLOCKHART, B. D.,	443, 484	MEEKS, FRANK R.,	455
FREUND, ISAAC,	392	MILLER, I. R.,	23
FUJINO, KIYOHISA,	262, 411	MIYAMOTO, KIHACHIRO,	411
G		MOREHEAD, F. F.,	327
GAVIS, JEROME,	375	MYSELS, KAROL J.,	462, 474, 481
GRAHAM, DONALD,	182	O	
GRAHAME, D. C.,	23	OTTER, RAYMOND J.,	462, 474
GUCKER, FRANK T.,	68	OTTEWILL, R. H.,	581
H		OVERBEEK, J. Th., G.,	501, 595
HANSEN, ROBERT S.,	549	P	
HEALY, T. W.,	609	PAK, CHARLES Y. C.,	513
HELLING, J. O.,	199	PATRICK, R. L.,	93
		PAYNE, G. O., JR.,	93
		PETERSON, EDWARD C.,	87

PLAZEK, DONALD J.,
PONTRELLI, GENE,

101

438

R

RAJAGOPAL, E. S.,
RIES, HERMAN E., JR.,
ROMO, LUIS A.,
RUMSCHEIDT, F. D.,

41

361

139

210, 238

S

SAUNDERS, FRANK L.,
SCHULMAN, STEPHEN,
SENSHU, KAZUO,
SHINODA, KŌZŌ,
SLATTERY, JOHN C.,
STEWART, P. R.,
STREET, N.,
SUBIRANA, J. A.,

13

438

262

85

431

192

192

618

T

TINCHER, ALLAN H.,
TSCHOEGL, N. W.,

87

89

V

VAN DEN TEMPEL, M.,
VEGUILLA, L. A.,
VENKATASUBRAMANIAN, V. S.,
VOLD, MARJORIE J.,

284

455

41

1

W

WALKER, DONALD C.,
WITTEN, LOUIS,
WOLFRAM., ERVIN,
WOODBIDGE, R. F.,

361

127

195

581

Y

YANG, J. T.,
YIN, THEODORE P.,

345

166

SUBJECT INDEX

A

- Acids, aliphatic, at water-air interface,
HANSEN, 549
Adsorption, of rutile, ROMO, 139
Amylopectin, and cetylpyridinium chlo-
ride, FISHMAN AND FREUND, 392

C

- Carbon black, morphology, GRAHAM
AND KAY, 182
Cellulose, properties of crystallites,
MARCHESSAULT *et al.*, 327
Colloidal particles, van der Waals inter-
action, VOLD, 1

D

- Decyl sulfate, conductivity, MYSELS AND
KAPAUAN, 481
Detergents, ethanol-water solutions,
FLOCKHART, 443
Diffusion, concentration product in
counterdiffusion, MEEKS AND
VEGUILLA, 455
Drop, liquid drop and interface, CHAP-
PELEAR, 186; water drops and wetta-
bility, WOLFRAM, 195

E

- Electrical resistance, of a polymer,
KAWASAKI, 405
Electrokinetic potentials, LYKLEMA AND
OVERBEEK, 501
Electrokinetics, and dielectric constant,
HUNTER, 190
Emulsification, ultrasonic, KRISHNAN
et al., 41
Emulsion, demulsification by resin
membrane, SHINODA, 85
Expansion, Schaefer's patterns, ARANOW
AND WITTEN, 127

F

- Fatty acid, multilayers, molecular tilt,
BATEMAN AND COVINGTON, 531

- Ferric oxide, solid and colloidal, equi-
librium, SCHULMAN *et al.*, 438

G

- Gas, gas bubbles and gas/liquid inter-
face, ALLAN *et al.*, 150

I

- Interface, solid sphere and rigid plane
interface, MACKEY AND MASON, 632

L

- Latexes, rheological properties, SAUN-
DERS, 13; size of polystyrene latexes,
DEŽELIĆ AND KRATOCHVIL, 561
Light, scattered from aerosol droplets,
GUCKER AND EGAN, 68

M

- Mercury surfaces, polyelectrolyte ad-
sorption, MILLER AND GRAHAME, 23
Methylacrylate, copolymers, FUJINO *et*
al., 262
Micelles, properties of mixed micelles,
MYSELS AND OTTER, 462, 474; critical
micelle concentration, FLOCKHART,
484
Mixed compounds, films, RIES AND
WALKER, 361
Monolayers, and moduli, TSCHOEGL, 89

O

- Oil, viscosities of crude oils, LORENZ *et*
al., 493

P

- Paper, properties and structure, LITT,
297
Plastic disperse systems, at small de-
formations, VAN DEN TEMPEL, 284
Poly-ethyl butyl methacrylate, proper-
ties, YIN AND FERRY, 166

- Poly (methyl acrylate), monolayers, LLOPIS AND SUBIRANA, 618
 Polystyrene, viscosity, McCORMICK, 635
 Polyvinyl alcohol, polymers, FUJINO *et al.*, 411
 Protein, films, and sucrose, MACRITCHIE AND ALEXANDER, 57; monofilm expansion, PAK AND ARNOLD, 513
- Q
- Quartz, and polyacrylamide, HEALY, 609
- R
- Ramie, properties of crystallites, MARCHESAULT *et al.*, 345
- S
- Silver bromide, isoionic point of emulsions, HERZ AND HELLING, 199; preparation of monodisperse sols, OTTEWILL AND WOODBRIDGE, 581
 Silver iodide, electrochemistry, LYKLEMA AND OVERBEEK, 595
- Stearic acid, desorption, PATRICK AND PAYNE, 93
 Streaming potential, and turbulence, STEWART AND STREET, 192
 Surface, surface-active compounds, BECHER, 49; liquids at solid surfaces, LESTER, 315; liquids flowing past surfaces, GAVIS AND KOSZMAN, 375; compression of surface films, BROOKS AND MACRITCHIE, 442; measurement of surface tensions, KUFFNER, 497
 Suspension, particle motions in sheared suspensions, RUMSCHEIDT AND MASON, 210, 238
- T
- Turbidity, standard, PETERSON AND TINCHER, 87
- V
- Viscometer, cone-plate viscometer, SLATTERY, 431
 Viscosity, viscoelastic dispersion of polydimethyl siloxane, PLAZEK *et al.*, 638

INDEX OF BOOK REVIEWS

- CHARGAFF, E., AND DAVIDSON, J. M. (eds.), *The Nucleic Acids*. Vol. III (STEINHARDT, J.), 312
 MYSELS, K. J., *Introduction to Colloid Chemistry* (ALEXANDER, A. E.), 91
 PAYNE, H. F., *Organic Coating Technology* (HOCHBERG, S.), 313
 Saline Water Conversion (LA MER, V. K.), 311
 SHEDLOVSKY, T., *Scientific Russian Reader* (SYNIAWSKA, N. A.), 638

JOURNAL OF COLLOID SCIENCE

EDITOR-IN-CHIEF

VICTOR K. LA MER
Columbia University, New York

ADVISORY BOARD

A. E. ALEXANDER	JOHN D. FERRY	ROBERT SIMHA
STEPHEN BRUNAUER	J. J. HERMANS	R. H. SMELLIE
J. A. CHRISTIANSEN	L. G. LONGSWORTH	HARRY SOBOTKA
P. J. W. DEBYE	S. G. MASON	JACINTO STEINHARDT
B. DERJAGUIN	KAROL J. MYSELS	TORSTEN TEORELL
D. G. DERVICHIAN	J. TH. G. OVERBEEK	A. C. ZETTMEOYER
JOHN T. EDSALL	J. H. SCHULMAN	BRUNO H. ZIMM
I. FANKUCHEN	LEO SHEDLOVSKY	W. A. ZISMAN
	THEODORE SHEDLOVSKY	

Volume 16
1961



ACADEMIC PRESS
New York and London

COPYRIGHT ©, 1961, BY ACADEMIC PRESS INC.

ALL RIGHTS RESERVED

NO PART OF THIS VOLUME MAY BE REPRODUCED IN ANY
FORM, BY PHOTOSTAT, MICROFILM, OR ANY OTHER MEANS,
WITHOUT WRITTEN PERMISSION FROM THE PUBLISHERS.

Made in the United States of America

Contents of Volume 16

NUMBER 1, FEBRUARY 1961

MARJORIE J. VOLD. The Effect of Adsorption on the Van Der Waals Interaction of Spherical Colloidal Particles.....	1
FRANK L. SAUNDERS. Rheological Properties of Monodisperse Latex Systems. I. Concentration Dependence of Relative Viscosity....	13
I. R. MILLER AND D. C. GRAHAME. Polyelectrolyte Adsorption on Mercury Surfaces. Differential Capacity in the Presence of Poly 2- and 4-Vinyl Pyridines.....	23
R. S. KRISHNAN, V. S. VENKATASUBRAMANIAN, AND E. S. RAJAGOPAL. Studies on Ultrasonic Emulsification.....	41
PAUL BECHER. Nonionic Surface-Active Compounds. IV. Micelle Formation by Polyoxyethylene Alkanols and Alkyl Phenols in Aqueous Solution.....	49
F. MACRITCHIE AND A. E. ALEXANDER. The Effect of Sucrose on Protein Films. I. Spread Monolayers.....	57
FRANK T. GUCKER AND JAMES J. EGAN. Measurement of the Angular Variation of Light Scattered from Single Aerosol Droplets.....	68
LETTERS TO THE EDITOR	
KÖZÖ SHINODA. Demulsification by the Use of Ion-Exchange Resin Membrane.....	85
EDWARD C. PETERSON AND ALLAN H. TINCHER. Turbidity Standard.....	87
N. W. TSCHOEGL. Compressional and Young's Moduli in Monolayers.....	89
BOOK REVIEW	
A. E. ALEXANDER. Introduction to Colloid Chemistry.....	91

NUMBER 2, APRIL 1961

R. L. PATRICK AND G. O. PAYNE, JR. The Rate of Desorption of Stearic Acid from Planar Surfaces—A New Technique.....	93
DONALD J. PLAZEK, WALTER DANNHAUSER, AND JOHN D. FERRY. Viscoelastic Dispersion of Polydimethyl Siloxane in the Rubberlike Plateau Zone.....	101
R. H. ARANOW AND L. WITTEN. A Theory of Schaefer's Expansion Patterns.....	127
LUIS A. ROMO. Adsorption Selectivity and Electrostatic Fields of Rutile Powders.....	139

R. S. ALLAN, G. E. CHARLES, AND S. G. MASON. The Approach of Gas Bubbles to a Gas/Liquid Interface.....	150
THEODORE P. YIN AND JOHN D. FERRY. Dynamic Mechanical Properties and Creep of Poly-2-Ethyl Butyl Methacrylate.....	166
DONALD GRAHAM AND WALTER S. KAY. The Morphology of Thermally Graphitized P-33 Carbon Black in Relation to its Adsorbent Uniformity.....	182

LETTERS TO THE EDITOR

D. C. CHAPPELEAR. Models of a Liquid Drop Approaching an Interface.....	186
R. J. HUNTER. The Dielectric Constant in the Equations of Electrokinetics.....	190
P. R. STEWART AND N. STREET. Streaming Potential and Turbulence.....	192
ERVIN WOLFRAM. Comment on the Paper, "Study of Wettability of Polymers by Sliding of Water Drops," by Koji Kawasaki...	195

NUMBER 3, JUNE 1961

A. H. HERZ AND J. O. HELLING. The Isoionic Point of Silver Iodide Sols and Silver Bromide and Bromiodide Emulsions.....	199
F. D. RUMSCHEIDT AND S. G. MASON. Particle Motions in Sheared Suspensions XI. Internal Circulation in Fluid Droplets (Experimental).....	210
F. D. RUMSCHEIDT AND S. G. MASON. Particle Motions in Sheared Suspensions XII. Deformation and Burst of Fluid Drops in Shear and Hyperbolic Flow.....	238
KIYOHISA FUJINO, KAZUO SENSU, AND HIROMICHI KAWAI. Tensile Stress Relaxation Behavior of Methylmethacrylate and Methylacrylate Copolymers.....	262
M. VAN DEN TEMPEL. Mechanical Properties of Plastic-Disperse Systems at Very Small Deformations.....	284
MORTON LITT. Macroscopic Properties and Microscopic Structure in Paper.....	297

BOOK REVIEWS

VICTOR K. LAMER. Saline Water Conversion.....	311
JACINTO STEINHARDT. The Nucleic Acids. Vol. III.....	312
SEYMORE HOCHBERG. Organic Coating Technology. Vol. II.....	313

NUMBER 4, AUGUST 1961

G. R. LESTER. Contact Angles of Liquids at Deformable Solid Surfaces	315
R. H. MARCHESSAULT, F. F. MOREHEAD, AND M. JOAN KOCH. Some Hydrodynamic Properties of Neutral Suspensions of Cellulose Crystallites as Related to Size and Shape.....	327

R. H. MARCHESSAULT, M. JOAN KOCH, AND J. T. YANG. Some Hydrodynamic Properties of Ramie Crystallites in Phosphate Buffer. . .	345
HERMAN E. RIES, JR., AND DONALD C. WALKER. Films of Mixed Horizontally and Vertically Oriented Compounds.	361
JEROME GAVIS AND IHOR KOSZMAN. Development of Charge in Low Conductivity Liquids Flowing Past Surfaces: A Theory of the Phenomenon in Tubes.	375
MYER M. FISHMAN AND ISAAC FREUND. The Interaction of Amylopectin with Cetylpyridinium Chloride.	392
KOJI KAWASAKI. On the Variation of Electrical Resistance of a Polymer as a Function of the Extent and Nature of Sorbed Water. . .	405
KIYOHISA FUJINO, TUNEO HORINO, KIHACHIRO MIYAMOTO, AND HIROMICHI KAWAI. Tensile Stress Relaxation Behavior of Partly to Completely Acetylated Polyvinyl Alcohol Polymers.	411
JOHN C. SLATTERY. Analysis of the Cone-Plate Viscometer.	431
STEPHEN SCHULMAN, GENE PONTRELLI, AND FRANK BRESCIA. Equilibrium Between Solid and Colloidal Ferric Oxide.	438
LETTER TO THE EDITOR	
J. H. BROOKS AND F. MACRITCHIE. An Alternative Method for the Compression of Surface Films.	442

NUMBER 5, OCTOBER 1961

B. D. FLOCKHART. The Vapor Pressures of Ethanol-Water Solutions of Detergents.	443
FRANK R. MEEKS AND L. A. VEGUILLA. Some Properties of the Concentration Product in Counterdiffusion.	455
KAROL J. MYSELS AND RAYMOND J. OTTER. Conductivity of Mixed Sodium Decyl and Dodecyl Sulfates—The Composition of Mixed Micelles.	462
KAROL J. MYSELS AND RAYMOND J. OTTER. Thermodynamic Aspects of Mixed Micelles—Application to an Empirically Established Equilibrium.	474
KAROL J. MYSELS AND PAZ KAPAUAN. Electric Conductivity of Sodium Decyl Sulfate Solutions.	481
B. D. FLOCKHART. The Effect of Temperature on the Critical Micelle Concentration of Some Paraffin-Chain Salts.	484
P. B. LORENZ, R. J. BOLEN, H. N. DUNNING, AND I. A. ELDIR. Ultracentrifugation and Viscosities of Crude Oils.	493
ROY J. KUFFNER. The Measurement of Dynamic Surface Tensions of Solutions of Slowly Diffusing Molecules by the Maximum Bubble Pressure Method.	497
J. LYKLEMA AND J. TH. G. OVERBEEK. On the Interpretation of Electrokinetic Potentials.	501

CHARLES Y. C. PAK AND JOHN D. ARNOLD. A Simple Apparatus for Measurement of Protein Monofilm Expansion at Air-Water Interface in Response to Soluble Reactants in the Subsolution.	513
J. B. BATEMAN AND E. J. COVINGTON. Molecular Tilt in Fatty Acid Multilayers	531

NUMBER 6, DECEMBER 1961

ROBERT S. HANSEN. Diffusion and the Kinetics of Adsorption of Aliphatic Acids and Alcohols at the Water-Air Interface.	549
GJURO DEŽELIĆ AND JOSIP P. KRATOHVIL. Determination of the Particle Size of Polystyrene Latexes by Light Scattering.	561
R. H. OTTEWILL AND R. F. WOODBRIDGE. The Preparation of Monodisperse Silver Bromide and Silver Iodide Sols.	581
J. LYKLEMA AND J. TH. G. OVERBEEK. Electrochemistry of Silver Iodide. The Capacity of the Double Layer at the Silver Iodide-Water Interface.	595
T. W. HEALY. Flocculation-Dispersion Behavior of Quartz in the Presence of a Polyacrylamide Flocculant.	609
J. LLOPIS AND J. A. SUBIRANA. Thermodynamics of Poly(Methyl Acrylate) Monolayers.	618
LETTERS TO THE EDITOR	

G. D. M. MacKAY AND S. G. MASON. Approach of a Solid Sphere to a Rigid Plane Interface.	632
H. W. McCORMICK. Concentration Dependence of the Dilute Solution Viscosity of Polystyrene.	635

BOOK REVIEW

Theodore Shedlovsky. Scientific Russian Reader.	638
Erratum.	638
Author Index.	639
Subject Index.	641
Index of Book Reviews.	642

METHODS IN HORMONE RESEARCH

Edited by RALPH I. DORFMAN

The Worcester Foundation for Experimental Biology, Shrewsbury, Massachusetts

All of the methods are presented in succinct and comprehensive descriptions including equipment, preparation, procedures, accuracy, and evaluation of results. Each of the contributors is an expert in the method represented. As a source of complete information regarding the many important methods, this treatise will contribute to many varied disciplines in chemistry.

Volume 1: Chemical Determinations

December 1961, 423 pp., approx. \$12.00

JOHN R. K. PREEDY, Estrogens
RALPH I. DORFMAN, Assay of
17-Ketosteroids and Testosterone
JOSEF ZANDER, Progesterone
ARNOLD I. KLOPPER, Pregnanediol and
Pregnanetriol
MICHAEL FINKELSTEIN, Pregnanetriolone,
Abnormal Urinary Steroid

FERNAND G. PERON,
Adrenocorticosteroids
S. A. S. TAIT and J. F. TAIT, Assay of
Aldosterone and Metabolites
FRED ELMADJIAN, Adrenaline and
Noradrenaline
S. B. BARKER, Chemical Assay of
Thyroxine-Like Materials
AUTHOR INDEX—SUBJECT INDEX.

Volume 2: Bioassay

January 1962, 750 pp., approx. \$22.00

Part 1: Statistical Methods
C. W. EMMENS, Statistical Methods

Part 2: Steroid Hormones and
Related Substances

C. W. EMMENS, Estrogens
RALPH I. DORFMAN, Anti-Estrogenic
Compounds

TAMOTSU MIYAKE, Progestational
Substances

ELVA G. SHIPLEY, Anti-Gonadotrophic
Steroids, Including Inhibition of
Ovulation and Mating

RALPH I. DORFMAN, Adrogens and
Anabolic Steroids

RALPH I. DORFMAN, Anti-Androgenic
Substances

RALPH I. DORFMAN, Corticoids and
Anti-Inflammatory Agents

Part 3: Protein Hormones and
Related Hormones and
Substances

F. ELMADJIAN, Epinephrine and
Norepinephrine

C. W. TURNER and
B. N. PREMACHANDRA,
Thyroidal Substances

K. L. SMITH, Insulin

WILLIAM W. BROMER and
OTTO K. BEHRENS, Glucagon

R. H. THORP, Parathyroid Hormone

R. H. THORP, Posterior Pituitary Hormones

F. W. LANDGREBE, Melanophore
Expanding Activity

BERNARD G. STEINETZ, VIVIAN L.
BEACH, and ROBERT L. KROC, Relaxin

ALBERT SEGALOFF, The Gonadotrophins

ALBERT SEGALOFF, Prolactin

C. W. TURNER, Thyrotropic Hormone

JOSEPH FISCHER, Adrenocorticotrophic
Hormone

Part 4

RALPH I. DORFMAN, Standard Methods
Adopted by Official Organizations

HAROLD PAPKOFF and CHOH HAO LI,
Hypophyseal Growth Hormone

AUTHOR INDEX—SUBJECT INDEX.



ACADEMIC PRESS, NEW YORK and LONDON

111 Fifth Avenue, New York 3, New York
17 Old Queen Street, London, S.W.1, England

PHYSICAL METHODS in CHEMICAL ANALYSIS

Edited by WALTER G. BERL

Applied Physics Laboratory, The Johns Hopkins University

Volume 4

August 1961, 476 pp., \$16.00

Dialysis

By CHARLES W. CARR, *University of Minnesota*

Separations with Molecular Sieves

By TUDOR L. THOMAS and ROLLAND L. MAYS, *Union Carbide Corporation, Tonawanda, New York*

Separations with Foams

By MILTON E. WADSWORTH, *University of Utah*

Electromagnetic Separations

By A. E. CAMERON, *Union Carbide Nuclear Company, Oak Ridge, Tennessee*

Ion Exchange

By WILLIAM RIEMAN, III, *Rutgers University*, and ROGER SARGENT, *The Dow Chemical Company, Midland, Michigan*

Analytical Applications of

Inclusion Compounds

By MAXIMO BARON, *Atanor S.A.M., Buenos Aires, Argentina*

Separation of Gases and Liquids

by Thermal Diffusion

By G. DICKEL, *University of Munich, West Germany*

Solvent Extraction

By F. A. VON METZSCH, *Th. Goldschmidt A. G., Essen, Germany*

AUTHOR INDEX—SUBJECT INDEX.

Volume 2

Second Edition, Revised

1962, in preparation

TENTATIVE CONTENTS

Polarography

By JAROSLAV HEYROVSKY and PETR ZUMAN, *Czechoslovak Academy of Sciences, Prague*

Conductometric Analysis

By H. T. S. BRITTON, *University of Exeter*

Potentiometric Analysis

By H. A. LAITINEN, *University of Illinois*

Electrography and Electro-Spot

Testing

By H. W. HERMANCE and H. V. WADLOW, *Bell Telephone Laboratories, Murray Hill, New Jersey*

Magnetic Methods of Analysis

By A. R. KAUFMANN, *Massachusetts Institute of Technology*

The Determination of the Area

of the Surfaces of Solids

By GEORGE JURA, *University of California, Berkeley*

Vacuum Techniques and Analysis

By BENJAMIN B. DAYTON, *Consolidated Electrodynamics Corporation, Pasadena, California*

Gas Analysis by Methods Depending on Thermal Conductivity

By E. R. WEAVER, *National Bureau of Standards, Washington, D. C.*

The Measurement of Radioactivity for Tracer Applications

By ALOIS LANGER, *Westinghouse Research Laboratories, East Pittsburgh, Pennsylvania*

Statistical Analysis

By J. SHERMAN, *Philadelphia Naval Shipyard*

Chromatographic Analysis

By WALTER G. BERL, *Applied Physics Laboratory, The Johns Hopkins University*

AUTHOR INDEX—SUBJECT INDEX.

PREVIOUSLY PUBLISHED

Volume 1, (Second Edition, Revised).....1960, 686 pp., \$19.00

Volume 31956, 652 pp., \$15.00



ACADEMIC PRESS, NEW YORK AND LONDON

111 FIFTH AVENUE, NEW YORK 3, NEW YORK
17 OLD QUEEN STREET, LONDON, S.W.1

Protein Structure

By HAROLD A. SCHERAGA, *Cornell University, Ithaca, New York*

August 1961, 306 pp., \$8.00

The primary aim of this book is to present some of the quantitative aspects of the physicochemical approach to the protein structure problem, including both gross and internal structure. In discussing gross structure, polymer principles have been applied. In considering the more detailed aspects of internal structure, attention has been directed to interactions between polar groups and nonpolar ones. The material is developed from first principles, assuming only a background of elementary physical chemistry.

The book has evolved from a series of lectures given for C.S.I.R.O. in Melbourne, based on research carried out in the author's laboratory during the past decade. It will be of interest to all students and research workers engaged in the study of the structure of biological activity of proteins. It will also be of value to workers in other biological sciences in which the principles of protein structure and activity are of interest.

CONTENTS:

Hydrodynamic Properties of Protein Solutions
Internal Structure; Effect of Hydrogen Bonding
on Side-Chain Reactivity
Limited Proteolysis
Denaturation

Limited Proteolysis and Aggregation in the
Fibrinogen-Fibrin Conversion
Some Experimental Methods
Configurational Studies of Insulin, Lysozyme,
and Ribonuclease
REFERENCES—SUBJECT INDEX.

Protein Biosynthesis

*Proceedings of the Symposium held under the auspices of
U.N.E.S.C.O., at Wassenaar, August 29—September 2, 1960
Edited by R. J. C. HARRIS, Imperial Cancer Research Fund, London*

June 1961, 409 pp., \$14.00

Contents available upon request.

This international symposium was sponsored jointly by U.N.E.S.C.O., C.I.O.M.S., and the Netherlands Cancer Institute. This book includes not only the papers but also the major contributions to the discussion. It provides the first authoritative and complete account of progress in this rapidly expanding field.

The treatment is primarily biochemical. All major research groups in this field were represented. This volume will be useful not only to biochemists but also to those cytologists, biophysicists, and chemists who are interested in such topics as the function of nucleic acids, the structure of cytoplasm, the properties of ribosomes, the biosynthesis of viruses, and the synthesis of antibodies.

Amino Acids, Proteins and Cancer Biochemistry

*Papers presented at the JESSE P. GREENSTEIN MEMORIAL SYMPOSIUM, Division
of Biological Chemistry, American Chemical Society, September 16, 1959*

Edited by JOHN T. EDSALL, Harvard University

Preface by SIDNEY W. FOX and JULIUS SCHULTZ

1960, 244 pp., \$7.00

"We believe that this book, which includes all of the papers given at the Symposium, will make an important contribution in portraying some of the

major current developments in amino acid and protein chemistry and in the biochemistry of cancer—the two great fields in which Greenstein's work was preeminent."

—From the Preface



ACADEMIC PRESS, NEW YORK AND LONDON

111 FIFTH AVENUE, NEW YORK 3, N. Y.
17 OLD QUEEN STREET, LONDON S.W. 1

Announcing

International Edition ANGEWANDTE CHEMIE — in English —

Volume 1, Number 1, January 1962

The *international edition* of ANGEWANDTE CHEMIE is under the editorial supervision of Dr. W. Foerst who is also chief editor of the German-language ANGEWANDTE CHEMIE, founded in 1888. This journal has achieved great distinction in chemical literature and has often been chosen as the medium of publication by many distinguished scientists, including many Nobel Laureates.

Each number of ANGEWANDTE CHEMIE/*international edition* contains

- * review articles
from all fields of chemistry written by authorities, concise,
easy to read, well documented
- * selected papers
from the affiliated journal "Chemie-Ingenieur-Technik"
- * communications
from all fields of chemical research, carefully selected to assure
highest standards
- * conference reports
abstracts of lectures given at the most important European
chemical meetings, covering unpublished results
- * selected abstracts
reporting the highlights from international chemical literature —
fast, reliable
- * book reviews

chosen from the semimonthly issues of the German edition.

Volume 1, about 600 pages ($\frac{3}{4}$ of the German edition), will consist of 12 issues, to be released monthly.

Subscription price: \$15.00 (plus postage)

Please place your order with your subscription agent or with one of the publishers.

A limited supply of sample issues, representing a complete translation of Volume 72, No. 22, November 21, 1960, has been prepared. A detailed brochure is available from one of the publishers:

ACADEMIC PRESS

111 Fifth Avenue
New York 3, New York
U. S. A.

17 Old Queen Street
London, S. W. 1
England

VERLAG CHEMIE, G.m.b.H.

Pappelallee 3
Weinheim/Bergstr.
Germany

